Vol. 63 July, 1959 No. 7

THE JOURNAL OF PHYSICAL CHEMISTRY

(Registered in U. S. Patent Office)

CONTENTS

THE JOURNAL OF PHYSICAL CHEMISTRY

(Registered in U. S. Patent Office)

Published monthly by the American Chemical Society at 20th and Northampton Sts., Easton, Pa.

Second-class mail privileges authorized at Easton, Pa. This publication is authorized to be mailed at the special rates of postage prescribed by Section 132.122.

The *Journal of Physical Chemistry* is devoted to the publication of selected symposia in the broad field of physical chemistry and to other contributed papers.

Manuscripts originating in the British Isles, Europe and Africa should be sent to F. C. Tompkins, The Faraday Society, 6 Gray's Inn Square, London W. C. 1, England.

Manuscripts originating elsewhere should be sent to W. Albert Noyes, Jr., Department of Chemistry, University of Rochester, Rochester 20, N. Y.

Correspondence regarding accepted copy, proofs and reprints should be directed to Assistant Editor, Allen D. Bliss, Department of Chemistry, Simmons College, 300 The Fenway, Boston 15, Mass.

Business Office: Alden H. Emery, Executive Secretary, American Chemical Society, 1155 Sixteenth St., N. W., Washington 6, D. C.

Advertising Office: Reinhold Publishing Corporation, 430 Park Avenue, New York 22, N. Y.

Articles must be submitted in duplicate, typed and double spaced. They should have at the beginning a brief Abstract, in no case exceeding 300 words. Original drawings should accompany the manuscript. Lettering at the sides of graphs (black on white or blue) may be pencilled in and will be typeset. Figures and tables should be held to a minimum consistent with adequate presentation of information. Photographs will not be printed on glossy paper except by special arrangement. All footnotes and references to the literature should be numbered consecutively and placed in the manuscript at the proper places. Initials of authors referred to in citations should be given. Nomenclature should conform to that used in *Chemical Abstracts*, mathematical characters marked for italic, Greek letters carefully made or annotated, and subscripts and superscripts clearly shown. Articles should be written as briefly as possible consistent with clarity and should avoid historical background unnecessary for specialists.

Notes describe fragmentary or incomplete studies but do not otherwise differ fundamentally from articles and are subjected to the same editorial appraisal as are articles. In their preparation particular attention should be paid to brevity and conciseness. Material included in Notes must be definitive and may not be republished subsequently.

Communications to the Editor are designed to afford prompt preliminary publication of observations or discoveries whose value to science is so great that immediate publication is imperative. The appearance of related work from other laboratories is in itself not considered sufficient justification for the publication of a Communication, which must in addition meet special requirements of timeliness and significance. Their total length may in no case exceed 500 words or their equivalent. They differ from Articles and Notes in that their subject matter may be republished.

Symposium papers should be sent in all cases to Secretaries of Divisions sponsoring the symposium, who will be responsible for their transmittal to the Editor. The Secretary of the Division by agreement with the Editor will specify a time after which symposium papers cannot be accepted. The Editor reserves the right to refuse to publish symposium articles, for valid scientific reasons. Each symposium paper may not exceed four printed pages (about sixteen double spaced typewritten pages) in length except by prior arrangement with the Editor.

Remittances and orders for subscriptions and for single copies, notices of changes of address and new professional connections, and claims for missing numbers should be sent to the American Chemical Society, 1155 Sixteenth St., N. W., Washington 6, D. C. Changes of address for the *Journal of Physical Chemistry* must be received on or before the 30th of the preceding month.

Claims for missing numbers will not be allowed (1) if received more than sixty days from date of issue (because of delivery hazards, no claims can be honored from subscribers in Central Europe, Asia, or Pacific Islands other than Hawaii), (2) if loss was due to failure of notice of change of address to be received before the date specified in the preceding paragraph, or (3) if the reason for the claim is "missing from files."

Subscription Rates (1959): members of American Chemical Society, $8.00 for 1 year; to non-members, $16.00 for 1 year. Postage free to countries in the Pan American Union; Canada, $0.40; all other countries, $1.20. Single copies, current volume, $1.35; foreign postage, $0.15; Canadian postage $0.05. Back volumes (Vol. 56–59) $15.00 per volume; (starting with Vol. 60) $18.00 per volume; foreign postage, per volume $1.20, Canadian, $0.15; Pan-American Union, $0.25. Single copies: back issues, $1.75; for current year, $1.35; postage, single copies: foreign, $0.15; Canadian, $0.05; Pan-American Union, $0.05.

The American Chemical Society also publishes *Journal of the American Chemical Society, Chemical Abstracts, Industrial and Engineering Chemistry, Chemical and Engineering News, Analytical Chemistry, Journal of Agricultural and Food Chemistry, Journal of Organic Chemistry* and *Journal of Chemical and Engineering Data*. Rates on request.

THE JOURNAL OF PHYSICAL CHEMISTRY

(Registered in U. S. Patent Office) (© Copyright, 1959, by the American Chemical Society)

VOLUME 63 JULY 20, 1959 NUMBER 7

SUBSTRATE EFFECTS ON THE DECOMPOSITION OF ALKYL HYDROPEROXIDES AND THEIR INFLUENCE UPON AUTOXIDATION[1]

BY J. R. THOMAS AND O. L. HARLE

California Research Corporation, Richmond, California

Received May 5, 1958

Rates of decomposition of tetralin hydroperoxide were measured in the presence of phenyl-α-naphthylamine in medicinal white oil. Data are presented to show that the amine is an effective radical trap in the system under study and that the measured rates represent rates of primary reactions, unattended by radical chain reactions. The decomposition is apparently first order to at least 50% decomposition, but the rate constants are dependent upon the initial concentration of hydroperoxide. Extrapolated to zero concentration, these rate constants give an activation energy of 31.4 kcal./mole over the temperature range 121.5–166.3°. The rate of decomposition is found to vary with the nature of the solvent, being much faster in certain olefins than in saturated hydrocarbons. In these olefinic solvents, the activation energy for decomposition is about 20 kcal./mole, indicating that the reaction is not unimolecular. A correlation is found to exist between the rate of decomposition of tetralin hydroperoxide in a number of solvents and the rates of autoxidation of these solvents.

Although the decomposition of alkyl hydroperoxides to give free radicals is an important reaction in the autoxidation of hydrocarbons, little is known about it with certainty. The reaction is known to be complex, frequently due to the presence of secondary chain reactions.[2] In addition, there is evidence that the primary reaction is second order under some conditions and first order under others.[3–5] Furthermore, it has been observed that the rate of decomposition of hydroperoxides is influenced by the nature of the solvent, although in these cases the role of the solvent was complicated by its influence upon the above-mentioned effects.

This paper describes a study of the thermal decomposition of tetralin hydroperoxide in medicinal white oil in the presence of an inhibitor to eliminate secondary reactions induced or propagated by free radicals. The decomposition is studied as a function of concentration under these conditions, which permits the first-order decomposition to be isolated from reactions of higher order. The influence of solvent upon the first-order decomposition is studied for a variety of solvents, and the results are correlated with the ease of autoxidation of the solvent.

Experimental

Rate Measurements.—For high boiling solvents, decomposition rates were determined by withdrawing aliquots for peroxide determination from glass-stoppered vials immersed in an oil-bath thermostated to within ±0.1°. The surface above the liquid in the vials was blanketed with oxygen-free nitrogen. Sealed ampules were used for lower boiling solvents. Temperature was measured with a thermocouple. Hydroperoxide was determined by reaction with potassium iodide in a glacial acetic acid–chloroform mixture under carbon dioxide, followed by titration with standard sodium thiosulfate.

A series of experiments following the procedure of Morse[6] also was performed. The decomposition of tetralin hydroperoxide in medicinal white oil was studied in an apparatus modeled upon hers, with the modification that the sweeping gases (helium and oxygen-free nitrogen) could be entirely recovered after sweeping at a carefully controlled rate and analyzed by mass spectrography for the hydrogen, oxygen and water which might be produced by the decomposition of the hydroperoxide.

In experiments to test the effectiveness of the inhibitor, the decomposition of tetralin hydroperoxide was induced by di-*t*-butyl peroxide in the presence of phenyl-α-naphthylamine (PAN) in degassed sealed ampules, and the decomposition rate was measured.

Materials.—Tetralin hydroperoxide, prepared by the method of Hock and Susemihl,[7] recrystallized from hexane; di-*t*-butyl peroxide, purified by distillation; medicinal white oil, commercial product, used without further purification;

(1) Presented before the Petroleum Division of the American Chemical Society Meeting, San Francisco, Calif., April 13–18, 1958.

(2) F. H. Seubold, Jr., F. F. Rust and W. E. Vaughan, *J. Am. Chem. Soc.*, **73**, 18 (1951).

(3) A. Farkas and E. Passaglia, *ibid.*, **72**, 3333 (1950).

(4) L. Bateman and H. Hughes, *J. Chem. Soc.*, 4594 (1952).

(5) V. Stannett, A. E. Woodward and R. B. Mesrobian, THIS JOURNAL, **61**, 360 (1957).

(6) B. K. Morse, *J. Am. Chem. Soc.*, **79**, 3375 (1957).

(7) H. Hock and W. Susemihl, *Ber.*, **66**, 61 (1933).

TABLE I

FIRST-ORDER DECOMPOSITION RATE CONSTANTS

Tetralin hydroperoxide in medicinal white oil. Influence of phenyl-α-naphthylamine and inert gases.

T, °C.	(ROOH), m	(PAN), m	Sweeping gas	$k \times 10^4$, sec.$^{-1}$
	0.06	0	None	1.68
	.054	0	7.12 cc./min. N_2	1.60
	.06	0.018	None	1.05
150.6	.054	.041	15.6 cc./min. N_2	0.91
	.053	.041	8.7 cc./min. He	1.03
	0.22	0	6.0 cc./min. He	2.99
	.22	0.08	7.1 cc./min. He	1.39
150.6	.24	.018	None	1.42
	.24	.037	None	1.37
	.24	.073	None	1.41
	0.24	0.018	None	4.33
166.3	0.24	0.037	None	4.33
	0.24	0.018	None	0.43
135.6	0.24	0.037	None	0.42

polybutene, commercial product, percolated through active alumina; phenyl-α-naphthylamine (PAN) and 2,6-di-*t*-butyl-*p*-cresol, commercial materials recrystallized from benzene–alcohol; all other solvents, commercial products percolated through active alumina and then carefully distilled under nitrogen.

Autoxidation Inhibition Periods.—The method has been described previously.[8] The inhibited substrate is stirred by a very fast magnetic stirrer in a closed system to which oxygen is delivered as consumed at atmospheric pressure from a recording gasometer.

Results

Influence of Inhibitor and Inert Gas Sweeping.—Phenyl-α-naphthylamine was used as an inhibitor to eliminate chain and radical-induced decomposition, as previously described.[9] From the data given in Table I, it is seen that small concentrations of this material decrease the observed rate of decomposition, but that further increases in concentration are without effect. A second inhibitor, 2,6-di-*t*-butyl-*p*-cresol, was found to behave similarly at 150.6° and to give a similar fully inhibited value. Also included in Table I are the results of experiments in which a gas stream is continually swept through the solution by the method of Morse.[6] Data are given for oxygen-free nitrogen and helium. It is seen that it makes no difference whether or not the solutions are continuously swept with an inert gas. This is in contrast to the work of Morse who reports that removal of oxygen by sweeping with an inert gas greatly accelerates the rate of decomposition of *t*-butyl hydroperoxide. In preliminary experiments at 98.5° with *t*-butyl hydroperoxide in dodecane, using apparatus patterned after that of Morse, we have been unable to reproduce Morse's results. We find the principal cause of *t*-butyl hydroperoxide disappearance from the reactor to be volatilization. If a Dry Ice trap is inserted in the flowing gas stream following the water condenser and the results are corrected for the hydroperoxide collected there, we find a rate of thermal decomposition similar to that observed in sealed glass ampules. This result is to be expected from the vapor pressure of *t*-butyl hydroperoxide at 20°, the temperature of the water condenser in the Morse apparatus. We also find a negligible yield of oxygen from the decomposition, *i.e.*, <1%.

Gaseous Products.—In Table II are given yields of several gaseous products from tetralin hydroperoxide decomposition recovered in the experiments using inert gas sweeping. Several points are of interest. First, the yield of oxygen is very low under all conditions. Second, the yield of hydrogen is appreciable at high concentration of hydroperoxide but is reduced to zero in the presence of PAN. Third, the yield of water is approximately 50%, based on peroxide OH, in the absence of PAN but becomes close to 100% in the presence of PAN.

TABLE II

YIELD OF GASEOUS PRODUCTS, MOLES/MOLE TETRALIN HYDROPEROXIDE DECOMPOSED

(ROOH), m	(PAN), m	H_2O	O_2	H_2
0.054	0	0.38–0.51	0.01	0.03
.054	0.041	.77–0.89	0.01	nil
.22	0	.46–0.47	nil	0.16
.22	0.081	.94–1.01	nil	nil

Order of Reaction, Hydroperoxide Decomposition.—Plots of log (RO_2H) *versus* time showed no departure from linearity except those at the lower temperature and higher concentrations. Typical behavior is shown in Fig. 1 for an initial peroxide concentration of 0.06 mole liter^{-1} at 150.5°. Where departure from linearity was observed, the effect was very small and could not be distinguished at less than about 50% decomposition. In these instances the initial slope was used as a measure of the first-order rate constant. The first-order rate constant so derived was dependent upon the initial concentration of hydroperoxide, showing the presence of a reaction of higher order than first. For example, the rate constants at 121.5° were 0.71, 0.83, 1.0 and 1.5 × 10^{-5} sec.$^{-1}$ at peroxide concentrations of 0.03, 0.06, 0.12 and 0.24 mole liter^{-1}, respectively. Linear extrapolation of these values to zero concentration gives, with very slight error, the true first-order rate constant uncomplicated by reactions of higher order. Table III gives the fraction of the total initial decomposition occurring by higher order reactions at a series of temperatures and at two concentrations of hydroperoxide. These data show that the extent of the higher order reaction decreases with increasing temperature and decreasing concentration. These observations are consistent with Bateman's[4] suggestion that the frequently observed second-order decomposition of hydroperoxides results from dimerization in solution, although they do not constitute proof.

TABLE III

PER CENT. DECOMPOSITION BY HIGHER ORDER REACTIONS

T, °C.	% at 0.06 mole l.$^{-1}$	% at 0.24 mole l.$^{-1}$
121.5	28	60
135.6	19	52
150.5	8.7	26
166.3	8.5	21

(8) O. L. Harle and J. R. Thomas, Paper 22 presented at the General Session of the Petroleum Division of the ACS, April 12, 1957; Preprints, Vol. 2, No. 1, p. 43.

(9) J. R. Thomas, *J. Am. Chem. Soc.*, **77**, 246 (1955).

Similar behavior was found when 2-ethylhexene-1 was used as a solvent. Again, the effect of increasing inhibitor concentration quickly approaches a limit, and the apparent first-order decomposition rate constant is dependent upon hydroperoxide concentration. At 130° the rate constants were 1.08, 1.29 and 1.69 $\times 10^{-4}$ sec.$^{-1}$ at 0.06, 0.12 and 0.24 mole liter^{-1}, respectively.

Di-*t*-butyl Peroxide-induced Decomposition of Tetralin Hydroperoxide.—In order to test the efficiency of phenyl-α-naphthylamine as an inhibitor of free radical-induced reactions, its effect on the di-*t*-butyl peroxide catalyzed decomposition of tetralin hydroperoxide was studied. The results of this study are shown in Table IV where the first-order rate constants for peroxide disappearance are given for various concentrations of tetralin hydroperoxide, di-*t*-butyl peroxide and PAN. All experiments gave first-order plots to within experimental error. Typical plots are shown in Fig. 2. Points calculated on the basis of a mechanism discussed later also are shown. Acetone and *t*-butyl alcohol, products of di-*t*-butyl peroxide decomposition, were found to have no effect on the hydroperoxide decomposition rate.

TABLE IV

INDUCED DECOMPOSITION OF TETRALIN HYDROPEROXIDE BY DI-*t*-BUTYL PEROXIDE, 150.5°

Solvent	(ROOH), *m*	(DTB), *m*	(PAN), *m*	$k \times 10^4$, sec.$^{-1}$
White Oil	0.06	0	0.091	1.05
	.06	0.025	0	3.3
	.03	.05	.091	1.63
	.06	.05	0	4.6
	.06	.05	.091	1.51
	.12	.05	.091	1.56
	.06	.05	.045	1.58
	.06	.05	.022	2.01
	.06	.025	.091	1.28
	.06	.10	.091	2.13

Effect of Solvent upon First-order Decomposition.—Comparing the first-order rate constants for tetralin hydroperoxide at 130° in medicinal white oil and 2-ethylhexene-1, one finds that the decomposition is 5.7 times as fast in the latter solvent as in the former solvent. Similar studies were made with other solvents, except that the rate constants were not extrapolated to zero concentration. The measurements were made at as low a concentration as feasible (0.06 mole liter^{-1} in all cases). Judging from data given above, these values should be in error by not more than 10–20%. Inhibitor was used in all cases. The rate constants for tetralin hydroperoxide decomposition in these solvents are given in Table V at 170°. The value for isooctane was measured at this temperature. Also given in Table V are the activation energies, where these were determined, and these values were used to extrapolate data from lower temperatures to 170°. Where activation energies were not determined, a value of 29.0 kcal./mole was used, except for 2,4,4-trimethylpentene-1 and polypropylene, where a value of 19.8 kcal./mole, that of 2-ethylhexene-1, was used. The activation energy in medicinal white oil of 31.4 kcal./mole arises from the data given in a previous section. The plot of $-\log k$ *versus* $1/T$ is given in Fig. 3.

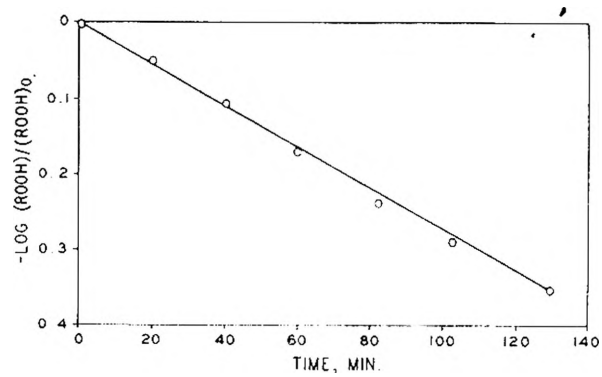

Fig. 1.—Log (ROOH)/(ROOH)$_0$ *vs.* time, tetralin hydroperoxide, 150.5°.

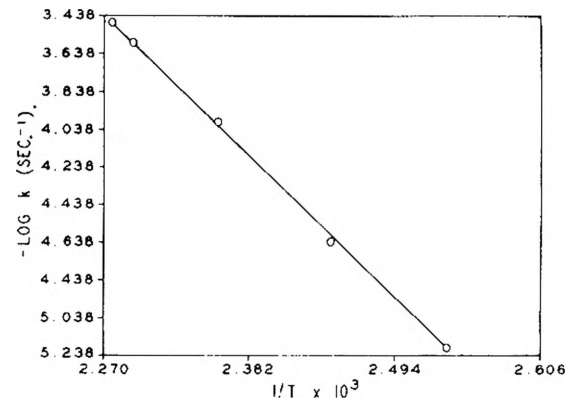

Fig. 2.—Decomposition of tetralin hydroperoxide; log *k* *vs.* $1/T$.

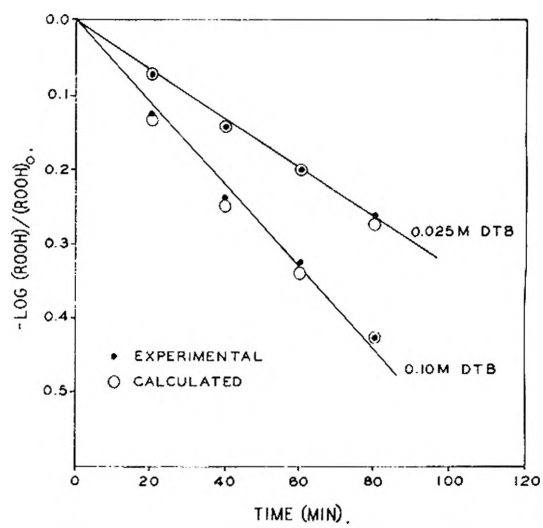

Fig. 3.—Log (ROOH)/(ROOH)$_0$ *versus* time. Tetralin hydroperoxide decomposition catalyzed by di-*t*-butyl peroxide (DTB)-0.091 *M* PAN.

Discussion

The decomposition of a hydroperoxide in solution is complex. In any given experiment without inhibitor there exists a primary first-order reaction, a secondary reaction which, together with the primary reaction, gives a first-order rate, and a reaction of higher order. Our purpose is to isolate as nearly as possible the primary reaction, since the

TABLE V

EFFECT OF SOLVENT UPON RATE OF DECOMPOSITION OF TETRALIN HYDROPEROXIDE AT 170°

	$k \times 10^4$, sec.$^{-1}$	ΔE_{Act}, kcal./mole
Isoöctane	1.31	...
n-Butyl stearate	1.47	30.0
n-Tetradecane	2.32	...
n-Octadecane	2.54	28.5
White oil	4.82	31.4
Hexadecene-1	7.92	28.0
Dioctyl ether	14.5	29.0
2-Ethylhexene-1	12.6	19.8
2,4,4-Trimethylpentene-1	16.7	...
Polybutene	21.7	18.7
Polypropylene	25.0	...

influence of hydroperoxide decomposition upon inhibited autoxidation appears to involve primarily this reaction. This is the case because the hydroperoxide concentration during the induction period is very low and because the inhibitor should greatly reduce the likelihood of free radical-induced secondary peroxide decomposition reactions.

First let us emphasize that we find essentially no oxygen evolved as a result of the decomposition of tetralin hydroperoxide under our conditions. Furthermore, we do not find an effect of sweeping a decomposing solution of tetralin hydroperoxide with inert gas as did Morse for *t*-butyl hydroperoxide, nor have we been able to reproduce Morse's results, as discussed above. Consequently, this complication need not be considered.

A most important question for our purpose is that of the efficiency with which PAN acts as a radical trap, since we use it to eliminate the free radical-induced secondary reactions. To determine its effectiveness, the induced decomposition of tetralin hydroperoxide by di-*t*-butyl peroxide was studied. The results presented in Table IV show that such an induced decomposition does occur and that PAN greatly inhibits it. For example, at a tetralin hydroperoxide concentration of 0.06 *M* and a di-*t*-butyl concentration of 0.05 *M* the observed first-order rate constant for hydroperoxide decomposition is 4.6×10^{-4} sec.$^{-1}$. In the presence of 0.045 and 0.091 *M* PAN the rate constants drop to 1.56 and 1.51×10^{-4} sec.$^{-1}$, respectively. The fully inhibited rate constant for tetralin at 0.06 *M* without added di-*t*-butyl peroxide is 1.05×10^{-4} sec.$^{-1}$. Unfortunately, the PAN does not entirely eliminate the effect of the di-*t*-butyl peroxide. The most likely reason for this is that di-*t*-butyl peroxide and tetralin hydroperoxide react in a bimolecular reaction. Such a bimolecular reaction is known for hydroperoxides alone, and it seems reasonable that a dialkyl peroxide and a hydroperoxide might react similarly. Evidence for this can be obtained from the data presented in Table IV.

Assuming that the fully inhibited tetralin hydroperoxide decomposition rate represents the primary first-order reaction (at 0.06 *M* and 150° the higher order reaction is very slight), and assuming a bimolecular reaction between peroxide and hydroperoxide, the rate equation for hydroperoxide disappearance is

$$-\ln \frac{(\mathrm{ROOH})_t}{(\mathrm{ROOH})_0} = k_1 t + k_2(\mathrm{DTB})_0 \int_0^t e^{-\{k_3 t + (k_2/k_{obs})(\mathrm{ROOH})_0(1 - e^{-k_{obs}t})\}} dt \quad (1)$$

where k_1 is the first-order rate constant for the primary decomposition of hydroperoxide, k_3 is the first-order decomposition rate constant for di-*t*-butyl peroxide decomposition, k_2 is the second-order rate constant for the hydroperoxide–peroxide reaction, and k_{obs} is the experimentally observed first-order rate for tetralin hydroperoxide disappearance. Graphical integration of this expression yields values of k_2 for the series of inhibited runs with varying concentrations of di-*t*-butyl peroxide. A constant value of k_2 of $16 \pm 1 \times 10^{-4}$ mole liter^{-1} sec.$^{-1}$ is obtained over the fourfold range of concentration studied, indicating the proposed mechanism to be correct. Integration of equation 1 for the series at constant di-*t*-butyl peroxide concentration but with varying concentrations of tetralin hydroperoxide shows that the observed first-order rate constant should vary by only 7% over the fourfold change of concentration reported in Table IV. This is in excellent agreement with the experimentally observed values and demonstrates further the soundness of the proposed mechanism. In the above calculations, k_3 was taken to be 1.49×10^{-4} sec.$^{-1}$ from the data of Lossing and Tickner.[10] Equation 1, using the value of k_2 found above, predicts essentially first-order hydroperoxide disappearance within experimental error for inhibited runs reported in Table IV to at least 50% decomposition. Calculated points are compared with experimental points in Fig. 3. Further indication that PAN effectively inhibits free radical-induced secondary reactions is evident from the gaseous products of decomposition presented in Table II. It will be noted that in the absence of PAN considerable hydrogen is evolved, but that in the presence of PAN the hydrogen evolution is eliminated. One likely explanation is that either the RO· radical or the S· radical derived from the solvent decomposes to give hydrogen. Alternatively, the RO· radical might decompose to give α-tetralone which might then react with hydroperoxide to give an α-hydroxy peroxide, which decomposes to give hydrogen in a manner discussed by Durham, Wurster and Mosher.[11] In any event, the inhibitory action of PAN upon hydrogen evolution suggests that it traps the radicals which might be involved in free radical-induced secondary decomposition of the hydroperoxide. The change in water yield is also indicative of its effectiveness.

These arguments demonstrate that PAN is an effective radical trap in our systems and that the first-order rate constants for tetralin hydroperoxide, extrapolated to infinite dilution, represent the primary first-order decomposition reaction quite well. The linear extrapolation of the observed rate constants to infinite dilution used here is not rigorous. However, since the observed first-order rate constants are a linear function of initial concentration and since the extrapolated value and the

(10) F. Lossing and A. W. Tickner, *J. Chem. Phys.*, **20**, 907 (1952).

(11) L. J. Durham, C. F. Wurster and H. S. Mosher, *J. Am. Chem. Soc.*, **80**, 332 (1958).

lowest measured concentration value never differ by more than 15%, the extrapolated values cannot be in error by more than several per cent.

The influence of solvent upon the rate of decomposition is much larger than that expected or ordinarily found for truly unimolecular reactions. Bawn and Mellish[12] found only a slight effect of solvent upon the unimolecular decomposition of benzoyl peroxide. Szwarc,[13,14] *et al.*, studying acetyl peroxide, found the rate to be independent of the solvent, and very close to that measured in the vapor phase. This behavior is to be expected since the transition state resembles the initial state so closely that the influence of solvent on both states should be the same.[15] The large effect of solvent found here indicates that the decomposition of hydroperoxide in solution is not truly unimolecular. This appears to be clearly the case with certain of the olefinic solvents, where the low activation energy indicates a different reaction from that occurring in the saturated solvents. The effect of olefinic solvents has been noted in the case of cyclohexene hydroperoxide by Farkas and Passaglia,[3] and in the case of *t*-butyl hydroperoxide by Walling and Chang.[16] In both instances, chain decomposition was considerable; however, evidence was obtained that the primary rate of bond cleavage was enhanced by the olefinic solvent. Walling and Chang suggest reaction (2) to account for this behavior

$$ROOH + CH_2 = CHC_6H_5 \longrightarrow ROO\cdot + CH_3\dot{C}HC_6H_5 \quad (2)$$

Nandi and Palit[17] observe that hydrogen peroxide functions as an initiator of vinyl polymerization at moderate temperatures and observe an effect of solvent upon the rate of initiation.

While the behavior of hydroperoxides in olefinic solvents may reasonably be explained by a reaction of the type shown above, (2), it is more difficult to suggest a reasonable mechanism for the influence of saturated solvents. A reaction such as (3) can be postulated, although it has no counterpart as far as we are aware.

$$ROOH + RH \longrightarrow RO\cdot + R\cdot + H_2O \quad (3)$$

A further indication that some such solvent effect is operable arises from the magnitude of the activation energy of the decomposition. The measurements reported here show clearly that the activation energy of the first-order tetralin hydroperoxide decomposition is about 31 kcal./mole. The complicating effects of induced decomposition and reactions of higher order appear to be absent, on the basis of the data presented. Previous data for other hydroperoxides show similarly low values of the activation energy.[9] When compared with the dissociation energies of hydrogen peroxide, 48 kcal./mole, and dialkyl peroxides, 32–36 kcal./mole,[18] this value seems abnormally low. The only other hydroperoxide for which the approximate first-order decomposition rate constant for the primary decomposition apparently has been determined is *t*-butyl hydroperoxide in *n*-octane.[19] The investigators relied solely upon extrapolation of rate data to infinite dilution, which might, but does not necessarily, eliminate induced decomposition. The activation energy in this case was found to be 39.0 kcal./mole, close to that found for di-*t*-butyl peroxide by the same investigators. Walling[20] suggests that this value appears low, in view of the value for hydrogen peroxide, and suggests that solvent is possibly involved in the cleavage process. In this case, however, the kinetic data agree closely with the dissociation energy calculated from heats of formation of the hydroperoxide and the resulting radicals. Mosher[21] recently has redetermined the heat of combustion of *t*-butyl hydroperoxide in agreement with Bell,[22] *et al.*, and calculates a dissociation energy of 41 ± 3 kcal./mole. It seems unlikely, thus, that the *n*-octane solvent plays a role in the decomposition in this case.

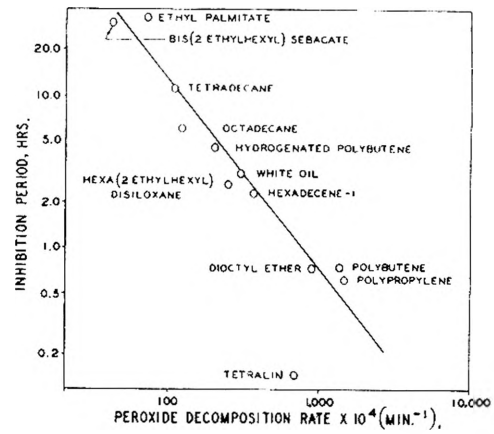

Fig. 4.—Inhibition period *versus* rate of thermal decomposition of tetralin hydroperoxide; 171°, 0.2% inhibitor.

The wide variations in the first-order decomposition rate constants with solvent suggests that this effect could be of importance in the rate of autoxidation of the solvent. This would be particularly true in inhibited oxidations, since the maximum hydroperoxide concentration during the inhibition period will be quite low, and higher order reactions will be unimportant. To test this idea, the inhibition period resulting from a given concentration of phenyl-α-naphthylamine in a number of fluids was determined at 171°. The log of the inhibition period is plotted against the log of the decomposition rate constant for tetralin hydroperoxide in those fluids in Fig. 4. It will be seen that the inhibition period is inversely proportional to the decomposition rate constant for all of the fluids studied except tetralin. In a previous report, it was shown[8] that the inhibition period is given by

(12) C. E. H. Bawn and S. F. Mellish, *Trans. Faraday Soc.*, **47**, 1216 (1951).

(13) A. Rembaum and M. Szwarc, *J. Chem. Phys.*, **23**, 909 (1955).

(14) J. Smid, A. Rembaum and M. Szwarc, *J. Am. Chem. Soc.*, **78**, 3315 (1956).

(15) S. Glasstone, K. J. Laidler and H. Eyring, "The Theory of Rate Processes," McGraw-Hill, Inc., New York, N. Y., 1941, p. 407.

(16) C. Walling and Y. W. Chang, *J. Am. Chem. Soc.*, **76**, 1878 (1954).

(17) U. S. Nandi and S. R. Palit, *J. Polymer Sci.*, **17**, 65 (1955).

(18) T. L. Cottrell, "The Strengths of Chemical Bonds," Academic Press, Inc., New York, N. Y., 1954.

(19) E. R. Bell, J. H. Raley, F. F. Rust, F. H. Seubold and W. E. Vaughan, *Disc. Faraday Soc.*, **10**, 242 (1951).

(20) C. Walling, "Free Radicals in Solution," John Wiley and Sons, New York, N. Y., 1957, p. 504.

(21) H. S. Mosher, private communication.

(22) E. R. Bell, F. H. Dickey, J. H. Raley, F. F. Rust and W. E. Vaughan, *Ind. Eng. Chem.*, **41**, 2597 (1949).

$$t_i = \frac{[IH]_0}{k_d k_L} \int_1^F \frac{d([IH]/[IH]_0)}{\frac{k_i}{k_d k_L} - \ln \frac{[IH]}{[IH]_0}} \qquad (4)$$

where

$[IH]_0$ = initial inhibitor concn.
$[IH]$ = instantaneous inhibitor concn.
k_d = rate constant for oxidation chain initiation by hydroperoxide decomposition
k_L = chain length constant, where chain length = $k_L/[IH]$
k_i = rate of chain initiation by reactions not involving hydroperoxide
F = fraction of inhibitor remaining at end of inhibition period (chosen to be arbitrarily small or zero)

It can be shown that the integral has a constant value for the conditions studied here.[8] The correlation shown in Fig. 4 suggests that the chain length constant k_L is approximately the same for the materials studied here, with the exception, possibly, of tetralin. The chain length constant for tetralin has been shown by Bolland[23] to be about 170 times as large as that for *n*-decane at 60°, which probably accounts for its very short inhibition period. Other materials with widely differing chain length constants should show similar deviations. The peroxides which catalyze the oxidation during the inhibition period are, of course, those native to the fluid. The effect of structure upon the thermal stability of hydroperoxides has been shown to be slight,[9] however, and the rate of decomposition of tetralin hydroperoxide should be close to that expected from the native peroxides in a given solvent.

(23) J. L. Bolland, *Quart. Rev.*, 358 (1948).

Summary

1. Phenyl-α-naphthylamine is shown to be an effective radical trap for the radicals produced when a hydroperoxide is decomposed in hydrocarbon solvents. By its use, free radical-induced secondary decomposition of the peroxide can be eliminated.

2. The primary first-order decomposition of tetralin hydroperoxide is strongly solvent dependent, suggesting that the radical-producing reaction involves reaction of the hydroperoxide with solvent.

3. The PAN inhibition period for autoxidation of a hydrocarbon is found to be inversely proportional to the rate at which tetralin hydroperoxide decomposes in that solvent. Since most hydroperoxides decompose at nearly the same rate in a given hydrocarbon solvent, the rate of the solvent–hydroperoxide reaction is seen to be an important factor in determining the rate of autoxidation of the hydrocarbon.

THE DEUTERIUM EXCHANGE ACTIVITIES OF SOME SUPPORTED PLATINUM CATALYSTS

BY C. G. MYERS, D. J. SIBBETT AND F. G. CIAPETTA

Contribution from Socony Mobil Oil Company, Inc., Research and Development Laboratory, Paulsboro, New Jersey

Received July 18, 1958

The kinetics of two different deuterium exchange reactions were studied over platinum on nine different supports. The reactions were (1) *n*-butane plus *n*-trideuteriobutane and (2) *n*-butane plus deuterium. The catalysts were, generally, platinum–acidic oxide materials having hydrogenation–dehydrogenation sites and "acid" sites. Their "dehydrogenation activities" were characterized by cyclohexane conversion to benzene; their "acid activities" by *p*-xylene isomerization. In either reaction, equilibrium product compositions matched those calculated by probability methods assuming (1) that all of the hydrogen atoms of *n*-butane are equally replaceable by deuterium atoms, and (2) that there is no isotope effect on the equilibrium compositions. In the butane–deuterium reaction, equilibration among the hydrogen isotopes of the system was reached first; equilibrium was next established for the distribution of deuterium atoms between hydrogen molecules and butane molecules; slowest was equilibration in the butane–deuteriobutane portion of the system. Catalyst activity toward each deuterium exchange reaction was found to parallel dehydrogenation activity primarily, and "acidity," as measured by xylene isomerization, secondarily. Reaction rate and apparent activation energy varied from catalyst to catalyst. Frequency factors and activation energies exhibited the "Compensation Effect." The kinetics suggest that the number of deuterium atoms combining with a butane molecule per collision of butane with deuterium also paralleled catalyst "acidity." The data, taken together, may mean that acid sites and platinum sites coact to promote this latter effect.

Catalytic exchange of deuterium between a low molecular weight paraffin and its deutero analog[1] involves catalyst interaction with only one chemical species, the hydrocarbon. On the other hand, another species, hydrogen, is present in the more commonly studied reaction of deuterium itself with paraffins.[2–5] In this work, these two reaction types are compared using *n*-butane. The catalysts were, generally, platinum on acidic oxide materials having both hydrogenation–dehydrogenation and "acid" activities.[6–10]

(1) G. Parravano, E. F. Hammel and H. S. Taylor, *J. Am. Chem. Soc.*, **70**, 2269 (1948).

(2) (a) C. Kemball, *Proc. Roy. Soc. (London)*, **A207**, 539 (1952); (b) **A217**, 376 (1951); (c) **A223**, 377 (1954); (d) J. R. Anderson and C. Kemball, *ibid.*, **A223**, 361 (1954).

(3) S. O. Thompson, J. Turkevich and A. P. Irsa, *J. Am. Chem. Soc.*, **73**, 5213 (1951).

(4) (a) A. Farkas and L. Farkas, *Trans. Faraday Soc.*, **35**, 917 (1939); (b) A. Farkas, *ibid.*, **36**, 522 (1940).

(5) (a) C. Horrex, R. K. Greenhalgh and M. Polanyi, *ibid.*, **35**, 511 (1939); (b) R. K. Greenhalgh and M. Polanyi, *ibid.*, **35**, 520 (1939).

(6) G. A. Mills, H. Heinemann, T. H. Milliken and A. G. Oblad, *Ind. Eng. Chem.*, **45**, 134 (1953).

(7) (a) M. J. Fowle, R. D. Bent, F. G. Ciapetta, P. M. Pitts and L. N. Leum, *Advances in Chem. Ser.*, No. 5, 76 (1951); (b) F. G. Ciapetta and J. B. Hunter, *Ind. Eng. Chem.*, **45**, 147 (1953); (c) F. G. Ciapetta, U. S. Patent 2,651,598.

(8) V. Haensel and G. R. Donaldson, *Ind. Eng. Chem.*, **43**, 2102 (1951).

(9) P. B. Weisz and E. W. Swegler, *Science*, **123**, 887 (1957).

(10) V. Haensel, U. S. Patent 2,623,860.

TABLE I

CATALYST CHARACTERIZATION

Cat. no.	Support	Pt concn. (wt. %)	Cl concn. (wt. %)	Surface area (sq. m./g.)	Dehyd. act.,[a] μmole/g./sec.	Isom. act.,[b] μmole/g./sec.
1	Al_2O_3[c]	0.59	0.15	430	4000	1.1
2	Al_2O_3[c]	.56	.69	410	3700	1.4
3	Al_2O_3[c]	.56	.01	180	1200	0.6
4	Al_2O_3[c]	.35	.35	350	400	1.2
5	Al_2O_3[d]	.49	1.0	90	1000	0.8, 0.9
6	SiO_2-Al_2O_3[e]	.47	...	390	1700	...
7	Cat. no. 6 treated with 0.5 M K_2CO_3			370	700	...
8	SiO_2[f]	0.47	...	680	1200	...
9	Act. C	0.56	...	1080	50	...

[a] Cyclohexane dehydrogenation activity. [b] p-Xylene isomerization activity. [c] Mostly eta Al_2O_3. [d] F-10 Al_2O_3. [e] 10% Al_2O_3. [f] 0.07% Al_2O_3.

Experimental

Materials.—Matheson C.P. n-butane (>99.8%) and Stuart Oxygen Co. deuterium (>99.5%) were used without further treatment. Phillips pure grade cyclohexane and p-xylene were each percolated through silica gel before use. Hydrogen was passed through Deoxo cylinders (palladium catalyst) to convert traces of oxygen to water, and then dried over silica gel.

The deuteriobutane was made by reaction at 316° and 1 atmosphere of 3 moles of deuterium with each mole of n-butane over the more active catalysts of this study. Space velocities were the same as those of the experiments reported below. The reaction product was frozen at liquid nitrogen temperatures, after which the non-condensable hydrogens were removed by evacuation. The remaining solidified butanes were gasified, refrozen, out-gassed and regasified. The charge for the butane–deuteriobutane experiments was made by dilution of 1 volume of the resulting deuteriobutanes with 3 volumes of n-butane.

The catalysts (Table I) were made by impregnation of the supports with aqueous chloroplatinic acid. The potassium "poisoned" catalyst[7e,11,12] was made by treating catalyst no. 6 with an equal volume of 0.5 M aqueous K_2CO_3 at room temperature for 30 min., filtering, washing and drying overnight at 280°. Each catalyst was reduced in flowing hydrogen at atmospheric pressure for 2 hours at 232°, 2 hours at 510°, and (for deuterium exchange reactions) overnight at 482° in place in the reactor.

Procedures.—Four kinds of hydrocarbon reactions were carried out; the two main types of deuterium exchange reactions and two indicator reactions, cyclohexane dehydrogenation to benzene and p-xylene isomerization.

The exchange reactions were carried out in an all-glass semi-automatic flow type apparatus. Premixed charge gas was displaced from a calibrated thermostated buret by mercury from a levelling bulb. This bulb rested in a harness which was raised at a constant speed by a cord winding on the spindle of an electrically driven "Zero-Max" torque converter. Charge rate depended on the setting of the torque converter and was reproducible to about ±4%.

The charge gas passed into a conventional spiral preheater (3 ft. of 1 mm. i.d. capillary tubing) and reactor tube ($^6/_{16}$ in. o.d. tubing). The bottom 8 cm. of the reactor contained the 2.0 cc. of 40/60-mesh catalyst. Preheater and reactor were together heated in thermostated (±0.5°) oil- or lead-baths.

Product gases passed from the reactor through about 2 ft. of unheated capillary tubing (2 mm. i.d.) into the top of a thermostated calibrated buret. This receiver was initially filled with mercury which could run out of it through a valve actuated by an "Asco" solenoid. The electrical circuit which operated the solenoid was made and broken by a manometric constant pressure regulator connected to the reactor. Thus, flow out of the reactor into the receiver was controlled by the pressure regulator. Pressure was constant to within ±1 mm. of mercury during an experiment.

Just before an experiment, hydrogen was evacuated from the reactor and replaced by charge gas. The first 30 to 40 cc. of product gas was discarded, then two 30 to 40 cc. product-samples were taken for analysis and, finally, residual reaction gas was evacuated and replaced with flowing hydrogen. Normally, three such experiments were done in one day, the earlier being at the lower temperature. At the end of the day any given catalyst sample was discarded. These arbitrary procedures almost eliminated the appearance of "erratic" results; those which persisted are reported.

The two indicator reactions were carried out in bench-scale high pressure equipment. For cyclohexane dehydrogenation, 350 p.s.i., 399°, 4 moles of hydrogen per mole of cyclohexane charge, and a liquid hourly space velocity of 5000 were used, giving conversions generally below 5%. For xylene isomerization, 175 p.s.i., 482°, 4 moles hydrogen per mole of p-xylene charge, and a space velocity of 100 gave conversions from 1 to 20%. Further details are given elsewhere.[13]

For these two indicator reactions, catalyst activity was characterized by reaction rate at conversion levels well below equilibrium values. Dehydrogenation activity is reported as micromoles of benzene produced per second per gram of catalyst after correction to eliminate effects of diffusional limitations on reaction rate. p-Xylene isomerization activity is in micromoles of isomers per second per gram. The repeatability of each is ±10%.

Mixtures of xylene isomers were analyzed by infrared absorption; all other reaction products, by mass spectrometry.

Equilibrium

Reaction of Deuterium with n-Butane.—Ideally, the reaction of an equimolar mixture of n-butane and deuterium would be

$$n\text{-}C_4H_{10} + D_2 \rightleftharpoons n\text{-}C_4H_9D + HD$$

In practice, however, all deuteriobutanes and all hydrogen isotopes are produced to some extent.

Equilibrium in this system may be considered as a combination of three simpler equilibria. First, there is an equilibrium with respect to introduction of deuterium atoms into butane. It is indexed by the proportion of the total deuterium atoms of the system which appear in the deuteriobutanes, the remaining atoms appearing as deuterium molecules or hydrogen deuteride. Secondly, there is the equilibrium among the various deuteriobutanes. Thirdly, there is an equilibrium among the hydrogen isotopes.

Each of these equilibria has been considered in

(11) A. P. Ballod, I. V. Patsevich, A. S. Feldman and A. V. Frost, *Doklady Akad. Nauk, U.S.S.R.*, **78**, 509 (1951); *C. A.*, **45**, 7861 (1951).

(12) M. O. Baker, S. D. Chestnutt and T. P. Weir, Jr., THIS JOURNAL, **52**, 1364 (1948).

(13) C. G. Myers and G. W. Munns, Jr., *Ind. Eng. Chem.*, **50**, 1728 (1958).

TABLE II

EQUILIBRIUM: BUTANE–DEUTERIUM EXCHANGE

$C_4H_{10}:D_2 = 1:1$; 125°; 1 atm.; Pt/SiO_2–Al_2O_3

Av. residence time (sec.)	5.5	5.5	8.0	8.0	18.3	18.3	27.9	27.9	50.2	50.2		
Compn., mole %		[a]		[a]		[a]		[a]		[a]	Calcn.	[b]
H_2	41.7	41.9	41.8	41.7	41.7	41.9	41.7	41.2	41.7	41.8		41.69
HD	7.8	7.7	7.8	7.9	8.0	7.7	7.9	8.3	7.9	7.8		7.88
D_2	0.5	0.4	0.5	0.4	0.4	0.4	0.4	0.5	0.4	0.4		0.43
n-C_4H_{10}	7.7	7.8	7.6	7.5	8.0	7.8	7.6	7.8	7.5	7.5	15.3	
n-C_4H_9D	15.6	15.4	15.2	15.4	15.6	15.5	15.2	15.4	15.5	16.1	30.5	
n-$C_4H_8D_2$	14.6	14.5	15.0	14.6	14.5	14.5	14.5	14.4	14.7	14.5	29.1	
n-$C_4H_7D_3$	8.3	8.1	8.2	8.3	8.0	8.1	8.4	8.3	8.3	8.0	17.3	
n-$C_4H_6D_4$	2.9	3.3	3.2	3.2	2.9	2.8	3.3	3.1	3.2	3.1	6.2	
n-$C_4H_5D_5$	0.8	0.9	0.8	0.9	0.9	1.3	0.9	0.9	0.9	0.7	1.6	
n-$C_4H_4D_6$	.04	.04	.1	.1	.1	0.04	.1	.1	.1	.1	tr.	
Atom wt. of D combined in												
Hydrogens/100 mole gas	8.8	8.5	8.8	8.7	8.8	8.5	8.7	9.3	8.7	8.6	Statistical	Calcd.
Butanes/100 mole gas	85.3	86.4	87.2	87.4	85.3	86.5	87.7	86.6	87.7	85.6		
Fraction of total D in												
Hydrogens	0.093	0.090	0.091	0.090	0.093	0.089	0.090	0.096	0.090	0.092		
Butanes	0.907	0.910	0.090	0.910	0.907	0.911	0.910	0.904	0.910	0.908		

[a] Second of two successive samples. [b] Calculated using $\mu = 0.0437$—see text.

the literature of exchange between paraffins and deuterium over films of transition metals. To check for consistency with the literature, the five experiments of Table II were made with the platinum–silica–alumina catalyst at 125° and at average residence times varying from 5 to 50 seconds. Two successive samples were taken during each run. The analyses of these 10 samples are the same within analytical repeatability (±2.5%). Clearly, the gas composition of Table II is time-independent when approached from a 1:1 mixture of deuterium and n-butane. To show that this is an equilibrium composition, it would also be necessary to obtain it from the corresponding mixture of deuteriobutanes and hydrogen. This was not attempted. Rather, the complete agreement which is shown below with the pertinent literature was considered justification for taking the compositions of Table II to represent equilibrium.

1. Introduction of Deuterium into the Butanes.—For the experiments reported in Table II, 90.8 ± 0.2% of the deuterium atoms of the system had become combined in the butanes, the remainder being in the hydrogen isotopes. Farkas[4b] determined that the ratio of H atoms to D atoms in the hydrogens divided by that ratio in the butanes lies between 1.89 and 2.43 at equilibrium. From the averaged data of Table II, the experimental ratio is 2.19.

$$\frac{\text{H/D in hydrogens}}{\text{H/D in butanes}} = \frac{[2(50.02) - 8.74]/8.74}{[10(49.98) - 86.57]/86.57} = 2.19$$

Thus, the experiments produced equilibrium in this respect. Moreover, the value of 2.19 is close to that of 1.91 calculated by Wirtz[14] on the basis that all of the hydrogen atoms of the butane molecule enter into the exchange.

2. Equilibration among the Deuterated Butanes.—Kemball[2c] found the distribution of the various butanes in the equilibrium products to be statistical. That is, they match those calculated by probability methods[15] assuming that (1) all ten positions occupied by hydrogen atoms in n-butane are equivalent, (2) a deuterium atom is equivalent to a hydrogen atom, and (3) these factors and charge composition determine equilibrium composition. This statistical method was used to calculate the equilibrium composition to be expected in the butane portion of the reaction products from the equimolar butane–deuterium mixture (Table II, column 11). Clearly, the distribution of the deuteriobutanes in the experimental products matches the equilibrium distribution.

3. Equilibration among the Hydrogen Isotopes.—The third equilibration to be considered is that among the hydrogens.

$$H_2 + D_2 \rightleftarrows 2HD$$

It has been thoroughly studied; the literature is summarized by Kirshenbaum.[16]

Following the method of Twigg,[17] the equilibrium constant may be expressed as a function of the total content of deuterium (both combined and uncombined) in the hydrogen fraction of the product gas. Thus, if μ is the total mole fraction of D_2 (both combined and uncombined) in the hydrogen fraction from the butane–deuterium reaction, and if n_i is the mole fraction of component i

$$\mu = {}^1/_2 n_{HD} + n_{D_2} \text{ and}$$

$$0.5 = \sum_i n_i = n_{H_2} + {}^1/_2 n_{HD} + \mu$$

because half of the product gas was hydrogen isotopes. At equilibrium

$$K = \frac{n^2_{HD}}{(0.5 - \mu - 0.5 n_{HD})(\mu - 0.5 n_{HD})}$$

(14) Wirtz, *Z. Elektrochem.*, **43**, 662 (1937).

(15) T. I. Taylor, "Hydrogen Isotopes," in P. H. Emmett, "Catalysis," Vol. V, Reinhold Publ. Corp., New York, N. Y., 1957, p. 354.

(16) I. Kirshenbaum, "Physical Properties of Heavy Water," National Nuclear Energy Series, Div. III, 4A (1951). See also *C. A.*, **46**, 8443 (1952).

(17) G. H. Twigg, *Trans. Faraday Soc.*, **33**, 1329 (1937).

At 125°, the value of $K = 3.48$.[16] The average value of μ for the 10 experiments of Table II is 0.0437. Using these values, the concentration of HD to be expected at equilibrium is 7.88 mole %. The corresponding concentration of D_2 is 0.43 mole %. The experimental distribution of the hydrogen isotopes in Table II matches this equilibrium distribution.

4. Comparative Rates of Approach to Equilibrium.—The introduction of deuterium into butane molecules produces, necessarily, either HD or H_2. As soon as either is formed, it exchanges with the other hydrogen isotopes present in the system. The three hydrogen isotopes equilibrate very rapidly. Even though very little deuterium and *n*-butane had reacted in some of the experiments, upwards of 90% of equilibrium among the hydrogens was achieved in all experiments. In most cases, complete equilibration among the hydrogens resulted.

Next most rapid was the rate of introduction of deuterium into butanes. That is, for products which were not quite at equilibrium in all respects, (1) the hydrogen isotopes would be completely equilibrated, (2) the ratio (H/D) in the hydrogens/(H/D) in the butanes would equal 2.19, but (3) the distribution of deuterated butanes would not be "statistical." Therefore the slowest of the three reactions is the equilibration among the butane "isotopes."

Reaction of Butane with Deuterobutane.—

$$n\text{-}C_4H_7D_3 + n\text{-}C_4H_{10} \rightleftharpoons n\text{-}C_4H_8D_2 + n\text{-}C_4H_9D, \text{ etc.}$$

Table III presents the product distributions from the reaction of the butane–deuteriobutane mixture over two active catalysts, platinum on F-10 alumina and platinum on silica–alumina. Each product is from the experiment having the longest residence time at each of three temperatures in the range from 291 to 608°. The distributions agree with each other and with the "statistical" equilibrium distribution (within analytical precision). Thus not only is the equilibrium distribution statistical in this system too, but it is also independent of both temperature and type of catalyst support in the ranges studied. In fact, the temperature-independence of the equilibrium distribution in the butane fractions from both reactions—and also in the hydrogen fraction[17]—is a reflection of the statistical nature of the equilibration process.

Kinetics

The Reaction of Butane with Deuteriobutane.—Harris[18] developed a generalized equation for the rate of an exchange reaction, assuming the reaction to be first order in the exchanged species (here, deuterium atoms). It was adapted by Anderson and Kemball[2d] to exchanges between deuterium and the light paraffin hydrocarbons. Anderson and Kemball found that their data for the reactions of deuterium with ethane, propane and isobutane over metal films in static systems fitted this adaptation of Harris' equation.

Rate constants were calculated from the results of the present work using the Anderson and Kemball equation

(18) G. M. Harris, *Trans. Faraday Soc.*, **47**, 710 (1951).

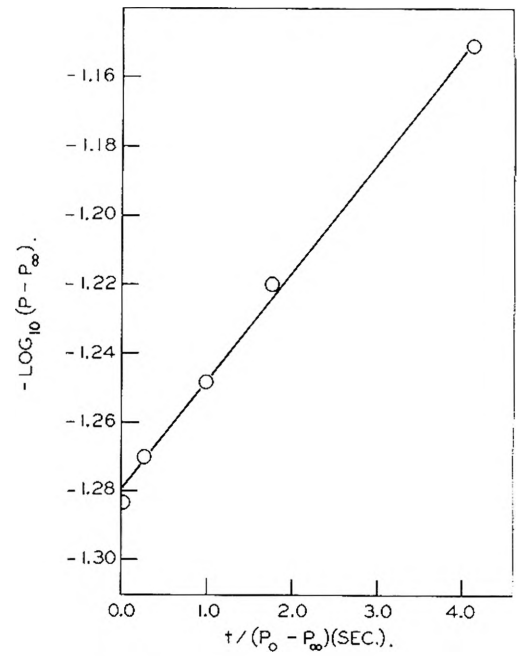

Fig. 1.—Butane–deuteriobutane exchange: rate (k_B) determination for Pt/SiO_2–Al_2O_3; 75°, 1 atm.

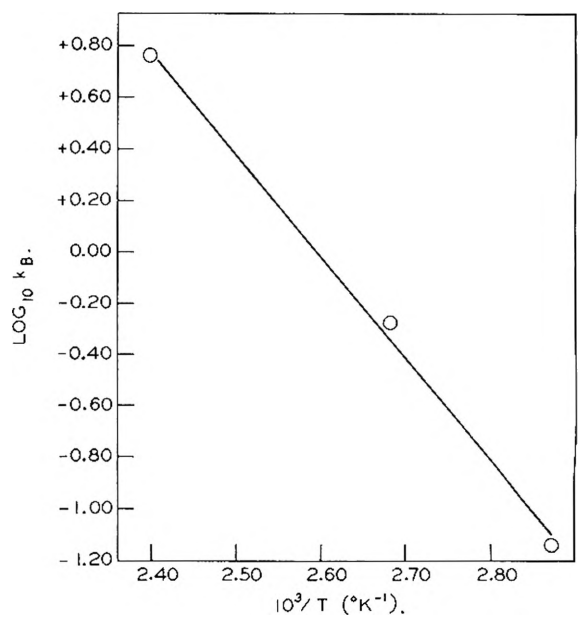

Fig. 2.—Butane–deuteriobutane exchange: activation energy determination for Pt/SiO_2–Al_2O_3; 1 atm.

$$-\log(P - P_\infty) = k_B t/2.30(P_0 - P_\infty) + \text{constant} \quad (1)$$

Here, t is the average residence time in the catalyst bed, and k_B is the specific rate of exchange in per cent. per second per gram. P, P_0 and P_∞ are the mole percentages of *n*-butane in the product gas, in the charge gas and in the equilibrium gas, respectively. P and P_0 were experimentally determined; P_∞ was calculated by statistical methods. This treatment expresses concentration in terms of the amount of undeuterated butane left in the product gas compared with the amount which would be found in the equilibrium product. It reduces the results of experiments with slightly different charge compositions to a common basis.

TABLE III

EQUILIBRIUM: BUTANE–DEUTERIOBUTANE EXCHANGE STATISTICAL CALCULATION *vs.* EXPERIMENTAL DETERMINATION

Catalyst	...	...	...	5	5	5	6	6	6	
Charge no.	2	3	5	5	2	2	2	2	3	
Temp. (°F.)	...	...	...	293	408	608	291	446	608	
Press. (mm.)	...	...	...	758	761	757	758	755	752	
GHSV @ STP ($hr.^{-1}$)	...	...	...	68.5	83.5	69.0	70.5	64.0	70.5	Statistical Calcn.
Av. res. time (sec.)	...	...	...	17.1	12.7	12.0	16.7	15.2	11.7	
Compn., mole %										
H_2	0.5	...	0.4	0.9	0.9	0.6	1.2	0.1	3.2	...
HD	.3	...	0.2	...	...	0.2	0.1	0.1	...	...
D_2	.3	...	...	...	...	...	...	...	...	...
n-C_4H_{10}	77.9	78.4	77.9	49.0	49.1	48.9	48.1	48.7	47.8	50.0
n-C_4H_9D	2.8	3.0	5.6	35.3	35.5	35.4	34.7	35.3	34.4	35.9
n-$C_4H_8D_2$	5.0	4.9	4.2	11.9	11.8	11.9	12.0	12.0	11.7	11.6
n-$C_4H_7D_3$	5.5	5.7	4.8	2.5	2.3	2.5	2.8	2.4	2.4	2.2
n-$C_4H_6D_4$	4.2	4.5	3.7	0.3	0.4	0.4	0.7	0.5	0.4	0.3
n-$C_4H_5D_5$	2.3	2.3	2.0	0.1	0.1	0.1	0.3	0.1	0.1	0.02
n-$C_4H_4D_6$	0.8	0.9	0.8	t	t	t	0.1	...	...	...
n-$C_4H_3D_7$	.3	0.3	.3	...	...	...	t	...	...	...
n-$C_4H_2D_8$	.1	t	.1	...	...	...	...	...	...	...

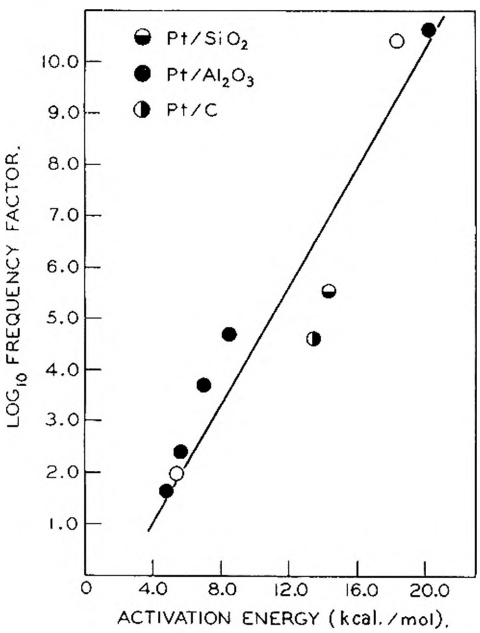

Fig. 3.—Butane–deuteriobutane exchange: compensation effect, 1 atm.

Figure 1 presents the rate determination for the platinum on silica–alumina catalyst. The data fit the first-order law (equation 1) as they must with only one species, butane, in the gas phase. (Hydrogen isotopes were not produced in the experiments, hydrogen concentrations reported in Table II being probably due to uncertainty in analysis of these complex deuteriobutane mixtures.) Figure 2 presents an "Arrhenius" plot of the effect of changing temperature on the rate constant of the butane–deuterobutane reaction over the platinum/silica–alumina catalyst. The apparent activation energy is 18.2 kcal./mole. Apparent activation energies and frequency factors (calculated from the Arrhenius equation) for all of the catalysts are listed in Table IV. The apparent activation energies and frequency factors exhibit the "Compensation Effect"[19] in which the log of the frequency factor increases linearly with increasing activation energy (Fig. 3). As is often the case with multicomponent catalysts such as the ones used here, this effect may be apparent rather than real. The available data do not permit ready interpretation. They imply, though, that the "activation energies" of Table IV are not at all conceptually simple.

TABLE IV

SUMMARIZED KINETIC RESULTS
BUTANE–DEUTERIOBUTANE EXCHANGE

Catalyst no.	Apparent activation energy (E_a) (kcal./mole)	Log frequency factor (log z)	Temp. range (°C.)
5	20.1	10.6	75–144
6	18.2	10.4	75–144
8	14.3	5.5	230–320
9	13.5	4.6	230–320
2	8.5	4.7	50–150
1	7.0	3.7	50–150
3	5.6	2.4	75–200
7	5.3	2.0	75–319
4	4.7	1.6	100–200

Reaction of Deuterium with Butane.—Kinetics of the reaction of equimolar deuterium and n-butane are treated in two ways. The first adopts the Anderson and Kemball rate equation 1 which has already been used for the butane–deuteriobutane experiments. Concentration terms are formulated as before except that P, P_0 and P_∞ represent mole percentages of the butane fraction of the gas only. (Thus, in the third column of Table II, $P = 7.6/0.499$, $P_0 = 49.9/0.499$, and P_∞ is calculated to be 15.0.) Thus, the resulting kinetics are those of the slowest equilibration (that among the deuteriobutanes). This treatment enables direct comparison of the kinetics of the butane–deuteriobutane experiments with those of the butane–deuterium experiments.

(19) E. Cremer, "The Compensation Effect in Heterogeneous Catalysis" in W. G. Frankenburg's "Advances in Catalysis," Vol. VII, Academic Press, New York, N. Y., 1955.

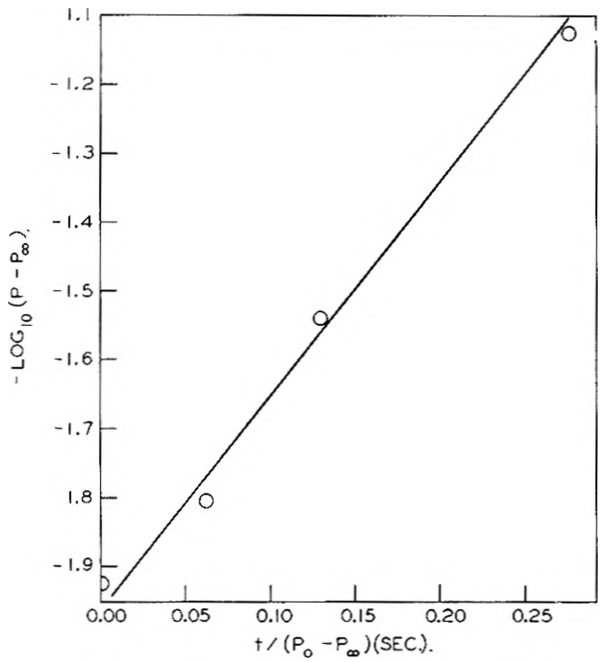

Fig. 4.—Butane–deuterium exchange: rate (k_B) determination for Pt/SiO_2–Al_2O_3; 75°, 1 atm.

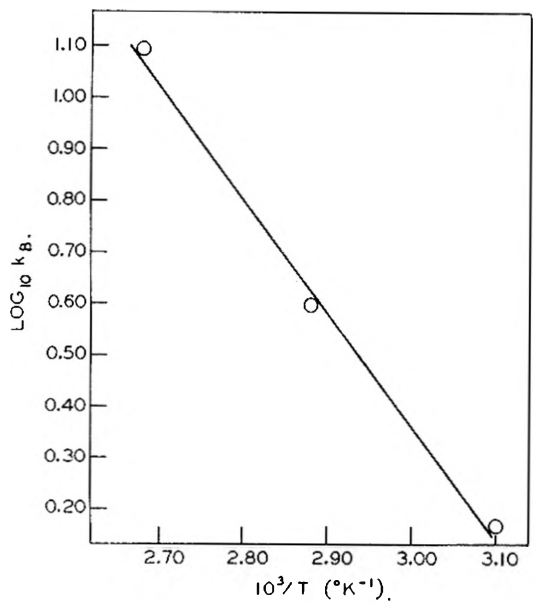

Fig. 5.—Butane–deuterium exchange: activation energy determination for Pt/SiO_2–Al_2O_3; 1 atm.

1. Analogous Characteristics of the Two Systems.—Figures 4 through 6 and Table V present for the reaction of butane with deuterium the data analogous to the results reported in Figs. 1 through 3 and Table IV for the reaction of butane with deuteriobutane. Results for the two systems differed. First, the catalysts are not lined up the same way in the two systems with respect to activation energy. The obvious distinction between the systems is that only butanes contact the catalyst in one, whereas butanes and hydrogens must compete with each other for the catalyst surface in the other. This may be—but is not necessarily—responsible for the observed differences. Secondly—and in spite of the different ordering of catalysts in

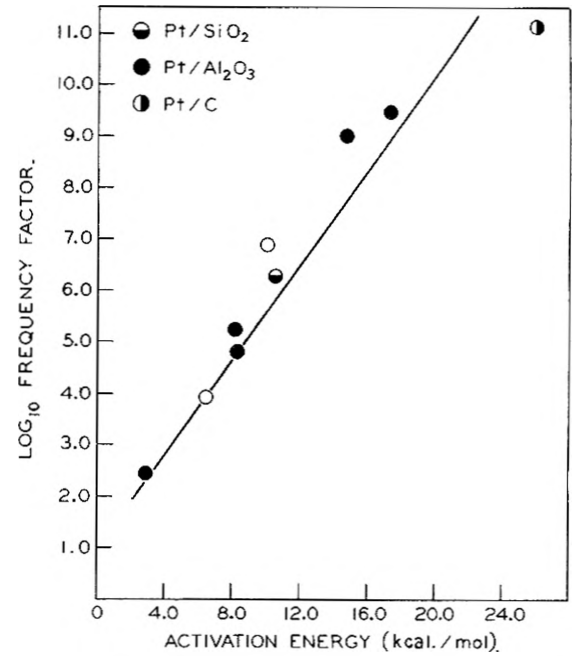

Fig. 6.—Butane–deuterium exchange: compensation effect; 1 atm.

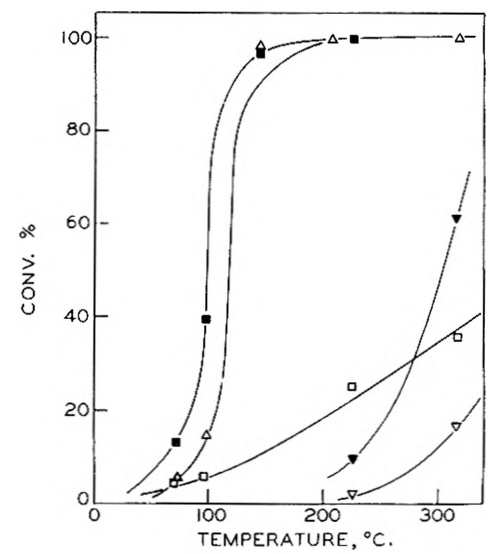

Fig. 7.—Butane–deuteriobutane exchange; GHSV = 71 hr.$^{-1}$, press. = 1 atm., non-alumina base catalysts: △, catalyst no. 5; ■, catalyst no. 6; □, catalyst no. 7; ▼, catalyst no. 8; ▽, catalyst no. 9.

the two systems—eight of the nine catalysts were more active in the butane–deuterium system than in the butane–deuteriobutane system. This is shown for the platinum on silica–alumina catalyst by comparison at constant temperature of the rate constants of Figs. 2 and 5. For the catalysts in general, it is shown by comparison of Fig. 7 with Fig. 8 and of Fig. 9 with Fig. 10. (Conversion in these latter plots is defined by analogy with the rate equations.)

$$\% \text{ Conversion} = \left[1 - \frac{(P - P_\infty)}{(P_0 - P_\infty)}\right] 100 \qquad (2)$$

It would be conventional to ascribe this greater activity to "activation" of the platinum by the extra hydrogen of the butane–deuterium system. How-

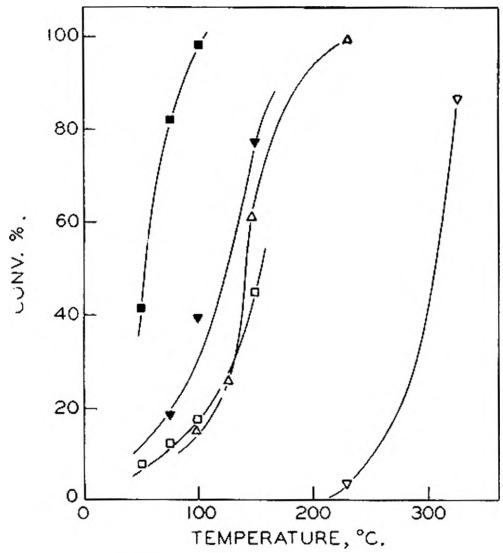

Fig. 8.—Butane-deuterium exchange; GHSV = 71 hr.$^{-1}$, press. = 1 atm., non-alumina-base catalysts: △, catalyst no. 5; ■, catalyst no. 6; □, catalyst no. 7; ▼, catalyst no. 8; ▽, catalyst no. 9.

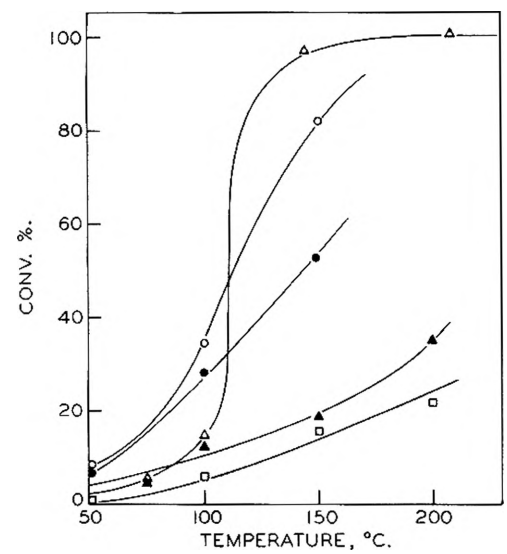

Fig. 9.—Butane-deuteriobutane exchange; GHSV = 71 hr.$^{-1}$, press. = 1 atm., Pt/Al_2O_3 catalysts: ●, catalyst no. 1; ○, catalyst no. 2; ▲, catalyst no. 3; □, catalyst no. 4; △, catalyst no. 5.

TABLE V

SUMMARIZED KINETIC RESULTS
BUTANE–DEUTERIUM EXCHANGE

Catalyst no.	Apparent activation energy (E_a) (kcal./mole)	Log frequency factor (log z)	Temp. range (°C.)
9	26.0	11.1	230–320
3	17.4	9.5	75–200
1	14.8	9.0	75–200
8	10.4	6.2	75–150
6	10.0	6.9	50–100
5	8.2	4.8	100–231
4	8.1	5.2	100–200
7	6.6	3.9	50–150
2	2.8	2.4	100–200

ever, nothing in these data necessarily points in this direction.

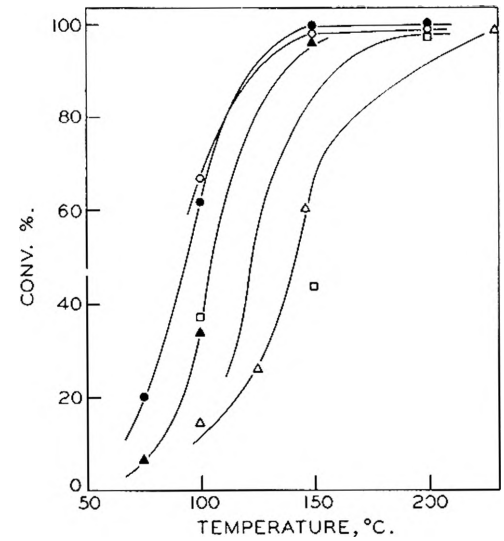

Fig. 10.—Butane–deuterium exchange; GHSV = 71 hr.$^{-1}$, press. = 1 atm., Pt/Al_2O_3 catalysts: ●, catalyst no. 1; ○, catalyst no. 2; ▲, catalyst no. 3; □, catalyst no. 4; △, catalyst no. 5.

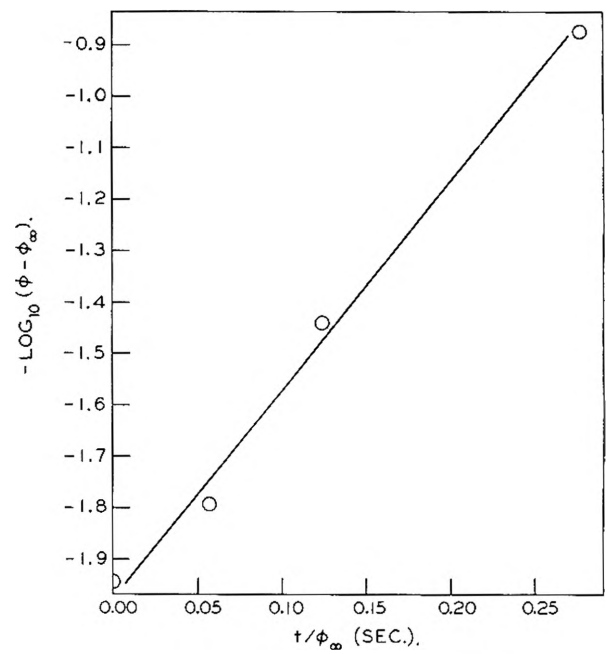

Fig. 11.—Butane–deuterium exchange: rate (k_D) determination for Pt/SiO_2–Al_2O_3; 75°, 1 atm.

2. Kinetics of the Introduction of Deuterium into Butane.—Instead of the rate of disappearance of C_4H_{10} (by reaction either with D_2 or with polydeuteriobutanes), the rate of introduction of D atoms into all butane "isotopes" can be used as a parameter of the exchange. From this point of view, Kemball[2c] found that the isobutane–deuterium reaction followed the first-order equation

$$-\log(\phi - \phi_\infty) = k_D t/2.303\phi_\infty + \text{constant} \quad (3).$$

Here, ϕ equals $\sum_{n=0}^{10}(n)$ (mole % of $C_4H_{10-n}D_n$). It measures the total number of D atoms which have entered the 50 molecules of butane in each 100 molecules of charge. Its equilibrium value is ϕ_∞. Then k_D is the number of D atoms entering 50 bu-

tane molecules per unit time per gram of catalyst.

Our data fit this expression; a plot of $-\log(\phi - \phi_\infty)$ *versus* t/ϕ_∞ is shown for the platinum/silica–alumina catalyst at 75° in Fig. 11. However, since residence time was varied by changing space velocity at constant pressure, the actual order of the reaction may be masked by the nature of the "integral" reactor used.[20,21] A fit of the data to equation 3 only characterizes the reaction as first order if the results include high conversion experiments in which the back reaction does not introduce disturbing factors. (The back reaction presents no problems here because of the simplicity of the system.) Most of the determinations of k_D include results from high conversion (>50%) experiment. In these determinations plots of $-\log(\phi - \phi_\infty)$ against t/ϕ_∞ also give straight lines. For example, Fig. 11 shows that the butane–deuterium reaction *is* first order in the exchanged species over the platinum on silica–alumina catalyst.

The rate $2k_D$ is comparable with k_B which is the rate of disappearance of butane molecules per hundred.

The ratio $2k_D/k_B$ compares the rate of entry of deuterium atoms into butane molecules with the rate of disappearance of butane molecules because they gain deuterium. That ratio, then, measures the average number of deuterium atoms which enter a butane molecule when that molecule collides and reacts with a source of deuterium atoms. Initially, the only source of deuterium atoms is deuterium molecules. As conversion goes up, hydrogen deuteride will become an increasingly important source—then polydeuteriobutanes will enter the picture as yet another source of D atoms. Thus, at low conversions of butane to deuteriobutanes, the ratio $2k_D/k_B$ will measure the number of deuterium atoms entering a butane molecule when that molecule collides and reacts with D_2 or HD.

The values of $2k_D/k_B$ at low conversions are given in Table VI for 8 of the catalysts. (No low conversion data were available for catalyst no. 1.) It should be noted that low conversion values correspond to lower temperatures for more active catalysts than for less active catalysts. A difference between the values of $2k_D/k_B$ for two catalysts may, therefore, reflect—in general—either differences in the temperature coefficients of the rates, or differences in the number of D atoms entering a butane molecule during each reactive collision of butane with D_2 or HD. Clearly, interpretation of Table VI will not be unambiguous; it will be only qualitative at best.

TABLE VI

AV. NO. OF D ATOMS ENTERING PER EXCHANGE

Catalyst	$2k_D/k_B$	Catalyst	$2k_D/k_B$
6	4.3	8	3.3
4	4.0	1	2.6
5	3.7	9	2.1
2	3.7	7	2.0
3	3.4		

(20) A. O. Hougen and K. M. Watson, "Chemical Process Principles," John Wiley & Sons, New York, N. Y., 1943, p. 962.

(21) C. D. Prater and R. M. Lago, "The Kinetics of the Cracking of Cumene by Silica–Alumina Catalyst" in W. G. Frankenburg's "Advances in Catalysis," Vol. VIII, Academic Press, New York, N. Y., 1956.

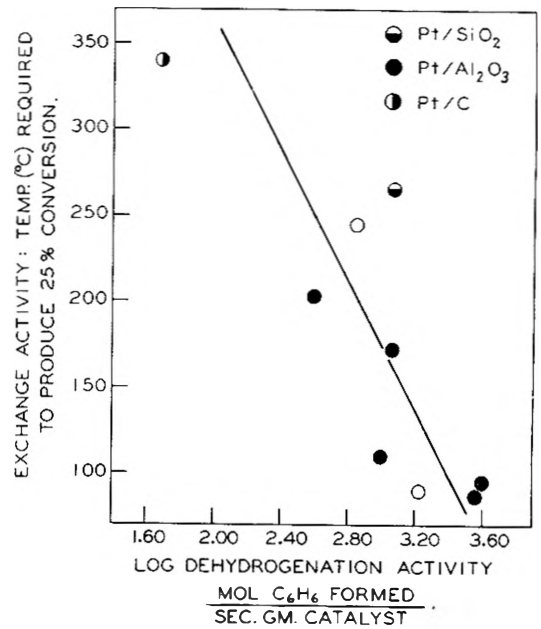

Fig. 12.—Butane–deuteriobutane exchange: exchange activity *vs.* dehydrogenation activity; GHSV = 71 hr.$^{-1}$, press. = 1 atm.

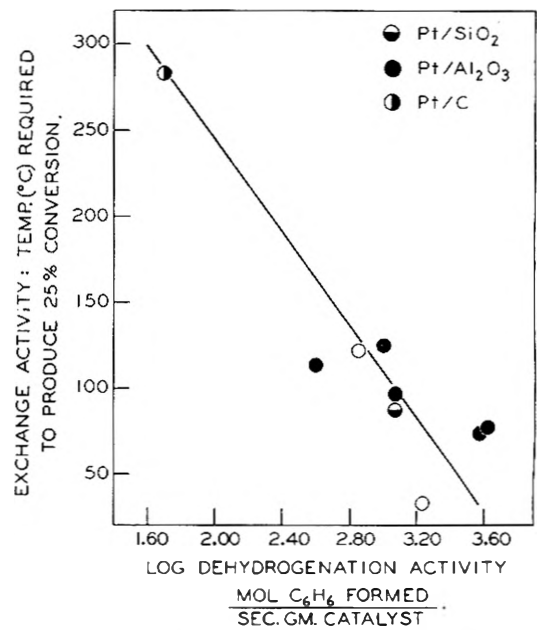

Fig. 13.—Butane–deuterium exchange: exchange activity *vs.* dehydrogenation activity; GHSV = 71 hr.$^{-1}$, press. = 1 atm.

Catalyst Comparisons.—Catalyst activity toward either exchange reaction may be expressed arbitrarily as the temperature required to give 25% conversion under fixed conditions (gas hourly space velocity of 71, atmospheric pressure, constant charge stock). In either case, conversion, being defined by equation 2, is measured in terms of the events in the butane fraction of the gas. As in the analogous kinetic treatment, this allows direct comparison of catalyst activities in the butane–deuteriobutane experiments with those of the butane–deuterium experiments.

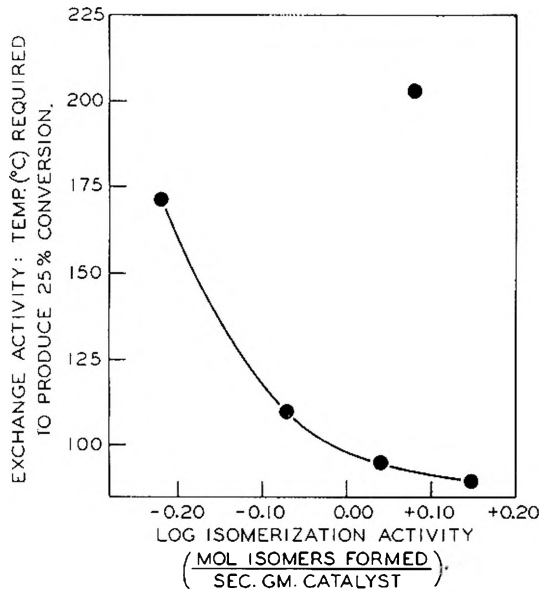

Fig. 14.—Butane-deuteriobutane exchange: exchange activity *vs.* xylene isomerization; GHSV = 71 hr.$^{-1}$, press. = 1 atm., Pt/Al_2O_3 catalysts.

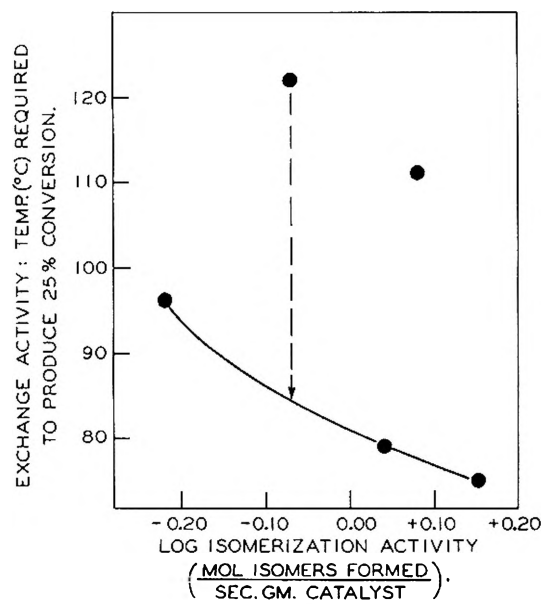

Fig. 15.—Butane-deuterium exchange: exchange activity *vs.* xylene isomerization; GHSV = 71 hr.$^{-1}$, press. = 1 atm., Pt/Al_2O_3 catalysts.

As was the case with respect to activation energy, the catalysts are not lined up the same way in the two systems with respect to exchange activity, thus defined. (Exchange activities may be read off from Figs. 7 through 10.) In spite of this, for either reaction, exchange activity roughly parallels activity of the catalysts toward dehydrogenation of cyclohexane to benzene. This is shown in Figs. 12 and 13. This suggests that the platinum site of the catalyst—which is primarily responsible for the dehydrogenation activity—also is the seat of the deuterium exchange activity. This suggestion is, moreover, consistent with the failure of the only support tested, silica–alumina, to catalyze the exchange even at 320°. (Silica–alumina was chosen for this test in view of the observation by Hansford, Waldo, Drake and Honig[22] and by Hindin, Mills and Oblad[23] of slow exchange between *n*-butane and deuterated silica–alumina in one hour at 200 to 280°. However, several differences exist between the types of experiments. In ours, residence times were less than one minute, and the silica–alumina may never have been deuterated by the gaseous deuterium.)

These catalysts also vary in "acidity." "Acidity" is here quite arbitrarily characterized by the rate of isomerization of *p*-xylene over the catalyst. Catalysis of this reaction is customarily explained by an ionic carbonium ion mechanism[24] which probably does not depend on formation of olefin intermediates. Therefore, xylene isomerization indexes a kind of catalyst "acidity" which should be fairly independent of the dehydrogenation activity inherent in the catalysts because of their platinum contents.

Xylene isomerization activities are available for only the five alumina based catalysts of Table I. "Acid" activities, so defined, are plotted against the corresponding butane–deuteriobutane exchange activities in Fig. 14. With the exception of the results with catalyst 4, greater "acidity" corresponds to greater exchange activity. Catalyst 4, which is rather "acid," is not very active toward the exchange: its dehydrogenation activity (400) is also very low. Presumably, this very low dehydrogenation activity exerts an over-riding depressing effect on the exchange activity. Thus, the dehydrogenation, isomerization and exchange data—all taken together—suggest that this exchange activity parallels dehydrogenation activity primarily, and "acidity" secondarily.

The relationship between catalyst "acidity" and exchange activity is less clear-cut in the butane–deuterium system. Four out of the five platinum–alumina catalysts bear the same relative positions in Figs. 14 and 15; the one out of line is catalyst 5. This, interestingly enough, is also the *one* catalyst which was not more active toward the butane–deuterium reaction than toward the butane–deuteriobutane reaction. It is possible that the experiment with the butane–deuterium mixture over this catalyst was in error; unfortunately the equipment was dismantled before this matter could be checked.

Finally, granting the difficulties in interpretation of Table VI, nevertheless the more "acidic" catalysts exchanged the larger number of D atoms during each reactive collision of D_2 or HD with a butane molecule. That is, the catalyst prepared with the most acidic base, silica–alumina, heads the list. Platinum on aluminas, wherein acidity is derived from presence of combined chlorine, follow with high chlorine content catalysts in the lead. Platinum on silica and platinum on carbon bring up the rear. Now, the results using unplatinized silica–alumina show that this could not be due to a direct contribution of the acid sites to transfer of deute-

(22) R. C. Hansford, P. G. Waldo, L. C. Drake and R. E. Honig, *Ind. Eng. Chem.*, **44**, 1108 (1952).

(23) S. G. Hindin, G. A. Mills and A. G. Oblad, *J. Am. Chem. Soc.*, **73**, 278 (1951).

(24) R. C. Hansford, in A. Farkas, "Physical Chemistry of the Hydrocarbons," Vol. II, Academic Press, New York, N. Y., 1953, p. 291.

rium from one molecule to another. It would have to be due to some co-action of the acid sites and the platinum sites.

Acknowledgment.—The authors are grateful to members of the Analytical Section of the Research and Development Laboratory of the Socony Mobil Oil Company, Inc., for devising the scheme for analysis of mixtures of deuteriobutanes, and to R. W. Baker, G. W. Munns, Jr., and R. L. Smith for determination of catalyst activities toward cyclohexane dehydrogenation of *p*-xylene isomerization.

CALCULATION OF STABILITY CONSTANTS FROM CRYOSCOPIC MEASUREMENTS BY THE PROJECTION STRIP METHOD

BY F. J. C. ROSSOTTI AND HAZEL ROSSOTTI

Contribution from the Department of Chemistry, The University of Edinburgh, Edinburgh, Scotland

Received September 8, 1958

It is shown that the formation curve, $\bar{n}(\log a)$, for a system of mononuclear complexes may be calculated readily from cryoscopic measurements in a constant ionic medium. If $N \leqslant 2$, stability constants are best obtained from the formation curve by the projection strip method, which is illustrated by recalculation of Kenttämaa's cryoscopic data for the sulfato complexes of magnesium, nickel(II), copper(II) and zinc. Methods are indicated for calculating stability constants for systems in which $N > 2$, and the limitations of the cryoscopic method are discussed.

Introduction

Although acid dissociation constants of aldehydes were calculated from freezing point measurements over fifty years ago[1-2] cryoscopy has been little used for quantitative studies of equilibria in solution. Data for solutions of weak electrolytes in pure water must be expressed in terms of both equilibrium constants and activity coefficients.[3-5] Even if only one complex is formed, the calculated value of the equilibrium constant then depends upon an arbitrary choice of activity coefficient,[5] and interpretation is even more difficult if two or more complexes coexist. Calculation is simpler if all activity coefficients can be taken to be unity, as in studies of association of neutral molecules in organic solvents[6-9] and of ionic equilibria in concentrated sulfuric acid.[10]

Ionic equilibria in aqueous solution are best investigated in the presence of a large excess of inert electrolyte, which keeps the activity coefficients effectively constant[11]; changes in the number of solute species may then be followed by measuring changes in a eutectic, or transition point.[12] A number of workers[13-17] have calculated one, or, at the most, two equilibrium constants for data of this type, but the relationship between the equations used, and the contemporary treatment of mononuclear step-equilibria, is not immediately obvious. It is shown below that the formation function, and hence the stability constants, of a mononuclear system may be obtained readily from cryoscopic measurements in a constant ionic medium. The method is illustrated by recalculation of data[15] for some sulfato complexes of bivalent metal ions.

(1) F. Auerbach, *Ber.*, **38**, 2833 (1905).
(2) H. von Euler, *ibid.*, **39**, 344 (1906).
(3) M. Randall and C. Allen, *J. Am. Chem. Soc.*, **52**, 1814 (1930).
(4) J. S. Johnson and K. A. Kraus, *ibid.*, **79**, 4436 (1952).
(5) P. G. M. Brown and J. E. Prue, *Proc. Roy. Soc.* (*London*), **232A**, 320 (1955).
(6) B. C. Barton and C. A. Kraus, *J. Am. Chem. Soc.*, **73**, 4561 (1951).
(7) M. Davies and D. M. L. Griffiths, *Z. physik. Chem.*, (*Frankfurt*), **2**, 353 (1954); **6**, 143 (1956).
(8) J. A. Davison, *J. Am. Chem. Soc.*, **67**, 228 (1945).
(9) N. E. White and M. Kilpatrick, THIS JOURNAL, **59**, 1044 (1955).
(10) R. J. Gillespie, E. D. Hughes and C. K. Ingold, *J. Chem. Soc.*, 2473 (1950).
(11) G. Biedermann and L. G. Sillén, *Arkiv Kemi*, **5**, 425 (1953).
(12) E. Darmois, *Bull. soc. chim. France*, 1 (1950).
(13) P. Hagenmüller, *Ann. chim.*, **12**:**6**, 1 (1951).
(14) J. Kenttämaa, *Suomen kemistilehti*, **29B**, 59 (1956).
(15) J. Kenttämaa, *Acta Chem. Scand.*, **12**, 1323 (1958).
(16) R. Schaal, *J. chim. phys.*, **52**, 719 (1955).
(17) P. Souchay and R. Schaal, *Bull. soc. chim. France*, 819 (1950).

Theory

1. Calculation of the Degree of Formation of Mononuclear Systems.—The formation of a mononuclear complex BA_n from a central group B and n ligands A in a constant ionic medium may be represented by the equilibria

$$B + nA \rightleftharpoons BA_n \quad \beta_n \tag{1}$$

and

$$BA_{n-1} + A \rightleftharpoons BA_n \quad K_n \tag{2}$$

where charges are omitted. The equilibrium constants β_n and K_n are the over-all and stepwise stoichiometric stability constants of BA_n, valid for the particular ionic medium and temperature. The degree of formation of the system is given by[18]

$$\bar{n} = \frac{A - a}{B} \tag{3}$$

$$= \frac{\sum_0^N n[BA_n]}{B} \tag{4}$$

where B and A are the total concentrations of central group and ligand, a is the free ligand concentration, and N is the maximum value of n. The sum, S, of the concentrations of solute species is related to the observed lowering, θ, of the eutectic or transition point, and to the appropriate cryoscopic constant, λ, by the expression

$$S = \theta\lambda^{-1} = A + B - \sum_0^N n[BA_n] = A + B(1 - \bar{n}) \tag{5}$$

(18) J. Bjerrum, "Metal Ammine Formation in Aqueous Solution," P. Haase and Sons, Copenhagen, 1941.

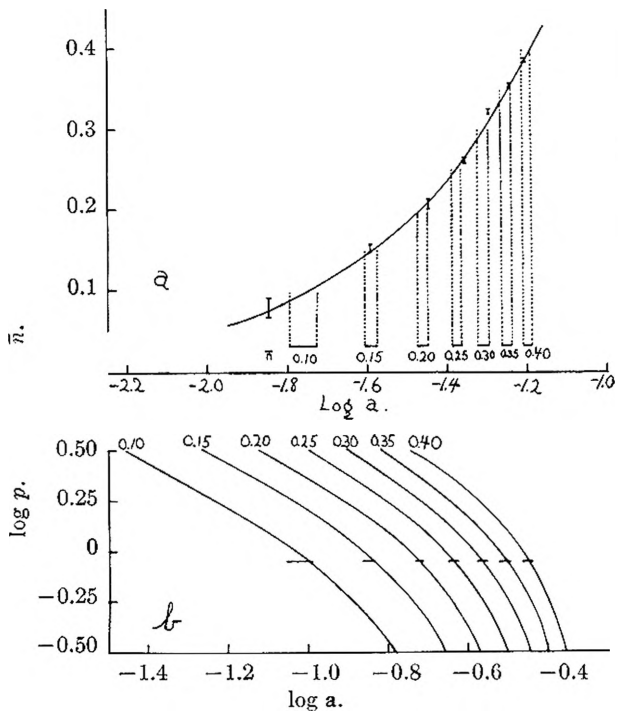

Fig. 1.—Calculation of stability constants of nickel sulfate complexes in 1.151 molal aqueous potassium nitrate at $-3.06 \pm 0.19°$: (a) projection strip of experimental points, $\bar{n}$, log a, calculated from Kenttämaa's measurements,[18] and theoretical formation curve calculated for log $\beta_1 = 0.70$ and log $\beta_2 = 1.50$; (b) projection strip superimposed on normalized curves log p(log a)$\bar{n}$ in position corresponding to log $p = -0.50$ and $^1/_2$ log $\beta_2 = 0.75$.

Thus $\bar{n}$ may be calculated readily from θ provided that A and B are known from the analytical composition of the solution, and that λ has previously been determined (*e.g.*, by means of a completely dissociated electrolyte). If the compound B_qA_r is the sole source of both central group and ligand, then $A = rq^{-1}B$, and equation 5 reduces to

$$\theta\lambda^{-1} = B(rq^{-1} + 1 - \bar{n}) \qquad (6)$$

Once $\bar{n}$ has been determined, the corresponding free ligand concentration may be calculated from equation 3, except in the case of such stable complexes that $\bar{n} \sim A/B$, and a is indistinguishable from zero.

Equations 5 and 6 are only valid in the absence of reactions other than (1) and (2). They cannot be used if polynuclear complexes are formed in solution, or if A or B take part in competitive equilibria involving protons or hydroxyl ions.

2. Computation of Stability Constants from Data $\bar{n}$,a.—Since

$$B = \sum_0^N [BA_n] \qquad (7)$$

equation 4 may be written

$$\sum_0^N (n - \bar{n})\beta_n a^n = 0 \qquad (8)$$

and the N stability constants $\beta_1, \beta_2, \ldots, \beta_N$ may in principle be calculated, provided that at least N pairs of values $\bar{n}$,a have been determined. Of the many methods (*e.g.*, ref. 19–20) which have been described for computing stability constants of mononuclear complexes, the most satisfactory are those in which plots of experimental functions are compared with normalized curves.[20]

Systems in which $N \leqslant 2$.—If it is found that $\bar{n} \leqslant 2$, it is possible that $N \leqslant 2$ and that no complexes higher than BA_2 are present under the conditions used. If only the first two complexes are formed, equation 8 may be transformed to

$$\left(\frac{\bar{n}}{1-\bar{n}}\right)\frac{1}{\mathbf{a}} - \left(\frac{2-\bar{n}}{1-\bar{n}}\right)\mathbf{a} = p \qquad (9)$$

where

$$\mathbf{a} = \beta_2^{1/2}a \qquad (10)$$

Thus $\bar{n}$ is a function of the normalized variable **a** and of the parameter

$$p = \beta_1\beta_2^{-1/2} = (K_1/K_2)^{1/2} \qquad (11)$$

which fixes the shape of the formation curve $\bar{n}$(log a). Systems described by two parameters and two variables, one of which can be normalized, are best treated by the projection strip method.[21] Since this device has not yet been used to calculate stability constants of mononuclear complexes, its application to systems in which $N \leqslant 2$ will be described in some detail. The family of theoretical curves log p (log **a**)$_{\bar{n}}$ are calculated from equation 9, using a number of convenient values of $\bar{n}$. Values in the range $0.1 \leqslant \bar{n} \leqslant 1.0$ are shown in Table I, and those in the range $1.0 \leqslant \bar{n} \leqslant 2.0$ readily may be obtained using the symmetry relationship

$$\log \mathbf{a}_{\bar{n}=1-d} = -\log \mathbf{a}_{\bar{n}=1+d} \qquad (12)$$

where $0 \leqslant d < 1$.

The experimental formation curve is plotted with the same abscissa scale as that used for the plots of log p against log **a**. For each value of $\bar{n}$ used to calculate the family of theoretical curves, the value of log a, together with the experimental uncertainty in this value, is marked off on the log a axis (Fig. 1a). This projection strip (log a)$_{\bar{n}}$ is superimposed on the family of theoretical curves, parallel to the log **a** axis, and in such a position that the best fit is obtained for all values of $\bar{n}$ used (Fig. 1b). The value of log p is then obtained as the ordinate corresponding to the best position of the strip. The maximum limits of error in this value may be estimated from the vertical distance through which the projection strip may be moved, whilst allowing the calculated values of (log a)$_{\bar{n}}$ to remain within the experimental uncertainty. The value of β_2 is given by the equation

$$\log a_0 = -\,^1/_2 \log \beta_2 \qquad (13)$$

where log a_0 is the point of intersection of the log p axis (log **a** = 0) with the projection strip. The maximum error in $^1/_2$ log β_2 is then given by the permissible horizontal displacement of the strip.

If $N = 1$, the projection strip will fit the normalized curves for $\bar{n} \leqslant 1.0$ for any value of log p above a lower limit, log p_{min}, which depend on the range of free ligand concentration over which the plateau value $\bar{n} = 1$ has been observed. The correct value of log β_1 is obtained from equations 11 and 13, regardless of the value of p chosen; an upper limit for log β_2 may be calculated from the value of log p_{min}.

(19) F. J. C. Rossotti and H. S. Rossotti, *Acta Chem. Scand.*, **9**, 1166 (1955).

(20) L. G. Sillén, *ibid.*, **10**, 186 (1956).

(21) F. J. C. Rossotti, H. S. Rossotti and L. G. Sillén, *ibid.*, **10**, 203 (1956).

TABLE I

THE FAMILY OF NORMALIZED FUNCTIONS LOG p (LOG a)$_{\bar{n}}$

−log a	log p								
	$\bar{n}$ = 0.1	$\bar{n}$ = 0.2	$\bar{n}$ = 0.3	$\bar{n}$ = 0.4	$\bar{n}$ = 0.5	$\bar{n}$ = 0.6	$\bar{n}$ = 0.7	$\bar{n}$ = 0.8	$\bar{n}$ = 0.9
1.60	0.641	0.996	1.230	1.423	1.599	1.776	1.968	2.202	2.554
1.40	.433	.792	1.028	1.221	1.398	1.575	1.767	2.001	2.353
1.20	.212	.582	0.818	1.017	1.195	1.372	1.565	1.800	2.152
1.00	− .046	.357	.607	0.806	0.987	1.166	1.360	1.596	1.949
0.90	− .210	.231	.491	.695	.879	1.059	1.255	1.492	1.848
.80	− .436	.087	.365	.578	.766	0.950	1.147	1.385	1.741
.70	− .868	− .092	.221	.449	.645	.834	1.035	1.275	1.632
.60	− ∞	− .367	.040	.298	.509	.707	0.914	1.159	1.519
.50		−1.102	− .231	.102	.345	.561	.779	1.032	1.398
.40		− ∞	− .961	− .213	.120	.380	.617	0.884	1.261
.35			− ∞	−0.521	− .032	.254	.517	.798	1.184
.30				− ∞	− .308	.093	.395	.697	1.095
.25					−1.039	− .155	.234	.584	0.996
.20					− ∞	− .771	− .016	.407	.865
.15						− ∞	− .641	− .147	.693
.10							− ∞	− .569	.414
.08								− ∞	.223
.05									− .532
.045									−1.184
.04									− ∞

The family of curves log p (log a)$_{\bar{n}}$ also may be used to calculate theoretical formation curves for systems in which β_1 and β_2 are known. Values of log a corresponding to the appropriate value of log p are marked off as a theoretical projection strip for a number of values of $\bar{n}$. This strip is placed along the abscissa of the formation curve so that the point log a = 0 on the strip is superimposed on the point log a = $^1/_2$ log β_2. The points of the theoretical strip are then projected back to their ordinate positions.

Systems in which $N > 2$.—Experimental values of $\bar{n} > 2$ indicate that, in addition to BA and BA$_2$, higher species BA$_n$($n \geqslant 3$) are present in appreciable concentrations. Higher complexes may also be important in cases where a projection strip of a formation curve for which $\bar{n} \leqslant 2$ cannot be satisfactorily fitted on the family of curves log p (log a)$_{\bar{n}}$; however, other factors, such as experimental error, or the formation of mixed or polynuclear complexes, also must be considered.

The stability constants for systems in which $N > 2$ cannot be obtained from data $\bar{n}$,a by direct curve-fitting in two dimensions. Data $\bar{n}$,a for systems in which $N = 3$ may be transformed conveniently by means of Fronaeous' integral[22]

$$\alpha_0^{-1} = \exp \int_0^a \bar{n}\, d \ln a \qquad (14)$$

The required values of β_1, β_2 and β_3 may be obtained simultaneously from the resultant function $\alpha_0^{-1}(a)$ by Sillén's curve-fitting procedure.[20] If $N > 3$, the stability constants cannot be calculated simultaneously from the functions $\bar{n}(a)$ or $\alpha_0^{-1}(a)$. Data at high and low free ligand concentrations may be treated separately, preferably by curve-fitting, and the approximate constants so obtained refined by successive approximations.[20] Alternatively, the data $\bar{n}$, a may be treated by the method of successive extrapolations.[19]

(22) S. Fronaeous, "Komplexsystem hos Koppar," Gleerupska Universitets Bokhandeln, Lund, 1948.

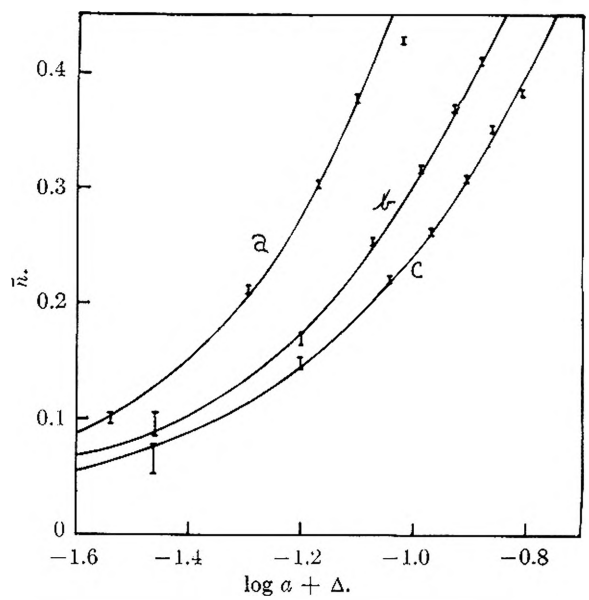

Fig. 2.—Formation curves of sulfato complexes in 1.151 molal aqueous potassium nitrate at −3.06 ± 0.19°. The points are calculated from Kenttämaa's data,[15] and the full curves from the best values of the stability constants obtained by the projection strip method (Table II): (a) Mg(II), Δ = 0; (b) Zn(II), Δ = 0.20; (c) Cu(II), Δ = 0.40.

Calculations

Kenttämaa[15] measured the effect of concentration of dissolved magnesium, nickel(II), copper(II) and zinc sulfates on the eutectic temperature, −2.831°, of saturated aqueous potassium nitrate. For sulfates of bivalent metal ions, $r = q$, $A = B$ and equations 6 and 3 reduce to

$$\bar{n} = 2 - \frac{\theta}{\lambda B} \qquad (15)$$

and

$$a = \frac{B(1 - \bar{n}) = \theta\lambda^{-1} - B}{} \qquad (16)$$

The functions $\bar{n}$(log a) were calculated from Kenttämaa's data B, $\theta\lambda^{-1}$ using equations 15 and 16.

The results for the nickel sulfate system are shown in Fig. 1a, and those for the other systems are plotted in Fig. 2.

It was found that $0.07 < \bar{n} < 0.43$ for all four systems, and the functions $\bar{n}(\log a)$ were analyzed by the projection strip method. As preliminary inspection indicated that, in each case, $-1 < \log p < 1$, additional theoretical curves $\log p(\log a)_{\bar{n}}$ for values of $\bar{n} = 0.15$, 0.25 and 0.35 were calculated in this range. The resultant family of curves is shown in Fig. 1b, together with the projection strip for the nickel sulfate system, superimposed in the position of best fit. The values of the stability constants obtained by the projection strip method, and the maximum limits of error, are shown in Table II, together with the values calculated by Kenttämaa, who obtained β_1 as the intercept, and β_2 as the slope, of the linear plot of $(2B - \theta\lambda^{-1})/(\theta\lambda^{-1} - B)^2$ against $\theta\lambda^{-1}$. From equations 15 and 16, it is apparent that this procedure is identical with that used by Irving and Rossotti[23] for treatment of the data $\bar{n},a$; the disadvantages of linear plots of this type are discussed elsewhere.[20,23]

Table II

Stability Constants[a] of Sulfato Complexes in 1.151 Molal Aqueous Potassium Nitrate at −3.06 ± 0.19°

	log β_1		log β_2	
	This work	Kenttämaa[15]	This work	Kenttämaa[15]
Mg(II)	0.38 ± 0.07	0.38	1.41 ± 0.08	1.40[b]
Ni(II)	.70 ± .04	.69	1.50 ± .05	1.53
Cu(II)	.72 ± .03	.72	1.50 ± .04	1.49
Zn(II)	.64 ± .04	.64	1.54 ± .05	1.56

[a] On the molal scale. [b] The value $\beta_2 = 15$ in the original paper[15] appears to be a misprint for $\beta_2 = 25$.

The stability constants obtained by Kenttämaa are well within the maximum limits of error in the values obtained by the projection strip method. The strips fitted the normalized curves satisfactorily over the whole concentration range studied. Thus there is no evidence for the presence of higher complexes than BA_2, as indeed would be expected since $\bar{n}$ never rises above 0.43.

Discussion

The values of β_n calculated from the depression of a eutectic point are stoichiometric stability constants, or concentration quotients, valid only for the particular temperature and ionic medium used. They depend on (i) the appropriate activity quotient $\{BA_n\}/\{B\}\{A\}^n$, (ii) the activity coefficients of the species B, A and BA_n, and (iii) the extent of association of the metal ion and ligand with the bulk electrolyte. Factors (ii) and (iii) will only be constant if the background salt is in considerable excess of the metal ion and ligand under investigation. This condition is not strictly fulfilled in Kenttämaa's work with the potassium nitrate eutectic,[15] since the variation (from ±0.03 to ±0.04 molal in the four systems) of the free metal ion concentration from its mean value is not negligible compared with the concentration (1.151 molal) of the background salt. Although it cannot be assumed that the activity coefficients remain constant, the variation is probably not so gross as to invalidate the use of Kenttämaa's data to illustrate the proposed method for analyzing cryoscopic measurements. Allowance for the formation of metal nitrate, or potassium sulfate, ion-pairs (factor (iii)) could be applied readily but no attempt has been made to eliminate these effects since reliable values of the necessary stoichiometric stability constants, valid for the same temperature and ionic medium, are not available.

Cryoscopy is too inflexible a method to be widely applicable to the study of equilibria in solution. Measurements in a given medium can only be made at one temperature, and, if a salt background is used to control activity coefficients, the solutions must be saturated with respect to the supporting electrolyte. The choice of a background salt is limited to those (*e.g.*, potassium chlorate,[15] potassium perchlorate,[14-15] potassium nitrate,[13-16] and sodium sulfate[16-17]) which have suitable eutectic or transition points. The method is unsuitable for studying systems which take part in competitive reactions with protons (*e.g.*, complexes of metal ions which are readily hydrolyzed, or of ligands which are conjugate bases of weak acids). Although B and A are usually varied by changing the concentration of the salt B_qA_r, they may also be varied independently by adding the appropriate B and A salts of an inert anion and cation, respectively; allowance must be made for the contributions of these inert ions to the total concentration of species present.

In spite of its limitations, cryoscopy is a reasonably accurate method for studying complex formation in a few types of system, provided that adequate mathematical analysis is made of the experimental data. The calculation of the function $\bar{n}(a)$ from cryoscopic measurements has several advantages over procedures used previously. Inspection of the formation curve $\bar{n}(\log a)$ may indicate the number of complexes present, and reveal random errors; systematic errors may also be recognized, and sometimes corrected for.[20] Coincidence of the functions $\bar{n}(\log a)_B$ for several values of B is evidence that the system is entirely mononuclear or homonuclear. If $N \leq 2$, stability constants may be computed readily from the formation curve by the projection strip method. This device treats a large number of data simultaneously and gives a realistic estimate of the limits of error in both β_1 and β_2. It is extremely quick and easy to use. The function $\bar{n}(a)$ also serves as a convenient starting point for the calculation of stability constants for systems in which $N > 2$.

Acknowledgments.—We are grateful to the Earl of Moray Endowment Committee for the purchase of a calculating machine and to David Martin, B.Sc., for computing the functions given in Table I.

(23) H. M. Irving and H. S. Rossotti, *J. Chem. Soc.*, 3397 (1953).

THE WETTING OF INCOMPLETE MONOMOLECULAR LAYERS. II. CORRELATION WITH MOLECULAR SIZE AND SHAPE[1]

BY L. S. BARTELL AND R. J. RUCH

Department of Chemistry, Iowa State College, Ames, Iowa

Received October 6, 1958

The contact angles of several liquids having the same surface tension were studied on complete and depleted monomolecular films of long-chain amines adsorbed on chromium slides. Controlled depletions with benzene or ether were measured quantitatively by a polarimetric optical method. Advancing contact angles on close-packed monolayers were all found to be roughly the same but, upon depletion, the layers showed an ability to discriminate between liquids of different molecular shapes and sizes. Direct observation by the optical method of the tracks of drops receded across monolayers revealed a similar distinction. Different liquid molecules exhibited markedly different abilities to enter spaces between adsorbed molecules and become an integral part of the film. An interpretation of the results is presented in terms of molecular size and shape and the probable structure of the depleted films.

Introduction

One of the most conspicuous properties of adsorbed films on solids is the marked alteration of wettability that may accompany adsorption. Although advantage is taken of this property in numerous technical applications, and many studies of adsorbed films have been reported, very little quantitative research has been undertaken on the relationship between contact angle and extent of adsorption. The first contribution of this series,[2] on the wetting of films of *n*-octadecylamine by water and *n*-hexadecane, represents one of the first direct studies ever undertaken of the problem. The most striking result observed was that the advancing contact angle of hexadecane remained constant until somewhat more than one-half of the film was depleted, after which the angle dropped abruptly to zero as depletion continued. The abruptness suggested that a specific solid–liquid interaction was operative, occasioned by the structural similarity between the liquid molecules and exposed hydrocarbon tails of the adsorbed molecules. At small to moderate depletions of the film, the hexadecane molecules might enter the holes and play the role of the well oriented hydrocarbon chains around them. Thus a droplet of hexadecane could not distinguish a complete from a depleted monolayer until the holes in the film reached a critical size too great for the amine molecules to support orientation of the anchorless hexadecane molecules all the way across them. Beyond this depletion the film would have a disordered structure and be wet by hexadecane.

The above hypothesis rests upon effects of molecular orientation which should be strongly dependent upon molecular size and shape. The present investigation consists of a series of experiments designed to test the hypothesis with liquids of similar surface tensions but substantially different molecular architecture.

Experimental Details

Monomolecular films of *n*-octadecylamine and of *n*-dodecylamine were formed on chromium plated slides by adsorption from solutions in *n*-hexadecane, 0.1% by weight and nearly saturated, respectively. The amines, donated by Armour and Company, and *n*-hexadecane, purchased from the Eastman Kodak Company, were purified as described earlier.[2,3] Chromium plated steel and brass slides, 1″ × 2.5″, were cut from commercial ferrotype plates, rinsed with pure benzene and flamed gently just before using. Other methods of cleaning were tried but none was simpler or appreciably more effective.

Adsorption generally was allowed to proceed for a few minutes after which the slides could be withdrawn from solution, apparently dry. Previous tests[2] indicated that such films contain a trace of the solvent, hexadecane, equivalent to a small fraction of a monolayer but that this has virtually no effect on the wetting properties of undepleted films. Since the hexadecane is immediately extracted during the depletion of films, it can be expected to have no significant effect on the present experiments. Wetting properties were not observed to depend upon the time of adsorption whether it was a few minutes or many hours.

Depletions of monolayers were made by dipping the slides into pure benzene or ether. It was found that depletions could be stopped at an earlier stage if cold ether were used instead of benzene which was used in the earlier study.[2] It is doubtful, however, whether this extra delicacy was particularly effective, since the liquids used in measurements of contact angles were comparable to benzene in solvent action. It was found that butyl alcohol was more effective than benzene in dissolving the more firmly adsorbed molecules but that it was difficult to remove quantitatively.

The liquids used in wetting experiments were *n*-tetradecane, *n*-hexadecane, 1,3,5-trimethylbenzene and Kel-F #3. The tetradecane and hexadecane, both products of the Eastman Kodak Company, were purified by treatment with concentrated H_2SO_4, dilute NaOH, anhydrous Na_2SO_4 and percolation through alumina and silica gel. Trimethylbenzene from the Eastman Kodak Company and Kel-F #3, supplied through the courtesy of the M. W. Kellogg Company, were used as obtained.

The liquids were contained in 1-cc. syringes and could be advanced onto and receded from the surface with fine control through hypodermic needles, the tips of which were cut parallel to the surface. Along with each liquid a control was run simultaneously on an adjacent area of the same film using the reference liquid, *n*-hexadecane. Advancing and receding contact angles of small droplets were measured directly using a low power microscope with a filar micrometer eyepiece mounted in a graduated rotating object holder.

The amount of material adsorbed was measured with an optical instrument similar to the ellipsometer described by Rothen.[4] The setting of the quarter-wave plate was kept constant for any particular run. In the calculations of per cent. depletion of the monolayers it was assumed that the analyzer readings of the optical instrument were a linear function of the average amount of adsorbate per area. Recent tests with radioactive films have confirmed this assumption to a reasonable degree of approximation.[5] The instrument was sensitive to a few per cent. of a monolayer.

No attempt was made to control the temperature during experiments and it varied from 22 to 25°.

(1) (a) Work supported by The American Petroleum Institute; (b) presented at the 133rd Meeting of the American Chemical Society, San Francisco, California, April 17, 1958.

(2) L. S. Bartell and R. J. Ruch, THIS JOURNAL, **60**, 1231 (1956).

(3) W. C. Bigelow, D. L. Pickett and W. A. Zisman, *J. Colloid Sci.*, **1**, 513 (1946).

(4) A. Rothen, *Rev. Sci. Instr.*, **16**, 26 (1945).

(5) L. S. Bartell and J. F. Betts, to be published.

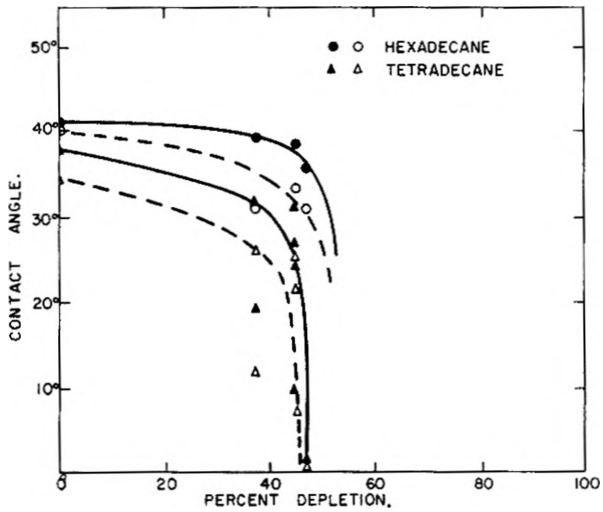

Fig. 1.—Contact angles of *n*-hexadecane and *n*-tetradecane on depleted monolayer of *n*-octadecylamine. Solid points represent advancing angles, open points represent receding angles.

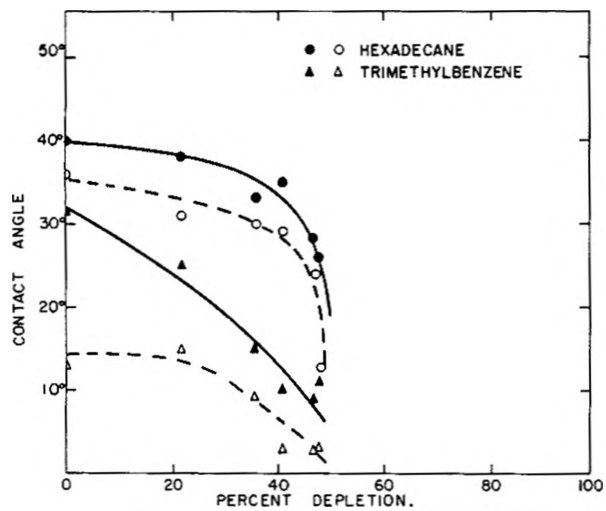

Fig. 2.—Contact angles of *n*-hexadecane and 1,3,5-trimethylbenzene on depleted monolayer of *n*-octadecylamine. Solid points represent advancing angles, open points represent receding angles.

Results

Wetting Experiments.—In order to test the role of molecular orientation in the wettability of depleted monolayers of octadecylamine several liquids with approximately the same surface tension as the reference liquid, *n*-hexadecane, were selected. At 20° the surface tensions reported for the liquids chosen, namely, *n*-tetradecane, *n*-hexadecane, 1,3,5-trimethylbenzene and Kel-F #3, are 26.7, 27.6, 28.5 and 28 dynes/cm., respectively. The area per adsorbed molecule of octadecylamine in undepleted films was estimated to be about 23 Å.^{2} by comparison with Langmuir–Blodgett films. This is somewhat greater than the area of 20.5 Å.^{2} observed for amines in close-packed films on water,[6] possibly because of the inclusion of hexadecane discussed above.[7] The results of the wetting experiments are illustrated in Figs. 1–3. The exact values of contact angle as a function of depletion of film were not sufficiently reproducible from slide to slide to warrant the plotting of all measured values for a given liquid on a single curve. Nevertheless, the general shapes of the curves of wetting *vs.* depletion were reproducible, and characteristic curves, established by many experiments, are drawn through one set of representative experimental points for each liquid.

An experiment also was run in which the size of the adsorbed molecules rather than the liquid molecules was varied. Figure 4 shows the wetting of *n*-dodecylamine by *n*-hexadecane. Dodecylamine did not adsorb as compactly as octadecylamine, giving an area of about 26 A.^{2} per molecule in undepleted films. The first point on the curve in Fig. 4 was obtained with a droplet nearly saturated with dodecylamine to prevent partial dissolution of the film.

Direct optical studies of the difference in penetration into films of octadecylamine by the above liquids were made and are discussed in the interpretation of wetting results below.

Discussion

Theoretical Considerations.—The wetting of simple surfaces by liquids can be correlated at least qualitatively by means of Young's equation

$$\gamma_{SV} - \gamma_{SL} = \gamma_{LV} \cos\theta \qquad (1)$$

where θ is the contact angle of the liquid on the solid and the γ_{ij} are the appropriate boundary tensions. Zisman, in a classic series of experiments,[8] has shown that on low energy surfaces θ varies quite smoothly as a function of γ_{LV} for a given solid, and equally smoothly with changes in γ_{SV} for a given liquid. The implication in terms of Young's equation is that, barring specific interactions, interfacial tension tends to be a predictable function of the surface tensions of the two separated phases involved. A function explicitly asserting this relationship has been proposed recently by Berghausen, *et al.*,[9] and in its simplest form is given by

$$\gamma_{ab} \approx \gamma_a + \gamma_b - 2(\gamma_a\gamma_b)^{1/2} \qquad (2)$$

As pointed out by the authors, eq. 2 is derived for a model system of such severe simplicity that it cannot be expected to apply accurately to any real system. It is successful, nevertheless, coupled with eq. 1, in correlating a great number of wetting experiments at least qualitatively,[10] and its failures in individual systems help reveal the magnitudes of specific interactions involved. Such failures, shown,

(6) N. K. Adam, *Proc. Roy. Soc.* (*London*), **A126**, 526 (1930).

(7) O. Levine and W. Zisman, THIS JOURNAL, **61**, 1068 (1957), cite evidence indicating that solvent may not be included in adsorbed films if true adsorption equilibrium is attained.

(8) See, for example, A. H. Ellison and W. A. Zisman, *ibid.*, **58**, 260 (1954), and the articles to which this reference refers.

(9) P. Berghausen, R. Good, G. Kraus, B. Podolsky and W. Soller, Technical Report to Air Force (contract No. AF 33 (616)-231 University of Cincinnati), Feb., 1955.

(10) It is interesting to note that eq. 2 actually seems to be more successful in correlating contact angles with surface tensions than in deducing interfacial tensions between immiscible liquids. This may be due in part to the fact that equilibrium interfacial tensions measured for liquid–liquid interfaces are complicated by solubility effects omitted from the model. In wetting experiments, on the other hand, the effective instantaneous boundary tensions for moving drops may be unconfused by such effects since the rate of advance of a boundary expressed in time per molecule traversed may be fast compared with relaxation times of the molecules in the solid surface. For a discussion of this principle see R. S. Hansen and M. Miotto, *J. Am. Chem. Soc.*, **79**, 1765 (1957).

for example, in the ability of a solid surface to discriminate between liquids of the same surface tension in wetting experiments, result from several factors, two of the most important of which are as follows.

First, deviations will result if intermolecular forces across an interface fail to approximate the geometric mean of the forces in the separate phases. If the forces are exclusively dispersion forces this can occur if the sizes of the molecules on the two sides of the interface are different. It can occur even more strikingly if specific attractions such as hydrogen bonds can be formed across the interface. Zisman has demonstrated this type of discrimination in many systems. A second factor arises if the surface has a structure with a markedly stronger capacity for orienting some kinds of molecules than others. In the present investigation the discrimination arising from the second effect predominates over the first.

It is appropriate to examine the conditions for finite contact angles on adsorbed monolayers. The failure of hydrocarbon oils to wet completely the hydrocarbon tails of adsorbed fatty molecules was first explained by Langmuir[11] as being due to the difference between "properties" of surfaces rich in methylene groups (liquids) and those rich in methyl groups (oriented monolayers). Methylene groups, linked together by short covalent bonds, concentrate more atoms and hence a greater number of attractive van der Waals contacts per unit area than do the rather widely spaced, bulky methyl groups. Accordingly it is clear from a qualitative correlation of free surface energy with work of cohesion that methylene (liquid) surfaces tend to be higher in energy and resist spreading over methyl surfaces. It often has been stressed that non-wetting requires a dense packing of methyl groups. It should be noted, however, that it is not the highness of density of surface atoms that reduces the wetting but, more importantly, the ability of the structure to prevent penetration of the liquid into the monolayer. That is to say, if during depletion of monolayers, gaps in the layer were formed that did not admit liquid molecules, the interfacial van der Waals contacts would decrease, lowering the solid–liquid adhesion, and the contact angle would tend to *increase* with increased depletion. If, on the other hand, the gaps allowed free entry of unoriented liquid, the interfacial van der Waals contacts would increase, and the contact angle would tend to decrease with increased depletion. It appears that the gaps formed in our experiments always permit entry of the liquid molecules, at least by the time that depletion has become readily measurable. With liquids near the critical surface tension for wetting a complete layer, therefore, it is only when the penetrating molecules in a depleted layer stay in the film and heal over the gaps with a "low energy" end that a depleted film can avoid becoming more readily wetted than a complete film.

Interpretation of Wetting Experiments.—Tetradecane, with a slightly lower surface tension than hexadecane, exhibits a slightly lower contact angle on a complete monolayer. Depletion experiments suggest, nonetheless, that it also has a significant tendency to orient in the vacancies of depleted films, as indicated in Fig. 1 by the relatively small decrease in contact angle with initial depletion. The resultant surface after entry seems to present not too ragged an aspect to the liquid despite the fact that tetradecane is not long enough to fill up holes completely. Its shortness becomes apparent when depletion is continued, for the wetting curve is less abrupt than for hexadecane and the critical depletion is reached sooner. Perhaps also correlated with its shortness is its greater sensitivity to inhomogeneities in depleted films. At intermediate coverages low contact angles were sometimes observed.

Trimethylbenzene is short and wide compared with octadecylamine chains and is unable to orient in holes in a monolayer. Kel-F #3 is a polymer composed, on the average, of five chlorotrifluoroethylene units with terminal chlorine atoms. It is incapable of favorable atomic registry upon packing

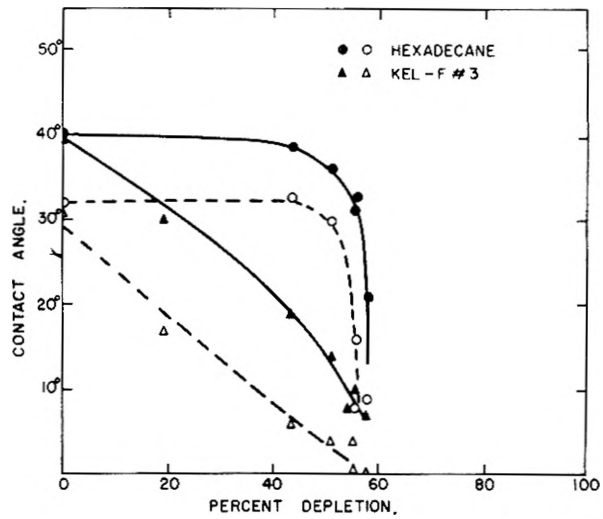

Fig. 3.—Contact angles of *n*-hexadecane and Kel-F #3 on depleted monolayer of *n*-octadecylamine. Solid points represent advancing angles, open points represent receding angles.

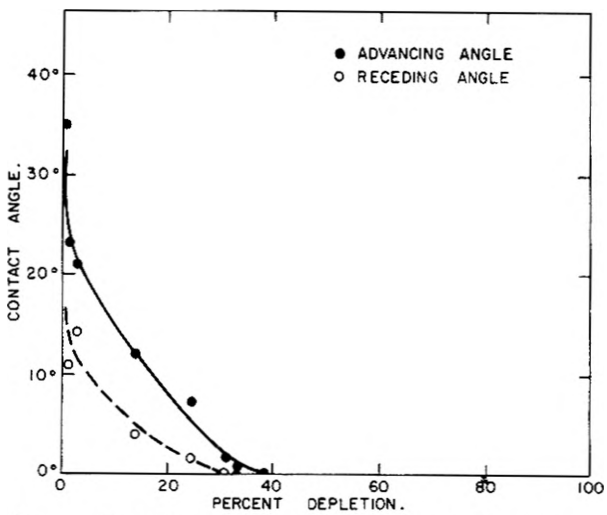

Fig. 4.—Contact angle of *n*-hexadecane on depleted monolayer of *n*-dodecylamine.

(11) I. Langmuir, *Pub. Am. Assoc. Adv. Sci.* [7], *Recent Adv. in Surf. Chem. and Chem. Phys.*, 9 (1939).

with hydrocarbon chains and is nearly as unsuited for orientation as trimethylbenzene. These molecules present particularly interesting cases because, according to Fox and Zisman,[12] alkyl benzenes wet surfaces of close-packed methyls most readily and halocarbons among the least readily of a wide variety of liquids of a given surface tension. *n*-Alkanes are intermediate. Figures 2 and 3, extrapolated backwards toward surface packings of methyl groups corresponding to those found for crystals of long chain hydrocarbons, are consistent with this picture. In the present experiments, however, the effect of orientation after substantial depletion of a monolayer can be seen to swamp the above specificity of intermolecular forces across the interface. This is indicated by a more rapid decrease of contact angle with depletion of film for trimethylbenzene and Kel-F #3 than for hexadecane.

When the length of the adsorbed molecules was altered rather than the length of the molecules of the liquid, an even greater change in wetting behavior was observed. On undepleted films of dodecylamine, a contact angle with hexadecane was obtained approaching that observed on octadecylamine, providing the hexadecane contained enough amine to prevent partial dissolution of the film. Bigelow and Brockway[13] showed earlier that close-packed monolayers of dodecanoic acid on glass are as poorly wet even by pure hexadecane as are those of octadecanoic acid. Figure 4 illustrates how rapidly the ordered surface structure of dodecylamine is destroyed by depletion of the monolayer. Even if hexadecane molecules were to orient strongly in holes in the film, their ends would stand above the shorter neighboring dodecyl chains and tend to spoil the compact array of surface methyls required for poor wetting. An experiment suggesting the same conclusion was described by Schaefer[14] who found lower contact angles of petrolatum on mixed Langmuir–Blodgett films composed of 15 carbon and 20 carbon acids than on films of pure 18 carbon acid. It is altogether likely in the present case, though, apart from the mismatch of length of the molecules, that the dodecylamine has a much feebler capacity for inducing orientation than does octadecylamine, and that this contributes strongly to the difference in wetting curves. In our experiments the dodecylamine molecules were about 15% less compactly adsorbed than the octadecylamine molecules, implying a greater disorder in the shorter adsorbed molecules themselves. More direct evidence of the greater disorder in the shorter chains has been provided by Bigelow and Brockway.[13] They showed by electron diffraction experiments with adsorbed films of fatty acids that the randomness of orientation of the adsorbed molecules increases sharply as the chain length is reduced beneath 18 carbon atoms, and that diffraction evidence for orientation vanishes altogether for the 12 carbon chain. The temperatures in the above experiments were 5 to 20° below the bulk melting points of the dodecyl derivatives. It is possible, especially for our depleted films, that the monolayers were above their effective melting points and were essentially liquid-like. The work of Mentor and Tabor[15] on transition temperatures in monolayers is compatible with this view.

A possible model for explaining the discrimination of a depleted monolayer between various liquids is one in which depletion of monolayers leaves more or less independent vacancies the size of single alkyl chains. Such vacancies would show strong selectivity in admitting molecules of the liquid. It is much more probable, however, that film structure is determined kinetically and that depletion starts from a limited number of "nuclei" which rapidly grow into depleted patches very much larger than the size of molecules. The activation energy of removing long chain molecules must be less at the edge of bare patches than in intact regions where molecules are hemmed in on all sides by neighbors. It is clear from many lines of evidence that the lateral cohesion of neighboring chains to each other is large. When adsorbed films of octadecylamine are severely depleted they still give electron diffraction patterns characteristic of compact clumps of molecules coöperatively holding each other upright rather than patterns of sparsely distributed independent molecules. It is reasonable to conclude then that during depletion the further depletion around existing holes soon proceeds faster than the depletion associated with making new holes. This implies that the holes in depleted films are so large that they cannot induce orientation of liquid molecules solely by virtue of their geometric shape. In the second model of film structure, then, the importance of the natural capacity of the liquid molecules to orient, given a meager framework, overshadows the orientational effect induced, as in the first model, by simple penetration of long, thin molecules into long, thin holes. Lending support to the hypothesis that long chain hydrocarbons may orient easily on surfaces in a direction perpendicular to the surface is an observation[16] by electron diffraction that very thin films of *n*-hydrocarbons with eighteen or more carbon atoms naturally assume this orientation. This is in contradistinction to a large body of literature in which it is conjectured that hydrocarbon chains must lie down on surfaces. The essential key to the problem undoubtedly lies in the coöperative interactions of the chains which are capable of holding together groups of upright molecules. Advantage may be taken of the low surface energy of methyl groups in this packing arrangement.

Observations of Penetration into Monolayers.—Additional evidence of the ability of adsorbed films to discriminate between various kinds of liquids was afforded by the optical method. Indeed, it is difficult to conceive of any other way all of the following phenomena could have been detected. The optical method permits instantaneous observations and rapid measurements of local surface concentrations of molecules, for example, in the molecular wake of a non-wetting droplet being pulled across a surface. The interaction of tetradecane, hexadecane and Kel-F #3 with films of octadecylamine was

(12) H. W. Fox and W. A. Zisman, *J. Colloid Sci.*, **7**, 428 (1952).
(13) W. C. Bigelow and L. O. Brockway, *ibid.*, **11**, 60 (1956).
(14) V. J. Schaefer, THIS JOURNAL, **45**, 681 (1941).
(15) J. W. Mentor and D. Tabor, *Proc. Roy. Soc.* (*London*), **A204**, 514 (1951).
(16) L. S. Bartell and C. L. Sutula, to be published.

examined. It was found that all of the liquids tended to dissolve virgin monolayers partially, to the extent of perhaps 10 to 30% if droplets of the pure liquids were pulled across the films. This behavior was conspicuous with Kel-F #3 but, curiously, was not visibly apparent with hexadecane if measurements were made shortly after the droplets were receded. Only after many minutes of standing did the paths traversed by hexadecane become visible as the hydrocarbon, which had taken the place of the dissolved amine molecules, evaporated. Tetradecane behaved similarly to hexadecane if the droplet was left near the region examined, but evaporated much faster than hexadecane when the droplet was removed.

The effect was striking when droplets were receded across monolayers that were already depleted by 40 or 50% with benzene. Then the tracks of the hydrocarbon droplets stood out boldly against the background of the surrounding depleted film and gave an optical thickness as great as the original film had been before depletion. Kel-F #3 was also found to penetrate into holes of depleted films, but, in general, it built up the optical thickness only to about two-thirds that of an undepleted film.

When optical observations were made directly while the drops were moving across depleted films it was found that hexadecane not only filled the vacancies in the films but that it left a fleeting multilayer in the track that rapidly evaporated to the monolayer level. No such multilayer was noted with Kel-F #3, although its vapor pressure is similar to that of hexadecane. It is interesting to note the seemingly anomalous implication that the apparent adhesion, as inferred from the case of adsorption of multilayers on the film, would appear to be greater for the liquid giving the poorer wetting. Whether the effect is a kinetic illusion, owing to faster evaporation of Kel-F #3, or real is uncertain.

No lateral diffusion of liquids into depleted areas not traversed by the droplets was observed. It is probable, nevertheless, that the molecules of the liquid penetrate into holes in the film far enough beyond the periphery of the drop that the effective boundary tension of the solid is one for which holes are fairly well filled by adsorbed liquid molecules. The transfer of molecules from the drop into depleted areas probably takes place whenever the drop edge touches such a region through the spontaneous surface diffusion of a liquid-like film into the bare regions. With the liquids in the present investigation the advance into holes bordering the drop should be much faster than normal rates of advance of the bulk drop. Adsorption by transport through the vapor phase may be appreciable, also.

To what extent the hexadecane molecules, after entering the large holes in a film, diffuse outward and form a true two-dimensional solution with the adsorbed molecules is not clear. Hexadecane has been shown by Vold and Vold[17] to enter liberally the three-dimensional lattice of certain phases of alkali stearates. In the adsorbed films, however, about one-third of the molecules appear to be so firmly adsorbed in tight clusters that there is some doubt as to whether they would be involved in two-dimensional solutions.

Finally, it is to be emphasized that the curves of wetting *versus* depletion presented here are not those to be expected in general. Commonly, where wetting is poor, the surface tension of the liquid exceeds the effective tension[18] of the solid by a substantial amount and complete wetting may occur only at essentially complete removal of the adsorbed film. Such behavior has been recorded with water on fatty amines adsorbed on quartz[19] and on Pt and Cr,[20] and with organic liquids on fluorocarbon films.[21] In the present investigation, the boundary tensions were delicately balanced, and complete wetting occurred at intermediate surface coverages. The system was then particularly sensitive to structural effects and revealed clearly the discrimination of an adsorbed monolayer between liquids of different molecular size and shape.

(17) M. J. Vold and R. D. Vold, *J. Colloid Sci.*, **5**, 1 (1950).

(18) The term "effective tension" is used instead of an unqualified term such as "free surface energy" to refer the description of wetting phenomena to the frame of reference offered by Zisman's experiments on low energy surfaces (ref. 8). When Young's equation is applied to the wetting of an adsorbed film (which may include significant amounts of the contact angle liquid) it is arbitrary whether the interfacial free energy between the solid and film is included in the terms γ_{SV} and γ_{SL} of eq. 1. If it is omitted the resulting γ_{SV} may frequently be low enough for the "effective surface" probed by the liquid to qualify as a low energy surface. Further, the effective tension may not have a true thermodynamic meaning. In experiments of the present variety, the composition, and hence tension, that is relevant in the region of the film being traversed by drop boundary, may be quite different from that of a film which has achieved thermodynamic equilibrium with the drop.

(19) A. M. Gaudin, "Flotation," 2nd ed., McGraw-Hill Book Co. New York, N. Y., 1957, p. 269.

(20) R. J. Ruch and L. S. Bartell, to be published.

(21) J. W. Shepard and J. P. Ryan, Paper No. 41, Colloid Division, 134th National ACS Meeting, Chicago, September 11, 1958.

SURFACE PROPERTIES OF MAGNESIUM OXIDE. II[1]

By R. I. Razouk and R. Sh. Mikhail

Contribution from the Department of Chemistry, Faculty of Science, Ain Shams University, Cairo, Egypt, UAR

Received October 28, 1958

In continuation to an earlier communication, work has been extended to study the effect of the temperature of preparation and of the duration of heating on the activity of magnesium oxide obtained by the thermal decomposition *in vacuo* of two specimens of precipitated magnesium hydroxide, precipitated magnesium carbonate and native magnesite. MgO prepared from precipitated $Mg(OH)_2$ or $MgCO_3$ behaves like that obtained from brucite, in that the maximum activity is developed on decomposition at 350°, whereas the oxide prepared from magnesite at 650° shows maximum activity. Sintering develops at higher temperatures and its extent is greater the larger is the surface area of the oxide and the higher the temperature. It is suggested that in the dehydration of $Mg(OH)_2$, the development of the surface area is a direct consequence of the reaction, whereas in the decomposition of $MgCO_3$ a process of activation occurs as well, so that the surface area of the product increases far more than corresponds to the fraction decomposed. The results are interpreted as a consequence of the interaction of three rate processes, namely, decomposition, recrystallization and sintering. It is concluded that the development of the activity of the product obtained by the thermal decomposition of different parent materials varies according to the mechanism associated with its decomposition.

The surface properties of magnesium oxide prepared by the dehydration of brucite were the subject of an earlier investigation.[1] In view of the controversial results obtained by various authors regarding the conditions of maximum activity of oxides produced by thermal decomposition[2] and the variation of activity with heat treatment, the work has been extended to the study of oxides obtained by the dehydration of two specimens of precipitated magnesium hydroxide and the decomposition of precipitated and native magnesium carbonate. Experiments have been confined to oxides prepared *in vacuo*, since the presence of air has been found to influence the surface properties in a complicated manner.[1] The effect of the temperature of decomposition and of the duration of heating at fixed temperatures on the activity of magnesium oxide was studied, the activity being arbitrarily measured by the specific surface area as determined from the monolayer capacity of adsorbed cyclohexane in the manner described earlier.[1]

Experimental

The apparatus, technique and the method of preparation of cyclohexane were described earlier.[1]

Four groups of oxide were prepared by thermal decomposition, *in vacuo*, of precipitated $Mg(OH)_2$ A and $Mg(OH)_2$ B, precipitated $MgCO_3$ C and native magnesite $MgCO_3$ M. Details of the methods of preparation are described elsewhere.[3] Decomposition temperatures varied between 350 and 1250°, and duration of heating between 10 min. and 20 hr. The oxide content of each product is given in the text.

Results

I. Effect of Temperature of Preparation.—The adsorption isotherms of cyclohexane on the various decomposition products obtained from the hydroxide and carbonate of magnesium by heating *in vacuo* for 5 hr. are all Type II of the Brunauer classification.[4] The adsorption seems to be purely physical in nature, and outgassing at room temperature brings about almost complete removal of the adsorbate.

The surface area of the various products has been estimated from the B-point of the isotherms, taking the molecular area of cyclohexane as 39 Å.^{2}.[5] It has been shown[1] that estimates of the surface area based on the adsorption isotherm of cyclohexane on magnesium oxide agree with the values obtained from the low-temperature nitrogen adsorption using the BET method. Table I shows a summary of the surface area values of the various oxides prepared by the decomposition *in vacuo* of precipitated magnesium hydroxide and carbonate and of magnesite at various temperatures. It should be noted that the decomposition was complete in all cases except with precipitated $MgCO_3$ C at 350°, when the decomposition was 1.2% short of completion.

Table I

Specific Surface Area of Magnesium Oxide Prepared at Various Temperatures

Temp. of preparation, °C. \ Parent material	$Mg(OH)_2$ A, m.^{2}/g.	$Mg(OH)_2$ B, m.^{2}/g.	$MgCO_3$ C, m.^{2}/g.	$MgCO_3$ M, m.^{2}/g.
25 (undec.)	1	89	8	6
350	34	310	426	
500	25	280	156	285
650	18	190	73	550
800		121	42	480
950	13	77	28	392
1100	7	13	17	197
1250				54

The results in Table I are shown in Fig. 1, in which are plotted also the areas of the dehydration products of brucite for the sake of comparison. It is evident that the oxides prepared from brucite and precipitated hydroxide or carbonate behave in a similar way. Thus the maximum activity is developed on decomposition at 350°, and sintering soon develops at higher temperatures, its extent being the greater the larger is the surface area of the produced oxide. However, the oxide prepared from magnesite shows a striking difference; for here the maximum activity develops when the oxide is formed at 650°, and the temperature at which it becomes "deadburnt" and thus possesses a very low surface area, is distinctly above that for the other parent materials. It seems therefore that

(1) Part I, R. I. Razouk and R. Sh. Mikhail, This Journal, **61**, 886 (1957).

(2) S. J. Gregg, "The Surface Chemistry of Solids," London, 1951.

(3) R. I. Razouk and R. Sh. Mikhail, This Journal, **62**, 920 (1958).

(4) S. Brunauer, "Physical Adsorption of Gases and Vapors," Oxford Press, New York, N. Y., 1945.

(5) N. Smith, C. Pierce and H. Cordes, *J. Am. Chem. Soc.*, **72**, 5595 (1950).

below 650° there is an activation process while above this temperature the ordinary sintering process occurs.

It is worth mentioning that although the surface area of $Mg(OH)_2$ A is very close to that of brucite (about 1 $m.^2/g.$[1]), yet the maximum surface area of the oxide obtained from the latter is about four times as much as the value obtained for the oxide prepared from the former.

Comparison of the results obtained with the hydroxides $Mg(OH)_2$ A and $Mg(OH)_2$ B and their dehydration products shows in a striking manner how differences in the details of preparation lead to large changes in the surface activity. Thus the surface area of the oxide prepared from $Mg(OH)_2$ B at temperatures between 350 and 800° is about ten times as big as that of the product obtained from $Mg(OH)_2$ A. Even if the surface area of the original hydroxide is subtracted from the area of the product, the ratio of the two areas still remains about 7:1.

It is interesting to note that whereas the various oxides experimented with possess surface areas which may vary up to 20-fold, variations of the water uptake at saturation do not generally exceed 30%, so that one cannot escape the conclusion already arrived at by the authors[3,6] that the sorption of water by magnesium oxide is not merely a surface phenomenon but mainly a bulk effect.

II. Effect of Time of Heating.—The effect of the duration of heat treatment on the surface area of magnesium oxide has been studied using $Mg(OH)_2$ B, $MgCO_3$ M and $MgCO_3$ C as starting materials.

Figure 2 shows the variation of the specific surface area of MgO B with duration of heating for various temperatures of dehydration, the time of heating representing the total time commencing with the parent material. The surface area falls sensibly with increase of time of heating for the oxides prepared at 1100 and 950°, but a limiting area is obtained on heating the hydroxide for 10 hr. This area is characteristic of the temperature of dehydration, and longer heat-treatment does not produce any effect, in agreement with the results obtained with dehydrated brucite.[1] However, Gregg, Packer and Wheatley[7] found that the surface area of magnesium oxide prepared by the calcination of the precipitated hydroxide diminishes continuously with increase of time of heating over a period of more than 300 hr. This difference may be due to the varying conditions of preparation of the parent material and of its heat-treatment especially with respect to the absence or presence of air during the decomposition of the hydroxide.

Magnesium oxide prepared at 800 and 650° behaves in a similar way, though to a much less extent, and the surface area falls slightly with increase of time of heating, reaching a limiting value after 10 hr. also.

On the other hand, when $Mg(OH)_2$ B is dehydrated *in vacuo* at 500°, the surface area of the product increases slightly with time but soon tends to a limiting value. Thus the area of the product

(6) R. I. Razouk and R. Sh. Mikhail, THIS JOURNAL, **59**, 636 (1955).
(7) S. J. Gregg, P. K. Packer and K. H. Wheatley, *J. Chem. Soc.*, 46 (1955).

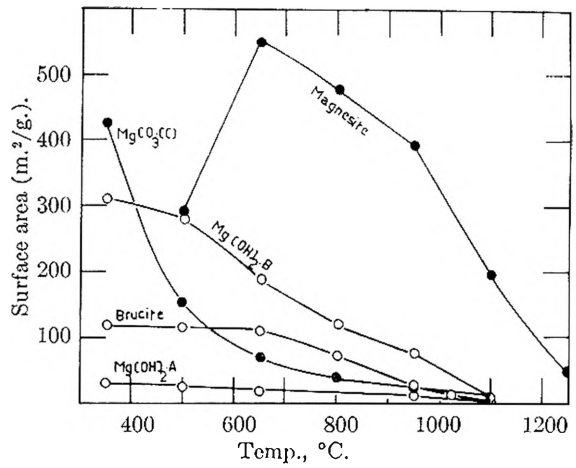

Fig. 1.—Effect of temperature of preparation on the surface area of magnesium oxide obtained from brucite, $Mg(OH)_2$ A, $Mg(OH)_2$ B, $MgCO_3$ C and $MgCO_3$ M.

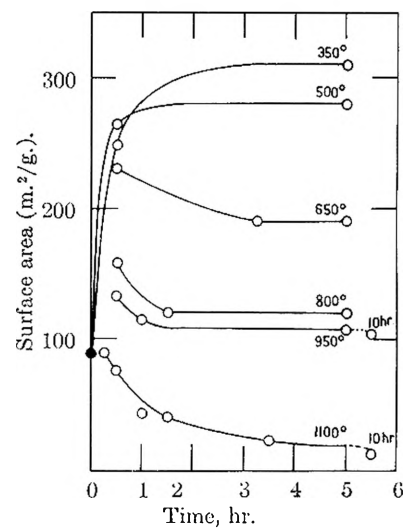

Fig. 2.—Effect of duration of heating on the surface area of magnesium oxide prepared from $Mg(OH)_2$ B at various temperatures (●, original hydroxide).

of dehydration obtained after heating the hydroxide for 0.5 hr. is 264 $m.^2/g.$, while that of the oxide obtained after 5 hr. is 280 $m.^2/g.$ However, it has been found that shock heating at this temperature for 0.5 hr. is not sufficient to bring about complete dehydration but results in a loss of 28.7% as compared with the theoretical value of 30.9%. Now if the area is corrected for incomplete dehydration it rises to 278 $m.^2/g.$ which is very close to the value of the completely dehydrated specimen obtained after 5 hr. of heating.

Similar results are obtained with the product prepared at 350°. Thus when the hydroxide was heated for 0.5 hr. at this temperature, it lost 22.4% of its weight, and the specific surface area of the product was found to be 249 $m.^2/g.$ of the dehydration product, whereas when the area is referred to the weight of magnesium oxide actually present, it becomes 309 $m.^2/g.$ as compared with the value of 310 $m.^2/g.$ obtained with the oxide prepared by dehydration for 5 hr. at the same temperature.

It may thus be concluded that in the case of MgO prepared from precipitated $Mg(OH)_2$ B, the development of the surface is a direct consequence of the

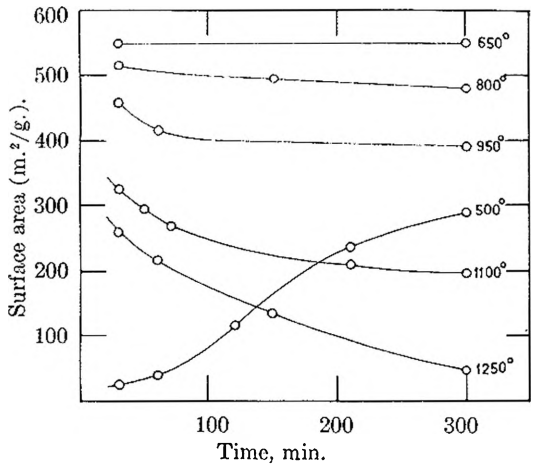

Fig. 3.—Effect of duration of heating on the surface area of magnesium oxide prepared from $MgCO_3$ M at various temperatures.

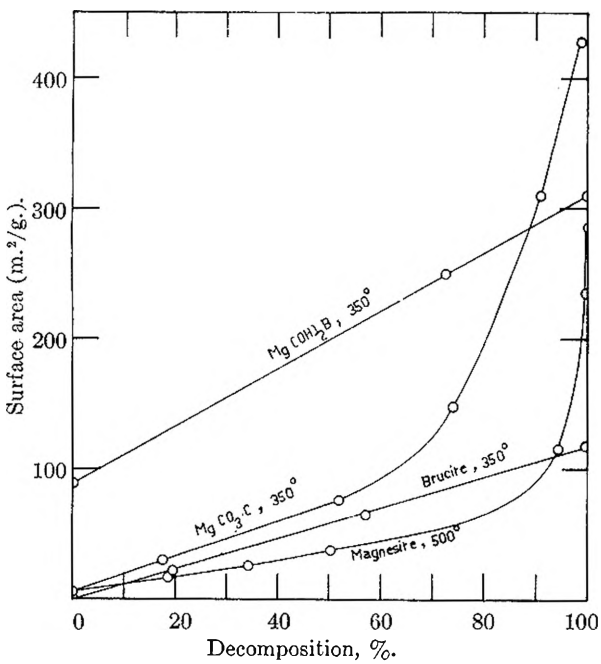

Fig. 4.—The surface area of magnesium oxide prepared from brucite, $Mg(OH)_2$ A, $Mg(OH)_2$ B, $MgCO_3$ C and $MgCO_3$ M as a function of the fraction decomposed.

decomposition of the hydroxide, and that the process of sintering becomes sensible only above 650°.

The effect of the duration of heating on the surface area of the product of decomposition of native magnesite, $MgCO_3$ M, is shown in Fig. 3. It is evident that at temperatures above 650°, the behavior is essentially the same as that of the dehydration products of magnesium hydroxide, namely, that the surface area decreases continuously with the increase of the time of heating until a limiting value is obtained with the oxide prepared by heating magnesite for 5 hr.

However, the oxide prepared from magnesite at 650° represents a special and critical case; for the duration of heating has apparently no effect on the surface area of specimens heated for periods varying between 0.5 and 5 hr. and, under these conditions, the oxide possesses the maximum surface area of 550 m.²/g. It is to be noted that heating for 0.5 hr. at this temperature brings about complete decomposition of magnesite.

The results of experiments on the products prepared by decomposition at 500° are more interesting. Specimens heated for 0.25, 0.5, 1, 2, 3.5 and 5 hr. at this temperature and having lost 9.6, 17.8, 26.2, 49.3, 52.07 and 52.20% of their weight as carbon dioxide, possess surface areas of 17, 26, 39, 116, 237 and 285 m.²/g. of the product, respectively. These values show that the area increases far more than corresponds to decomposition, indicating that in the case of magnesite the development of the surface is not a direct consequence of decomposition, but proceeds either with a slower rate than decarbonation, or develops even after it has ceased. A similar increase in the ratio of area to percentage decomposition also has been observed by Gregg, Packer and Wheatley[7] using MgO from $Mg(OH)_2$ and by Glasson[8] using CaO from $Ca(OH)_2$.

Precipitated $MgCO_3$ C showed the same behavior. Thus the products prepared by decomposition *in vacuo* at 350° for intervals of 10 min., 1, 1.5, 3 and 5 hr. and having lost 9.2, 27, 39, 47.5 and 51.6% of their weight possess surface areas of 31, 76, 147, 310 and 426 m.²/g. of the product of decomposition, respectively; the increase in area far exceeding the extent of decomposition.

Figure 4 summarizes the results of the measurements of the surface area of the products of decomposition of brucite,[1] precipitated $Mg(OH)_2$ B, magnesite $MgCO_3$ M and precipitated $MgCO_3$ C as a function of the percentage of decomposition. The curves show clearly that in the case of natural and precipitated hydroxide, the surface area of the product is a direct consequence of decomposition, whereas in the case of natural and precipitated magnesium carbonate a process of activation takes place in the mean time at the lower temperatures of preparation.

Discussion

The surface properties of magnesium oxide produced by thermal decomposition have been the subject of many investigations. According to the general theory of Gregg for the preparation of active solids,[9] the formation of magnesium oxide by thermal decomposition may proceed in one of two ways. Thus during the decomposition of the parent material, one nucleus of the oxide may first form within each crystallite, and then the lattice rearranges by growth of this nucleus, a process which is a function of both temperature and time. Under these conditions, one would expect limited activation of the oxide, the development of much strain and slight variation of surface area.[10] But none of these effects has been observed. Indeed, the present investigation reveals that the effect of heat treatment is a pronounced variation in the surface area, while Thomas and Baker[11] could not detect the presence of lattice strain in their X-ray studies, and even suggested that the line broaden-

(8) D. R. Glasson, *ibid.*, 1506 (1956).

(9) S. J. Gregg, *ibid.*, 3940 (1953).

(10) D. T. Livey, B. M. Wanklyn, M. Hewitt and P. Murray, *Trans. Brit. Ceram. Soc.*, **56**, 217 (1957).

(11) D. Thomas and T. W. Baker, "X-Ray Diffraction Studies of Active Magnesium Oxide," quoted in ref. 10.

ing given by some specimens of oxide is rather due to changes in the particle size.

Alternatively, each crystallite of the parent material, immediately on decomposition, may give rise to a large number of nuclei, and the original lattice collapses as a result of decomposition. The development of some lattice strain cannot, however, be overlooked, especially with specimens prepared at the lower temperatures, when the oxide is formed at first in the form of a pseudo-lattice, with the ions of Mg^{++} and O^{--} still occupying the same positions that they held in the original lattice. Thus Fricke and Lüke[12] found that the active oxide possessed an energy content 67 cal./g. higher than the sintered oxide. But the pseudo-lattice has probably a short-life existence, since it has not been detected by X-ray examination,[13] and this form soon collapses to yield a great number of magnesium oxide crystallites corresponding to the number of nuclei formed in the parent material. This process, which is associated with the disappearance of the original structure of the parent material and the formation of the new lattice of the oxide, may be designated "recrystallization," and accounts for the activation and the development of large surface areas of the products.

Both decomposition and recrystallization are rate processes, and the variation of the surface area with percentage decomposition is dependent on the rate-determining step. When the decomposition of the parent material is rate-determining, the area of the product will be a linear function of the fraction decomposed, as in the production of magnesium oxide from precipitated and natural hydroxide. On the other hand, if recrystallization is the rate-determining process, then further activation of the product may occur, resulting in an increase of the surface area far more than corresponds to the fraction decomposed, and this is the case with precipitated and native carbonate. Thus the development of activity of the product obtained by the thermal decomposition of different starting materials, varies according to the mechanism associated with its decomposition.

Accompanying the process of recrystallization, a third rate process is of frequent occurrence, namely, the growth of the formed magnesium oxide crystallites which is usually called sintering. Increase in the grain size of the particles by sintering has been illustrated in a striking manner by a set of electron micrographs taken by Birks and Friedman[14] using magnesium oxide prepared from commercial magnesite. Raising the temperature invariably increases sintering until a temperature is reached when the oxide becomes "deadburnt." The effect of time is also to increase sintering. The activity generally diminishes exponentially with time, but it has been found in the present investigation that a limiting value of the surface area always has been obtained for each temperature. It is interesting to note that the oxides which possess higher surface areas sinter more rapidly. This may be understood in view of the higher surface energy associated with finer powders, facilitating thus the process of surface adhesion and surface diffusion which are so important in the process of sintering.[15] Furthermore, two other effects may contribute to the easier sintering of finer particles, namely, the presence of edge and corner energies[16] and the considerable rise in the surface energy due to the screening effect of the cations and the consequent approach of the whole structure to a disordered lattice as predicted by Weyl.[17]

The net result of the interaction of the three above-mentioned processes, *viz.*, decomposition, recrystallization and grain growth of the product may lead under certain conditions to the appearance of a maximum in the surface area–temperature curves. Before the maximum is reached the first two processes are predominating, whereas beyond it sintering becomes more significant.

Finally, the conclusion could be drawn that temperature or duration of heating can no longer be arbitrary in the production of active magnesium oxide by thermal decomposition. Heating must be conducted at temperatures and for periods ensuring complete decomposition as well as maximum activation and avoiding any sintering effects. The use of parent materials possessing large surface areas will generally favor sintering at comparatively lower temperatures of preparation.

(12) R. Fricke and I. Lüke, *Z. Elektrochem.*, **41**, 174 (1935).
(13) R. Sh. Mikhail, Ph.D. Thesis, Ain Shams University, 1957.
(14) L. S. Birks and H. Friedman, *J. Appl. Phys.*, **17**, 687 (1946).
(15) G. F. Huttig, *Kolloid Z.*, **98**, 263 (1942); **99**, 262 (1942).
(16) B. Weissenbach, *Radex-Rundschau*, **6**, 257 (1951).
(17) W. A. Weyl, "Structure and Properties of Solid Surfaces," Ed. R. Gomer and C. S. Smith, Univ. of Chicago Press, Chapter IV 1952.

DETONATION PROPAGATION IN LIQUID OZONE–OXYGEN

BY RILEY O. MILLER

Lewis Research Center, National Aeronautics and Space Administration, Cleveland, Ohio

Received October 26, 1958

Velocities and approximate composition limits of detonation propagation were determined for the liquid O_3–O_2 system at −177°. Detonations in vertical tubes were photographed with a rotating-mirror streak camera. Glass tubes, 5 and 8 mm. i.d., and stainless steel and lead tubes, 11 mm. i.d., were used. Initiation was either by direct spark or by a 100% ozone booster charge. Initial pressure was either 1.5 or 21 plus atmospheres. In general, the detonation behavior was as follows: (a) from about 50 to 100% by weight O_3, Chapman–Jouguet-type propagation was obtained; (b) from about 35 to 50% O_2, propagating reactions were inefficient, or did not occur; (c) below about 35% O_3, no propagation was obtained. The detonation velocity for 100% ozone was about 6000 m./sec. and varied as the square root of the weight fraction of ozone in the mixture. The experimental velocities were compatible with elementary solid state model theory.

Introduction

Liquid ozone detonations are of both practical and theoretical interest. The dangerous detonable character of liquid ozone has been known for years; now engineers need to know how to use it safely in rockets and other industrial equipment. Liquid ozone detonations lend themselves to analytical treatment; the chemistry and physics is simple compared to that of other condensed explosives. Detonations in liquid ozone, for example, should give information on how oxygen behaves at high pressures and temperatures. The work described here was done to fulfill partially a need for quantitative data on these detonations.

Experimental

General Description.—The apparatus consisted of a closed system for the preparation and concentration of the ozone, a detonation tube in which the mixture was made and detonated, and equipment to measure the detonation velocity. The detonation tube was submerged in a bath of liquid oxygen contained in a glass refrigerant tube which was inside a sealed tank of larger diameter. The tank had two narrow vertical glass windows on opposite sides for observation and photography of the detonation tube.

In each experiment, the required volumes of pure liquid ozone and then oxygen were distilled into the detonation tube. Helium pressure, if desired, was applied inside the tube and the mixture was remotely stirred and then detonated either by direct spark or by a 100% ozone booster charge. The detonation was photographed by a rotating-mirror strip camera.

Detonation Tube Assembly.—Detonation tubes of borosilicate glass, stainless steel and lead were used. At the bottom of each tube was either a 0.05 mm. spark gap or a booster cell separated from the experimental section of the tube by a thin diaphragm. The length of the booster cell was 3 to 4 cm. and its diameter was somewhat larger than that of the tube's experimental section. At the bottom of the booster cell was a spark gap. The walls of the tubes were about 1 mm. thick.

The experimental section of all tubes was about 25 cm. long. Mixtures were stirred by 1 or 2 steel balls which were made to go up and down the length of the experimental section by a reciprocated magnet. The stirring time was 15 to 20 minutes, depending upon tube diameter. In later experiments the tubes were pressurized with helium before stirring. The balls were held above the liquid when not being used.

During the experiment liquid oxygen was continuously admitted to the refrigerant tube. To prevent the O_3–O_2 mixture in the detonation tube from separating into two liquid phases,[1] the temperature in the tube was kept at about −177° by maintaining the pressure inside the tank at 1.5 atmospheres.

Materials.—The ozone was made from commercial dry oxygen which first was passed through a copper oxide catalyst bed at about 700° to oxidize impurities and then through beds of calcium sulfate and sodium hydroxide–asbestos to remove water and carbon dioxide, respectively. The ozonator was similar to one described elsewhere.[2] Ozone and some oxygen were condensed in a glass bulb. The oxygen was later removed at reduced pressure, some being distilled into a second bulb. These stocks were used immediately to prepare the mixture in the detonation tube.

The purity of the undiluted ozone probably was greater than 99.95%. In computations involving densities of liquids at −177° the values 1.554 and 1.117 g./cm.^{3} were used for ozone and oxygen, respectively. The densities of mixtures were assumed to be additive.

Materials in contact with the ozone and oxygen were borosilicate glass, stainless steel and fluoroethylene polymers. Before assembly all internal parts were washed with C. P. acetone or chromic acid and dried. Before an experiment most of the system was treated for several minutes with fluorine gas.

In an attempt to reduce initiation of explosion in the detonation tube during stirring, a few tenths of one per cent. carbon tetrafluoride was added to the mixture in a few of the experiments. As indicated by these and other experiments, this amount of additive does not measurably affect detonations already initiated.

Helium used to pressurize the tube was first passed through a trap cooled to −196°.

Measurements.—In glass detonation tubes the mixture composition was measured directly in the tube with a cathetometer, the volume of the experimental section having been calibrated for this purpose. The accuracy of mixture composition in a glass tube is estimated to be within ±0.3%.

When metal detonation tubes were used the volumes of the liquids were measured prior to distillation into the tube. The accuracy of the composition in metal tubes is probably within ±2.5%.

The streak photograph was made of a reflected image which was adjusted for vertical alignment by a mirror next to the tank window. Two pilot lights above and below the outside of the tank window were photographed to give a length scale and horizontal reference lines on the film.

Measurements of the streak photographs were made from the negatives with an optical comparator. The detonation velocity was assumed to be proportional to the slope of the leading edge of the detonation streak and the rotational speed of the camera, which was recorded at the time the spark was fired. The velocity measurements were influenced in some cases by the judgment of the person reading the film. The data reported herein are mid-points of maxima and minima of several readings made on each of two or more occasions. The reported values are usually near the arithmetic mean. The possible error is indicated with the data and includes differences in interpretation plus an estimate of other experimental error.

Results and Discussion

Streak Photographs.—Straight streaks were obtained from detonations of higher concentrations of ozone in both glass and metal tubes. Although some light conceivably may have come from sources other than the detonation products themselves, a

(1) C. Brown, A. W. Berger and C. K. Hersh, *J. Chem. Phys.*, **23**, 1340 (1955); A. C. Jenkins, F. S. Di Paolo and C. M. Birdsall, *ibid.*, **23**, 2049 (1955).

(2) A. L. Henne and W. L. Perilstein, *J. Am. Chem. Soc.*, **65**, 2183 (1943).

reasonable assumption is that in a steady-state detonation the small time delay in excitation of possible secondary emitters is constant. The slope of the leading edge of a straight streak is therefore accepted to be proportional to a detonation velocity.

Curved streaks, indicating decaying velocities, were obtained from some boosted explosions in glass tubes at lower concentrations.

2. Composition Limits for Detonation Propagation. A. Glass tubes.—The limits for spark initiated detonation is estimated to be about 50% by weight ozone (Table I). Five spark-initiated detonations at this and lower concentrations definitely did not propagate; another failed halfway up the tube. High initial pressure and small diameter probably have a repressing effect on detonation from a spark. One photograph of pure ozone in a small tube at high pressure shows the spark followed by a slow, scarcely luminous reaction which suddenly changed to a high order detonation at the center of the tube. Similar but longer delays may have occurred in the small tubes containing 66 and 55% ozone.

When the detonations in glass tubes were overboosted with 100% ozone, the composition limit was indicated to be several per cent. lower and the effects of pressure were more apparent. When the tube was pressurized to 21 atmospheres or higher, the steady state was reached quickly or else detonation failed completely. On the other hand, at 1.5 atmospheres velocities were initially high and decayed slowly. These slowly decaying reactions were considered incomplete because delayed explosions occurred in the tank several minutes after the booster charge was fired. Decaying waves were observed in mixtures containing as little as 35% by weight ozone. The reaction at 35%, however, was very weak, as was shown by the character of the glass breakage.

The reason that decay was slow at 1.5 atmospheres may be local heating due to adiabatic compression of tiny oxygen bubbles which reinitiate the decomposition of ozone mixtures that are below the limit for steady propagation. Conditions are favorable for bubbles, inasmuch as the oxygen in the mixture is near its boiling point. The bubble-initiation explanation is based on other observations in the literature.[3]

B. Stainless Steel Tubes.—Experiments with stainless steel tubes corroborated the fact that detonations of decreased efficiency will propagate from a booster detonation in mixtures containing less than 50% by weight ozone. A steady-state detonation was obtained in 49% ozone, and mixtures of about 40% propagated detonations that fragmented the steel. The efficiency was less when the initial pressure was high. The lower efficiency was indicated by after-explosions and by less fine fragmentation of the tube.

Mixtures containing 35 to 31% by weight ozone did not propagate at initial pressures of 1.5, 28 and 69 atmospheres. Non-propagation was indicated because the tubes from these experiments were not fragmented but only splayed at the bottom by the booster detonation. After-explosions in the tank also occurred.

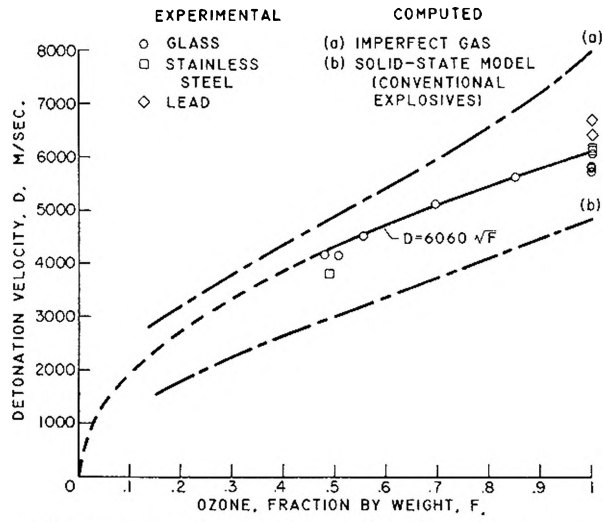

Fig. 1.—Detonation velocities in liquid ozone–oxygen.

C. General.—The experiments with glass and stainless steel tubes show that Chapman–Jouguet-type detonations may propagate in liquid ozone–oxygen mixtures containing about 50% or more ozone by weight. Both types of tubes also show that at lower concentrations less efficient detonations can be made to propagate from a stronger booster detonation, but at 35 to 30% by weight ozone these detonations fail.

The experiments also show that in addition to the Chapman–Jouguet-type detonations, there can be other modes of decomposition in liquid ozone. In one experiment 67% ozone in a stainless steel tube was initiated by a booster charge which was not in contact with the diaphragm at the bottom of the tube. The part of the tube containing the liquid was split open by a low order explosion instead of being fragmented as usual. There were no after-explosions in the tank. A visible flash occurred, but this was not caught on the streak photograph. This may have been the same type of reaction that sometimes occurred from direct spark in the small glass tubes when no streak photographs were obtained. Further studies of low order explosions in liquid ozone may be of practical and theoretical interest.

3. Detonation Velocities.—The steady-state velocities are shown plotted in Fig. 1 against mixture composition. One point is included from an experiment in which detonation failed halfway up the tube. This velocity was constant to the point where detonation ceased, and was considered representative of what steady-state velocity would be for this composition.

The solid curve which is fitted to the experimental data is the parabola

$$D = 6060\sqrt{F} \qquad (1)$$

where D is the detonation velocity, meters per second, and F is the fraction by weight ozone in the mixture. This relation is suggested by the fact that the Chapman–Jouguet equations can be solved approximately to give an expression[4,5]

(3) F. P. Bowden and A. D. Yoffe, "Initiation and Growth of Explosion in Liquids and Solids," Cambridge Univ. Press, 1952.

$$D \approx \varphi\sqrt{8.372 \times 10^3\ \Delta E_c} \qquad (2)$$

where ΔE_c is the heat of explosion (cal./g.) and φ is a variable dependent upon hydrodynamic and thermodynamic relations.

When φ was evaluated for individual experiments it was found to be essentially constant. Least squares fits for φ were obtained for several cases. Maximum and minimum values of D, indicated in Table I, were used to weight D in favor of the more precise data. The average values for φ were then

(a)	Glass tubes, 8 mm. i.d.	2.59
(b)	All glass tubes	2.59
(c)	Glass and stainless steel	2.60
(d)	All tubes	2.65

The latter value of φ was used and equation 1 results when this is substituted into (2). The heat of explosion is represented by an appropriate function of the composition, $\Delta E_c = QF$, where Q is the heat of formation per gram of pure ozone, cal./g.

The average velocity in 100% ozone in glass was slightly less than would be predicted from the velocities at lower concentration. The velocities from two experiments with lead tubes were higher than the other data at 100%. The latter may reflect the influence of greater confinement because of greater tube-wall density.[6]

Various semi-empirical relations for the computation of detonation velocities exist in the literature. Two of the more simple ones have been evaluated here for the conditions of the liquid ozone–oxygen detonations and the calculated velocities are also plotted in Fig. 1.

The top curve (a) is based on the assumption that the products behave as a gas which follows a simplified virial equation of state

$$\frac{pv}{nRT} = 1 + \frac{b}{v} + 0.625\,\frac{b^2}{v^2} + 0.287\,\frac{b^3}{v^3} + 0.193\,\frac{b^4}{v^4} \qquad (3)$$

where b is independent of temperature and specific volume. The value of b is taken to be 0.953, the value of the second virial coefficient for oxygen as calculated from an imperfect gas model.[4] The quantity v, cm.^{3}/g., is the specific volume at the Chapman–Jouguet condition. A procedure described by Taylor[4] was used; the data were computed numerically. Presence of small amounts of O and O_3 in the product gas was neglected. This method has been used with success in predicting detonation velocities of several conventional explosives.

The bottom curve (b) is from equation (4), which was derived from a solid-state model[5]

$$D^2 = 8.372 \times 10^3\ \gamma(\gamma + 2)\Delta E_c \qquad (4)$$

The quantity γ is the Grüneisen parameter defined, for example, by $\nu = a/V^\gamma$ where ν is an average vibrational frequency in a solid, V is volume, and a is a constant. Empirical values of γ for several conventional condensed explosives have been evaluated[5] and it was found that

(4) J. Taylor, "Detonation in Condensed Explosives," Clarendon Press, Oxford, 1952, Ch. VII.

(5) W. H. Andersen and R. B. Parlin, "New Approaches to the Determination of Thermodynamic-Hydrodynamic Properties of Detonation Processes," Tech. Rep. No. 28, Inst. for Study of Rate Processes, Univ. Utah, 1953 (Contract N7-onr-45107).

(6) H. Eyring, *et al.*, *Chem. Revs.*, **45**, 112 (1949).

TABLE I

DETONATION PROPAGATION BEHAVIOR

Ozone, % by wt.	Charge diameter, mm.	Initial pressure, atm.	Propagation mode	Detonation velocity, m./sec.
		Glass: direct spark		
100.0	4.8	1.0	Steady	5730 ± 460
100.0	4.8	28	Delayed[a]	6040 ± 410
100.0	8	1.5	Steady	5800 ± 150
100.0	8	28	Steady	5810 ± 70
85.0	8	21	Steady	5600 ± 60
69.5	8	28	Steady	5100 ± 180
65.6	4.8	1.5	Brisant[b]	
54.6	4.8	32	Less brisant[b]	
55.5	8	1.5	Steady	4500 ± 80
50.7	4.8	1.5	Failed[c]	4130 ± 100
49.7	8	1.5	None	
47.6	4.8	28	None	
47.8	8	28	None	
39.7	4.8	1.5	None	
38.0	4.8	28	None	
		Glass: ozone booster		
48.4	4.8	1.5	Decaying	6100 to 5600[d]
48.0[e]	8	21	Steady	4160 ± 140
42.0	4.8	1.5	Decaying	5800 to 4100[d]
41.1[f]	8	28	Failed[c]	4700 to 4100[d]
37.6	8	1.5	Decaying	5800 to 4800[d]
37.9[f]	4.8	21	None	
35.4[f]	4.8	1.5	Decaying	6700 to 4400[d]
34.3	8	28	None	
		Lead: direct spark		
100.0	11	1.5	Steady	6390 ± 100
100.0	11	1.5	Steady	6670 ± 630
		Stainless steel: direct spark		
100.0	5	1.5	Steady	6060 ± 190
100.0	11	28	Steady	6110 ± 210
		Stainless steel: ozone booster		
49[f]	11	28	Steady	3790 ± 110
41	11	1.5	Brisant[b]	
40[f]	11	28	Less brisant[b]	
35	11	1.5	None	
35	11	69	None	
32	11	1.5	None	
33	11	28	None	
31	11	69	None	

[a] Low order reaction first 1/2 of charge. [b] Detonation delayed or non-luminous. [c] Narrow bright streak stopped abruptly halfway. [d] Approximate initial and final velocities. [e] 0.5% CF_4 added. [f] 0.1% CF_4 added.

$$\gamma = 0.89\rho_0 - 0.049 \qquad (5)$$

where ρ_0 is the loading density in g./cm.^{3} This function was used to obtain the values of γ which were used to construct curve (b).

As shown by Fig. 1, curves (a) and (b) are widely separated at the conditions of the ozone detonations. The experimental velocities fall between them. Theory developed for conventional explosives does not seem to apply *per se* to the ozone data. In its original context, however, the Grüneisen γ is constant. Now when γ in equation 4 is evaluated in terms of the experimental data (eq. 1), γ is a constant having a value 1.84.

For comparison an independent value of γ can

be estimated from the following considerations. Slater[7] has derived the following equation from the equation of state for a solid at absolute zero and a Taylor's series expansion of the Morse equation

$$\gamma = \frac{ar_e}{2} + \frac{1}{3} \qquad (6)$$

where r_e is the equilibrium distance between atoms, and a is the constant coefficient in the exponents of the Morse equation. It is further shown[7] that values of r_e and a for several elements are about the same in the solid as in the diatomic state. Values of γ (eq. 6) for the solids agree with the values from the respective diatomic molecules, within 20%. Now if γ is computed from tabulated values of a and r_e for diatomic oxygen, γ takes the value 1.94 which is only 5% higher than 1.84 found in these experiments. The magnitude and constancy of the γ from these experiments is consistent with the fundamental ideas of the solid-state model.

(7) J. C. Slater, "Introduction to Chemical Physics," McGraw-Hill Book Co., Inc., New York, N. Y., 1939, p. 452 ff.

EVALUATION OF THE EFFECT OF SECONDARY REACTIONS IN CONTROLLED POTENTIAL COULOMETRY

By David H. Geske and Allen J. Bard

Contribution from the Department of Chemistry, Harvard University, Cambridge, Mass.

Received October 27, 1958

Controlled potential coulometry is an effective tool in studying electrode reactions. When a primary electrode reaction is followed by a secondary chemical reaction which regenerates or consumes the electroactive material, the apparent number of faradays per mole of reactant is in general a function of experimental variables. This paper presents a mathematical treatment of several reaction schemes in which secondary reactions occur. A method for evaluating the true n-value as well as the kinetic parameters of the secondary chemical reaction is given.

Introduction

Electrolysis at controlled potential is an experimental technique which is widely employed in the study and elucidation of electrode reactions. Experimental determination of n, the number of faradays per mole of electroactive material, yields the data which allows prediction of the primary electrode reaction products. This is of particular importance in the treatment of organic substances where n may be larger than three or four. The principles and methodology of controlled potential electrolysis have been thoroughly reviewed by Lingane.[1]

The interpretation of coulometric data is straightforward when integral n values are obtained. Non-integral n values will in general be obtained when there are secondary chemical reactions between the product of the electrode reaction (or substances derived from the primary product) and the original electroactive species, or when there are secondary chemical reactions leading to the regeneration of the electroactive substance. This paper presents a mathematical treatment for several of these cases. This work is intended to serve as a guide for the determination of the true n-value as well as for the evaluation of kinetic parameters from coulometric data.

Classification.—It is convenient to classify the possible reaction schemes in terms of the behavior of the reaction product, R. The electrode reaction is represented as

$$C \pm ne^- \longrightarrow R$$

where C is the electroactive material and R is the soluble primary product of the electrode reaction. It is assumed that only a single electrode reaction occurs, thus induced reactions are not treated here. In the reactions below, W, X, Y, and Z represent electrolytically inert materials.

Case I. R Undergoes No Further Reaction.—This case, which is most frequently encountered, involves only integral values of n; the characteristics of the current–time curves have been derived and verified by Lingane.[2] Under these circumstances, R is the experimentally observed reaction product.

Case II. R Undergoes a Single Secondary Reaction.—

(a) $R + Z \longrightarrow X$
(b) $R + C \longrightarrow Y$
(c) $R + Z \longrightarrow C$

Case III. R Undergoes Parallel Secondary Reactions.—

(a) $R + W \longrightarrow X$
$R + Z \longrightarrow Y$
(b) $R + C \longrightarrow X$
$R + Z \longrightarrow Y$
(c) $R + Y \longrightarrow C$
$R + Z \longrightarrow X$

Cases IIa and IIIa are essentially identical to Case I, except that the final product is different from the primary electrode reaction product. Cases IIb, IIc, IIIb and IIIc are similar in that experimental n-values will in general be non-integral and dependent upon some experimental parameters such as (C_i), the initial concentration of electroactive material. Cases IIc, IIIb and IIIc are derived under the restrictive assumption of (Z) being large enough that $d(Z)/dt \simeq 0$.

Other cases, such as the occurrence of three parallel reactions or the formation of the reactive intermediate R from a slow chemical reaction following the electrode reaction, can be treated by

(1) J. J. Lingane, "Electroanalytical Chemistry," 2nd Ed., Interscience Publishers, Inc., New York, N. Y., 1958, p. 222.

(2) Ref. 1, pp. 225–229.

suitable modification of the procedure outlined below.

Mathematical Treatment. General Considerations.—Controlled potential coulometry is usually performed in a stirred solution with the electrode maintained at a potential such that a single electrode reaction occurs. The potential of the electrode is chosen so that the rate of the reaction given in equation 1

$$C \pm ne^- \longrightarrow R \qquad (1)$$

is controlled by the rate of mass transfer of C from the bulk of the solution to the electrode. Under these conditions, the rate of the reverse reaction is considered negligible.

The current i is given by equation 2

$$i = nFm[(C) - (C_0)] \qquad (2)$$

where F is the faraday, (C) is the concentration of C in the bulk of the solution, (C_0) is the concentration at the electrode surface, and m is a constant dependent on prevailing mass-transfer conditions. Under conditions of the Nernst diffusion layer treatment[3] m is AD/δ, where A is the area of the electrode, D is the diffusion coefficient of C, and δ is the thickness of the "diffusion layer." More recent studies[4] have defined m in terms of several hydrodynamic parameters.

When limiting current conditions prevail, $(C_0) \simeq 0$, equation 2 becomes

$$i = nFm(C) \qquad (3)$$

Current, taken as a positive quantity, is related to the rate of consumption of C by

$$i = -nFV\left(\frac{d(C)}{dt}\right)_{elec.\ rxn.} \qquad (4)$$

where V is the total volume of the solution and the minus sign is affixed because $(d(C)/dt)_{elec.\ rxn.}$ is a negative quantity. Combining (4) and (3) gives the rate of concentration change caused by the electrode reaction

$$\left(\frac{d(C)}{dt}\right)_{elec.\ rxn.} = -p(C) \qquad (5)$$

where $p = m/V$.

The apparent number of electrons per mole n_{app} is determined experimentally and is defined as

$$n_{app} = \frac{\int_0^t i\,dt}{FV[(C_i) - (C)]} \qquad (6)$$

The following assumptions have been made in the derivations given below—(a) the electrolysis solution is homogeneous except for the solution at the electrode surface, the "diffusion layer," (b) volume of the electrolysis solution is large in comparison with that of the "diffusion layer," (c) where chemical equations are written, any equilibrium is displaced far to the right.

Case IIb.—The occurrence of a single secondary reaction consuming C

$$R + C \xrightarrow{k_2} Y \qquad (7)$$

will lead to integral values of n^0_{app} when k_2 is either very large or very small. The symbol n^0_{app} refers to evaluation of n_{app} at completion of the electrolysis where (C) approaches zero. Similar superscript notation is used below for (R), (X) and (Y) with the same meaning. For $k_2 \simeq 0$ the reaction is essentially identical with Case I and $(R^0) = (C_i)$ and $n^0_{app} = n$. When k_2 is large, $(R^0) \simeq 0$ and $n^0_{app} = n/2$. The evaluation below is applicable for intermediate k_2 values.

The system is described by the equations[5]

$$\frac{d(C)}{dt} = -p(C) - k_2(R)(C) \qquad (8)$$

$$\frac{d(R)}{dt} = p(C) - k_2(R)(C) \qquad (9)$$

Dividing (8) by (9) and solving for (C) with (R) $= 0$ at $t = 0$, letting $k_2/p = \gamma$, gives

$$(C) = (C_i) + (R) + \frac{2}{\gamma}\ln[1 - \gamma(R)] \qquad (10)$$

It is convenient to evaluate n_{app} by noting that

$$\int_0^t i\,dt = nFm\int_0^t (C)\,dt \qquad (11)$$

From equations 9 and 11

$$\int_0^t i\,dt = nFm\int_{R=0}^{R}\frac{d(R)}{p - k_2(R)} = -\frac{nFV}{\gamma}\ln[1 - \gamma(R)] \qquad (12)$$

Substitution of (12) into (6) along with (10) gives

$$n_{app} = \frac{n}{2}\left\{1 - \frac{(R)}{(R) + \frac{2}{\gamma}\ln[1 - \gamma(R)]}\right\} \qquad (13)$$

An implicit relation for (R^0) as a function of (C_i) and γ is obtained from (10).

$$(R^0) + (C_i) = -\frac{2}{\gamma}\ln[1 - \gamma(R^0)] \qquad (14a)$$

A similarity was noted between the n^0_{app}–(C_i) dependences of Case IIb and IIIb and it was found that equation 14a could be approximated by

$$(R^0) \simeq \frac{1}{2\gamma}\ln[2\gamma(C_i) + 1] \qquad (14b)$$

Evaluation of n^0_{app} can be done by appropriate combination of (13) and (14a) giving the alternate expressions

$$n^0_{app} = \frac{n}{2}\left[1 + \frac{(R^0)}{(C_i)}\right] \qquad (15a)$$

$$n^0_{app} = -\frac{n}{\gamma(C_i)}\ln\left[1 - \gamma(C_i)\left(\frac{2n^0_{app}}{n} - 1\right)\right] \qquad (15b)$$

The approximate explicit form is

$$n^0_{app} \simeq \frac{n}{2}\left\{1 + \frac{1}{2\gamma(C_i)}\ln[2\gamma(C_i) + 1]\right\} \qquad (15c)$$

It is evident from examination of equation 14a that $(R^0) \leq 1/\gamma$. Equations 14a and 15a,b predict the expected values of n^0_{app} for very large and very small values of γ, *i.e.*, $n^0_{app} = n/2$ and $n^0_{app} = n$, respectively.

(3) W. Nernst, *Z. physik. Chem.*, **47**, 52 (1904).

(4) See *e.g.*, B. Levich, *Acta Physicochim. U.R.S.S.*, **17**, 257 (1942).

(5) The total rate of concentration change is of C

$$\frac{d(C)}{dt} = \left[\frac{d(C)}{dt}\right]_{electrode} + \left[\frac{d(C)}{dt}\right]_{rxn.\ (7)}$$

$$\left[\frac{d(C)}{dt}\right]_{rxn.\ (7)} = -k_2(C)(R)$$

Combination of these equations with (5) gives (8). Equation 9 is derived in a similar manner.

Figure 1 shows the variation of n^0_{app} with (C_i) at several values of γ. It can be seen that variation of n^0_{app} with (C_i) will take place at usual concentrations, only when $10^4 > \gamma > 1$. Consideration of the experimental n^0_{app} values allows evaluation of γ.

Evaluation of γ can also be done from data for (R^0) or (Y^0) as a function of (C_i) by means of equation 14a.

It was not possible to obtain closed-form solutions for (C) and (R) as a function of t. Numerical solutions of differential equations 8 and 9 were obtained with the aid of the IBM 650 computer. It was found that $(C)/(C_i)$ was a function of the parameters $\gamma(C_i)$ and pt. Representative solutions are shown in Fig. 2. Deviations in linearity of the log $(C)/(C_i)$ *vs.* pt plot occur only in the early part of the electrolysis.

Case IIc.—A single secondary reaction regenerating C

$$R + Z \xrightarrow{k_2} C \qquad (16)$$

is the case recently treated mathematically by Meites and Moros[6] under the assumption of a first-order regenerative reaction. The presentation below arrives at the same conclusions as those of Meites and Moros, but the results are expressed somewhat differently to allow comparison with the other three cases in this paper. The system is described by equations 17, 18 and 19

$$\frac{d(C)}{dt} = -p(C) + k_2(R)(Z) \qquad (17)$$

$$\frac{d(R)}{dt} = p(C) - k_2(R)(Z) \qquad (18)$$

$$(R) = (C_i) - (C) \qquad (19)$$

For purposes of this discussion (Z) will be assumed to be present in large excess so that $d(Z)/dt \simeq 0$.

Combining (17) and (19) and solving for (C) with the initial condition (C) = (C_i), $t = 0$, gives

$$(C) = (C_i)\left[\frac{\gamma' + e^{-p(1+\gamma')t}}{1+\gamma'}\right] \qquad (20)$$

where $\gamma' = k_2(Z)/p$.

It is evident from equation 20 that at large values of t

$$(C) = \frac{\gamma'(C_i)}{1+\gamma'} \qquad (21)$$

and hence (C) can approach zero only when $p >> k_2(Z)$. Thus evaluation of γ' can be done by determining $(C)/(C_i)$ *in situ* when the current reaches a steady value.

Solution for n_{app} is conveniently done by combination of (17), (19) and (11)

$$n_{app} = n\left[\frac{1}{1+\gamma'} + \frac{p\gamma' t}{1 - e^{-p(1+\gamma')t}}\right] \qquad (22)$$

It is of interest that n_{app} is *independent* of (C_i), but is time dependent. Variation of n_{app} with time under ordinary experimental conditions will be noted only when $\gamma' \geq 0.1$.

Case IIIb.—This case concerns the parallel competitive secondary reactions

(6) L. Meites and S. A. Moros, *Anal. Chem.*, **31**, 23 (1959).

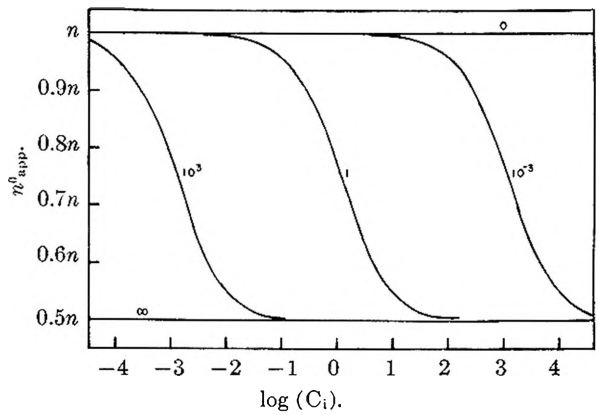

Fig. 1.—Case IIb: dependence of apparent number of faradays per mole, n^0_{app} *vs.* logarithm (C_i); data for various values of γ, liter mole^{-1}.

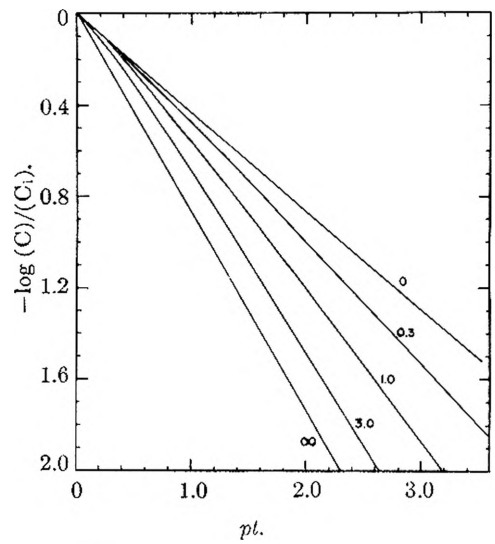

Fig. 2.—Case IIb: variation of $-\log (C)/(C_i)$ *vs.* pt plot with variation of γ (C_i). Values of γ (C_i) given on plot.

$$R + C \xrightarrow{k_2} X \qquad (23)$$

$$R + Z \xrightarrow{k_3} Y \qquad (24)$$

and is described by equations 25 and 26

$$\frac{d(C)}{dt} = -p(C) - k_2(C)(R) \qquad (25)$$

$$\frac{d(R)}{dt} = p(C) - k_2(C)(R) - k_3(Z)(R) \qquad (26)$$

Assuming the concentration of Z is so large that it remains essentially constant throughout the reaction, and making the stationary state assumption $d(R)/dt \simeq 0$

$$(R) = \frac{p(C)}{k_2(C) + k_3'} \qquad (27)$$

where $k_3' = k_3(Z)$.

Introducing (27) into (25) and solving for (C) under the initial conditions (C) = (C_i) at $t = 0$, gives

$$(C) = \frac{(C_i)e^{-2pt}}{2K(C_i)+1}\left[K(C_i) + \{K^2(C_i)^2 + [2K(C_i)+1]e^{2pt}\}^{1/2}\right] \qquad (28)$$

where $K = k_2/k_3'$.

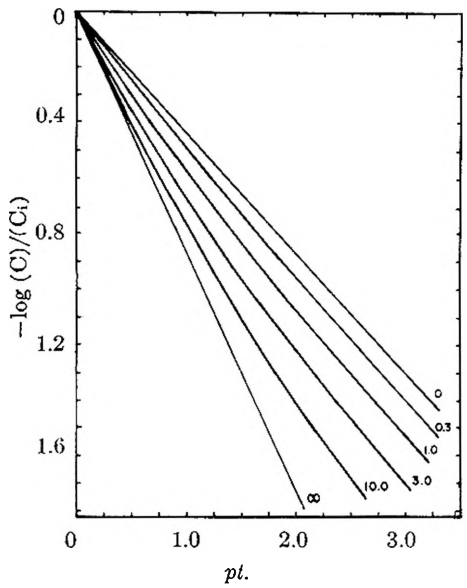

Fig. 3.—Case IIIb; variation of $-\log (C)/(C_i)$ *vs.* pt plot with variation of $K(C_i)$. Values of $K(C_i)$ given on plot.

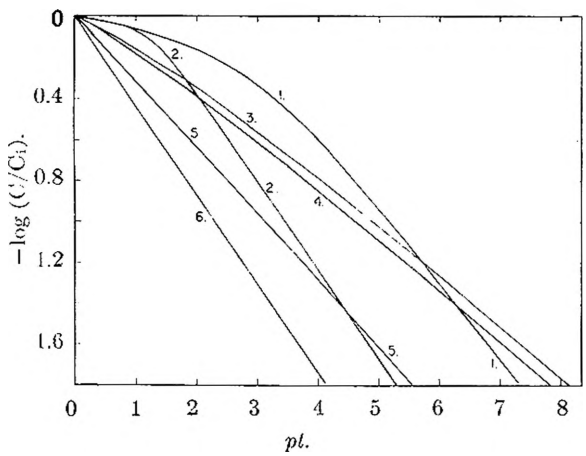

Fig. 4.—Case IIIc: numerical computation of $-\log (C)/(C_i)$ *vs.* pt: 1, $(C_i) = 4$ mM, $(Y_i) = 8$ mM, $K' = 1000$ liter mole^{-1}; 2, $(C_i) = 10$ mM, $(Y_i) = 10$ mM, $K' = 1000$ liter mole^{-1}; 3, $(C_i) = 1$ mM, $(Y_i) = 2$ mM, $K' = 1000$ liter mole^{-1}; 4, $(C_i) = 8$ mM $(Y_i) = 16$ mM, $K' = 100$ liter mole^{-1}; 5, $(C_i) = 2$ mM, $(Y_i) = 4$ mM, $K' = 100$ liter mole^{-1}; 6, $K' = 0$.

The current decay follows the expression [from (3) and (28)]

$$i = \frac{nFm(C_i)e^{-2pt}}{2K(C_i) + 1}\left[K(C_i) + \{K^2(C_i)^2 + [2K(C_i) + 1]e^{2pt}\}^{1/2}\right] \quad (29)$$

This expression can be compared with the equivalent expression for case I[2]

$$i = nFm(C_i)e^{-pt} \quad (30)$$

As $K \rightarrow 0$, (Case IIa), equation 29 becomes identical with (30). As K approaches infinity, equation 29 becomes

$$i = nFm(C_i)e^{-2pt} \quad (31)$$

since C reacts with R as soon as it is formed.

Figure 3 shows typical current–time curves for this case. For $K(C_i)$ values larger than approximately twenty, a log $[(C)/(C_i)]$ *vs.* t plot is not useful in evaluating K. In the suitable range of values K can be evaluated from current–time data and independent evaluation of p by appropriate solution of eq. 29.

Solution for n_{app} is done by combination of (25), (27) and (11)

$$n_{app} = \frac{n}{2}\left\{1 - \frac{1}{2K[(C_i) - (C)]}\ln\left[\frac{2K(C) + 1}{2K(C_i) + 1}\right]\right\} \quad (32)$$

and

$$n^0_{app} = n\left\{\frac{1}{2} + \frac{1}{4K(C_i)}\ln [2K(C_i) + 1]\right\} \quad (33)$$

It can be seen that $n^0_{app} = n$ at $K = 0$, and $n^0_{app} = n/2$ as $K \rightarrow \infty$, as would be expected from the reaction scheme.

The variation of n^0_{app} with (C_i) is approximately the same as that shown in Fig. 1 for Case IIIb, where K values in liter mole^{-1} are substituted for values of γ. Variation of n^0_{app} with (C_i) takes place at usual concentrations only when $K > 1$ liter mole^{-1}.

At the completion of the electrolysis the concentrations of X and Y are

$$(X^0) = \frac{1}{4K}\{2K(C_i) - \ln [2K(C_i) + 1]\} \quad (34)$$

$$(Y^0) = \frac{1}{2K}\ln [2K(C_i) + 1] \quad (35)$$

Experimental determination of these quantities provides an alternate method of evaluating K.

The stationary state assumption used in the treatment requires that (R) be very small at all times, or that

$$k_2(C) + k_3' >> p(C) \quad (36)$$

Thus the range of k_2 and k_3' that can be examined using this derivation depends upon the experimental choice of p.

Case IIIc.—The "catalytic" reaction scheme

$$R + Y \xrightarrow{k_2} C \quad (37)$$

$$R + Z \xrightarrow{k_3} X \quad (38)$$

is described by the equations

$$\frac{d(C)}{dt} = -p(C) + k_2(R)(Y) \quad (39)$$

$$\frac{d(R)}{dt} = p(C) - k_2(R)(Y) - k_3'(R) \quad (40)$$

$$\frac{d(Y)}{dt} = -k_2(R)(Y) \quad (41)$$

where $k_3' = k_3(Z)$, *i.e.*, Z is present in much larger quantity than C or Y.

Writing the stationary state approximation for (R), *i.e.*, $d(R)/dt \simeq 0$

$$(R) = \frac{p(C)}{k_2(Y) + k_3'} \quad (42)$$

substituting it into (39) and (41) and solving the two equations gives

$$(C_i) - (C) = \frac{k_3'}{k_2}\ln\frac{(Y_i)}{(Y)} \quad (43)$$

where (Y_i) is the initial concentration of Y.

It is not possible to obtain an explicit expression for (C) as a function of time. Numerical computation for a number of cases, Fig. 4, showed that $(C)/(C_i)$ is a function of pt, (Y_i), (C_i), and K', where $K' = k_2/k_3'$. It is seen from Fig. 4 that in all cases the slope of the log $(C)/(C_i)$ *vs.* pt plot is

smaller than when no catalytic regeneration occurs.

Evaluation of n_{app} is done by substituting (42) into (41), integrating, and substituting into (11). The resulting expression is substituted into (6) along with (43) to give

$$n_{app} = \frac{n\left[(Y_i) - (Y) + \frac{1}{K'}\ln\frac{(Y_i)}{(Y)}\right]}{\frac{1}{K'}\ln\frac{(Y_i)}{(Y)}} \quad (44)$$

At the completion of the electrolysis where (C) approaches zero, evaluation of (Y^0) from (43) and substitution into (44) gives

$$n^0_{app} = n\left\{1 + \frac{(Y_i)}{(C_i)}\left[1 - e^{-K'(C_i)}\right]\right\} \quad (45)$$

The dependence of n^0_{app} on $(Y_i)/(C_i)$ and K′ is depicted in Fig. 5.

If (Y_i) is large in comparison to (C_i)

$$(C) = (C_i)e^{-pt/(K''+1)} \quad (46)$$

where $k_2' = k_2(Y_i)$ and $K'' = k_2'/k_3'$, then

$$n^0_{app} = (K'' + 1)n \quad (47)$$

Discussion

At first examination the reaction schemes for Cases IIb and IIIb appear highly unlikely. It is indeed true that the limitation of electrolytic inertness imposed on W, X, Y, Z suggests that the indicated reaction schemes will be found only infrequently. Most frequent application of the derivations for Cases IIb and IIIb probably can be made to organic species, for instance in a coupling reaction between R and C. In this case the oxidation (or reduction) of the product of the secondary reaction could well occur at a more oxidizing (or reducing) potential than the primary electrode reaction. This present paper was prompted by an experimental study of the electro-oxidation of the tetraphenylborate ion in acetonitrile, an example of Case IIb.[7]

The variation of n-values for the reduction of picric acid with initial concentration[8] may be an example of Case IIb or IIIb. Meites and Meites suggest that the dependence of n on the original concentration of picric acid is caused by a competition between further electroreduction of a partially reduced intermediate and a chemical rearrangement of the intermediate. The data also could be explained in terms of Case IIb or IIIb. Numerous examples of catalytic electrode reactions, corresponding to case IIc or IIIc have been investigated by polarographic techniques.[9] For example, in the presence of hydroxylamine, titanium(III), from the electroreduction of titanium(IV), is chemically oxidized to titanium(IV) by hydroxylamine. Moros and Meites[10] made a coulometric study of the reduction of manganese(II) to manganese(I) in cyanide media and concluded that water was reduced by manganese(I), an example of case IIc. These same authors[6] report evidence showing that the reduction of vanadium(IV) to vanadium(II) involves catalytic currents or induced currents or both.

(7) D. H. Geske, THIS JOURNAL, **62**, 1062 (1959).

(8) L. Meites and T. Meites, *Anal. Chem.*, **28**, 103 (1956).

(9) P. Delahay, "New Instrumental Methods in Electrochemistry," Interscience Publishers, Inc., New York, N. Y., 1954, p. 108 ff.

(10) S. A. Moros and L. Meites, unpublished, see ref. 6.

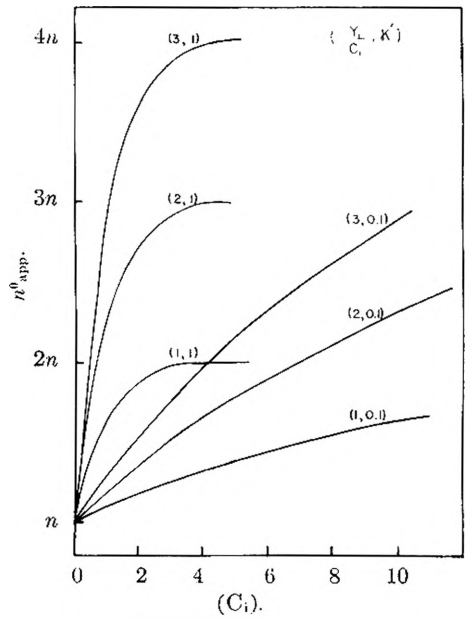

Fig. 5.—Case IIIc: dependence of n^0_{app} on $(Y_i)/(C_i)$ and K′.

The preceding treatment points to three alternate methods for determining kinetic rate constants (or ratios of rate constants) of the secondary chemical reactions. The three types of useful information are current-time data, variation of n^0_{app} with (C_i) or t, and quantitative analysis of the solution. Selection of the most appropriate method will depend on the peculiar characteristics of each case. In cases IIb and IIIb the true n-value may be evaluated directly by extrapolation of n^0_{app} data to low (C_i), or by extrapolation of n^0_{app} values to high (C_i) values where $n^0_{app} = n/2$. In case IIc an extrapolation of n_{app} to zero time gives the true n-value, while in case IIIc, n^0_{app} is obtained by extrapolation to zero (C_i).

The range of values of rate constants accessible for evaluation by methods indicated above depends upon the particular case. In case IIb the range is dependent on the value of p, which would ordinarily range from 10^{-1} to 10^{-4} sec.$^{-1}$, hence limiting k_2 to 10^{-4} to 10^3 liter mole^{-1} sec.$^{-1}$. For case IIIb the ratio of rate constants K could be obtained over the range 1 to 10^4 from n^0_{app}–(C_i) data.

Whereas treatment of catalytic cases by voltammetric techniques is feasible for values of $k_2(Z)$ larger than 0.1 sec.$^{-1}$, controlled potential coulometry is concerned with somewhat slower catalytic reactions. In case IIc, γ' can range from approximately 10^{-1} to 10, thus giving a range of $k_2(Z)$ of 10^{-5} to 1 sec.$^{-1}$.

The accessible range of K′ values for case IIIc depends on (Y_i). Since K′ is a ratio of rate constants, independent measurement of one of the constants is necessary for absolute evaluation of the other.

Single secondary reactions too rapid for treatment by cases IIb and IIc may be made accessible by purposely introducing a competing parallel reaction and treating the system by case IIIb or IIIc.

Experimental elucidation of an electrode reaction

where secondary reactions occur certainly must include solution analysis. Clearly, the electrochemical data are extremely useful and in certain circumstances may furnish kinetic data which otherwise would be difficult to obtain. It should be noted that where some estimate of diffusion coefficient is available the true n-value for a reaction may be obtained from polarographic and chronopotentiometric data. Since n^0_{app} is dependent on p at a particular (C_i) value in cases IIb and IIc and is independent of p for cases IIIb and IIIc an experimental means is at hand for distinguishing parallel and single secondary reactions.

This treatment has assumed that limiting current conditions are in force at the electrode throughout the electrolysis. Thus potentiostats whose voltage output is so inadequate that limiting current conditions are not attained until the electrolysis has proceeded for some time, cannot be used in an experimental study based on the mathematical expressions derived above.

The expressions derived can be applied with minor modifications to millicoulometric determinations,[11] where only a part of the electroactive material is consumed.

Non-integral n-values alone are not a sufficient condition for concluding that the case under consideration is one of the cases discussed here. Higher order secondary reactions, induced reactions,[6] competing secondary electrode reactions or other complex reaction schemes can also result in non-integral n-values. For example, Lanza, *et al.*,[12] report an n of 1.26 in the millicoulometric reduction of phenyl and benzyl thiocyanate. The postulated reaction scheme was

$$RSCN + e \longrightarrow RS\cdot + CN^-$$
$$RS\cdot + {}^1/_2Hg \longrightarrow {}^1/_2Hg(RS)_2$$
$${}^1/_2Hg(RS)_2 + e^- \longrightarrow {}^1/_2Hg + RS^-$$

The n-value was explained by the authors as caused by the loss of mercuric mercaptide through diffusion away from the dropping mercury electrode.

Acknowledgment.—The authors are grateful to Dr. Gordon Goodman for his assistance in computer programming and operation.

(11) R. D. Weaver and G. C. Whitnack, *Anal. Chim. Acta*, **18**, 51 (1958).

(12) P. Lanza, L. Griggia and G. Semerano, *Ricer. Sci.*, **26**, *S* 230 (1956).

THE ELECTROOXIDATION OF THE TETRAPHENYLBORATE ION; AN EXAMPLE OF A SECONDARY CHEMICAL REACTION FOLLOWING THE PRIMARY ELECTRODE PROCESS

BY DAVID H. GESKE

Contribution from the Department of Chemistry, Harvard University, Cambridge, Mass.

Received October 27, 1958

Voltammetric and chronopotentiometric studies with platinum electrodes have shown that tetraphenylborate ion in acetonitrile solution undergoes a two-electron oxidation. Controlled potential coulometric data for n^0_{app}, the apparent number of faradays per mole, varied from 1.02 to 1.8 over the concentration range 1.0×10^{-2} to $8.9 \times 10^{-5} M$. This variation indicated that a secondary chemical process was consuming tetraphenylborate ion. A reaction scheme is proposed in which the products of the primary electrode process are biphenyl and diphenylboronium ion. A secondary reaction between tetraphenylborate ion and hydrogen ion, which is generated by reaction of diphenylboronium ion with the solvent system, produces benzene and triphenylboron. Solution analysis data are presented in support of the proposed reaction scheme. Reasonable agreement was found between the experimental dependence of n^0_{app} on the concentration of tetraphenylborate ion and that calculated on basis of the rate of the secondary reaction and the electrode parameter.

In the decade since the preparation of lithium tetraphenylborate by Wittig, *et al.*,[1] a voluminous literature has accumulated on the chemistry of the tetraphenylborate ion (TPB). Nearly two hundred literature references are listed in recent bibliographies.[2] The bulk of the work has been concerned with application of TPB as an analytical reagent for various cations, including potassium.

This present study was prompted by the observation that TPB could be electrolytically oxidized at a platinum electrode in anhydrous acetic acid, N,N-dimethylformamide and acetonitrile. The work reported below was done employing acetonitrile as solvent.

A number of preliminary studies of the homogeneous *chemical* oxidation of TPB have been made under diverse conditions. The reaction

$$2LiB(C_6H_5)_4 + 2CuCl_2 \longrightarrow 2CuCl + 2LiCl + 2B(C_6H_5)_3 + (C_6H_5)_2$$

has been reported in ether solution.[3] Spier[4] developed an oxidimetric method for determination of potassium in which precipitated potassium TPB was treated with acidic ceric ammonium nitrate at 92°. One mole of potassium TPB consumed 72 equivalents of ceric ion, whereas total oxidation of TPB to boric acid, carbon dioxide and water would require 120 equivalents. Razuvaev and Brilkina[5] heated anhydrous ferric chloride and potassium TPB in acetone "on the water-bath" for 30 minutes. On basis of the analysis of the reaction mixture, this reaction scheme was suggested

$$LiB(C_6H_5)_4 + 3FeCl_3 \longrightarrow LiCl + C_6H_5BCl_2 + 3FeCl_2 + (C_6H_5)_2 + \cdot C_6H_5$$

(1) G. Wittig, G. Keicher, A. Rückert and P. Raff, *Ann.*, **563**, 110 (1949).

(2) A. J. Barnard, Jr., *Chemist-Analyst*, **44**, 104 (1955); **45**, 110 (1956); A. J. Barnard, Jr., and H. Büechl, *ibid.*, **46**, 16 (1957); **47**, 46 (1958).

(3) G. Wittig and P. Raff, *Ann.*, **573**, 195 (1951).

(4) H. W. Spier, *Biochem. Z.*, **322**, 467 (1952).

(5) G. A. Razuvaev and T. G. Brilkina, *Zhur. Obschei Khim.*, **24**, 1415 (1954); English translation, *J. Gen. Chem. U.S.S.R.*, **24**, 1397 (1954).

$$\cdot C_6H_5 \xrightarrow{\text{acetone}} C_6H_6$$

Controlled potential electrolysis was utilized in the present work so that a single well-defined oxidation reaction could be carried out. This procedure simplified the task of ascertaining the nature of the oxidized species.

Results and Discussion

Voltammetry.—It is not possible to oxidize TPB on a platinum electrode in aqueous solutions because of the interfering evolution of oxygen. When acetic acid is used as solvent the oxidation wave obtained with a rotating platinum microelectrode is quite drawn-out and ill-defined. The oxidation in N,N-dimethylformamide occurs with a half-wave potential of 1.20 v. *vs.* aq. sat. calomel; however, the residual current is quite large in the same potential region.

It is evident from the residual current trace in Fig. 1 that acetonitrile is a useful solvent for anodic voltammetry because of its wide potential region.[6] As shown in Fig. 1, TPB in acetonitrile solution gives a well-defined oxidation wave on a rotating platinum electrode. Using a scan rate of 1.18 mv./sec. there is an indication of a second wave at 1.4 volts in the current–potential curve of a 0.143 m*M* solution, trace 2, Fig. 1. The current decrease at more anodic potentials is caused by formation of an interfering film. At a higher TPB concentration, trace 3, Fig. 1, the film interference prevents observation of the second wave.

It was established that the current decrease was caused by film formation since repetition of the voltage scan after the first trace on a clean electrode resulted in grossly lowered currents. When the electrode was cleaned in nitric acid a current–potential trace identical with the first was obtained. Film formation has been observed previously in the oxidation of organic compounds.[7]

While the major effort was directed toward elucidation of the electrode reaction corresponding to the first wave, it is interesting to note that diphenyl has a current peak in the same region as the second wave of TPB. Lund[7] reported a deformed oxidation wave for biphenyl with an $E_{1/2}$ of 1.48 v. (*vs.* Ag, $AgNO_3$ electrode).

The concentration dependence of the half-wave potential of the first wave is given by

$$E_{1/2} = 0.51 - 0.07 \log (C)$$

where (C) is the millimolar concentration of TPB. A plot of $\log i/(i_l - i)$ *vs.* E for a typical wave approximates a straight line with a slope of 80 mv. These observations indicate that the electrode process is irreversible.

There was no change in voltammetric behavior when the hydrogen ion environment was modified by employing solutions with 0.01 *M* picric acid, 0.16 m*M* tetramethylammonium hydroxide and 1.8 *M* water successively present. These data strongly suggest that hydrogen ion is not involved in the primary electrode process.

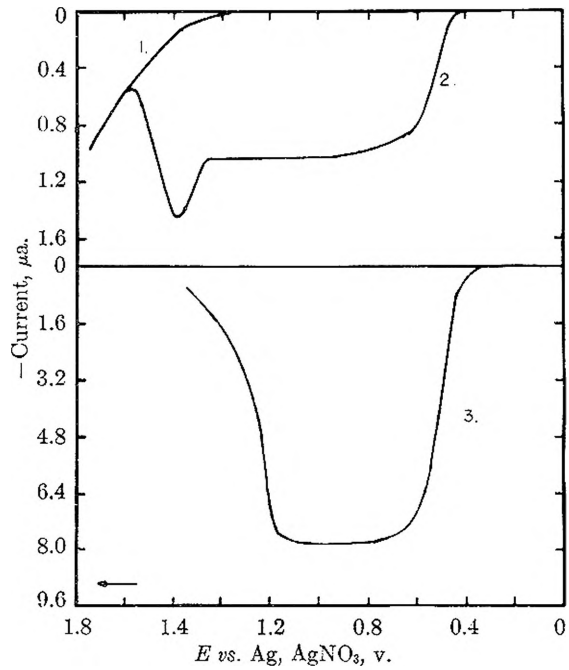

Fig. 1.—Voltammetry, current–potential curves; current, μa. *vs.* potential in volts (*vs.* Ag, $AgNO_3$, scale). Data obtained with rotating platinum microelectrode using polarization from cathodic to anodic potentials: 1, residual current, 0.1 *M* lithium perchlorate; 2, 1.43×10^{-4} *M* sodium tetraphenylborate in acetonitrile; 3, 1.20×10^{-3} *M* sodium tetraphenylborate in acetonitrile.

Precision evaluation of the limiting current constant, $i_l/(C)$, gave a value of 6.50 ± 0.05 μa. l./mmole. This same electrode with the same stirring conditions gave a current constant of 4.81 μa. l./mmole for the oxidation of iodide ion to iodine in acetonitrile.

The limiting current constant I_l may be written as

$$\frac{i_l}{(C)} = I_l = nkD\alpha \qquad (1)$$

where n is the number of faradays per mole, k is an arbitrary constant which is peculiar to the electrode under given stirring, D is the diffusion coefficient and α is a constant. Since according to the Nernst derivation the diffusion coefficient for an ionic species is directly proportional to its limiting ionic conductance, equation 1 may be rewritten

$$I_l = nk'(\lambda^\circ)\alpha \qquad (2)$$

where λ° is the limiting ionic conductance. The limiting ionic conductance for iodide ion in acetonitrile as evaluated from the data of Walden and Birr[8] and Popov and Skelly[9] is 102.4.

Thus, equation 2 for iodide ion oxidation, a one-electron process, is

$$4.81 = k'(102.4)\alpha \qquad (3)$$

The value for the ionic limiting conductance of TPB obtained from combination of the data of

(6) A recent study by H. Schmidt and J. Noack, *Z. anorg. allgem. Chem.*, **296**, 262 (1958), on the electrolysis of perchlorate in acetonitrile, offers evidence on the limiting anodic process. The reactions postulated were

$$ClO_4^- - e \longrightarrow \cdot ClO_4$$
$$\cdot ClO_4 + CH_3CN \longrightarrow HClO_4 + \cdot CH_2CN$$
$$2\cdot CH_2CN \longrightarrow (CH_2CN)_2$$

(7) H. Lund, *Acta Chem. Scand.*, **11**, 1323 (1957).

(8) P. Walden and E. J. Birr, *Z. physik. Chem.*, **144**, 269 (1929).

(9) A. I. Popov and N. E. Skelly, *J. Am. Chem. Soc.*, **76**, 5309 (1954).

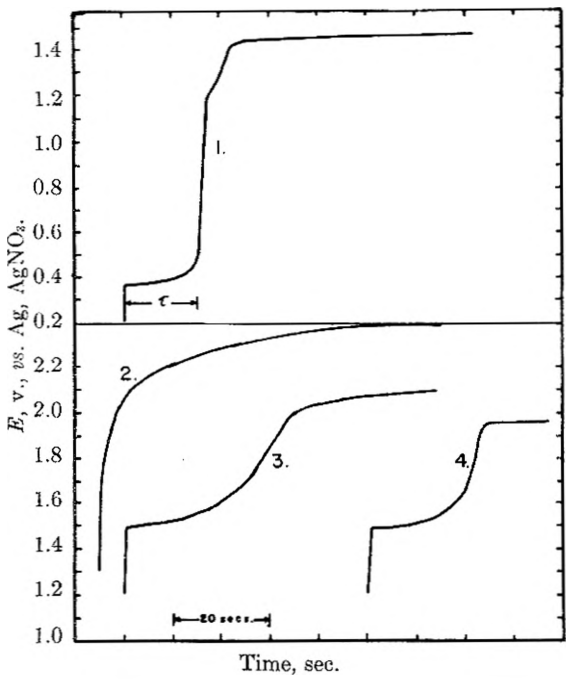

Fig. 2.—Chronopotentiometry, potential–time curves; potential in volts (*vs.* Ag, $AgNO_3$ scale) *vs.* time in seconds. 1, 1.01×10^{-3} *M* sodium tetraphenylborate in acetonitrile, $i = 61.1$ μa.; 2, supporting electrolyte, 0.1 *M* lithium perchlorate, $i = 30.53$ μa.; 3, 1.01×10^{-3} *M* sodium tetraphenylborate in acetonitrile, $i = 300$ μa.; 4, 1.32×10^{-3} *M* diphenyl, $i = 200$ μa.

French and Muggleton[10] and Fuoss, *et al.*,[11] is 56.3. Equation 2 for TPB oxidation is

$$6.50 = nk'(56.3)^{\alpha} \qquad (4)$$

Nightingale[12] empirically obtained an α-value of 0.66 for rotated microelectrodes. Using this value for α in a solution of eq. 3 and 4 gives $n = 2.01$.[13]

Chronopotentiometry.—A typical potential–time curve for oxidation of TPB at constant current is given in Fig. 2, trace 1. The quantity $i\tau^{1/2}/(C)$, where τ is the transition time and i is the current, was found to be independent of concentration and current in the ranges studied, 0.2 to 1.0 m*M* and 10 to 100 μa. The value of the transition time constant, $i\tau^{1/2}/(C)$, was 0.250 amp. sec.$^{1/2}$ liter mole^{-1}.

As with the voltammetry, an interfering film formed on the electrode at highly anodic potentials. Repetition of a trace resulted in grossly shortened transition times because of the increased current density.

Chronopotentiometric data for the one-electron oxidation of triiodide ion to iodine was obtained with the same electrode. The transition time constant was 0.173 amp. sec.$^{1/2}$ l. mole^{-1}.

Equation 4,[14a] where F is the number of coulombs per faraday and A is the area of the electrode

$$\frac{i\tau^{1/2}}{(C)} = \frac{n\pi^{1/2}FAD^{1/2}}{2} \qquad (4a)$$

can be used to calculate the n-value for the TPB reaction. The limiting ionic conductance of triiodide ion, which is proportional to the diffusion coefficient, has a value of 98.6 as evaluated from the data of Walden and Birr[8] and Popov, *et al.*[15] Combining chronopotentiometric data for triiodide ion and TPB with limiting ionic conductances gives an n of 1.91. Thus, both voltammetric and chronopotentiometric data indicate a two-electron primary electrode process.

Further information on the electrode processes in the 1.5 v. region was obtained from the chronopotentiometric data. As shown in trace 3, Fig. 2, a second discrete wave occurs in the oxidation of TPB. (The transition time for the first inflection point is so short that it is not apparent in trace 3, Fig. 2.) The $i\tau_2^{1/2}/(C)$ value for the second inflection was 1.33 amp. sec.$^{1/2}$ l. mole^{-1}.

The oxidation of biphenyl, trace 4, Fig. 2, occurs in the same potential region as the second transition for TPB. The transition time constant for biphenyl was 0.850 amp. sec.$^{1/2}$ l. mole^{-1}. This evidence suggests that the second oxidation wave of TPB (approx. 1.5 volts) involves oxidation of biphenyl. However, a rather puzzling aspect is that the ratio of the two transition times, τ_2/τ_1, is approximately 28 as calculated from the transition time constants. It is possible to estimate the number of electrons in the second step from the relation[14b]

$$\frac{\tau_2}{\tau_1} = 2\left(\frac{n_2}{n_1}\right) + \left(\frac{n_2}{n_1}\right)^2$$

where n_2 and n_1 are the number of faradays per mole for the first and second steps, respectively. The ratio is 24 when n_2 is 8. This n-value seems inordinately large, especially when it is noted that Lund[7] observed a two-electron reaction for the electrolytic oxidation of anthracene in acetonitrile.

Controlled Potential Electrolysis.—The major portion of this study was devoted to examination of solutions obtained from the electrolysis of TPB at 0.7 v., *i.e.*, to the elucidation of the two-electron reaction. Data are summarized in Table I.

Coulometric evaluation of n^0_{app}, the *apparent* number of faradays per mole as defined in footnote *a*, Table I, gave values ranging from 1.02 to 1.8. The concentration dependence of n^0_{app} as shown in Fig. 3, clearly indicated that a secondary chemical reaction was consuming TPB.

Proposed Reaction Scheme.—The reaction scheme (5) to (8) is proposed. Supporting evidence for each reaction is subsequently presented.

$$B(C_6H_5)_4^- - 2e \xrightarrow{\text{electrode}} B(C_6H_5)_2^+ + (C_6H_5)_2 \qquad (5)$$

$$B(C_6H_5)_2^+ + H_2O \xrightarrow{k_1} (C_6H_5)_2BOH + H^+ \qquad (6)$$

$$H^+ + B(C_6H_5)_4^- \xrightarrow{k_2} B(C_6H_5)_3 + C_6H_6 \qquad (7)$$

(after completion of electrolysis)

$$B(C_6H_5)_3 + {}^1/_2O_2 \longrightarrow (C_6H_5)_2BOC_6H_5 \qquad (8)$$

(10) C. M. French and D. F. Muggleton, *J. Chem. Soc.*, **61**, 2131 (1957).

(11) R. M. Fuoss, J. B. Berkowitz, E. Hirsch and S. Petrucci, *Proc. Natl. Acad. Sci.*, **44**, 27 (1958).

(12) E. R. Nightingale, Jr., *Anal. Chim. Acta*, **16**, 493 (1957).

(13) The value for α may be subject to some variation with the particular experimental conditions. However, even with the extreme limits of 0.5 and 0.75 for α, the n-values of 1.82 and 2.12, respectively, are still clearly indicative of a two-electron process.

(14) P. Delahay, "New Instrumental Methods in Electrochemistry," Interscience Publishers, Inc., New York, N. Y., 1954, (a) p. 184; (b) p. 192.

(15) A. I. Popov, R. H. Rygg and N. E. Skelly, *J. Am. Chem. Soc.*, **78**, 5740 (1956).

TABLE I

CONTROLLED POTENTIAL ELECTROLYSES (25 ml. solution-volume)

(C_i), mM	n^0_{app}[a]	(H^+), mM	$\frac{(H^+)}{(C_i)}$	$[(C_6H_5)_2]$, mM	$\frac{n^0_{app}(C_i)}{2}$, mM	(C_6H_6), mM	$\left[1-\frac{n^0_{app}}{2}\right](C)_i$, m$M$	$a_{m\,240m\mu}$, $(C_6H_5)_2BOH \times 10^{-3}$
0.55	1.31							
0.99$_4$	1.31	0.3	0.3					
9.63	1.05	.5	.05					
0.16$_2$	1.54	[b]		0.11	0.12			
10.39	1.02	.11	.011	5.0	5.3			
10.39[c]	1.02			4.9$_3$	5.3	4.6	4.9	
0.089$_5$	1.8[d]			0.08	0.08			20.9
2.02$_5$	1.14	.16	.08	1.08	1.15	0.7	0.86	17.4
2.02$_5$[e]	1.43	.79	.39	1.33	1.43	0.4$_6$	0.56	17.0
2.02$_5$	1.21	.42	.21					
4.54	1.03	.10$_5$	.02$_3$	2.36	2.34	2.0$_7$	2.20	16.8$_5$
5.28	1.15$_6$	.47	.09	3.14	3.05	2.0	2.12	
5.28	1.05	.12	.02	2.68	2.78	2.9	2.50	16.0
5.04[f]	1.84			4.5	4.65		0.4	20.3
10.39[g]	1.93							

[a] Defined as $\int_0^t i\,dt/FV(C_i)$. [b] No indicator change detected. [c] 20 ml. solution volume. [d] Residual current correction introduced a 5% uncertainty. [e] Solution made 0.22 M in H_2O. [f] Acetate buffer media; 0.16 M $(CH_3)_4N^+CH_3COO^-$, 0.2 M $HC_2H_3O_2$. Prolonged electrolysis necessary because of interfering film formation. [g] Picrate buffer media; 0.07 M sodium picrate (satd.), 0.1 M picric acid.

One obvious requirement for the validity of this scheme is that only TPB undergoes an electrode reaction at 0.7 v. This was verified by examining the voltammetry of the various species in the scheme.

Primary Electrode Process.—The fraction of TPB which undergoes reaction at the electrode is simply $n^0_{app}/2$, and the concentration of the electrode reaction product then is $n^0_{app}(C_i)/2$ (assuming 1:1 stoichiometry). Figure 4 is a plot of the concentrations of biphenyl observed in the electrolyzed solutions *vs.* $n^0_{app}(C_i)/2$. The fact that the data closely fit the straight line which has the theoretical slope of one is taken to mean that biphenyl is a product of the primary electrode process.

The occurrence of biphenyl and not benzene as an electrode reaction product offers some evidence on the mechanism of the reaction. If phenyl radicals were liberated into the solution they would abstract a hydrogen from acetonitrile to form benzene.[16,17] Since biphenyl is formed, the dimerization must occur very soon after the removal of the two electrons from TPB.

Evidence for occurrence of the diphenylboronium ion, $B(C_6H_5)_2^+$, in the primary electrode process is discussed in a later section.

Secondary Reaction.—Observation of a small hydrogen ion concentration in the electrolyzed solution suggested that the secondary reaction might involve hydrogen ion. Wittig, *et al.*,[1] report that in hydrochloric acid solution at 80°, TPB decomposes to benzene and triphenylboron. A number of other workers[18,19] have noted the instability of TPB in acidic media.

Controlled potential electrolyses were carried out in picrate and acetate buffer media (see last two entries, Table I). The fact that the n^0_{app} value for a 10.39 mM TPB solution was increased from 1.02 to 1.93 when the solution was buffered was taken as conclusive evidence that the competing secondary reaction involved hydrogen ion.

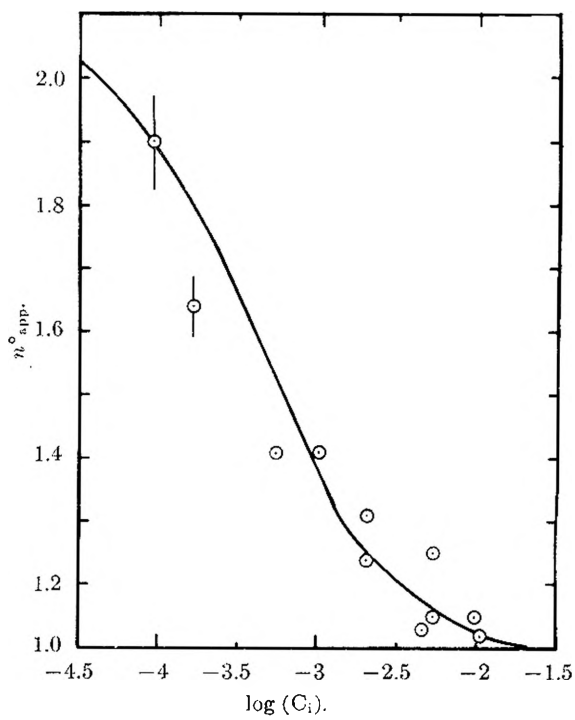

Fig. 3.—Variation of $n^0_{app.}$ apparent number of faradays per mole, with log (C_i), initial concentration of sodium tetraphenylborate in moles/liter.

Evidence that the reaction in acetonitrile occurred as written in equation 7 is (a) quantitative consumption of one hydrogen ion per TPB as established by addition of a measured amount of TPB to excess perchloric acid in acetonitrile followed by titration of excess acid with diethylamine; (b) presence of benzene in stoichiometric amount in a reaction mixture as shown from reduced pressure distillation (details given in Ex-

(16) W. A. Waters, *J. Chem. Soc.*, 113 (1937).
(17) W. E. Hanby and W. A. Waters, *ibid.*, 1792 (1939).
(18) K. Sporek and A. F. Williams, *Analyst*, **80**, 347 (1955).
(19) H. Flaschka and F. Sadek, *Chemist-Analyst*, **45**, 20 (1956).

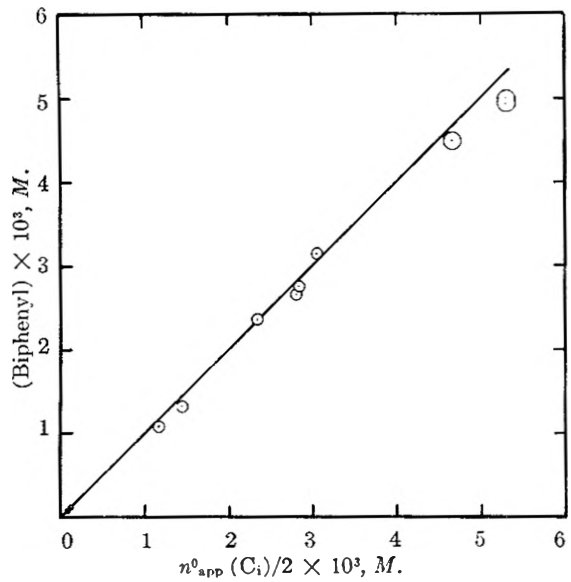

Fig. 4.—Biphenyl concentration in electrolyzed solutions, mM, *vs.* n^0_{app} (C$_i$)/2, mM.

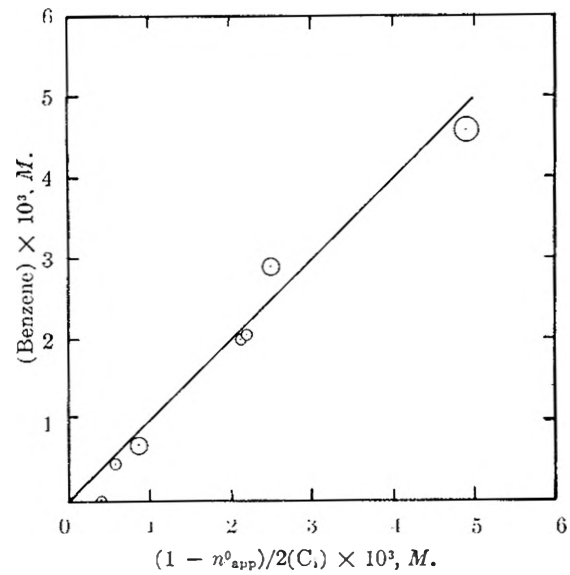

Fig. 5.—Benzene concentration in electrolyzed solutions, mM *vs.* (1 − n^0_{app}/2) (C$_i$), mM.

perimental section); (c) spectra of reaction solutions exposed to oxygen after completion of reaction were essentially identical to spectra of oxygenated triphenylboron solutions (see section on Triphenylboron Solution Chemistry). It is important to note that in acid solution oxygen is a strong enough oxidant to oxidize TPB. Thus oxygen was removed in all electrolysis and kinetic studies.

Neu[20] has reported preparation of tetraphenyldiboroxide, $[(C_6H_5)_2B]_2O$, by treatment of Na-TPB with 1 M aqueous hydrochloric acid. We have examined this reaction and have found that it proceeds in a stepwise manner; rather rapid formation of triphenylboron, as evidenced by its precipitation, is followed by slower hydrolysis to diphenylboronous acid, $(C_6H_5)_2BOH$, which is later converted to the anhydride. Evidence cited in the previous paragraph shows that only the first step occurs in reaction of hydrogen ion and TPB in acetonitrile solution.

An exhaustive kinetic study of the hydrogen ion–TPB reaction in acetonitrile was beyond the scope of this project. However, preliminary investigation showed that in the millimolar concentration region the reaction was first order in both hydrogen ion and TPB and had a rate constant of approximately 7.5 liter mole^{-1} sec.$^{-1}$

If reaction 7 is indeed the secondary reaction which consumes TPB, the fraction of TPB reacting with hydrogen ion, $1 - n^0_{app}/2$, multiplied by the initial concentration of TPB, (C$_i$), should be equal to the observed benzene concentration. Available data are plotted in Fig. 5 and show reasonable agreement with the straight line which is drawn with the theoretical slope of one.

If it is assumed that the reaction which produces hydrogen ion in solution is much faster than reaction 7, the proposed reaction scheme is an example of Case IIb as treated by Geske and Bard.[21] One of the expressions applicable to a reaction scheme of this type is

$$n^0_{app} = \frac{n}{2}\left[1 + \frac{(R^0)}{(C_i)}\right] \qquad (9)$$

In the present system n is 2 and (R^0) is the hydrogen ion concentration. Figure 6 shows the extent of agreement of experimental data with equation 9.

Reaction Generating Hydrogen Ion.—When it was shown that biphenyl was a product of the electrode reaction it was logical to consider diphenylboronium ion, $B(C_6H_5)_2^+$, as the other product. Davidson and French[22] reported the existence of diphenylboronium ion in methyl ethyl ketone and nitrobenzene solutions. They suggest that in solvents with readily available lone pairs of electrons compounds of the diaryl boron chloride type will be solvated, and the boron atom will become isoelectronic with the central carbon atom of arylmethyl chlorides. It was shown that when aluminum trichloride was added to an ethyl methyl ketone solution of diphenylboron chloride (DPBC) the conductivity increased and an absorption maximium appeared at 337 mμ. Close agreement between the position of this maximum and the value predicted from molecular-orbital calculations for diphenylboronium ion was cited as evidence for the presence of the ion in solution. Another evidence was that silver chloride was precipitated when silver perchlorate was added to a nitrobenzene solution of DPBC.

The occurrence of diphenylboronium ion in the primary electrode scheme offers a possibility for the generation of hydrogen ion in the solution. As written in equation 6, hydrolysis of diphenylboronium ion by traces of water in the solvent system affords diphenylboronous acid and hydrogen ion.

A series of experiments were performed with DPBC and silver perchlorate in acetonitrile in an attempt to determine the chemical behavior of di-

(20) R. Neu, *Chem. Ber.*, **87**, 802 (1954).

(21) D. H. Geske and A. J. Bard, THIS JOURNAL, **63**, 1057 (1959).

(22) J. M. Davidson and C. M. French, *J. Chem. Soc.*, 114 (1958).

phenylboronium ion in acetonitrile. Reactions were carried out in a dry-box so that as closely anhydrous conditions as possible would be obtained. Using rigorously dried reagents, reaction of 5 ml. of 20.6 m*M* DPBC with 5 ml. 48 m*M* silver perchlorate did yield a precipitate of silver chloride. The solution was filtered and a portion was titrated with diphenylguanidine[23] using crystal violet as indicator. (The precipitation of silver chloride apparently was not complete since a small amount of silver chloride precipitated during the titration.) The titration indicated a hydrogen ion concentration of 9.22 m*M* for the reaction solution, or 89.4% of the stoichiometric amount for production of one hydrogen ion per diphenylboronium ion. The spectrum of the reaction solution, after correction for dilution, was essentially identical with that of the original DPBC solution, *i.e.*, a broad peak with a maximum at 230 mμ, $a_m = 12.9 \times 10^3$. Restating the results, hydrogen ion had been generated in almost quantitative amount, but the product of the reaction was not diphenylboronous acid.

This series of experiments was repeated (in dry box) using 0.1 *M* lithium perchlorate solution in preparing the stock solutions. The use of lithium perchlorate solutions, with a water content of 9 m*M*, more closely corresponded to the actual conditions of the electrolysis solution. Results were similar to those described in the preceding paragraph. The spectrum of the DPBC stock solution showed a maximum at 235 mμ, $a_m = 15.4 \times 10^3$, probably indicating partial hydrolysis to diphenylboronous acid. After filtering the silver chloride from reaction of 5 ml. 18.0 m*M* DPBC with 5 ml. 48 m*M* silver perchlorate, titration of a portion of the filtrate showed 90% generation of hydrogen ion. After correction for dilution the spectrum of the reaction solution was quantitatively identical with the spectrum of the DPBC stock solution. However, when the cell spacer was lifted so that the solution was briefly exposed to atmospheric moisture, the absorption peak shifted to the 238 mμ position characteristic of diphenylboronous acid.

These results substantiate the following conclusions: (a) diphenylboronium ion in acetonitrile reacts to produce an almost stoichiometric amount of hydrogen ion; (b) the intermediate boron compound is readily hydrolyzed to diphenylboronous acid by atmospheric moisture. Thus reaction 6 in the proposed reaction scheme represents the *over-all* reaction since in the process of examining the solution the intermediate boron compound would be hydrolyzed. The exact identity of this intermediate is not known.

Triphenylboron Solution Chemistry.—The occurrence of triphenylboron in the reaction scheme required that its solution behavior be investigated. Razuvaev and Brilkina[5,24] characterized triphenylboron by its reaction with oxygen to give phenyl diphenylborinate, $(C_6H_5)_2BOC_6H_5$, which was then hydrolyzed by water to diphenylboronous acid, $(C_6H_5)_2BOH$, and phenol. Rondestvedt, *et al.*,[25] found that when a methanolic solution of triphenylboron was refluxed in nitrogen atmosphere, the major product was phenyl diphenylborinate. The oxidation was attributed to trace impurities, possibly oxygen or formic acid.

Experimental observation of acetonitrile solutions of triphenylboron showed that the uptake of oxygen was very rapid. When a triphenylboron solu-

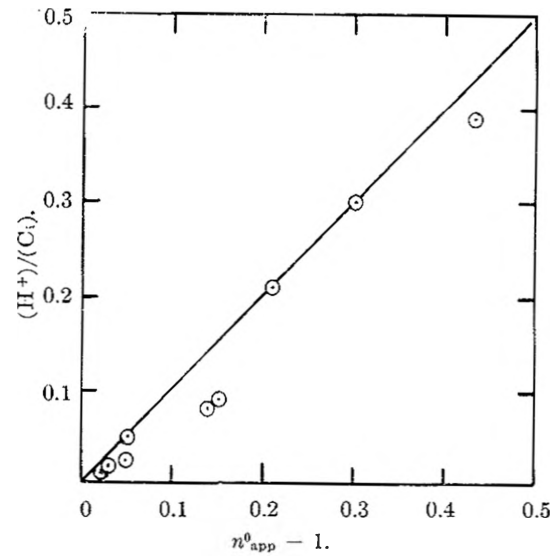

Fig. 6.—Ratio of hydrogen ion concentration of electrolyzed solution to initial concentration of sodium tetraphenylborate, $(H^+)/(C_i)$, *vs.* $n^0_{app} - 1$.

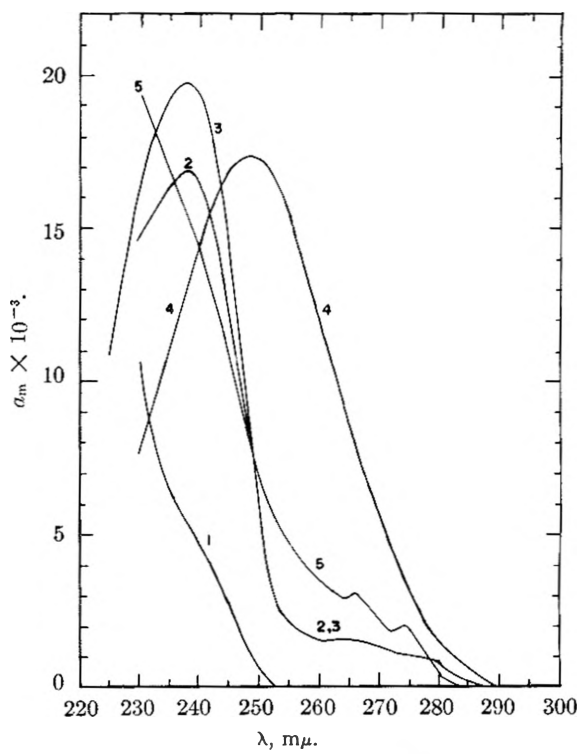

Fig. 7.—Absorption spectra in acetonitrile, molar absorbance indexes, liter mole^{-1} cm.$^{-1}$ *vs.* wave length, mμ: 1, triphenylboron, oxygen excluded; 2, triphenylboron, oxygenated; 3, phenyl diphenylborinate, $(C_6H_5)_2BOC_6H_5$, and diphenylboronous acid, $(C_6H_5)_2BOH$; 4, biphenyl $(C_6H_5)_2$; 5, sodium tetraphenylborate.

(23) Diphenylguanidine does not react with silver ion under the conditions employed here.

(24) G. A. Razuvaev and T. G. Brilkina, *Doklady Akad. Nauk U.S.S.R.*, **85**, 815 (1952).

(25) C. S. Rondestvedt, Jr., R. M. Scribner and C. E. Wulfman, *J. Org. Chem.*, **20**, 9 (1955).

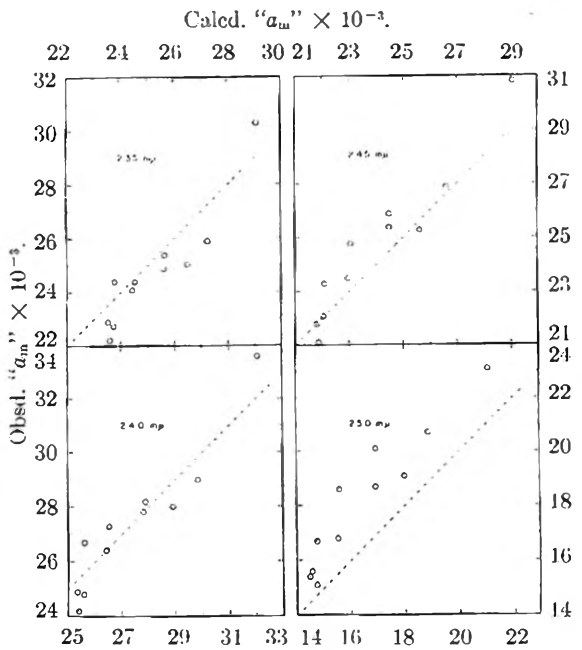

Fig. 8.—Comparison of observed and calculated molar absorbance indexes, liter mole^{-1} cm.$^{-1}$ × 10^{-3}, at various wave lengths.

tion was prepared and the absorption cell filled in a nitrogen atmosphere, absorption spectrum 1, Fig. 7, was obtained. Brief exposure to oxygen gave a solution with spectrum 2, Fig. 7. Methanolic solutions of triphenylboron showed similar sensitivity to oxygen. The spectrum of a known sample of phenyl diphenylborinate in acetonitrile is essentially identical with the spectrum of diphenylboronous acid, Fig. 7, number 3.[26]

If the suggestion that triphenylboron reacts with oxygen to give phenyl diphenylborinate is correct, then it is obvious from comparison of spectra in Fig. 7 that the reaction is not quantitative in acetonitrile since the molar absorbance indices observed for oxygenated triphenylboron are lower than those for phenyl diphenylborinate. Molar absorbance data for various oxygenated triphenylboron solutions showed up to 7% variation from the value given in Fig. 7. This suggests that the reaction may be somewhat more complex. It seems satisfactory to conclude that phenyl diphenylborinate is the *major* product when acetonitrile solutions of triphenylboron are exposed to oxygen.

Although electrolyses were carried out in a nitrogen atmosphere, the electrolyzed solution was inevitably exposed to atmospheric oxygen before a spectrum could be obtained. Thus it was necessary to obtain spectral data for triphenylboron under the same conditions.

Absorptimetric Data.—Taken as a whole the various evidences for the proposed reaction scheme seem to offer substantial confirmation of the scheme's validity. One further correlation is obtained from examination of the absorption spectra of the electrolyzed solutions.

The observed spectra, which had a maximum at 240 mμ, qualitatively appeared to be a summation of the C_6H_5BO absorption[26] and biphenyl absorption, Fig. 7. (Spectrum of TPB is included in Fig. 7 for comparison.) Quantitative evaluation of the spectra was done as follows. At the completion of the electrolysis, after exposure of the solution to oxygen

$$[(C_6H_5)_2] = [(C_6H_5)_2BOH] = \frac{n^0_{app}(C)_i}{2} \quad (10)$$

$$[C_6H_6] = [B(C_6H_5)_3,oxyg.] = \left(1 - \frac{n^0_{app}}{2}\right)(C_i) \quad (11)$$

At any wave length, the absorbance A_s is

$$\frac{A_s}{b} = a_{(C_6H_5)_2}\frac{n^0_{app}}{2}(C_i) + a_{(C_6H_5)_2BOH}\frac{n^0_{app}}{2}(C_i) + a_{B(C_6H_5)_3,oxyg.}\left(1 - \frac{n^0_{app}}{2}\right)(C_i) \quad (12)$$

where b is the cell path length and a_x is the respective molar absorbance index. The absorption of benzene is negligible in comparison with other species and so is omitted from equation 12. Rearranging equation 12 and dividing by C_i gives

$$\frac{A_s}{b(C_i)} = "a_m" = \frac{n^0_{app}}{2}[a_{(C_6H_5)_2} + a_{(C_6H_5)_2BOH} - a_{B(C_6H_5)_3,oxyg.}] + a_{B(C_6H_5)_3,oxyg.} \quad (13)$$

Calculated and experimental "a_m" values for several wave lengths are compared in Fig. 8. The dotted line is the calculated line with a slope of one. In a number of cases the experimental data show considerable divergence from the calculated value. This probably is a reflection of the complexity of the oxygenation reaction of triphenylboron.

In the extraction analysis of the electrolyzed solution as described in the Experimental Section, all of the boron species should be present as diphenylboronous acid in the cyclohexane extract of the acid solution. The molar absorbance index for this absorption (calculated on the basis of the concentration in acetonitrile) should be independent of n^0_{app} and should be precisely the a_m value for diphenylboronous acid in cyclohexane, 21.4 × 10^3 at 240 mμ. Agreement of available data, Table I, with this criterion is only approximate.

Comparison of Results with Mathematical Treatment.—As indicated in a preceding paragraph, the proposed reaction scheme is an example of case IIb[21] if the reaction producing hydrogen ion is much faster than the hydrogen ion–TPB reaction. If this is the case it should be possible to compare the experimental and calculated dependence of n^0_{app} on (C_i).

An implicit relation for n^0_{app} was previously derived, equation 15b, reference 21. Evaluation for $n = 2$ gives

$$n^0_{app} = \frac{-2}{\gamma(C_i)}\ln[1 - \gamma(C_i)(n^0_{app} - 1)] \quad (14)$$

The symbol γ represents k_2/p, where k_2 is the rate constant for reaction 7, and p is a constant dependent on the particular electrode employed (area, stirring) and the solution volume (see ref. 21 for detailed treatment).

The solid line in Fig. 3 which gives a reasonable fit for the data is the n^0_{app}-(C_i) relation where

(26) Apparently the 238 mμ peak with the 260–280 mμ shoulder is characteristic of the $(C_6H_5)_2BO$— chromophore in acetonitrile. This is supported by the fact that the spectrum of tetraphenyldiboroxide, $(C_6H_5)_2BOB(C_6H_5)_2$, is just twice as intense as that of $(C_6H_5)_2BOH$.

$\gamma = 3 \times 10^3$ liter mole.$^{-1}$. The p-value[27] for the electrode used here with a 25-ml. solution volume was 2×10^{-3} sec.$^{-1}$. The experimental estimate of k_2, as given in a preceding paragraph, was 7.5 liter mole^{-1} sec.$^{-1}$, corresponding to $\gamma = 3.75 \times 10^3$ liter mole. We feel that the substantial agreement between the calculated function and observed data as shown in Fig. 3 is another support of the proposed reaction scheme.

Addition of 0.2 M water to a 2.02 mM TPB solution increased n^0_{app} from 1.14 to 1.43. This can be accounted for easily in terms of a decrease in the rate constant k_2 with addition of water. We have qualitatively observed that the hydrogen ion–TPB reaction is in fact slower in water than in acetonitrile.

Current–time curves were obtained, but variation of stirring conditions with positioning of the electrode in the cell significantly modified the data. Thus no quantitative comparison with the calculated current–time curves[21] was attempted.

Solution of the mathematical problem corresponding to electrolysis in a buffered medium, where $d(H^+)/dt = 0$, is done easily by following the procedure outlined for case IIb, reference 21. The expression obtained is

$$n^0_{app} = n\left[\frac{p}{p + k_2(H^+)}\right] \qquad (15)$$

Using the dissociation constant for picric acid as determined by Kilpatrick and Kilpatrick,[28] 1.26×10^{-5}, a buffer system of 0.07 M sodium picrate and 0.1 M picric acid in acetonitrile would have a hydrogen ion concentration of 1.8×10^{-5} M. The experimental n^0_{app} value, 1.93, is in reasonable agreement with the calculated value, 1.87. Since the data obtained for the acetate buffer were complicated by interfering film formation the derivation given above is not applicable.

When the various evidences presented in support of the proposed reactions are considered as a unit, the validity of the reaction scheme seems to be established satisfactorily.

Experimental

Reagents.—Technical grade acetonitrile (Union Carbide) was purified by the usual method.[29] The boiling point was 81.5 ± 0.2° at 760 mm. Water content as determined by Karl Fischer titration was approximately 1 mM. N,N-Dimethylformamide (Eastman "Spectro Grade"), biphenyl (Eastman) and cyclohexane (Fisher "Spectranalyzed") were used as obtained.

Sodium tetraphenylborate (Baker) was purified by preparing a concentrated solution in acetonitrile, filtering off suspended material and then removing solvent from the filtrate under vacuum. "Anhydrous" lithium perchlorate (G. F. Smith and Co.) contained 3–5% water and so was dried in an air oven at 160° and then in a vacuum oven at 180°. Water content of material treated in this way was 0.5% so that 0.1 M lithium perchlorate solutions had a total water content of at least 5 mM.

Trimethylammonium tetraphenylborate was obtained by mixing aqueous solutions of trimethylammonium chloride and sodium tetraphenyl borate, and washing and drying the resulting precipitate. Triphenylboron was prepared by pyrolysis of trimethylammonium tetraphenylborate as described by Wittig, *et al.*[3] Acidimetric analysis using the mercuric chloride reaction[1] showed 94–96% purity. The remainder was biphenyl as shown by cyclohexane extraction experiments (see below). Absorption spectra of triphenylboron were corrected for the biphenyl impurity.

Tetraphenyldiboroxide, $(C_6H_5)_2B]_2O$, as prepared according to Neu,[20] was 97.4% pure as determined by titration. Diphenylboronous acid, $(C_6H_5)_2BOH$, was prepared according to Abel, *et al.*,[30] by hydration of the anhydride. The refractive index was 1.592 in agreement with the literature value. Phenyl diphenylborinate was obtained by reaction of phenol and tetraphenyldiboroxide as described by Lappert, *et al.*[31] Diphenylboron chloride was supplied by Prof. M. F. Lappert.

After drying picric acid (Baker) at 80° *in vacuo* the compound contained less than 0.5% water. Sodium picrate from neutralization of picric acid with sodium hydroxide contained no more than 0.1% water. Solid tetramethylammonium hydroxide was obtained by evaporation of a 10% aqueous solution (Eastman). Tetramethylammonium acetate from neutralization of tetramethylammonium hydroxide and acetic acid tenaciously retained water even on prolonged vacuum treatment. The sample employed in preparation of the acetic acid–acetate buffer, Table I, contained 12.5% water. Acetic anhydride was added to the acetonitrile solution to react with the water.

Diethylamine was purified by distillation. Standard solutions in acetonitrile were standardized against perchloric acid in acetic acid. Tetramethylammonium triiodide was prepared by the method of Chattaway and Hoyle[32] and showed 99.4% purity by iodometric titration.

Prepurified nitrogen was passed over hot copper turnings and barium oxide and then bubbled through acetonitrile.

Apparatus and Measurements.—All potential measurements in this paper are referred to the Ag, 0.01 M $AgNO_3$, (CH_3CN) arbitrary zero.[33] Actual measurements were made using an aqueous saturated calomel reference electrode in the manner described by Kolthoff and Coetzee;[34] conversion to the silver, silver nitrate scale was done using the value of 0.29 v. for the potential of the cell, silver, silver ion *vs.* aqueous saturated calomel.

Voltammetric measurements with a rotating platinum electrode (0.29 mm.^{2} apparent area, rotation at 600 r.p.m.) were obtained on a Sargent XXI recording polarograph. Traces from cathodic to anodic potentials were obtained at a scan rate of 1.18 mv./sec. An all-glass cell was equipped with fritted inlets for reference electrode and nitrogen. The sample was thermostated at 25.0° by passing water from a constant temperature bath through a jacket surrounding the cell. Current–potential traces were corrected for residual current and "iR" drop across the electrolysis cell.

Chronopotentiometric measurements were obtained using conventional circuitry. A General Radio power supply, type 1204-B, with appropriate ballast resistors was used to supply a constant current. Potential measurements between reference and indicator electrodes were made using a Leeds and Northrup pH indicator, no. 7664, and feeding the output into a Varian G-10 recorder. The time scale, 3.75 sec./div., was established by the synchronous motor used to drive the strip chart. The auxiliary electrode, a mercury pool, was placed in a compartment separated from the sample solution by two fritted discs. The platinum indicator electrode was planar and had an apparent area of 0.40 cm.^{2} Water at 25.0° was circulated through the jacket surrounding the sample cell.

A Lingane–Jones potentiostat was used to carry out the

(27) Evaluation of p was done by obtaining the p for oxidation of iodide ion, 3.0×10^{-3} sec.$^{-1}$, under the same stirring and volume conditions. The p value for TPB then is 2.0×10^{-3} sec.$^{-1}$ as evaluated from equations 1–4 of this paper together with equations 3–5, reference 21. The p-value for oxidation of ferrocene, $Fe(C_5H_5)_2$, to ferricinium ion, $Fe(C_5H_5)_2^+$, was $2.0_6 \times 10^{-3}$ sec.$^{-1}$, which is reasonable under the assumption that ferrocene and TPB would have similar diffusion coefficients.

(28) M. Kilpatrick, Jr., and M. L. Kilpatrick, *Chem. Revs.*, **13**, 131 (1933).

(29) S. Wawzonek and M. E. Runner, *J. Electrochem. Soc.*, **99**, 457 (1952).

(30) E. W. Abel, W. Gerrard and M. F. Lappert, *J. Chem. Soc.*, 3833 (1957).

(31) E. W. Abel, W. Gerrard and M. F. Lappert, *ibid.*, 112 (1957).

(32) F. D. Chattaway and G. Hoyle, *J. Chem. Soc.*, **123**, 654 (1923).

(33) V. A. Pleskov, *Zhur. Fiz. Khim.*, **22**, 351 (1948).

(34) I. M. Kolthoff and J. F. Coetzee, *J. Am. Chem. Soc.*, **79**, 870 (1957).

controlled potential electrolyses. At higher currents where the output voltage of the potentiostat was inadequate a manually-operated auxiliary power supply was employed. The potential of the working electrode was maintained at 0.70 v. *vs.* Ag, $AgNO_3$. The electrode, which was rotated at 600 r.p.m. in the Sargent Synchronous Rotator, was a spiral of platinum wire (B. & S. No. 22, apparent area, 6.0 cm.^{2}) wound 1 mm. away from a 6 mm. glass tube. The auxiliary electrode, a mercury pool, was in a compartment separated from the sample compartment by two fritted discs. Resistance between the platinum and reference, and platinum and mercury electrodes, was 900 and 1300 ohms, respectively. Solutions were not thermostated.

Current integration was done with the permanent magnet d.c. motor (Electro Methods, Ltd., Caxton Way, Stevenage, Herts, England) using the calibration technique developed by Lingane.[35] For electrolysis of solutions less concentrated than 1 m*M* a strip chart record of current was obtained and the current–time curve was integrated by weighing the paper.

The absence of TPB at the completion of the electrolysis was verified by adding thallium perchlorate to a small portion of solution. Electrolysis of the supporting electrolyte solution showed that no detectable hydrogen ion was generated by the small residual current.[6]

All electrodes were cleaned in nitric acid and then immersed in acidic ferrous ammonium sulfate solution to remove oxides. All sample solutions were degassed with nitrogen and nitrogen was passed over the solution during the electrolysis.

Spectrophotometric measurements were made with a Cary model 11 recording spectrophotometer. Where necessary, spacers were used in 1 cm. cells so that path lengths of 0.1 and 0.005 cm. were also available.

Kinetic measurements were made by measuring the limiting current at the rotating platinum electrode (at +0.7 v.) as a function of time. Acetonitrile solutions of perchloric acid were freshly prepared for each run. Essentially anhydrous solutions were obtained by diluting anhydrous 1 *M* perchloric acid in acetic acid with acetonitrile.[34]

Solution Analysis.—Two extraction procedures were used to investigate the electrolyzed solutions. A 2-ml. aliquot portion was added to a saturated aqueous solution of mercuric chloride. This converted all the phenyl boron compounds into boric acid and phenylmercuric chloride, the latter being insoluble in water. This heterogeneous system was extracted with 10 ml. of cyclohexane. Biphenyl and benzene are quantitatively extracted under these conditions. Phenylmercuric chloride, while partially soluble in cyclohexane, has a molar absorbance index of only 288 at 258 mμ[36] and thus its absorption as well as that due to benzene ($a_m^{255m\mu} = 202$) can be neglected in comparison with biphenyl (Fig. 7). The fact that biphenyl was the absorbing species in the cyclohexane extract was established by dividing the observed absorbances by the molar absorbance indices for biphenyl. The quotients, apparent concentrations of biphenyl, were constant within 5% over the wave length region 230–270 mμ.

When a 2-ml. aliquot was treated with 1 *M* sodium hydroxide and extracted with cyclohexane, biphenyl was again the only strongly absorbing species in the cyclohexane. It was shown by experiment that under these conditions phenyl diphenylborinate (from oxygenation of triphenylboron) hydrolyzed to diphenylboronite and phenolate ions and thus remained in the aqueous phase. Acidification of the aqueous portion was followed by another cyclohexane extraction. The diphenylboronous acid quantitatively extracted into the cyclohexane. The extraction of phenol under these conditions is not complete. This is of no consequence since the weak phenol absorption in cyclohexane occurs at longer wave lengths than the diphenylboronous acid peak at 240 mμ. The identity of the biphenyl and diphenylboronous acid absorption in the two cyclohexane extracts was established in the way described in the preceding paragraph.

Benzene was estimated in acetonitrile by carrying out a reduced pressure distillation. The receiver was cooled in a Dry Ice–acetone mixture. After approximately one-half of the 15-ml. aliquot had distilled over the distillation was stopped and the volume of distillate was accurately measured. Since the benzene–acetonitrile azeotrope is more volatile than the biphenyl azeotrope it is possible to analyze for benzene spectrophotometrically using the base-line technique to eliminate errors from background absorbance.

Acknowledgment.—The gift of a quantity of diphenylboron chloride from Prof. M. F. Lappert is gratefully acknowledged. This research was supported in part by the Higgins Fund.

(35) J. J. Lingane, *Anal. Chim. Acta*, **18**, 349 (1958).

(36) G. Leandri and A. Tundo, *J. Chem. Soc.*, 3377 (1954).

SOME COMMENTS ON THE VALUES OF ΔS^0 FOR IONIC REACTIONS AND THE VALUES OF THE ENTROPY OF SOLUTION OF IONS

BY EDWARD L. KING[1]

Contribution No. 2360 from the Gates and Crellin Laboratories of Chemistry, California Institute of Technology, Pasadena, Cal.

Received August 11, 1958

The values of ΔS^0 for certain series of closely related acid dissociation reactions, with a correction applied for the difference of the symmetry numbers of the acid and conjugate base, are correlated by equations of the form $\Delta S^0_{cor} = a - b\Delta Z^2$. The entropies of solution of the gaseous ions Na^+, K^+, Rb^+, Cs^+, Mg^{++}, Ca^{++}, Sr^{++} and Ba^{++} are not, however, functions of Z^2. For the ions of each charge type the entropy of solution is consistent with an equation $\Delta S^0_{soln} = \alpha + \beta/r$; the value of β shows no stronger a dependence upon Z than first power.

In seeking a correlation between the standard entropy changes in ionic reactions and some function of the charges on the reactants and products, one should consider only reactions with the same value of Δn, where Δn is the net increase in the number of solute species in the reaction. The relative values of ΔS^0 for reactions with different values of Δn can be altered simply by a change in the concentration scale (*i.e.*, by a change in the choice of standard state).[2] Laidler[3] has correlated the values of ΔS^0 for a large number of diverse reactions having variable values of Δn with the values of ΔZ^2 for the reaction, where ΔZ^2 is the difference between the sum of the squares of the charges on

(1) John Simon Guggenheim Foundation Fellow, 1957–1958; permanent address, Department of Chemistry, University of Wisconsin, Madison, Wisconsin. This study was supported in part by the Research Committee of the Graduate School, The University of Wisconsin.

(2) The failure to take this into account vitiates some discussions of the values of ΔS^0 in complex ion reactions (*e.g.*, R. J. P. Williams, THIS JOURNAL, **58**, 121 (1954)) as has been pointed out by H. A. Bent, *ibid.*, **60**, 123 (1956). (See also A. W. Adamson, *J. Am. Chem. Soc.*, **76**, 1578 (1954).)

(3) K. J. Laidler, *Can. J. Chem.*, **34**, 1107 (1956); *J. Chem. Phys.*, **27**, 1423 (1957).

the products and the sum of the squares of the charges on the reactants. Scott and Hugus[4] have pointed out, however, that the correlation is marred by the variation of Δn among the reactions considered.

It is anticipated that factors other than charge also play a role in establishing the value of $\bar{S}^0$ for solute species in water[5] and thus in the present paper a possible correlation with ΔZ^2 of the values of ΔS^0 for only series of closely related reactions is investigated. Three series of acid dissociation reactions, all with $\Delta n = 1$, do, in fact, have values of ΔS^0_{cor} at 25° which conform to the equation

$$\Delta S^0_{cor} = a - b\Delta Z^2 \qquad (1)$$

(The ΔS^0_{cor} values being considered are corrected for any difference in the symmetry numbers of acid and conjugate base;[6] this correction must be made before the values of ΔS^0 are scrutinized for a possible dependence upon ΔZ^2.) The three series of reactions are[7]

$$H_nPO_4^{n-3} = H_{n-1}PO_4^{n-4} + H^+ \qquad n = 3,2,1 \quad (A)$$

$$H_nCit^{n-3} = H_{n-1}Cit^{n-4} + H^+ \qquad n = 3,2,1 \quad (B)[8]$$

$$(CH_2NH_2)_2H_n^n = (CH_2NH_2)_2H_{n-1}^{n-1} + H^+ \qquad n = 2,1 \quad (C)$$

$$(CH_2CO_2)_2H_n^{n-2} = (CH_2CO_2)_2H_{n-1}^{n-3} + H^+ \qquad n = 2,1$$

The values of the parameters a and b for each series as well as the observed and calculated values of ΔS^0_{cor} are presented in Table I. The ions in each of these series are large and the total charge is undoubtedly distributed onto several of the peripheral atoms. The correlation of ΔS^0_{cor} with ΔZ^2 may be, therefore, somewhat fortuitous since nearby solvent molecules certainly do not see a localized charge of magnitude Z.

It appears that there is some inconsistency between the observed correlation of ΔS^0_{cor} for the phosphoric acid dissociation reactions and the equation proposed by Connick and Powell[9] which correlates the conventional values of the entropies of oxy-anions $(HO)_mXO_n^{-Z}$ (*i.e.*, the values based upon $\bar{S}^0_{H^+} = 0$) with the equation

$$\bar{S}_Y^0 = 43.5 - 46.5(Z - 0.28n) \qquad (2)$$

In the dissociation of any oxy-acid

$$(HO)_mXO_n^{-Z} = (HO)_{m-1}XO_{n'}^{-Z'} + H^+$$

with $n' = n + 1$ and $Z' = Z + 1$, the values of both n and Z increase by one unit. Thus equation 2 predicts a value of $\Delta S^0 = -33.5$ e.u. for the acid dissociation reaction of all oxy-acids which are ions. Connick and Powell do not suggest that equation 2 is valid for species with $Z = 0$. The observed values of this quantity for the limited number of oxy-acids which are ions (HCO_3^-, $H_2PO_4^-$, HSO_4^- and $HPO_4^=$) are not constant but lie in the range -26 to -43 e.u.[10]

(4) P. C. Scott and Z. Z. Hugus, *ibid.*, **27**, 1421 (1957).

(5) H. S. Frank and M. W. Evans, *ibid.*, **13**, 507 (1945).

(6) S. W. Benson, *J. Am. Chem. Soc.*, **80**, 5151 (1958).

(7) It is to be noted that only a series of reactions consisting of three or more members provides a valid test of the form of equation 1.

(8) It is assumed that, because of the presence of the adjacent hydroxyl group, the first acid dissociation of citric acid, $HOC(CH_2CO_2H)_2(CO_2H)$, involves the middle carboxyl group. This has relevance in making the symmetry number correction.

(9) R. E. Connick and R. E. Powell, *J. Chem. Phys.*, **21**, 2206 (1953).

(10) K. S. Pitzer, *J. Am. Chem. Soc.*, **59**, 2365 (1937).

TABLE I

VALUES OF ΔS^0_{cor} FOR ACID DISSOCIATION REACTIONS

Reactions	a	b	n	ΔS^0_{cor} values: Obsd.[a]	Calcd.
A	−5.5	5.9	3	−16.8	−17.3
			2	−29.5	−29.1
			1	−40.2	−40.9
B	+0.1	4.9	3	− 9.6	− 9.8
			2	−19.8	−19.6
			1	−29.2	−29.4
C	−6.6	4.1	2[b]	1.5	1.6
			1[b]	− 6.6	− 6.6
			2[c]	−17.0	−14.8
			1[c]	−22.7	−23.0

[a] Values of ΔS^0_{cor} are calculated from experimental values of ΔS^0 reported in the papers: phosphoric acid, K. S. Pitzer, *J. Am. Chem. Soc.*, 59, 2365 (1937); citric acid, R. G. Bates and G. D. Pinching, *ibid.*, 71, 1274 (1949); ethylenediammonium ion, D. H. Everett and B. R. W. Pinsent, *Proc. Roy. Soc.* (*London*), 215A, 416 (1952); succinic acid, T. L. Cottrell and J. H. Wolfenden, *J. Chem. Soc.*, 1019 (1948). The correction factor to be subtracted from the value of ΔS^0 to obtain ΔS^0_{cor} is $R \ln \sigma_A/\sigma_B$, where σ_A and σ_B are the symmetry numbers of the acid and conjugate base.[6] These correction factors for the successive reactions in each series are: A, 0.8, −0.8 and −2.8 e.u.; B, −1.4, 0.0 and −2.8 e.u.; C, 3.6, 0.8, 0.0 and −2.8 e.u. [b] Ethylenediammonium ion. [c] Succinic acid.

In connection with this correlation of values of ΔS^0 for the dissociation reactions of phosphoric acid with the value of ΔZ^2, it is of interest to note that Altshuller[11] has found the values of the entropy of solution of gaseous oxy-anions are a function of Z^2 and not Z.[12] Couture and Laidler[13] have also correlated the "absolute" values of $\bar{S}^0$ for oxy-anions with an equation involving Z^2.

The dependence of the values of $\bar{S}^0$ for monatomic cations (or the values of ΔS^0 for the process $M^+_{(g)} = M^+_{(aq.)}$) upon the value of Z is open to some question and appears to be unsettled.[3,4] While Laidler[3] is correct in pointing out that, in general, a physically meaningful correlation of $\bar{S}^0$ upon Z should involve the "absolute" values of $\bar{S}^0$, the form of the equations which have been used to correlate $\bar{S}^0$ (or ΔS^0_{soln}) with Z and r are such that the use of the conventional ionic entropies (based upon $\bar{S}^0_{H^+} = 0$) is appropriate in discerning the power to which Z is raised in the correlation of $\bar{S}^0$ or ΔS^0_{soln} with Z. The various equations which have been suggested for this correlation have in common the incorporation of the dependences upon Z and r in the same term

$$\Delta S^0_{soln} = \alpha - \frac{\beta(Z)}{r^n} \qquad (3)$$

The value of $\beta(Z)$ obtained from the correlation with r of ΔS^0_{soln} for ions of a particular charge does not depend upon the origin with respect to which the values of $\bar{S}^0$ are reckoned. The value of $\beta(Z)$ which correlates the dependence of ΔS^0_{soln} of ions of a particular charge upon the radius depends in a critical way upon the choice of radius values

(11) A. P. Altshuller, *J. Chem. Phys.*, **24**, 642 (1956).

(12) Altshuller[11] used S_2^0 values based upon $\bar{S}_{H^+}^0 = 0$. If one uses $\bar{S}_{H^+}^0 = -5$ e.u.[16b] instead, the correlation of ΔS^0_{soln} with Z^2 is not marred. For the isoelectronic sequence ClO_4^-, SO_4^{-2} and PO_4^{-3}, the "absolute" value of $\Delta(\Delta S^0_{soln})/\Delta(Z^2) = -10.5 \pm 0.5$ e.u.

(13) A. M. Couture and K. J. Laidler, *Can. J. Chem.*, **35**, 202 (1957).

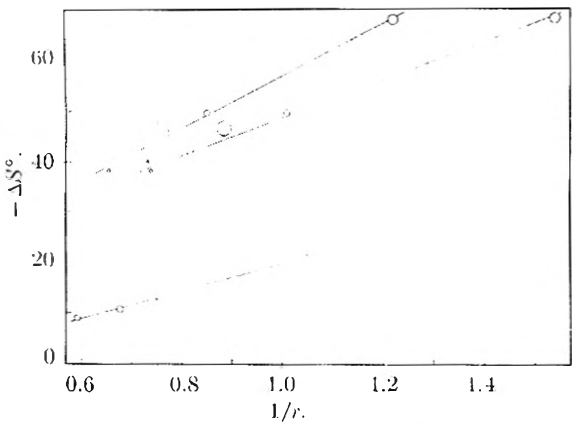

Fig. 1.—The values of $\Delta S°_{298}$ for the process: M^{+n} (g., 1 atm.) = M^{+n} (aq., hyp. 1 *m* soln.). Reading from top to bottom the lines are: divalent ions, $\Delta S° = -5.0 - 52.0/r_u$; divalent ions, $\Delta S° = -9.8 - 37.9/r_c$; univalent ions, $\Delta S° = 7.4 - 27.2/r_c$. (The radius of each circle indicates the uncertainty in the value of $\bar{S}°_2$ as given by K. K. Kelley, Bureau of Mines Bull. 477, 1950 (except in case of $\bar{S}°_{Ca^{++}}$, which is from C. C. Stephenson, *J. Am. Chem. Soc.*, 66, 1436 (1944)).

which are appropriate. Latimer[14] has used the crystal radii in equation 3 with $n = 1$. Powell and Latimer[15] have used "effective" radii which were taken as the crystal radii values plus 2.00 Å. with $n = 2$. Laidler[3] has used Pauling's univalent radius values with $n = 1$. As Gurney has made clear, the balancing of attractive and repulsive forces which determines the equilibrium separation of particles makes the size of ions in solution different than their size in crystals.[16] The size of ions in solution is expected to be larger, which suggests that Powell and Latimer's use of an additive constant and Laidler's use of univalent radius values for polyvalent ions are corrections in the right direction. Neither of these approaches can be defended as being rigorous, however, nor does it appear possible to decide at this time upon the proper radius values to use.

One may seek, nevertheless, for correlations between $\Delta\bar{S}^0_{soln}$ and crystal radii, r_c, or univalent radii, r_u. Because of uncertainties in the values of $\bar{S}^0_2$ and/or the values of the ionic radius for many ions, particularly those of charge +3 and +4, attention will be confined to the alkali metal ions Na^+, K^+, Rb^+ and Cs^+, and the alkaline earth ions which are isoelectronic with these alkali metal ions *i.e.*, Mg^{++}, Ca^{++}, Sr^{++} and Ba^{++}. The plots of $\Delta\bar{S}^0_{soln}$ *versus* $1/r$ are given in Fig. 1. The value of β for the +1 ions being considered is 27.2; for the +2 ions the value of β is 52 if Pauling's univalent radius values are used and is 37.9 if Pauling's crystal radii values are used.

The dependence of β upon Z is certainly not the second power dependence expected on the basis of the Born equation under the assumption that r is not a function of T.[17] The approximately first power dependence of β upon Z, obtained if the univalent radius values are used, is viewed as fortuitous. The corresponding values of α are not at all consistent with values of the "absolute" entropy of hydrogen ion in the range -2 to -6, e.u. obtained by various methods.[18] If a value of -5 e.u. is used for the value of $\bar{S}^0_{H^+}$, the values of α for the +1 and +2 ions are $+7.4 - 5 = 2.4$ and $-5.0 - 2(5) = -15.0$. While equation 3, with $n = 1$, adequately represents the radius dependence of the entropies of solution of a limited number of gaseous monatomic ions of a particular charge, the dependence upon charge cannot be incorporated in this equation without allowing both α and β to be functions of Z. This limited group of spherically symmetrical cations, with values of both $\bar{S}^0$ and r_c which are relatively certain, should be ideally suited for testing simple dependences of $\Delta\bar{S}^0_{soln}$ upon Z. A simple dependence is not suggested by the data. It would appear that the suggested first[15] and second[3] power dependences upon Z for much more extensive groups of ions are fortuitous consequences of the choice of r values.

It seems overly optimistic to expect a good correlation of the values of the entropy of solution of gaseous monatomic ions as a simple function of the charge and radius of the ion. Perhaps if the appropriate account were taken of cation hydration, the entropies of solution of these hydrated species would show the dependence upon Z^2 which is shown by the polyatomic anions.[11] Such hydrated species would more closely resemble the polyatomic ions involved in the acid dissociation reactions already considered than do the unhydrated cations. Sufficient information is not now available to allow the calculation of the entropy of solution of hydrated gaseous ions.

(14) W. M. Latimer, *Chem. Revs.*, **18**, 351 (1936).

(15) R. E. Powell and W. M. Latimer, *J. Chem. Phys.*, **19**, 1139 (1951); see also R. E. Powell, THIS JOURNAL, **58**, 528 (1954).

(16) R. W. Gurney, "Ionic Processes in Solution," McGraw-Hill Book Co., Inc., New York, N. Y., 1953, Chap. 16.

(17) See, however, the suggestion that $dr'/dT \propto r'/Z$, where r' is an effective radius, $r_c + 0.85$ (W. M. Latimer, *J. Chem. Phys.*, **23**, 90 (1955)).

(18) (a) Some methods are reviewed by B. E. Conway and J. O'M. Bockris in Chap. II of "Modern Aspects of Electrochemistry," Academic Press, New York, 1954; (b) R. W. Gurney, "Ionic Processes in Solution," McGraw-Hill Book Co., Inc., New York, N. Y., 1953, Chap. 10.

THE THERMODYNAMICS OF ALUMINUM(III) FLUORIDE COMPLEX ION REACTIONS. THE GRAPHICAL EVALUATION OF EQUILIBRIUM QUOTIENTS FROM $\bar{n}([X])$[1]

BY EDWARD L. KING AND PATRICK K. GALLAGHER

Contribution from the Department of Chemistry, University of Wisconsin, Madison, Wisconsin

Received November 29, 1959

The existing data, $\bar{n}([F^-])$, of Brosset and Orring on the stability of aluminum(III) fluoride complexes are treated by a newly devised graphical procedure to obtain values of $Q_n = [AlF_n^{+3-n}]/[AlF_{n-1}^{+4-n}][F^-]$, for $n = 1$ to 5. These Q_n values valid for $I \leq 0.5$ are corrected to the ionic strength values of the calorimetric work of Latimer and Jolly and used in interpreting this work to give values of ΔH_n and ΔS_n°. These values of ΔS_n° corrected for the symmetry numbers of the reactant and products species agree with the values calculated by the equation $\Delta S_{cor} = 12.8 - 2.9\Delta Z^2$ with an average difference of 0.4 e.u.

The correlation with ΔZ^2 of the corrected entropy changes in series of closely related acid dissociation reactions presented in the companion paper[2] suggests that such a correlation may also exist in complex ion formation reactions. The aluminum(III)–fluoride complex ion formation reactions

$$AlF_{n-1}^{+4-n} + F^- = AlF_n^{+3-n} \quad Q_n = \frac{[AlF_n^{+3-n}]}{[AlF_{n-1}^{+4-n}][F^-]}$$

are an ideal series in which to seek such a correlation for there are equilibrium data by Brosset and Orring[3] providing ΔF^0_n values for the reactions with $n = 1$ to 5 in solutions of ionic strength 0.5 which can be coupled with the calorimetric data of Latimer and Jolly[4] to give ΔH_n and ΔS^0_n values.[5] With n varying from 1 to 5, ΔZ^2 varies from -6 to $+2$. The calculation of the values of ΔS^0_n has, of course, been carried out already by Latimer and Jolly.[4] It is possible, however, to subject the equilibrium data[3] to a more careful analysis than has been done. The variation in ionic strength existing in the solutions used in the calorimetric work also makes desirable certain corrections which were not applied in the original paper.[4] The present paper deals with a reinterpretation of the equilibrium and calorimetric data to yield values of the equilibrium quotients Q_1 to Q_5 for $I \cong 0.5$; these Q values are corrected to values appropriate for the ionic strength of each calorimetric run before being used to calculate the concentrations of the several aluminum(III) fluoride species present. The values of ΔS^0_{cor}, the entropy change corrected for the change in symmetry number, obtained from this treatment of the data do fit the equation

$$\Delta S^0_{cor} = a - b\Delta Z^2 \qquad (1)$$

which has the same form as that which correlates the values of ΔS^0_{cor} for the acid dissociation reactions.[2]

The Evaluation of the Equilibrium Quotients.—Brosset and Orring[3] obtained $\bar{n}$, the average number of fluoride ions bound per aluminum(III) ion, as a function of the concentration of fluoride ion in media of ionic strength ~0.5 at 25°. With potassium nitrate as the principal electrolyte present, the range of $\bar{n}$ was 0.49 to 3.29; with ammonium nitrate present, the range of $\bar{n}$ was 2.23 to 4.65. It is to be noted that with a maximum observed value of $\bar{n}$ of 4.65, the value of Q_6 cannot possibly be established with much certainty. The data indicate that different sets of Q_n values are appropriate for each of the two media, potassium nitrate solution and ammonium nitrate solution. In the calculation of the Q_n values, Brosset and Orring used six points from the smooth curve of $\bar{n}$ *versus* $-\log [F^-]$ for the potassium nitrate solutions.

Use can be made of all the appropriate experimental points in the evaluation of each Q_n by a newly devised graphical procedure. The experimental points most appropriate for the evaluation of a particular equilibrium quotient Q_a are those with $(a - 0.9) < \bar{n} < (a - 0.1)$. If such points do not establish the value of Q_a, none will. This graphical procedure is suggested by a derivation given below. The general equation for $\bar{n}$ as a function of $[F^-]$ is

$$\sum_{n=0}^{n=N} (n - \bar{n})[F^-]^n Q_0 Q_1 \ldots Q_n = 0$$

with $Q_0 \equiv 1$. This equation can be rearranged to give

$$\frac{\sum_{n=0}^{n=a-1} (\bar{n} - n)[F^-]^{n-a-1} Q_0 \ldots Q_n}{(a + 1 - \bar{n})Q_0 Q_1 \ldots Q_{a-1}} = \frac{(a - \bar{n})Q_a}{(a + 1 - \bar{n})[F^-]} + Q_a Q_{a+1} + \frac{\sum_{n=a-2}^{n=N} (n - \bar{n})[F^-]^{n-a-1} Q_0 Q_1 \ldots Q_n}{(a + 1 - \bar{n})Q_0 Q_1 \ldots Q_{a-1}}$$

which is the form suggesting the plot for the evaluation of Q_a, the values of Q_0, Q_1, . . . and Q_{a-1} having already been determined by similar plots. A plot of

$$\frac{\sum_{n=0}^{n=a-1} (n - \bar{n})[F^-]^{n-a-1} Q_0 \ldots Q_n}{(a + 1 - \bar{n})Q_0 Q_1 \ldots Q_{a-1}}$$

versus

$$\frac{(a - \bar{n})}{(a + 1 - \bar{n})[F^-]}$$

(1) Supported in part by a grant from the U. S. Atomic Energy Commission (Contract AT(11-1)-64, Project No. 3).

(2) E. L. King, THIS JOURNAL, **63**, 1070 (1959).

(3) C. Brosset and J. Orring, *Svensk kem. Tid.*, **55**, 101 (1943).

(4) W. M. Latimer and W. L. Jolly, *J. Am. Chem. Soc.*, **75**, 1548 (1953).

(5) The standard values of ΔS and ΔF, indicated in the present work with the usual zero superscript, correspond to the standard state for solute species being a hypothetical one molar solution of the species in an aqueous solution of ionic strength under consideration.

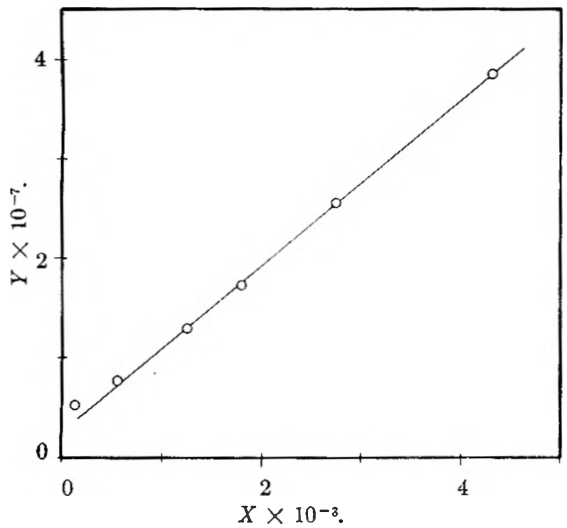

Fig. 1.—The graphical evaluation of Q_3 which is the slope of this plot of

$$Y = \left\{ \frac{\sum_{n=0}^{n=2} (\bar{n} - n)[F^-]^{n-4} Q_0 \ldots Q_n}{(4 - \bar{n}) Q_0 Q_1 Q_2} \right\}$$

versus

$$X = \frac{(3 - \bar{n})}{(4 - \bar{n})[F^-]}$$

The values of Q_1 and Q_2 have been obtained previously from analogous plots. The points shown in this figure are, from left to right, for $\bar{n}$ values of 2.94, 2.80, 2.66, 2.58, 2.49 and 2.37.

will be a straight line if the third term on the right-hand side of the equation is negligible; the slope of this line is the value of Q_a. In making such a plot, there is little point in using $\bar{n}$ values less than $\sim(a - 1.2)$ or greater than $\sim(a - 0.1)$. If at the highest concentration of fluoride ion being considered, *i.e.*, at $\bar{n} \cong (a - 0.1)$, the species of composition AlF_{a+2}^{+1-a}, AlF_{a+3}^{-a}, ... are not present at significant concentrations, the condition for linearity is satisfied. Although the value of Q_{a+1} is obtainable from the intercept in this plot, the experimental points most relevant to establishing the value of Q_{a+1} have not been used; it is preferable to use a different plot for the evaluation of each Q_n.

A number of methods have been proposed for the determination of Q_n values given $\bar{n}([X])$.[6,7] Some of these have been reviewed and compared by Sullivan and Hindman[6a] and by Rossotti and Rossotti.[6c] The latter authors have also proposed a graphical procedure somewhat related to the present one but which leads to values of the over-all equilibrium quotients, $\beta_n = [MX_n]/[M][X]^n$. Such equilibrium quotients correspond to reactions which are not, except for $n = 1$, the principal equilibria existing in any of the solutions. It is difficult, therefore, to decide which of the experimental points are particularly relevant in the establishment of a particular Q_n. While the functions plotted in the method described in this paper are derived from the original data by a relatively laborious calculation, the advantages of the present method justify the labor. The principal advantage of the present method is simply that in each plot one uses only the data which are relevant to the establishment of the Q_n under consideration. The stepwise reaction forming AlF_a^{+3-a} corresponds closely to the principal equilibrium in the solutions with $\bar{n} \cong (a - 0.5)$ and thus it is obvious which of the data are relevant.

In Fig. 1 is presented a typical plot, the one having a slope which is the value of Q_3 in potassium nitrate medium. In Table I are presented the Q_n values obtained by this treatment. The average difference between the observed values of $\bar{n}$ and the values calculated using the Q_n values obtained in this paper is 0.01_9 for the 16 points in potassium nitrate solution and 0.03_6 for the 19 points in ammonium nitrate solution.

TABLE I

THE VALUES OF THE EQUILIBRIUM QUOTIENTS FOR ALUMINUM(III) FLUORIDE COMPLEX ION FORMATION REACTIONS AT 25°

$I \cong 0.5$

	Calcd. in this paper		Brosset and Orring smoothed values[a]
	NH_4NO_3 soln.	KNO_3 soln.	
Q_1		1.46×10^6	1.36×10^6
Q_2		1.13×10^5	1.04×10^5
Q_3	3.7×10^3	8.2×10^3	7.17×10^3
Q_4	4.4×10^2	5.1×10^2	5.50×10^2
Q_5	2.9×10^1	$(2.9 \times 10^1)^b$	4.26×10^1
Q_6	$(1.1)^b$		2.94

[a] These correspond to potassium nitrate solution. [b] Very uncertain value.

The Correction of Q_n Values for their Dependence upon I.—Latimer and Jolly[4] made calorimetric measurements upon solutions of ionic strength ranging from ~0.016 to ~0.20. They used the Q_n values derived by Brosset and Orring from smoothed data at $I \cong 0.5$ without correction. Of the tacit assumptions in this procedure, (a) that the distribution of aluminum(III)–fluoride species is not a function of the ionic strength and (b) that the dependence of the ΔH values upon I is small compared to the experimental uncertainty, certainly the first is not justified. It is difficult, of course, to predict the exact dependence of each Q_n upon I. In the present work it is assumed that the dependence of $\log Q_n$ upon I is a function of the value of $(\Delta Z^2)_n$, the difference between the square of the charges on the products and reactants in the nth reaction. The relationship

$$(1/\Delta Z^2) \log Q/K = \frac{A\sqrt{I}}{1 + Ba\sqrt{I}}$$

with $a = 6.80$ nicely correlates the dependence of $Q = [CrNCS^{++}]/[Cr^{+++}][SCN^-]$ from $I = 0.016$ to 0.6.[8] The Davies equation[9]

$$(1/\Delta Z^2) \log Q/K^0 = \left\{ \frac{A\sqrt{I}}{1 + \sqrt{I}} - 0.1\, I \right\}$$

has also been much used, although generally only to

(6) (a) J. C. Sullivan and J. C. Hindman, *J. Am. Chem. Soc.*, **74**, 6091 (1952); (b) G. Scatchard, method presented in the paper: J. T. Edsall, G. Felsenfeld, D. S. Goodman and F. R. N. Gurd, *ibid.*, **76**, 3054 (1954); (c) F. J. C. Rossotti and H. S. Rossotti, *Acta Chem. Scand.*, **9**, 1166 (1955).

(7) J. Z. Hearon and J. B. Gilbert, *J. Am. Chem. Soc.*, **77**, 2594 (1955).

(8) C. Postmus and E. L. King, THIS JOURNAL, **59**, 1208 (1955).

(9) C. W. Davies, *J. Chem. Soc.*, 2093 (1938).

a lower maximum value of I. The values of $(Q/K^0)^{1/\Delta Z^2}$ at $I = 0.5$ calculated by each of these two equations differ by a factor of two. The plot of log $\gamma_\pm$ for sodium chloride *versus* I lies between the plots of $(1/\Delta Z^2)$ log Q/K^0 *versus* I calculated using each of the two equations. This plot of log $(\gamma_\pm)_{NaCl}$ *versus* I is assumed to give the ionic strength dependence of $(1/\Delta Z^2)$log Q_n for each of the aluminum-(III) fluoride reactions.

The Calorimetric Evaluation of ΔH_n.—Each Q_n value was corrected by the means just outlined to the ionic strength of the final solution in each of the calorimetric runs; these Q_n values were used to evaluate the distribution of aluminum among the several forms. The Q_n values from the potassium nitrate series were used for the calorimetric runs carried out in sodium fluoride solution and the Q_n values from the ammonium nitrate series were used for the runs carried out in ammonium fluoride solution. Latimer and Jolly reported the results of eleven calorimetric experiments for which the values of $\bar{n}$ of the final solutions, calculated using the corrected Q_n values, were 0.217, 0.738, 1.34, 1.91, 2.96, 3.16, 3.58, 4.05, 4.67, 4.93 and 4.94. In the last two solutions, the calculated extent of formation of AlF_6^{-3} is approximately 10%. Certainly little confidence can be placed in any value of ΔH_6 obtained from considering the results of these two experiments. Whether one considers the eleven experiments and six unknowns, ΔH_1 through ΔH_6, or the nine experiments (with $\bar{n} \leqslant 4.67$) and five unknowns, ΔH_1 through ΔH_5, has little effect on the calculated values of ΔH_1 through ΔH_5. The value of ΔH_5, which is the most affected, differs by 0.3 kcal. in the two treatments. The simultaneous equations have been treated by the method of averages; in this treatment, it is assumed, of course, that the value of ΔH_n for each n is independent of the ionic strength. The values of ΔH_1 through ΔH_5 derived in this manner from Latimer and Jolly's calorimetric work are presented in Table II. Using these ΔH_n values and the corrected Q_n values, one calculates values of the net heat absorbed per mole of aluminum(III) which differ from the observed values by an average of 36 cal. These values of ΔH_n do not differ greatly from those reported by Latimer and Jolly; the largest difference is 390 cal. in the case of $n = 5$.

Results and Discussion

The calculated ΔH_n values have been coupled with ΔF_n° values calculated from the Q_n values corrected to $I = 0.07$, a value in the middle of the ionic strength range of the calorimetric studies, to allow the calculation of ΔS_n° values; these ΔS_n° values are assumed to be appropriate for an aqueous solution with $I = 0.07$. The Q_n values from Table I which were corrected to $I = 0.07$ were for $n = 1, 2$, and 3, the values obtained from the studies on potassium nitrate solution, for $n = 4$, the average of the values obtained in the two different media and for $n = 5$, the value obtained from the studies on ammonium nitrate solution. A list of the derived thermodynamic quantities is given in Table II.

Before scrutinizing the values of ΔS^0 for a possible dependence upon the value of ΔZ^2, it is necessary that they be corrected for the symmetry number factor in the value of ΔS^0; this is equivalent to considering the so-called intrinsic value of the equilibrium quotient.[10] In making this correction, it was assumed that all of the aluminum species are octahedral $Al(OH_2)_{6-n}F_n^{+3-n}$, with the relative amounts of any geometrical isomers being dictated solely by statistical considerations.[11] These values of ΔS°_{cor} are nicely correlated with equation 1 with $a = 12.8$ and $b = 2.9$. For reactions with $n = 1$ to 5, the average difference between the observed and calculated values is 0.4 e.u. (There is very poor agreement in the case of the reaction with $n = 6$ but, as has been stated, the experimental data tell us very little about this reaction.)

The observed correlation of ΔS°_{cor} with ΔZ^2 neither confirms nor denies that a contribution to the value of ΔS^0 is that due to the replacement of a water molecule by a fluoride ion as suggested by Latimer and Jolly.[4] This contribution, +15.6 e.u., is the same for each step and thus does not influence the value of b. It is to be noted that the approximate symmetry in the residual charge effect upon ΔS^0, as calculated by Latimer and Jolly, is somewhat fortuitous since these reactions are ones in which $\Delta n \neq 0$; the actual values of ΔS^0 for such reactions depend upon the arbitrary choice of standard state.

This correlation of ΔS°_{cor} with the value of ΔZ^2, like the similar correlation in the companion paper, is somewhat surprising since the net charge on the

TABLE II

THERMODYNAMIC QUANTITIES FOR THE REACTIONS

$$AlF_{n-1}^{+4-n} + F^- = AlF_n^{+3-n}$$

n	$T = 25°$ ΔF^0, kcal.	$I = 0.07$[a] ΔH,[b] kcal.	ΔS^0,[c] e.u.	$(\Delta S^0 + R \ln \sigma_P/\sigma_R)$,[d] e.u.	Calcd. value of ΔS^0 (cor.) e.u.
1	−9.02	+1.06	33.8	30.2	30.2
2	−7.32	0.92	27.6	25.8	24.4
3	−5.54	.18	19.2	18.6	18.6
4	−3.66	.04	12.4	13.0	12.8
5	−1.82	− .36	4.9	6.7	7.0

[a] See text for discussion of the assumed dependence of Q_n values upon I. [b] The values of ΔH presented by Latimer and Jolly[4] for $n = 1$ to 5 are 1.15, 0.78, 0.19, 0.28 and −0.75 kcal., respectively. [c] The values of ΔS° presented by Latimer and Jolly[4] for $n = 1$ to 5 are 32, 26, 18, 13 and 5 e.u., respectively. [d] The entropy change corrected for the change of symmetry numbers of the reactant (σ_R) and product (σ_P).

(10) S. W. Benson, *J. Am. Chem. Soc.*, **80**, 5151 (1958).

(11) In the cases of *cis*- and *trans*-$Cr(OH_2)_4(NCS)_2^+$ and $Cr(OH_2)_4Cl_2^+$, the *trans* isomer is present in an amount ~2 times that expected statistically (J. T. Hougen, K. Schug and E. L. King, *ibid.*, **79**, 519 (1957); E. L. King, Sr. M. J. M. Woods, O. P. and H. S. Gates, *ibid.*, **80**, 5015 (1958)). In the case of *cis*- and *trans*-$Cr(OH_2)_4F_2^+$, the *trans* isomer is present at a relative concentration ~1.5 times that expected statistically (E. L. King and Y. T. Chia, forthcoming publication). The nuclear magnetic resonance study on aluminum(III)-fluoride complexes suggests that one or the other of the two isomers of difluoroaluminum(III) ion is present predominantly (R. E. Connick and R. E. Poulsen, *ibid.*, **79**, 5153 (1957)). If the predominant isomer of difluoroaluminum(III) ion is the *cis* isomer, the appropriate correction for the symmetry number change is very similar to the value given above. For $n = 2$, the correction would be −1.4 e.u. rather than the −1.8 e.u. calculated under the assumption of statistical distribution. On the other hand if the predominant isomer is the *trans* isomer, the correction would be +1.4 e.u.; if this were the true situation, the correlation of ΔS°_{cor} with ΔZ^2 would be less striking. The question of the distribution of isomers also exists for trifluoroaluminum(III) and the correlation of all of the reactions would necessitate information regarding its isomeric composition.

polyatomic aquofluoroaluminum(III) species is undoubtedly spread out over the peripheral atoms. Whatever the cause of the correlation, its existence is unmistakable. The validity of equation 1 does raise a question regarding the proposed correlation of $\bar{S}^0$ values of complex ions with the first power of Z.[12,13]

(12) J. W. Cobble, *J. Chem. Phys.*, **21**, 1446 (1953).
(13) P. George, G. I. H. Hanania and D. H. Irvine, *ibid.*, **22**, 1616 (1954).

EFFECTS OF INTERPARTICLE CONDENSATION ON HEATS OF ADSORPTION AND ISOTHERMS OF POWDER SAMPLES[1]

BY CONWAY PIERCE

Department of Chemistry, University of California, Riverside, California

Received November 1, 1958

Additional heat of immersion measurements for graphite in benzene confirm a previous conclusion that there is extensive capillary condensation in voids between particles when powder samples adsorb vapor at high relative pressure. Heats of adsorption, computed from heats of immersion, show that beyond the first 2–3 layers practically all the net heat is due to destruction of film surface as the interparticle spaces fill. The contribution of capillary condensation to nitrogen adsorption isotherms for powders is measured by comparing isotherms with an ideal isotherm which gives that part of the adsorption due to multilayers on the free surface. The ideal isotherm follows the equation $(V/V_m)^{2.75} = \frac{1.30}{\log p_0/p}$ at all relative pressures above 0.2. The ideal isotherm is applied to experimental data to (1) determine surface area independently of a BET plot, (2) evaluate the contribution of interparticle condensation to the isotherm, (3) measure the adsorption in small pores that fill at low relative pressure and (4) explain abnormalities in isotherms of graphite samples whose surfaces are exceptionally homogeneous. Studies of many powder sample isotherms show that interparticle condensation normally occurs, to an extent determined by the size and shape of particles and their tightness of packing.

It was shown in a preceding publication[2] that when a powdered graphite sample is equilibrated with benzene vapor there is capillary condensation in the voids between particles. The evidence for this is that the area of the liquid film surface adsorbed on the particles is only 15% the area of the dry powder. The powder used in the preceding study had been prepared by grinding and nothing was known about the particle size distribution. It was felt desirable, therefore, to repeat the measurements using a sample of known particle size. The one selected was a graphitized carbon black prepared by the Cabot laboratories,[3] designated as Elf 4(2700°). Electron microscope studies[4] on the original black have shown that the particles are spherical and quite uniform in size, with an arithmetic mean diameter of 260 Å. The nitrogen area before heating is 120 m.^{2}/g. After heating the area is 85–100 m.^{2}/g.

Details of the calorimetric measurements have been described.[2] Results are shown in Fig. 1A, which gives the heat of immersion per gram as a function of the weight of benzene preadsorbed. These data show that for this sample also there is capillary condensation between particles, as previously observed for two other powder samples. It appears, therefore, that such condensation is normal for adsorption by powder samples.

Effects of Interparticle Condensation on Heat of Adsorption.—As discussed in the preceding paper[2] the heat of immersion for a dry sample is the sum of three effects, first noted by Harkins and Jura.[5]

$$H_w = E - E_L + H_s \qquad (1)$$

where H_w is the heat of immersion, $E - E_L$ is the *integral* net heat of adsorption and H_s is the heat due to destruction of the adsorbed film when immersed in bulk liquid. H_s is the product of the film area by the unit enthalpy of the surface. It follows from (1) that H_w for a sample equilibrated with vapor at p_0 can be used to measure the area of the adsorbed film. When there is no condensation between particles the area so measured is that of the dry surface (plus a small correction for the thickness of the film). Harkins and Jura[5] used this relation to make an absolute measurement of area for an anatase powder.

This absolute method cannot be used when there is capillary condensation between sample particles. As shown in Fig. 1A, H_w for this sample is 0.63 cal./g. when 0.6 g. of benzene has been adsorbed. Converting to ergs and dividing by the enthalpy[6] of benzene gives an area of 39 m.^{2}/g., less than half that of the dry powder.

If there were no condensation between particles the H_w curve of Fig. 1A should level out as indicated by the dotted line. The value at saturation should be the enthalpy–area product (an area of 85 m.^{2}/g. was assumed). In the region where the dotted line first leaves the experimental values it represents an estimate only, based on the Harkins–Jura results for a sample that had little or no interparticle condensation.

The difference between H_w for a dry sample and one for preadsorbed vapor is the integral net heat of adsorption for the amount of vapor adsorbed. This relation is used to replot the data of Fig. 1A as heats of adsorption, Fig. 1B. The upper curve shows experimental values and the middle curve

(1) Presented at Symposium on Energetics of Surfaces and Interfaces, 134th National Meeting, American Chemical Society.
(2) C. Pierce, J. Mooi and R. E. Harris, THIS JOURNAL, **62**, 655 (1958).
(3) Provided through courtesy of Drs. W. R. Smith and W. B. Spencer, Godfrey L. Cabot, Inc., Cambridge, Massachusetts.
(4) "Cabot Carbon Blacks Under the Electron Microscope," Godfrey L. Cabot, Inc., 1953.
(5) W. D. Harkins and G. Jura, *J. Am. Chem. Soc.*, **66**, 919, 1362 (1944).
(6) F. E. Bartell and R. M. Suggitt, THIS JOURNAL, **58**, 36 (1954).

the ideal values that would be obtained if H_w followed the dotted curve of Fig. 1A. The difference between these two, shown by the lower curve of Fig. 1B, is the heat due to destruction of film surface as pore spaces between particles fill. This curve is of course only an approximation at adsorption below saturation, but is probably a fairly close one. Values taken from this curve may be used to compute the film area lost in filled spaces when a given amount is adsorbed. For example, at 0.2 g. of benzene adsorbed the area lost is about 17 m.^{2}/g.

The slopes of the curves of Fig. 1B are the *differential* net heats of adsorption. If there were no interparticle condensation this heat should be approximately the same as the change in free energy ($\Delta F = RT \ln p/p_0$) after the first few layers are completed. When measured net heats of adsorption are greater than the computed ΔF value the excess heat is due to the decrease in enthalpy as surface is lost by interparticle condensation.

Effect of Interparticle Condensation on the Isotherm.—An experimental adsorption isotherm represents the total adsorption, the sum of that due to capillary condensation and that due to building up a multilayer film on exposed surface. In the past it generally has been assumed that when the isotherm is type II almost all the adsorption is in the exposed film. The present results show that this is not necessarily true. All of the samples whose heats of immersion were measured have type II nitrogen isotherms. It is unsound to assume that the isotherm for any powder sample is completely free of interparticle condensation.

It is of interest, therefore, to separate the effects of interparticle condensation and exposed film adsorption, so that for a given isotherm the contributions of the two can be evaluated independently. This can be done by comparing the experimental nitrogen isotherm with a normal isotherm which gives the multilayer adsorption only. Data for a normal nitrogen isotherm are summarized in Table I, as the number of statistical layers, n, adsorbed at given relative pressures. The n values were obtained by combining data for many powder samples at the lower relative pressures with Bowers' data[7] for a single sheet of metal foil at the high relative pressures where the powders might have some interparticle condensation. The values finally selected from the composite data were found to be in good agreement with those of Shull[8] in the relative pressure range below $0.95p_0$. They are lower than those previously used by the author,[9] which were based on isotherms that are now known to have considerable interparticle condensation.

After selecting composite n values these were tested by a Frenckel–Halsey–Hill plot, as has previously been done by Halsey[10] and by Bowers[7] for experimental isotherms of individual samples. It was found that all values from 0.20 to $0.99p_0$ fall on a straight line whose equation is

$$n^{2.75} = (V/V_m)^{2.75} = \frac{1.30}{\log p_0/p} = \frac{2.99}{\ln p_0/p} \qquad (2)$$

(7) R. Bowers, *Phil. Mag.*, [7] **44**, 4676 (1953).
(8) C. G. Shull, *J. Am. Chem. Soc.*, **70**, 1405 (1948).
(9) C. Pierce, THIS JOURNAL, **57**, 149 (1953).
(10) G. Halsey, *J. Chem. Phys.*, **16**, 931 (1948).

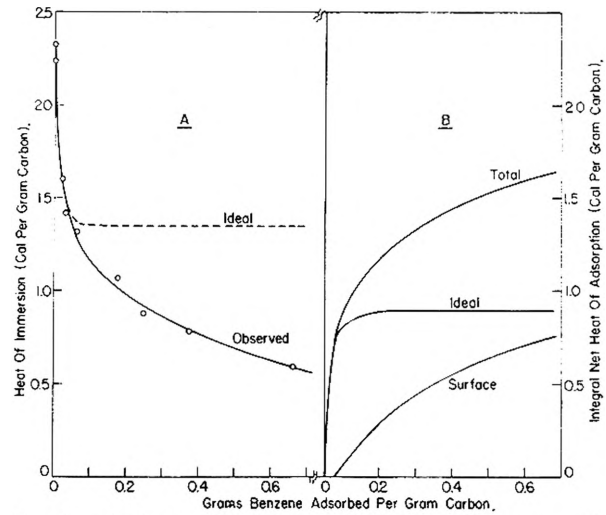

Fig. 1.—A, heat of immersion, graphite in benzene; B, integral net heat of adsorption, benzene on graphite.

TABLE I

COMPOSITE ISOTHERM FOR MULTILAYER ADSORPTION OF NITROGEN

p/p_0	No. of layers, n	p/p_0	No. of layers, n
0.20	1.25	0.80	2.58
.30	1.39	.85	2.90
.40	1.54	.90	3.35
.50	1.70	.925	3.80
.60	1.90	.950	4.40
.70	2.17	.975	5.70
.75	2.34	.990	7.85

Reasons for a fit by this equation below 2 statistical layers, where a given site must hold either 1 or 2 layers, have been suggested by Halsey.[10] Frenckel[11] and Hill[12] have given a general derivation applicable at higher relative pressure, but they use an exponent of 3. The experimentally determined value is 2.75.

Applications of the n values to many experimental isotherms has shown that the multilayer adsorption seems to be remarkably free of effects due to the specific solid used. This is shown in the data of Tables II and III and in Figs. 2, 3 and 4. The n values are found to fit isotherms for many surfaces, including carbon, metals, oxides and ionic crystals. They undoubtedly are true relative to one another, but it is possible that they are not true on an absolute basis, since they are for each sample relative to the volume assumed to fill the first layer.

It has been found that testing experimental isotherms by the n values yields useful information, some of it not previously attainable. Some of the applications are illustrated in the following sections.

1. Determination of V_m.—In general a BET plot for determination of V_m is based upon the isotherm values in the region 0.05 to $0.3p_0$. The n values may be used to calculate V_m independently. This is done by determining the ratio V/n for different relative pressures and taking the average value as V_m. Typical determinations are shown in Table

(11) J. Frenckel, "Kinetic Theory of Liquids," Oxford University Press, London, 1946.
(12) T. L. Hill, "Address in Catalysis," Vol. IV, Academic Press, New York, N. Y., 1932.

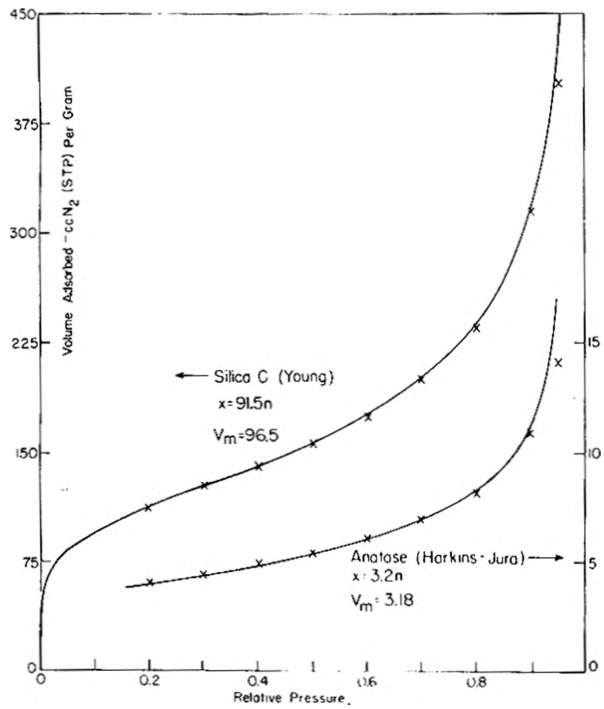

Fig. 2.—Isotherms for adsorption of nitrogen by powder samples. The crosses are computed by the n values of Table I: upper curve, Silica C data from Young[15]; lower curve, Harkins-Jura data for anatase.[5]

II, along with BET values for comparison. The V/n ratios, designated as V'_m, are averages for all relative pressures up to the start of interparticle condensation. It has been found in tests of several dozen isotherms that agreement between the BET value and V'_m is always within a few per cent.

TABLE II

DETERMINATION OF MONOLAYER ADSORPTION BY COMPARISON WITH STANDARD n VALUES

		V/n values from isotherm data, cc.				
p/p_0	n	a	b	c	d	e
0.20	1.25	1.07	0.87	3.12	26.4	91.5
.30	1.39	1.12	.87	3.20	27.0	91.5
.40	1.54	1.12	.89	3.18	27.3	91.5
.50	1.70	1.13	.90	3.24	27.4	91.5
.60	1.90	1.12	.89	3.25	27.7	91.5
.70	2.17	1.11	.88	3.22	(28.8)	93.0
.80	2.58	1.07	.86	3.25	(32.0)	94.5
.90	3.35	1.07	.84	3.25		93.0
.95	4.40	1.16	(.91)	(3.87)		
.975	5.70	(1.22)				
Av. (V_m)		1.11	0.875	3.21	27.2	92
V_m from BET plot		1.074	.872	3.18	27.6	96.5

[a] Catalyst, J. M. Holmes, private communication.[13] [b] Catalyst, J. M. Holmes, private communication.[13] [c] Anatase, Harkins and Jura.[5] [d] Spheron 6 pellets, Joyner and Emmett.[14] [e] SiO_2 powder, G. J. Young, private communication.[15]

2. Detection of Interparticle Condensation.—Deviations of type II isotherms from the normal n values at relative pressures above 0.7 may be due either to capillary condensation between particles or to condensation in large macro pores within particles. Usually when the latter effect is present the isotherm is type IV or V, but interparticle condensation may occur when the isotherm appears to be type II. The normal n values may, however, be used to show the existence of this effect. Isotherm values below $0.7p_0$ are used to compute V'_m, from the average V/n ratio as in Table II. The product nV'_m is then compared with experimental values at various relative pressures, as shown in Fig. 2 and Table III.

TABLE III

TEST OF EXPERIMENTAL ISOTHERMS FOR INTERPARTICLE CONDENSATION

	Obsd.[a]	$10.4n$	Obsd.[b]	$0.65n$	Obsd.[c]	$25.8n$	Obsd.[d]	$27.2n$
p/p_0	(μg. N_2)		(cc. N_2)		(cc. N_2)		(cc. N_2)	
0.20	13.0	13.0	0.76	0.79	32	33	33.0	34.0
.30	14.5	14.5	0.84	0.87	36	36	37.5	37.8
.40	15.8	16.0	0.94	0.97	39	40	42.0	42.0
.50	17.5	17.7	1.07	1.07	44	44	46.5	46.2
.60	19.8	19.8	1.23	1.20	49	49	52.5	51.7
.70	23.0	22.6	1.42	1.37	55	56	62.5	59.0
.80	27.5	26.6	1.68	1.60	64	66	82.7	70.2
.90	35.0	34.8	2.19	2.14	86	88		
.95	45.0	45.5			114	114		
.975					186	147		

[a] N_2 on aluminum foil, Bowers.[7] [b] N_2 on KCl crystals, J. M. Holmes, private communication.[13] No condensation below $0.9p_0$. [c] N_2 on carbon black, Andries Voet, private communication.[16] Condensation starts near $0.975p_0$. [d] Spheron 6, Joyner and Emmett.[14] Condensation begins near $0.7p_0$.

The two isotherms of Fig. 2 were selected to illustrate powders whose adsorption indicates little interparticle condensation. The silica sample[15] has an area near 400 m.²/g. but it is very fluffy and loosely packed. It begins to show interparticle condensation at $0.95p_0$. The anatase sample is the one used by Harkins and Jura,[5] one of the first powder isotherm studies carried to high relative pressure. Apparently some interparticle condensation starts above $0.9p_0$. The data of Table III indicate varying degrees of interparticle condensation.

3. Capillary Condensation in Porous Samples.—When most of the surface lies in pores the shapes of the isotherm indicate the disappearance of surface as pores fill. If the pores are small the isotherm is type I. Filling of large pores leads to type IV or type V isotherms. If, however, a sample has some micropores that fill at low relative pressure and extensive open surface outside of these pores, the isotherm may be type II. The n values may be used to interpret such isotherms. The isotherm for Carbolac I (Fig. 3) is an example of this situation. Carbolac I is a finely divided ink[4] black of nitrogen area about 1000 m.²/g., but with an electron microscope area of about 250 m.²/g. The discrepancy between the two values (a roughness factor of 4) leads to the belief that the particles contain small pores that fill at low relative pressure, so that the volume held in these pores is included in the V_m value. Analysis by the n values shows that this interpretation is correct and permits computa-

(13) J. M. Holmes, Carleton University, Ottawa, Canada.

(14) L. G. Joyner and P. H. Emmett, *J. Am. Chem. Soc.*, **70**, 2353 (1948).

(15) G. J. Young, College of Mineral Industries, The Pennsylvania State University. The sample is described in *J. Coll. Sci.*, **13**, 67 (1958). The isotherm indicates a very slight desorption hysteresis after equilibration at p_0.

(16) Andries Voet, J. M. Huber Corporation, Berger, Texas.

tion both of the volume held in the small pores and the free surface area not in these pores.

When there is adsorption both in small pores and in free surface outside of these pores we have the relation

$$\text{Volume adsorbed} = V_c + nV_m' \qquad (3)$$

where V_c is the gas volume held in the pores and V_m' is the volume to form a monolayer on free surface. Using the data of Emmett and Cines[17] we have

$$\text{at } 0.6p_0 \quad 340 \text{ cc.} = V_c + 1.90V_m'$$
$$\text{at } 0.2p_0 \quad 272 \text{ cc.} = V_c + 1.25V_m'$$

Solving, V_c = 142 cc. and V_m' = 104 cc. This gives an area of 460 m.²/g. outside of the small pores, a value in much better agreement with the electron microscope area than the uncorrected nitrogen area. A roughness factor of 1.8 would account for this difference. The values of V_c and V_m' are used to compute adsorptions at various relative pressures, Fig. 3. Good agreement is found up to $0.9p_0$ where apparently some interparticle condensation begins.

4. Packing in First Layer.—Graphitized carbon blacks[3] have been used extensively in adsorption studies, because they appear to have very uniform surfaces. Nitrogen isotherms for these blacks have an unusual shape, first noted by Joyner and Emmett,[14] with an abrupt rise between 0.25 and $0.4p_0$. In the past this rise has been attributed to lateral interaction in the second layer. An analysis of recent data[18] by using the n values suggests a different interpretation. When V/n ratios are computed a nearly constant value is obtained from 0.4 to $0.975p_0$ but from 0.2 to 0.4 the ratio is low. The nV_m' values fit experimental ones closely from 0.4 to $0.975p_0$ but are too high below $0.4p_0$, as shown by the crosses of Fig. 4. This suggests that perhaps the first layer is not packed to the same degree as in most nitrogen adsorption. V'_m is 1.78 cc. whereas V_m (BET) is 1.44 cc. If V'_m represents a true first layer value the area is 7.75 m.²/g. as compared with a BET area of 6.3 m.²/g. If these deductions are correct the rise between 0.25 and $0.4p_0$ indicates that added vapor is crowding into the first layer as the pressure is increased.

As might be expected from the particle size, over 5000 Å. in diameter, there is no detectable interparticle condensation for the sample of Fig. 4. The nV'_m values agree closely with experimental ones up to the highest pressure measured, $0.975p_0$.

Acknowledgments.—This research was supported in part by a grant from the Petroleum Research Fund administered by the American Chemical Society. Grateful acknowledgment is hereby made to the donors of this fund. We also wish to thank the Department of Chemistry, University of Chicago, for providing space and facilities for this work, W. R. Smith and W. B. Spencer of the Godfrey L. Cabot Co. for the samples used, T. F. Young for helpful comments and discussions, and G. J. Young, J. M. Holmes and Andries Voet for isotherm data.

(17) P. H. Emmett and M. Cines, THIS JOURNAL, **51**, 1329 (1947).
(18) J. M. Holmes and R. A. Beebe, *ibid*., **61**, 1684 (1957).

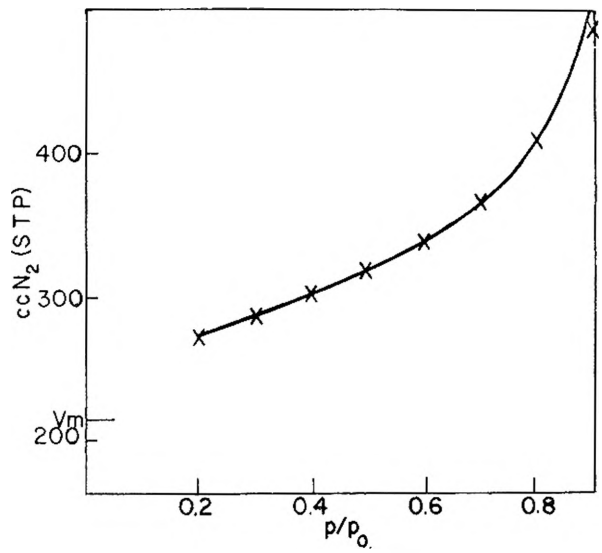

Fig. 3.—Analysis of isotherm for Carbolac I: solid line, data of Emmett and Cines[17]; crosses, computed from n values, with V_m' = 104 cc. (STP) and V_c = 142 cc. (STP).

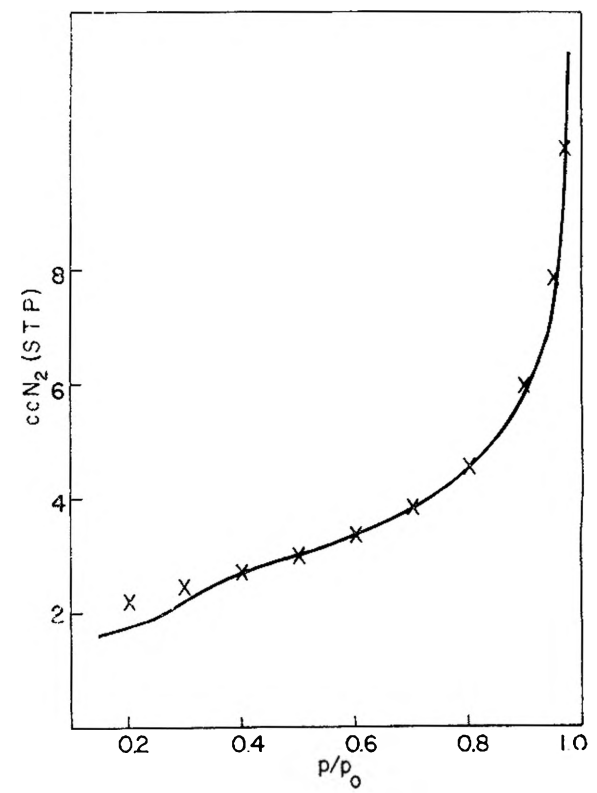

Fig. 4.—Analysis of isotherm for Sterling MT (3000°): solid line, data of Holmes and Beebe[18]; crosses, computed from n values.

MODEL CALCULATION OF THE TEMPERATURE DEPENDENCE OF SMALL MOLECULE DIFFUSION IN HIGH POLYMERS[1]

BY W. WILFRIED BRANDT[2]

Polytechnic Institute of Brooklyn, Brooklyn, N. Y.

Received November 3, 1958

An expression has been derived for the activation energy of small molecule diffusion in high polymers in terms of the intermolecular and intramolecular interactions and of the number of degrees of freedom involved in the molecular motion. The result has been used to calculate diffusion coefficients and their temperature dependence on the basis of Barrer's "zone" theory. The resulting Arrhenius activation energies are 30 to 75% of the experimental ones. The reason for this is discussed. The approach indicates that the change of the activation energy at the glass transition found experimentally in many polymers can be understood as a consequence of the change of the thermal expansion coefficient at this point. Certain details of molecular structure, such as the shape of the potential barrier of hindered rotation and the number of degrees of freedom per monomer unit, are found to have only a small effect on the resultant diffusion properties. The calculated effect of the penetrant molecule's size on the activation energy is in good agreement with experimental data.

Introduction

The diffusion of small molecules in solid high polymers is an activated process and is frequently described by the activation energy E_D appearing in an Arrhenius-type equation

$$D = D_0 \exp(-E_D/RT) \qquad (1)$$

where D is the diffusion coefficient, D_0 is a temperature independent frequency factor, and R and T have their usual meaning.

Several workers[3-6] found E_D to be an increasing function of the penetrant molecule's diameter, but to be nearly independent of the molecular structure of the penetrant.[7] This implies that E_D will be, after the penetrant size effect has been taken into account, a function of the high polymer molecular properties, such as the chain geometry or the chain stiffness and the intermolecular forces.

The relative effect of different structure variables, however, is unknown and is unlikely to be established by experiment alone since in comparing two polymers one has to realize that several or all conceivable structure parameters may be different.

Another complication of the relation between molecular structure variables and quantities like E_D, which are intended to describe the activated state, exists in that rate processes in polymers in general may proceed by various types of motion which are most sensitive to different structure variables. For example, certain diffusion "jumps" involving only very short chain segments are liable to impose a severe strain in these segments and their chance of occurring will be controlled by the chain stiffness. Conversely the frequency of diffusion jumps involving long segments of the polymer chains will largely depend on how well the different parts of a long segment will coöperate to allow the required rearrangement.

Eyring's[8] and Wilkens'[9] theories of diffusion do not account for the presence of different segment lengths while the so-called "zone" theory of Barrer[6] does. In none of these theories has an attempt been made to estimate the activation energy from a consideration of the molecular structure.

In this work a simple molecular model will be defined and its consequences will be examined on the basis of Barrer's theory. Although the molecular model used is probably not the only one possible, it will be interesting to compare the predictions of the model calculations with experimental results so as to gain insight into which molecular structure parameters are of prime importance to the diffusion mechanism of small molecules in high polymers.

Description of the Molecular Model Used.—The molecular model to be used in this work is best described by listing the assumptions which will enter the formal development of the next section.

1. The activated state is taken to involve two polymer chains which have moved apart to permit the passage of the penetrant molecule (Fig. 1a). It is of little consequence whether the chains are thought to be originally exactly parallel or only approximately so.

2. The activation energy is assumed to consist of two contributions (a and b):

a. An intermolecular term due to the repulsion the bent molecular chains will experience from their neighbors on making room for the penetrant molecule. The internal pressure will be taken as a measure of this repulsion, since it is readily available from various experimental data.

b. An intramolecular term due to the resistance of the molecular chains to bending. Since bond distances and bond angles are changed only with difficulty it is assumed that the bending of chains involves a partial rotation of chain units out of their equilibrium position against a hindering potential of internal rotation.

3. The molecular motions which lead to the activated state shown in Fig. 1 are assumed to involve the partial rotation of each backbone chain unit against the hindering potential, such that the total torsional strain is distributed evenly over the entire segment.

4. The number of degrees of freedom found in a

(1) The paper is in part evolved from the author's doctoral dissertation, Polytechnic Institute of Brooklyn, 1956.

(2) Polychemicals Department, E. I. du Pont de Nemours & Co., Inc., Du Pont Experimental Station, Wilmington, Delaware.

(3) G. J. van Amerongen, *J. Polymer Sci.*, **5**, 307 (1949).

(4) (a) S. N. Zhurkov and G. Ya. Ryskin, *J. Tech. Phys.* (*U.S.S.R.*), **24**, 797 (1954); (b) G. Ya. Ryskin, *ibid.*, **25**, 458 (1955).

(5) P. Meares, *Trans. Faraday Soc.*, **53**, 101 (1957).

(6) R. M. Barrer, THIS JOURNAL, **61**, 178 (1957) and references given there.

(7) F. A. Long, Lecture at the Nat. Bur. Standards, Washington, D. C., March, 1958.

(8) S. Glasstone, K. J. Laidler and H. Eyring, "The Theory of Rate Processes," McGraw-Hill Book Co., Inc., New York, N. Y., 1941.

(9) J. B. Wilkens, Dissertation, Cornell, 1957.

segment of the chain is assumed to be proportional to the segment length.

5. The probability that the f degrees of freedom contained in a segment will coöperate in a diffusion step is $\rho_f = (1/m)^f$. m will be taken equal to 2 in most of this work. This may be plausible since a rotation against a hindering potential may proceed in two different directions,[6] and since the degrees of freedom connected to such motions are thought to be the only ones of interest.

Formal Treatment.—Barrer's[6] theory leads to an expression for the diffusion coefficient D

$$D = \frac{\nu}{2} d^2 \sum_{f=1}^{f_{max}} \rho_f [(E/RT)^{f-1} \{(f-1)!\}^{-1}] \exp(-E/RT) \quad (2)$$

where ν is the thermal vibration frequency of the penetrant molecule, d is the jump distance, f is the number of degrees of freedom involved in a particular motion, f_{max} is the value of f for which the expression in square brackets has a maximum, and E is the total energy of the activated "zone" under consideration. The term $\exp(-E/RT)$ is the probability that the total energy E is available at the temperature T. The expression in the square bracket gives the probability that the energy E is distributed over f degrees of freedom, and ρ_f, the probability of f degrees to coöperate, is the quantity mentioned in assumption 5 of the last section. Barrer[10] assumed that one of the terms of the sum is sufficiently large to permit the neglect of all other terms. In this work it will be shown that this simplification is unwarranted, and also that E is strongly dependent on f which necessitates a numerical evaluation of the sum of equation 2.

The total energy found within f degrees of freedom can, on the assumptions (1) and (2) of the last section, be expressed as

$$E = E_i + E_b + E_{th} \quad (3)$$

where E_i is the intermolecular term, E_b is the intramolecular term, and E_{th} is the thermal energy which is not part of the activation energy but of the total energy. E_i, E_b and E_{th} will now be expressed in terms of f and other molecular parameters.

The intermolecular contribution to the activation energy E_i will be taken to be the product of the volume that has to be swept out by the molecular chains if they are to allow the diffusing molecule between them, ΔV, and of $(\partial U/\partial V)_T$, where U is the internal energy and V is the volume. $(\partial U/\partial V)_T$ and $T(\partial p/\partial T)_V$ are very large compared to the external pressure, p.[11] Consequently, one can write

$$E_i = \left(\frac{\partial U}{\partial V}\right)_T \Delta V = \left[T\left(\frac{\partial p}{\partial T}\right)_V - p\right] \Delta V \backsimeq T\left(\frac{\partial p}{\partial T}\right)_V \Delta V = P_i \Delta V \quad (4)$$

where P_i is the internal pressure which by definition is equal to $T(\partial p/\partial T)_V$. ΔV can be expressed approximately in terms of the molecular dimensions by reference to Fig. 2. One finds

$$\Delta V = 4 \frac{\overline{AB} \times \overline{BE}}{2} \sigma_c N$$

(10) R. M. Barrer, *Trans. Faraday Soc.*, **39**, 237 (1943).

(11) F. C. Collins, W. W. Brandt and M. H. Navidi, *J. Chem. Phys.*, **25**, 581 (1956).

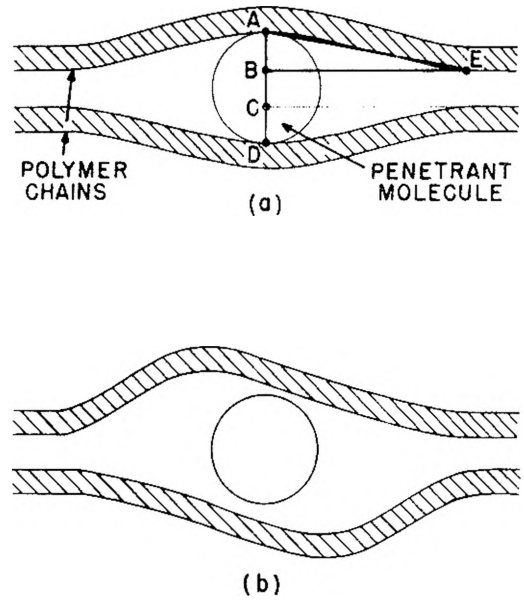

Fig. 1.—(a) Symmetrical model for the activated state used in calculation; (b) unsymmetrical model (see text).

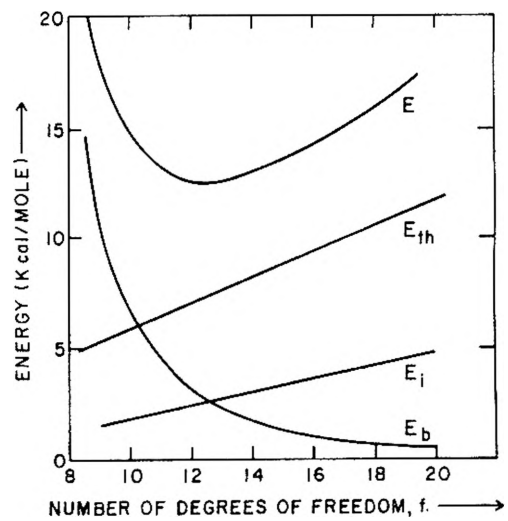

Fig. 2.—The total energy E and its components E_i, E_b and E_{th} as a function of the number of degrees of freedom f (case 2 of Table I).

where σ_c is the average diameter of the high polymer molecules, and N is Avogadro's number. Setting

$\overline{AE}$ = $s/2$, where s is the segment length

$\overline{AD}$ = σ_p, the penetrant molecule's diameter and

$\overline{BC}$ = $\frac{1}{2}\varphi^{1/2}$, with φ as defined below, one obtains

$$\Delta V = 2\,\overline{AB} \times \overline{BE} \times \sigma_c \times N$$
$$= 2\,\overline{AB}^2(\overline{AE}^2 \times \overline{AB}^{-2} - 1)^{1/2} \quad \sigma_c N$$
$$\Delta V = \tfrac{1}{2}(\sigma_p - \varphi^{1/2}/2)^2[(s^2/(\sigma_p - \varphi^{1/2}/2)^2 - 1)]^{1/2}\,\sigma_c N$$

φ is the free volume per unit length of the chain molecule and can be calculated as the free volume per repeat unit divided by the length of the repeat unit in the direction of the chain axis. Thus φ is actually a "free area" and its square root is approximately equal to the linear distance perpendicular to the chain axis through which a chain may move freely.

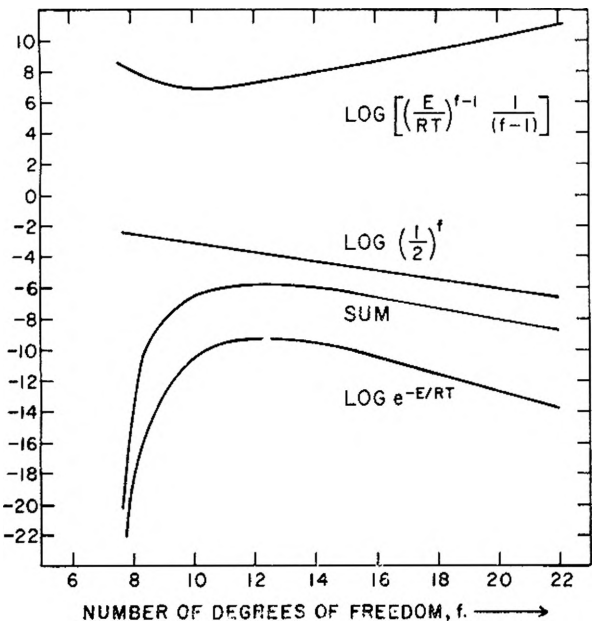

Fig. 3.—The terms of the sum of equation 2 and the factors contained in these terms (on a logarithmic scale) against the number of degrees of freedom f (case 2 of Table I).

The intramolecular contribution to the activation energy E_b is considered to arise from the bending of two molecular chains over the segment length s such that the number of backbone chain bonds which are distorted is equal to $2s/\lambda$, where λ is the length of one backbone chain bond measured along the chain axis. The angle $\delta = <AEB$ divided by the number of backbone chain bonds per half segment, is taken as an approximation of the average angle of rotation ϑ against the hindering potential, $V(\vartheta)$, which each bond within the segment has to sustain when this segment is bent. This approximation is most accurate for small values of the angle ϑ. One gets $\vartheta = \delta \times 2\lambda/s$. The potential of hindered rotation $V(\vartheta)$ is taken to be[12]

$$V(\vartheta) = \frac{V_0}{2}(1 - \cos 3\vartheta) = \frac{V_0}{2}(1 - \cos 6\delta\lambda/s)$$

Also, for relatively small values of ϑ one can approximate the potential well of hindered rotation by a parabola, hence

$$V(\vartheta) = \frac{V_0}{2} \times \frac{1}{2}(6\delta\lambda/s)^2 = 9V_0\delta^2\lambda^2/s^2$$

Finally, on approximating δ^2 by $\tan^2\delta$

$$\delta^2 = \left(\sigma_p - \frac{\varphi^{1/2}}{2}\right)^2 \Big/ \left(s^2 - \left(\sigma_p - \frac{\varphi^{1/2}}{2}\right)^2\right)$$
$$= \left(s^2 \Big/ \left(\sigma_p - \frac{\varphi^{1/2}}{2}\right)^2 - 1\right)^{-1}$$

and

$$V(\vartheta) = 9V_0\delta^2\lambda^2/s^2$$
$$= 9V_0\lambda^2 s^{-2}\left(s^2 \Big/ \left(\sigma_p - \frac{\varphi^{1/2}}{2}\right)^2 - 1\right)^{-1} \quad (5)$$

The intramolecular strain energy in the two polymer molecules which moved apart is then

$$E_b = 2s\lambda^{-1}V(\vartheta)$$
$$= 18V_0\lambda s^{-1}(s^2/(\sigma_p - \varphi^{1/2}/2)^2 - 1)^{-1} \quad (6)$$

(12) S. Mizushima, "Structure of Molecules and Internal Rotation," Academic Press, New York, N. Y., 1954.

Both E_i and E_b are seen to involve s, the segment length, and this must be expressed in terms of the number of degrees of freedom involved in the motion such that the summation of equation 1 can be carried out. This is accomplished by setting, according to assumption 4

$$f = 2s\lambda^{-1}z \quad (7)$$

where z is a proportionality constant which represents the number of degrees of freedom associated with one backbone chain bond. In most of the calculations to follow $z = 1$. This estimate is shown to be reasonable in Appendix I.

The thermal energy stored in f degrees of freedom will be taken to be

$$E_{th} = fRT \quad (8)$$

Inserting equation 5 into equation 4, equation 7 into equations 4 and 6, and equations 4, 6 and 8 into equation 3, one obtains

$$E = E_i + E_b + E_{th}$$
$$= {}^1/_2(\sigma_p - \varphi^{1/2}/2)^2[\{f\lambda/2z(\sigma_p - \varphi^{1/2}/2)\}^2 - 1]^{1/2}\sigma_c NP_i$$
$$+ 36V_0 f^{-1}[\{f\lambda/2z(\sigma_p - \varphi^{1/2}/2)\}^2 - 1]^{-1} + fRT \quad (9)$$

Summary of the Results.—The total energy E is plotted in Fig. 2 against the number of degrees of freedom involved in the diffusion jump f for a typical case. E_b is very high for small values of f (short segments), while E_i increases steadily as f becomes larger. Consequently the quantity $(E_b + E_i)$ which is the activation energy, has a distinct minimum at an intermediate number of degrees of freedom, f_{min} which in this case is 16. Figure 3 shows the terms $e^{-E/RT}$, $[(E/RT)^{f-1}/(f-1)!]$ and $\rho_f = (1/2)^f$ on a logarithmic scale plotted against f. The sum of these curves is also shown and it is obvious that several terms of the sum in equation 2 are of nearly the same magnitude. Table I summarizes the results of a series of calculations. Cases 1, 2 and 3 may be considered the standard results. The other cases are generated by assuming different values for the internal pressure, the factor $\rho_f^{1/f}$, the thermal expansion coefficient α the number of degrees of freedom per backbone chain bond z, the constant V_0 measuring the chain stiffness, the chain thickness σ_c and the penetrant molecule's diameter, σ_p.

Discussion

The values of $2D/\nu d^2$ obtained in these calculations according to equation 2 are listed in Table I and have been used to derive apparent activation energies E_D from Arrhenius' equation 1. It is this quantity and its calculated dependence on molecular structure variables which will be discussed in relation to experimental data found in the literature.

The E_D values obtained (Table I) are all too low by about 25 to 70%. The data chosen in most cases (that is, cases 1 to 9 and 11 to 16) would be appropriate to the diffusion of ethane in polyethylene for which the experimental value of E_D is 13.3 kcal./mole.[13] One reason for this may be that the molecular motions chosen as a basis for these calculations and shown schematically in Fig. 1a are not the only ones leading to successful diffu-

(13) W. W. Brandt, *J. Polymer Sci.*, to be published.

TABLE I

SUMMARY OF RESULTS

Case	T (°K.)	P_i (atm.)	$\rho_f^{1/f}$	$a \times 10^3$ (deg.$^{-1}$)	z	V_0 (cal./mole)	σ_c (Å.)	σ_D (Å.)	$(E_b + E_i)_{min}$ (cal./mole)	f_{min}	f_{opt}	$\frac{2D}{\nu d^2}$	E_D (cal./mole)
1	273	3375[a]	1/2[c]	0.772[d]	1[e]	2750[f]	4.07[h]	5.08[k]	4940	16	12	2.92×10^{-6}	3790
2	298	3250[a]	1/2	.772[d]	1	2750	4.07	5.08	4730	16	12	5.27×10^{-6}	3930
3	323	3125[a]	1/2	.772[d]	1	2750	4.07	5.08	4520	16	12	8.81×10^{-6}	
4	273	6760[b]	1/2	.772[d]	1	2750	4.07	5.08	8240	13–14	12	0.170×10^{-6}	10580
5	298	5770[b]	1/2	.772[d]	1	2750	4.07	5.08	7220	14	12	$.890 \times 10^{-6}$	9180
6	323	4970[b]	1/2	.772[d]	1	2750	4.07	5.08	6390	14–15	12	2.94×10^{-6}	
7	273	3375[a]	1[g]	.772[d]	1	2750	4.07	5.08	4940	16	18		
8	298	3250[a]	1	.772[d]	1	2750	4.07	5.08	4730	16	17		
9	323	3125[a]	1	.772[d]	1	2750	4.07	5.08	4520	16	16		
10	273	3315	1/2[c]	0.355[e]	1	2750	4.07	5.08	4840	16	12	3.23×10^{-6}	3140[m]
11	298	3250	1/2	.772	0.75[g]	2750	4.07	5.08	4730	12	10	2.44×10^{-5}	4180
12	323	3125	1/2	.772	.75	2750	4.07	5.08	4520	12	9	4.22×10^{-5}	
13	298	3250	1/2	.772	1	5500[g]	4.07	5.08	5660	19	14	0.87×10^{-6}	4280
14	323	3125	1/2	.772	1	5500	4.07	5.08	5410	19	14	1.57×10^{-6}	
15	298	3250	1/2	.772	1	2750	4.63[i]	5.08	5230	15	12	3.93×10^{-6}	4260
16	323	3125	1/2	.772	1	2750	4.63	5.08	4990	15	12	6.86×10^{-6}	
17	298	3250	1/2	.772	1	2750	4.07	7.45[l]	8320	19	16	4.09×10^{-8}	6710
18	323	3125[a]	1/2[a]	.772	1	2750	4.07	7.45	7990	19	16	9.08×10^{-8}	

[a] Assuming $P_i = 3250$ atm. at 25°, see J. M. Lupton A.C.S. Meeting, Chicago, Sept. 1958, and $P_i \propto v^{-2}$ where v is the molecular volume. See J. Hildebrand and R. L. Scott, "The Solubility of Nonelectrolytes," Reinhold Publ. Corp., New York, N. Y., 1950, p. 97. [b] Reference (11), for volume data see ref. *a*, for specific heats see B. Wunderlich, M. Dole, *J. Polymer Sci.*, 24, 201 (1957), for sonic velocity data see S. P. Kabin, *Sov. Phys. Tech. Phys.*, 26, 2542 (1956), and Yo. Maeda, *Chem. High Pol. (Japan)*, 14, 442 (1957). [c] Estimated values, $\rho_f = 1/2$ from assumption (3) and ref. 6, $z = 1$ from Appendix I. [d] H. A. Stuart, "Die Physik der Hochpolymeren," Vol. III, Springer, Berlin, 1955, p. 264. Value for polyethylene above the glass transition. [e] Same as *d* but for temperatures below transition. [f] Reference 12, p. 68, value for ethane. [g] Arbitrary. [h] Calculated from $\sigma_c = [(v_{CH_2}/\lambda)(v_0/v)]$ where v_{CH_2} is volume per CH_2 group, λ is length of backbone C–C bond projected on chain axis, v the specific vol. at 25°, v_0 the extrapolated specific volume at °K. [i] Calculated from $\sigma_c = (v_{C_6H_6}/\lambda)$. [k] Ref. *d*, Vol. I, p. 89, value for ethane. [l] Same as ref. *k*, value for benzene. [m] E_D calculated from cases 2 and 10.

sion jumps. For example, if two molecules were to move apart in an unsymmetrical fashion (Fig. 1b) rather than symmetrically as assumed in the calculations of Table I, then E_i, E_b and E_D would be larger. The difficulty of counting the various possible motions prevents this refinement of the molecular model used for the present.

Another reason for the low E_D values obtained lies in the fact that the internal pressure as obtained from PVT data (ref. *a* of Table I) is a very low value; it is the value that would pertain if the chain molecules were to move apart very slowly, that is, over a period of a few hours. Since the diffusion event occurs on a much smaller time scale one should use a higher estimate of the (average) internal pressure to calculate E_i. In cases 4, 5 and 6 such a higher estimate as suggested by Collins, *et al.*,[11] has been used and it is to be noted that the resulting E_D is much closer to, but still lower than, the experimental value of about 13 kcal./mole.

The segment length which contributes most to the diffusion coefficient is given by $s_{opt} = f_{opt}\lambda/2z$, where f_{opt} and z are listed in Table I. The relatively low values obtained for s_{opt} (6 to 8 chain units long) in all these calculations are in agreement with the experimental result that D is independent of the polymer molecular weight and long chain branching.[13] Small molecule diffusion may thus be considered to proceed predominantly by short range motions.

In spite of this qualitative agreement little weight may be attached to the actual values of f_{opt}, since cases 7, 8 and 9 show them to be strongly dependent on the factor $\rho_f^{1/f}$. If one were to include the unsymmetrical motions which may be present (Fig. 1b) in these calculations, then one might also have to account for the fact that the number of possible chain contortions increases with the number of degrees of freedom present. This might be accomplished by introducing a factor of the form $\tau_f = n^f$, where n is a constant. τ_f and ρ_f are, for the present, inseparable and unknown. It is noteworthy that E_D itself is affected only slightly by the change in ρ_f or τ_f as used in cases 7, 8 and 9.

It is very interesting to investigate the effect of a glass transition on the activation energy E_D. Case 10 has been calculated by assuming that the polymer, unlike real polyethylene, has a sharp glass transition at 298°, resulting in a lower thermal expansion coefficient and temperature coefficient of the internal pressure below this temperature. The activation energy derived from cases 10 and 2 is indeed lower than that from cases 1 and 2 which is in qualitative agreement with experimental data for several branched polymers listed in Table II. If unsymmetrical motions had been included in these calculations, $(E_i + E_b)$ would have assumed larger values, thus bringing the change in E_D at the glass transition more in line with that assumed for the thermal expansion coefficient at this point. Implicit in assumption (3) made earlier is the neglect of internal rotation as contributing to the diffusion process. This neglect appears to be justified because an activation energy which is in part due to the passage of rotational barriers will be even less dependent on the free volume and on the thermal ex-

pansion coefficient than the one calculated here. The model defined in this work would predict essential constancy of $(E_i + E_b)$ and therefore of E_D in passing a glass transition under constant volume conditions. Also there appears to be no significant change of the optimum segment length in agreement with the fact that D itself does not change abruptly near the glass transition.

TABLE II

EFFECT OF GLASS TRANSITION ON THERMAL EXPANSION COEFFICIENTS AND ACTIVATION ENERGIES

$\alpha>$ and $\alpha<$ are the thermal expansion coefficient above and below glass transition. $E_{D>}$ and $E_{D<}$ are the activation energies for the diffusion of methanol above and below the glass transition.

Polymer	$\alpha>/\alpha<$	$E_{D>}/E_{D<}$	$\frac{\alpha>/\alpha<}{E_{D>}/E_{D<}}$
Polymethyl methacrylate	2.14[a]	1.74[b]	1.23
Polymethyl methacrylate	1.96[a]	1.53[b]	1.28
Poly-*n*-butyl methacrylate	1.61[a]	1.30[b]	1.23
Polystyrene	2.27[c]	1.80[b]	1.26
Calculations Cases 1, 2, 10	2.17	1.21	1.79

[a] S. S. Rogers and L. Mandelkern, THIS JOURNAL, 61, 985 (1957). [b] Reference 4, values for methanol. [c] R. N. Work, *J. Appl. Phys.*, 27, 69 (1956).

Next the constant z requires discussion. Cases 11 and 12 show the activation energies and the segment lengths to be affected only slightly by a change in z. The optimum number of degrees of freedom, however, is changed. In the Appendix, it will be shown that the values selected for z are quite reasonable.

The chain stiffness is described in this model by z and V_0. The latter quantity is essentially a measure of the narrowness of the potential well of hindered rotation. Yet the cases 13 and 14 show that E_D is affected only slightly by a change; s, however, appears to be larger for such a stiff molecule.

The polymer chain thickness σ_c is varied in cases 15 and 16 with respect to the standard cases 2 and 3. The effect on E_D is small, that on f_{opt} is negligible.

The penetrant molecule's diameter σ_p is seen to affect the apparent activation energy quite strongly (cases 17 and 18 of Table I). This is in accord with the experimental findings of van Amerongen[3] and of Ryskin.[4]

TABLE III

CALCULATION OF THE PARAMETER z FROM THE FREE VOLUME EQUATION OF STATE (SEE APPENDIX I)

	kT/P_i[a] (Å.^{3})	v_0[b] (Å.^{3})	v (Å.^{3})	z
n-Pentane	23.4	137.6	191.3	1.07
n-Heptane	21.6	183.8	243.1	1.08
n-Nonane	21.4	230.2	296.9	1.06
n-Hexadecane	22.9	392.8	486.4	0.92

[a] From ultrasonic data, ref. (11). [b] See ref. (14).

Appendix I

It is of interest to estimate the number of degrees of freedom per backbone chain bond z by an independent method. The degrees of freedom in question are those which are responsible for the existence of the internal pressure in the high polymer and they are assumed to be those connected to the internal rotation.

The free volume equation of state can be written as

$$\frac{kT}{P_i} = \left[1 - \left(\frac{v_0}{v}\right)^{1/3}\right] v \qquad (10)$$

where v_0 is the "incompressible volume" and the other quantities have been defined previously. Taking now for v that volume which is associated with three degrees of freedom, that is, setting

$$v = \frac{3}{z} v_m$$

where v_m is the volume per chain bond length, one gets

$$z = \left[1 - \left(\frac{v_0}{v}\right)^{1/3}\right] v_m 3 \frac{P_i}{kT}$$

The free volume is given by

$$v_f = \frac{4\pi}{3}\left[1 - \left(\frac{v_0}{v}\right)^{1/3}\right]^3 v = (v - v_0)$$

leading to

$$z = \left(\frac{v - v_0}{v}\frac{3}{4\pi}\right)^{1/3} v_m 3 \frac{P_i}{kT}$$

Table III shows values of z calculated for some lower hydrocarbons. It is seen that z is indeed of the order of unity.

(14) A. K. Doolittle, *J. Appl. Phys.*, **22**, 1471 (1951).

THE KINETICS OF ADSORPTION OF ORGANIC ACIDS AT THE WATER-AIR INTERFACE[1]

BY ROBERT S. HANSEN AND TERRY C. WALLACE

Institute for Atomic Research and Department of Chemistry, Iowa State College, Ames, Iowa. Contribution No. 676. Work was performed in the Ames Laboratory of the U. S. Atomic Energy Commission

Received November 5, 1958

The vibrating jet method with theory modified for non-uniform velocity profile is applied to determination of dependence of surface tensions of aqueous solutions of pentanoic acid, heptanoic acid, octanoic acid and heptanol-1 on concentration and time. Results are independent of orifice and flow rate for orifices designed to permit the necessary theoretical treatment, and extrapolate uniformly to results obtained by Addison for decanoic acid, and Dervichian for hendecanoic acid, by conventional surface tension methods. Where π is the spreading pressure at time t, and π_∞ the equilibrium spreading pressure, the empirical equation 4 was found to represent well the data obtained in the present work as well as the data of Addison and Dervichian. No mechanism of adsorption could be devised leading explicitly to this relation. Observed rates of surface tension depression in the systems studied were too slow to correspond to diffusion controlled mechanisms, but could be well represented by a second-order kinetic mechanism implying a dimeric transition state located substantially in the surface film. Equations based on this model are derived and shown to agree well with experimental results.

Introduction

A number of workers have studied the time dependence of the surface tension of aqueous solutions of surface active organic compounds for nearly new surfaces and have suggested kinetic explanations for their observations. Bond and Puls,[2] obtaining results by vibrating jet and sheet methods, proposed a theory for their explanation based on diffusion-limited kinetics. Boutaric and Berthier[3a] studied the time dependence of the surface tension of aqueous saponin solutions using the ring method and expressed their results in a form suggesting first-order kinetics[3b] rather than diffusion limited kinetics. Additional evidence for diffusion limited kinetics in the depression of the surface tension of aqueous solution has been furnished by Addison,[4] Burcik[5] and Ross[6] with results in each case obtained by the vibrating jet method.

It is somewhat remarkable that the bulk of the evidence for the diffusion-limited mechanism of surface tension depression has been obtained by the vibrating jet method. On the contrary, evidence obtained by conventional surface tension methods (drop weight, Wilhelmy plate) in systems showing relatively slow rates of surface tension depression such as aqueous solutions of decanoic acid and hendecanoic acid studied by Addison[7] and Dervichian,[8] respectively, agree poorly with a diffusion-limited adsorption model. Finally, critical theoretical studies of the adsorption mechanism by Ward and Tordai[9] and by Sutherland[10] contraindicate diffusion controlled mechanisms of surface tension depression in systems so far studied.

Recent work in this Laboratory[11] has demonstrated that the surface age near the orifice in a vibrating jet system is markedly greater than the quotient of axial distance from the orifice by mean stream velocity, and has presented an accurate method for deriving surface ages. An approximate treatment of this problem had been presented earlier by Sutherland and Rideal.[12] We have also shown that the surface tension near the orifice cannot be calculated by Rayleigh's formula because of the non-uniform velocity profile and have presented a method for its correct calculation.

The purposes of the present work are twofold: first, to demonstrate that meaningful results for time dependent surface tensions can be obtained by the vibrating jet method if correctly applied, and that these results are concordant with those obtained by other methods; and second, to present a kinetic mechanism adequate for representation of data obtained by us and by others for similar systems.

Experimental

The following reagents were used in this investigation: distilled water redistilled from alkaline permanganate solution; pentanoic acid, heptanoic acid, octanoic acid and heptanol-1, in each case center fractions from the distillation of the corresponding Eastman best grade reagent through a 30-plate Oldershaw column at a reflux ratio in excess of 10:1; methanol, ethanol and butanol-2 central fractions from a similar distillation of Baker and Adamson reagent grade absolute methanol, Commercial Solvents Gold Shield absolute ethanol, and Eastman best grade butanol-2 after purification by the method of Lund and Bjerrum.[13] The apparatus and experimental procedure have been described previously[11] except that a thermometer was placed at the constant level reservoir exit. Orifices used are described in Table I. Surface tensions were calculated from observed

TABLE I

Orifice	Major radius (cm.)	Minor radius (cm.)	Mean radius (cm.)	Length (cm.)
D	0.0501	0.0445	0.0472	0.890
E	.0508	.0474	.0491	.648
F	.0513	.0481	.0495	.646

wave length and flow rate from the formula developed in our previous work,[11] namely

(1) Based in part on a dissertation submitted by Terry C. Wallace to the Graduate School at Iowa State College in partial fulfillment of the requirements for the degree of Doctor of Philosophy, Sept. 1958.

(2) W. N. Bond and H. O. Puls, *Phil. Mag.*, Seventh Series, **24**, 864 (1937).

(3) (a) A. Boutaric and P. Berthier, *J. chim. phys.*, **36**, 1 (1939); (b) A. Dognon and L. Gougerot, *ibid.*, **40**, 127 (1943).

(4) C. C. Addison, *J. Chem. Soc.*, 535 (1943); 252, 477 (1944); 98 (1945).

(5) E. J. Burcik, *J. Colloid Sci.*, **5** 421 (1950); **8**, 520 (1953).

(6) S. Ross and R. M. Haak, 32nd National Colloid Symposium, Urbana, Ill., June 19–21, 1958; THIS JOURNAL, **62**, 1260 (1958).

(7) C. C. Addison, *J. Chem. Soc.* 579 (1946).

(8) D. G. Dervichian, *Kolloid-Z.*, **146**, 96 (1956).

(9) A. F. H. Ward and L. Tordai, *J. Chem. Phys.*, **14**, 453 (1946).

(10) K. Sutherland, *Australian J. Sci. Research Ser.*, **A5**, 683 (1952).

(11) R. S. Hansen, M. E. Purchase, T. C. Wallace and R. W. Woody, THIS JOURNAL, **62**, 210 (1958).

(12) E. K. Rideal and K. L. Sutherland, *Trans. Faraday Soc.*, **48**, 1109 (1952).

(13) H. Lund and J. Bjerrum, *Ber.*, **94**, 149 (1920).

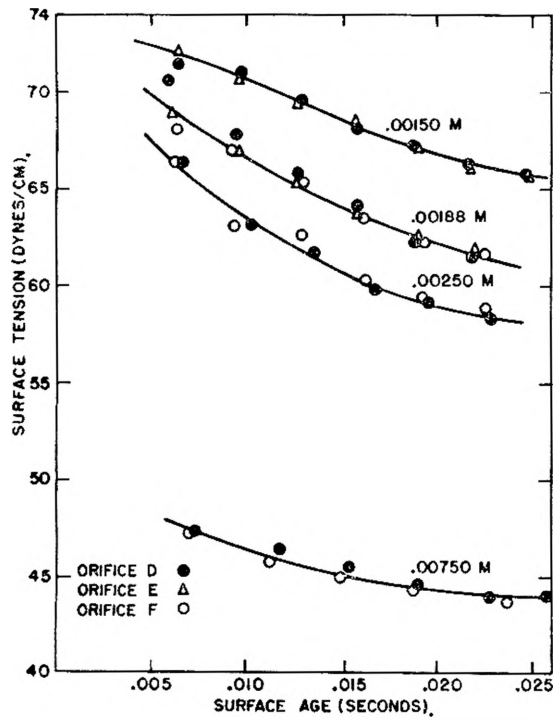

Fig. 1.—Dependence of surface tension of aqueous heptanoic acid solutions on concentration and time as determined with different orifices.

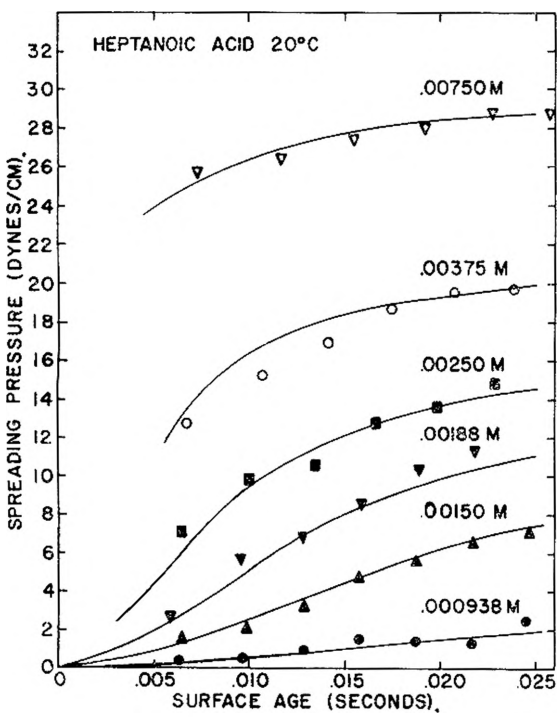

Fig. 2.—Dependence of spreading pressure of aqueous heptanoic acid solutions on concentration and time. Curves are from eq. 4, points are experimental.

$$\gamma = \gamma_a\{V(1, Z)\}^n \qquad (1)$$

where γ is the true surface tension and γ_a the apparent surface tension given by

$$\gamma_a = \frac{\rho k^2 v^2 r^3}{6}\left\{1 - \frac{5}{12}k^2r^2 + \frac{85}{576}k^4r^4 + 2\left(\frac{2\mu}{\rho v k r^2}\right)^{3/2} + 3\left(\frac{2\mu}{\rho v k r^2}\right)^2 + \frac{37}{24}\left(\frac{b}{r}\right)^2\right\} \qquad (2)$$

In equation 2, $k = 2\pi/\lambda$, λ is the wave length, v the mean velocity, r the jet radius, μ the viscosity, b the jet amplitude and ρ the liquid density. $V(1,Z)$ is the ratio of surface to mean stream velocity whose dependence on the dimensionless group $Z = \mu z/\rho v r^2$, where z is the axial distance from the orifice, has been established. In a vertical stream such as those used in the present work the stream radius changes slightly with distance from the orifice; a simple hydrodynamic treatment of this effect[11] leads to a prediction of a variation of the leading term v^2r^3 in equation 2 by a factor $(1 + 2gz/v_0^2)^{1/4}$ with distance z from the orifice. Accurate measurements of stream diameter over the range of measurement indicated, however, that the actual variation amounted to a factor $(1 + 2gz/v_0^2)^{1/2}$, or about twice the expected variation; we have used the observed variation in treating our data rather than the predicted one and are unable to explain the discrepancy. The correction is in any event small. Surface ages were calculated as previously described,[11] with modification for the acceleration of gravity. Thus if z_i were the ideal axial distance at surface age t, the actual axial distance z_a will be

$$z_a = z_i + \frac{1}{2}gt^2 \qquad (3)$$

Assuming $z_i = z_a$, a first approximation to t is obtained and used to obtain a corrected z_i from observed z_a by means of eq. 3. A second approximation to t is obtained from the corrected z_i, and the process iterated to convergence. (The second approximation was usually adequate.)

At very low discharge rates the liquid issuing from the orifice tended to wet the face of the orifice, so that a frustum was formed whose base was about half again the diameter of the orifice and which extended about 2 mm. down the jet. Talcum powder deposited on this frustum tended to remain there, showing that the liquid surface was stagnant there. When the face of the orifice was painted with Beckman "Desicote," a silicone based water repellent, the frustum was eliminated. Validity of application of our theoretical treatment[11] to the Desicoted orifices was demonstrated by repeating the experiments therein described with these orifices; water, methanol, ethanol and 2-butanol were used to test orifice D, and water to compare orifices D, E and F. Equation 1 was found to represent data obtained with Desicoted orifices excellently, the value of n obtained (0.645 ± 0.015) agreeing within experimental error with the value obtained for untreated orifices (0.650 ± 0.013). The Desicoted orifices therefore were used throughout the remainder of this research.

Solution temperatures were measured before and after the solution had passed through the orifice and did not differ by more than 0.2°.

The dependence of surface tension of aqueous solutions of heptanoic acid on time and concentration was investigated using orifices D, E and F and solutions of four different concentrations at 20°. Similar measurements at this same temperature were made for heptanol-1 solutions of six different concentrations, octanoic acid solutions of three different concentrations and pentanoic acid solutions of two different concentrations.

Results

Dependence of spreading pressure (surface tension of solvent less surface tension of solution) on concentration and time was found to be well represented, for all systems studied in this work, by the empirical equation

$$\frac{\pi}{\pi_\infty - \pi}\exp\left(-b\frac{\pi}{\pi_\infty}\right) = k\pi_\infty{}^2 t \qquad (4)$$

in which π is the spreading pressure at time t, π_∞ is the equilibrium spreading pressure, and b and k are constants for a given solute. Results are presented graphically in Figs. 1–4, in which experimental points are compared with curves calculated by means of eq. 4. Experimental results of Addison[7] for aqueous decanoic acid solution (obtained by the drop weight method) and of Dervichian[8] for aqueous hendecanoic acid solution (obtained by the

Wilhelmy plate method) are compared with curves calculated from Eq. 4 in Figs. 5 and 6. Values of π_∞ were obtained from smoothed curves through the equilibrium surface tension data presented by King[14] for pentanoic acid and heptanoic acid, Weber and Sternganz[15] for heptanoic acid, Posner, Anderson and Alexander[16] for heptanol-1, and Frumkin[17] for octanoic acid. Values of the parameters b and K used in calculating the curves shown in Figs. 1–6 are presented in Table II.

TABLE II

Solute	b	K, cm.²/dynes² sec.
Pentanoic acid	1.12	2.62
Heptanoic acid	1.04	1.35×10^{-1}
Octanoic acid	1.14	1.50×10^{-2}
Decanoic acid	0.80	1.91×10^{-4}
Hendecanoic acid	1.07	7.80×10^{-6}
Heptanol-1	0.93	1.28×10^{-1}

Discussion

Figure 1 shows that the same surface tension–time curves can be obtained with different orifices provided surface tensions and surface ages are correctly calculated. While the range of orifices investigated was not great orifice D was approximately 40% longer than orifices E and F so that dependence of surface age on axial distance and ratios of surface to mean velocity differed appreciably. An orifice prepared as described[11] was rejected only if it failed to produce a stable jet. Further, no significant variation of results with discharge rate was observed. In contrast to our findings, Rideal and Sutherland[12] have reported that apparent surface tension–time curves obtained by the vibrating jet method depend markedly on the orifice used. We conclude that this dependence will not occur if the orifice meets certain minimum specifications, namely: 1. flow at the orifice exit must be non-turbulent. High speed motion pictures of the flow of small ink increments injected into a water stream before the orifice entrance demonstrated that no turbulence occurred in the exit jets of our orifices, and the flow appeared to be perfectly axial. The character of the exit stream in the bell shaped orifices of Rideal and Sutherland is unknown, but the damping of a turbulence developed in an orifice entrance should be more effective the greater the length of the orifice.

2. There should be no stagnant portions in the exit jet. In our work such portions were eliminated by "Desicoting" the orifice exit face.

3. The orifice design must be such that the exit flow pattern can be predicted, permitting calculation of surface age from axial distance and true surface tensions. We have shown[11] that such calculations can be made if the orifice is approximately a right circular cylinder. The corresponding development for the bell-shaped orifices of Rideal and Sutherland does not exist. We conclude that, subject to the restrictions indicated, the vibrating jet method is an absolute method for measuring surface tensions and their dependence on time. It is not, in our experience, a highly precise method; experimental errors, arising chiefly from uncertainties in measurement of wave length, total approximately 1% in surface tension.

It can hardly be overemphasized that surface

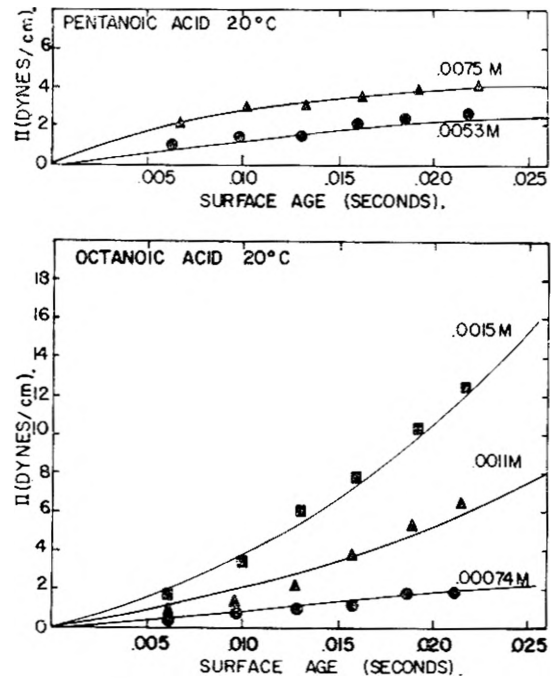

Fig. 3a, 3b.—Dependence of spreading pressure of aqueous pentanoic and octanoic acid solutions on concentration and time. Curves are from eq. 4, points are experimental.

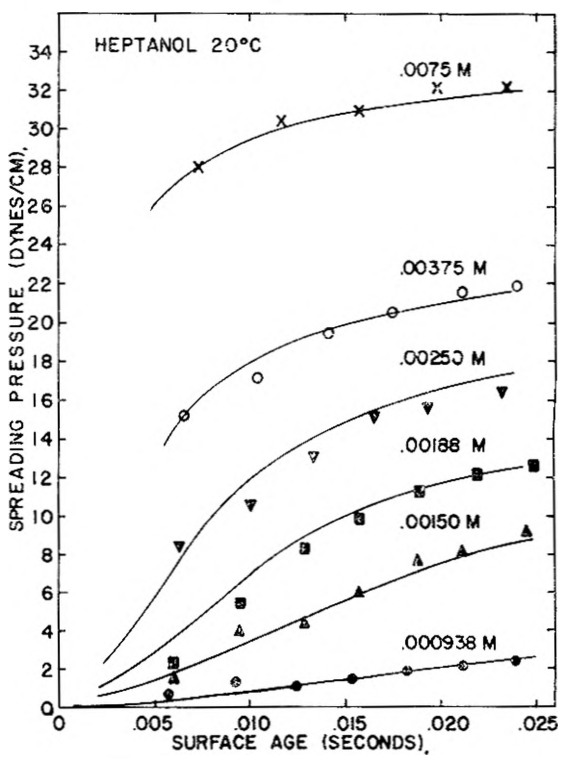

Fig. 4.—Dependence of spreading pressure of aqueous heptanol-1 solutions on concentration and time. Curves are from eq. 4, points are experimental.

(14) H. H. King, *Kans. State Agr. Coll. Tech. Bull.*, No. 9, 1922.

(15) L. I. Weber and P. Sternganz, *Z. physik. Chem.*, **169**, 241 (1934).

(16) A. M. Posner, J. R. Anderson and A. E. Alexander, *J. Colloid Sci.*, **7**, 623 (1952).

(17) A. Frumkin, *Z. physik. Chem.*, **116**, 498 (1925).

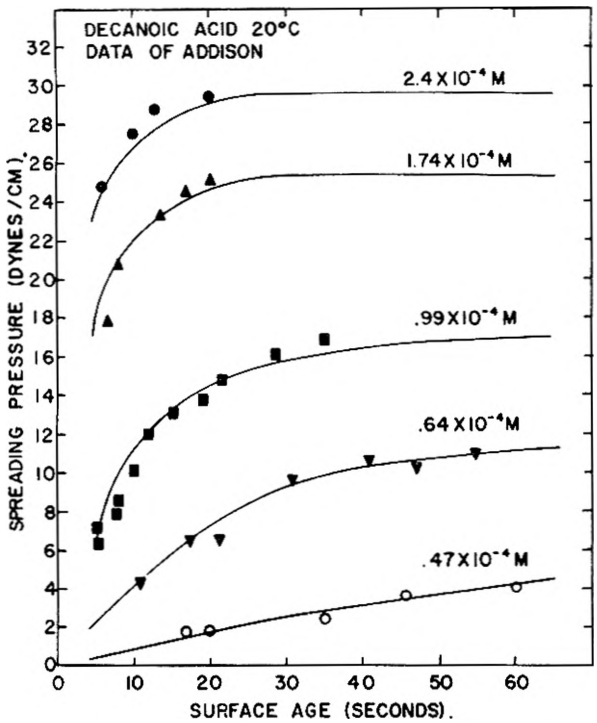

Fig. 5.—Dependence of spreading pressure of aqueous decanoic acid solutions on concentration and time. Curves are from eq. 4, points from experimental data of Addison.[7]

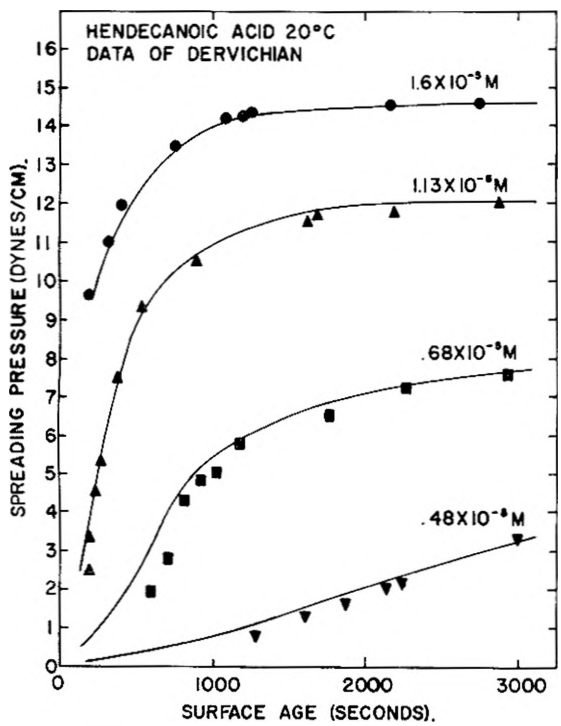

Fig. 6.—Dependence of spreading pressure of aqueous solutions of hendecanoic acid on concentration and time. Curves are from eq. 4, points are from experimental data of Dervichian.[8]

age differs *markedly* from the quotient of axial distance by mean velocity near the orifice (as much as 40% in the first observable waves)—sufficiently so, as we shall see, that the mechanistic conclusion reached may well depend on whether or not the surface age is correctly calculated. It can also hardly be overemphasized that the surface tension calculated from Rayleigh's formula may differ *markedly* (as much as 15 dynes/cm.) from the true surface tension and that calculated from eq. 1 in the neighborhood of the orifice.

Figures 1–6 and Table II show that the dependence of spreading pressure on solute concentration and time is represented by a single empirical equation for the aliphatic acids having from 5 to 11 carbons, and for 1-heptanol. Of particular interest is the fact that the same equation represents the data obtained in this work by the vibrating jet method, the data obtained by Addison using the drop weight method, and the data obtained by Dervichian using the Wilhelmy plate method. It will be observed that the parameter b does not vary systematically with chain length (it is approximately 1.0 for all systems) and the parameter K decreases systematically with increasing chain length. The systematic character of this variation is made evident in Fig. 7, in which $\log K$ is plotted against the logarithm of the aliphatic acid solubility in water (data from work of Eggenberger, Broom, Ralston and Harwood[18] and Ralston and Hoerr[19]). The dependence is almost linear, extending over 5 orders of magnitude in K and nearly 4 in solubility. When it is considered that the present experimental work, the work of Addison and that of Dervichian cover five orders of magnitude in time scale and include three different methods of investigation the general harmony of results obtained is striking and provides added evidence for the reliability of results obtained by a correctly executed vibrating jet technique.

An excellent example of the consequences of an inaccurate calculation of surface age is furnished by the work of Bond and Puls.[2] (This work is selected for comment because in contrast to work published by Addison,[4] Burcik[5] and Ross[6] in which a similar error appears to have been made the orifices are of such a character and their technique sufficiently well described to permit estimation of true surface ages from their data.) Bond and Puls found that their data could be represented by eq. 5

$$\log \frac{\gamma - \gamma_\infty}{\gamma_0 - \gamma_\infty} = -\alpha t^{1/2} \qquad (5)$$

and because of the indicated $t^{1/2}$ dependence at small times, concluded that the adsorption of soaps at the water–air interface was diffusion controlled. Their jet radius is given as 0.082 cm., and from an earlier paper by Bond[20] its length is estimated to be 0.40 cm. Since their jet was horizontal it may be inferred that they used the highest mean velocity possible (to minimize curvature of the stream) consistent with a Reynold's number less than 2000 (to avoid turbulence) or about 200 cm./sec. Using these figures, the true surface ages in the work of Bond and Puls were calculated from their apparent surface ages. The resulting data are better represented by eq. 6

$$\log \frac{\gamma - \gamma_\infty}{\gamma_0 - \gamma_\infty} = -kt \qquad (6)$$

(18) D. N. Eggenberger, P. K. Broome, A. W. Ralston and H. J. Harwood, *J. Org. Chem.*, **14**, 1108 (1948).

(19) A. W. Ralston and C. W. Hoerr, *ibid.*, **7**, 546 (1942).

(20) W. N. Bond, *Proc. Phys. Soc. (London)*, **A47**, 549 (1935).

than their original data were represented by eq. 5; the dependence on time is now to the first power, and a principal argument for their diffusion controlled mechanism is eliminated. The two treatments are compared in Fig. 8.

Theory

In order to infer adsorption mechanisms from the dependence of surface tension on concentration and time some assumption is necessary as to the dependence of surface tension on surface excess in non-equilibrium systems. We make the following assumption explicitly, and consider that it is not a trivial one: *Assumption: The surface tension depends only on the surface excess, whether the system is at equilibrium or not.* This means that an observed spreading pressure will be taken as implying the same surface excess as would correspond to that spreading pressure at equilibrium, so that dynamic surface excesses may be inferred from dynamic spreading pressures by the use of equilibrium spreading pressure–surface excess curves.

While this assumption has been implicit in all previous interpretations of time dependent surface tensions to the best of our knowledge (see particularly the work of Bond and Puls,[2] Ward and Tordai[9] and Sutherland[10]) it contains theoretical implications the validity of which is at present unknown. Precisely, it implies that the rate-determining step in the adsorption occurs prior to or in the act of entering the surface, and that subsequent rearrangements or reorientations in the surface film are either fast or do not affect the surface tension. The surface potential studies of Posner and Alexander[21] suggest strongly that slow orientation processes occur in surface films, but also suggest that these result in negligible changes in surface tension. We are unaware of other work having a direct bearing on this problem. Theoretically, such reorientations should be accompanied by a decrease in surface tension, and the work of Posner and Alexander is the only justification for assuming this decrease to be negligible.

With the assumption stated, we were unable to find a kinetic mechanism which led to eq. 4. Briefly, the difficulty results from the fact that the implied rate of surface tension depression varies as $(\pi_\infty - \pi)^2$, rather than, for example, as $\pi_\infty^2 - \pi^2$, which implies an unlikely coupling of forward and reverse rates. Therefore a general rate of adsorption theory was developed, and eq. 4 was used for estimating slopes and rounding experimental data.

The possibility of diffusion controlled kinetics was first investigated. Important theoretical treatments of diffusion-controlled adsorption kinetics have been published by Ward and Tordai[9] and by Sutherland[10]; Sutherland's treatment provides the dependence of surface excess on concentration and time in terms of tabulated functions, but is limited to the linear portion of the adsorption isotherm, and therefore we have tested our results in terms of the more tedious but general theory of Ward and Tordai. If C_0 is the bulk concentration of the solution, $C(0,t)$ the "subsurface" concentration at time t, $U(t) = C(0,t)/C_0$, $\Gamma(t)$ is the surface excess at time t, and D_a is the apparent diffusion coefficient, the results of Ward and Tordai are given by eq. 7

$$\Gamma(t) = 2C_0\sqrt{\frac{D_a}{\pi}}\left\{t^{1/2} - \int_0^{t^{1/2}} U(t-\xi^2)\,d\xi\right\} \quad (7)$$

The experimental data, equilibrium surface tension data, and equation of state data[22] then permit calculation of $\Gamma(t)$ from observed dependence of surface pressure on time, and permit calculation of $U(t)$ assuming surface and subsurface are in equilibrium. Equation 7 then permits calculation of the apparent diffusion coefficient D_a; if the adsorption kinetics are diffusion controlled D_a should be independent of concentration and time, and equal to the actual diffusion coefficient. The results of this investigation were qualitatively in accord with those of Ward and Tordai; the apparent diffusion coefficient for all substances studied here increased with time, increased with concentration and at all times and concentrations was less than the true diffusion coefficient. With aqueous solutions of heptanoic acid, for example, ranges of D_a calculated in the range 5 to 25 milliseconds for those surface tension–time curves showing appreciable structure were as follows: $C_0 = 9.38 \times 10^{-4}\ M$, $0.22 \leqslant 10^6 D_a \leqslant$

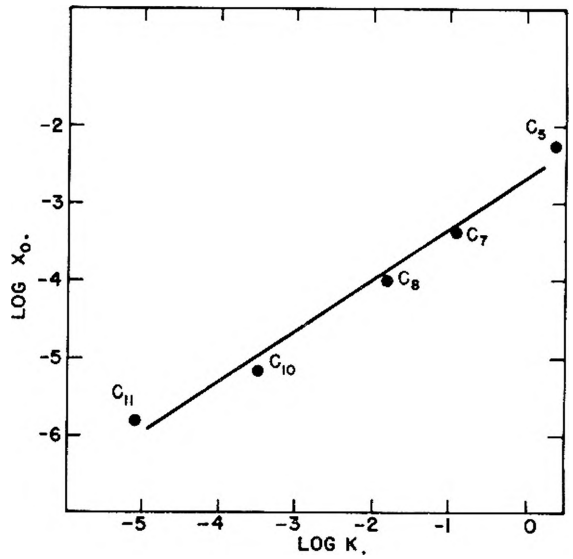

Fig. 7.—Dependence of rate constant k, eq. 4, on aliphatic acid solubility.

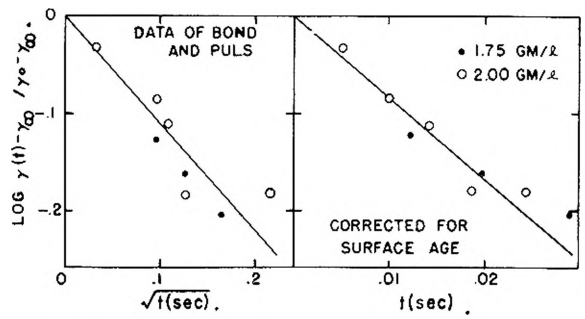

Fig. 8.—Incorrect inference of adsorption mechanism resulting from over-simplified calculation of surface age. Data of Bond and Puls[2] using their surface ages (left) and corrected surface age (right).

(21) A. M. Posner and A. E. Alexander, *Trans. Faraday Soc.*, **45**, 651 (1949).

(22) R. K. Schofield and E. K. Rideal, *Proc. Roy. Soc.* (*London*), **A109**, 57 (1925); **A110**, 167 (1926).

0.45; $C_0 = 15.0 \times 10^{-4} M$, $0.34 \leqslant 10^6 D_a \leqslant 2.02$; $C_0 = 18.8 \times 10^{-4} M$, $0.86 \leqslant 10^6 D \leqslant 5.40$; $C_0 = 25.0 \times 10^{-4}$, $2.90 \leqslant 10^6 D_a \leqslant 6.50$. In each case the apparent diffusion coefficient increased almost uniformly with time. The true diffusion coefficient may be estimated[23] to be 8×10^{-6} cm.²/sec. We therefore conclude that the adsorption kinetics in the present systems are not diffusion controlled; the theory to be developed to represent these systems carries a second-order dependence on concentration, and it is therefore to be expected that in systems at sufficiently high concentrations the diffusion process (which is essentially first order in concentration) will become rate limiting.

Suppose the transition state involves m molecules from the bulk solution (B molecules) where their activity is A_B and n molecules from the surface film (S molecules) where their activity is A_S; the transition state then can be represented as B_mS_n, its activity as $\mathfrak{A}^{\pm}$, its concentration by $C^{\pm}$ and its activity coefficient by $\gamma^{\pm}$. The adsorption process can then be represented by

$$m\mathrm{B} + n\mathrm{S} \underset{}{\overset{K_a}{\rightleftharpoons}} \mathrm{B}_m\mathrm{S}_n \xrightarrow{k_a} (m - r)\mathrm{B} + (n + r)\mathrm{S} \quad (8)$$

The principle of microscopic reversibility then determines that the reverse reaction must be of the form

$$(m - r)\mathrm{B} + (n + r)\mathrm{S} \overset{K_d}{\rightleftharpoons} \mathrm{B}_m\mathrm{S}_n \xrightarrow{k_d} m\mathrm{B} + n\mathrm{S} \quad (9)$$

and the net rate of adsorption $d\Gamma/dt$ must therefore be of the form

$$\frac{d\Gamma}{dt} = \frac{k_a K_a \mathfrak{A}_B^m \mathfrak{A}_S^n}{\gamma^{\pm}} - \frac{k_d K_d \mathfrak{A}_B^{m-r} \mathfrak{A}_S^{n+r}}{\gamma^{\pm}} \quad (10)$$

Further development will be limited to the special case $m = 2, n = 0, r = 1$ which proved to represent our data very well. In this case we have

$$\frac{d\Gamma}{dt} = \frac{\mathfrak{A}_B}{\gamma^{\pm}} [k_a K_a \mathfrak{A}_B - k_d K_d \mathfrak{A}_S] \quad (11)$$

We now define standard states and indicate assumptions concerning activity coefficients.

1. The standard state for the solute in bulk is taken such that $\lim_{C \to 0} \alpha_B/C_B = 1$ where C_B is the molar bulk concentration of solute; in the case of the dissociating fatty acids C_B is the concentration of undissociated fatty acid. The highest concentration studied in this work was 7.5×10^{-3} molar; under these circumstances we may assume $\alpha_B = C_B$ for all systems studied.

2. The standard state for the surface molecules is taken to be the same as that for bulk molecules. With this definition $\alpha_S = \alpha_B = C_B$ at equilibrium, and therefore $k_a K_a = k_B K_B = \beta$. The surface fugacity f may be defined in terms of the surface pressure π by

$$\ln \frac{f}{\pi} = \int_0^{\pi} \left(\frac{\bar{A}}{RT} - \frac{1}{\pi}\right) d\pi = \int_0^{\pi} \frac{\phi}{\pi} d\pi \quad (12)$$

where $\phi = \pi\bar{A}/RT - 1$ may be obtained from the surface Amagat diagrams of Schofield and Rideal[22] and from similar diagrams prepared from the work of Addison[7] and Dervichian.[8] The reference fugacity f_0 must then be such that, at equilibrium, $f/f_0 = C_B$. Evidently f_0 is equal to the Traube constant, *i.e.*, $f_0 = \lim_{C \to 0} \pi/C_B$, and is available from the equilibrium surface tension data cited.[7,8,14-17] Therefore also $\mathfrak{A}_S = f/f_0$, $\mathfrak{A}_B = f_\infty/f_0$, where f_∞ is the equilibrium surface fugacity.

3. The standard state for the transition state is taken to be such that $\lim_{\pi \to 0} \gamma^{\pm} = 1$.

With these definitions eq. 10 can be rewritten in the two equivalent forms eqs. 13 and 14

$$\frac{d\Gamma}{dt} = \frac{\beta C_B}{\gamma^{\pm}} (C_B - f/f_0) \quad (13)$$

$$\frac{d\Gamma}{dt} = \frac{\beta \gamma_S C_B}{\gamma^{\pm} f_0} \left\{ \pi_\infty \exp\left[\int_\pi^{\pi_\infty} \frac{\phi}{\pi} d\pi\right] - \pi \right\} \quad (14)$$

where $\gamma_S = \exp\left[\int_0^{\pi} \phi/\pi \, d\pi\right]$ is the activity coefficient of adsorbed molecules at spreading pressure π. Further

$$\frac{d\Gamma}{dt} = \frac{d\Gamma}{d\pi}\frac{d\pi}{dt} \quad (15)$$

the values of $d\pi/dt$ are available analytically from eq. 4 and the values of $d\Gamma/d\pi$ are available from the cited equation of state data. This information suffices to establish the ratio $\beta\gamma_S/\gamma^{\pm}$, since all other quantities in eqs. 13 and 14 are known. Further since by definition $\lim_{\pi \to 0} \gamma^{\pm} = 1$, $\lim_{\pi \to 0} \gamma_S = 1$ it follows that $\lim_{\pi \to 0} \beta\gamma_S/\gamma^{\pm} = \beta$, establishing β. Since γ_S is known as a function of π, $\gamma^{\pm}$ can now be established as a function of π, and perhaps of C_B and t as well. Now eq. 11 implies that the rate-determining step in the adsorption process occurs in or near the surface film, and if this is true the activity coefficient $\gamma^{\pm}$ should depend explicitly on π only, and only implicitly on concentration and time. In other words, for a given solute $\gamma^{\pm}$ should have a definite value for a given value of π whether this value of π is reached in short times with high concentrations or in long times with low concentrations. Further, the variation of $\gamma^{\pm}$ with π should be physically reasonable if the mechanism proposed is correct.

Figure 9 presents a plot of $\log \beta\gamma_S/\gamma^{\pm}$ against π, including data from all systems studied in the present work as well as those of Addison and Dervichian. Surprisingly, the data for these different systems do not differ sufficiently to justify separate curves to be drawn through them, and the common curve corresponds to a common value of β of 0.8 ± 0.3 and a common dependence of $\gamma^{\pm}$ on π. Considering that the calculation of the ratio $\beta\gamma_S/\gamma^{\pm}$ involves addition of errors in the original surface tension–time data, representation of these data by an empirical equation, equation of state data, and Traube's constant data the scatter of results covering three orders of magnitude in concentration and five orders of magnitude in time seems to us remarkably small.

Figure 10 compares the dependence of the surface activity coefficient for octanoic acid at the water–air interface, butyric acid at the water benzene interface (both from work of Schofield and Rideal[22]) and octanoic acid in the transition state (from the present work). An ideal film would have an activity coefficient (with standard states as defined) of

(23) W. Jost, "Diffusion," Academic Press, New York, N. Y., 1952, p. 475.

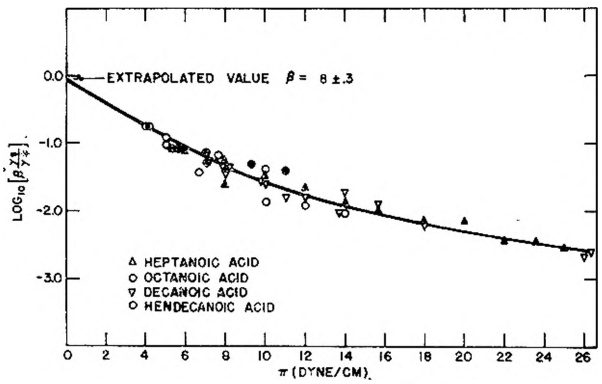

Fig. 9.—Dependence of $\beta(\gamma_s/\gamma^+)$ (β = second-order rate constant, γ_s and γ^+, surface and transition state activity coefficients) on spreading pressure (see eq. 14 in text).

unity independent of spreading pressure. The initial decrease in activity coefficient of octanoic acid at the water–air interface with increasing spreading pressure reflects the attractive interaction of the hydrocarbon chains at this interface; the decrease does not occur at the water–benzene interface because no energetic advantage accrues to molecules in the interfacial film by addition of nearest neighbors since their interaction with benzene is substantially equally favorable. With increasing spreading pressure the activity coefficient increases, and at sufficiently high spreading pressures the logarithm of the activity coefficient varies almost linearly with spreading pressure, reflecting the finite cross sectional areas of the adsorbed molecules. The slopes of these portions permit estimation of the cross sectional areas as ~25 Å.^{2} in both cases. The calculated activity coefficient for the transition state shows no initial decrease; the plot of log $\gamma^{\pm}$ against π is almost linear, resembling the corresponding curve for the water–benzene interface but having a steeper slope. The cross sectional area indicated by this slope is ~100 Å.^{2}. The lack of an initial decrease indicates no stabilization of the transition state by molecules already in the film. Both this and the large effective cross sectional area suggest that the transition state is poorly oriented for strong interaction with molecules already in the film, and the area defended by a poorly oriented octanoic acid dimer could easily be of the order of magnitude calculated.

It is improbable that the rate constants β and transition state activity coefficients are strictly independent of chain length, but more likely that small systematic variations (probably such that β decreases, and $\gamma^{\pm}$ increases with increasing chain length) have been masked by the accumulation of experimental and computational errors previously mentioned.

We conclude that equations (11 and 13) well represent the kinetics of adsorption of aliphatic acids of from 5 to 11 carbons at the water–air interface, that the transition state activity coefficient involved varies reasonably with spreading pressure, and that neither the transition state activity coefficient nor the rate constant varies appreciably with chain length. The adsorption kinetics are not diffusion controlled, but involve a dimeric transition state located (substantially) in the surface film.

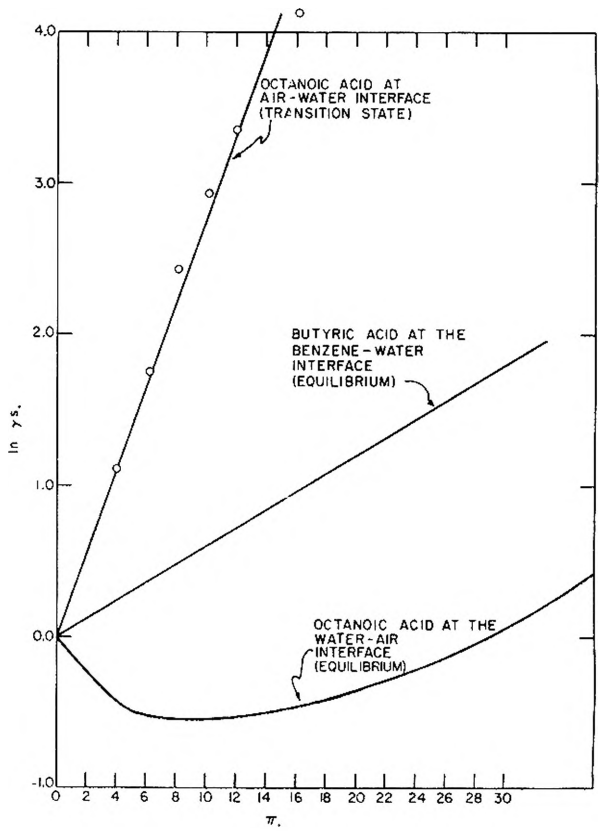

Fig. 10.—Dependence of transition state activity coefficient on spreading pressure compared with equilibrium activity coefficient-spreading pressure data from work of Schofield and Rideal.[22]

EVALUATION OF DIFFUSION COEFFICIENTS FROM SEDIMENTATION VELOCITY MEASUREMENTS

BY HIROSHI FUJITA[1]

Department of Chemistry, University of Wisconsin, Madison 6, Wisconsin

Received November 5, 1958

For two-component systems in which the sedimentation coefficient s is a linear function of solute concentration C, a procedure is developed which permits determination of the diffusion coefficient D from sedimentation velocity measurements. The basis of the development is an approximate equation derived recently by Fujita for the height–area ratio of the sedimentation boundary curves in such systems. This procedure is tested by using the height–area data of Baldwin for bovine plasma albumin, and it is found that the values of D computed by the present method agree satisfactorily with those predicted from the free diffusion experiment of Gosting.

Introduction

Data for the height–area ratio, H/A, from sedimentation velocity experiments may be used to evaluate the diffusion coefficient of a given two-component system, provided that an adequate theoretical equation for H/A is available and the values of other parameters involved in the equation are experimentally known. Such an equation previously has been derived[2] for the case in which both the diffusion coefficient D and the sedimentation coefficient s are independent of solute concentration C. However, because s generally varies with C, its applicability is quite limited. In fact, it has been shown quite recently by Baldwin[3] that even a slight dependence of s upon C causes an appreciable inaccuracy in the determination of D when use is made of the equation which neglects this effect. Fujita[4] derived an equation for H/A from his approximate solution of the ultracentrifuge equation of Lamm[5] in which s is a linear function of C and D is constant. However, no practical procedure was given by which his equation could be utilized to evaluate D from experimental H/A data. In an application of the equation given by Fujita to data for bovine plasma albumin, Baldwin[3] has used a method of successive approximations to determine the values for D from measurements of H/A. This method is useful when an approximate value for the diffusion coefficient of the system concerned is known in advance. However, since this is not generally the case, it is worthwhile to devise a procedure for the evaluation of D which permits straightforward application of Fujita's equation to observed data. In this paper, such a procedure is presented and tested by using Baldwin's data[3] on bovine plasma albumin.

Method

It was shown[4] that the height–area ratio, H/A, of a sedimentation boundary in a two-component system where s has a concentration dependence of the form

$$s(C) = s(0)(1 - kC) \tag{1}$$

and where D is constant is given by

$$\frac{H}{A} = \frac{e^{-(\tau/2)}}{r_0[1 + (1 - \lambda)^{1/2}][\epsilon(1 - e^{-\tau})]^{1/2}} F(\xi_m) \tag{2}$$

Here

$$F(\xi_m) = \frac{2e^{-\xi_m^2}}{(\pi)^{1/2}[1 + \Phi(\xi_m)]} + 2\xi_m \tag{3}$$

$$\xi_m = \frac{\beta(\lambda)^{1/2}}{1 + (1 - \lambda)^{1/2}} \tag{4}$$

$$\beta = (\alpha/\epsilon)^{1/2} \tag{5}$$

$$\lambda = \alpha(1 - e^{-\tau}) \tag{6}$$

and

$$\Phi(x) = \frac{2}{(\pi)^{1/2}} \int_0^x e^{-q^2} dq \tag{7}$$

The other symbols appearing in these equations have the significance

$$\alpha = kC_0,\ \tau = 2\omega^2 s(0)t,\ \epsilon = 2D/[r_0^2\omega^2 s(0)] \tag{8}$$

where ω is the angular velocity of the rotor, r_0 is the radial distance from the axis of the rotor to the initial boundary formed between solution and solvent, and C_0 is the concentration (weight per unit volume of solution) of the starting solution.

Equation 2 may be rewritten in the form

$$G(\xi_m) = 2\alpha r_0(H/A) \sinh(\tau/2) \tag{9}$$

where

$$G(x) = 2x\left[\frac{1}{x} + \frac{e^{-x^2}}{(\pi)^{1/2}[1 + \Phi(x)]}\right] \tag{10}$$

Because equation 2 was derived under the assumption that $\tau << 1$, equation 9 may be written in the approximate form[6]

$$G(\xi_m) = \alpha r_0(H/A)\tau \tag{11}$$

Equation 11 may be solved for ξ_m to give

$$\xi_m = G^{-1}(\eta) \tag{12}$$

where

$$\eta = \alpha r_0(H/A)\tau \tag{13}$$

and G^{-1} is the inverse function of G. In terms of the original variables equation 13 may be written

$$\eta = 2r_0\omega^2 s(0)kC_0(H/A)t \tag{14}$$

On the other hand, equation 4 for ξ_m may be expanded in powers of τ, and we have finally

$$\xi_m = \frac{r_0\omega^2 s(0)kC_0}{2(D)^{1/2}}\left[1 - \frac{1}{2}(1 - kC_0)\omega^2 s(0)t\right](t)^{1/2} \tag{15}$$

Here terms of order τ^2 have been neglected in comparison with unity to conform to the approximation used in deriving equation 11.

Substitution of equations 14 and 15 into equation 12 yields

(1) On leave from the Physical Chemistry Laboratory, Department of Fisheries, University of Kyoto, Maizuru, Japan.

(2) T. Svedberg and K. O. Pedersen, "The Ultracentrifuge," Clarendon Press, Oxford, 1940.

(3) R. L. Baldwin, *Biochem. J. (London)*, **65**, 503 (1957).

(4) H. Fujita, *J. Chem. Phys.*, **24**, 1084 (1956).

(5) O. Lamm, *Arkiv Mat. Astron. Fysik*, **21B**, No. 2 (1929).

(6) The approximation involved here is such that terms of order $\tau^2/24$ are neglected in comparison with unity.

$$\left[1 - \frac{1}{2}(1 - kC_0)\omega^2 s(0)t\right](t)^{1/2} = \frac{2(D)^{1/2}}{r_0\omega^2 s(0)kC_0} G^{-1}(2r_0\omega^2 s(0)kC_0(H/A)t) \quad (16)$$

Thus in the range of t for which $\tau = 2\omega^2 s(0)t << 1$ a plot of $[1 - (1/2)(1 - kC_0)\omega^2 s(0)t](t)^{1/2}$ *vs.* $G^{-1}(2r_0\omega^2 s(0)kC_0(H/A)t)$ should form a straight line with a slope of $2(D)^{1/2}/[r_0\omega^2 s(0)kC_0]$. The value of the diffusion coefficient D then is determined from this slope, provided that the values of r_0, ω^2, C_0, $s(0)$ and k are known. The first three of these parameters are directly available from given experimental conditions. The values of $s(0)$ and k may be obtained from measurements of the movement of the boundary peak by using the procedure described previously.[4] Accordingly, if values of the height–area ratio, H/A, are determined as a function of time t from a series of schlieren boundary photographs and if the functional form of G^{-1} is known, we can calculate values of $[1 - (1/2)(1 - kC_0)\omega^2 s(0)t](t)^{1/2}$ and $G^{-1}(2r_0\omega^2 s(0)kC_0(H/A)t)$ for each value of t at which the boundary photograph was taken. Then the necessary plot may be prepared.

As mentioned above, G^{-1} stands for the inverse function of G. This means that $G^{-1}(x)$ as a function of x satisfies the equation

$$x = 2G^{-1}(x)\left\{G^{-1}(x) + \frac{\exp[-(G^{-1}(x))^2]}{(\pi)^{1/2}[1 + \Phi(G^{-1}(x))]}\right\} \quad (17)$$

Because this equation cannot be solved explicitly for $G^{-1}(x)$, the form of $G^{-1}(x)$ may be obtained only in graphical or tabular form. Figure 1 shows the curve of this function in the range of x, $0 < x < 10$. Numerical values of $G^{-1}(x)$ in a wider range of x are listed in Table I. When using the above method it is recommended that a large scale graph of $G^{-1}(x)$ be prepared, using the data given in this table and then desired values of $G^{-1}(x)$ may be read from the graph.

Application

We now apply the above described method to the height–area ratio data of Baldwin[3] for bovine plasma albumin in a buffer. He showed that the sedimentation coefficient of this solute in the given buffer decreases almost linearly with increasing solute concentration over the range studied. A slight downward curvature is observed in the plot of s *vs.* C at high concentrations. When applying the above method to his H/A data, this effect may be approximately taken into account by changing slightly the values of $s(0)$ and k in equation 1 in accordance with the initial concentration of a particular experiment concerned. Table II records his H/A data for $C_0 = 0.67$ and 1.35 g./100 ml.,[7] together with the values of the parameters necessary for computations. That the values of $s(0)$ and k are slightly different in the two cases results from the fact that a slight deviation from linearity of the observed plot of s *vs.* C has been taken approximately into consideration. These values are the same as those originally assigned by Baldwin[3] in his application of equation 2 to the H/A data shown in Table II.

(7) Only for these two initial concentrations did Baldwin measure boundary areas and maximum heights.

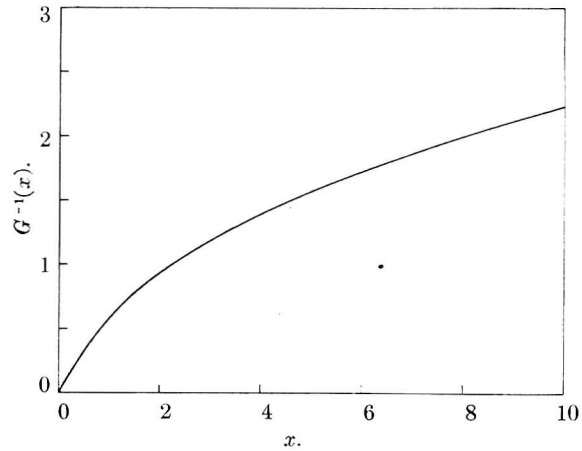

Fig. 1.—Graph of $G^{-1}(x)$ *versus* x.

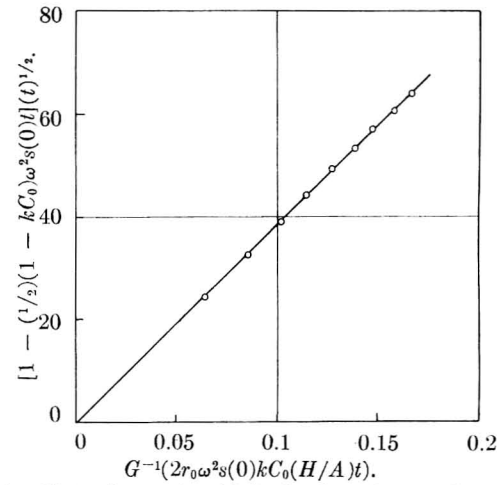

Fig. 2.—Test of equation 16 for bovine plasma albumin at $C_0 = 0.67$ g./100 ml.

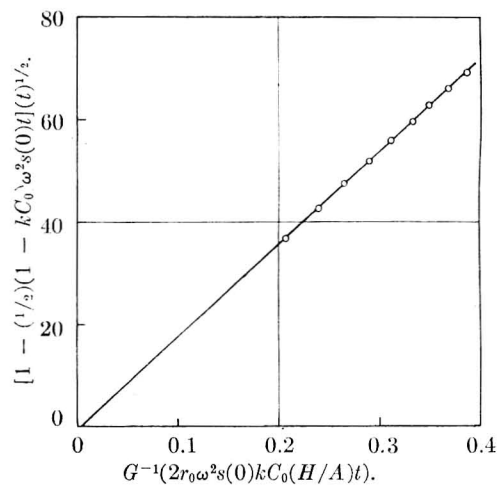

Fig. 3.—Test of equation 16 for bovine plasma albumin at $C_0 = 1.35$ g./100 ml.

Figures 2 and 3 show the plots of $[1 - (1/2)(1 - kC_0)\omega^2 s(0)t](t)^{1/2}$ *vs.* $G^{-1}(2r_0\omega^2 s(0)kC_0(H/A)t)$ calculated from these data for $C_0 = 0.67$ and for 1.35 g./100 ml. It is seen that in both cases the plotted points fall well on a straight line, in agreement with the prediction. According to equation 16 these straight lines should pass through the coördinate origin, and, in fact, the data for $C_0 = 0.67$ g./100

TABLE I

NUMERICAL VALUES OF $G^{-1}(x)$

x	$G^{-1}(x)$	x	$G^{-1}(x)$	x	$G^{-1}(x)$
0.00000	0.00	0.7471	0.48	5.5068	1.65
.02286	.02	0.7890	.50	5.8337	1.70
.04632	.04	0.8984	.55	6.1715	1.75
.07039	.06	1.0145	.60	6.5200	1.80
.09508	.08	1.1378	.65	6.8792	1.85
.1204	.10	1.2684	.70	7.2491	1.90
.1464	.12	1.4068	.75	7.6296	1.95
.1731	.14	1.5532	.80	8.0207	2.00
.2005	.16	1.7080	.85	8.8344	2.10
.2285	.18	1.8714	.90	9.6898	2.20
.2573	.20	2.0438	.95	10.5866	2.30
.2869	.22	2.2253	1.00	11.5243	2.40
.3172	.24	2.4162	1.05	12.5027	2.50
.3483	.26	2.6169	1.10	13.5217	2.60
.3802	.28	2.8274	1.15	14.5810	2.70
.4129	.30	3.0479	1.20	15.6806	2.80
.4464	.32	3.2788	1.25	16.8204	2.90
.4808	.34	3.5200	1.30	18.0002	3.00
.5160	.36	3.7717	1.35	20.4801	3.20
.5522	.38	4.0340	1.40	23.1200	3.40
.5893	.40	4.3070	1.45	25.9200	3.60
.6273	.42	4.5907	1.50	28.8800	3.80
.6662	.44	4.8853	1.55	32.0000	4.00
.7061	.46	5.1906	1.60	35.2800	4.20

TABLE II

SUMMARY OF BALDWIN'S DATA ON BOVINE PLASMA ALBUMIN

C_0 = 0.67 g./100 ml.		C_0 = 1.35 g./100 ml.	
$s(0) = 4.86 \times 10^{-13}$ (sec.)		$s(0) = 4.92 \times 10^{-13}$ (sec.)	
$k = 0.057$ (100 ml./g.)		$k = 0.059$ (100 ml./g.)	
$\omega^2 = 3.919 \times 10^7$ (rad.^{2} sec.$^{-2}$)		$\omega^2 = 3.919 \times 10^7$ (rad.^{2} sec.$^{-2}$)	
$r_0 = 5.901$ cm.		$r_0 = 5.938$ cm.	
Temp. = 24.50°		Temp. = 25.07°	
t (sec.)	A/H (cm.)	t (sec.)	A/H (cm.)
0.60×10^3	0.688×10^{-1}	1.40×10^3	0.956×10^{-1}
1.08	0.909	1.88	1.086
1.56	1.093	2.36	1.206
2.04	1.252	2.84	1.309
2.52	1.389	3.32	1.406
3.00	1.522	3.80	1.478
3.48	1.635	4.28	1.572
3.96	1.729	4.76	1.642
4.44	1.828	5.24	1.699

ml. fulfill this condition. The reason that the data for C_0 = 1.35 g./100 ml. are not in accordance with the prediction is not clear, although it is possible to draw a straight line so that it represents all plotted points adequately and passes through the origin. The slopes of the straight lines drawn in Figs. 2 and 3 give for D values of 6.79×10^{-7} and 6.93×10^{-7} cm.^{2}/sec., respectively. These values may be compared, respectively, to 6.85×10^{-7} and 6.94×10^{-7} cm.^{2}/sec. as estimated by Baldwin[3] from the free diffusion experiments of Gosting.[8] The corresponding values of D obtained by Baldwin[3] from his sedimentation velocity experiments are 7.02×10^{-7} and 6.76×10^{-7} cm.^{2}/sec.; he started his iteration procedure with the D values predicted from Gosting's work and obtained these values in the second step of the iteration. Further iterations may lead to values for D which are closer to the predicted ones.

It is seen that the values of D derived by the method presented above agree with the predicted ones to within 1%. Such agreement is better than one has reason to expect because the precision of height–area ratio measurements from the schlieren boundary photographs currently obtainable is not so high as to warrant such accuracy. It is significant that D can be evaluated directly with a reasonable accuracy from sedimentation velocity measurements only, provided that the given system obeys equation 1.

(8) Measurements quoted in R. L. Baldwin, L. J. Gosting, J. W. Williams and R. A. Alberty, *Disc. Faraday Soc.*, **20**, 13 (1955).

Discussion

Equation 2 was derived with an initial condition consisting of a sharp boundary formed between solution and solvent. Experimentally, this type of initial condition can be obtained only in the recently developed synthetic boundary cells.[9,10] Strictly speaking, equation 2 is inapplicable to Baldwin's data, because they were obtained in a conventional ultracentrifuge cell initially filled with only one uniform solution. Thus the fairly good agreement obtained between the calculated and predicted D values may be fortuitous. However, at least an approximate justification for the direct analysis of Baldwin's data in terms of equation 2 is obtained from a recent study by Fujita and MacCosham[11]; they showed that when D is sufficiently small and s is sufficiently large, as in the system studied by Baldwin, the "zero-time correction" which is associated with the presence of the cell meniscus is negligible. This means that under such conditions a sedimentation boundary which originates from the initial condition obtained in the conventional cell behaves as if it originated from a sharp boundary formed between solution and solvent at the position corresponding to the meniscus. Thus equation 2 may be applied to Baldwin's data, with the single modification that r_0 is taken as the radial distance from the axis of rotation to the meniscus.

Recently Fujita[12] derived an equation similar to equation 16 from a study of differential sedimentation boundaries; here a differential boundary is defined as one which originates from a sharp boundary formed between solutions of slightly different concentrations. The data for the function $G^{-1}(x)$ given in Table I are also useful when evaluating the diffusion coefficient from height–area ratio measurements of such differential boundaries. A practical procedure for the determination of D for this case has been described.[12]

Acknowledgments.—The author wishes to thank Professor R. L. Baldwin for placing his original data at the author's disposal. The help of Dr. P. J. Dunlop in the preparation of this manuscript is gratefully acknowledged.

(9) G. Kegeles, *J. Am. Chem. Soc.*, **74**, 5532 (1952).

(10) E. G. Pickels, W. F. Harrington and H. K. Schachman, *Proc. Natl. Acad. Sci.*, **38**, 943 (1952).

(11) H. Fujita and V. J. MacCosham, *J. Chem. Phys.*, **30**, 291 (1959).

(12) H. Fujita, *ibid.*, in press.

The work was supported by a grant to Professor J. W. Williams from the National Institutes of Health G-4912. The author wishes to express his gratitude both to individual and to institution.

SURFACE PROPERTIES OF GERMANIUM

BY Y. L. SANDLER AND M. GAZITH

Westinghouse Research Laboratories, Pittsburgh 35, Pa.

Received November 20, 1958

Some physical and chemical properties of germanium films sputtered by a discharge in an inert atmosphere have been studied. A detailed investigation of the ortho–para conversion of hydrogen catalyzed by the germanium between 77°K. and room temperature reveals a twofold origin of the conversion, magnetic and chemical; the activity due to either mechanism is remarkably high. Both mechanisms are believed to be due to a high concentration of single or very weakly coupled electrons in the defect surface. The oxygen adsorption on the films at 77°K. was studied by measuring adsorption isotherms and by investigating the influence of different amounts of oxygen and of absorbed light on the activity of the films. A weakly adsorbed layer of oxygen was found at low relative pressures at 77°K. Failure of this oxygen layer to induce a magnetic conversion in hydrogen indicates that this reversible adsorption is a weak chemisorption. It is shown to be the precursor of a stronger chemisorption at room temperature. The reversible nature of this adsorption and its interaction with unsaturated surface electrons and with the space charge layer of the germanium is discussed.

In this paper we report an investigation of some magnetic, catalytic and electrical properties of germanium and of their changes by adsorption of oxygen. Germanium was chosen because it is available in a state of very high chemical purity and because its semi-conducting properties are relatively well understood.

Adsorption properties of clean germanium surfaces have been investigated in recent years by various research groups,[1–6] and some work on the catalytic properties of germanium at elevated temperature also has been reported.[7,8] The scarcity of work until recently on the catalytic properties may be due to the high sensitivity of germanium to oxygen poisoning and the resulting technical difficulties[8] in studying its properties.

In the present work a new approach was chosen: the parahydrogen conversion at low temperatures was used to probe the bare surface and the adsorbed oxygen layers. As is known, the parahydrogen conversion on surfaces can have two distinct mechanisms,[9] both of which were found to be operative in the present case. One of these mechanisms, mainly found at low temperatures, is a purely physical process consisting of the inversion[10] of the nuclear spins of a hydrogen molecule in a strong inhomogeneous magnetic field. This type of conversion requires no activation energy and is generally caused by the presence of unpaired electrons in the surface on which the hydrogen is adsorbed. As previously shown in the case of TiO_2,[11] a study of this type of conversion reveals the existence of free valences in the bare surface and also enables us to distinguish between paramagnetic and diamagnetic forms of adsorbed oxygen.

The second mechanism in the parahydrogen conversion has a "chemical" origin; it involves the activation of the H–H bond and it is analogous to the hydrogen–deuterium exchange reaction which we also have studied. A thorough study of the kinetics of the ortho–para conversion was carried out in order to differentiate between the two mechanisms.

The adsorption and desorption of oxygen at low temperatures and its influence on the reactivity of the solid also was investigated. In this way different types of adsorption could be distinguished. Electrical conductivity changes and the influence of absorbed light were studied to elucidate the nature of the interaction between semiconductor and adsorbed oxygen.

A convenient technique of sputtering a germanium film by an electric gas discharge was adopted in the present experiments. It gave films of relatively high surface area, and new films could be sputtered on top of old ones to give excellent reproducibility.

Experimental

Vacuum System.—Some initial experiments were carried out with an ultra-high vacuum system.[12] However, because of the catalytic activity of the metal valves, this system was abandoned in favor of a good conventional vacuum system.

Mercury pumps and liquid nitrogen traps were used giving (in the later experiments with "thick films") a vacuum of 10^{-8} mm. or better, as measured by an ion gauge at the entrance to the reaction vessel. For isolating the reaction vessel, a greased stopcock was used with liquid nitrogen traps on either side of it; it was well ground and polished and required only a very thin film of grease (Apiezon N) for lubrication. After extended degassing, a vacuum of better than 10^{-6} mm. could be maintained for many hours in the closed reaction vessel (without the presence of a gettering film).

Reaction Vessel.—The reaction vessel, made of Nonex glass, had a volume of about 90 cc. It contained two pieces of intrinsic germanium having an impurity concentration of less than 10^{13}/cc. The pieces were perforated and slipped over tungsten leads. Before the leads were sealed in the tube, the germanium was etched in an H_2O_2–HF

(1) J. A. Dillon and H. E. Farnsworth, *J. Appl. Phys.*, **28**, 174 (1957).

(2) P. Handler in "Semiconductor Surface Physics," University of Pennsylvania Press, Philadelphia, Pa., 1956, p. 23.

(3) M. Green, J. A. Kafalas and P. H. Robinson, ref. 2, p. 349.

(4) J. T. Law, THIS JOURNAL, **59**, 543 (1955).

(5) R. M. Dell, *ibid.*, **61**, 1584 (1957).

(6) S. P. Wolsky, *J. Appl. Phys.*, **29**, 1132 (1958).

(7) K. Tamaru and M. Boudart in "Advances in Catalysis," Vol. IX, Academic Press, New York, N. Y., 1957, p. 699.

(8) S. Z. Roginskii and V. M. Frolov, *Doklady Akad. Nauk SSSR*, **111**, 623 (1956).

(9) A. Farkas, "Orthohydrogen, Parahydrogen and Heavy Hydrogen," Cambridge University Press, Cambridge, 1935, p. 89.

(10) E. Wigner, *Z. physik. Chem.*, **B23**, 28 (1933).

(11) Y. L. Sandler, THIS JOURNAL, **58**, 54 (1954).

(12) D. Alpert, *J. Appl. Phys.*, **24**, 860 (1952).

solution and outgassed *in vacuo* in a quartz vessel, heated to 800° for 2 days. The tube contained 2 strips of evaporated gold serving as electrodes for conductivity measurements on part of the film. Tungsten leads and molybdenum springs were used for making electrical contact with the strips. The vessel was degassed for 3 days at 300°. It was similarly treated overnight each time before a fresh film was deposited over an old film.

The molybdenum springs ceased to make contact after repeated heating and cooling of the vessel. Conductivity measurements thus could be made only in the initial experiments on thin films.

Conductivity Measurements.—These were carried out in a screened Wheatstone bridge circuit with 1.5 volt d.c. The imbalance due to conductivity changes was measured with a Keithley VTVM, type 200B.

Pressure Measurements.—The vacuum system contained what we call a "Toepler Gauge," as previously described.[11] This was used for calibrating volumes, mixing gases, and for calibrating the thermistors.

One of the thermistor gages was connected directly to the reaction vessel and one to the gas inlet before the vessel. They were used for ad- and desorption measurements with oxygen, hydrogen and krypton. The electric setup was roughly the same as used by Rosenberg.[13] The calibration curves (log pressure *versus* log voltage) for oxygen gave an almost straight 45 degree line between 3×10^{-4} mm. (1.5 mv.) and 3×10^{-1} mm. (1.5 v.). For calculating the pressure in the reaction vessel when below room temperature, the thermal transpiration corrections of Bennett and Tompkins[14] were used.

Hydrogen Analyses.—Ortho–para analyses were carried out by the Farkas micro-method.[15] In hydrogen–deuterium exchange experiments, samples were taken off the system and analyzed by mass spectrometer.[16]

Gases.—O_2, Kr (for surface area determinations) and He (for sputtering the film) were of spectroscopic purity. H_2 and D_2 were purified by passage through hot palladium tubes. Parahydrogen and orthodeuterium were prepared by adsorption on charcoal at solid nitrogen and liquid hydrogen temperatures, respectively. Equilibrium hydrogen was obtained by keeping hydrogen in a vessel containing charcoal impregnated with a paramagnetic salt; it was kept in the same temperature bath as the reaction vessel.

Because the films were found to be extremely sensitive to traces of oxygen, the gases in the initial experiments were passed over a freshly evaporated magnesium film before entering the reaction vessel. No ortho–para conversion took place in parahydrogen during the short contact time. In later adsorption experiments the film was discarded. When using normal hydrogen directly from the palladium tube, it was found that no poisoning of the film occurred. The other gases used generally caused a certain loss in activity due to impurities. Therefore the change in activity was frequently checked by remeasuring the rate of conversion of normal hydrogen to equilibrium hydrogen under standard conditions, *viz.*, at 77.2°K. and 4.5 mm. pressure. All curves given in the paper are corrected for changing activity.

Sputtering of Films.—The transparent "thin films" used in the first experiments were obtained by a discharge in 0.3 mm. helium, applying 1600 volts, 2 ma. d.c. for 10 minutes with the reaction vessel in a liquid nitrogen bath. "Thick films" of about 1 μ thickness (estimated from interference colors) were produced in the following manner: A strong discharge was passed in krypton between the two germanium electrodes, the gas being replaced a number of times. The electrodes became red hot in this process and thus were further freed from active gases. After degassing the coating produced by this discharge, at 300° *in vacuo*, new germanium was sputtered under milder conditions onto this coating in 4 mm. helium (300 volts, 35 ma., 30 minutes, 77°K.). The films were of rather non-uniform thickness; they had a geometric surface area of about 20 cm.^{2}.

(13) A. J. Rosenberg, *J. Am. Chem. Soc.*, **78**, 2929 (1956).

(14) M. J. Bennett and F. C. Tompkins, *Trans. Faraday Soc.*, **53**, 185 (1957).

(15) Ref. 9, p. 25.

(16) The authors are indebted to W. M. Hickam and his group for carrying out the analyses.

Results

The first films ("thin films;" see Experimental Section) were produced under poorer vacuum conditions than later films, and also before the additional cleaning of the germanium electrodes by a strong krypton discharge. They produced only a very slow conversion in hydrogen adsorbed at 77°K. (in a static system). The first film gave a half-life τ for the parahydrogen conversion of 25 hours. The activity of the films increased each time when a fresh film was sputtered on top of the old film. When the conversion was remeasured after certain time intervals, the rate was found to fall off gradually. This loss of activity was probably caused by adsorption of oxygen due to the residual oxygen pressure in the system.

The hydrogen reaction was found to have the characteristics of a magnetic spin inversion. No chemical activity was found: after the exposure of a 20-hour film, (*i.e.*, a film giving a half-life with light hydrogen of 20 hours at 77°K. and 4.5 mm. pressure) to a hydrogen–deuterium mixture, no measurable amount of HD was found after 16 hours; the exchange reaction must have been at least 100 times slower than the parahydrogen conversion.

With light hydrogen, the conversion at 89.8°K. proceeded 2.27 times more slowly than at 77.1°K. The negative temperature coefficient of the reaction again shows that the mechanism cannot be a chemical one; moreover it shows that the magnetic reaction itself is the rate determining step (and not desorption of the hydrogen).

The order of the reaction $n_k = 1 - (\partial \log \tau/\partial \log p)_T$ was found to be 0.8. We can evaluate the heat of adsorption Q of the hydrogen from the experimental activation energy E, assuming that for a magnetic conversion the "true activation energy" E_s is negligibly small. From the relation[17]

$$E = E_s - (n_k Q - RT) \qquad (1)$$

we find $Q = 1400$ cal./mole, a reasonable value for the molecular heat of adsorption of hydrogen. Later experiments made it clear that the surface of the thin films was not atomically clean. The results are characteristic of a surface containing a complete monolayer of strongly chemisorbed oxygen.

Reaction Mechanism with "Thick Films."—The following experiments were carried out with "thick films" (see Experimental Section). They were found to be much more active than the first thin films. Each fresh coating sputtered onto an old film gave a reproducible high activity. The parahydrogen conversion at 77°K. and 4.5 mm. pressure ("standard conditions") gave a half-life $\tau = 13.5 \pm 0.5$ minute. This value increased in some cases by up to 20% after the film was allowed to warm up to room temperature *in vacuo* for a short time to release the trapped helium.

A measurable hydrogen–deuterium exchange was now found to take place at 77°K.; it was 12 times slower than the parahydrogen conversion. This shows that also the conversion, at least in part, must involve a chemical exchange reaction of the

(17) Y. L. Sandler, *J. Chem. Phys.*, **21**, 2243 (1953).

same type. The H_2–D_2 exchange generally proceeds at a lower rate because of the smaller zero-point energy of adsorbed deuterium. However, the following investigation showed that in the hydrogen conversion an additional mechanism—the magnetic type of conversion—is operative which predominates at 77°K.

The ortho–para conversion in deuterium was measured under the same conditions; it proceeded 4 times more rapidly than the H_2–D_2 exchange. This shows that zero-point energy differences alone cannot explain the discrepancy between the rates of the hydrogen conversion and the H_2–D_2 exchange. The relative rates[18] for light and heavy hydrogen for a magnetic surface conversion cannot be predicted with certainty; their ratio usually lies between 1 and 4 at liquid air temperature. The ratio 3 found in the present case thus is within the expected range for the almost purely magnetic reaction at 77°K.

There is still another difference in the detailed mechanism that could in principle account for the difference in reaction rates of the ortho–para conversions (of H_2 as well as D_2) and the hydrogen–deuterium exchange reaction. In a chemical parahydrogen conversion the two atoms desorbing from the surface can come from the same parent molecule, while the exchange reaction obviously requires the exchange of atoms coming from different molecules. For this reason the kinetics of the two reactions was further studied.

Figure 1 shows the half-life at 4.5 mm. pressure, plotted on a logarithmic scale, *versus* the inverse absolute temperature. Here a less active film of 83 minutes standard half-life was used, produced by adding traces of oxygen; this made it possible to extend the measurements to higher temperatures, where reaction rates with clean films became too fast.

The exchange reaction gives a practically straight line between 77 and 180°K. The activation energy corresponding to this line is $E = 1600$ cal./mole. It follows from the shape of the two curves that the mechanism of the two reactions must be essentially the same in the higher temperature region (above 120°K.). In the low temperature region, however, the conversion curve is seen to bend down (faster rates). Here evidently another mechanism becomes predominant.

Figure 2 shows the pressure dependence of the conversion at 77 and 90°K. for an almost fresh film of 23 minutes standard half-life (lower curves), and the same for an oxidized film of 4.5 hours half-life (upper curves). Log τ is plotted *vs.* log p. The reaction order $n_k = 1 - (\partial \log \tau/\partial \log p)_T$ can be calculated from these curves. It was low and varied rapidly in the measured region. For example, at 77°K. for the faster film it changed from 0.35 at 2.5 mm. to practically 0 at 20 mm. pressure.

With the more strongly poisoned film (upper curves) we see that the two curves for 77 and 90°K. cross over near 4 mm. pressure. Thus, in the lower pressure region the half-life actually begins to decrease again with decreasing temperature. We have here a region of "negative activation energy" E characteristic of the magnetic conversion. It follows from equation 1 that for a magnetic conversion ($E_s \approx 0$) E will be negative, unless $n_k \approx 0$ (as is the case in the higher pressure region). The leveling off of the conversion curve (Fig. 1) at 77° K. can only be explained on the basis of a mechanism that is magnetic, at least to a large extent.

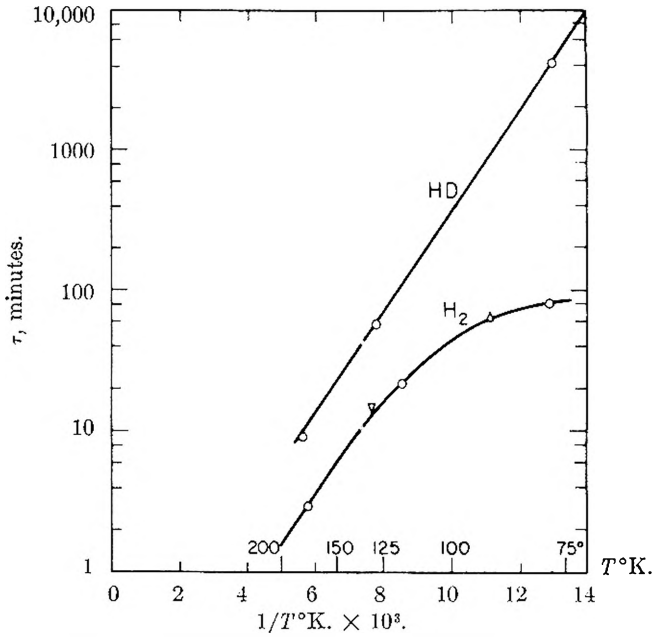

Fig. 1.—Half-life of parahydrogen conversion (H_2) and of hydrogen-deuterium exchange (HD) *vs.* the inverse temperature.

Practically no hydrogen–deuterium exchange was found with the more strongly poisoned film; the exchange proceeded about 1/200th as fast as the conversion. The initial results obtained with thin films (a large ratio τ_{HD}/τ_{H_2} and a negative activation energy) are characteristic for films inactivated by oxygen.

Effect of Oxygen at Very Low Pressures.—Figure 3 shows the effect on the conversion at 77°K. of measured amounts of oxygen, adsorbed at very low pressures at 77°K. The surface was exposed to increasing amounts of oxygen which were taken up quantitatively. The initial pressures, before adsorption, were between 1.5×10^{-5} and 2.2×10^{-4} mm. The number of adsorbed oxygen molecules is plotted against the percentage loss in activity $= (1 - \tau_0/\tau) \times 100$, τ_0 of the fresh film being 16 minutes in the present case. It is seen that the activity loss is not a linear function of the amount of oxygen taken up. The initial decrease in activity to one-half is caused by an amount of oxygen only enough to cover 0.4 cm.^{2}. On a plot of the amount taken up *versus* activity loss on logarithmic scales, a roughly straight line was obtained for 2 films.

The oxygen adsorption in this region of very low pressures is believed to have taken place on the

(18) Y. L. Sandler, *Can. J. Chem.*, **32**, 258 (1954).

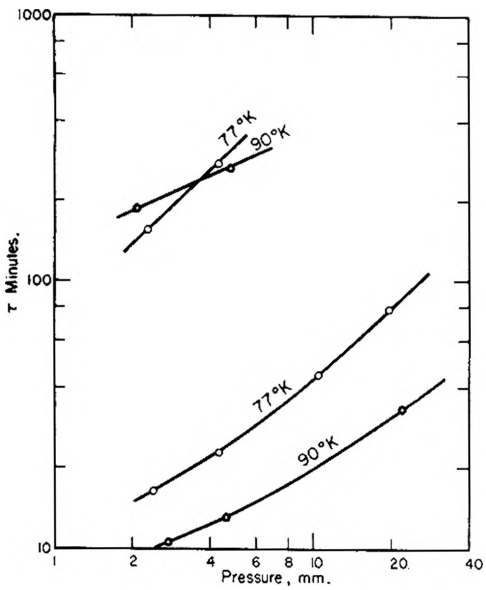

Fig. 2.—Pressure dependence of half-life for two films of different activity.

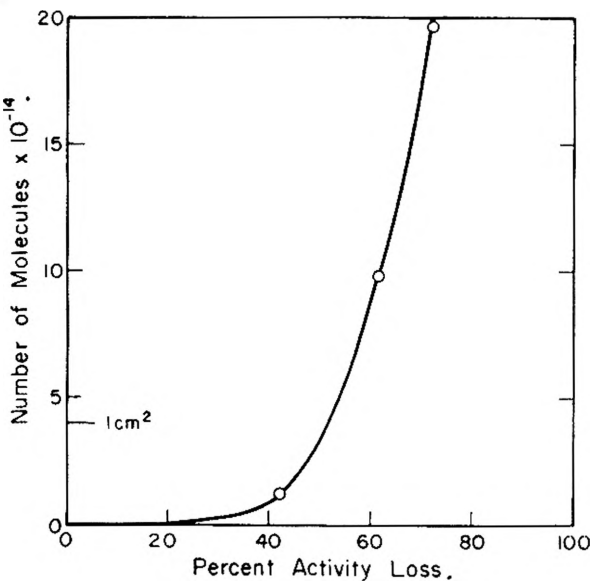

Fig. 3.—Number of adsorbed oxygen molecules *versus* activity loss.

atomically clean parts of the surface. The larger part of the activity for the parahydrogen conversion is due to this bare part of the surface. The H_2–D_2 exchange reaction apparently can occur only on the clean parts of the surface. We have previously seen that it is almost completely quenched on more strongly poisoned films, while some conversion activity persists.

A number of adsorption experiments also were carried out at room temperature with fresh films at pressures of 10^{-4} to 10^{-3} mm. Again a remarkably small oxygen uptake was found corresponding to about 1 cm.² coverage. The smallness of the uptake was quite unexpected in view of the high activity of the films. The reason for this behavior may be found in the micro-porous structure of the active surface. The pores may be closed by relatively small quantities of oxygen and, therefore, there may be no direct relationship between the amount of oxygen adsorbed and the active surface area for the parahydrogen conversion (see Discussion).

The experiments described from here on were all carried out at higher oxygen pressures or with films already containing a monolayer of strongly adsorbed oxygen.

Adsorption Isotherms.—The adsorbing surface area of the films ("thick films") was determined by the BET method, using krypton at 77°K. The film surface area was found to be 400 cm.², after allowance had been made for adsorption on the bare glass surface (~150 cm.²).

The oxygen adsorption isotherms for the same films at 77°K. were determined at pressures between 3×10^{-4} and 5×10^{-2} mm. This was done by two different methods giving essentially the same results, except at the lowest pressures. In one method oxygen was adsorbed on the film in increasing amounts at constant temperature. In the other method a measured amount of oxygen was let into the reaction vessel at room temperature. The vessel then was closed and cooled to 77°K. After 20 minutes a pressure reading was taken again. From the pressure drop the amount of adsorbed gas was calculated (taking into account the temperature change and the thermal transpiration effect). The vessel then was pumped at 77°K. and slowly warmed up again, before a fresh amount of gas was let in. These curves were taken with higher pressures first, going to lower pressures. Both methods gave practically identical results for films which had been in contact with oxygen.

In Fig. 4 two such curves are shown plotted on a logarithmic scale. The upper curve was obtained with a fresh film by the first method; the lower curve was obtained by the second method, starting with higher pressures first. The adsorption is seen to be reversible to a large extent. Adsorption was practically instantaneous at the higher pressures. Below 10^{-3} mm. a slow adsorption was observable which was completed after about 10 minutes.

The highest point taken (5×10^{-2} mm.) corresponds to a coverage of 300 cm.², *i.e.*, 75% of the BET area, provided that one oxygen molecule is adsorbed per two germanium sites (assuming 8×10^{14} sites/cm.²). Unfortunately no higher points could be measured to indicate whether the curve levels off, because the thermistors became insensitive at higher pressures. At any rate, the reversible adsorption extends to at least a large fraction of a monolayer.

From the upper curve and from a few points taken at 90°K., a heat of adsorption of 2.8 kcal./mole was evaluated for the low-pressure end of the curve (at 5×10^{-4} cc. coverage, 20 cm.²); it should be even lower at higher pressures. The relative pressures p/p^0 of the region investigated here are between 1.5×10^{-6} and 2.5×10^{-4}. This should be a region between the first strongly chemisorbed layer and the physically adsorbed layer (BET region).

Dependence of Conversion on O_2 Pretreatment.—When increasing amounts of oxygen at 77°K. were adsorbed on a fresh film, the film was increasingly poisoned for the parahydrogen conver-

TABLE I

INFLUENCE OF OXYGEN ON ACTIVITY

	Pretreatment of film	Adsorpt. T, °K.	O_2 press., mm.	Contact, min.	Pumping, hr.	Pumping T, °K.	τ, hr.
(1)	Fresh film	77	5×10^{-2}	60			22.3
	Same film				22	77	7.6
	Same, slowly warmed up				1	77 to 296	1.6
(2)	3 fresh films	296	5×10^{-2}	10	0.7	296	5.5
			3×10^{-3}	10	0.7	296	5.5
			1×10^{-1}	10	0.7	296	5.5
(3)	Fresh film	296	1.2×10^{-1}	20	0.8	296	7.2
	Same film				44		7.1
(4)	13 hour film	296	10^{-1}		5	600	3.6

sion. The half-life τ varied from 13 minutes for the fresh film to 22 hours for 5×10^{-2} mm. oxygen pressure. (This pressure which is the upper limit for the adsorption curve, coincides with the upper pressure limit at which the presence of oxygen in the hydrogen did not influence the ortho–para analysis.)

In Table I some typical experiments are summarized. The standard half-life resulting from different pretreatments of the film is given.

From example 1 it is seen that a film poisoned to 22 hours at 77°K. could be reactivated to a certain extent by pumping at 77°K. When the film was slowly warmed up to room temperature, the activity increased to a half-life of 1.6 hours.

On the other hand, if adsorption was carried out at room temperature, (examples 2, 3), the gas became much more strongly adsorbed. Pumping restores a good vacuum almost immediately. The activity is restored to a lesser extent than when ad- and desorbing at low temperatures. Example 4 shows that, with a film strongly poisoned at room temperature, even at 300° only partial regeneration occurs.

Influence of Light.—With the initial "thin films" changes in the electric conductivity and in the conversion activity were observed when the film was illuminated. From the experiments described above, it seems clear that they were covered from the start with a complete monolayer of oxygen.

The initial resistivity of a 20 hour film was 4.6×10^9 ohm/square. When left in a vacuum for one month, the resistivity increased to 1.3×10^{10} ohm/square, while the conversion half-life increased from 25 to 45 hours.

The 1 month old film was subjected to illumination by an incandescent lamp, the light being focused through the liquid nitrogen bath onto the inside surface of the film. The resistivity ρ was now found to decrease with time, obeying within the experimental error a logarithmic law

$$\rho = \rho_0 - \text{const.} \times \log (\text{time}) \qquad (2)$$

between 10 seconds and 18 hours after the start of illumination. The resistivity during this period decreased from 1.388×10^{10} to 1.269×10^{10} ohm/square ($\pm 0.003 \times 10^{10}$). In the dark it increased again, but at a lower time rate. The logarithmic law (2) observed for the conductivity change is equivalent to a logarithmic adsorption law ("Elovitch equation"). After improving the vacuum by degassing the traps, the rate of change of resistance

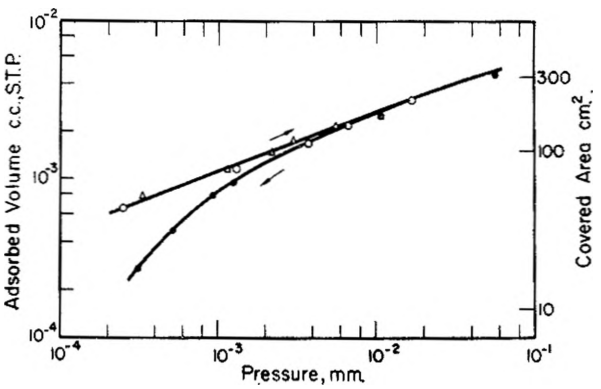

Fig. 4.—Reversible oxygen adsorption at 77°K.

on illuminating the film considerably decreased. From this and the slowness of the conductivity changes, it follows that a reversible gas adsorption must have been involved.

The films probably were p-type; films from intrinsic germanium have a tendency to be p-type at low temperatures owing to electrons trapped in surface states.[2] In the present case the old films must have been covered with a chemisorbed layer of oxygen. This is known to lead to an electron transfer into the surface, thus making the space charge layer more p-type. Reversible adsorption of oxygen seems to have led to the observed decrease in conductivity. This change in a p-type layer means that an electron transfer took place from the surface to the space charge layer. Conversely, illumination led to an electron transfer back into the surface and desorption of oxygen.

The effect of light on the conversion was studied with a film having a half-life of 134 minutes. When the film was illuminated in the course of a conversion experiment, no effect of the light could be detected. However, on pre-illumination of the film for a longer period, a small but significant effect was found.

TABLE II

EFFECT OF PRE-ILLUMINATION ON HALF-LIFE

Pretreatment	H_2 pressure, mm.	Temp., °K.	Half-life, min.
Dark	4.4	77.3	134
24 hr. light	4.2	77.2	138
22 hr. dark	4.0	77.0	155
22 hr. light	3.8	76.9	156
24 hr. dark	3.7	77.1	190

In Table II results are summarized showing the

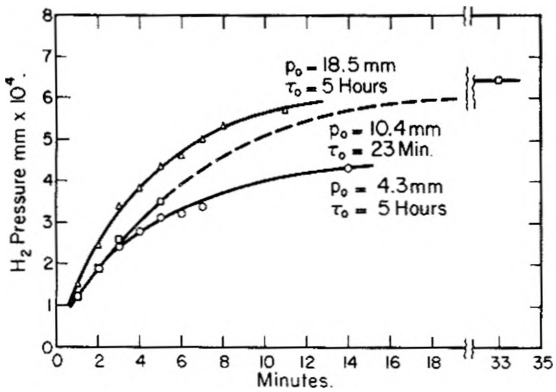

Fig. 5.—Hydrogen pressure at 77°K. *vs.* desorption time after one minute pumping, for films of different standard half-life and for different initial pressures.

influence of illumination on the parahydrogen conversion at 77°K. The half-life measurements are accurate to better than 1%. It is seen that after illumination of one day the half-life remained roughly the same, while after an equal period of darkness the half-life went up. The usual drift to longer half-lives in the dark (due to oxygen uptake in an imperfect vacuum) is counteracted by light.

The experiments with controlled amounts of oxygen have shown that addition of oxygen always leads to a slowing down of the conversion. We thus conclude that the slow effect of light on the conversion is caused by desorption of reversibly adsorbed oxygen, which uncovers a paramagnetic surface.

Desorption of Adsorbed Hydrogen.—For calculating the absolute conversion rate on our surfaces, the fraction of hydrogen in the adsorbed phase must be known. This fraction seemed too small to be determined by a conventional adsorption experiment. Therefore, the following procedure was adopted, giving us the minimum amount of hydrogen adsorbed.

Hydrogen was admitted to the reaction vessel at a known pressure p_0. The reaction vessel was then pumped for 60 seconds. After this time the vacuum indicated by the thermistor (connected to the reaction vessel) was less than 3×10^{-5} mm. The reaction vessel then was isolated and the pressure increase was determined as a function of time. Figure 5 shows three such curves. The two outer curves were taken with the same 5-hour film at different initial pressures p_0, while the middle curve was obtained with a relatively fresh film (τ = 23 min.). Within the limit of reproducibility of the amount desorbed for different films (~30%), no significant difference was found between fresh and oxidized films.

From the 4.3 mm. curve we find that at least 60% of the hydrogen desorbed in 10 minutes; the total amount was found by warming up to room temperature. From this amount we calculate that at least 1×10^{-4} of the total amount of hydrogen present in the reaction vessel must have been adsorbed in a conversion experiment at 77°K. and 4.5 mm. pressure. The coverage corresponds to 10^{-2} monolayers. This seems to be a reasonable value for adsorbed molecular hydrogen and is not likely to be too low to a considerable extent.

Discussion

It appears from our experiments that we may distinguish between three different types of surfaces having a different effect on the conversion: (1) the "bare" part of the surface, which causes the larger part of the magnetic activity at 77°K. with a fresh film and also causes the chemical activity; (2) the surface which contains a monolayer of strongly chemisorbed oxygen. This type of surface is believed to account for a part of the magnetic activity but it is chemically inactive; and (3) the surface covered by a layer of loosely bound oxygen; this surface appears to be completely inactive.

(1) The source of the high magnetic and the chemical activity of the bare part of the surface appears to be the same; both are connected with the existence of free valences.

It is not known with certainty whether the surface electrons must be unpaired to give a "surface paramagnetism" (as defined by the ability to catalyze the magnetic parahydrogen conversion). It seems probable that if the spins are far enough apart from each other, they may cause a conversion even if they are weakly coupled. When in coordination with one of the spins, the relatively small hydrogen molecule may be subjected to an inhomogeneous magnetic field that is of similar order of magnitude as in case of independent spins. At any rate, the conversion would be caused by highly unsaturated valences.

(2) The half-life of the magnetic conversion on a film with one chemisorbed oxygen layer is of the order of 1 hour. Films contacted with oxygen at 77°K. can be restored to have a half-life of about 1.5 hours by a slow warm-up *in vacuo* (Table I), while heating an oxidized film to 300° *in vacuo* gave a film of 3.5 hours. Experiments by various authors[1,6,19] on the regeneration of oxidized germanium surfaces by heating *in vacuo* show that no regeneration to a clean surface occurs below 400°. The partial restoration of activity in our experiments shows that the surface containing a monolayer of oxygen must be at least partly paramagnetic too. The same result is indicated by the illumination experiments with thin films; here we concluded that light causes desorption of reversible oxygen and uncovers a paramagnetic surface. This must have been a surface already covered with a monolayer of strongly adsorbed oxygen.

The paramagnetism of this surface is believed to be caused by residual unsaturated valences. The oxygen adsorbed in the form of O^- ions on intrinsically diamagnetic faces could also be a source of paramagnetism.

(3) The second layer is loosely bound at 77°K. Most of the gas can be desorbed at 77°K. or a somewhat higher temperature. When, however, a surface partly covered with a second layer of oxygen is allowed to warm up to room temperature, the oxygen is much more strongly bound. The reversible oxygen adsorption at 77°K. is different from the stronger activated adsorption known to exist at room temperature.[3] Formation of an

(19) A. J. Rosenberg, P. H. Robinson and H. C. Gatos, Lincoln Laboratory Quarterly Progress Report, group 35, Nov. 1, 1957, p. 16.

adsorption layer of the latter kind requires an activation energy (5.5 kcal. at monolayer coverage) and probably involves displacement[20] of surface atoms. The weak adsorption at 77°K. is, therefore, the precursor of the activated adsorption at room temperature.

The build-up of the weakly adsorbed layer is accompanied by a continuous decrease in the conversion rate. This, in principle, might be due to a combination of lower hydrogen adsorption and a lower transition probability. A much more likely explanation, however, is that this layer is diamagnetic. It cannot then consist of physically bound oxygen molecules which would be paramagnetic. The adsorption apparently is a weak chemisorption involving the pairing of the π-electrons of the oxygen molecules with the surface. (The tendency of oxygen molecules to form weak chemical bonds is, for instance, apparent in the formation of diamagnetic dimers[21] in gaseous and liquid oxygen.) The free valences causing the surface paramagnetism would be used up in this process, possibly by formation of a weak peroxide bond

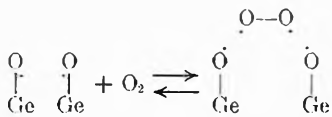

Bond formation will thus decrease the electron affinity of the surface and result in some transfer of negative charge from the surface back to the bulk. This would explain the observed photoconductivity changes.

Law[4] has found similar adsorptions of other gases (H_2, N_2, CO, CO_2) on a germanium single-crystal filament at low relative pressures. In view of the low heats of adsorption found, Law considered these to be "purely physical" adsorptions and therefore to have no effect on the conductivity of the solid. Our results with oxygen indicate that adsorption of these other gases is also caused by unsaturated valences on the surface and that the gases may cause a small conductivity change.

A similar type of weak adsorption also seems to cause the chemical parahydrogen conversion at low temperatures on metal surfaces.[22,23] Like the reversible oxygen adsorption, the reversible hydrogen adsorption causes a conductivity change[26] opposite to the initial change produced by the strongly adsorbed gas. The weak hydrogen adsorption is the forerunner of a slow adsorption[24-26] at higher temperatures, which in most cases is probably an activated adsorption (similar to the activated adsorption of oxygen on germanium at room temperature) and not bulk solution, as has often been assumed.[24,26]

It will be of interest to compare the rates found with the results of previous experiments with paramagnetic surfaces. We have reported previously that magnetic conversions seem to proceed at fairly consistent rates[11,27] when reduced to an equal number of paramagnetic centers and an equal fraction of hydrogen adsorbed on the surface.

It was found[11] that 1×10^{13} adsorbed oxygen molecules/cm.^{2} cause a "true" half-life of $\tau_s = 30$ seconds; by definition, $\tau_s = \tau \times f$, where f is the fraction of adsorbed hydrogen. On our surfaces the maximum density of paramagnetic centers would be about 8×10^{14}/cm.^{2} and $f = 1 \times 10^{-4}$. On 400 cm.^{2} surface (BET area), this would lead to an expected half-life of the order of 1 hour; or about 3 hours, if we correct for the ratio of the squares of the magnetic moments of an electron and an oxygen molecule.

It is seen that the strongly chemisorbed layer (2) causes a conversion of the expected magnitude, if we assume that a considerable percentage of the surface sites is paramagnetic. On the other hand, the residual conversion on the surface covered with reversibly adsorbed oxygen (3) is low, owing to the formation of the weak chemisorption bond.

The very fast conversion on what we termed the "bare surface" (1) is striking. The oxygen poisoning experiments at the lowest pressures at 77°K., as well as the adsorption experiments at room temperature, indicate that the active surface area is only of the order of 1 cm.^{2}. Supposing that the density of adsorbed hydrogen on the bare surface was roughly the same as on the oxygen covered parts of the surface, then $f = 1/400 \times 10^{-4}$. The conversion half-life of 13 minutes found for this surface then is more than 10^3 shorter than expected.

A more extended adsorption of hydrogen[4] on the bare part of the surface cannot explain this large discrepancy. We conclude that the area accessible to hydrogen is considerably larger than the area accessible to oxygen. The active surface apparently is located in micro-pores which are plugged up by a relatively small amount of oxygen. The effect probably is a consequence of the mode of preparation of the germanium. It is quite possible that these "pores" are dislocations not located in the film but in the solid germanium piece used as a cathode. In any case the strong surface paramagnetism of the "bare surface" is shown to be a consequence of a highly disordered structure, and not to be a property of certain perfect surface planes (previously considered a possibility[28,29]).

The same surface caused a high chemical activity. The fact that no low temperature activity for the hydrogen–deuterium exchange was found by Tamaru and Boudart[7] with their germanium films (produced by the decomposition of germane),

(20) M. Green, ref. 2, p. 372.
(21) G. N. Lewis, *J. Am. Chem. Soc.*, **46**, 2027 (1924).
(22) D. D. Eley, *Proc. Roy. Soc.* (*London*), **A178**, 452 (1941).
(23) A. Farkas and L. Farkas, *J. Am. Chem. Soc.*, **64**, 1594 (1942).
(24) O. Beeck, "Advances in Catalysis," Vol. 2, Academic Press, New York, N. Y., 1950, p. 161.
(25) F. C. Tompkins, *Z. Elektrochem.*, **56**, 360 (1952).
(26) J. H. Singleton, THIS JOURNAL, **60**, 1606 (1956).
(27) Y. L. Sandler, ref. 18, p. 257.
(28) Y. L. Sandler, *Phys. Rev.*, **108**, 1642 (1957).
(29) If the active area was really small (which does not appear likely), we could not completely rule out the possibility that small patches of metallic impurities, produced in the sputtering process, may have caused the activity. Therefore, to confirm our conclusions, we recently carried out a conversion experiment on germanium powder which had not come in direct contact with metal. The powder was produced by crushing a crystal in an ultra-high vacuum. Again a conversion was found at 77°K., but the rate per unit area now was considerably lower because of the more nearly perfect structure of the crushed crystals.

again points to the conclusion that the activity in our case is a structural property.

We might compare the chemical parahydrogen conversion at −78° on our films with the conversion at the same temperature on nickel films, investigated by Singleton.[26] Although the activation energies are about the same (1400 cal./mole), the germanium is about 75 times more active, if the active area is assumed to be only 1 cm.^{2}. This remarkably high activity again suggests that the true active area is larger than 1 cm.^{2}.

Even so, this surface area is not likely to have been much larger than the measured BET area (~400 cm.^{2}) because we would have found this from the hydrogen desorption experiments carried out with films of different cleanliness. We thus conclude that the activity of our films even when related to the true active area, is remarkably high.

In the case of transition metals and their oxides it has been demonstrated convincingly[30] that the strong low-temperature activity for the hydrogen-deuterium exchange is due to surface unsaturation connected with an intrinsic property of the catalyst, *viz.*, the existence of unfilled d-shells. It is interesting that structural unsaturation, as found in the present experiments, may lead to catalytic activity of a similar order of magnitude.

(30) D. A. Dowden, N. Mackenzie and B. M. W. Trapnell, ref. 7, p. 65.

STUDIES OF THE HYDROGENATION OF ETHYLENE OVER COPPER–NICKEL ALLOYS

BY W. KEITH HALL AND P. H. EMMETT*

Mellon Institute, Pittsburgh, Pa.

Received November 15, 1958

The hydrogenation of ethylene has been studied over a series of copper–nickel alloy catalysts. The activation energies obtained were relatively constant with composition over most of the range and with pretreatment, indicating that the observed changes in specific activities came about through changes in the frequency factors. No abrupt drop in specific reaction rate near the critical composition of 60 atom % copper was observed. The microcatalytic technique employed was particularly well adapted for studies of promoting and poisoning effects and allowed the characterization of a large promoting effect of chemisorbed hydrogen on the reaction rate. In the copper-rich range, this effect was so pronounced that these promoted alloys were more active than pure nickel. Relationships between the present work and current theories of catalysis are discussed.

Several years ago, Reynolds[1] studied the hydrogenations of styrene and benzene over a series of copper–nickel alloy catalysts. In both instances, the isothermal catalytic activity fell to a very small fraction of a fairly high initial activity, as the critical composition of 60% copper–40% nickel was approached from the nickel-rich side. This critical composition corresponds to that for which the band theory of metals predicts that the d band should be just filled. The magnetic moments at a fixed field strength of 5,000 gauss also were measured for these catalysts and found to fall as expected from the theory. From arguments presented by Dowden[2] this behavior could be expected if positive ions were involved in the reaction mechanism, and when copper is alloyed with nickel, the activation energy might be expected to increase and the frequency factor to decrease near the critical composition.

Considering the behavior of styrene as observed by Reynolds,[1] it was a little surprising from the experimental viewpoint that a totally different behavior in the ethylene hydrogenation was observed by Best and Russell[3] over a similar series of alloy catalysts. These workers observed activities several orders of magnitude higher than that of the pure nickel catalyst in the copper-rich range, where the d bands of the metals are filled. From the theoretical standpoint, however, this discrepancy could be explained in a multiplicity of ways.

According to the theoretical development of Dowden,[2] the behavior of the activation energies as a function of catalyst composition would be expected to be a better criterion of the nature of the surface processes involved than the isothermal reaction rates, as the frequency factors may contain factors which cannot be properly evaluated. Since the present authors had previously found interesting relationships between activation energy and composition with these same catalysts in the hydrogenation of benzene,[4] such data were obtained for the hydrogenation of ethylene and are reported herein.

Experimental

Catalysts.—Copper and nickel form a continuous series of homogeneous-substitutional solid solutions. For the present work, a series of unpromoted, high purity copper–nickel alloys, a pure copper and a pure nickel catalyst were made. It will suffice to say here that the preparation procedure followed quite closely Best and Russell's modification[3] of the method of Long, Fraser and Ott.[5] This involved coprecipitation of the metals as the basic carbonates followed by roasting to the mixed oxide phases. The latter were reduced to the metal phase with hydrogen at temperatures not exceeding 350°. Further details concerning their nature, preparation and purity are to be found in earlier

* Department of Chemistry, The Johns Hopkins University, Baltimore, Md.

(1) P. W. Reynolds, *J. Chem. Soc.*, 265 (1950).

(2) D. A. Dowden, *ibid.*, 242 (1950); *Ind. Eng. Chem.*, **44**, 977 (1952).

(3) R. J. Best and W. W. Russell, *J. Am. Chem. Soc.*, **76**, 838 (1954).

(4) W. K. Hall and P. H. Emmett, THIS JOURNAL, **62**, 816 (1958).

(5) J. H. Long, J. C. W. Fraser and E. Ott, *J. Am. Chem. Soc.*, **56**, 1101 (1934).

papers.[4,6] In one of these,[5] it was possible to show that any fluctuation in composition could not have exceeded 3%, proving that their bulk phases, at least, were very homogeneous. The designations and analyses of the reduced binary alloys in order of decreasing *atom per cent.* nickel are[4]: VIII = 100, V = 84.8, VI = 72.4, VII = 53.8, IX = 45.5, X = 34.3, IV = 20.6, XI = 14.7, III = 7.8 and II = 0.0%.

Preliminary experiments revealed that the activity of these catalysts for the low temperature hydrogenation of ethylene was quite sensitive to the amount of hydrogen left on the catalyst after reduction. This was controlled in an empirical way and three separate sets of studies were carried out. The catalysts were reduced at 350° and then treated with flowing purified helium carrying gas for 30 to 45 minutes at the same temperature. This helium treatment may be presumed to be equivalent to an evacuation of the same duration. After activity measurements had been made in this condition, the catalyst was again reduced overnight at 250°, but cooled in hydrogen to the reaction temperature and retested; after activity measurements had been made, the catalyst was reduced again overnight at 250°, but treated this time in helium, as before, and its activity redetermined.

Experimental Procedure.—With the exception of new samples of catalysts V and VI, the samples of the catalysts used in the study of the hydrogenation of benzene[4] were used again (after rereduction) in the study of the hydrogenation of ethylene. In preliminary experiments, in which an attempt was made to study the steady-state reaction over these beds, the reaction was found to be so exothermic that it could not be controlled, nor could a significant measure of the catalyst temperature be obtained. Above some very low conversion, the reaction would suddenly go to complete conversion. When this occurred, the catalyst could be cooled as much as 30° without a decrease in reaction rate. It was thought probable that the catalyst was forming a "hot spot" near the gas inlet. In an attempt to improve heat transfer, the catalyst tubes were opened under an atmosphere of carbon dioxide and mixed with an approximately equal volume of copper shot which had been screened through six and onto ten mesh U.S. standard screens. (Separate experiments with this shot had shown that it was inactive in the hydrogenation of ethylene at temperatures as high as 360° and that its surface area was immeasurably small, probably the order of the sum of the geometric areas of the individual beads.) This resulted in improved heat transfer, but still left much to be desired. (These beads were left in the tubes throughout all subsequent experiments.)

Because of the difficulties encountered in attempts at steady-state operation, another technique was adopted. At about this time, a new microcatalytic technique was under development in our laboratory.[7] The manner in which it was adapted to the requirements of the present experiments has been described in detail elsewhere.[8] Briefly, the technique involved establishing a fixed rate of flow (about 40 cc./min.) of purified helium gas over the catalyst. This gas which was inert to the catalyst was used to pass measured volumes of the purified hydrogen–ethylene gas over the catalyst with an unavoidable minimum of mixing. Eight milliliter slugs of the reactant gas were measured out in the special dosing device[8] and carried over the catalyst. With complete reaction, only about two calories of heat could be released by a given slug in the entire tube, so that the problem of heat removal no longer existed and the reactor became essentially isothermal. After reaction, the slug emerged from the tube and was carried directly over a charcoal adsorption chromatographic column for analysis.

Gases Used.—As it was discovered early in the work that these catalysts appeared to be particularly sensitive to small amounts of poison, the ultimate practical limit of purification of all the gases used was sought. Thus, to the already existing purification train in the hydrogen line consisting of a Deoxo purifier, anhydrous magnesium perchlorate, platinized asbestos at 375°, and more anhydrous magnesium perchlorate, a trap containing approximately 25 g. of high area charcoal was added. This was thermostated at −195° during experiments and was baked out under high vacuum at 375° at weekly intervals. A similar trap was built into the helium carrying gas line. Thus, the hydrogen and helium used in this work were of extreme purity.

Both a prepurified 60/40 hydrogen–ethylene gas mixture supplied by the Matheson Co. and synthetic blends of separately purified ethylene and hydrogen were used in this study. Both gases yielded essentially the same results. The Matheson gas was further purified using a chromous chloride scrubber such as described by Schuit and de Boer[9] for use with hydrogen. To their system, however, an extra Dry Ice trap packed with glass wool was added to ensure nearly complete removal of water. The purified gas was allowed to wash through the doser for approximately 15 minutes between experiments. When a slug was required, it was trapped and sent over the catalyst. A separate blend of synthesis gas was prepared and stored in two 5-liter bulbs. In this instance, high purity ethylene was run over a large sample of carefully reduced, high area commercial nickel catalyst to ensure the removal of poisons that might affect the test catalysts. No detectable ethane was present in the purified gas. To this was added hydrogen, purified as described below, to make the composition of the blend approximately the same as that supplied by the Matheson Co. This was transferred to the evacuated doser through the use of a buret system attached to a conventional high vacuum system. The fact that the data obtained, using the blends interchangeably in the various experiments, fitted the same curve was taken as evidence of their mutual purity.

The catalysts were protected from Hg vapor by small, gold-leaf traps. These consisted of 23 karat gold leaf, such as used for lettering on glass, wrapped around a solid glass rod. This assembly fitted loosely into a glass sleeve in such a way that the trap represented a constriction in the line rather than a mixing chamber for the slug with the carrying gas. The catalysts were further protected by a 15-cm. length of capillary tube (forming part of the catalyst tubes) immersed in the temperature control bath, which in nearly all cases ran from −20 to −100°. Without the traps, the capillary always showed visual evidence of the collection of Hg on lowering the bath; with the traps no trace of a Hg mirror was observed.

Temperature Control.—The cryostat used to maintain the catalysts at the various sub-zero test temperatures deserves special mention. It was a simple, homemade, unsilvered, unevacuated Dewar or double-walled flask, so arranged that the heat leak between the walls could be fixed by controlling the nature and pressure of the gas between the walls. The outer wall was made of 100-mm. Pyrex tubing and the two walls created an annular space about 1.5 mm. wide. When the bath was filled with pentane and the flask was immersed in liquid nitrogen, the heat leak between the walls was sufficient to produce a temperature decrease of about 1.5° per minute when the annular space was open to the atmosphere. This heat leak was balanced with a knife heater controlled by a thyratron circuit using a commercial-grade platinum resistance thermometer as a sensing element; the thermostated liquid was stirred by a rapid bubbling of compressed air introduced at the bottom of the bath. In operation, it was found that temperatures could be maintained for long periods of time or reproduced within ±0.3°. It was, therefore, particularly useful in this work because the temperature could be rapidly varied; in the 20 to 30-minute period required for the analysis of one slug, the temperature could be varied upward or downward by as much as 30°.

Treatment of Data.—The experimental procedure[8] consisted of selecting four to six temperatures, chosen so as to give conversions in the range between 10 and 90%, and cycling these temperatures from two to three times, obtaining a test conversion at each temperature, each time. These test conversions were plotted as a function of slug number and points taken at the same temperature were connected. In many cases, the extent of reaction was independent of slug number, but unfortunately in many others it varied with slug number either upward or downward to a greater or less degree. From the curves drawn through points taken at a single temperature, the data required for the construction of an activation energy curve could be picked off at any given slug number. In general, the data quoted herein were taken at the 12th slug. The calculated activation energies, however, were not strong functions of slug number, if they varied at all.

(6) W. K. Hall and L. Alexander, THIS JOURNAL, **61**, 242 (1957).

(7) R. J. Kokes, H. Tobin, Jr., and P. H. Emmett, *J. Am. Chem. Soc.*, **77**, 5860 (1955).

(8) W. K. Hall and P. H. Emmett, *ibid.*, **79**, 2091 (1957).

(9) G. C. A. Schuit and N. H. de Boer, *Rec. trav. chim.*, **72**, 909 (1953).

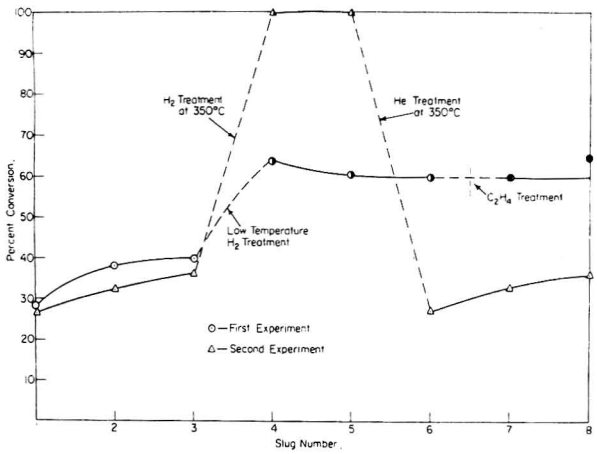

Fig. 1.—Effect of pretreatment on Cu–Ni catalyst X (34.3 atom % Ni).

The kinetics of a heterogeneous reaction taking place in a flowing system can only be rigorously discussed in terms of the differential reaction rate at some point or points in the catalyst bed. Since such a treatment generally involves a large multiplication of the required experimental data, true kinetics for catalytic flow systems are not frequently reported in the literature. In the present work, the usual formalism was adopted of quoting fractional conversions of the entering ethylene (under conditions of constant flow rate of carrying gas) and apparent activation energies, defined as the product of RT^2 and the observed temperature coefficient of the logarithm of these conversions. Since in general the catalyst was held in a constant volume of about 5 cc., the reactant gas passed through the bed at constant space velocity. Specific activities then were obtained by dividing total conversions by the total surface area contained in the tube. (Distinction should be made between the procedure adopted here and that used in our earlier work[4] where the flow rate per gram of catalyst was kept constant and specific activities were obtained by dividing the conversions by area per gram.) As the reaction is known to be first order in hydrogen,[13–17] an excess of this gas was used. Since the object of this study was not to elucidate the reaction mechanism and since variations in reaction rate of several orders of magnitude were expected and observed, this procedure was deemed satisfactory.

Results

Sensitivity to Poisons.—When the microcatalytic technique was adopted for the study of the ethylene hydrogenation, no difficulty from poisoning was anticipated. The catalysts to be studied had surface areas exceeding 1 m.²/g. and each tube contained a gram or more of reduced catalyst. The volume of each slug of gas was approximately 8 cc. (NTP); by this technique, therefore, no more than 180 cc. of synthesis gas passed any catalyst in a single set of experiments. Thus a simple calculation shows that even if the gas contained up to 0.01% of a poison, in a day's time only enough poison could be collected to cover from 5–10% of the total surface. It was surprising, therefore, when the first experiments with pure Ni catalyst VIII indicated that the catalyst was losing an appreciable fraction of its activity with the passage of the first few slugs. Because of the precautions taken to assure high purity of the reactants, it seemed unlikely that this effect could be due to poisons present in the reactant gas. Furthermore, helium had been adopted as the carrying gas for these experiments because it was particularly amenable to exceedingly high purification. By passing it slowly through a relatively large amount of high area charcoal at liquid nitrogen temperatures, it can be essentially quantitatively cleaned of any and all impurities except small traces of hydrogen. Consideration of these factors suggested that the observed effects should be attributable to some product of the reaction, possibly a carbonaceous residue of the type suggested by Beeck[10] or more recently by Jenkins and Rideal.[11] In the following paragraphs it will be demonstrated that while such a poisoning action is definitely a factor, with the pure nickel catalyst at least, it is a relatively minor factor as compared to the more powerful promoting and/or poisoning action of hydrogen. More specifically, it will be shown that while cooling from reduction to reaction temperature in hydrogen (rather than in He) strongly inhibited the low temperature hydrogenation of ethylene over the pure nickel catalyst, a similar treatment strongly promoted the reaction over all of the copper–nickel alloys.

In the example given in an earlier paper,[8] the plot of per cent. conversion *versus* slug number was relatively independent of slug number. This behavior was followed fairly well by all of the copper–nickel alloy catalysts in the hydrogen-treated condition, as well as by the pure copper catalyst regardless of the pretreatment. With the pure nickel catalyst, however, the per cent. conversion decreased strongly with slug number under all conditions of pretreatment. With the copper–nickel alloy catalysts, on the other hand, the catalytic activity increased strongly with slug number when the catalysts were treated in flowing helium for 30 minutes at 350° and cooled in helium; similar treatment at 250° yielded similar results with a somewhat less strong dependence. That the observed increase in activity as a function of slug number was due to the very slow adsorption of hydrogen at the low temperature was established by the experiments shown in Fig. 1. In the first experiment, a fresh sample of catalyst X was reduced overnight (17 hours) at 350° in carefully purified hydrogen gas. It was then treated with helium for 30 minutes at the same temperature and cooled in helium to −42.5°. A series of three slugs of synthesis gas were passed over the catalyst at this low temperature (circles). After the third slug had passed the catalyst, the hydrogen stream was turned back over the catalyst at the same low temperature for 30 minutes, following which it was swept out with the helium carrying gas, and the catalytic activity redetermined. With the next three slugs, the activity was found to have nearly doubled and to have leveled off to a fairly constant value. A similar treatment, after the sixth slug, with purified ethylene, appeared to have no further effect on the catalyst activity. Following the eighth slug, the catalyst was again reduced overnight in hydrogen at 350° and treated with helium at that temperature. On adjusting the temperature in the flowing helium gas to −42.5° and redetermining the activity, the data (triangles) obtained were found to be in excellent agreement with the corresponding results from the previous day as well as with the final three points of this experi-

(10) O. Beeck, *Disc. Faraday Soc.*, **8**, 118 (1950).
(11) G. I. Jenkins and E. Rideal, *J. Chem. Soc.*, 2490 (1955).

ment (discussed below). In this second experiment, the method of hydrogen treatment was changed so that the catalyst was warmed in the hydrogen flow to 350°, held at this temperature for 30 minutes and then cooled back to the lower reaction temperature by simply removing the furnace and allowing the catalyst to cool to room temperature before replacing the cryostat. On redetermining the catalyst activity (slug numbers 4 and 5), complete conversion of the reacting gas was obtained. When, however, the temperature was again raised to 350° in the flowing helium stream, and then recooled to the reaction temperature, data in almost perfect agreement with those obtained in the first part of the experiment were obtained. Such cycles as the one just described could be carried out many times on the same catalyst with excellent reproducibility as long as the conditions of pretreatment were strictly reproduced. Moreover, it could be demonstrated that the effect did not involve the reaction of a portion of the C_2H_4 with H_2 added at the high temperature. As could be anticipated from the lack of an effect of treatment with C_2H_4 gas, as shown in Fig. 1, when a slug of pure C_2H_4 was passed over a hydrogen treated catalyst, no C_2H_6 appeared on the chromatogram. Thus, it seems clear that the hydrogen taken up by the catalyst at high temperature became part of the catalyst itself with respect to the low temperature hydrogenation and acted as a promoter. The present data do not, however, eliminate the possibility that the primary action of this hydrogen was on the equilibria between various hydrocarbon intermediates and/or residues on the surface. However, the nature of a related phenomenon, observed by Kummer and Emmett[12] in this Laboratory several years ago, suggests a more fundamental change in the properties of the catalyst surface. In this instance, it was observed that the para-hydrogen conversion was poisoned by hydrogen chemisorbed above 100° on an iron synthetic ammonia catalyst, but not by that chemisorbed at −78°.

The effect of H_2 shown in Fig. 1 for catalyst X was general for all of the copper–nickel alloys. With pure nickel, the effect was equally dramatic, but in the opposite direction. In this case it was found that under the experimental conditions chosen, the conversion could be controlled at about 50 or at 95% by pretreatment with H_2 or He, respectively.

The poisoning effects of carbonaceous residues of the type[10,11] mentioned earlier may be superimposed on the effects of alteration of the hydrogen contents of the catalysts. In this case, alterations in conversion as a function of slug number with the hydrogen treated catalysts should provide some index of the possible magnitude of the poisoning action of the carbonaceous material. As the activities of the alloy catalysts in this condition were nearly independent of slug number, it may be inferred that with these, such poisoning is relatively unimportant. In any case, with these a decrease in activity could correspond to a desorption of H_2.

(12) J. T. Kummer and P. H. Emmett, THIS JOURNAL, **56**, 258 (1952).

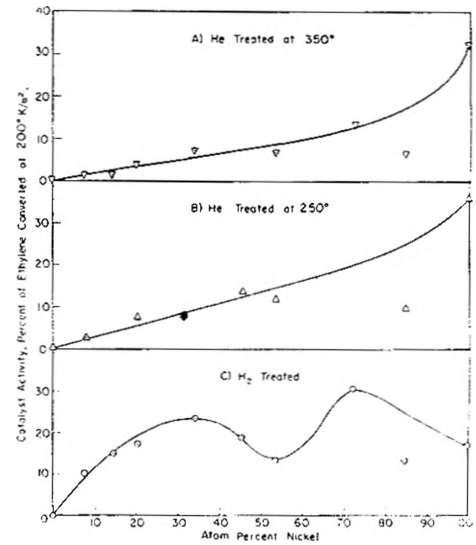

Fig. 2.—Catalytic activity of series of copper–nickel alloys at 200°K. in the hydrogenation of ethylene.

The only completely unambiguous example available, therefore, is that provided by the pure nickel catalyst. Here the conversion of the hydrogen treated catalyst fell from 95 to about 82% over a series of 16 slugs, or less than one third the primary effect of the H_2 treatment mentioned above.

Effect of Alloy Composition.—Three sets of standard pretreatment procedures were used, namely: (a) treatment with helium at 350°; (b) treatment with helium at 250°; and (c) cooling the freshly reduced catalyst in hydrogen to the reaction temperature.

Activation energy curves were obtained for each catalyst for each of the pretreatment procedures outlined above, utilizing the method described in reference 8. The specific activities are compared in Fig. 2 at 200°K. for each of these pretreatment procedures; this temperature was chosen because a value for all catalysts except pure copper catalyst II could be obtained from the activation energy curves without extrapolation. The point for nickel-rich catalyst V appeared in all three cases to be too low to be in agreement with the remainder of the data. It was not rechecked with another sample of catalyst because for the present purposes it makes little difference whether or not this catalyst should be twice as active. It has been ignored in drawing the curves.

The upper two curves for the helium-treated catalysts are quite similar and could be represented by straight lines to a good first approximation. Since these curves were the least affected by the promoting effect of hydrogen, they may be taken as most nearly representing the activity of the catalyst prior to promotion with adsorbed hydrogen. It seems important, therefore, that there is absolutely no evidence of any discontinuity in the curves at the critical composition of 40% nickel–60% copper. This is the more surprising when it is recalled that Reynolds,[1] when testing the hydrogenation of styrene to ethylbenzene found a curve which fell linearly to zero near 40% copper in a fashion reminiscent of that observed by the present authors for the hydrogenation of benzene.[4] It is

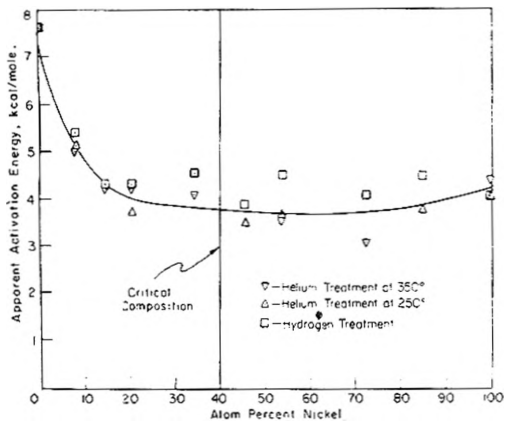

Fig. 3.—Complete set of activation energy data for the hydrogenation of ethylene on a series of copper–nickel alloys.

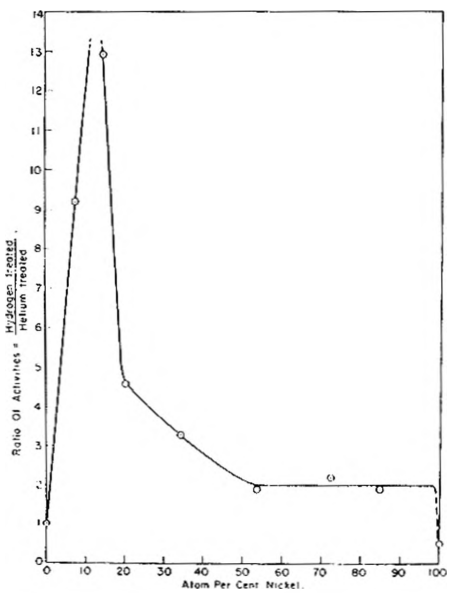

Fig. 4.—The promoting effect of preadsorbed hydrogen as a function of catalyst composition.

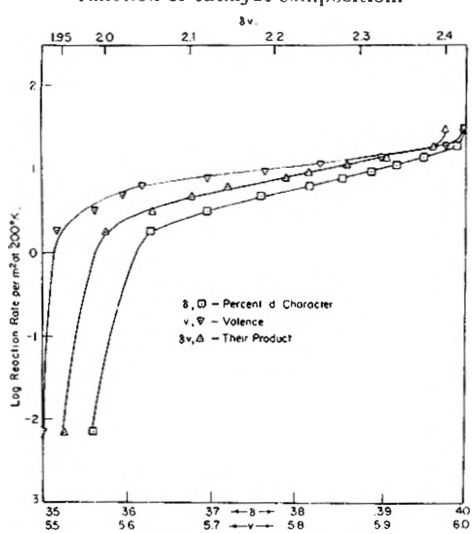

Fig. 5.—Correlation of catalytic activity with per cent. d character; data for He cooled sample used.

quite evident, therefore, that the mechanisms of the hydrogenation of ethylene and of styrene differ in an important way.

There has been much controversy in recent years as to the true mechanism of the hydrogenation of ethylene; proponents can be found for practically every conceivable path.[13–17] The present data indicate that the correct mechanism must be one in which, whatever electronic properties of the solid are relevant, variations in this series of catalysts largely cancel each other out. This is re-emphasized by the activation energy data plotted in Fig. 3; virtually no change in activation energy was observed over 85% of the composition range. The constancy over the greater part of the range is in agreement with the findings of Beeck[17] and of Best and Russell,[3] although in both of these instances, the absolute magnitude of the activation energy was considerably higher. Nevertheless, the former workers with a series involving many of the transition metals, and the latter workers with copper–nickel alloys observed no marked changes in activation energy, in spite of changes in activity of up to five orders of magnitude, in their respective studies. The data of Rienäcker[18] behave somewhat differently, although here too the frequency factor was dominant.

Data for the hydrogen-treated catalysts shown in Fig. 3 indicate that the activation energies for the catalysts in the hydrogen-treated state are as high as or a little higher than the corresponding values in the helium-treated state. Taking this fact into account and making a comparison of the activities of the hydrogen-treated catalyst shown in Fig. 2C to those of the helium-treated catalyst in Figs. 2A and 2B, it is again found that the relatively large changes in activity come about through changes in the frequency factors, rather than through changes in the activation energies.

The same conclusion may be reached by viewing the relative constancy of the activation energy over most of the composition range together with the gradations in the activity shown in any single curve of Fig. 2. This point is re-emphasized in Fig. 4, where ratios of the activities for the hydrogen-treated catalyst to those of the catalyst treated with helium at 350° are plotted as a function of composition. Over the range where relatively little change in activation energy was observed and where the activation energies of the hydrogen-treated catalysts were always higher, the activities of the hydrogen-treated catalysts were from two to four times those of the helium-treated catalysts. With catalyst XI (14.7% nickel), where the activation energies were found to be nearly identical, the activity was 13 times as high with the hydrogen-treated catalyst. Thus in the hydrogenation of ethylene, as in the hydrogenation of benzene studied earlier,[4] the variations in activity found in the present work must be largely attribut-

(13) D. D. Eley, "Catalysis," Vol. III, edited by P. H. Emmett, Reinhold Publ. Corp., New York, N. Y., 1955, p. 49 ff.

(14) H. Eyring, C. Colburn and B. J. Zwolinski, *Disc. Faraday Soc.*, **8**, 39 (1950).

(15) K. Laidler, *ibid.*, **8**, 47 (1950); "Catalysis," Vol. I, edited by P. H. Emmett, Reinhold Publ. Corp., New York, N. Y., 1954, p. 158 ff; p. 221.

(16) G. H. Twigg, *Disc. Faraday Soc.*, **8**, 152 (1950).

(17) O. Beeck, *Rev. Mod. Phys.*, **17**, 61 (1945); *Rec. Chem. Progr.*, **8**, 105 (1947).

(18) G. Rienäcker and E. A. Bommer, *Z. anorg. allgem. Chem.*, **242**, 302 (1939).

able to variations in frequency factor rather than variations in activation energy—both as a function of catalyst composition and as a function of hydrogen promotion.

The point for pure nickel shown in Fig. 4 lies much below the remaining points, reflecting the poisoning action of hydrogen on the reaction over nickel. With pure copper, no effect was observed; this is probably because the reaction was run in the temperature range (75 to 125°) where the chemisorption was rapidly reversible so that the effect just could not be observed. From the data of McCabe and Halsey,[19] it may be inferred that were this catalyst tested at a lower temperature, the ordinate for this point would be between eight and ten.

It is the data in Fig. 2C for the hydrogen-treated catalyst that should be compared with the data of Best and Russell[3] (and with our earlier work[4]). It should be recalled that these workers found that their alloys (which fell in the copper-rich region) had higher activities than those of their pure nickel catalyst. Although the variations in rate found in the present work were not nearly as large as those observed by Best and Russell, a similar result was obtained and a possible reason for this unusual observation appears to be established. The differences in magnitude between the two sets of data can perhaps be reconciled by consideration of the differences in techniques employed and/or the differences in the reduction temperatures.

Discussion and Conclusions

According to Beeck's correlation between catalytic activity in the hydrogenation of ethylene and lattice parameter,[17] the activities of this series of alloys would be expected to increase markedly between pure nickel and pure copper, while on the basis of his correlation of the same activity data with Pauling's per cent. d character,[20] the activities would be expected to decrease as copper is alloyed with nickel. The data for the helium cooled samples studied in the present work are in agreement with the latter correlation, indicating that electronic factors are controlling the kinetics rather than geometric factors.

The most satisfactory correlations found for the present data are shown in Fig. 5, where the logarithm of the specific activity is plotted against the per cent. d character of the orbitals used by the bonding electrons of the metal, the valence and the product of these quantities. These parameters were obtained by a route which is given in detail in Appendix I; they all increase continuously with composition from copper to nickel. As shown, a nearly linear correlation was obtained with all of these parameters for all catalysts tested except the pure copper catalyst II and to a lesser degree with pure nickel catalyst VIII. Catalyst II may be excused on the grounds of its much higher activation energy. When Schuit's correlation[21] of Beeck's data (for the product of the per cent. d character and the valence) is normalized (so that coincidence is obtained for nickel) by adding 3.8 to the log reaction rate quoted by Beeck,[22] satisfactory agreement with the data shown in Fig. 5 is obtained. Beeck used the correlation with per cent. d character as an aid in the interpretation of his data for the heats of adsorption of hydrogen and of ethylene and the rates of hydrogenation of ethylene on thin metal films of the transition elements. Since the heats of adsorption decreased and the reaction rates increased with the per cent. d character, and since in these experiments all variations in rate were due to variations in frequency factor, the following explanation was offered. A low heat of adsorption gives rise to a high frequency factor. In turn, the low heat of adsorption stems from a high per cent. d character (because in this case a large fraction of the available d orbitals is required to bond the crystal together, leaving only a small fraction available to bond adsorbate to the surface). Hence, the higher the d character, the lower the heat of adsorption and the higher is the catalytic activity.

If the data obtained in the present work are interpreted in a similar way, the heat of adsorption of ethylene on nickel would be expected to be lower than on the alloys and the heat would be expected to increase as more and more copper was alloyed with nickel. These data are not available, but the point is open for experimental verification.

The present data do not include figures for the amount of hydrogen left on the catalyst after any pretreatment. It is presumed that a catalyst cooled in hydrogen had a great deal more hydrogen left on its surface than one that had been treated with helium. The alloy catalysts were all promoted by hydrogen, whereas the pure nickel catalyst was poisoned by this gas. The promoting effect became greater in the copper-rich region where the d band was filled. Where hydrogen acted as a promoter, a small but consistent increase in the activation energy occurred, although with the pure nickel catalyst, where it acted as a poison, there appeared to be a small decrease in activation energy. It should be noted that in most of the earlier work[1,3,4] the catalysts used were in the "hydrogen-treated" condition and, that, so far, little attention has been directed toward this important factor.

The most pertinent related work is that of McCabe and Halsey,[19] who studied the hydrogenation of ethylene over a pure copper catalyst at 0°. From their data, it was concluded that hydrogen adsorbed between 100 and 140° fixed the activity of the catalyst. However, the adsorption of the critical hydrogen took place at 0° at a much lower rate but, once it was adsorbed, it was not removed by the reaction at 0° (as shown by the fact that a stable catalytic activity could be maintained with the hydrogen supplied at 0°); hence, it became part of the catalyst and was not a reactant.

More recently, Singleton[23] has shown that the rate of the ortho–para hydrogen conversion over evaporated nickel films depends critically upon the amount of slow-sorbed hydrogen. The rate was found to decrease with increasing amounts of slow

(19) C. L. McCabe and G. D. Halsey, *J. Am. Chem. Soc.*, **74**, 2732 (1952).

(20) L. Pauling, *Phys. Rev.*, **54**, 899 (1938); *J. Am. Chem. Soc.*, **69**, 542 (1947); *Proc. Roy. Soc. (London)*, **A196**, 343 (1949).

(21) G. C. A. Schuit, *Disc. Faraday Soc.*, **8**, 205 (1950).

(22) O. Beeck, *ibid.*, **8**, 118, 126 (1950).

(23) J. H. Singleton, THIS JOURNAL, **60**, 1606 (1956).

sorption, similar to the behavior observed by Kummer and Emmett[12] for synthetic ammonia catalysts.

Amano and Parravano[24] report a marked promoting effect of preadsorbed hydrogen on the benzene hydrogenation over ruthenium on alumina catalysts at 0°. Interestingly enough, here also the differences in rate observed for ruthenium–alumina, rhodium–alumina and platinum–alumina are all attributable to the pre-exponential factor rather than to any effect on the activation energy. Limitation of space prohibits further documentation of many related observations.[25–34]

Any attempt to provide a detailed explanation of these observations must of necessity be in the nature of speculation. Nevertheless, it would be expected that the observed effect of preadsorption of (promotion with) hydrogen would come about through the alteration of some fundamental property of the catalyst. In the experiments of McCabe and Halsey,[19] as in our own, there was ample evidence to support the contention that the hydrogen became part of the catalyst itself and did not enter into the reaction to any appreciable extent. In becoming part of the catalyst surface, the energetics of the process were changed, leading to the promoting effect. Alteration of the work function of the catalyst would appear to be a likely candidate for this role. Following the de Boer hypothesis[35] discussed in more detail in our earlier work,[4] it is to be observed that were the electronic chemical potential to be increased by the preadsorption of hydrogen, then an exponential term would appear as part of the frequency factor in such a way as to increase it also.

Two final comments seem in order. In the first place, it is of some interest to compare the activation energies found in this study with those reported in the literature for nickel catalysts. The following values have been reported: 3.2, 3.6, 4.6, 6.0, 8.2 and 10.7 kcal./mole.[13] The last value, due to Beeck,[17,22] was obtained on evaporated thin metal films of nearly all of the transition elements. Because of the technique employed, it is generally considered to be the most reliable. Nevertheless, as pointed out by Beeck himself, this value was obtained on surfaces highly poisoned by acetylenic complexes. Since, in general, the effect of a poison is to increase the apparent activation energy, it seems entirely possible that the values reported herein may be more representative of the true activation energy for the reaction than that of Beeck. On the other hand, if the surface was less covered by carbonaceous material in the present experiment, than in those instances of steady-state operation, hydrogen may have adsorbed with a higher average heat of adsorption and have lowered the apparent activation energy correspondingly. Finally, it should be noted that the data collected in the present work clearly indicate the difficulty of observing the kinetics of any catalytic process over uncontaminated alloy surfaces. It is clearly demonstrated that the choice of the copper–nickel alloy system is a particularly poor one to be used for the correlation of activity data to unmeasured properties of the solid state. That this has been found to be true for the present alloy system may be taken to indicate that similar results may be anticipated in many other situations, thereby emphasizing the futility of such an approach under ordinary circumstances. Nevertheless, special circumstances may be found which may allow such correlations to be made, *e.g.*, where the properties being correlated can actually be measured under conditions of reaction.

Acknowledgment.—This work was sponsored by the Gulf Research & Development Co., as a part of the research program of the Multiple Fellowship on Petroleum. Thanks are due to Professor H. S. Frank, Head, Department of Chemistry, University of Pittsburgh, for many helpful discussions in the course of this work.

Appendix I

Derivation and Calculation of Parameters from Resonating Valence Bond Theory of Metals for Copper–Nickel Alloys.—Correlations have been made by previous workers[10,20] between the logarithms of the specific activities of catalysts of various metals in the hydrogenation of ethylene and their per cent. d characters, and also between the logarithms of these same activities and the products of their per cent. d characters and their metallic valences (as defined below). It was, therefore, deemed desirable to test the data obtained in the present work for the same reaction in similar correlations.

Pauling[20] has supplied the necessary parameters for the pure metals and these values were used in the earlier correlations. So far, however, such calculations have not been reported in the literature for alloy systems. It was necessary, therefore, to attempt to extend this treatment to the copper–nickel alloy system.

Two simple courses are open for estimation of the per cent. d characters of alloy systems; both treatments are in keeping with the semi-empirical approach used by Pauling,[20] in that in both cases the assumption is made implicitly that the copper and nickel atoms retain their identity in the hybrids used to make up the giant crystal molecule in the same sense as metal atoms are conceived to do in the theory of directed covalency. In the first instance, it may be assumed that the copper and nickel atoms in the alloys retain the same d character as in the pure metals. In this case, the per cent. d character of the alloy system would be a linear function of composition; the results of

(24) A. Amano and G. Parravano, "Advances in Catalysis," Academic Press, Inc., New York, N. Y., Vol. IX, p. 716 ff., 1957.

(25) R. E. Cunningham and A. Gwathmey, ref. 24, p. 25 ff.

(26) K. Abelsova and S. Roginski, *Z. physik. Chem.*, **A174**, 449 (1935).

(27) K. Abelsova and T. Zellinskaya, *Acta Physicochim. U.R.S.S.*, **7**, 121 (1937).

(28) K. Abelsova, S. Roginski and T. Zellinskaya, *Doklady Akad. Nauk S.S.S.R.*, **30**, 29 (1941).

(29) S. Roginski, *ibid.*, **30**, 23 (1941).

(30) M. Babkova and I. Mochan, *ibid.*, **30**, 32 (1941).

(31) K. Zhadanovskaya, V. Korolev and I. Mochan, *ibid.*, **30**, 26 (1941).

(32) A. Rawdel and F. Yudin, *ibid.*, **30**, 37 (1941).

(33) L. Kh. Freidlin and N. I. Ziminova, *ibid.*, **74**, 955 (1950); *Izvest. Akad. Nauk S.S.S.R., Otdel. Khim. Nauk*, 659 (1950); 145 (1951).

(34) H. A. Smith, A. J. Chadwell and S. S. Kirslis, THIS JOURNAL, **59**, 820 (1955).

(35) J. H. de Boer, *Disc. Faraday Soc.*, **8**, 208 (1950).

TABLE I

SUMMARY OF CALCULATIONS OF PARAMETERS FROM VALENCE BOND THEORY

N_2	a_0[a]	f_{1A}	f_{2A}	Valence, v	δ	δ[b]	δ[c]	$(V\delta)$	log rate
0	3.5175	0.30	0	6.0	0.400	0.400	0.400	2.400	1.509
.10	3.5260	.278	.3915	5.978	.399	.400	.396	2.385	1.308
.20	3.5345	.250	.2483	5.899	.395	.396	.391	2.331	1.176
.30	3.5430	.214	.2183	5.831	.392	.393	.387	2.285	1.079
.40	3.5511	.1667	.2067	3.765	.389	.390	.383	2.241	1.000
.50	3.5595	.100	.1962	5.696	.386	.388	.379	2.213	0.909
.60	3.5680	0	.1827	5.619	.382	.386	.374	2.145	.820
.70	3.5772	0	.2115	5.596	.376	.379	.370	2.104	.699
.80	3.5871	0	.2273	5.564	.370	.371	.366	2.057	.519
.90	3.5978	0	.2319	5.517	.363	.364	.361	2.002	.225
1.00	3.6077	0	.250	5.500	.357	.357	.357	1.951	−2.144

[a] Reference 36. [b] For comparison, the value of δ calculated on the assumption that the decrease in valence is linear with composition, is listed here. This amounts to assuming that the ratio Cu (A)/Cu (B) is invariant with composition. [c] This column of figures was calculated on the assumption that the per cent. d character of the alloy was a linear function of composition.

such calculations are listed in Table I. This method is, however, inconsistent with the other physical data (magnetic moments and lattice parameters) used by Pauling in formulating the generalities expressed in (1) and (2), below. Thus, although the log reaction rates correlate as well, or better, with the per cent. d characters obtained by this method as to the values of this parameter calculated by the consistent method described below (Fig. 5), this approach will not be discussed further here or mentioned elsewhere in the text.

In the other possible approach, an alloy system may be considered to be made up of the proper combination of the hybrids where v is the hybrid

		3d	4s	4p	Hybrid
N_1	NiA; $v = 6$	⇅ ↑ ↑ . .	.	. . .	d^2sp^3
	NiB; $v = 6$	⇅ ⇅ . . .	.	. . o	d^3sp^3
N_2	CuA; $v = 7$	⇅ ⇅ . . .	.	. . .	d^3sp^3
	CuB; $v = 5$	⇅ ⇅ ⇅ . .	.	. . o	d^2sp^3

valence and N_1 and N_2 are the atom fractions Ni and Cu, respectively, with $N_1 + N_2 = 1$. Also defined are

f_{1A} = atom fraction of Ni (A) in Ni (A) + Ni (B)
f_{1B} = atom fraction of Ni (B) in Ni (A) + Ni (B)
f_{2A} = atom fraction of Cu (A) in Cu (A) + Cu (B)
f_{2B} = atom fraction of Cu (B) in Cu (A) + Cu (B)
n = bond order = valence/coördination number = $v/12$
R_n = atom radius in bonding of order n
R_1 = single bond radius
z = $10 + N_2$ = av. no. of electrons per atom outside the last closed shell
δ = % d character of the metal bond
a_0 = length of cubic cell

It should be noted that in the hybrid diagrams, dots and open circles represent orbitals which are hybridized d^2sp^3 and/or d^3sp^3 to form the bonding orbitals of the crystal—the dots indicating that an electron is available to populate the orbital, and the open circle, indicating that there is not. Thus, in the assembled crystal, dots represent orbitals in which paired electron bonds are to be found, whereas the open circles represent vacant orbitals into which electrons can be pushed by an impressed electromotive force and are, therefore, responsible for the high electrical conductivity of the crystal. It should also be noted that the number of dots in a hybrid corresponds to its valence and that the d^2sp^3 forms have $^1/_3$ d character, whereas the d^3sp^3 forms have $^3/_7$.

Nickel (A) deserves special mention. Here, the d^2sp^3 form is supposed to have two unpaired electrons in two of the three unhybridized *atomic d orbitals* (represented by arrows). That this should be the case follows directly from Hund's rule provided that only six electrons are available to occupy the five orbitals and that only two of the five are used in the hybridization. This gives rise to the magnetic moment of the high nickel alloys and allows the ratio of Ni (A)/Ni (B) (or f_{1A} and f_{1B}) to be fixed *a priori*. This fact (known values of f_{1A} and f_{1B} as a function of composition) is used in the following development.

It will be noted that both forms of nickel have the same valence (namely, 6), whereas Cu (A) and Cu (B) have valences 7 and 5. The net valence of the alloy-crystal is unknown, but enters in an important way into the binding energy and, hence, into the observed lattice parameter. This fact is used to fix the ratio of Cu (A) to Cu (B) below. From Pauling[20]:

$$R_n = R_1 - 0.300 \log n = R_1 - 0.300 \log v/12 \quad (1)$$

$$R_1(\delta, z) = 1.825 - 0.043z - (1.600 - 0.100z)\delta \quad (2)$$

For the face centered cubic structure

$$R_n = \sqrt{2}/4a_0 \quad (3)$$

Define

$$v = 6 - x; \quad 0 < x < 0.5 \quad (4)$$

because

$$5.5 < v < 6$$

Combining (1), (3) and (4)

$$\sqrt{2}/4a_0 = R_1 - 0.300 \log (6 - x)/12$$

or

$$\sqrt{2}/4a_0 = R_1 + 0.300 \log 2 - 0.300/2.303 \ln (1 - x/6)$$

Expanding the logarithm for small x

$$\sqrt{2}/4a_0 = R_1 + 0.0903 + 0.300/2.302(x/6) \quad (5)$$

the higher terms being entirely negligible to the required accuracy. Substituting (4) back into (5) and rearranging

$$R_1 = \sqrt{2}/4a_0 - 0.2206 + 0.0217v \quad (6)$$

Eliminating R_1 from equations 2 and 6 yields

$$\sqrt{2}/4a_0 + 0.0217v = 2.0456 - 0.043z - (1.6 - 0.1z)\delta \quad (7)$$

It is now convenient to redefine v and δ

$$v = 6N_1 + 7N_2f_{2A} + 5N_2f_{2B}$$
$$f_{2A} + f_{2B} = 1$$
$$v = 6N_1 + 5N_2 + 2N_2f_{2A} \quad (8)$$

and

$$\delta = {}^1/_3N_1f_{1A} + {}^3/_7N_1f_{1B} + {}^3/_7N_2f_{2A} + {}^1/_3N_2f_{2B}$$

or

$$\delta = N_1[{}^3/_7 - f_{1A}({}^3/_7 - {}^1/_3)] + N_2[{}^1/_3 + f_{2A}({}^3/_7 - {}^1/_3)] \quad (9)$$

Substitution of (8) and (9) into (7) and rearranging yields

$$f_{2A} = \frac{1.9370 - [\sqrt{2}/4a_0 + 0.043z + (1.6 - 0.1z)({}^1/_3N_2 + N_1[{}^3/_7 - f_{1A}({}^3/_7 - {}^1/_3)]) + 0.0217N_1]}{N_2[0.0432 + (1.6 - 0.1z)({}^3/_7 - {}^1/_3)]} \quad (10)$$

As noted earlier, all parts of the right-hand member are fixed for a given composition either by the known value of a_0 or by the known magnetic moment. Thus f_{2A} can be calculated and from it, the valence and the per cent. d character. The results of these calculations are also listed below in Table I. It is rather surprising that it appears to make little difference in the values of δ obtained whether these laborious calculations are used or whether the simple assumption is made that the valence is a linear function of composition. In these calculations the lattice parameter data of Owen and Pickup[36] are used. It should be added that, although both Pauling and Owen and Pickup quote figures and equations in terms of ångström units, both works actually are in terms of kX units.

(36) E. A. Owen and L. Pickup, *Z. Krist.*, **88**, 116 (1935).

THE PHASE DIAGRAM OF THE CERIUM–CERIUM TRICHLORIDE SYSTEM

By G. W. Mellors and S. Senderoff

Research Laboratories, National Carbon Company, Division of Union Carbide Corporation, P. O. Box 6116, Cleveland 1, Ohio

Received November 14, 1958

The solubility of cerium in cerium trichloride is 9.3 mole % with a temperature coefficient of nearly zero between 777 and 950°. The solubility of $CeCl_3$ in cerium is not greater than 0.2 mole % at 950°. Above 777° and 9.3 mole % added cerium the system consists of two immiscible liquids in equilibrium and has a consolute temperature that is too high to estimate from these data. The data from thermal and chemical analysis reported here are consistent with e.m.f. measurements on the system reported previously.

Introduction

The phase relationships in the cerium–cerium trichloride system were investigated by Cubicciotti.[1] He observed definite freezing point depressions and concluded that this melt must be a true solution rather than an emulsion or colloidal dispersion as supposed in this type of system by Lorenz.[2] Cubicciotti's results may be summarized as follows: the melting point of pure cerium chloride was 802° and successive additions of cerium metal resulted in a linear depression of the freezing point until at 33 mole % cerium the melting point was about 720°. This he considered to be the maximum solubility of the metal in the salt; no further depression of the freezing point was observed on the addition of more cerium metal and, probably, two immiscible liquids were formed. At one temperature (810°) the compositions of the two liquids in equilibrium were measured; a mixture of salt and metal was equilibrated, quenched and analyzed. The upper (salt-rich) phase was a black friable solid which contained 33% cerium metal and the lower phase (which had the appearance of the original metal) contained an insignificant amount of cerium chloride.

In an investigation of the e.m.f. of the cell Mo (or W)|$CeCl_3(x)Ce(1-x)$||$CeCl_3$|Cl_2(graphite) it was found that the measured potential remained constant (at constant temperature) from about 9 to 33 mole % cerium.[3] Below 9 mole % cerium the e.m.f. exhibited a variation with concentration as predicted by theory. The slope of the e.m.f.–concentration curve corresponded to a 2-electron change and it was concluded that Ce^{1+} and Ce^{3+} were the species present in melt. However, it was puzzling that the potential showed a "buffering" effect above 9 mole % cerium; this might be explained by the presence of a reservoir for Ce^{1+} in an un-ionized particle or a complex ion or, as suggested by Flood and Hill[4] for Fe_2O_3–FeO systems, in vacancies in the structure. At this stage measurements of density and electric conductance were commenced, since these would yield structural information on the melts; these measurements have now been completed and will be described in a succeeding paper.

During density measurements it was noted that compositions containing more than 10 mole % cerium were viscous and the results irreproducible. This was thought to be owing to imperfect homogenization; however, prolonged holding and stirring at 1000° failed to improve the situation. On several occasions cerium metal adhered to the density bob after such treatment.

Approximate measurements of the freezing points of compositions containing 20, 26 and 31 mole % cerium yielded results differing largely from those previously reported.[1] A redetermination of

(1) D. D. Cubicciotti, *J. Am. Chem. Soc.*, **71**, 4119 (1949).

(2) R. Lorenz, "Die Electrolyse Geschmolzener Salze," W. Knapp, Halle A-S (1906).

(3) S. Senderoff and G. W. Mellors, *J. Electrochem. Soc.*, **105**, 224 (1958).

(4) H. Flood and S. G. Hill, *Z. Elektrochem.*, **61**, 18 (1957).

the phase diagram of this molten system was then commenced.

Experimental

Materials.—$CeCl_3$ and Ce metal were prepared as described in a previous paper.[3]

All weighings and transfers were performed in a dry box. Argon was purified by passage through titanium chips at 900°.

Furnace and Crucibles.—The furnace was a tensile test type made by Marshall Products Company. The bore was 3.5" and an iron tube 3.25" o.d., 1/4" wall thickness served as a baffle between the furnace windings and the "Vycor" tube containing the crucible. The cell envelope was a 51 mm. o.e. "Vycor" tube, 30" in length, completely closed at the lower end by a 10 1/2 rubber stopper. Through the upper 10 1/2 stopper passed a 6 mm. o.d. molybdenum thermowell, an argon inlet tube and an aperture for a 1/8" o.d. molybdenum stirrer. A deep drawn molybdenum crucible, 1 5/8" o.d., 2 5/8" in height (Fansteel Metallurgical Corporation, North Chicago) contained the melt. The pedestal supporting the crucible was solid alumina, the crucible was enclosed in a graphite crucible, and an alumina tube, whose i.d. was approximately equal to the i.d. of the molybdenum crucible, rested on the top of the latter and extended to within 1/2" of the top of the 51 mm. "Vycor" envelope. In this experimental arrangement it was possible to attain a temperature constancy of better than 1° over the center 3.5" of the furnace containing the crucible and melt.

Temperature.—Chromel-alumel thermocouples were used, protected by 6 mm. o.d. molybdenum sheaths closed at the lower end. The thermocouple was positioned in the center of the melt, equidistant from the walls of the crucible and the surface of the melt. The temperature of this measuring element was indicated on an L and N Azar Recorder. A reference junction at 0° was provided. It is possible on this type of recorder to suppress all but a small fraction of the thermocouple output, displaying 10, 5, 2 or 1 mv. as full scale deflection of the "Speedomax" recorder. In this way a greater accuracy of temperature reading was obtained. Generally the first cooling curve was made with 5 mv., the second with 2 or 1 mv. full scale deflection. In the latter case the temperature could be read to within 0.25°. The chart speed of the recorder was 0.5 inch per minute and the cooling rate of the sample was 2.5° per minute. With some compositions, cooling arrests as long as 2 inches were observed by this procedure.

The temperature of the furnace was controlled by a "Wheelco" controller with an independent thermocouple adjacent to the winding.

General Procedure.—The apparatus was charged with an amount of $CeCl_3$ previously calculated to give a satisfactory depth of melt in the crucible (approximately 120 g.), together with the appropriate amount of Ce metal to give the intended composition. All joints in the apparatus were sealed with "Unichrome" stopoff (Metal and Thermit Corporation) prior to commencement of a run. The apparatus was flushed with argon for several hours and then heated slowly to about 950°. The melt was stirred and held at this temperature for several hours to ensure homogenization, the furnace power was then switched off and a cooling curve obtained on the recorder chart. The temperature was then raised and the cooling curve repeated. Unless agreement of inflection temperatures to better than 1° was obtained between the two runs, the results were discarded since a variation invariably indicated contamination. A further weighed amount of cerium metal then was added and the cooling curves repeated for this new composition. In experiments involving quenching from the high temperatures the entire "Vycor" envelope, with argon atmosphere maintained, was removed from the furnace and immersed in iced water.

Results

In Fig. 1b is shown the low cerium end of the diagram plotted from cooling curve data from some of the 60 compositions examined. Below 5 mole % Ce it was difficult to obtain the second inflection at about 777° as is frequently the case in phase diagrams of this type. Also it was observed that above about 9 mole % Ce the temperature of the first inflection remained virtually constant, falling no more than 2–3° up to 44 mole % added cerium. Between 9 and 44 mole % Ce a second inflection at 725° was obtained, this becoming more pronounced with increasing Ce content. It could be shown readily that between 777 and 725° the system consisted of a solid and a liquid in equilibrium, since it was possible to stir the contents of the crucible.

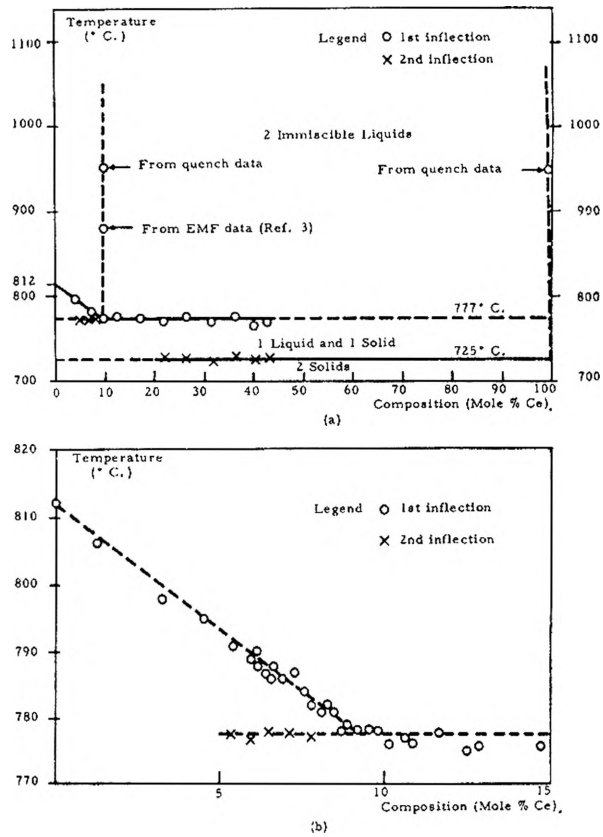

Fig. 1.—Phase diagram of Ce–$CeCl_3$ system: (a) complete diagram; (b) low Ce end.

It was now apparent that above 777° and between about 9 and possibly up to 99 mole % Ce, the system consisted of two immiscible liquids. Two samples containing about 20 mole % Ce were held, with stirring, at 950° for 2 hours, then allowed to stand at this temperature without stirring for a further four hours and finally quenched, solidifying within a minute. Visual examination of the quenched material showed the presence of two phases, the lower of which appeared to be cerium metal. Analyses showed the composition (in mole fraction) of the upper phase to be 0.097 Ce, 0.903 $CeCl_3$ and the lower to be 0.998 Ce, 0.002 $CeCl_3$. These results, therefore, give the compositions of the two liquids in equilibrium at 950°. Figure 1a shows the entire diagram for the system. It will be seen that a further point on the salt-rich vertical is obtained from e.m.f. data, *viz.*, the point of inflection of the log Ce^{1+}/Ce^{3+} *versus* e.m.f. curve.[3] It is apparent that no meaningful estimate of the consolute temperature of this system may be made since this line is so nearly vertical as far as it has been determined.

The horizontal line at 777° represents the freez-

ing point of the left hand (*i.e.*, $CeCl_3$-rich) liquid, while between this temperature and 725° the system consists of this material, now solid, in equilibrium with the right hand (*i.e.*, Ce-rich) liquid, the freezing point of the latter being 725°.

Discussion

As described in the introduction to this paper, the e.m.f. of the cell Mo(or W)|$CeCl_3(x)Ce(1-x)$||$CeCl_3$|Cl_2(graphite) remained constant from about 9 to 33 mole % cerium. The explanation of this behavior is now apparent from the redetermined phase diagram; addition of cerium metal beyond about 9 mole % does not change the cerium ion activity and the Ce^{1+}/Ce^{3+} ratio remains constant. It follows also that the e.m.f. remains constant.

One may calculate the heat of fusion of $CeCl_3$ from the phase diagram by the well-known equation

$$\Delta H_f = \frac{\nu x R T_0 T}{T_0 - T}$$

where ΔH_f = heat of fusion, ν = foreign particles/mole of added solute, x = mole fraction of solute, R = gas constant, T_0 = melting point of $CeCl_3$, T = melting point of solution. The value of νx to be used in the equation depends upon the nature of the solute and solvent. Thus, if ΔH_f were known, this calculation could be used to identify the species present in the solution. Unfortunately the only value for ΔH_f which is available (8 kcal./mole)[5] is derived from the phase diagram of Eastman, *et al.*[6] This diagram has now been shown to be in error. It may be noted that the calculated values of ΔH_f for Ce^0, Ce^+ salts and Ce^{2+} compounds as the assumed species of the solute are, respectively, 6.0, 9.0 and 18.[7]

Acknowledgments.—The authors gratefully acknowledge informative and enlightening discussions with H. R. Bronstein of Oak Ridge National Laboratory, L. M. Litz and E. R. Van Artsdalen of these laboratories. In addition they wish to thank J. C. Fisher, Jr., for generous help in the preparation of cerium chloride in these laboratories.

(5) L. Brewer, *et al.*, Paper 6, Page 76 *et seq.*, "Chemistry and Metallurgy of Miscellaneous Materials: Thermodynamics," ed. L. L. Quill, National Nuclear Energy Series.

(6) E. D. Eastman, D. D. Cubicciotti and C. D. Thurmond, Paper 2, Page 10, "Chemistry and Metallurgy of Miscellaneous Materials: Thermodynamics," ed. L. L. Quill, National Nuclear Energy Series.

(7) The solvent, $CeCl_3$ is assumed to contain Ce^{3+}, Cl^- and all possible complexes of Ce^{3+} and Cl^- in amounts such that they are not appreciably affected by a small addition (*i.e.*, 10^{-2} mole fraction) of solute.

VOLUME EFFECTS ON MIXING IN THE LIQUID Bi–$BiBr_3$ SYSTEM[1]

BY F. J. KENESHEA, JR., AND DANIEL CUBICCIOTTI

Stanford Research Institute, Menlo Park, California

Received November 15, 1958

Volume effects on mixing in the liquid Bi–$BiBr_3$ system have been determined by measuring the density as a function of temperature for mixtures varying in composition from pure $BiBr_3$ to 0.4 mole fraction of bismuth. It was found that there is a decrease in the total volume of the system on mixing. In the mixtures studied, the partial molar volume of the $BiBr_3$ is approximately the same as the molar volume of $BiBr_3$ and increases with temperature. The partial molar volume of the bismuth in the solutions is less than the molar volume of pure bismuth and decreases with increasing temperature. These effects are analogous to the volume changes found previously in the Bi–$BiCl_3$ system and are interpreted in terms of the same model of an interstitial type of solution, with the added bismuth entering into empty octahedral holes in the liquid quasi-lattice. Above a temperature of 300° the partial molar volume of bismuth becomes negative at infinite dilution. It is suggested that this contraction in volume is brought about when added bismuth enters into the interstitial holes in the expanded bromide lattice and pulls the surrounding bromides more closely together.

Introduction

In previous reports in our study of metal–salt interactions we have discussed the results obtained in the investigation of vapor pressures in the Bi–$BiCl_3$ and Bi–$BiBr_3$ systems[2,3] and volume effects in the Bi–$BiCl_3$ system.[4] As a continuation of this work we have measured the volume changes in the Bi–$BiBr_3$ system. As has been pointed out previously,[3] the phase diagram for the bromide system is very similar to that for the chloride. At 300° as much as 40 to 45 mole % bismuth can be dissolved in $BiBr_3$; at higher concentrations and at 300°, two liquid phases coexist.[5] In the present study only salt-rich homogeneous liquid solutions of bismuth in $BiBr_3$ were investigated.

Experimental

As in the chloride experiments, the densities of liquid Bi–$BiBr_3$ mixtures were determined by a pycnometric method, the details of which have been reported already.[4]

The $BiBr_3$ was prepared by reaction of Bi_2O_3 with aqueous HBr and then evaporation of the water under N_2. Before use, the $BiBr_3$ was distilled twice under 5 mm. of dry N_2, the final distillation being made directly into the Pyrex pycnometer containing a weighed amount of bismuth. The pycnometer was sealed under vacuum. The material in the pycnometer was always premelted by heating with a torch before being transferred to the furnace, which was already heated to a temperature of about 300°. This was done to prevent breaking of the bulb by expansion of the solid salt if the material were allowed to come to temperature in the furnace.

The $BiBr_3$ prepared in the above fashion was found by analysis to contain 46.36% Bi (determined gravimetrically as $BiPO_4$); the theoretical amount for $BiBr_3$ is 46.56%.

A cooling curve taken on a 100-g. sample of the pure $BiBr_3$ showed a halt corresponding to the freezing point at 218.5°.

(1) This work was made possible by the financial support of the Research Division of the United States Atomic Energy Commission.

(2) D. Cubicciotti, F. J. Keneshea, Jr., and C. M. Kelley, THIS JOURNAL, **62**, 463 (1958).

(3) D. Cubicciotti and F. J. Keneshea, Jr., *ibid.*, **62**, 999 (1958).

(4) F. J. Keneshea, Jr., and D. Cubicciotti, *ibid.*, **62**, 843 (1958).

(5) (a) B. G. Eggink, *Z. physik. Chem.*, **64**, 449 (1908); (b) L. Marino and R. Becarelli, *Atti accad. nazl. Lincei*, **24**, 625 (1915); **25**, 105 (1916); **25**, 171 (1916).

This compares with a value of 218° for the melting point listed by the National Bureau of Standards.[6]

Results

The densities of the Bi–$BiBr_3$ solutions were calculated in the same way as was described for the chloride system. The experimental densities obtained for solutions ranging in composition from pure $BiBr_3$ to 0.4 mole fraction of bismuth are shown as a function of temperature in Fig. 1. The straight lines drawn through the points were obtained from a least squares treatment of the data to fit an equation of the form $\rho = a - bt$, where ρ is the density in g./cc., a and b are constants and t is the temperature in °C. The constants for the equations are shown in Table I, along with the experimental temperature range and the standard error.

TABLE I

DENSITY EQUATIONS FOR Bi–$BiBr_3$ MIXTURES

Mole fraction Bi	$\rho = a - bt$ (g./cc.) a	$b \times 10^3$	Standard error (g./cc.)	Exptl. temp. range (°C.)
0	5.248	2.40	0.001	224–394
0.0129	5.260	2.33	.001	223–318
.0792	5.367	2.25	.001	227–363
.1308	5.433	2.15	.001	230–356
.1562	5.484	2.15	.002	216–393
.2935	5.702	1.85	.002	343–446
.4001	5.920	1.65	.002	355–447

The density of pure $BiBr_3$ as measured in this study was 1% higher than the value found by Jaeger and Kahn[7] at 250° and 2% higher at 400°. Jaeger and Kahn state that the melting point of their material was about 250°, which is considerably higher than that observed for our material (see Experimental).

From the density, the molar volume of the solution $\tilde{V}$ was calculated by means of the equation

$$\tilde{V} = \frac{M_1 x_1 + M_2 x_2}{\rho}$$

where M_1 and M_2 are the molecular weights of $BiBr_3$ and Bi, respectively, and x_1 and x_2 the corresponding mole fractions. The molar volume as a function of composition is shown in Fig. 2 for temperatures of 250, 300, 350 and 400°.

From the molar volume curves the partial molar volumes $\bar{V}$ of $BiBr_3$ and bismuth were determined by the method of intercepts. The values of these partial molar volumes for several compositions and temperatures are given in Table II. The error in the values for the molar volume is estimated to be ±0.1%. This error is greatly magnified in determining the partial molar volume of bismuth $\bar{V}_2$ at low concentrations because of the long extrapolation that must be made. Thus, at infinite dilution the error in $\bar{V}_2$ is estimated to be ±10 cc., and at concentrations between 0.1 and 0.3 mole fraction of bismuth it is ±2.5 cc. These errors were obtained by drawing the molar volume curve (Fig. 2) with its maximum plus and minus deviation and constructing tangents in each case to find the spread in the values for the partial molar

(6) "Selected Values of Chemical Thermodynamic Properties," Circular 500, National Bureau of Standards.

(7) F. M. Jaeger and Jul. Kahn, *Proc. Acad. Sci. Amsterdam*, **19**, 381 (1916).

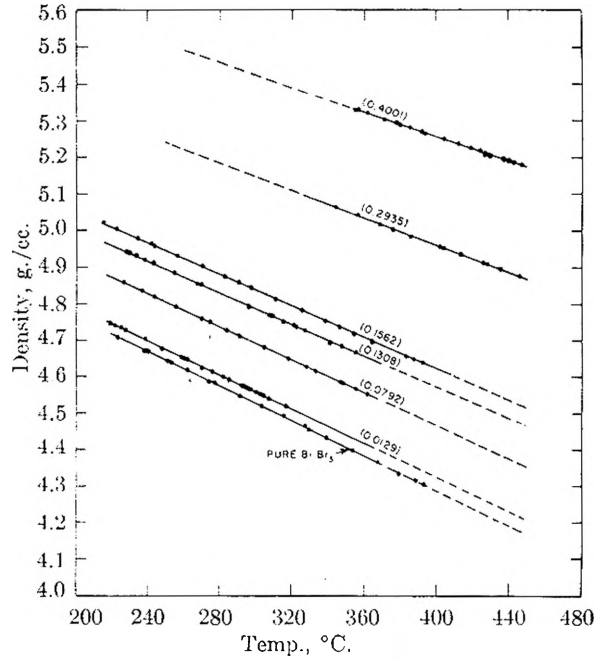

Fig. 1.—Density of Bi–$BiBr_3$ mixtures as a function of temperature. Numbers on curves indicate mole fraction Bi.

volumes. In using the method of intercepts in this work, $\bar{V}_1$ was determined graphically and $\bar{V}_2$ was calculated from $\tilde{V}$ and $\bar{V}_1$, using the expression

$$\tilde{V} = x_1 \bar{V}_1 + x_2 \bar{V}_2$$

The tangents to the curves were constructed from the normals, which in turn were obtained by holding a mirror across the curve and applying the "squint test."[8]

Discussion

The molar volume curves of Fig. 2 show that when bismuth is mixed with $BiBr_3$ there is a decrease in the total volume. Comparison of the bromide with the chloride system indicates they are quite similar in that respect, with a slightly larger decrease in the bromide case. For example, the largest decrease in the bromide system was 6% (at 400° and $x_2 \sim 0.4$) as compared to 5% for the chloride system (at 400° and $x_2 \sim 0.35$).

The partial molar volumes in this system follow the same pattern observed with the chloride. The partial molar volume of $BiBr_3$, $\bar{V}_1$, is essentially the same as the molar volume for $x_2 < 0.1$ and differs from the molar volume by only 1% up to $x_2 = 0.3$. Thus in the salt-like phase the volume of the $BiBr_3$ behaves almost ideally. The partial molar volume of the bismuth $\bar{V}_2$ is considerably smaller in dilute solutions than the molar volume of bismuth but increases as the bismuth concentration increases, reaching values of the order of those of pure bismuth when the solution becomes saturated. For a given composition $\bar{V}_2$ decreases with increasing temperature.

In the chloride system it was suggested that the results could be interpreted by postulating that the bismuth atoms, or ions formed by loss of electrons, enter into interstitial octahedral holes in the liquid

(8) A. G. Worthing and J. Geffner, "Treatment of Experimental Data," John Wiley and Sons, Inc., New York, N. Y., 1943, p. 88.

TABLE II

PARTIAL MOLAR VOLUMES IN Bi–$BiBr_3$ MIXTURES

Mole fraction Bi	250°	300°	350°	400°
		$\bar{V}_{BiBr_3}$, cc.		
0	96.6 ± 0.1	99.1 ± 0.1	101.8 ± 0.1	104.6 ± 0.1
0.1 to 0.2	95.9 ± 0.1	98.2 ± 0.2	100.9 ± 0.2	103.5 ± 0.2
.3	95.1 ± 0.2	97.8 ± 0.2	100.3 ± 0.2	103.5 ± 0.2
.4	[a]	95.1 ± 0.3	98.2 ± 0.3	100.9 ± 0.3
		$\bar{V}_{Bi}$, cc.		
0	−4 ± 10	−8 ± 10	−24 ± 10	−29 ± 10
0.1 to 0.2	14.5 ± 2.5	14.2 ± 2.5	11.3 ± 2.5	10.6 ± 2.5
.3	17.5 ± 2.5	15.2 ± 2.5	13.8 ± 2.5	10.8 ± 2.5
.4	[a]	19.7 ± 0.8	18.0 ± 0.8	16.7 ± 0.8
1.0	20.76 ± 0.02[b]	20.90 ± 0.02	21.03 ± 0.02	21.16 ± 0.02

[a] A mixture containing 0.4 mole fraction bismuth at 250° is in the two-phase region of the phase diagram. [b] The molar volume for pure bismuth was obtained from previous work.[4] The liquid molar volume at 250° (below the melting point) was obtained by extrapolation from higher temperatures.

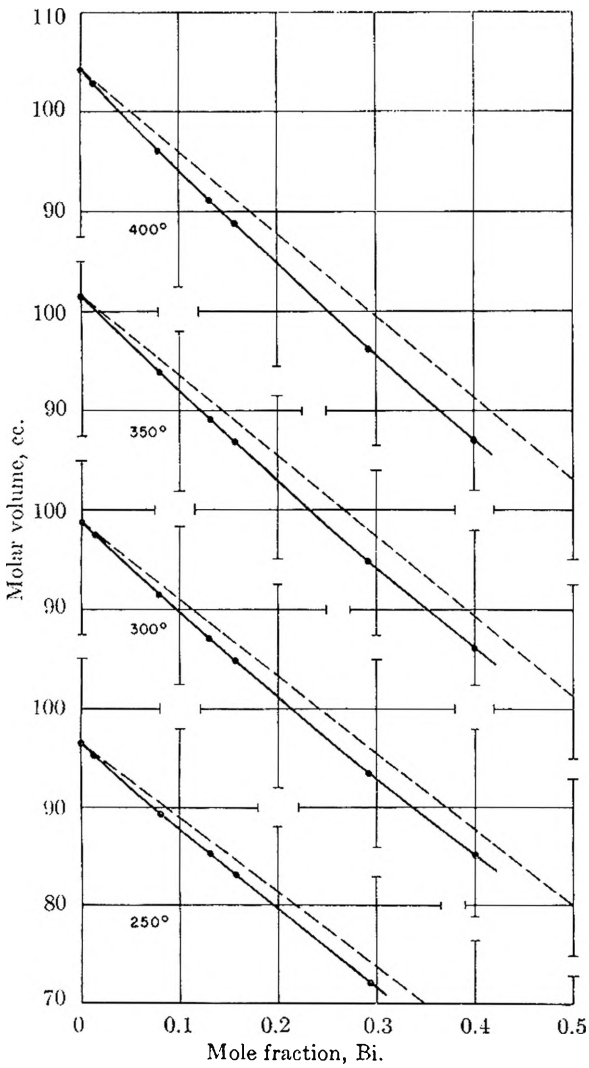

Fig. 2.—Molar volume of Bi–$BiBr_3$ mixtures as a function of composition. The dashed line in each case represents additive volumes.

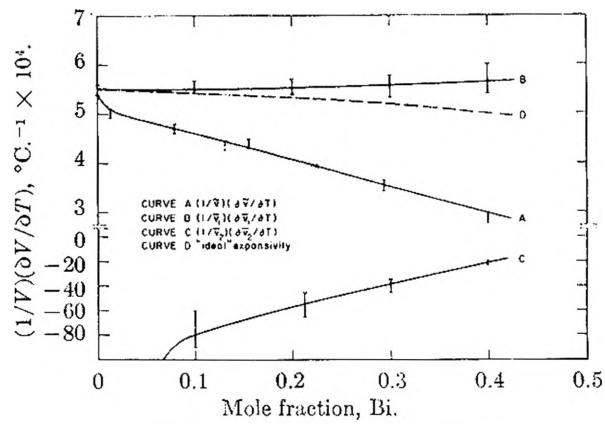

Fig. 3.—Expansivity of Bi–$BiBr_3$ solutions at 400°.

$BiCl_3$ quasi-lattice. The same model can be applied to the present system since the results are similar. The model accounts for the net decrease in volume on mixing because the bismuth, on dissolving, occupies holes that are already available in the original salt. (However, in dilute solution the volume decrease is too great to arise entirely from this effect, as will be seen.) The model also accounts for the decrease in $\bar{V}_2$ with an increase in temperature because the thermal expansion of the bromide lattice allows the added bismuth to be more readily accommodated.

As in the chloride case calculations of the partial molar volume of bismuth based on filling of the octahedral holes in a close-packed bromide lattice lead to results which are inconclusive in determining the bismuth species involved.

In dilute solutions $\bar{V}_2$ becomes negative, having a value of −30 cc. at 400° and infinite dilution (Table II). This effect can be included in the model if one postulates that on entering the hole the added bismuth causes a contraction of the bismuth and bromine species in its vicinity. At 400° the pure $BiBr_3$ has expanded by 8% over its value at 250°, as calculated from the change in molar volume. It does not seem unreasonable to suggest that the local structure around an octahedral hole can be reduced by at least this amount when bismuth is added to $BiBr_3$ at 400°. For the expanded close-packed structure assumed here the large negative value of $\bar{V}_2$ can be explained by a reduction of a few per cent. in the volume of the eight octahedra immediately surrounding an octahedral hole.

The expansivity of the bromide solutions, like that of the chloride system, exhibits negative deviations from additivity due to the fact that $\partial \bar{V}_2/\partial T < 0$. This is illustrated graphically in Fig. 3, where

the expansivity at 400° is shown as a function of mole fraction of bismuth. The total expansivity of the solution, $(1/\bar{V})\ (\partial\bar{V}/\partial T)$, is given by curve A, and the expansivities of the $BiBr_3$ and Bi, $(1/\bar{V})$, $(\partial\bar{V}/\partial T)$, are given by curves B and C, respectively. (The expansivities in this instance are plotted *versus* mole fraction rather than volume fraction as in the chloride case[4] to avoid using negative volume fractions, which would be obtained at dilute concentrations due to negative values of $\bar{V}_2$.) For an ideal solution, the expansivity of the Bi–$BiBr_3$ mixtures when plotted against mole fraction (curve D of Fig. 3) does not give a straight line as it would if plotted against volume fraction. The expansivity of the $BiBr_3$ in the solution, shown by curve B, was calculated from the values of $\bar{V}_1$ given in Table II, whereas values of the expansivity of the Bi in solution, curve C, were obtained from curves A and B and the relationship

$$\frac{1}{\bar{V}}\left(\frac{\partial\bar{V}}{\partial T}\right) = \left[\frac{x_1\bar{V}_1}{x_1\bar{V}_1 + x_2\bar{V}_2}\right]\frac{1}{\bar{V}_1}\left(\frac{\partial\bar{V}_1}{\partial T}\right) + \left[\frac{x_2\bar{V}_2}{x_1\bar{V}_1 + x_2\bar{V}_2}\right]\frac{1}{\bar{V}_2}\left(\frac{\partial\bar{V}_2}{\partial T}\right)$$

In accord with the behavior of $\bar{V}_1$ the expansivity of the $BiBr_3$ in the solution, $(1/\bar{V}_1)(\partial\bar{V}_1/\partial T)$, is essentially constant, showing that the $BiBr_3$ in solution acts much the same as pure $BiBr_3$. On the other hand, because of the decrease in $\bar{V}_2$ with increasing temperature, the bismuth expansivity is negative for $x_2 > 0.04$ and approaches $-\infty$ at about $x_2 = 0.04$ where $\bar{V}_2 = 0$. For $x_2 < 0.04$, $(1/\bar{V}_2)(\partial\bar{V}_2/\partial T) > 0$ and approaches $+\infty$ at $x_2 = 0.04$. The positive values arise because for $x_2 < 0.04$, both $\bar{V}_2$ and $\partial\bar{V}_2/\partial T$ are negative and hence the product $(1/\bar{V}_2)(\partial\bar{V}_2/\partial T)$ is positive. Over the range of compositions studied, the behavior of the bismuth in the solution leads to negative deviations of the total expansivity from the ideal curve, as in Fig. 3. Evidently the attraction of the added bismuth for the surrounding bromides as described above leads to a tighter binding than would be obtained in an ideal mixture.

Acknowledgments.—The authors are indebted to Mr. W. Wilson and W. Robbins for assistance in the experimental and computational work, and to Dr. C. M. Kelley for helpful suggestions.

A METHOD FOR ESTIMATING THE HEAT OF FORMATION OF THE HALIDES[1]

By Howard W. Anderson and LeRoy A. Bromley

Department of Chemical Engineering and Radiation Laboratory, University of California, Berkeley, California

Received November 20, 1958

In thermochemical calculations it is frequently necessary to estimate the standard heat of formation of compounds for which experimental data are unavailable. Although there are several methods that may be used, none is completely reliable or general. It was the purpose of this research to develop a more reliable and/or more general method of estimation or correlation. To do this several modifications were made to the work done by Pauling[10] in developing a scale of electronegativity. The result is the simple equation 2 with a set of parameters x and Y. Each valence state of each element may be assigned a value x and a value Y. Where these parameters have not been determined, they may be calculated for any cation when experimental heats of formation of two halide compounds of the cation are known. The average deviation obtained for a set of the halides of twenty-two metals was 0.93 kcal./mole. Except for certain fluorides an error of less than 10 kcal./mole may generally be expected in estimating an unknown using only two experimental values.

I. Introduction

In the estimation of chemical equilibria or the stability of chemical bonds it is often necessary to estimate the free energy of formation of chemical compounds. One way of doing this is to consider separately the contributions of the heat of formation and the entropy of formation. These two quantities may be estimated individually when they are not tabulated.

Let us consider the heat of formation. It may be defined as the enthalpy change for the reaction

$$nA + mB \longrightarrow A_nB_m$$

where A and B are elements. When both reactants and products are at an arbitrarily defined standard state, *e.g.*, 25° and 1 atm., the enthalpy change is the standard heat of formation at those conditions. Several methods[2-4,6-8,11,12] for estimating this quantity are available. None of these methods is sufficient in itself as a general method with reliable accuracy. The purpose of this research was to develop a more general and/or more reliable method of estimation which also would be easy to apply. The work done by Pauling[10] in developing a scale of electronegativities of the elements was taken as the starting point.

Pauling's approximate equation relating the heat of formation to electronegativity is

$$-\Delta H_f = \sum_{A-B}(x_B' - x_A')^2 - 55.1n_N - 24.2n_0 \quad (1)$$

where

(1) Howard W. Anderson, Master's Thesis, Univ. of Calif., Berk., 1958. Also UCRL 8152.

(2) Brewer, Bromley, Gilles and Lofgren, *Natl. Nucl. Energy Ser. Div.* IV, **19B**, 76 (1949).

(3) V. V. Fomin, *Zhur. Fiz. Khim.*, **27**, 1689 (1953).

(4) A. Gosselin, *Bull. soc. chim. Belg.*, **12**, 61 (1945).

(5) N. W. Gregory, *J. Am. Chem. Soc.*, **75**, 6054 (1953).

(6) A. F. Kapustinskii, *Izvest. Akad. Nauk. S.S.S.R. Otdel. Khim. Nauk*, 568 (1948).

(7) A. F. Kapustinskii and Yu. M. Golutvin, *ibid.*, 3 (1951).

(8) O. Kubaschewski and E. L. Evans, "Metallurgical Thermochemistry," John Wiley and Sons, Inc., New York, N. Y., 1956.

(9) R. S. Mulliken, *J. Chem. Phys.*, **3**, 586 (1935).

(10) L. Pauling, "The Nature of the Chemical Bond," Cornell University Press, Ithaca, N. Y., 1945.

(11) P. Sue, *J. chim. phys.*, **42**, 45 (1945).

(12) F. Trombe, *Compt. rend.*, **218**, 457 (1944).

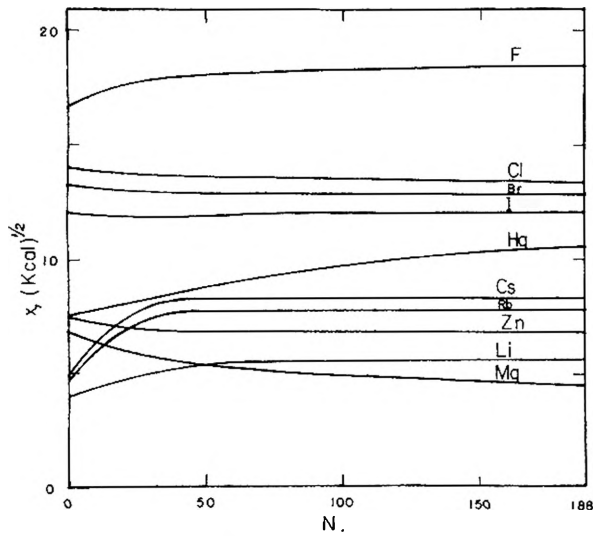

Fig. 1.—Iterative solution of eq. 4; x *vs.* N.

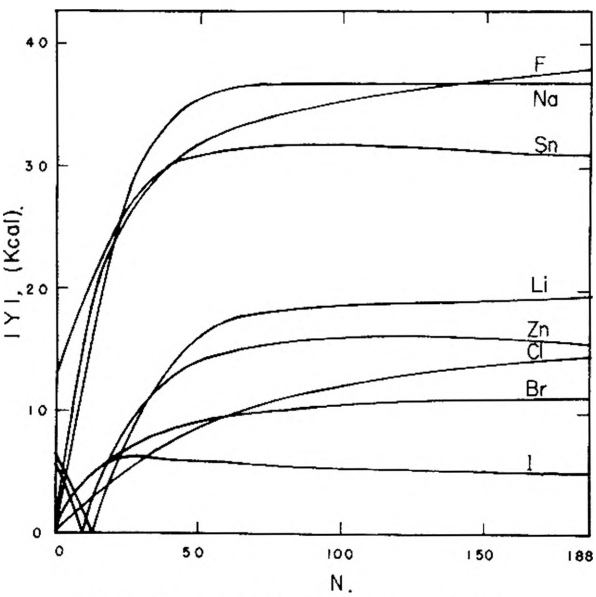

Fig. 2.—Iterative solution of eq. 4; Y *vs.* N.

x' is electronegativity (in kcal.$^{1/2}$)
n is the no. of atoms of nitrogen or oxygen in the molecule
ΔH_f is the standard heat for formation (in kcal.)

The summation is taken over the apparent number of single bonds. The corrections for nitrogen and oxygen are a result of their excessive stability in the standard state in comparison with the energy of single N–N or O–O bonds.

Although Pauling's equation was developed strictly empirically, Mulliken later gave some theoretical justification for its form.[9]

Let us now consider methods of improving the accuracy of equation 1. Pauling's use of correction factors for the standard states of nitrogen and oxygen suggests that this type of correction might also be employed for the other elements. It was decided to assign such a constant, designated Y, to each element. These constants can be used to correct for changes in the standard states of the elements. It should be pointed out that constants resulting from an empirical fitting process do not necessarily have physical significance.

The Pauling scale of electronegativity was determined initially as a unit for a small group of nonmetallic elements and then extended one value at a time for the metallic elements. It should be possible as well as desirable to evaluate the whole set at once. A set of Y values could be determined simultaneously. That is, we take eq. 1 as the form of our tentative relation. We use a complete set of Y values but do not assign values for x or Y, and obtain

$$-\Delta H_f = \nu_{AB}(x_B - x_A)^2 + \nu_A Y_A + \nu_B Y_B \quad (2)$$

where

ν_{AB} is the apparent no. of single bonds
ν_A is the no. of atoms of element A
ν_B is the no. of atoms of element B

Although the equation is written for binary compounds, it is not restricted to them. It is readily adapted for more general compounds. For example, if a compound contains anion C in addition to anion B, we write

$$-\Delta H_f = \nu_{AB}(x_B - x_A)^2 + \nu_{AC}(x_C - x_A)^2 + \nu_A Y_A + \nu_B Y_B + \nu_C Y_C \quad (3)$$

Since all the data used in this study are for compounds of only one cationic and one anionic species, the binary form of the equation is used throughout. This does not affect the generality of the results.

To evaluate the set of x and Y, we may utilize the technique of least squares to fit the equation to the experimental data. Let

$$\Delta = (-\Delta H_f)_{exptl} - (-\Delta H_f)$$

$$\frac{\partial}{\partial \xi}[\Sigma \Delta^2] = 0 = \Sigma \frac{\partial}{\partial \xi} \Delta^2 = 0$$

$$\xi = x_{A_n}, x_{B_m}, Y_{A_n}, Y_{B_m}$$

The result is

$$\xi = x_{B_m}: \sum_{i=A_1}^{A_n} 2\Delta\nu_{A_iB_m}(x_{B_m} - x_{A_i}) = 0 \quad (4a)$$

$$\xi = x_{A_n}: \sum_{j=B_1}^{B_m} -2\Delta\nu_{A_nB_j}(x_{B_j} - x_{A_n}) = 0 \quad (4b)$$

$$\xi = Y_{B_m}: \sum_{i=A_1}^{A_n} \Delta\nu_{B_m} = 0 \quad (4c)$$

$$\xi = Y_{A_n}: \sum_{j=B_1}^{B_m} \Delta\nu_{A_n} = 0 \quad (4d)$$

There result $2(m + n)$ equations in $2(m + n)$ unknowns, variables inseparable, to be solved simultaneously.

Results and Discussion

Solution of Equations 4.—This set of equations is non-linear and implicit in x. The method of solution chosen was the use of an iterative procedure. The particular method selected is discussed in detail by Anderson.[1]

Equations 4c and 4d are linear in Y and present no difficulty as far as the iterative solution is concerned. Equations 4a and 4b, on the other hand, are cubic in x and pose a problem in root selection. Preliminary hand calculations indicated that for the cations one root was greater than the anion electronegativities, one was approximately equal to the average of the anion values, and one was less.

NOMENCLATURE

Symbol	Definition	Units
$a,b,c,\ldots$	Numerical constants	
A	Designates a cation	
B	Designates an anion	
N	Iteration number	
x	Electronegativity (primed values denote Pauling's values)	$(\text{Kcal./mole})^{1/2}$
Y	Synthetic parameter	Kcal./atom
δ	$(-\Delta H_f)_{\text{exp.}} - (-\Delta H)_{\text{calcd}}$	Kcal./mole
ΔH_f	Standard heat of formation at 25°, 1 atm.	Kcal./mole
ν_{A-B}	Apparent number of single bonds A–B in compound A_nB_m	
$\nu_{A,B}$	Number of atoms of A or B per molecule	

The first root is contrary to the Pauling scale and the general theory. The second leads to a solution in which all the electronegativities are nearly the same. This is also contrary to the electronegativity concept. The third root is in agreement with the scale of Pauling and is thus the root of interest. A similar situation was found for the anion roots. Owing to the nature of the equations, these roots were evaluated by trial-and-error calculations.

The calculations required for the iterative solution and the trial-and-error evaluation of roots are readily performed by high-speed digital computers. In this case the problem was programmed for the IBM 701. The experimental data used in the solution were the heats of formation of the halides of twenty-two metals. The halides were selected because they are chemically similar and should pose no great problem in radical behavior. Unfortunately the program chosen did not allow for heats of formation larger than 250 kcal./mole and hence the heats of the alkaline earth fluorides were not used.

A plot of several x values as a function of the number of iteration is given in Fig. 1, and a set of Y values is plotted in Fig. 2. There is a tendency for the system to converge, although a few values seem particularly recalcitrant. The slopes of these curves are plotted in Figs. 3 and 4. Initially there appears to be a decided tendency toward convergence. However, as the solution continues, the rate of change of the x values seems to be heading toward a common value, as are the rates for Y. Although the rates at the end of 188 cycles are generally small, there is no indication that convergence on a unique set of values would be obtained in any finite number of additional cycles. The system at 188 cycles may be thought of as a pseudo solution; it approximately satisfies the set of equations, yet unique values have not been found for x and Y.

A plot of the total deviation from experiment of values of $-\Delta H_f$ calculated from sets of c and Y at different iteration numbers indicates that the agreement is continually improving and tending toward a minimum. The log of the slope of this curve plotted as a function of the log of the iteration number results in a straight line of slope minus 2.0 to within the accuracy of the data. That is

$$\frac{d\Sigma\delta}{dN} = bN^{-2} \qquad (5)$$

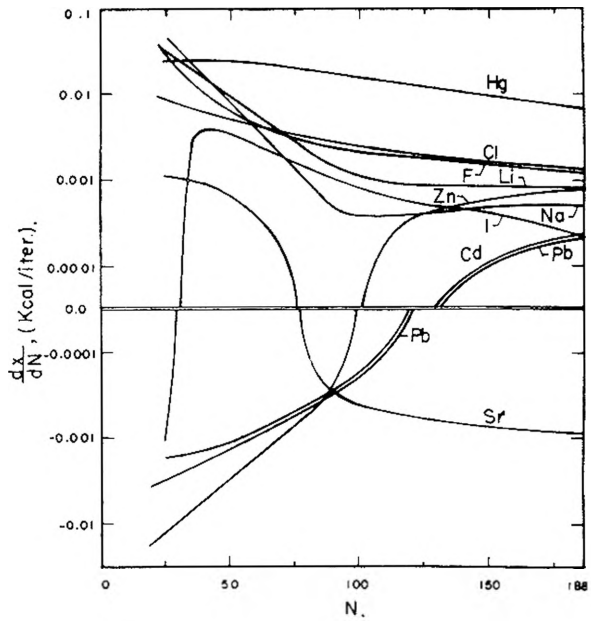

Fig. 3.—Iterative solution of eq. 4; dx/dN *vs.* N.

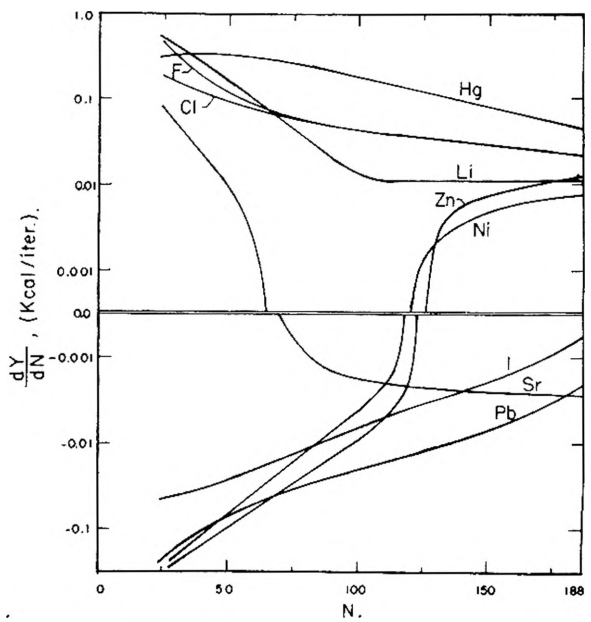

Fig. 4.—Iterative solution of eq. 4; dy/dN *vs.* N.

Graphically, b is 1.60×10^3. Integrating from $N = d$ to infinity, one obtains

$$\int_d^\infty \frac{d\Sigma\delta}{dN}\,dN = (\Sigma\delta)_{n=\infty} - (\Sigma\delta)_{n=d} = -\frac{1.60 \times 10^3}{d}$$

Let d be 188; then one gets

$$(\Sigma\delta)_{n=\infty} - (\Sigma\delta)_{n=188} = -8.5 \text{ kcal.}$$

Thus, if the slope of $\Sigma\delta$ *vs.* N were to continue to decrease in accordance with equation 5, $\Sigma\delta$ would be reduced by 8.5 kcal. after an infinite number of iterations. Although this is to be considered only as an approximation, it is indicative of the extent to which correlation may be improved by continuing the iterative procedure. For the present purposes, this amount of gain in agreement with experiment does not warrant the time or the financial investment in computer time that is

required to obtain it. The system at 188 iterations will be considered a "solution" and evaluated as such. It is given in Table I.

TABLE I

ITERATIVE SOLUTION OF EQUATIONS 4
VALUES OF x AND Y FOR ITERATION 188

Ion	x (kcal.$^{1/2}$)	Y (kcal.)	Ion	x (kcal.$^{1/2}$)	Y (kcal.)
Sn^{++}	6.858	−30.91	Mg^{++}	4.522	−36.60
Pb^{++}	7.220	−18.30	Ca^{++}	4.788	10.70
Zn^{++}	6.858	−15.58	Sr^{++}	4.618	13.70
Cd^{++}	7.255	−10.16	Ba^{++}	4.533	19.38
Hg^{+}	9.554	2.53	Li^{+}	5.595	19.61
Cu^{+}	10.107	6.68	K^{+}	7.553	54.00
Cu^{++}	6.980	−60.47	Rb^{+}	7.794	55.90
Ag^{+}	9.134	− 0.79	Cs^{+}	8.295	61.93
Ni^{++}	6.480	−50.73	F^{-}	18.449	−37.97
Co^{++}	6.620	−44.70	Cl^{-}	13.411	14.67
Fe^{++}	6.534	−42.14	Br^{-}	12.840	11.31
Mn^{++}	6.853	− 3.35	I^{-}	12.076	5.22
Cr^{++}	6.770	−17.14			

Evaluation of Solution.—The experimental data and back-calculated heats are listed in Table II. The agreement with the experimental data is considerably better and comparable in order of magnitude with the expected error in the experimental values. Continuing the iterative procedure further can indeed result only in minor gains.

During the calculation of the average deviation it was observed that for chromium the deviation from experimental values was much larger than for any other element: the average error for three values of $-\Delta H_f$ was 3.90. A check of the experimental data revealed that they were in serious disagreement with the latest information; the error in the value for CrI_2 was 13.9, for $CrCl_2$ was 2.4[5] kcal. New x and Y values for chromium were calculated from the latest data using equations 4b and 4d. The average error was reduced to 1.45. This demonstrated that the present method might detect some large deviations in experimental determinations.

Extension of the x and Y Scale.—Additional individual values can be calculated readily, as was done in correcting the chromium constants, if a set of values of x and Y is available. It would increase the range of applicability of the equations if the scale could be extended to include oxygen, sulfur and also radicals like the carbonate and sulfate. That is, consider the radicals as acting as entities in the equations instead of a combination of elements. Such a calculation was made using carbonate, nitrate, sulfate and acetate radicals. Constants for oxygen and sulfur were calculated at the same time. These calculations were again made on the IBM 701, using a modification of the original program to solve equations 4a and 4c for each anion. The results indicated that two constants per element are inadequate to produce a satisfactory correlation.[1]

TABLE II

SOLUTIONS OF EQUATIONS 4 FOR HALIDES
COMPARISON OF EXPERIMENTAL DATA AND BACK-CALCULATION FOR $-\Delta H_{f298}$

All data in kcal./mole.

Compd.	Exptl.	Calcd.	Compd.	Exptl.	Calcd.
LiF	146.3	146.87	Hg_2Cl_2	63.32	64.14
LiCl	97.70	95.37	Hg_2Br_2	49.42	49.27
LiBr	83.72	83.41	Hg_2I_2	28.91	28.22
LiI	64.79	66.84	$HgCl_2$	55.0	54.48
NaF	136.0	136.46	$HgBr_2$	40.5	42.02
NaCl	98.232	96.27	HgI_2	25.2	24.19
NaBr	86.030	85.60	$SnCl_2$	83.6	84.31
NaI	68.84	70.74	$SnBr_2$	63.6	63.28
KF	134.46	134.75	SnI_2	34.4	33.99
KCl	104.18	102.98	PbF_2	158.5	157.93
KBr	93.73	93.26	$PbCl_2$	85.85	87.68
KI	78.31	79.67	SrF_2	(290.3)	(320.35)[a]
RbF	131.28	131.46	$SrCl_2$	198.0	197.67
RbCl	102.91	102.11	$SrBr_2$	171.1	171.52
RbBr	93.03	92.67	SrI_2	135.5	135.39
RbI	78.5	79.45	BaF_2	(286.9)	(330.75)[a]
CsF	126.9	127.07	$BaCl_2$	205.56	206.34
CsCl	103.5	102.77	$BaBr_2$	180.4	180.0
CsBr	94.3	93.89	BaI_2	144.0	143.61
CsI	80.5	81.45	CrF_2	181.0	181.38
MgF_2	(263.5)	(275.38)[a]	$CrCl_2$	97.0	94.82
$MgCl_2$	153.40	150.75	CrI_2	40.3	42.11
$MgBr_2$	123.7	124.38	MnF_2	189.0	189.66
MgI_2	86.0	87.96	$MnCl_2$	115.3	112.00
CaF_2	(290.3)	(308.01)[a]	$MnBr_2$	90.7	90.96
$CaCl_2$	190.0	188.74	MnI_2	59.3	61.66
$CaBr_2$	161.3	162.98	$FeCl_2$	81.5	81.77
CaI_2	127.8	127.37	$FeBr_2$	60.02	60.00
CuI	16.2	15.77	FeI_2	29.98	29.72
CuF_2	126.9	126.67	CoF_2	159.0	159.22
$CuCl_2$	49.2	51.58	$CoCl_2$	77.80	76.87
$CuBr_2$	33.2	30.82	$CoBr_2$	55.50	55.30
CuI_2	1.7	1.91	CoI_2	24.40	25.28
AgF	48.5	48.02	NiF_2	159.5	159.86
AgCl	30.362	32.17	$NiCl_2$	75.5	74.69
AgBr	23.78	24.25	$NiBr_2$	54.2	52.79
AgI	14.91	13.09	NiI_2	20.5	22.35
$ZnCl_2$	99.40	99.63	CuCl	32.2	32.26
$ZnBr_2$	78.17	78.60	CuBr	25.1	25.45
ZnI_2	49.98	49.31	$PbBr_2$	66.21	67.48
CdF_2	164.9	164.50	PbI_2	41.85	39.30
$CdCl_2$	93.00	94.95			
$CdBr_2$	75.15	74.83			
CdI_2	48.0	46.75			

[a] Not used in evaluating constants for these cations.

Acknowledgment.—One of the authors is grateful to the National Science Foundation which provided the fellowship which made these studies possible. This work was performed under the auspices of the U. S. Atomic Energy Commission.

A STUDY OF AMORPHOUS SiO

By George W. Brady

Bell Telephone Laboratories, Murray Hill, New Jersey

Received November 24, 1958

A Fourier analysis of the scattered intensity from the material described as "amorphous SiO" indicates that the material is a stoichiometric mixture of SiO_2 + Si.

Introduction

When SiO_2 is heated with a reducing agent such as Si or C, it vaporizes to SiO.[1] Solid SiO is obtained by quenching this vapor. The resulting substance is brown-black, resinous looking, and X-ray and electron diffraction studies show an amorphous diffraction ring corresponding to a spacing of 3.60 Å. Hoch and Johnston[2] claimed to have made crystalline SiO by heating a mixture of Si and SiO_2 at 1300°. The basis for their claim was the development of a series of new X-ray diffraction lines. Geller and Thurmond,[3] however, presented an alternative interpretation of this work, supplemented by further experiments; the powder data given by Hoch and Johnson indicate the presence of β-SiC and β-cristobalite, and not a crystalline modification of SiO. Brewer and Edwards[1] estimate that SiO is unstable below 1450°K. and that the quenched material disproportionates at a considerable rate at temperatures around 400–700°.

Aside from the observation that the diffraction pattern of the amorphous material exhibits a characteristic halo, no detailed examination of the structure has been made, particularly in the room temperature range. Accordingly it appeared worthwhile to do an analysis of the X-ray scattering in the hope that a more complete understanding of this unusual substance would result therefrom.

Experimental and Calculations

The experimental details and method of calculation have been described fully in previous publications.[4,5] The diffraction patterns were recorded with Mo Kα radiation. The effective numbers of electrons of Si and O, calculated from the scattering factors, were K_{Si} = 14.9 and K_O = 7.1, respectively. The SiO sample was obtained from the Kemet Co., Cleveland, Ohio. According to their description, it was made by condensing SiO vapor at 500°.

Discussion

The intensity pattern, corrected for polarization and incoherent scattering, is shown in Fig. 1. The characteristic halo can be seen at s = 1.7; further maxima are evident at other s values. The amount of detail in a diffraction pattern is in a general way indicative of the amount of order in the specimen, but without a proper analysis of the data it is not safe to ascribe these maxima to characteristic distances on the basis of a Bragg's law relation.

The radial distribution function calculated from the data of Fig. 1 is shown in Fig. 2. The distribution curve shows a well-resolved peak at 1.63 Å., two overlapping peaks in the region between 2 and 3 Å., and what appears to be a peak superimposed on a broad background, at 4.1 Å. The first peak distance is equivalent to the Si–O distance and can be attributed to this interaction. The area under the peak is 450 els.[2] The nearest neighbor Si–O peak would have an area of

$$2 \times K_{Si} \times K_O \times n_1 \qquad (1)$$

where n_1 is the number of nearest O's around Si. When the values of K_{Si} and K_O are inserted and the resulting expression equated to the measured area, there results a value of n_1 = 2.1. This is a rather surprising result and immediately raises the question as to whether the true chemical nature of the substance is expressed by the formula SiO. If the formula were written as ($^1/_2$ SiO_2 + $^1/_2$ Si), the expression 1 would be multiplied by the coefficient $^1/_2$ which would give a value for n_1 of 4.2, consistent with the tetrahedral nearest neighbor configuration in the silicates. This would imply that the substance is a stoichiometric mixture of SiO_2 and Si, and therefore there should be exhibited in the radial distribution curve an Si–Si peak at 2.36 Å. and an O–O tetrahedral edge peak at 2.65 Å. Examination of Fig. 2 shows that the two unresolved peaks between 2 and 3 Å. have maxima at roughly these positions. We can then proceed to attempt a resolution of the peaks.

For example, if we compute the area due to a tetrahedral edge O–O interaction we get 7.1 × 7.1 × 6 = 302 els. When this peak is subtracted from the distribution curve (see Fig. 2), the Si–Si peak with maximum at 2.35 Å. is resolved. The area is 410 els.[2] From this we then calculate the nearest neighbor number n_2 of Si's around Si. It is equal to $410/(^1/_2 \times K^2_{Si})$, which gives a value for n_2 of 3.7. This indicates that the tetrahedral Si structure is present as a separate phase and that quantitatively as well as qualitatively, the X-ray results are completely consistent with the description of "SiO" as being a stoichiometric mixture. We could equally well have assumed that the peak with maximum at 2.35 Å. resulted from the Si tetrahedral structure, subtracted its computed area, and resolved the O–O peak at 2.64 Å. This procedure gives within experimental error the correct value of 6 for the number of oxygen–oxygen neighbors.

It is not possible to deduce a structure having two nearest O neighbors for each Si which will reproduce the distribution function out to any reasonable distance from the origin. For example, if one had strings of Si's attached together with each Si attached to two O's this would require a maximum number of 2 for the Si–Si neighbors and also for the O–O nearest neighbors. The computed electron density of such a configuration would be less than the measured density by more than 100%. In addition, such a model would require a large

(1) L. Brewer and R. K. Edwards, This Journal, **58**, 351 (1954).
(2) M. Hoch and H. L. Johnston, *J. Am. Chem. Soc.*, **75**, 5224 (1953).
(3) S. Geller and C. D. Thurmond, *ibid.*, **77**, 5285 (1955).
(4) G. W. Brady, *J. Chem. Phys.* **27**, 300 (1957).
(5) G. W. Brady and J. T. Krause, *ibid.*, **27**, 304 (1957).

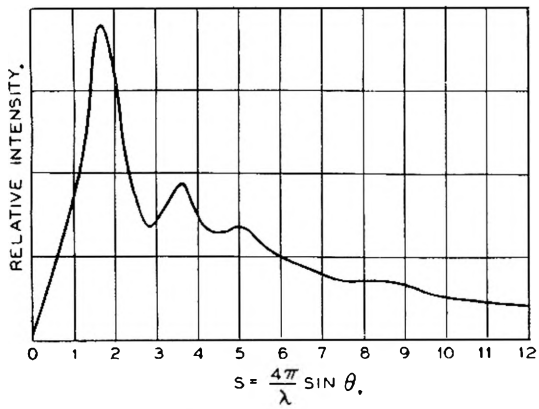

Fig. 1.—Diffraction pattern of SiO.

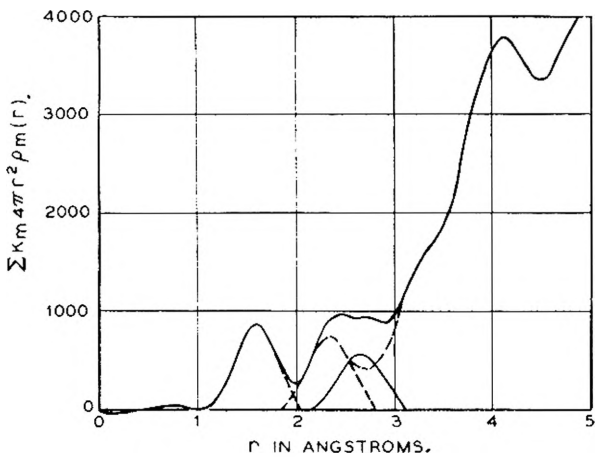

Fig. 2.—Radial distribution function calculated from the data in Fig. 1. The dotted peak is the calculated O–O area.

amount of distortion to reproduce the O–O peak at the tetrahedral distance.

An alternative method is to compare the "SiO" radial distribution curve with that of SiO_2, obtained by Warren and co-workers.[6] It is admittedly risky to attempt a quantitative comparison of distribution curves unless the data used in calculating them are obtained under similar experimental conditions, and cover the same angular range of intensity. However, it is to be noted that the Si–O peak at 1.62 Å. in both curves (Fig. 3) agrees reasonably well.[7] The procedure is illustrated in Fig. 3, where the "SiO" curve is represented in 3a, and the SiO_2 curve, with the ordinate multiplied by $^1/_2$, in 3b. The result of subtracting 3b from 3a is shown in 3c. There remain two peaks, the first at 2.35 Å., which as before we can immediately identify as the nearest neighbor Si–Si peak, and a peak at 3.8 Å. which can be identified with the second nearest

(6) B. E. Warren, H. Krutter and O. Morningstar, *J. Am. Ceram. Soc.*, **19**, 202 (1936).

(7) A detailed comparison of the two curves is not necessarily for the purpose of deciding whether the differences between the curves may be caused by the presence of a separate silicon phase.

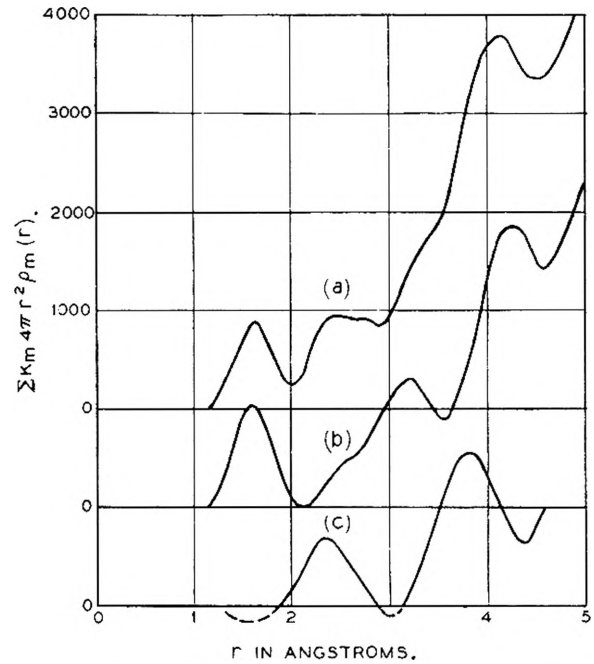

Fig. 3.—The result of subtracting the radial distribution function of $^1/_2$ SiO_2 from that of SiO is shown in 3c.

neighbor distance of the diamond type silicon structure. The areas of the peaks are, respectively, 425 and 900 el². The first peak is consistent with the nearest neighbor number of 4. The second nearest neighbor peak is not completely resolved and gives a value of ~8 for the second nearest neighbor number rather than the expected value of 6, but this difference can be attributed to the approximate nature of the procedure. The more important point is the position of this peak which is just right for the second nearest neighbor distance.

These results strongly support the view that amorphous "SiO" is in reality a stoichiometric mixture of SiO_2 + Si. This does not, of course, eliminate the possibility that the original material may have been SiO, which disproportionated after a time at room temperature.[8] However, it is questionable whether the presence of a "characteristic ring" in the X-ray pattern can be used unequivocally as evidence for the existence of SiO. The most intense peaks for SiO_2 and Si occur at Bragg angles of ~10.0° and ~13.0°, respectively,[8] while the "SiO" ring maximum occurs at ~11.3°. The line broadening produced by the fine state of subdivision of the material could result in considerable overlap of the two peaks to give this apparent maximum between them. Indeed, the half-maximum width of the peak in the intensity pattern is 8.5°, which is more than twice the angular distance between the maxima of the Si and SiO_2 peaks.

Acknowledgment.—We would like to thank S. Geller and C. D. Thurmond for discussion and criticism. The latter also supplied the samples.

(8) G. Haas, *J. Am. Ceram. Soc.*, **33**, 353 (1950).

ADSORPTION OF SOLUBLE FLUOROCARBON DERIVATIVES AT THE ORGANIC LIQUID-AIR INTERFACE[1]

BY A. H. ELLISON AND W. A. ZISMAN

Chemistry Division, U. S. Naval Research Laboratory, Washington 25, D. C.

Received November 24, 1958

Essential conditions are discussed for the adsorption of an amphipathic polar solute in an unassociated (or weakly associated) organic liquid. These are exemplified by consideration of the possibility of high surface activity by fluorocarbon compounds dissolved in hydrocarbons or in chlorinated hydrocarbons. A number of amphipathic polar fluorocarbon derivatives, which were prepared for this investigation, have been studied with emphasis on the effects of varying the molecular weight and structure of the oleophobic and oleophilic portions of the molecule and of the ratio of the number of fluorine and hydrogen atoms per molecule. Data are presented on many compounds including mono-, di-, tri- and tetra-functionality in the oleophilic portion of the amphipathic molecule. Adsorption of several promising types of compounds at the free surface of the liquid was studied by measuring the surface tension lowering as a function of solute concentration for solutions in hexadecane, hexachlorobutadiene and chlorinated biphenyl. Because some fluorinated solutes adsorb on smooth solids to increase considerably the contact angle of the solution, it was at times advisable to use methods of measuring the surface tension which were not dependent on the contact angle. This led to the use of the following methods: differential capillary rise, ring pull, maximum bubble pressure and pendant drop. The merits and deficiencies of each method when used with such liquids and solutes are summarized.

Because of the usual uncertainty about the thickness of the adsorbed surface phase, difficulties arose in computing from the Gibbs surface excess the extent of adsorption. Evidence is given for the formation in hexachlorobutadiene and chlorinated biphenyl of monolayer films of solute molecules. It is shown that the surface activity of a given solute increases exponentially with the difference between the surface tension of solvent and pure liquid solute. The problem of replacing all solvent molecules in the surface phase by solute molecules is discussed both in terms of the kinetics of competitive adsorption and the possibilities offered by appropriately synthesized materials. Because of solubility problems, it appears impossible to find a surface active solute which will operate with high efficiency in a wide variety of organic liquids.

Introduction

By analogy with the hydrophilic–hydrophobic nature of the amphipathic (or polar–non-polar) molecules which are most surface active in aqueous liquids, one would expect a substance dissolved in a hydrocarbon (or in any other unassociated or weakly associated organic liquid) to also be surface active provided that it has an analogous amphipathic molecular structure. Hence, at opposite portions of the solute molecule it should have oleophilic and oleophobic properties, respectively, with respect to the liquid phase.[2] Because adsorption of this type of solute can only proceed spontaneously when a lowering of the surface free energy of the liquid accompanies that process, the oleophobic portion of the molecule must have a higher probability of adsorbing and orienting at the free surface of the solution and of thereby lowering the surface free energy below that of the solvent.

Since surfaces comprising perfluoromethyl or perfluoromethylene groups have much lower free surface energies than those comprising the analogous hydrocarbon groups or any others studied to date,[3-7] the most promising surface active agents for use in organic liquids can be prepared using suitable highly fluorinated hydrocarbon derivatives as synthetic starting materials. One simple method of balancing appropriately the oleophobic and oleophilic properties of the molecule is to condense an alkanoic monocarboxylic acid with a perfluoroalkanoic alcohol, the number of carbon atoms in each of the two segments of the molecule being adjusted by the appropriate choice of the acid and alcohol used as starting materials. However, only when the method of linking the oleophobic and oleophilic portions of the molecule greatly alters the solubility is the choice critical; thus, a hybrid ether would also appear promising. Variations from a simple linear arrangement of oleophobic and oleophilic radicals, can be obtained by synthesis of branched molecules so constructed that 2, 3 or more fluorinated hydrocarbon groups would be free to adsorb simultaneously in the interface, the rest of the molecule being submerged in the liquid substrate.

This report is concerned with the surface tension depressant properties of a variety of soluble fluorocarbon–hydrocarbon hybrid molecules at the organic liquid-air interface and with their relation to the adsorptivity, solubility and molecular structure. Much of the experimental work with soluble fluorocarbon derivatives reported here was completed prior to our published work with the all-Teflon film balance on insoluble film-forming materials[7,8]; but unavoidable interruptions delayed completion of this paper.

Materials and Experimental Procedures

With the exceptions of the perfluorokerosene (FCD-330), ethyl ϕ-butyrate, bis-(t-butoxy)-bis-(ψ'-heptoxy)-silane, tris-(ψ'-amyl)-phosphate, tetrakis-(ψ'-pentoxy)-silane and bis-(t-butoxy)-bis-(ϕ'-octoxy)-silane, the fluorocarbon derivatives used here have already been described by O'Rear, Murphy and co-workers.[9] Their nomenclature will be used here as

ϕ-octanoic acid = $F(CF_2)_7COOH$
ϕ'-octanol = $F(CF_2)_7CH_2OH$
ψ-octanoic acid = $H(CF_2)_7COOH$
ψ'-octanol = $H(CF_2)_7CH_2OH$

(1) Presented at "Symposium on Surface Chemical Properties of Fluorochemicals" at joint meeting of Division of Colloid Chemistry and Fluorine Chemistry Subdivision of Division of Industrial Chemistry, American Chemical Society 134th meeting, Chicago, Illinois, September 11, 1958.

(2) W. A. Zisman and J. G. O'Rear, U. S. Patent 2,824,141 (Feb. 18, 1958).

(3) H. W. Fox and W. A. Zisman, *J. Colloid Sci.*, **5**, 514 (1950).

(4) H. W. Fox and W. A. Zisman, *ibid.*, **7**, 109, 428 (1952).

(5) F. Schulman and W. A. Zisman, *J. Am. Chem. Soc.*, **74**, 2123 (1952).

(6) H. M. Scholberg, R. A. Guenther and R. I. Coon, THIS JOURNAL, **57**, 923 (1953).

(7) A. H. Ellison and W. A. Zisman, *ibid.*, **59**, 1233 (1955).

(8) A. H. Ellison and W. A. Zisman, *ibid.*, **60**, 416 (1956).

(9) P. D. Faurote, C. M. Henderson, C. M. Murphy, J. G. O'Rear and H. Ravner, *Ind. Eng. Chem.*, **48**, 445 (1956).

Although an exceptional degree of purity was achieved in each synthesis, the last traces of adsorbable impurities were removed by slow percolation of the liquid preparation through a column filled with suitable adsorbents. Freedom from adsorbable impurities was determined by measuring the spreading coefficient of the compound on water using Washburn and Keim's method[10] using eicosyl alcohol as the "piston film."[8] Purity was judged to be adequate when the spreading coefficient was at a minimum and did not change on further treatment with adsorbents. Hydrolytically unstable compounds (*e.g.*, esters of ϕ-acids) could not be tested by this technique. The presence of very small traces of ϕ- or ψ-acids in the esters could be detected, however, by observing whether the ester would spread freely on a clean polished platinum foil. If spreading took place and no retraction occurred afterwards, the compound was adjudged free from such acids, since previous research had shown that very small concentrations of any of these acids readily adsorbed on the clean metal substrate to form a condensed monolayer on which the bulk liquid could not spread.[11-13]

Bis-(t-butoxy)-bis-(ψ'-heptoxy)-silane, tris-(ψ'-amyl)-phosphate, tetrakis-(ψ'-pentoxy)-silane and bis-(t-butoxy)-bis-(ϕ'-octoxy)-silane were synthesized and purified at this Laboratory by J. G. O'Rear. The perfluorokerosene FCD-330 (a perfluorolube oil fraction having a density d^{20}_4 1.9958 and boiling at 60–130° at 10 mm.) was supplied by E. I. du Pont de Nemours & Company, Incorporated. Ethyl ϕ-butyrate was obtained from Columbia Organic Chemicals Company. All of these substances were purified as described above. A commercial grade of n-hexadecane, having a surface tension at 20° of 27.6 dynes/cm., was used most frequently as the organic substrate in this study because it is not too volatile, has a low viscosity and can be readily freed from polar impurities by percolation through activated silica and alumina.

Solutions were prepared by adding a weighed amount of solute to a known volume of solvent. Saturated solutions were made by adding an excess of solute and then warming it slightly to ensure saturation. The concentration of a saturated solution was determined either from its density and the density *vs.* concentration relation of the unsaturated solutions or from its density alone (assuming ideal behavior).

Each of the fluorinated compounds was "screened" by measuring the depression of the surface tension of a saturated solution in n-hexadecane at 20°. This was taken as a measure of the maximum useful surface activity of the solute. However, in a few instances the solute was miscible or nearly so, and a 10% by weight solution was used instead. From this work several interesting compounds were selected for measurement of the surface tension *vs.* concentration (c) of solute in order to compute the adsorption excess Γ by applying the Gibbs equation

$$\Gamma = -\frac{c}{RT}\left(\frac{\partial\gamma}{\partial c}\right) \qquad \text{(i)}$$

Nearly all of the solutions studied exhibited non-zero equilibrium contact angles on glass and platinum and, therefore, no one method of measuring surface tension was always most satisfactory. Four methods therefore were used. These methods were the differential capillary rise (C), ring pull (R), differential maximum bubble pressure (B) and pendant drop methods (P).

A simple and precise differential capillary rise cell, which was easily disassembled and cleaned and needed only 0.25 ml. of liquid, was designed by our associate, H. W. Fox, and used in this investigation. It was constructed from two 6"-lengths of precision-bore, glass, capillary tubing which were approximately 0.1 and 0.05 cm. in internal diameter. Accurate diameters were determined by the mercury feed method. On the external surface of each tube was ground a flat area parallel to the bore. This permitted mounting both capillary tubes in parallel side by side and close enough together to be visible simultaneously in the field of view of the telescope of a slide micrometer. Three spacers cut from Teflon sheet ($^1/_{16}$" thick) were used to hold the pair of capillaries in place with their axes vertical in a heavy wall test tube 6" long. The heavy wall of the test-tube served to eliminate the buoyancy effect when the tube was partly immersed in the water thermostat-bath. By this arrangement the differential capillary rise with water or n-hexadecane could be read with a reproducibility of $\pm 3 \times 10^{-4}$ cm. and a precision of ± 0.02 dyne/cm. Excellent checks with the best surface tension values in the literature could be obtained with this device.

The maximum bubble pressure cell used here was much like that described by Sugden.[14] It was protected from the contaminating vapors of the incoming air and the manometer fluid by suitable cold traps and absorption towers. The Cenco–DuNuoy interfacial tensiometer was used with the corrections of Fox and Chrisman.[15] The pendant drop apparatus was much like the atmospheric pressure and temperature instrument described by Andreas, Hauser and Tucker.[16] Fordham's tables[17] were used with the data obtained. For convenience the various components were mounted on a single optical bench. The camera lens was separated from the camera in order to obviate problems with light leaks often associated with bellows-type cameras. Reproducibility of measurements with this method is decreased because of sensitivity of the drop to building vibration.

Our experience has shown that whereas the C and R methods depend on the solution exhibiting a zero contact angle on either glass or platinum, the B and P methods do not. Usually the precision of the C, B and R methods was better than ± 0.05; and that of the P method was ± 0.2 dyne/cm. due to vibration difficulties. Measurements with the C and P methods can be made with less than 1 cc. of sample, whereas the B and R methods require not less than 5 and 10 cc., respectively. With the C, P and R methods there is adequate time for the solute to diffuse to the interface since these are static methods; with the B method this can be assumed only when the rate of bubbling is very slow, *e.g.*, three bubbles per minute. The viscosity of the sample does not affect the measurement by the C, P and R methods, but it can be ignored with the B method only when the bubbling rate is slow. The time involved in making a measurement increases approximately in the order R < C < B < P.

The surface tension of the hexadecane used was measured by all four methods and good checks for consistency resulted. Surface tensions of the liquid solutes were determined by whichever was the most convenient method; the method used is indicated in Table I. Densities of solutions containing less than 0.5% by weight of the solute were assumed to be the same as that of the solvent; all others were measured at 20° using calibrated pycnometers. Pendant drop data were obtained at 24 ± 1°, all other surface tensions and densities were measured at 20 ± 0.5° and 50 ± 1% relative humidity.

Relative Surface Tension Depression in Hexadecane.—Surface tensions of the liquid fluorocarbon derivatives studied as solutes in n-hexadecane are given in the 4th column of Table I. The liquids are arranged in order of increasing surface tension. Surface tensions of the saturated solutions in n-hexadecane are given in the 5th column of the table. In the case of ψ'-undecyl acetate, the surface tension of the pure solute is estimated because it is solid at 20°.

Because of the lower surface tensions of the pure compounds and their amphipathic structures, the ϕ and ϕ' derivatives were more effective as surface tension depressants than the structurally analo-

(10) E. R. Washburn and C. P. Keim, *J. Am. Chem. Soc.*, **62**, 1747 (1940).

(11) A. H. Ellison, H. W. Fox and W. A. Zisman, THIS JOURNAL, **57**, 622 (1953).

(12) E. F. Hare, E. G. Shafrin and W. A. Zisman, *ibid.*, **58**, 236 (1954).

(13) H. W. Fox, E. F. Hare and W. A. Zisman, *ibid.*, **59**, 1097 (1955).

(14) S. Sugden, "The Parachor and Valency," Knopf, New York, N. Y., 1930.

(15) H. W. Fox and C. H. Chrisman, Jr., *J. Phys. Chem.*, **56**, 284 (1952).

(16) J. Andreas, E. Hauser and W. Tucker, *ibid.*, **42**, 100 (1938).

(17) S. Fordham, *Proc. Roy. Soc.* (*London*), **A141**, 1 (1948).

Table I

Surface Tensions of Liquid Fluorocarbon Derivatives in *n*-Hexadecane

(All data at 20°; surface tension in *n*-hexadecane = 27.6 dynes/cm.)

Order of increasing solubility	Fluorochemical solute	F/H	Surface tension (dynes/cm.) Solute	Satd. soln.	Method of measurement used	Density d^{20}_4
XIV	Ethyl ϕ-butyrate	1.4	16.3	18.2	Capillary rise	1.394
...	Bis-(*t*-butoxy)-bis-(ϕ'-octoxy)-silane	1.4	18.4	...	Ring pull	1.525
XII	Butyl ϕ-caprylate	1.7	18.7	19.8	Ring pull	1.5328
XV	Hexyl ϕ-butyrate	0.54	19.2	25.0[a]	Capillary rise	1.2315
III	Bis-(ϕ'-octyl)-3-methylglutarate	2.5	19.5	24.6	Ring pull	1.6894
...	Bis-(ϕ'-hexyl)-3-methylglutarate	1.8	19.9	...	Ring pull	1.6101
V	F.C.D. 330	∞	20.0	27.2	Capillary rise	1.9958
VI	Bis-(ϕ'-butyl)-3-methylglutarate	1.2	20.5	23.5	Ring pull	1.4968
...	1,6-Hexanediol bis-(ϕ-octanoate)	2.5	20.6	...	Ring pull	1.6687
VIII	Bis-(*t*-butoxy)-bis-(ψ'-heptoxy)-silane	1.0	21.0	22.6	Ring pull	1.474
I	1,2,3-Trimethylolpropane tris-(ϕ-butyrate)	1.9	21.2	27.4	Bubble press.	1.6137
IX	1,6-Hexanediol bis-(ϕ-butyrate)	1.2	21.5	25.3	Bubble press.	1.4696
X	ψ'-Heptyl methyl ether	3.5	22.1	26.7	Bubble press.	1.6294
...	Bis-(ϕ'-butyl)-sebacate	0.7	22.4	...	Ring pull	1.3837
XI	ψ'-Nonyl butyrate	1.6	22.7	25.7	Bubble press.	1.5780
XIII	1,10-Decanediol bis-(ϕ-butyrate)	0.70	23.0	24.0	Bubble press.	1.3594
...	ψ'-Nonyl 2-ethylhexanoate	0.89	23.1	...	Ring pull	1.4384
...	Tetrakis-(ψ'-pentoxy)-silane	2.7	24.5	...	Capillary rise	1.732
...	Bis-(ψ'-nonyl)-3-*t*-butyl adipate	1.5	24.9	...	Ring pull	1.6238
...	Bis-(ψ'-nonyl)-3-methylglutarate	2.3	24.9[b]	...	Ring pull	1.714
XVI	Octadecyl ϕ-butyrate	0.19	25.1	27.2[a]	Capillary rise	1.0560
...	Tris-(ψ'-amyl)-phosphate	2.7	25.2	...	Ring pull	1.772
...	Bis-(ψ'-heptyl)-3-methylglutarate	1.7	25.6	...	Ring pull	1.6484
VII	1,6-Bis-(ψ'-heptoxy)-hexane	1.3	25.8	26.8	Bubble press.	1.5776
...	1,6-Hexanediol bis-(ψ'-heptanoate)	1.7	25.9	...	Ring pull	1.6263
...	Bis-(ψ'-heptyl)-adipate	1.7	26.1	...	Bubble press.	1.6516
II	Bis-(ψ'-heptyl)-pinate	1.3	26.2	27.6	Capillary rise	1.6009
IV	ψ'-Undecyl acetate	3.7	21.0	27.4	Estimated	...

[a] 10% by wt. of solute. [b] Supercooled to 20° from m.p. of 25°.

gous ψ and ψ' derivatives. In fact, of the ψ and ψ' compounds only bis-(*t*-butoxy)-bis-(ψ'-heptoxy)-silane exhibited a notable surface tension lowering action in hexadecane. It is evident that several of these soluble fluorinated compounds are able to depress the surface tension of hexadecane by from 5 to 10 dynes/cm.; hence they may have future application. It is noteworthy that bis-(*t*-butoxy)-bis-(ψ'-heptoxy)-silane has a lower surface tension than tetrakis-(ψ'-pentoxy)-silane even though the latter has the greater fluorine to hydrogen ratio.

Obviously, a useful agent for depressing the surface tension of an organic liquid is one capable of giving the maximum possible depression with the minimum concentration of solute. An agent having a large absolute value of $\partial\gamma_{LV}/\partial c$ may have little usefulness, however, if the solubility is too low to allow the adsorbed phase to become saturated with the solute. Hence, an agent which is nearly insoluble has little utility. But, if it is too soluble, $\partial\gamma_{LV}/\partial c$ may be too small in magnitude, and the necessary concentration for a significant depression in the surface tension may be excessive. Table I shows these opposite effects, for at each extreme of solubility, the agents were able to achieve only a small fraction of the theoretically maximum possible depression—that of the pure solute. In Table II will be found comparisons of the largest possible and the maximum observed surface tension depressions of the structurally analogous compounds of Table I. In the last column is given the ratio, which may be called the "efficiency" of surface tension depression.

Table II

Effect of Structure on Surface Tension Depression and Adsorptivity in Saturated Solutions in *n*-Hexadecane

Solute	F/H	Largest possible depression in γ_{LV}, dynes/cm.	Obsd. depression in γ_{LV} dynes/cm.	Efficiency in depressing γ_{LV}, %
Ethyl ϕ-butyrate	1.4	11.3	9.4	83
n-Hexyl ϕ-butyrate[a]	0.54	8.4	2.6	31
n-Octadecyl ϕ-butyrate[a]	0.19	2.5	0.4	16
1,6-Hexanediol bis-(ϕ-butyrate)	1.2	6.1	2.3	38
1,10-Decanediol bis-(ϕ-butyrate)	0.7	4.6	3.6	78
Bis-(ϕ'-octyl)-3-methylglutarate	2.5	8.1	3.2	40
Bis-(ϕ'-butyl)-3-methylglutarate	1.2	7.1	4.1	58
ψ'-Undecyl acetate	3.3	6.6	0.2	3
ψ'-Nonyl butyrate	1.6	4.9	1.9	39
Butyl ϕ-caprylate	1.4	8.9	7.8	88

[a] Due to high solubility in hexadecane, data on γ_{LV} given for 10% solutions.

In the development of a surface active agent, it is usual to study a series of homologs in order to find the proper balance in the action of the groups or

TABLE III

EFFECT OF SURFACE TENSION OF SOLVENT ON SURFACE ACTIVITY OF DISSOLVED ψ'-NONYL BUTYRATE

(All data obtained at 20°)

Solvent	γ_{LV} Surface tension (dynes/cm.) of solvent	of satd. soln.	Surface tension depression $\Delta\gamma_{LV}$ (dynes/cm.)	Concd. satd. soln. Wt. %	Mole fraction of solute $N_s \times 10^2$	$\overline{\partial\gamma_{LV}/\partial c}$	$\left(\frac{\partial\gamma_{LV}}{\partial c}\right)_{in}$
n-Hexadecane	27.6	25.7	1.9	5.8	2.6	73	0.28
Hexachlorobutadiene	35.9	24.3	11.6	6.5	3.3	355	3.1
Trichlorobiphenyl (Arochlor 1242)	44.7	27.5	17.2	2.1	0.58	2970	17.8

radicals contributing to the solubility or insolubility of the molecule. In this way one obtains the greatest possible surface tension decrease per mole of solute. Generally in such a study, the structural changes which decrease the solubility increase the adsorptivity. This point is evident on comparing the structurally analogous compounds of Table II. Accordingly, in this investigation ψ'-undecyl acetate was synthesized on the basis of the results obtained with ψ'-nonyl butyrate. Although the anticipated decrease in solubility was found, the usually accompanying increase in adsorptivity was not found (see Table I). Another interesting example is that of 1,6-hexanediol bis-(ϕ-butyrate), which although less soluble than its 1,10-decanediol homolog, was not so well adsorbed. The cause in this instance is attributed to tendency of such molecules to adsorb as U-shaped configurations with both fluorocarbon terminal groups striving to remain in the air–liquid interface and the hydrocarbon portion of the molecules immersed in the substrate liquid. The 1,6-hexanediol derivative is much more sterically hindered from adsorbing in this manner than its 1,10 homolog.

Effect of Varying Surface Tension of Organic Solvent.—One would expect that the ability of the surface active solute to lower the surface tension of the organic solvent would be greater the higher the surface tension of the solvent because the free energy decrease on adsorption of solute would be greater. The correctness of this argument is shown in Table III on comparing the surface tensions of saturated solutions of ψ'-nonyl butyrate in hexadecane, hexachlorobutadiene and trichlorobiphenyl (Arochlor 1242). It is seen in column 4 that the surface tension depression $\Delta\gamma_{LV}$ is greater the higher the surface tension of the solvent. In order to compare $\Delta\gamma_{LV}$ on an equimolal basis, the mole fraction N_s of the solute is given in the 6th column. The average value of $\partial\gamma_{LV}/\partial N_s$ for each agent over the concentration range 0 to N_s is denoted as $\overline{\partial\gamma_{LV}/\partial c}$, and it can be taken as approximately equal to $\Delta\gamma/c$; this value is given in the 7th column. Note that $\overline{\partial\gamma_{LV}/\partial c}$ is about 5 times greater for the solution in hexachlorobutadiene than in *n*-hexadecane, and it is 40 times greater for that in trichlorobiphenyl. Hence a 60% increase in the surface tension of the solvent caused a 4000% increase in $\overline{\partial\gamma_{LV}/\partial c}$. Upon plotting the logarithm of $-\overline{\partial\gamma_{LV}/\partial c}$ against the difference between the surface tension of the liquid solute (γ_{solute}) and that of the solvent ($\gamma_{solvent}$), a good straight line results. Hence

$$\overline{\frac{\partial\gamma_{LV}}{\partial c}} = a \exp[b(\gamma_{solvent} - \gamma_{solute})] \qquad \text{(ii)}$$

This large rise in surface activity is not caused by the decrease in solubility of ψ'-nonyl butyrate, because in going from hexadecane to trichlorobiphenyl that property changed only 50%; furthermore, in going from hexadecane to hexachlorobutadiene there was a rise in solubility.

Surface Tension *vs.* Concentration and Application of the Gibbs Adsorption Relation.—Because of these observations a more intensive study was made of the surface tension lowering and adsorptivity of ψ'-nonyl butyrate and 1,10-decanediolbis-(ϕ-butyrate) each dissolved in hexadecane. Surface tension data for these solutions were obtained by the differential maximum bubble pressure method, and graphs of the results against the solution concentration are given in Fig. 1. A notable feature of curve A of Fig. 1 is that the curve exhibits a constant and negative slope from zero concentration to 10%, and then it becomes more negative as the concentration rises up to saturation at a concentration of 12%. This change of curvature at high concentrations is opposite to that observed with surface active agents in aqueous solutions. Curve B is defined by fewer experimental points, but the behavior is very much the same as satura-

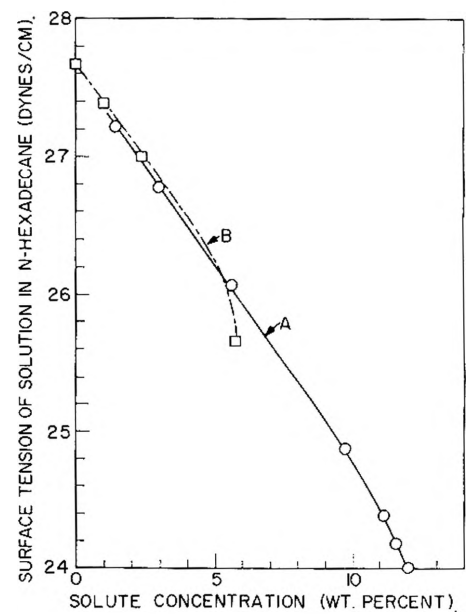

Fig. 1.—Surface tension *vs.* solute concentration in *n*-hexadecane; curve A, for 1,10-decanediol bis-(ϕ-butyrate); curve B, for ψ'-nonyl butyrate (all data at 20°).

tion is approached. Both curves of Fig. 1 reveal that a given addition of solute produces a greater surface tension depression when the solution is nearly saturated than when it is very dilute.

The observed behavior suggests several possible mechanisms of adsorption. The behavior near saturation could be caused by a change in the orientation of the adsorbed polar molecules. If this were the case, however, each curve in Fig. 1 would be expected to exhibit a much more rapid change in slope followed by a gradually decreasing slope at high concentrations. Another explanation could be based on the formation and adsorption of micelles of solute, but micelles were not found when these solutions were examined by the sensitive light-scattering methods of Arkin and Singleterry.[18] The most reasonable explanation is that the adsorbed film comprises a mixture of solute and solvent molecules, the behavior between concentrations of 10% and saturation indicating the desorption or displacement of solvent molecules from the surface phase. The fact that the change in slope near saturation is gradual and increases with the concentration is explained readily by the last mechanism.

A similar study of solutions of (*t*-butoxy)-bis-(ψ'-heptoxy)-silane in *n*-hexadecane was made at 24° using the pendant drop method. Results are given in Fig. 2. Here the surface tension was lowered about 2 dynes/cm. by a relatively small concentration of solute, and no significant additional lowering resulted with increased concentration until approximately 90% of saturation had been exceeded. If in the middle concentration region of the graph the surface phase had comprised a condensed film of adsorbed solute molecules, the surface tension would have been close to that of the pure solute (21.0 dynes/cm.) instead of the observed much higher value of 25.6 dynes/cm. Hence, it is concluded that in this region the adsorbed phase is either a mixed film of more than monolayer thickness comprising both solvent and solute molecules or else is a stable mixed monolayer of solute and solvent. However, as saturation is approached, the solvent molecules are driven out of the surface phase.

Results on the surface tension as a function of concentration of dissolved ψ'-nonyl butyrate in hexadecane, hexachlorobutadiene and trichlorobiphenyl are given in Table IV. Applying the Gibbs adsorption relation (i) using the concentration instead of activities because the solutions are assumed sufficiently dilute, the adsorption excess Γ was calculated and is given in the 4th column. If the adsorbed solute is assumed to be a monolayer, the area per adsorbed solute molecule is $A = 1/\Gamma$, and this value is given in the last column of Table IV. Graphs of Γ *vs.* solute concentration (c) are given in Fig. 3 for the ψ'-nonyl butyrate. In Fig. 4 is a similar graph for the adsorption of 1,10-decanediol di-(ϕ-butyrate) solution in hexadecane calculated from the data of curve A of Fig. 1. Similar calculations of Γ *vs.* concentration (c) were not made from the data of Fig. 2 because

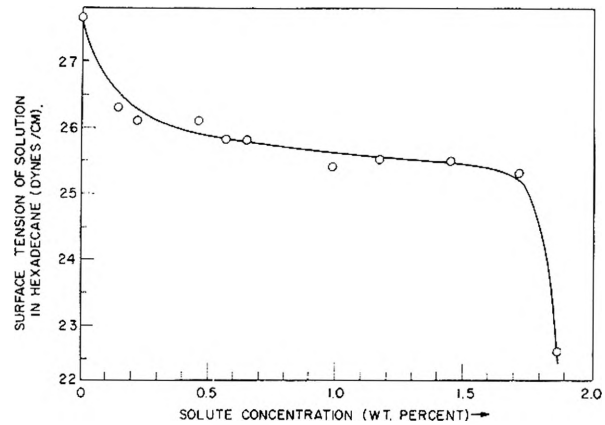

Fig. 2.—Surface tension of bis-(*t*-butoxy)-bis-(ψ'-heptoxy)-silane dissolved in *n*-hexadecane (all data at 24°).

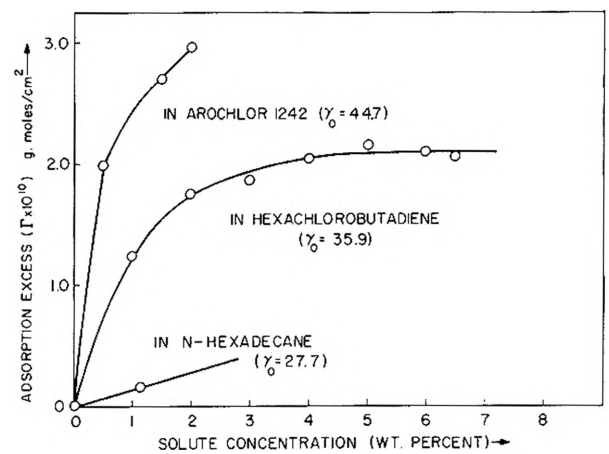

Fig. 3.—Adsorption excess *vs.* concentration of ψ'-nonyl butyrate in various solvents (all data at 20°).

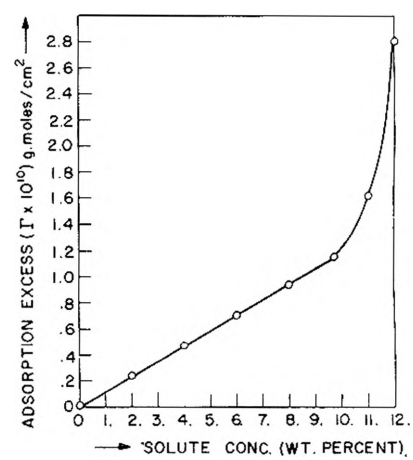

Fig. 4.—Adsorption excess *vs.* concentration of 1,10-decanediol bis-(ϕ-butyrate) in *n*-hexadecane (all data at 20°).

these surface tensions were measured by the pendant drop method and $(\partial\gamma_{LV}/\partial c)$ is not known precisely enough as a function of concentration to deserve an application of the Gibbs relation. However, it evidently will lead to an adsorption isotherm like the Type IV isotherm of Brunauer, Deming and Teller.[19]

(18) L. Arkin and C. R. Singleterry, *J. Am. Chem. Soc.*, **70**, 3965 (1948).

(19) S. Brunauer, L. S. Deming, W. E. Deming and E. Teller, *ibid.*, **62**, 1723 (1940).

Table IV

Effect of Varying Solvent on Surface Tension Depression and Adsorption of ψ'-Nonyl Butyrate

(All data obtained at 20°)

Solvent	Solute concn., wt. %	Soln. surface tension (γ_{LV}) (dynes/cm.)	Adsorption (calcd.) $\Gamma \times 10^{10}$, g. moles/cm.^{2}	Adsorption (calcd.) $A \times 10^{16}$, cm.^{2}/molecule
n-Hexadecane	0	27.67	0	0
	1.01	27.38		
	2.40	27.01	0.14 (av.)	1200 (av.)
	5.8 (satd.)	25.67		
Hexachlorobutadiene	0	35.9	0	0
	0.50	34.5		
	1.00	32.55	1.25	130
	2.00	30.02	1.74	94
	3.01	28.19	1.86	86
	4.01	26.59	2.04	77
	5.02	25.85	2.15	73
	6.02	24.79	2.09	74
	6.5 (satd.)	24.34	2.06	75
Trichlorobiphenyl	0	44.68	0	0
	0.50	36.29	1.99	83
Arochlor (1242)	1.50	29.68	2.69	62
	2.06 (satd.)	27.48	2.93	54

Referring to Fig. 3 and Table IV, it is seen that A of ψ'-nonyl butyrate has a value of around 1200 Å.^{2} in hexadecane over most of the concentration range except close to the solubility limit; it approaches a steady maximum of about 74 Å.^{2} in hexachlorobutadiene when the solute concentration is about 80% of the solubility limit; and it attains a value of between 60 and 80 Å.^{2} in trichlorobiphenyl at 50% of the solubility limit. Using the Stuart–Briegleb molecular models, it is found that if the molecule of ψ'-nonyl butyrate were adsorbed with the nine-carbon fluorocarbon chain in the surface and the hydrocarbon chain and ester group at right angles but immersed in the liquid phase, the surface area required at closest packing would be between 69 and 85 Å.^{2} depending on how the area contribution of the hydrocarbon chain is calculated. This leads to the conclusion that in the upper concentration range of the solutions in the solvents of higher surface tension, hexachlorobutadiene and trichlorobiphenyl, the molecules of ψ'-nonyl butyrate are adsorbed as a condensed monolayer with the highly fluorinated carbon chain probably lying in the interface and the rest of the molecule immersed in the liquid phase. In hexadecane the solute is adsorbed either as a thick film comprising both solute and solvent molecules or as a gaseous monolayer.

Turning to Fig. 4, A varies from 600–300 Å.^{2} at 2–3 wt. % concentration, which corresponds to gaseous or uncondensed monolayers, down to 95 Å.^{2} at a concentration of 11%. Only when the concentration is practically at saturation (12%) does A approach 56 Å.^{2} Thus, as inferred earlier from Figs. 1 and 2, we must conclude that this compound adsorbs in hexadecane as a mixed film which contains a high proportion of solvent molecules except very close to the solubility limit. But it is remarkable that at the solubility limit, A is rather close to the value for a condensed monolayer.

From the data of Table IV the initial slope $(\partial\gamma_{LV}/\partial c)_{init.}$ of the surface tension *vs.* concentration curves for ψ'-nonyl butyrate in *h*-hexadecane, hexachlorobutadiene and trichlorobiphenyl were calculated to be 0.28, 3.1 and 17.8, respectively. A graph of log $(\partial\gamma_{LV}/\partial c)_{init.}$ against $\gamma_{solvent}-\gamma_{solute}$ is a straight line. (γ_{solute} = 22.7 for ψ'-nonyl butyrate according to Table I). Hence as in equation ii, we can state that

$$-\left(\frac{\partial\gamma_{LV}}{\partial c}\right)_{init.} = \alpha \exp[\beta(\gamma_{solvent} - \gamma_{solute})] \quad \text{(iii.)}$$

Using equation i to replace $-\partial\gamma_{LV}/\partial c$ by $RT\Gamma/C$ we obtain

$$\left(\frac{\Gamma}{c}\right)_{init.} = \frac{\alpha}{RT} \exp[\beta(\gamma_{solvent} - \gamma_{solute})] \quad \text{(iv)}$$

This relation is not only useful but is suggestive in its statistical mechanical implications. Belton and Evans[20] have derived theoretically a similar relation for a binary liquid system which forms a perfect solution. When the mole fraction of solute is sufficiently small, their relation can be greatly simplified and reduces to

$$\Gamma = b_1 \exp\left(\frac{b_2(\gamma_{solvent} - \gamma_{solute})}{RT}\right) \quad \text{(v)}$$

General

An unavoidable conclusion from this investigation is that where close packed monolayers can be obtained only when the concentration is close to the solubility limit, the solute molecules must have a low average lifetime of adsorption in the interface. When the solute concentration is raised sufficiently to force the solute molecules to displace nearly all of the solvent molecules from the interface, the probability of collision between solute molecules becomes so high that nucleation and subsequent crystallization result. This last possibility can be made less probable by choosing solute molecules having low cohesional energies. This could occur through increasing the extent of fluorination, through appropriate location of groups to decrease association, or through sterically hindering molecular cohesion or alignment. It is re-

(20) J. W. Belton and M. G. Evans, *Trans. Faraday Soc.*, **41**, (1945).

markable that one can work so close to the solubility limit in these surface-chemical systems, and future research along such lines on surface activity in non-aqueous systems is inviting.

It should be noted that the fluorochemicals found most surface active by measurements of γ_{LV} *vs.* c and calculation of $\partial\gamma_{LV}/\partial c$ (or of Γ/c) are among those found most surface active by Jarvis and Zisman[21] through observation of the spreadability.

Under the most favorable conditions there may be a surface tension lowering $\Delta\gamma_{LV}$ of from 10 to 20 dynes/cm. with some fluorochemicals, and with such systems monolayer adsorption of solute may occur. This leads to the firm conclusion that fluorochemicals can have high surface activity in organic solvents. The effect is greatest with solvents of highest surface tension and solutes of lowest surface tension. Of course, the arrangement of the fluorine atoms in the molecules is important. A correct oleophobic–oleophilic balance is one of the necessary attributes. It also appears that the atomic proportion of fluorine to hydrogen in the molecule should not be less than 0.5 or more than 2.0 for best results.

(21) L. Jarvis and W. A. Zisman, THIS JOURNAL, **63**, 727 (1959).

NON-RESONANT MICROWAVE ABSORPTION IN CERTAIN HALOGEN SUBSTITUTED METHANES[1]

BY JAMES E. BOGGS AND HARMAN C. AGNEW

Department of Chemistry and Electrical Engineering Research Laboratory, The University of Texas, Austin, Texas

Received November 29, 1958

The absorption of microwave radiation of 9400 Mc. frequency by CH_3Cl, CH_3Br, CHF_3, $CHCl_2F$, $CHClF_2$, CH_2F_2, CBr_2F_2 and CCl_2F_2 has been studied over a pressure range from 0.2 to 2 atm. at 26°. Absorption in the first five gases is of the typical non-resonant type associated with molecular inversion transitions. CCl_2F_2 and CBr_2F_2 show no appreciable absorption and the absorption by CH_2F_2 appears to be due to nearby rotational lines.

A number of workers recently have concerned themselves with inversion transitions in non-planar gaseous molecules, studying the effect by measuring non-resonant absorption in the microwave region[2–6] or by examining the frequency variation of the dielectric constant of the gas.[7–10] For symmetric top molecules it has been found possible to calculate the observed intensity and frequency variation of the non-resonant microwave absorption from the Van Vleck–Weisskopf equation for the pressure-broadening of a spectral line using the dipole moment matrix element for inversion and assuming the resonant frequency of the inversion to be essentially zero.[5] The same model has led to the calculation of the observed difference between the dielectric constant of the gas at low frequency and that at microwave frequencies.[9] Both procedures require the evaluation of the quantity $\Sigma f_{JK} |\mu_{JK}|^2$ where f_{JK} is the fractional number of molecules occupying the JK rotational energy level and $|\mu_{JK}|$ is the dipole moment matrix element for inversion. This sum has been obtained in closed form only for symmetric top molecules so that the quantitative treatment has been limited to such substances. Dielectric constant measurements on gases of lower molecular symmetry, however, have shown that for these substances, also, the orientation polarization is lower at 9400 Mc. than at low frequency, suggesting the same sort of molecular inversion.[10] Certain non-planar molecules of C_{2v} symmetry (CH_2Cl_2, CH_2F_2, CH_2Br_2 and possibly CCl_2F_2) have been shown to have the same dielectric constant at 9400 Mc. as at low frequency within experimental error.[10]

We have now measured microwave absorption in $CHCl_2F$ and $CHClF_2$, for which dielectric constant data have been reported,[7] to determine whether or not the relationship between the absorption and the dielectric dispersion is that which would be predicted if both were caused solely by molecular inversion. We have also looked for absorption in CH_2F_2, CBr_2F_2 and CCl_2F_2 to see whether the absorption measurements give any indication of inversion.

Experimental

Two different methods were used to measure the absorption of microwave energy at 9400 Mc. over a pressure range from 0.2 to 2 atm. All measurements were made at 26 ± 2°. The first method was a fairly direct measurement of attenuation in a 100 foot coil of wave guide filled with the gas. A TS147/UP U.S. Navy radar test set fed the signal through a calibrated attenuator and the sample cell to a crystal detector, amplifier and power meter. Tunable transitions were used, and the system was tuned flat looking both ways from the sample container. A slotted section and tuning screw just before the sample cell allowed the voltage standing wave ratio to be monitored and controlled at that point. A directional coupler with power meter permitted the incident power to be monitored. In use, the sample cell was evacuated, the amplifier adjusted to indicate some given power level, the gas introduced to the desired pressure, and attenuation removed at the variable attenuator until the original power level was restored. This gave the attenuation coefficient of the gas from which the loss tangent could be calculated.

With this apparatus the average deviation in the loss tangent measurements obtained for a given gas was 2.0%,

(1) This work has been supported by Air Force Contract AF 33(616)-5581.

(2) W. D. Hershberger, *J. Appl. Phys.*, **17**, 495 (1946).

(3) J. E. Walter and W. D. Hersaberger, *ibid.*, **17**, 814 (1946).

(4) B. Bleaney and J. H. N. Loubser, *Proc. Phys. Soc.* (*London*), **A63**, 483 (1950).

(5) G. Birnbaum, *J. Chem. Phys.*, **27**, 360 (1957).

(6) Krishnaji and G. P. Srivastava, *Phys. Rev.*, **109**, 1560 (1958).

(7) J. E. Boggs, C. M. Crain and J. E. Whiteford, THIS JOURNAL, **61**, 482 (1957).

(8) J. E. Boggs, C. M. Thompson and C. M. Crain, *ibid.*, **61**, 1625 (1957).

(9) J. E. Boggs, *J. Am. Chem. Soc.*, **80**, 4235 (1958).

(10) J. E. Boggs, J. E. Whiteford and C. M. Thompson, THIS JOURNAL, **63**, 713 (1959).

although the absolute accuracy is felt to be considerably worse. The attainment of greater accuracy probably was prevented by the construction of the sample cell which consisted of a coil made up from eight semi-circular sections joined together. Each joint presented a small discontinuity to the radiation and produced some reflection of the wave. Although the wave was effectively flat before entering the sample, the reflections within the sample, which could not be tuned out, could interact so as to produce either an additive or subtractive effect on the apparent loss.

The second method made use of a bridge circuit constructed of x-band wave guide. The signal from the TS-147/UP test set passed through an attenuator to a magic tee which divided the power equally into the two arms of the bridge. One arm consisted of a phase shifter, the sample cell 1.05 meters in length and a variable attenuator. The other arm was similar with a physically identical sample container used to make the two arms of the bridge electrically equivalent. The signals from the two arms were summed by a second magic tee and fed into a third tee where the signal was mixed with the output from a local oscillator operating at a frequency 30 Mc. above or below 9400 Mc. The resultant 30 Mc. signal was amplified and displayed as power.

To make a measurement, the sample cell was evacuated and the bridge was balanced to minimum signal by adjusting the phase shifters and variable attenuators. The balance was sufficiently precise that the ratio of summed to subtracted signals was in excess of 60 db. at all times. The sample then was introduced and the bridge rebalanced to minimum signal using only the phase shifters, the power level of the minimum being noted. The sample cell was again evacuated, the bridge was rebalanced to maximum power using the phase shifters, and attenuation was introduced with the calibrated attenuator in the TS147/UP signal source until the power output of the bridge was reduced to the level of the minimum with the sample in the sample cell. This attenuation, read in decibels, is equal to 20 log $[(1 + e^{-\alpha l})/(1 - e^{-\alpha l})]$, where l is the length of the sample and α is the attenuation coefficient of the gas.

The accuracy obtained by this second method was again not as high as had been anticipated. The over-all accuracy can only be checked by comparison with measurements by other methods that have been reported for certain gases as shown below. While neither method of measurement gave results of as high accuracy as needed to study the fine details of the absorption, the accuracy was sufficient to answer the original questions proposed.

Results and Discussion

In order to evaluate the accuracy of the experimental methods, measurements were made on absorption by CH_3Cl, CH_3Br and CHF_3, for which loss tangents at 9400 Mc. have been reported by other investigators. As shown by Birnbaum,[5] if the loss tangent is measured at various gas pressures and if the loss is due entirely to a pressure-broadened low-frequency inversion transition, a plot of $p^2/\tan\delta$ against p^2 should give a straight line. The maximum absorption, $(\tan\delta/p)_{max}$, and line broadening constant, $\Delta\nu/p$, are related to the slope m and the intercept c of this line by the equations

$$\Delta\nu/p = (m/c)^{1/2}$$

and

$$(\tan\delta/p)_{max} = (4mc)^{-1/2}$$

Table I shows the observed loss tangent at one atmosphere pressure and the values of $(\tan\delta/p)_{max}$ in mm.$^{-1}$ and $\Delta\nu/p$ in cm.$^{-1}$/mm. for the reference gases. Of the various measurements shown, those by Birnbaum are probably most accurate.

The remaining gases were studied by the second method described above. For $CHCl_2F$ and $CHClF_2$ the typical non-resonant absorption curve was obtained in a plot of $p^2/\tan\delta$ against p^2. The curve was linear at the higher pressures with a curvature at low pressure caused by the effect of nearby rotational lines.

Table I

	$\tan\delta_{atm} \times 10^4$	$(\tan\delta/p)_{max} \times 10^7$	$\Delta\nu/p \times 10^4$
	CH_3Cl		
Method 1	2.5	4.6	1.8
Method 2	3.0	5.2	1.9
Bleaney and Loubser[4]			1.6
Birnbaum[5]	2.7	4.8	1.5
Krishnaji and Srivastava[6]			1.6
Theoretical[5]		5.4	
	CH_3Br		
Method 2	2.2	3.8	1.3
Bleaney and Loubser[4]			1.6
Birnbaum[5]	1.6	3.8	1.9
Krishnaji and Srivastava[6]			1.6
Theoretical[5]		4.1	
	CHF_3		
Method 2	4.2	14.8	0.8
Birnbaum[5]	3.7	16.3	0.7
Theoretical[5]		18.3	

The data for $CHCl_2F$ gave values of $(\tan\delta/p)_{max} = 6.5 \times 10^{-7}$ mm.$^{-1}$ and $\Delta\nu/p = 1.3 \times 10^{-4}$ cm.$^{-1}$/mm. If it is assumed that only a low-frequency inversion transition is responsible for the observed loss and also for the dielectric dispersion observed by Boggs, Crain and Whiteford,[7] the dielectric constant measurements can be used to calculate a value of 5.7×10^{-7} mm.$^{-1}$ for $(\tan\delta/p)_{max}$. This agreement is as good as can be expected considering the uncertainty in the dielectric constant measurements as well as those in the present investigation. The agreement would suggest that essentially all of the observed electrical interaction is due to the inversion transition and that the low-frequency rotational lines are weak enough to have little effect.

Absorption measurements also were made on $CHClF_2$. For this substance the plot of $p^2/\tan\delta$ against p^2 was again a straight line as expected, but the slope of the line was so small that major uncertainties were introduced into the calculation of $(\tan\delta/p)_{max}$ and $\Delta\nu/p$ from the graph. The published dielectric constant data[7] would predict a value of $(\tan\delta/p)_{max}$ of 6.6×10^{-7} mm.$^{-1}$, a value which at least is not inconsistent with our loss measurements.

Measurements were also made on CH_2F_2, CBr_2F_2 and CCl_2F_2 to check the dielectric constant data showing that there was no measurable dispersion in these gases. The interpretation of the absorption data is complicated by the fact that low-frequency rotational transitions can contribute to the loss at 9400 Mc. Thus, a measurement showing no loss is significant, while one showing appreciable loss would not necessarily be.

Measurements of microwave absorption in CBr_2F_2 and CCl_2F_2 showed that there is no measurable loss at 9400 Mc. Any loss which occurs must correspond to a $\tan\delta$ of less than 0.2×10^{-4} at 1 atmosphere pressure. Thus, for these two compounds the absorption measurements support the dielectric constant experiments in showing that low frequency radiation cannot produce an inversion

transition. Wilson[11] has shown that this is to be expected on the basis of the selection rules for molecules of C_{2v} symmetry.

For CH_2F_2 the measurements gave a value of $\tan \delta = 1.3 \times 10^{-4}$ at 1 atm. This is an appreciable loss, although it is less than that observed for any of the other gases. Significantly, the pressure dependence of the loss tangent is different from that observed for the other gases, the variation of loss tangent with pressure being much smaller. This is the type of effect that would be expected if the loss were due to a nearby rotational line rather than to the non-resonant absorption connected with inversion. The evidence for CH_2F_2 is not conclusive, but it is probable that the observed loss is due to nearby rotational transitions rather than to inversion.

(11) E. B. Wilson, Jr., THIS JOURNAL, **63**, Aug. (1959).

Conclusions

The absorption of microwave energy by $CHCl_2F$ is of the typical non-resonant type, giving a linear plot of $p^2/\tan \delta$ against p^2. This, in addition to the correlation between the value of $(\tan \delta/p)_{max}$ calculated from the absorption data and that computed from the dielectric constant measurements, gives strong support to the contention that the dielectric dispersion in this gas is of the same inversion type studied previously in symmetric top molecules. The absorption studies correlate also with dielectric constant measurements in indicating no measurable effects of inversion in molecules of C_{2v} symmetry.

Acknowledgments.—The authors wish to express their thanks to Mr. Andrew P. Deam and to Dr. Donald C. Thorn for valuable assistance in the design and construction of the equipment.

DIFFERENTIAL THERMAL ANALYSIS AND HETEROGENEOUS KINETICS: THE REACTION OF VITREOUS SILICA WITH HYDROFLUORIC ACID

BY AVROM A. BLUMBERG[1]

Mellon Institute, Pittsburgh 13, Pennsylvania

Received November 25, 1958

The method of Borchardt and Daniels, using differential thermal analysis to study the kinetics of reactions, has been extended to solid–liquid heterogeneous reactions. A simple method of determining the necessary thermal constants has been suggested. The heat of reaction was determined to be 33 ± 2 kcal. The rate of solution of vitreous silica can be described by the rate law $dM/dt = -(k_0 e^{-\Delta E/RT})S(HF)$ where the frequency factor k_0 is 0.120 ± 0.022 (g. SiO_2/sec. cm.^{2} HF molarity), and the activation energy is 9 ± 1 kcal.

Introduction

The reaction between vitreous silica and hydrofluoric acid[2]

$$6HF + SiO_2 \longrightarrow 2H_2O + H_2SiF_6$$

will be discussed in more detail in another paper. For the present, it is sufficient to know the stoichiometric coefficients of hydrofluoric acid and silica and something of the equilibria of the acid. Acid–fluoride systems are described by the equilibria

$$HF \longleftrightarrow H^+ + F^- \qquad K_1(25°) = 7 \times 10^{-4}$$
$$HF + F^- \longleftrightarrow HF_2^- \qquad K_2(25°) = 5$$

where the numerical values are averaged from those of several workers.[3] At high acidity it is possible to suppress the first reaction and to have virtually all the fluoride as the undissociated hydrofluoric acid. The work here does not employ hydrofluoric acid concentrations greater than 2.5 molal because there is evidence of polymer formation at higher concentrations.[4]

The earliest application of DTA to the study of kinetics is the work of Borchardt and Daniels[5] who developed the method for single phase liquid systems and we have used an adaptation of their procedure, extending it to the reaction of a solid with a liquid phase.

If we have in a bath, at temperature T_b which increases with time, two similar containers, one, designated by the subscript "1," with a reacting mixture, the other, designated by "2," with an inert mixture, then in a time interval dt, the temperature changes in the flask are described by

$$C_1\,dT_1 = dH + K_1(T_b - T_1)\,dt \qquad (1)$$
$$C_2\,dT_2 = K_2(T_b - T_2)\,dt \qquad (2)$$

where C_i is the heat capacity, K_i the thermal conductivity, T_i the temperature of each flask, and dH is the heat evolved during that time interval. By adjustment, we can make $C_1 = C_2 = C$ and $K_1 = K_2 = K$; by subtracting equation 2 from equation 1, and defining $\Delta T = T_1 - T_2$

$$dH = C\,d\Delta T + K\Delta T\,dt \qquad (3)$$

Integrating of equation 3 between $t = 0$ and $t = \infty$ and defining A as the total area under the ΔT *vs.* t curve, the total heat of evolution is

$$\Delta H = KA \qquad (4)$$

In the heterogeneous reaction

$$l\text{L(solution)} + m\text{M(solid)} \longrightarrow \text{product}$$

where l and m are the usual stoichiometric coefficients, we assume the rate of disappearance of either solid or soluble reactant to follow a law such as

$$k' = \left(\frac{L}{V}\right)^x S \qquad (5)$$

(1) Pittsburgh Plate Glass Company Fellowship.

(2) N. V. Sidgwick, "The Chemical Elements and Their Compounds," Vol. I, Oxford University Press, Oxford, England, 1950, p. 615.

(3) Ref. 2, Vol. II, p. 1105.

(4) R. P. Bell, K. N. Bascombe and J. C. McCoubrey, *J. Chem. Soc.*, 1286 (1956).

(5) H. J. Borchardt and F. Daniels, *J. Am. Chem. Soc.*, **79**, 41 (1957).

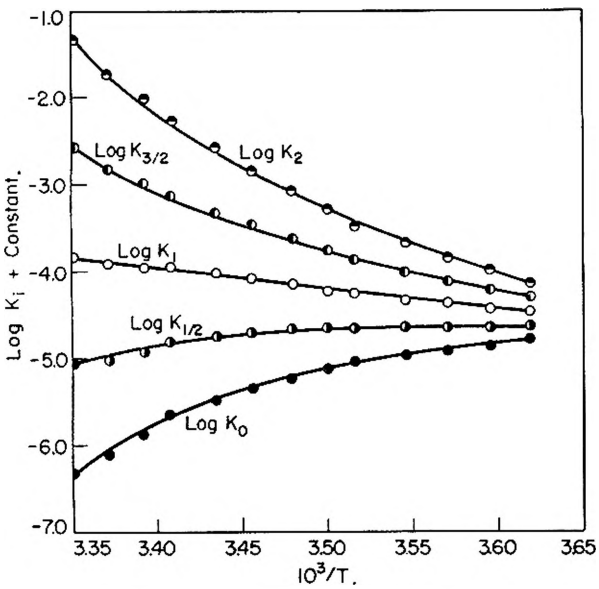

Fig. 1.—The logarithms of calculated rate constants, assuming certain orders of reaction, plotted against reciprocal temperature.

where L/V is now the concentration of the soluble reactant, (L moles in V kg. of water), S is the exposed area of the solid, and x is the order with respect to the soluble reactant. If we assume that (a) the mass change of the water is negligible during the course of reaction, so V is constant, and (b) the solid is consumed in a uniform manner with no significant change in shape, so

$$S = \frac{S_0}{M_0^{2/3}} M^{2/3}$$

where M is the mass of the solid phase, and S_0 and M_0 are the initial area and mass, then equation 5 may be rewritten

$$k = L^x M^{2/3} \qquad (6)$$

The assumption that the glass is attacked uniformly, so that the surface varies as the 2/3 power of the mass, was judged to be a valid one; microscope examination of powder samples before and after considerable attack revealed no changes in the general shape of the particles.

Case I. An Excess of Solid Reactant.—Suppose we start with L_0 moles of soluble reactant and M_0 grams of solid reactant (whose formula weight is w), and suppose further that there is an excess of solid reactant, *i.e.*, $M_0/mw > L_0/l$. At time t

$$M = M_0 - \frac{mw}{l}(L_0 - L) \qquad (7)$$

grams of solid reactant remain. Also

$$-\mathrm{d}L/\mathrm{d}t = \frac{L_0}{KA}[K\Delta T + C\,\mathrm{d}\Delta T/\mathrm{d}t] \qquad (8)$$

And

$$L = \frac{L_0}{KA}[K(A - a) - C\Delta T] \qquad (9)$$

where $a = \int_0^t \Delta T\,\mathrm{d}t$, is the area under the $\Delta T - t$ curve up to time t. From equations 7 and 9

$$M = M_0 - \frac{mw}{l}\frac{L_0}{KA}[Ka + C\Delta T] \qquad (10)$$

Equation 6 may be written

$$-\mathrm{d}L/\mathrm{d}t = kL^x M^{2/3}$$

or

$$k = \frac{-\mathrm{d}L/\mathrm{d}t}{L^x M^{2/3}} \qquad (11)$$

From the known values of K, C, L_0 and w, the stoichiometric coefficients m and l (which are 6 and 1, respectively, in the case of silica and hydrofluoric acid) and the experimentally determined ΔT, $\mathrm{d}\Delta T/\mathrm{d}t$, A and a, the rate constant k may be determined as a function of x as the only unknown parameter, for any temperature for which measurements are available. Only for one value of x will a plot of log k *vs.* $1/T$ produce a straight line, according to the Arrhenius law

$$k = k_0 e^{-\Delta E/RT}$$

This x is the order of the reaction with respect to the soluble reactant. Reaction orders commonly encountered are 0, 1/2, 1, 3/2 and 2. Such plots from one experiment are shown in Fig. 1. The slope of the straight line gives the energy of activation.

Case II. An Excess of Soluble Reactant.—Here

$$\mathrm{d}M/\mathrm{d}t = \frac{M_0}{KA}[K\Delta T + C\,\mathrm{d}\Delta T/\mathrm{d}t] \qquad (12)$$

$$M = \frac{M_0}{KA}[K(A - a) - C\Delta T] \qquad (13)$$

$$L = L_0 - \frac{l}{mw}\frac{M_0}{KA}(Ka + C\Delta T) \qquad (14)$$

Case III. An Excess of Neither Reactant.—Here

$$L_0/l = M_0/mw \qquad (15)$$

and equations 10 and 13 become identical, as do (9) and (14).

Experimental

I. Preparation of the Reaction Flasks and Thermocouples.—Both flasks were polyethylene pint bottles with tightly fitting screw caps. Thirty gauge copper–constantan thermocouples in two concentric polyethylene tubes (0.075" and 0.128" o.d.) were passed through the flask walls so that the junctions (treated with molten polyethylene to have them in contact with and completely surrounded by polyethylene) were immersed in the contained liquids. The differential thermocouples from the flasks were passed to a microvolt amplifier and then the signal to a recorder so that $\Delta T = T_1 - T_2$ could be read to 2.56×10^{-3}. On the same recorder the bath temperature, T_b, was printed directly to the nearest 1/8°; this was checked continually by a calibrated thermometer read to the nearest 0.1°.

If the bath temperature increases linearly with time

$$T_b = m + nt \qquad (16)$$

equations 1 (with $\mathrm{d}H = 0$, in the case of a suitable inert liquid) and (2) have the non-transient solutions

$$T_i = m + nt - n\,C_i/K_i \qquad (17)$$

or

$$T_i = T_b + T_{lag} \qquad (18)$$

Here T_{lag} is the amount by which each flask temperature lags behind the bath temperature, due to the finite heat transfer rate from bath to flask. From equation 17

$$\Delta T = n\left[\frac{C_2}{K_2} - \frac{C_1}{K_1}\right] \qquad (19)$$

When the two flasks are not balanced and are in a bath whose temperature is defined by equation 16, ΔT will reach a steady value represented by equation 19. Where T_b is non-linear with respect to time t, no steady value will be reached, but the drift will be slow for small coefficients of t^2 and higher terms.

Although exact matching is not essential since the steady value for ΔT can be taken as the base line (*in lieu* of $\Delta T = 0$) from which ΔT readings are taken during reaction, K values can be adjusted by wrapping waterproof tape around the flask with the higher thermal conductivity. Heat capacities are adjusted by varying the amount of liquid in either flask.

II. **Evaluation of the Terms K_1 and C_1.**—From equation 1 in the special case where flask "1" is filled with a suitable inert liquid (*i.e.*, $dH = 0$), and heated to some temperature $T_{1,0} > T_b$, then replaced in the bath (at T_b), where $T_2 = T_b$, T_1 will approach $T_b = T_2$ (*i.e.*, $\Delta T \rightarrow 0$) according to the relation

$$\ln \Delta T = \ln (T_{1,0} - T_2) - \frac{K_1}{C_1} t \qquad (20)$$

Thus from the slope K_1/C_1 and the known value C_1, K_1 may be calculated for the flask.

The nature of C_1 must be discussed. Both the fluid within and the flask itself cool to T_b. Since the flask has a heat capacity, its effect must be considered in the cooling (and in the regular reaction). The term K_1 includes the thermal conductivity of the flask material and also the two film coefficients on either side of the flask.[6] If the flasks are shaken so that the liquids within and without are similarly agitated, the temperature will be very nearly the average $\frac{1}{2}(T_1 + T_b)$. As will be apparent, the smaller the specific heat of the flask as compared to that of the solution within, the less serious is any error arising from the mean-wall temperature assumption. The heat capacity of the wall, C_w, will be taken to be that of the flask material alone (*i.e.*, the heat capacities of the films are neglected); C_f designates the heat capacity of the fluid. Then when the fluid temperature drops by dT_1, the mean-wall temperature drops by $\frac{1}{2} dT_1$; the total loss of heat is

$$C_f dT_1 + C_w(\tfrac{1}{2} dT_1) = C_1 dT_1$$

or

$$C_1 = C_f + \tfrac{1}{2} C_w \qquad (21)$$

The steps involved in determining K_1 and C_1 are: (a) with a suitable fluid in flask "1," cooling according to equation 20, and with C_1 defined by equation 21, the slope K_1/C_1 is obtained and from it the value K_1 for the flask; (b) with the reaction solution in flask "1," again cooling according to equation 21, and with the slope K_1/C_1 and K_1 from (a) above, C_1 for the reaction solution and flask is obtained.

Heat capacities of polyethylene were taken from literature values.[7] A typical set of curves is shown in Fig. 2. In practice the plot of $\ln \Delta T$ *vs.* t can be repeated several times by following the cooling on several sensitivities of the recording instrument. Also, K_1 and C_1 were evaluated both before and after each reaction.

This scheme is experimentally quicker and analytically simpler than that originally proposed.[5] From inspection of, for example, equations 8, 9 and 10 it is apparent that the ratio K/C is sufficient to determine both the order of reaction and activation energy. The heat of reaction (*vide* equation 4) depends on K and in this method ultimately on C. But the assumptions leading to equation 21 introduce errors in K less than those arising in measuring A.

III. Preparation of Materials.—Powdered vitreous silica was prepared by passing Corning fused silica 7940 lump cullet (analysis: less than 100 p.p.m. impurities) through a jaw crusher and a hammer mill and screening to sort the powder in five ranges between 100 and 270 mesh. This was followed by repeated washing with aqua regia (to remove iron, as indicated by thiocyanate test), and repeated sedimentation along a four-foot column of water (to remove fines, as indicated by the Tyndall effect and confirmed by microscopic examination). Impurities, determined by emission spectroscopy, were less than 88 p.p.m. after this processing. Surface areas were determined by krypton adsorption.

Hydrochloric acid was prepared from reagent grade stock and standardized against primary standard sodium carbonate. Hydrofluoric acid was prepared from reagent grade stock and standardized against sodium hydroxide solution (which, in turn, was standardized against the hydrochloric acid). The reaction solution was prepared from these by weighing out the proper amounts of each and enough distilled water to make a total of 300 g. for each run.

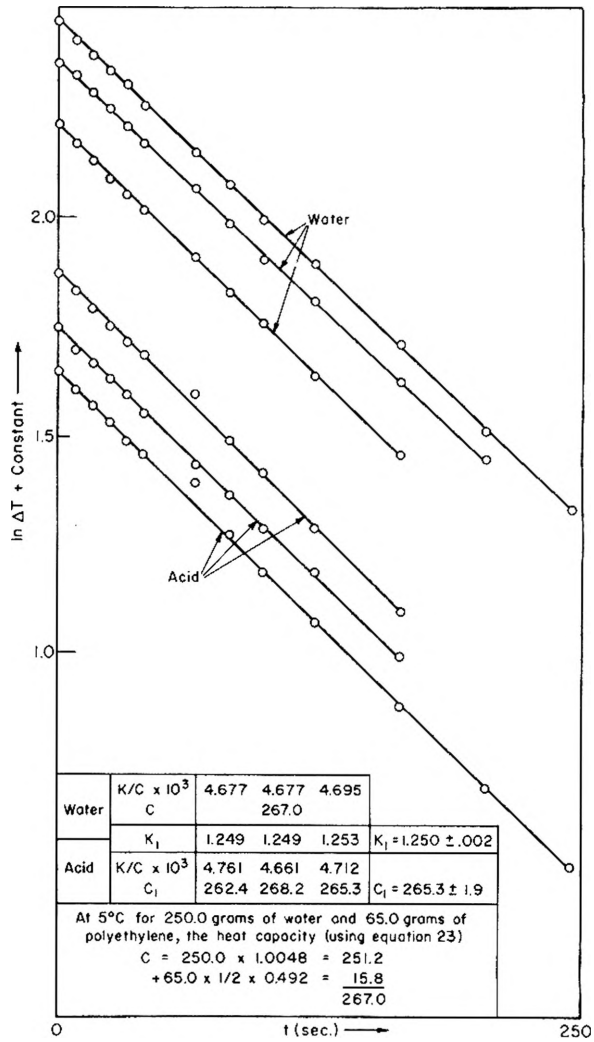

Water	K/C x 10³	4.677	4.677	4.695	
	C	267.0			
	K_1	1.249	1.249	1.253	K_1 = 1.250 ± .002
Acid	K/C x 10³	4.761	4.661	4.712	
	C_1	262.4	268.2	265.3	C_1 = 265.3 ± 1.9

At 5°C for 250.0 grams of water and 65.0 grams of polyethylene, the heat capacity (using equation 23)

C = 250.0 x 1.0048 = 251.2
+65.0 x 1/2 x 0.492 = 15.8
267.0

Fig. 2.—Evaluation of K_1 and C_1 from the rate of cooling of a warmed flask, according to the equation in $\Delta T = -K/Ct$ + constant.

IV. Conducting the Reaction.—The flasks were filled with equal masses of water, suspended from a wrist action shaker, shaken, immersed in and allowed to come to thermal equilibrium with the bath at constant temperature T_b. The thermal conductivities were adjusted, while T_b was increased linearly with time, according to equation 19. Then, with T_b constant and near the freezing point, K_1 was determined according to the procedure (IIa) of this section. Water was replaced with the reaction solution (water–hydrochloric– and hydrofluoric acids), and C_1 similarly was determined (IIb). Finally, with T_b increasing linearly with time, C_2 was adjusted to C_1 by adding to or removing from flask "2" an amount of water calculated by equation 19.

After these adjustments, the bath temperature was lowered to about the freezing point and one of two silica samples of equal mass (to the nearest milligram) was added to the inert flask. After $T_1 = T_2 = T_b$, the other silica sample was added to flask "1," the bath heater was turned on, shaking resumed, and both ΔT and T_b were recorded.

At the end of the reaction, which here is complete in about four hours, the heater was turned off (the bath by this time is usually at 30–35°), and K_1/C_1 determined for the spent reaction mixture—flask system at this higher temperature. Then, with water in the flask, K_1 is obtained.

(6) W. L. Badger and W. L. McCabe, "Elements of Chemical Engineering," McGraw-Hill Book Co., Inc., New York, N. Y., 1936, p. 128–131.

(7) M. Dole, W. P. Hettinger, Jr., N. R. Larson and J. A. Wethington, Jr., *J. Chem. Phys.*, **20**, 781 (1952).

TABLE I

DATA FOR THE ATTACK OF VITREOUS SILICA BY HYDROFLUORIC ACID, OBTAINED BY DTA

Initial mass of silica M_0 (g.)	Initial area of sample S_0 (cm.)²	In 300 g. of reaction soln. Moles of HF	Moles of HCl	Heat of reaction ΔH (kcal./mole SiO_2)	Activation energy ΔE (kcal.)/mole	Frequency factor k_0 (g. SiO_2/sec. cm.² HF molarity)
20.130	28,000	0.600	1.200	32.14	9.13	0.132
20.015	27,800	.600	1.200	30.29	10.5	.151
20.154	28,000	.600	1.200	35.82	6.82	.110
46.742	38,300	.600	1.200	34.10	7.28	.132
48.224	39,600	.600	1.200	31.89	8.55	.138
39.399	32,300	.600	1.200	30.63	11.3	.135
31.435	43,700	.450	0.900	36.10	7.66	.085
36.263	50,400	.450	0.900	36.93	7.22	.081

The K_1 and C_1 used in calculations are the average of the low and high temperature values.

The actual reaction temperature at any time can be calculated from T_b, ΔT and

$$T_{lag} = T_2 - T_b \qquad (18a)$$

so

$$T_1 = T_b + T_{lag} + \Delta T \qquad (22)$$

But T_{lag} will be negligible for small values of nC_2/K_2 (equation 19).

Results

The data for eight runs are presented in Table I. Two different samples of vitreous silica were used, 140–170 and 200–230 mesh with areas 820 and 1390 cm.²/g., respectively. The maximum temperature difference ΔT developed during the reaction ranged from 0.36° for samples with smaller areas, to 0.67°, for those with larger areas. In all runs the assumption of a first-order reaction with respect to hydrofluoric acid concentration gave a straight line in the log k *vs.* $1/T$ plot (Fig. 1).

Discussion

The method of studying the kinetics of a reaction by differential thermal analysis has been extended to a heterogeneous system, vitreous silica and hydrofluoric acid, by including with the original procedure of Borchardt and Daniels the assumption that the surface of a powder sample varies as the 2/3 power of the mass. In the case of isotropic substances (which include glasses but not crystalline quartz) where the rate of attack is uniform over the surface, linear ratios between dimensions can be expected to remain fairly constant for spheres, cubes and other solids whose surface-to-mass ratio is low, but not for rods and plates. The former class, which may be designated as pykna (from the Greek word for compact) is assumed to include the pulverized glass used in these experiments, since crushing has the general effect of making non-pyknic solids more nearly pyknic. Further, any errors arising from this assumption are less significant the less the solid is reduced in mass. For this reason the experiments here reported all used an excess of silica, with only from 12 to 30% of the solid consumed at completion of the reaction.

In addition, in order to have temperature differences large enough to measure with precision, it was necessary to use both an excess of silica (to provide a large area) and a high concentration of hydrofluoric acid. The latter was restricted to no greater than 2.5 molal for reasons discussed in the Introduction.

In the temperature range 0–35° the reaction can be described satisfactorily by a first-order kinetics law, with respect to the hydrofluoric acid concentration

$$\frac{dM}{dt} = -(k_0 e^{-\Delta E/RT}) S(HF)$$

where the frequency factor

$$k_0 = 0.120 \pm 0.022 \left(\frac{\text{g. } SiO_2}{\text{sec. cm.}^2 \text{ HF molarity}}\right)$$

and the activation energy

$$\Delta E = 9 \pm 1 \text{ kcal.}$$

The activation energy is of a magnitude expected either for a diffusion process or a heterogeneous reaction,[8] and so no decision can be made between these two processes on the basis of this work.

The heat of reaction was determined by this method to be 33 ± 2 kcal./mole of SiO_2. This agrees reasonably well with the literature values of 38 kcal./mole of SiO_2.[9]

Acknowledgments.—The author thanks the Messrs. Jay C. Fries and Edward R. Shuster of the Department of Research in Chemical Physics at Mellon Institute for their work in determining surface areas and impurities in the silica samples.

(8) S. Glasstone, K. J. Laidler and H. Eyring, "The Theory of Rate Processes," McGraw-Hill Book Co., Inc., New York, N. Y., 1941, p. 391, 525.

(9) K. S. Evstrop'ev and M. M. Skornyakov, *Akad. Nauk S. S. S. R.* 182 (1949); (see also *C. A.*, **46**, 10831 f, h (1952)).

THERMOCHEMISTRY AND VAPOR PRESSURE OF ALIPHATIC FLUOROCARBONS. A COMPARISON OF THE C–F AND C–H THERMOCHEMICAL BOND ENERGIES[1]

BY W. D. GOOD, D. R. DOUSLIN, D. W. SCOTT, ANN GEORGE, J. L. LACINA, J. P. DAWSON AND GUY WADDINGTON

Contribution No. 78 from the Thermodynamics Laboratory, Petroleum Experiment Station, Bureau of Mines, U. S. Department of the Interior, Bartlesville, Oklahoma

Received December 8, 1958

The heat of formation of four organic fluorine compounds, including three completely fluorinated aliphatic compounds, was determined by a rotating-bomb method of combustion calorimetry. An earlier technique that used sealed, fused-quartz ampoules for containing samples of volatile fluorine compounds was replaced by an improved technique that used sealed bags of a polyester film. For three of the compounds vapor pressure measurements were made by an improved method of comparative ebulliometry. The following values, in kcal. mole^{-1}, are reported for the standard heat of formation, $\Delta Hf°_{298.16}$, of these compounds from graphite and gaseous fluorine and hydrogen: *m*-fluorobenzotrifluoride(g), −184.17; perfluoromethylcyclohexane(g), −675.3; perfluoroethylcyclohexane(g), −769.7; and perfluoro-*n*-heptane(g), −789.0. These values were used with other thermochemical data to obtain a direct comparison of the C–F and C–H thermochemical bond energies in aliphatic compounds.

Systematic investigations of the thermodynamic properties of organic fluorine compounds are in progress in this Laboratory. One development of this program has been a precise method for determining the heat of combustion of fluorine-containing substances.[2] This paper reports a modification of previous techniques to allow combustion calorimetry of completely fluorinated compounds, such as fluorocarbons. Values of heat of combustion and formation were determined for *m*-fluorobenzotrifluoride (*m*,α,α,α-tetrafluorotoluene), perfluoromethylcyclohexane [undecafluoro-(trifluoromethyl)-cyclohexane], perfluoroethylcyclohexane [undecafluoro-(pentafluoroethyl)-cyclohexane] and perfluoro-*n*-heptane (*n*-hexadecafluoroheptane). Measurements of the vapor pressure of all except perfluoro-*n*-heptane were made by an improved method of comparative ebulliometry, and values of heat of vaporization were computed from the results. The values of heat of formation for the three fluorocarbons were used with other thermochemical data to obtain a direct comparison of the C–H and C–F thermochemical bond energies.

Experimental

The basic procedures used in this investigation for combustion calorimetry[2] and comparative ebulliometry[3] have been described. Only developments made in this investigation and procedures peculiar to it will be discussed here.

Combustion Calorimetry

Sample Containers Prepared from Polyester Film.—Bags of polyester film were employed to introduce samples of volatile organic fluorine compounds into the combustion bomb. The selection of containers for volatile samples has been a particularly troublesome problem in the combustion calorimetry of fluorine compounds. Previously, fused-quartz ampoules were used for compounds of relatively low fluorine content.[2] For compounds of high fluorine content, like those studied in this investigation, the reaction of fused quartz with the hydrofluoric acid in the combustion products would lead to large and uncertain thermochemical corrections (even if it were possible to make satisfactory thin-walled ampoules with the 3-ml. capacity required for fluorocarbons). As originally disclosed at the Calorimetry Conference of 1956, the bags of polyester film were devised to avoid the aforementioned difficulties and are expected to have numerous applications in combustion calorimetry. Therefore, their preparation and use will be described in detail.

The polyester film used to make the bags has a low permeability for organic compounds, including highly fluorinated materials. Compounds of widely differing properties, such as fluorocarbons, *m*-fluorobenzotrifluoride, benzene, toluene, commercial isohexanes, tetramethyllead and water, were sealed successfully in these bags and held for long intervals without evidence of swelling of the film or of loss of sample by permeation through the film.

Figure 1 illustrates preparation of a sample sealed in a polyester bag. The bag is made from a flat piece of film cut as shown in "a." This flat piece is folded and heat-sealed to make the empty bag shown in "b." The heat sealing is done with a small soldering iron held near, *but never touching*, the edges of the piece, which is held (with edges extending approximately $^1/_{16}$ inch) between metal templates. Such a bag may be made without detectable change in weight of the film.

The material that the bag is to contain is stored in a small, sealed glass vial and, immediately after the vial is opened, is transferred to the bag with a hypodermic syringe. Air is removed from the bag by applying slight pressure on the walls, and the neck of the bag is sealed with a special clamp. The gas space is reduced as much as possible to minimize errors in reduction of weights to *in vacuo* and errors caused by solution of gases in the liquid. Liquid is removed from the neck (outside the clamp) by swabbing it with filter paper. After the neck is thoroughly dry, the tip is held with tweezers and sealed as in "c." The mass of sample is determined by weighing the empty bag and then the bag and its contents, after filling and sealing. Because the film is prone to become electrostatically charged during these operations, it is discharged before each weighing. As the film is slightly hygroscopic, the bag is allowed to equilibrate with the atmospheric humidity prevailing in the balance case. After the final weighing the filled bag is rolled and placed inside the platinum crucible used in the combustion experiment. All of these operations of sample preparation are performed with the hands covered by thin cotton gloves to protect the film from contamination.

Use of the polyester sample containers simplified the comparison experiments[2] because it eliminated the "twin ampoules," as well as the need for H_2SiF_6 in the initial bomb solution. The reduction of the calorimetric data to standard states[2] also was simplified because the bomb solutions were not complicated by the presence of H_2SiF_6.

Polyester bags were compared with fused-quartz ampoules as sample containers in experiments with *m*-fluorobenzotrifluoride. This compound, empirical formula $C_7H_4F_4$, has as many fluorine atoms as hydrogen atoms in the molecule.

(1) This research was supported by the United States Air Force through the Air Force Office of Scientific Research of the Air Research and Development Command under Contract No. CSO-680-57-4. Reproduction in whole or in part is permitted for any purpose of the United States Government.

(2) W. D. Good, D. W. Scott and Guy Waddington, THIS JOURNAL, **60**, 1080 (1956).

(3) G. Waddington, J. W. Knowlton, D. W. Scott, G. D. Oliver, S. S. Todd, W. N. Hubbard, J. C. Smith and H. M. Huffman, *J. Am. Chem. Soc.*, **71**, 797 (1949).

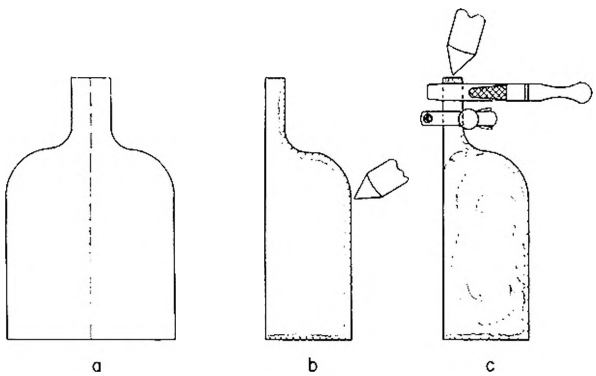

Fig. 1.—Preparation of polyester sample containers.

It was selected for the comparison as being intermediate in its properties between hydrocarbons and fluorocarbons. As shown in a later section on Calorimetric Results (Table III), concordant results were obtained with both sample containers, but improved precision was obtained with the polyester bags.

Calorimetric Procedures.—The calorimeter (laboratory designation BMR-2) and bomb (laboratory designation Pt-5) have been described.[2] Bomb Pt-5, internal volume 0.353 l., was used in all combustion experiments with *m*-fluorobenzotrifluoride, perfluoromethylcyclohexane and perfluoro-*n*-heptane. Bomb Pt-5 failed during the experiments with perfluoroethylcyclohexane and was replaced by a similar bomb, Pt-3b, internal volume, 0.349 l.

The ignition circuit differed from that used previously. A short piece of platinum wire, 0.002 inch diameter, was used to ignite a fuse of cotton thread. The energy evolved when the wire was connected momentarily across a 20-volt transformer was sufficient to fuse the wire. For the combustion experiments with *m*-fluorobenzotrifluoride, the electrical ignition energy was assumed to be small and constant and was included in the energy equivalent of the calorimetric system. For the combustion experiments with the fluorocarbons, an electronic device was used to measure directly the input of electrical energy. The circuit was patterned after that described by Pilcher and Sutton.[4] Observation of significant variations in values of electrical ignition energy suggests that the accuracy was improved by the direct measurement of electrical ignition energy.

The experimental procedures were essentially those described for combustion experiments with Teflon.[2] Samples of the discharge gases, freed from HF and sometimes reduced in oxygen content by scrubbing with sodium pyrogallate, were retained after representative combustion experiments for mass spectrometer scanning. No fluorine-containing gases other than CF_4 were detected. The bomb gas was tested occasionally for carbon monoxide, but none was detected.

For the combustion experiments with *m*-fluorobenzotrifluoride, perfluoromethylcyclohexane and perfluoro-*n*-heptane, the bomb was charged with oxygen to an initial pressure of 30 atm. An initial oxygen pressure of 40 atm. was necessary in the experiments with perfluoroethylcyclohexane to prevent the formation of a "sooty" deposit in the bomb. Brown resinous deposits remained on the crucible in preliminary experiments with perfluoroethylcyclohexanone and perfluoro-*n*-heptane. However, the formation of resinous deposits in experiments with the latter compound was prevented in most experiments by using enough hydrocarbon oil as promoter to produce about 30% of the total energy of the bomb process. Formation of trace amounts (never more than 0.5 mg.) could not be entirely eliminated in the experiments with perfluoroethylcyclohexane. Thermochemical corrections for incomplete combustion were applied on the assumption that the heat of combustion of the deposit was 5 ± 5 cal. mg.$^{-1}$.

Under the conditions of the combustion experiments, the fluorine in *m*-fluorobenzotrifluoride was converted quantitatively to HF. In the experiments with the fluorocarbons, more than half of the fluorine appeared in the combustion products as CF_4. The per cent. of fluorine appearing as CF_4 varied from 76 to 79% for perfluoromethylcyclohexane, 73 to 80% for perfluoroethylcyclohexane, and 62 to 64% for perfluoro-*n*-heptane. The proportion of fluorine that appeared as CF_4 was a function of the amount of hydrogen available in the reactants in auxiliary oil and/or polyester film.

Loss in weight of the platinum crucibles, up to 2 mg. per experiment, was observed. The loss probably was caused by formation of volatile platinum fluorides that later reacted with water to form hydrous oxides. The thermochemical effect of such a reaction was assumed to be negligible. For instance, if the net reaction was

$$Pt(c) + {}^1/_2O_2(g) + H_2O(liq) = Pt(OH)_2(c) \qquad (I)$$

then $\Delta H°_{298.16} = -18.9$ kcal.,[5] and reaction 2 mg. of platinum would evolve only 0.2 cal., or less than 0.003% of the total energy of the bomb process.

Comparative Ebulliometry

The comparative ebulliometer system described in Ref. 3 has been modified by addition of a third ebulliometer to the two for containing sample and water. The third ebulliometer contains benzene as a secondary reference substance and is used for comparative measurements in the range 70–145 mm. In this low pressure range, water does not boil steadily enough for precise results.

Units of Measurement and Auxiliary Quantities

All data reported are based on the 1951 International Atomic Weights[6a] and fundamental constants[6b] and the definitions: 0°C. = 273.16°K.; 1 cal. = 4.1840 abs. j. Measurements of temperature were made with platinum resistance thermometers calibrated in terms of the International Temperature Scale.[6c] All electrical and mass measurements were referred to standard devices calibrated at the National Bureau of Standards.

For use in reducing weights in air to *in vacuo*, in correcting the energy of the actual bomb process to the isothermal bomb process and in correcting to standard states, the values in Table I were used for density ρ, specific heat c_p, and $(\partial E/\partial P)_T$ of the various substances. These values were obtained from the literature or, in parentheses, estimated by analogy with structurally similar substances.

TABLE I

AUXILIARY QUANTITIES AT 25°

	ρ, g. ml.$^{-1}$	c_p, cal. deg.$^{-1}$ g.$^{-1}$	$(\partial E/\partial P)_T$, cal. atm.$^{-1}$ g.$^{-1}$
Polyester film	1.38	0.315	−0.00069
Perfluoromethylcyclohexane	1.788	(.235)	− .0066
Perfluoroethylcyclohexane	1.826	(.242)	− .0062
Perfluoro-*n*-heptane	1.718	.258	− .0069
m-Fluorobenzotrifluoride	1.289	(.289)	− .0066

Materials

***m*-Fluorobenzotrifluoride.**—*m*-Fluorobenzotrifluoride, which was supplied by the Illinois State Geological Survey Division through the courtesy of Dr. G. C. Finger, was distilled in an efficient fractionating column by C. J. Thompson and H. J. Coleman of the Chemistry and Refining Branch of this Station. The sample was a composite of selected fractions judged to be of highest purity on the basis of refractive index determinations and had a purity of 99.91 ± 0.05 mole % as determined by the time–temperature freezing point method. The material was dried by passing the vapor over freshly activated Molecular Sieve.

Perfluoromethylcyclohexane.—Crude perfluoromethylcyclohexane was supplied by the Minnesota Mining and Manufacturing Company through the courtesy of Dr. T. J. Brice. This material was first treated with a neutral permanganate solution to remove olefinic impurities by oxidation. The olefin-free material was purified by the Chemistry and Refining Branch of this Station by physical means.

(4) G. Pilcher and L. E. Sutton, *Trans. Roy. Soc. (London)*, **A248**, 23 (1955).

(5) F. D. Rossini, D. D. Wagman, W. H. Evans, S. Levine and I. Jaffe, "Selected Values of Chemical Thermodynamic Properties," N.B.S. Circular 500, 1952.

(6) (a) E. Wichers, *J. Am. Chem. Soc.*, **74**, 2447 (1952); (b) F. D Rossini, F. T. Gucker, Jr., H. L. Johnston, L. Pauling and G. W. Vinal, *ibid.*, **74**, 2699 (1952); (c) H. F. Stimson, *J. Research Natl. Bur. Standards*, **42**, 209 (1949).

TABLE II

SUMMARY OF TYPICAL CALORIMETRIC EXPERIMENTS

	m-Fluorobenzotrifluoride (fused quartz)	*m*-Fluorobenzotrifluoride (polyester)	Perfluoromethylcyclohexane	Perfluoroethylcyclohexane	Perfluoro-*n*-heptane
Comparison experiments					
m(benzoic acid), g.	1.22632	1.05125	0.98471	1.00652	1.15101
m(auxiliary oil), g.	0.01728				
m(succinic acid), g.			.56136	0.52154	0.21750
m(polyester), g.		0.25143			
$n^i(H_2O)$, mole	.5241	.5255	.4915	.4924	.5018
n^i(HF), mole	.03558	.03582	.04938	.04926	.06789
$n^i(H_2SiF_6)$, mole	.000741				
Δt_c, deg.	1.97936	2.00383	1.97429	1.97923	1.97789
$m\Delta Ec°/M$(benzoic acid), cal.	−7741.7	−6636.5	−6216.4	−6354.1	−7266.2
$m\Delta Ec°/M$(oil), cal.	−189.8				
$m\Delta Ec°/M$(succinic acid), cal.			−1695.2	−1674.9	−656.8
$m\Delta Ec°/M$(polyester), cal.		−1389.7			
$m\Delta Ec°/M$(fuse), cal.	−5.9	−6.3	−5.6	−5.3	−6.2
$-\Delta E^f$ dec. (HNO_3), cal.	−0.4	−0.4	−0.5	−1.4	−1.0
$-\Delta E$, cor. to st. states, cal.	−11.0	−11.5	−12.0	−13.6	−11.7
$-\Delta E_{ign.}$, cal.			−0.9	−0.8	−0.8
ε(cont.)(Δt_c), cal.	26.9	27.2	24.8	26.4	25.3
ε_{app}(calor.)($-\Delta t_c$), cal.	−7921.9	−8017.2	−7905.8	−7923.7	−7917.4
ε_{app}(calor.), cal. deg.$^{-1}$	4002.3	4001.0	4004.4	4003.4	4003.0
Combustion experiments					
m(compound), g.	1.64081	1.57512	5.75873	5.63880	4.51368
m(auxiliary oil), g.	0.01807				0.22478
m(polyester), g. (at % rel. hum.)		0.12062(40)	0.10623(51)	0.12842(32)	0.09992(27)
$n^i(H_2O)$, moles	0.5523	0.5523	0.5523	0.5523	0.5523
Δt_c, deg.	1.97217	2.00359	1.96523	1.96897	1.97488
ε_{app}(calor.)($-\Delta t_c$), cal.	−7893.1	−8016.3	−7869.5	−7882.6	−7905.4
ε(cont.)($-\Delta t_c$), cal.	−27.7	−28.1	−28.3	−29.9	−28.0
$\Delta E_{ign.}$, cal.			0.6	0.7	0.7
ΔE, cor. to st. states, cal.	11.5	12.1	21.3	24.8	17.1
ΔE^f_{dec} (HNO_3), cal.	0.5	0.4	0.3	0.1	0.5
$\Delta E^f_{hydr}(H_2SiF_6)$, cal.	27.2				
$-m\Delta E_c°/M$(fuse), cal.	6.0	6.3	5.2	4.7	6.6
$-m\Delta Ec°/M$(oil), cal.	198.5				2468.9
$-m\Delta Ec°/M$(polyester), cal.		659.3	580.4	702.2	546.5
Cor. to st. CF_4 conversion, cal.[a]			0.4	72.8	−20.0
Cor. for incomplete combustion, cal.				−2.4	
$m\Delta Ec°/M$(compound), cal.	−7677.1	−7366.3	−7289.6	−7109.6	−4913.1
$\Delta Ec°/M$(compound), cal. g.$^{-1}$	−4678.8	−4676.7	−1265.8	−1260.8	−1088.5

[a] Correction to the % of fluorine appearing as CF_4 in the combustion products corresponding to eq. IV, V and VI based on the value of the heat of hydrolysis of CF_4 determined in this Laboratory.[2]

The method (distillation in an efficient fractionating column followed by silica gel percolation of selected fractions of distilled material) was that developed by Blumkin, Orrick and Gibson,[7] but the limited amount of starting material did not permit purification to the degree achieved by those workers. Two samples were used for experimental studies—a "best" sample, hereinafter designated as "A" ($n^{20}D$ 1.2809$_1$) and a second sample, designated as "B" ($n^{20}D$ 1.2808$_6$), shown by infrared spectra to be significantly less pure. No quantitative value was obtained for the purity of either sample, but freezing curves, gas–liquid chromatograms and infrared spectra all indicated that the purity of even the "best" sample was only of the order of 98 mole %. The samples were dried by passing the vapor over freshly activated Molecular Sieve.

Perfluoroethylcyclohexane.—Crude perfluoroethylcyclohexane was obtained from the same source and was purified by the same methods as perfluoromethylcyclohexane. Two samples were used for experimental studies—a "best" sample, hereinafter designated "A" ($n^{20}D$ 1.2884$_8$), and a less pure sample, designated "B," which was a composite of fractions having refractive indices $n^{20}D$ between 1.2883$_5$ and 1.2285$_8$. Gas–liquid partition chromatograms yielded purity values of 96+ and 93+ mole % for samples "A" and "B," respectively. The samples were dried by passing the vapor over freshly activated Molecular Sieve.

Perfluoro-*n*-heptane.—The perfluoro-*n*-heptane used in this work was furnished by Carbide and Carbon Chemicals Company, under contract to the Atomic Energy Commission, through the courtesy of Karl E. Rapp. Two samples of significantly different but not definitely known purity, hereinafter designated as samples "A" and "B," were used. Time–temperature freezing point determinations of purity gave values of 99.8 and 99.4 mole % for samples "A" and "B," respectively, if the value used for the freezing point for zero impurity $T_f°$ was calculated from the experimental curves. However, this value of $T_f°$ differed significantly from the literature value of the triple point temperature.[8]

(7) S. Blumkin, N. C. Orrick and J. D. Gibson, "Purification and Some Physical Properties of Undecafluoro-(trifluoromethyl)-cyclohexane," Report No. K-623, Carbide and Carbon Chemicals Division, Union Carbide and Carbon Corporation, K-25 Laboratory Division, June 30, 1950.

These observations suggest that formation of solid solutions may have invalidated the freezing-point method of purity determination. Sample "A" showed no impurity band between 200 and 240 mμ in the ultraviolet spectrum,[9] and sample "B" had been treated chemically to remove impurities responsible for that band. The samples were dried with P_2O_5 and by passing the vapor over freshly activated Molecular Sieve.

Benzoic Acid, Auxiliary Oil and Succinic Acid.—The benzoic acid was National Bureau of Standards Sample 39g. The auxiliary oil and succinic acid were those described in ref. 2. More recent determinations of $\Delta Ec°/M$ gave the values (with uncertainty interval): auxiliary oil, -10983.7 ± 0.6 cal. g.$^{-1}$; succinic acid, -3019.8 ± 0.4 cal. g.$^{-1}$.

Polyester Film.—The polyester film, 100 gauge Mylar Type A, was purchased from the Film Department of E. I. du Pont de Nemours & Company, Inc. This polyester film, empirical formula $C_{10}H_8O_4$, is the condensation product of ethylene glycol and terephthalic acid. The amount of carbon dioxide obtained by combustion of the film was about 99.6% of that expected from the idealized formula. Less than 100% is reasonable because the film contains hydroxyl end groups, ash and, perhaps, trapped water. The film is very slightly hygroscopic. The amount of water it absorbs is approximately a linear function of the relative humidity, and the total amount absorbed in the change from 0 to 100% relative humidity is 0.46_2% of the weight of the particular sample of film used. The heat of combustion was determined for samples equilibrated with air of known relative humidity. The following equation was used to represent $\Delta Ec°/M$ of the film as a function of relative humidity

$$\Delta Ec°/M = -5476.1 - 0.2524 \text{ (relative humidity expressed in \%) cal. g.}^{-1} \quad \text{(II)}$$

Cotton Thread.—The sample of unmercerized cotton thread used as fuse material had the empirical formula $CH_{1.774}O_{0.887}$. For $\Delta Ec°/M$ of the cotton thread, the value -4050 cal. g.$^{-1}$ was determined.

Calorimetric Results

Calorimetric experiments selected as typical of each of the several series are summarized in Table II. The symbols of this table are the same as those of Ref. 2.

***m*-Fluorobenzotrifluoride.**—Five pairs of satisfactory combustion and comparison experiments were obtained by using fused-quartz ampoules as sample containers. Another five pairs of satisfactory experiments were obtained by using the new polyester bag technique. The values obtained for $\Delta Ec°/M$, summarized in Table III, refer to the reaction

$$C_7H_4F_4(\text{liq}) + 7O_2(g) + 60H_2O(\text{liq}) = 7CO_2(g) + 4HF\cdot 15H_2O(\text{liq}) \quad \text{(III)}$$

In the series of experiments with fused quartz ampoules, the corrections for chemical reaction of silica were large, 17 to 29 cal. per experiment. Uncertainties in these large quantities probably account for the poorer precision in that series. The appropriately weighted average value of $\Delta Ec°/M$ from both series is -4677.6 ± 0.4 cal. g.$^{-1}$.

Fluorocarbons.—The results for all combustion experiments with the fluorocarbons are listed in Table IV. The values of $\Delta Ec°/M$ refer to the equations

Perfluoromethylcyclohexane

$$C_7F_{14}(\text{liq}) + 3.5O_2(g) + 31.5H_2O(\text{liq}) = 3HF\cdot 10H_2O(\text{liq}) + 2.75CF_4(g) + 4.25CO_2(g) \quad \text{(IV)}$$

Perfluoroethylcyclohexane:

$$C_8F_{16}(\text{liq}) + 4O_2(g) + 31.5H_2O(\text{liq}) = 3HF\cdot 10H_2O(\text{liq}) + 3.25CF_4(g) + 4.75CO_2(g) \quad \text{(V)}$$

Perfluoro-*n*-heptane:

$$C_7F_{16}(\text{liq}) + 3O_2(g) + 63H_2O(\text{liq}) = 6HF\cdot 10H_2O(\text{liq}) + 2.5CF_4(g) + 4.5CO_2(g) \quad \text{(VI)}$$

TABLE III

m-FLUOROBENZOTRIFLUORIDE: COMPARISON OF METHODS

	$\Delta Ec°/M$, cal. g.$^{-1}$ (fused-quartz ampoules)	$\Delta Ec°/M$, cal. g.$^{-1}$ (polyester bags)
	−4675.3	−4677.1
	−4681.4	−4578.2
	−4677.7	−4676.7
	−4678.2	−4678.6
	−4678.8	−4676.5
Mean	−4678.3	−4677.4
Std. dev. of mean	±1.0	±0.4

The foregoing equations correspond closely to the stoichiometry of the actual bomb process.

The "A" samples of the fluorocarbons were of the highest purity that was practical to achieve. However, the purity fell far short of that usually desired for precision combustion calorimetry. To test for any effect of impurity, combustion calorimetry also was done on the "B" samples, which were of significantly lower purity. If the impurity had been material with a significantly different heat of combustion, different values of heat of combustion should have been observed for the samples of different purity. Actually, for none of the fluorocarbons was there any significant difference in the

TABLE IV

COMPARISON OF VALUES OF $\Delta Ec°/M$ FOR FLUOROCARBON SAMPLES OF DIFFERENT PURITY, IN CAL. G.$^{-1}$ AT 25°

	Perfluoromethylcyclohexane	Perfluoroethylcyclohexane	Perfluoro-*n*-heptane
"A" Sample	−1265.3	−1260.8	−1089.1
	−1265.5	−1261.6	−1087.5
	−1265.1	−1259.3	−1088.2
	−1265.8	−1259.4	−1088.8
	−1265.1	−1260.0	−1088.5
Av. value and stand. dev. of mean	−1265.4 ± 0.1	−1260.2 ± 0.4	−1088.4 ± 0.3
"B" Sample	−1266.0	−1259.9	−1090.1
	−1265.8	−1259.8	−1093.4
	−1266.2	−1260.5	−1083.9
	−1265.2	−1259.2	−1086.8
	−1264.5	−1258.5	−1086.9
			−1088.8
Av. value and stand. dev. of mean	−1265.5 ± 0.3	−1259.6 ± 0.3	−1088.3 ± 1.3
Av. value and stand. dev. of mean for all expt.	−1265.5 ± 0.2	−1259.9 ± 0.3	−1088.4 ± 0.7

observed values of heat of combustion for the two samples. This observation suggests that the impurity in the samples had a relatively small effect on the heat of combustion. Such would be the case if the impurities were isomeric or, at least, were other fluorocarbons.

Ebulliometric Results

Vapor Pressure.—The vapor pressures of *m*-fluorobenzotrifluoride, perfluoromethylcyclohex-

(8) G. D. Oliver and J. W. Grisard, *J. Am. Chem. Soc.*, **73**, 1688 (1951).

(9) D. Grafstein, *Anal. Chem.*, **26**, 523 (1954); D. N. Glew and L. W. Reeves, THIS JOURNAL, **60**, 615 (1956).

ane and perfluoroethylcyclohexane were determined by comparative ebulliometry. The "best" or "A" samples of perfluoromethylcyclohexane and perfluoroethylcyclohexane were used. The differences in the boiling and condensation temperatures of the samples at 1 atm. pressure were: *m*-fluorobenzotrifluoride, 0.001°; perfluoromethylcyclohexane, 0.004°; perfluoroethylcyclohexane, 0.005°. These small differences show that whatever impurity was in the samples had nearly the same volatility as the major component and, therefore, had little effect on the observed vapor pressure. The results are listed in Table V. The Antoine[10] and Cox[11] equations selected to represent these results are

m-Fluorobenzotrifluoride:

$$\log p = 7.00795 - 1305.692/(t + 215.766) \quad \text{(VII)}$$

$$\log (p/760) = A(1 - 373.759/T) \quad \text{(VIII)}$$

where

$$\log A = 0.864641 - 7.31027 \times 10^{-4}T + 6.91364 \times 10^{-7}T^2$$

Perfluoromethylcyclohexane:

$$\log p = 6.82184 - 1132.493/(t + 211.066) \quad \text{(IX)}$$

$$\log (p/760) = A(1 - 349.456/T) \quad \text{(X)}$$

where

$$\log A = 0.907847 - 10.32816 \times 10^{-4}T + 10.92653 \times 10^{-7}T^2$$

Perfluoroethylcyclohexane:

$$\log p = 6.85194 - 1217.729/(t + 205.674) \quad \text{(XI)}$$

$$\log (p/760) = A(1 - 374.135/T) \quad \text{(XII)}$$

where

$$\log A = 0.921458 - 10.09293 \times 10^{-4}T + 10.0873 \times 10^{-7}T^2$$

In these equations, p is in mm., t in °C. and T in °K. Comparisons of observed and calculated vapor pressure for both the Cox and Antoine equations are given in Table V. These comparisons show that the three-constant Antoine equations do not represent the observed vapor pressure accurately over the wide pressure range, but that the four-constant Cox equations do. The normal boiling points calculated from the Cox equation are: *m*-fluorobenzotrifluoride, 100.60° (373.76°K.); perfluoromethylcyclohexane, 76.30° (349.46°K.); and perfluoroethylcyclohexane, 100.98° (374.14° K.).

The vapor pressure of perfluoromethylcyclohexane was measured by Fowler, *et al.*,[12] whose results differ by as much as 4% from the more precise data of this research. No vapor pressure data for either of the other two compounds have been reported.

Heat of Vaporization.—Values of the heat of vaporization at 298.16°K. were computed from the Cox equations, the exact form of the Clapeyron equation and estimated values for the second virial coefficient. These values of the heat of vaporization, listed in Table VI, are strictly the heat of vaporization to the real gas, $\Delta Hv_{298.16}$, but are not significantly different from the standard heat of vaporization, $\Delta Hv°_{298.16}$. For perfluoro-*n*-heptane, Oliver and Grisard's value,[8] also obtained from vapor pressure measurements, was accepted.

(10) C. Antoine, *Compt. rend.*, **107**, 681 (1888).

(11) E. R. Cox, *Ind. Eng. Chem.*, **28**, 613 (1936).

(12) R. D. Fowler, J. M. Hamilton, Jr., J. S. Kasper, C. E. Weber, W. B. Burford III and H. C. Anderson, *Ind. Eng. Chem.*, **39**, 375 (1947).

Derived Thermochemical Data

Table VI lists the derived data for all four compounds. The uncertainties listed for $\Delta Ec°$ and $\Delta Hc°$ are the uncertainty intervals equal to twice the final "over-all" standard deviation. The latter includes uncertainties not only in the combustion and comparison experiments but also in the values of heat of combustion of benzoic acid, auxiliary oil, polyester film and succinic acid used in the comparison experiments. To compute values of the standard heat of formation, values of the heat of formation of carbon dioxide,[5] water,[5] hydrofluoric acid[5] and tetrafluoromethane[2] were used.

The value of the heat of formation of perfluoro-*n*-heptane was combined with entropy data from ref. 8 and entropy values for C(graphite)[5] and $F_2(g)$[13] to calculate values of the standard entropy of formation, free energy of formation and logarithm of the equilibrium constant of formation.

$$7C(c, \text{graphite}) + 8F_2(g) = n\text{-}C_7F_{16}(\text{liq}) \text{ or } (g) \quad \text{(XIII)}$$

	Liquid	Gas
$\Delta Hf°_{298.16}$, kcal. mole^{-1}	−797.7	−789.0
$\Delta Sf°_{298.16}$, cal. deg.$^{-1}$ mole^{-1}	−262.8	−238.2
$\Delta Ff°_{298.16}$, kcal. mole^{-1}	−719.3	−717.9
$\log Kf_{298.16}$	527.2	526.2

Thermochemical Bond Energy Comparison

The values of heat of formation of the three fluorocarbons studied in this investigation, of tetrafluoromethane,[2] and of structurally similar hydrocarbons,[14] with values of the heat of atomization of hydrogen[5] and fluorine,[13] made possible a comparison of the C–F and C–H thermochemical bond energies in aliphatic compounds.

The difference in thermochemical bond energies, E(C–F) − E(C–H), was derived from the hypothetical reactions

$$CF_4 + 4H = CH_4 + 4F \qquad \Delta H°_{298.16} = 67.7 \text{ kcal.}$$

$$n\text{-}C_7F_{16} + 16H = n\text{-}C_7H_{16} + 16F \qquad \Delta H°_{298.16} = 213.1 \text{ kcal.}$$

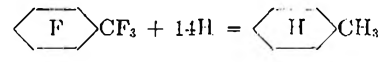

$$\Delta H°_{298.16} = 173.7 \text{ kcal.}$$

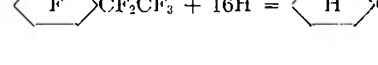

$$\Delta H°_{298.16} = 197.7 \text{ kcal.}$$

Since the molecular conformations of reactant and product in each of these reactions are the same, the heats of reaction depend primarily on the thermochemical bond energy of the ligands created or destroyed in the substitution of hydrogen for fluorine.

If a represents the difference in bond energies, E(C–F) − E(C–H), for the ≻CF group relative to the ≻CH group, b the difference for the >CF_2 group relative to the >CH_2 group, c the difference for the –CF_3 group relative to the –CH_3 group and d the difference for CF_4 relative to CH_4, then four equations may be written for the heats of the four reactions

(13) W. H. Evans, T. R. Munson and D. D. Wagman, *J. Research Natl. Bur. Standards*, **55**, 147 (1955).

(14) F. D. Rossini, K. S. Pitzer, R. L. Arnett, R. M. Braun and G. C. Pimentel, "Selected Values of Physical and Thermodynamic Properties of Hydrocarbons and Related Compounds," Carnegie Press, Pittsburgh, Pa., 1953.

TABLE V

VAPOR PRESSURE IN MM.

Ref. comp.[a] B.p., °C.	Ref. comp.[a] p(obsd.)[b]	*m*-Fluorobenzotrifluoride B.p., °C.	*m*-Fluorobenzotrifluoride p(obsd.) − p(calcd.) Antoine eq. VII	*m*-Fluorobenzotrifluoride p(obsd.) − p(calcd.) Cox eq. VIII	Perfluoromethylcyclohexane B.p., °C.	Perfluoromethylcyclohexane p(obsd.) − p(calcd.) Antoine eq. IX	Perfluoromethylcyclohexane p(obsd.) − p(calcd.) Cox eq. X	Perfluoroethylcyclohexane B.p., °C.	Perfluoroethylcyclohexane p(obsd.) − p(calcd.) Antoine eq. XI	Perfluoroethylcyclohexane p(obsd.) − p(calcd.) Cox eq. XII
19.061	71.87							38.098	0.00	0.00
21.720	81.64	40.448	+0.01	−0.02				40.834	− .02	− .01
24.388	92.52	43.210	+ .01	− .01				43.570	.00	+ .01
27.068	104.63	45.984	+ .01	.00				46.326	− .01	+ .01
29.757	118.06	48.764	+ .02	+ .02				49.086	+ .02	+ .03
32.460	132.95	51.560	.00	+ .01				51.864	+ .03	+ .04
35.174 / 60.000	149.41	54.372	− .05	− .03	32.618	−0.02	−0.01	54.667	− .04	− .03
65	187.57	60.008	− .06	− .03	37.909	− .01	− .01	60.275	+ .01	.00
70	233.72	65.684	− .05	− .02	43.247	+ .01	.00	65.941	+ .03	.00
75	289.13	71.398	.00	+ .01	48.634	+ .03	.00	71.653	+ .06	+ .01
80	355.22	77.155	+ .03	+ .02	54.069	+ .04	.00	77.418	+ .07	+ .01
85	433.56	82.954	+ .06	+ .03	59.551	+ .08	+ .02	83.233	+ .06	− .01
90	525.36	88.794	+ .07	+ .02	65.084	+ .06	.00	89.099	+ .01	− .04
95	633.99	94.675	+ .09	+ .03	70.665	+ .03	.00	95.011	.00	.00
100	760.00	100.598	+ .08	+ .02	76.296	− .03	.00	100.975	− .07	.00
105	906.06	106.563	+ .04	− .01	81.975	− 1.0	+ .01	106.990	− .20	− .03
110	1074.6	112.569	.0	.0	87.703	− .1	+ .1	113.055	− .3	.0
115	1268.0	118.615	− .1	− .1	93.481	− .3	.0	119.166	− .4	.0
120	1489.1	124.703	− .2	− .1	99.305	− .2	.0	125.326	− .2	.0
125	1740.8	130.830	.0	.0	105.176	+ .1	.0	131.532	+ .2	+ .1
130	2026.0	136.996	+ .1	.0	111.094	+ .5	.0	137.786	+ .8	.0

[a] The reference compound from 71.87 to 149.41 mm. was pure benzene and that from 149.41 to 2026.0 mm. was pure water. [b] From vapor pressure data for benzene ["Selected Values of Physical and Thermodynamic Properties of Hydrocarbons and Related Substances" by American Petroleum Institute Research Project 44, Carnegie Press, Pittsburgh, Pa., Table 21k] and for water [N. S. Osborne, H. F. Stimson and D. C. Ginnings, *J. Research Natl. Bur. Standards*, **23**, 261 (1939)].

TABLE VI

DERIVED DATA AT 298.16°K., KCAL. MOLE^{-1}

	State	*m*-Fluorobenzotrifluoride HF·15H$_2$O[a]	Perfluoromethylcyclohexane HF·10H$_2$O[a]	Perfluoroethylcyclohexane HF·10H$_2$O[a]	Perfluoro-*n*-heptane HF·10H$_2$O[a]
$\Delta Ec°$	Liquid	−767.61 ± 0.14	−443.01 ± 0.11	−504.05 ± 0.23	−422.38 ± 0.21
$\Delta Hc°$	Liquid	−767.61 ± 0.14	−440.94 ± 0.11	−501.68 ± 0.23	−420.01 ± 0.21
$\Delta Hf°$	Liquid	−193.24	−683.4	−778.9	−797.7
$\Delta Hv°$		9.07 ± 0.05	8.11 ± 0.05	9.20 ± 0.05	8.686
$\Delta Hf°$	Gas	−184.17	−675.3	−769.7	−789.0

[a] Concentration of HF to which $\Delta Ec°$ and $\Delta Hc°$ apply, eq. III–VI.

$4d = 67.7$ kcal. $\quad a + 10b + 3c = 173.7$ kcal.

$10b + 6c = 213.1$ kcal. $\quad a + 12b + 3c = 197.7$ kcal.

The solution of these equations is: $a = 7.2$ kcal., $b = 12.0$ kcal., $c = 15.5$ kcal. and $d = 16.9$ kcal. The increase in E(C–F) − E(C–H) is much greater than any structural variation in the carbon–hydrogen bond energy, E(C–H), and therefore represents a real increase in the carbon–fluorine bond energy, E(C–F), as more fluorine atoms are bonded to the same carbon atom. Resonance with structures of the type

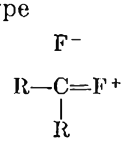

which is associated with the decrease in the C–F bond distance when more than one fluorine atom is bonded to the same carbon atom,[15] is probably also associated with the increase in the C–F bond energy.

The values given for E(C–F) − E(C–H) may be used to estimate the heat of formation of any aliphatic fluorocarbon if the heat of formation of the corresponding hydrocarbon is known.

(15) L. Pauling, "The Nature of the Chemical Bond," Cornell University Press, Ithaca, N. Y., 1945, p. 235.

TETRAMETHYLLEAD: HEAT OF FORMATION BY ROTATING-BOMB CALORIMETRY

BY W. D. GOOD, D. W. SCOTT, J. L. LACINA AND J. P. MCCULLOUGH

Contribution No. 79 from the Thermodynamics Laboratory, Petroleum Experiment Station, Bureau of Mines, U. S. Department of the Interior, Bartlesville, Oklahoma

Received December 8, 1958

Combustion calorimetry of tetramethyllead was done by a rotating-bomb method. The experiments gave for the reaction $(CH_3)_4Pb(liq) + 2HNO_3(in\ 40\ H_2O) + 7.5\ O_2(g) = Pb(NO_3)_2(c) + 7\ H_2O(liq) + 4\ CO_2(g)$ the value $\Delta H°_{298.16} = -886.8 \pm 0.3$ kcal. The heat of vaporization was calculated from the results of vapor pressure measurements. Derived values for the heat of formation from graphite, hydrogen gas and lead metal, $\Delta Hf°_{298.16}$, are 23.5 kcal. mole^{-1} for the liquid and 32.6 kcal. mole^{-1} for the gas.

Studies of the thermodynamic properties of tetramethyllead were made in this Laboratory as an outgrowth of earlier investigations of tetraethyllead.[1] Lippincott and Tobin have determined the heat of formation of tetramethyllead by the standard method of combustion calorimetry,[2] but their result is inconsistent with the more recent value for tetraethyllead. The standard techniques used by Lippincott and Tobin are not satisfactory for studies of organic lead compounds because the products of combustion include a complex mixture of solid inorganic compounds that is difficult to define either chemically or thermodynamically. As shown in the study of tetraethyllead, the rotating-bomb method of combustion calorimetry[1,3,4] provides a means for surmounting this difficulty. In the rotating-bomb method, a solution is used to dissolve the solid products of combustion and produce an easily defined final state for the combustion reaction.

This paper reports experimental values of the heat of combustion and vapor pressure of tetramethyllead and derived values of the heat of formation, heat of vaporization and other thermodynamic properties at 298.16°K.

Experimental

The principal features of the experimental method used for combustion calorimetry were: (a) the combustion reaction took place in a fused-quartz crucible that was relatively inert to the hot lead oxides produced; (b) a solution of nitric and arsenious acids was used in the bomb to convert all lead in the combustion products to Pb^{++} ion; and (c) suitable comparison experiments were used to refer the combustion reaction to solid $Pb(NO_3)_2$ as a product and to minimize errors in reduction of the data to standard states. Vapor pressure measurements were made by a static method described in a previous publication from this Laboratory.[5]

Procedure for Combustion Calorimetry of Tetramethyllead.—The use of unsealed, fused-quartz ampoules to contain samples, as was done with tetraethyllead,[1] was unsatisfactory with tetramethyllead. In exploratory experiments such ampoules were filled with enough tetramethyllead to give both 1 and 2° temperature increments within the calorimeter. The ampoules were placed in thin, fused-quartz crucibles with a kindler of auxiliary oil, as were the ampoules of tetraethyllead. Regardless of the sample size, oxygen pressure or mass of kindling material used outside the ampoule, the sample detonated violently within the bomb to produce audible noises, copious amounts of carbon, and mangled electrodes and internal fittings. Use of sealed polyester bags[6] as sample containers also failed to give complete combustion.

Detonation of tetramethyllead—the most likely cause of incomplete combustion—was eliminated by diluting the sample with auxiliary oil and sealing the solution in a polyester bag. Smooth combustion reactions occurred with solutions of tetramethyllead and auxiliary oil in such proportion that tetramethyllead evolved about half the total energy of the reaction. Use of significantly higher proportions of tetramethyllead gave incomplete combustion.

The auxiliary oil was placed inside a previously weighed polyester bag with a hypodermic syringe. The bag and its contents were reweighed to obtain the weight of auxiliary oil by difference. Tetramethyllead then was placed inside the bag with a hypodermic syringe. Care had to be exercised that neither the auxiliary oil nor the tetramethyllead touched the neck of the bag. Finally, most of the air was removed from the bag by pressure on its walls, and the neck of the bag was clamped and sealed. This procedure differed from that previously described,[6] because no material could be removed from the bag after the auxiliary oil and tetramethylead had been mixed. The sealed bag was weighed to obtain the mass of tetramethyllead by difference. The bag was rolled and placed inside a thin, fused-quartz crucible for the combustion experiment.

Heat of Solution of Auxiliary Oil and Tetramethyllead.—To refer the combustion reaction to pure tetramethyllead instead of a solution in auxiliary oil, it was necessary to know the heat of solution of tetramethyllead in the oil. The availability of the rotating-bomb calorimeter made possible a simple determination of the heat of solution. A small vessel, made vapor tight by means of a Teflon gasket, was constructed of brass as shown in Fig. 1. Auxiliary oil was placed in the inner chamber of the vessel and tetramethyllead in the outer chamber in the same ratios by weight as employed in the combustion experiments. The smooth lip of the inner chamber was covered by a small, smooth-surfaced brass plate. The vapor space above the liquids was small so that the heat effect from change in the amount of vapor when the liquids were mixed was negligible. The mixing vessel was placed inside the combustion bomb, and the bomb was placed inside the calorimeter as for an ordinary combustion experiment, except that the bomb was not inverted. The calorimeter was heated to an initial temperature slightly lower than the temperature of the isothermal jacket (25°). Time–temperature observations were made for an initial period, and rotation of the bomb was begun. When the bomb turned, the contents of the two chambers were mixed. The accompanying heat effect was observed by time–temperature measurements, which were continued until a steady rate of temperature change was obtained again. The heat of solution of the tetramethyllead and auxiliary oil was calculated from the known energy equivalent of the system. The solution of tetramethyllead in auxiliary oil, in the concentration used for the combustion experiments, about 19 wt. % oil, was found to be accompanied by the absorption of 0.16$_5$ cal./g. of tetramethyllead.

(1) D. W. Scott, W. D. Good and Guy Waddington, THIS JOURNAL, **60**, 1090 (1956).

(2) E. R. Lippincott and M. C. Tobin, *J. Am. Chem. Soc.*, **75**, 4141 (1953).

(3) W. N. Hubbard, C. Katz and Guy Waddington, THIS JOURNAL, **58**, 142 (1954).

(4) W. D. Good, D. W. Scott and Guy Waddington, *ibid.*, **60**, 1080 (1956).

(5) G. Waddington, J. W. Knowlton, D. W. Scott, G. D. Oliver, S. S. Todd, W. N. Hubbard, J. C. Smith and H. M. Huffman, *J. Am. Chem. Soc.*, **71**, 797 (1949).

(6) W. D. Good, D. R. Douslin, D. W. Scott, Ann George, J. L. Lacina, J. P. Dawson and Guy Waddington, THIS JOURNAL, **63**, 1133 (1959).

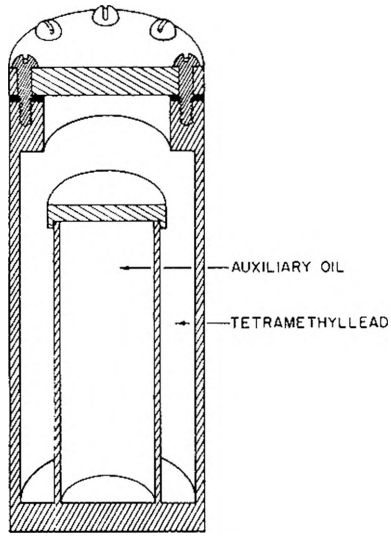

Fig. 1.—Heat of solution vessel.

Comparison Experiments.—The comparison experiments were similar to those used for tetraethyllead. The only significant difference was that the amount of auxiliary oil was chosen to give the same amount of carbon dioxide as in the combustion experiments, rather than the same evolution of energy. For this reason, the temperature increments were about 1.75° for the comparison experiments and 2.00° for the combustion experiments. Because the amounts of carbon dioxide were the same, the important corrections for solution of carbon dioxide in the bomb solutions should cancel almost exactly between combustion and comparison experiments.

Calibration Experiments.—To ascertain that use of different temperature increments did not introduce systematic errors, ordinary calibration experiments with benzoic acid also were done concurrently using samples of such size that both 1.75 and 2.00° temperature increments were obtained. To emphasize that the use of both 1.75 and 2.00° temperature increments did not introduce errors, the values obtained for ε (calor.), the energy equivalent of the calorimetric system, are given below. Values marked with an asterisk were measured with 1.75° increments, and the others were obtained with the ordinary 2.00° increments.

4057.29, 4057.72*, 4057.27, 4057.27*, 4057.67, 4057.83*

Average value and standard deviation of the mean = 4057.51 ± 0.11 cal. deg.$^{-1}$.

Calorimeter and Bomb, Initial Solution and Other Procedures.—Except for slight modifications, the calorimeter (BMR-2), bomb (B57I) and auxiliary equipment used were as described in earlier publications.[1,4,6] The initial bomb solution —50 ml. of a solution containing about 8.6 wt. % nitric acid and 0.15 wt. % arsenious acid—was similar to that used for tetraethyllead. The thermochemical corrections applied for oxidation of arsenious acid were in the range 9–13 cal. per combustion experiment. In all experiments the bomb was charged with oxygen to an initial pressure of 30 atmospheres. Other experimental and computational procedures were the same as those used for tetraethyllead.

Materials

Tetramethyllead.—Two samples of tetramethyllead were used, both contributed by the Ethyl Corporation through the courtesy of G. W. Thomson. The sample used for combustion calorimetry had been purified by three fractional crystallizations by a zone-melting method. Ordinary analytical methods and vapor chromatography failed to detect any impurity, so the purity was estimated conservatively to be 99.95 mole %. A less-pure sample was used for studies of vapor pressure, which were made before the high-purity sample was available. The purity of this sample was determined by calorimetric melting point studies to be, at most, 99.6 mole %.

Benzoic Acid, Auxiliary Oil, Polyester Film, Lead Nitrate and Oxygen.—The benzoic acid (National Bureau of Standards Sample 39g), auxiliary oil, polyester film, lead nitrate and oxygen have been described.[1,6]

Results

Units of Measurements and Auxiliary Quantities.—The results are expressed in terms of the thermochemical calorie equal to 4.1840 abs. j. and the 1951 International Atomic Weights[7a] and fundamental physical constants.[7b] Temperatures measured on the International Temperature Scale[8] by platinum resistance thermometry were converted to absolute temperatures by the relation 0° = 273.16°K. Values of physical properties of tetramethyllead used in the data reduction, all for 25°, are density, 1.979 g. ml.$^{-1}$; specific heat, 0.181 cal. g.$^{-1}$ deg.$^{-1}$; and $(\partial E/\partial P)_T$, −0.0044 cal. atm.$^{-1}$ g.$^{-1}$. The value of Bjellerup, *et al.*,[9] for the heat of oxidation of arsenious oxide to arsenic acid in aqueous solution was accepted.[10]

The Heat of Combustion of Tetramethyllead.—Six satisfactory combustion experiments were ob-

Table I[a]

Typical Pair of Combustion and Comparison Experiments with Tetramethyllead

	Combustion experiment	Comparison experiment
m(tetramethyllead), g.	1.31697	
m(auxiliary oil), g.	0.31502	0.65992
m(polyester), g. (at % rel. hum.)	0.09605(39)	
m[$Pb(NO_3)_2$], g.		1.63304
$n^i(H_2O)$, mole	2.6432	2.6563
$n^i(HNO_3)$, mole	0.07144	0.06158
$n^i(As_2O_3)$, mole	0.000379	0.000379
Δt_c, deg.	2.03364	1.76428
ε(calor.)$(-\Delta t_c)$, cal.	−8251.5	−7158.6
ε(cont.)$(-\Delta t_c)$, cal.	−102.9	−90.7
ΔE_{ign},[b] cal.	0.5	0.6
ΔE, cor. to st. states, cal.	19.5	20.3
ΔE^f_{soln} (SiO_2), cal.	−0.5	
ΔE^f_{soln} ($PbSiO_3$), cal.	−0.2	
ΔE^f_{dec} (As_2O_3), cal.	9.3	−0.2
$-m\Delta Ec^\circ/M$(fuse), cal.	7.1	4.5
$-m\Delta Ec^\circ/M$(oil), cal.	3460.1	7248.4
$-m\Delta Ec^\circ/M$(polyester), cal.	525.0	
$\Delta E_{soln.}$,[c] cal.	0.2	
$m\Delta Ec^\circ/M$(tetramethyllead), cal.	−4333.4	
$\Delta Ec^\circ/M$(tetramethyllead), cal. g.$^{-1}$	−3290.4	
ΔEc°(tetramethyllead), kcal. mole^{-1}	−879.6	
$m\Delta E^\circ/M$[$Pb(NO_3)_2$], cal.		24.3
$\Delta E^\circ/M$[$Pb(NO_3)_2$], cal. g.$^{-1}$		14.9
ΔE°[$Pb(NO_3)_2$], kcal. mole^{-1}		4.9

[a] The symbols of this table are the same as those used in ref. 1. [b] Ignition energy was measured directly by a method described in ref. 6. [c] $\Delta E_{soln.}$ is the thermochemical correction for the solution of tetramethyllead in auxiliary oil.

(7) (a) E. Wichers, *J. Am. Chem. Soc.*, **74**, 2447 (1952); (b) F. D. Rossini, F. T. Gucker, Jr., H. L. Johnston, L. Pauling and G. W. Vinal, *ibid.*, **74**, 2699 (1952).

(8) H. F. Stimson, *J. Research Natl. Bur. Standards*, **42**, 209 (1949).

(9) L. Bjellerup, S. Sunner and I. Wadsö, *Acta Chem. Scand.*, **11**, 1761 (1957).

(10) Use of the same value in reduction of the data for tetraethyllead yields a revised value of $\Delta Hf^\circ_{298.16}$(liq) = +12.7 kcal. mole^{-1}, 0.1 kcal. mole^{-1} lower than the value previously reported.[1]

tained in ten attempts. Results of four experiments were rejected because "soot" was formed or small amounts of inorganic lead compounds failed to dissolve. Results of a typical combustion experiment with tetramethyllead and the corresponding comparison experiment are summarized in Table I.

If the presence of small concentrations of As_2O_3 and As_2O_5 in the bomb solutions is neglected, the values of $\Delta Ec°$ (tetramethyllead) and of $-\Delta E°$ [$Pb(NO_3)_2$] in Table I refer to equations I and II below. Equations III and IV represent two small dilution corrections, one to correct for differences in concentration of the initial bomb solutions and one to refer each experiment to the same initial concentration of nitric acid, HNO_3 (in 40 H_2O).

$$(CH_3)_4Pb(liq) + 14.50HNO_3 \cdot 536.6H_2O(liq) + 7.5O_2(g) + 4.7H_2O(liq) = Pb(NO_3)_2 \cdot 12.50HNO_3 \cdot 548.3H_2O(liq) + 4CO_2(g) \quad (I)$$

$$\Delta E°_{298.16} = -879.6 \text{ kcal.}$$

$$Pb(NO_3)_2 \cdot 12.50HNO_3 \cdot 548.3H_2O(liq) = Pb(NO_3)_2(c) + 12.50HNO_3 \cdot 538.8H_2O(liq) + 9.5H_2O(liq) \quad (II)$$

$$\Delta E°_{298.16} = -4.9 \text{ kcal.}$$

$$12.50HNO_3 \cdot 538.8H_2O(liq) = 12.50HNO_3 \cdot 462.6H_2O(liq) + 76.2H_2O(liq) \quad (III)$$

$$\Delta E°_{298.16} = -0.1 \text{ kcal.}$$

$$2HNO_3 \cdot 80H_2O(liq) = 2HNO_3 \cdot 74H_2O(liq) + 6H_2O(liq) \quad (IV)$$

$$\Delta E°_{298.16} = 0.0 \text{ kcal.}$$

The sum of equations I through IV is

$$(CH_3)_4Pb(liq) + 2HNO_3(in\ 40H_2O) + 7.5O_2(g) = Pb(NO_3)_2(c) + 7H_2O(liq) + 4CO_2(g) \quad (V)$$

$$\Delta E°_{298.16} = -884.6 \text{ kcal.}$$

The results of all six pairs of combustion and comparison experiments are given in Table II. The value of $\Delta H°_{298.16}$ (eq. V) in Table II is the direct result of the calorimetric studies; aside from small thermochemical corrections, this value depends only on calorimetric experiments done in this Laboratory and the certificate value of the heat of combustion of the benzoic acid used for calibration.

Vapor Pressure and Heat of Vaporization.—The results of the vapor pressure measurements are listed in Table III. The first series of pressures was observed with $^1/_5$ of the original material distilled out of the sample container; the second series was observed with an additional $^3/_5$ distilled out so that only $^1/_5$ remained. The somewhat lower values of vapor pressure observed in the second series indicate that the sample contained a small amount of impurity of different volatility.

The following Antoine equation was selected to represent the vapor pressure data. The units are p in mm. and t in °C.

$$\log_{10}p = 6.93767 - 1335.317/(t + 219.084) \quad (VI)$$

The difference between the observed values and those calculated from eq. VI are included in Table III.

The heat of vaporization at saturation pressure, $\Delta Hv_{298.16}$, was calculated to be 9075 cal. mole^{-1} by use of eq. VI, the exact form of the Clapeyron equation, and an estimated value of -2.8 l. for the second virial coefficient, $V - RT/P$. The foregoing value differs from the standard heat of vaporization, $\Delta Hv°_{298.16}$, by an amount less than the experimental uncertainty.

TABLE II

SUMMARY OF CALORIMETRIC EXPERIMENTS WITH TETRAMETHYLLEAD

$\Delta Ec°$(Tetramethyllead) (eq. I), kcal. mole^{-1}	$\Delta E°[Pb(NO_3)_2]$ (eq. II), kcal. mole^{-1}	Dilution correction (eq. III, IV), kcal. mole^{-1}	$\Delta E°_{298.16}$ (eq. V), kcal. mole^{-1}
−879.9	−5.2	−0.1	−885.2
−879.5	−4.9	− .1	−884.5
−879.8	−4.8	− .1	−884.7
−880.3	−5.0	− .1	−885.4
−879.6	−4.9	− .1	−884.6
−879.5	−5.0	− .1	−884.6

$\Delta E°_{298.16}$(eq. V), mean −884.8 kcal. mole^{-1}
$\Delta H°_{298.16}$(eq. V) −886.9 kcal. mole^{-1}
Stand. dev. of the mean ±0.15 kcal. mole^{-1}
Uncertainty interval ±0.3 kcal. mole^{-1}

TABLE III

t, °C.	p(obsd.), mm. 1st	2nd	Mean	p(mean) − p(calcd), mm.
0.00	7.02	6.97	7.00	+0.04
15.00	17.12	17.06	17.09	− .02
20.00	22.55	22.50	22.52	.00
25.00	29.34	29.24	29.29	− .02
30.00	37.78	37.65	37.72	− .02
35.00	48.19	48.04	48.12	+ .01
40.00	60.91	60.65	60.78	+ .01
45.00	76.20	75.93	76.06	− .02
50.00	94.68	94.34	94.51	+ .06
55.00	116.45	116.14	116.30	− .04
60.00	142.46	142.03	142.24	.00

Derived Results.—The values in Circular 500[11] for the standard heat of formation of HNO_3 (in 40 H_2O), $Pb(NO_3)_2$(c), H_2O (liq) and CO_2(g) were used with the values determined for $\Delta H°_{298.16}$ (eq. V) and the heat of vaporization of tetramethyllead to calculate values of the heat of formation of tetramethyllead in the liquid and gaseous states. An unpublished value obtained in this Laboratory for the entropy of liquid tetramethyllead at 298.16° K., $S_{satd.} = 76.48 \pm 0.20$ cal. deg.$^{-1}$ mole^{-1}, was used to calculate the entropy of the ideal gas at 1 atm. pressure, as shown in Table IV. These values of the entropy of tetramethyllead were used with entropy values from Circular 500[11] for C (graphite), H_2(g) and Pb(c) to compute values of the standard entropy of formation, free energy of formation and logarithm of the equilibrium constant of formation. The derived thermodynamic properties are listed in Table V.

Comparison with Previous Work.—The value reported by Lippincott and Tobin[2] for $\Delta Hf°_{298.16}$ (g) of tetramethyllead, 3.2 ± 3 kcal. mole^{-1}, is in very poor agreement with the more accurate value of this research, 32.6 kcal. mole^{-1}. Before the development of rotating-bomb calorimetry, a method similar to that of Lippincott and Tobin was used in this Laboratory in an unpublished study of tetraethyllead. The early result for tetraethyllead

(11) F. D. Rossini, D. D. Wagman, W. H. Evans, S. Levine and I. Jaffe, "Selected Values of Chemical Thermodynamic Properties," N.B.S. Circular 500, 1952.

TABLE IV

THE MOLAL ENTROPY OF TETRAMETHYLLEAD IN CAL. DEG.$^{-1}$ AT 298.16°K.

S_{satd}(liq)	76.48 ± 0.20
Vaporization, $\Delta Hv/T$	30.44
S(ideal) − S(real), estimated	0.03
Compression, $R \ln P$	−6.47
S° (ideal gas at 1 atm.)	100.48 ± 0.20

TABLE V

THERMODYNAMIC PROPERTIES AT 298.16°K.

$4C(c, \text{graphite}) + 6H_2(g) + Pb(c) = (CH_3)_4Pb$ (liq or g)

	Liquid	Gas
$\Delta Hf°_{298.16}$, kcal. mole^{-1}	+23.5	+32.6
$\Delta Sf°_{298.16}$, cal. deg.$^{-1}$ mole^{-1}	−131.7	−107.7
$\Delta Ff°_{298.16}$, kcal. mole^{-1}	+62.8	+64.7
Log $Kf_{298.16}$	−46.0	−47.4

differed from the reliable one found subsequently by the rotating-bomb method by 39 kcal. mole^{-1}, but in the opposite direction from the difference found for tetramethyllead.

The Pb–C Thermochemical Bond Energy and Bond Dissociation Energy.—The Pb–C thermochemical bond energy was calculated from the heat-of-formation values of both tetramethyllead (Table V) and tetraethyllead (ref. 1). The heat of vaporization of tetraethyllead $\Delta Hv°_{98.16}$ was estimated to be 13 kcal. mole^{-1}, the values of heat of atomization of elements were obtained from Circular 500[11] and the other bond energies were assigned the values E(C–H) = 98.85 kcal. and E(C—C) = 83.1 kcal., given by Cass, *et al.*[12] The values obtained for E(Pb–C) are 34.9 kcal. for tetramethyllead and 31.7 kcal. for tetraethyllead. The difference of 3.2 kcal. corresponds to 12.8 kcal. in the heat of atomization. Thus, the assumption of constant bond energies is a poor approximation for these compounds.

The average Pb–C bond dissociation energy, one fourth of $\Delta H_{298.16}$ for the gas-phase reaction $PbR_4 = Pb + 4R$, was calculated by use of Field and Franklin's[13] values of 31 and 24 kcal. mole^{-1} for ΔHf of methyl and ethyl radicals, respectively. The values thus obtained were 34 kcal. for tetramethyllead and 32 kcal. for tetraethyllead, or approximately the same as the thermochemical bond energies calculated above.

(12) R. C. Cass, S. E. Fletcher, C. T. Mortimer, H. D. Springall and T. R. White, *J. Chem. Soc.*, 1406 (1958).

(13) F. H. Field and J. L. Franklin, "Electron Impact Phenomena and the Properties of Gaseous Ions," Academic Press, Inc., New York, N. Y., 1957, p. 129.

THE DISSOCIATION PRESSURE OF $ZnAs_2$

BY V. J. LYONS

International Business Machines Corporation, Research Laboratory, Poughkeepsie, New York

Received December 11, 1958

Two standard methods have been employed to measure the dissociation pressure of $ZnAs_2$ in the range 612 to 770°. A dew-point method was used from 612 to 759° and triple-point measurements covered the range 756 to 770°. The melting point of the compound was found to be 768 ± 1° at an arsenic pressure of 3.3 atmospheres. In the temperature range 612 to 740° the data may be represented by the equation $\log P = -12300/T + 15.0$. The heat of dissociation calculated from the slope of the equation is 18.8 kcal./mole.

Introduction

The compound $ZnAs_2$ is a semi-conductor having an energy gap of approximately 0.92 e.v. at 300°K.[1] During the course of investigation of various properties of the compound a degree of thermal instability, resulting from the dissociation of the compound, was observed. Since thermal dissociation introduces special problems relevant to the growth of single crystals and to the precision of subsequent physical measurements, a study was made of the dissociation reaction for the compound. Thus dissociation pressures were measured. The data presented herein cover the temperature range 600° to the melting point.

Experimental

The dissociation pressure of a solid compound may be defined as the sum of the vapor pressures of the dissociation products in equilibrium with the solid compound at a specified temperature.[2] In the case where only one of the dissociation products is volatile, the pressure may be expressed in terms of the volatile product in equilibrium with the solid compound. Dissociation of $ZnAs_2$ proceeds according to the reaction

$$ZnAs_2 = {}^1/_3Zn_3As_2{}^3 + {}^1/_3As_4$$

Since the vapor pressure of arsenic is considerably higher than the vapor pressures of Zn_3As_2 and $ZnAs_2$, the dissociation pressure is essentially equal to the arsenic pressure.[4]

Two different methods were used to measure the dissociation pressure of $ZnAs_2$. In the temperature range 600 to 759° a "dew-point" method was employed, while in the range 750° to the melting point, $ZnAs_x$ composition melting points were observed under various arsenic pressures thereby providing triple-point measurements. Overlapping of the temperature ranges covered by each method provided a means of checking the reliability of the methods.

In the "dew-point" method, measurement of the arsenic pressure in a closed system can be accomplished by observation of its condensation temperature, *i.e.*, its "dew-point."[5] Dissociation of the compound in order to provide an arsenic atmosphere for the measurement will result in the formation of a layer of Zn_3As_2 on the sample surface. In order to minimize the thickness of the Zn_3As_2 layer, a large sample surface area to reaction tube volume ratio is necessary. Therefore, approximately 10 g. of $ZnAs_2$ was broken into small pieces (1–2 mm. in diameter) prior to the runs. The

(1) W. J. Turner, A. S. Fischler, V. J. Lyons and W. E. Reese, "The Electrical and Optical Properties of $ZnAs_2$," presented at The American Physical Society Meeting, Chicago, Nov. 29, 1958.

(2) See for example, E. P. Egan, J. E. Potts and G. D. Potts, *Ind. Eng. Chem.*, **38**, 454 (1946).

(3) The compound Zn_3As_2 does not dissociate in the temperature range studied.

(4) Arsenic pressures were obtained from two sources: (a) "International Critical Tables," 3b. 207; (b) R. E. Honig, *R. C. A. Rev.*, **18**, No. 2, 195 (1957).

(5) K. Weiser, THIS JOURNAL, **61**, 513 (1957).

$ZnAs_2$ was synthesized at 775° by direct combination of Zn and As in a sealed quartz tube under an arsenic pressure of two atmospheres. A single crystal of the compound was grown by directional freezing in a temperature gradient. The material was stoichiometric $ZnAs_2$ as shown by wet chemical analysis.

The spectrographically pure monocrystalline $ZnAs_2$, contained in a carbon-coated quartz boat, was placed at one end of a quartz tube. The tube was then filled with H_2 to a pressure of 10 mm. prior to sealing off. Thermocouple wells were located at each end of the reaction tube for measuring decomposition and condensation temperatures. The reaction tube was placed in a furnace consisting of two contiguous windings of nichrome ribbon on a quartz tube providing separate heaters for decomposition and condensation. The furnace was enclosed in a second quartz tube such that the entire reaction tube was visible.

After the two heaters were raised to the same temperature, the temperature of the condensation furnace (T_2) was lowered in steps of 5° while the decomposition temperature (T_1) was maintained constant.[6] A 10 minute equilibration time was allowed after each change in T_2. A short blast of air then was directed into the thermocouple well (T_2) thus momentarily lowering the temperature 10–20° in the immediate area of the well. The air blast was used to ensure against errors which might occur due to supersaturation of the arsenic vapor.

The temperature was lowered in this manner until the air blast caused arsenic crystals to appear on the well. T_2 was then varied over a narrow range and the process was repeated until the condensation temperature was established through observation of the condensation and sublimation of the arsenic crystals. The decomposition temperature was then increased to a new value and equilibrated for 20–30 minutes prior to repeating the process. At a decomposition temperature of 612°, the arsenic condensation temperature could be determined with an accuracy of ±10°. At higher decomposition temperatures, however, the condensation temperatures were determined with 4–6° since the arsenic sublimed more rapidly at these temperatures.

In the temperature range 730 to 760° there was a noticeable increase in the quantity of Zn_3As_2 formed as a product of the dissociation. Two problems were thus encountered. The first problem involved the gradual sublimation of Zn_3As_2 away from the sample surface and subsequent condensation of the compound in the area of the temperature gradient between the two furnaces. Therefore, the decomposition pressures could be recorded only in the order of increasing sample temperature since reduction of the sample temperature, after decomposition at an elevated temperature, would result in recombination of As with Zn_3As_2 at two different temperatures: (1) the sample temperature, and (2) a lower temperature in the gradient area. The second problem was encountered when the sample reached the (Zn_3As_2-$ZnAs_2$) eutectic temperature (750°) and a liquidus phase appeared on the sample surface. As the sample temperature was increased the liquidus phase increased in volume and eventually covered the entire surface. Since this condition could not be distinguished visually from a completely molten phase, samples of larger surface area were used for the high temperature dissociation. This resulted in the observed presence of both solid and liquid phases at the decomposition temperature of 759°. Further dissociation at higher temperatures increased the possibility of the entire sample becoming a liquid solution of ($ZnAs_2$-Zn_3As_2) in which case the system becomes bivariant.

In order to increase the accuracy of the measurements made near the melting point of the compound, a different method was employed wherein arsenic vapor was maintained in equilibrium with a $ZnAs_x$ composition at the melting point of the sample. The primary objectives in employing this method were to establish the melting point of the stoichiometric compound and to determine the equilibrium arsenic pressure at the melting point. The method employed an apparatus similar to that used by van den Boomgaard and Schol[7] in their study of the compounds GaAs, InAs and InP. The furnace was the same as that used in the dew-point measurements. A quantity of $ZnAs_2$ was contained in a graphite boat and a large excess of arsenic was kept in a cylindrical reservoir at the opposite end of the reaction tube. The reaction tube was evacuated to 1×10^{-5} mm. prior to sealing.

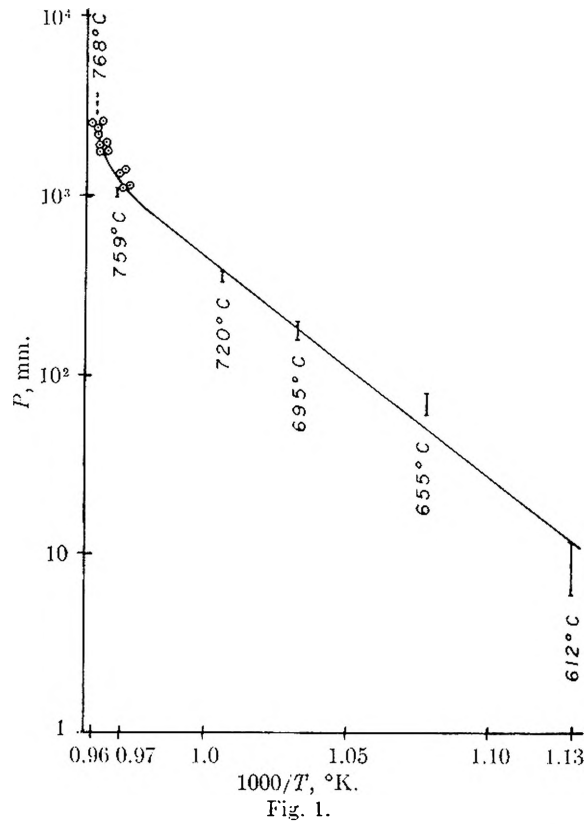

Fig. 1.

After melting the $ZnAs_2$ under an arsenic pressure determined by its temperature, the melt was maintained at a temperature of ~780° for periods of from two to six hours. This permitted the melt composition to adjust to the equilibrium composition represented by the arsenic vapor pressure. The melt was then frozen under the constant arsenic pressure. Accurate freezing points of the melt could not be recorded due to considerable supercooling of the melt. (Supercooling occurred over the entire temperature range covered by the experiment regardless of the melt composition.) The sample then was heated at the constant rate of 1°/min. The latent heat of fusion was thus observed as a plateau in the curve of sample temperature *vs.* heating time. Sample melting could be observed visually. Melting points of various compositions were measured under arsenic pressures of from 1.5 to 3.6 atmospheres. The melting points were recorded first in the order of increasing arsenic pressures and then with decreasing arsenic pressures. This provided a check on the established equilibrium of the system. There was no variation between melting points taken with increasing or decreasing arsenic pressure. A maximum in the melting point curve occurred at an arsenic pressure of 3.3 atmospheres. Since at this point arsenic was in equilibrium with both solid and liquid $ZnAs_2$, the pressure represents the dissociation pressure of $ZnAs_2$ at its melting point. The melting point of the compound was found to be 768 ± 1°. The previously reported melting point was 771°.[8]

Discussion

A plot of the experimental data is shown in Fig. 1. In the temperature range 600 to 740°, the data may be represented as a straight line and fitted to the equation

$$\log P = -\frac{12300}{T} + 15.0 \qquad (1)$$

(6) Temperatures were measured with Pt-Pt, 10% Rh thermocouples which were subsequently calibrated with an N.B.S. standardized Pt-Pt, 10% Rh thermocouple.

(7) Boomgaard and Schol, *Philips Res. Rpts.*, **12**, 127 (1957).

(8) M. Hansen, "Constitution of Binary Alloys," second edition, McGraw-Hill Book Co., Inc., New York, N. Y., 1958, pp. 185–186.

where P is pressure in millimeters of mercury and T is absolute temperature. The equilibrium constant for the dissociation reaction

$$ZnAs_2 \rightleftharpoons \frac{1}{3} Zn_3As_2 + \frac{1}{3} As_4 \qquad (2)$$

may be expressed as the arsenic pressure only since the vapor pressures of Zn_3As_2 and $ZnAs_2$ are negligible in the temperature range studied. The assumption of only As_4 molecules in the vapor state is based on a calculation of the fraction of As_4 molecules dissociated using data tabulated by Stull and Sinke.[9] In the temperature range 730 to 830° the fraction of As_4 molecules dissociated to form As_2 molecules is approximately 1×10^{-3}; hence the contribution due to As_2 molecules may be considered negligible. The equilibrium constant is then

$$K_p' = P^{1/3}_{As4} \qquad (3)$$

in the temperature range described for equation 1.

In the temperature range 750° to the compound melting point, the experimental data show an increase in the slope of the dissociation pressure curve. Since the Zn–As phase diagram indicates a degree of solubility of arsenic in liquid $ZnAs_2$, a positive slope would be expected for arsenic-rich compositions near the $ZnAs_2$ stoichiometry and, therefore, an infinite slope would occur at the $ZnAs_2$ melting point. Hence, an increase in the slope of the curve below the compound melting point, as suggested by the experimental data, is not altogether unexpected in this system. No attempt was made to determine the equilibrium constant near the melting point because of insufficient data on the reactions involved.

The over-all heat for the reaction corresponding to equation 2 as calculated from the slope of log P *vs.* $1/T$ using the straight line approximation[10]

$$\ln P = -\frac{\Delta H}{RT} + C$$

is 18.8 kcal./mole of solid $ZnAs_2$.

(9) D. R. Stull and G. C. Sinke, "Thermodynamic Properties of the Elements," Advances in Chemistry Series, No. 18, 1956.

(10) K. Denbigh, "Principles of Chemical Equilibrium," Cambridge University Press, 1955, Ch. 6.

TABLE I

TABULATION OF EXPERIMENTAL DATA

Dew Point Measurements

$ZnAs_2$, temp., °C.	As condensation temp., °C.	As pressure, mm.
612	420–440	6.03–11.5
655	498–507	62.2–79.0
695	535–541	160.7–199.8
720	569–573	357.1–390.7
759	619–623	1035.2–1122.0

Triple-point Measurements

$ZnAs_2$ m.p., °C.	As temp., °C.	As pressure, mm.
756.9	623.0	1122
754.9	624.0	1143
758.7	632.9	1361
757.4	633.8	1387
764.9	646.3	1762
763.7	647.5	1803
763.4	647.9	1815
764.4	655.0	2075
765.5	655.0	2075
766.9	660.7	2307
766.9	661.0	2317
766.9	663.4	2421
768.5	665.4	2512
767.8	665.6	2512
766.1	666.4	2559
765.7	666.5	2559

Acknowledgments.—The author wishes to express his thanks to Dr. G. A. Silvey and Dr. K. Weiser for their valuable suggestions and discussions.

THE SLOW STEP IN CHEMISORPTION. THE POSSIBLE ROLE OF THE SOLID ADSORBENT. II

BY G. PARRAVANO,[1] H. G. FRIEDRICK AND M. BOUDART

Department of Chemical Engineering, University of Notre Dame, Notre Dame, Indiana

Received December 12, 1958

The rates of adsorption of hydrogen and deuterium on a variety of zinc oxide samples are identical over a wide temperature range. It is concluded that the activated complex does not involve the adsorbed species. The slow step in this chemisorption process is associated with the thermal generation of active centers.

Introduction

In a previous paper under the same title,[2] the phenomenon of slow chemisorption was critically analyzed in the light of data existing at that time. It was recalled that the commonly accepted mechanism of "activated" adsorption was not acceptable in certain cases. This mechanism assumes that only a fraction of the molecules hitting vacant surface sites will be adsorbed, namely, the fraction possessing an excess energy E in translational motion. Such a simple picture of the activation energy E for adsorption leads to serious difficulties.

In particular, it provides no explanation for the fact that rates of slow chemisorption of hydrogen and deuterium should sometimes be identical, a striking experimental fact discovered at Princeton by Pace and Taylor[3] and confirmed by Kohl-

(1) Department of Chemical and Metallurgical Engineering, University of Michigan, Ann Arbor, Michigan.

(2) M. Boudart and H. Taylor, L. Farkas Memorial Volume, Research Council of Israel, Jerusalem, 1952, p. 223.

(3) J. Pace and H. S. Taylor, *J. Chem. Phys.*, **2**, 578 (1934).

schutter.[4] The complete lack of a kinetic isotope effect, over an extended temperature range, indicates that, at least for the oxide adsorbents studied in these investigations, the slow step in the adsorption process pertains to the *solid adsorbent* itself and not to the interaction between a site and the gaseous adsorbate. The slow step was tentatively ascribed to the thermal production of adsorption sites, so that the surface was of the type first described by Vol'kenshtein.[5] Unfortunately, it was not possible to specify the process of site production, since little was known about the solid state behavior of the adsorbents used in the Princeton work (zinc oxide–chromium oxide, chromium oxide gel, nickel on kieselguhr).

It seemed therefore important to repeat the critical experiment of Pace and Taylor, this time on an adsorbent which is better understood. Zinc oxide was selected for two reasons. First, a considerable amount of work has been done on the chemical[6] and physical[7] properties of zinc oxide surfaces. Secondly, some adsorption rate measurements have been published[8] which are at variance with the results of Pace and Taylor, in the case of hydrogen and deuterium on zinc oxide. It was decided to use a sensitive differential technique, able to detect minute differences in adsorption rates of the two isotopic molecules not only on pure zinc oxide, but on zinc oxide modified by uni- and trivalent impurities.

Experimental

Materials.—Zinc oxide was obtained by decomposition of C.P. zinc carbonate (Baker and Company) for 0.5 hour at 800° in a porcelain crucible. Gallia- and lithia-containing samples were prepared by impregnation of the pure oxide with known amounts of standard solutions of the corresponding nitrates. The impregnated materials then were dried at 120° and heated for 2 hours at 800°.

Hydrogen, from an electrolytic cell (25% potassium hydroxide), was purified by passage through a Pd–Al_2O_3 catalyst and magnesium perchlorate. Deuterium was obtained by electrolysis of heavy water and purified in a manner similar to hydrogen. Mass spectrometric analysis of deuterium gas showed that it contained 95.8% D_2.

Apparatus.—Measurements were taken in a differential adsorption apparatus. Two vessels, containing the same weight of oxide, were each connected to one side of a differential manometer, hydrogen or deuterium line, gas burets, and high vacuum line. The adsorption vessels were fitted into two holes of a stainless steel block. The differential manometer was filled with dibutyl phthalate, dyed with crystal violet, and variations in the meniscus height of the liquid were recorded on photographic paper, by means of an optical recording system.[9] The developed photographic paper yielded a black and white graph of meniscus height *vs.* time. In order to make sure that any observed variation of meniscus height was due to a difference in the adsorption rate of the two vessels, filled with hydrogen or deuterium, preliminary blank runs were made by filling both vessels with zinc oxide and hydrogen under conditions in which adsorption took place. No variation in meniscus height was observed. Pressure differences due to changes of the original volume following meniscus variations were found to be negligible.

Method.—Known amounts of hydrogen and deuterium were separately admitted into the two vessels, containing similar preparations of zinc oxide, suitably pretreated and the recording manometer was turned on. Runs were taken over a period of about 10 hours. After each run the amount adsorbed was read off from the hydrogen buret.

Results

Hydrogen and deuterium adsorption was followed at three different temperatures: 75, 200, 300° and constant pressure of 730 mm. Prior to a run, all zinc oxide samples were evacuated at 450° for 4 hours. Runs were performed in the order listed in Table I. No difference in adsorption rates could be detected in any of the test runs.

TABLE I

HYDROGEN AND DEUTERIUM ADSORPTION ON ZINC OXIDE
ORDER OF RUNS PERFORMED

No.	Kind of run	Catalyst	Temp., °C.
1	Blank	Pure ZnO	200
2	Blank	Pure ZnO	200
3	Test	Pure ZnO	200
4	Test	Pure ZnO	200
5	Test	Pure ZnO	200
6	Blank	Pure ZnO	300
7	Test	Pure ZnO	300
8	Test	Pure ZnO	75
9	Blank	ZnO + 0.35 mole % Ga_2O_3	200
10	Blank	ZnO + 0.35 mole % Ga_2O_3	200
11	Test	ZnO + 0.35 mole % Ga_2O_3	200
12	Test	ZnO + 0.35 mole % Ga_2O_3	200
13	Test	ZnO + 0.35 mole % Ga_2O_3	200
14	Blank	ZnO + 0.50 mole % Li_2O	200
15	Blank	ZnO + 0.50 mole % Li_2O	200
16	Test	ZnO + 0.50 mole % Li_2O	200
17	Test	ZnO + 0.50 mole % Li_2O	200
18	Test	ZnO + 0.50 mole % Li_2O	200

Typical data on the amount of gas adsorbed are recorded in Table II.

TABLE II

ADSORPTION OF HYDROGEN AND DEUTERIUM ON ZINC OXIDE
Time of adsorption, 10 hours

Catalyst	Temp., °C.	H_2 or D_2 adsorbed (mole/g. catalyst) × 10^6
ZnO	75	1.015
ZnO	200	1.225
ZnO	300	0.567
ZnO + 0.35 mole % Ga_2O_3	200	.242
ZnO + 0.50 mole % Li_2O	200	.117

The adsorption results clearly follow the pattern of previous investigations.[10]

Discussion

As is well known from the kinetic theory of gases, the number of molecules striking a surface per cm.^{2} per second is equal to $(c/4)n$ where c is the mean molecular velocity and n in the number of molecules per cm.^{3}. If there is an energy barrier E for adsorption so that only the fraction of molecules with translational energy $> E$ can be adsorbed, the rate of adsorption r given by

$$r = \frac{c}{4}\exp(-E/RT) = n$$

Now, c is inversely proportional to molecular

(4) H. W. Kohlschutter, *Z. physik. Chem.*, **A170**, 300 (1934).

(5) F. F. Vol'kenshtein, *Zhur. Fiz. Khim.*, **23**, 917 (1949).

(6) G. Parravano and M. Boudart, "Advances in Catalysis," Vol. VII, Academic Press, New York, N. Y., 1956, p. 50.

(7) S. Roy Morrison, ref. 6, p. 259.

(8) G. Natta and N. Agliardi, *Atti Acad. Naz. Lincei*, **344**, 500 (1947).

(9) C. R. Thomas and H. H. Lichtin, *Rev. Sci. Instr.*, **24**, 661 (1953).

(10) A. Cimino, E. Cipollini and E. Molinari, *Naturwissen.*, **43**, 58 (1956).

mass, so that $c_{H_2} = \sqrt{2}c_{D_2}$. Moreover, since hydrogen and deuterium are involved in the activated state E_{H_2} must also be different from E_{D_2}. In order to decide whether E_{H_2} is smaller or larger than E_{D_2}, recourse must be made to absolute rate theory of isotope kinetic effects.[11] If hydrogen nuclei are more tightly bound in the reactants than in the activated complex $E_{H_2} < E_{D_2}$. If, on the contrary, hydrogen nuclei are more tightly bound in the activated state than in the reactants, $E_{H_2} > E_{D_2}$.

In the classical "diving" mechanism of activated adsorption with dissociation, hydrogen nuclei are more tightly bound in the reactants[12] so that $E_{H_2} < E_{D_2}$. Then, at a given pressure, the rate of adsorption of hydrogen should be *at least* $\sqrt{2} = 1.41$ times faster than that of deuterium. The negative experiment reported here consequently rules out the classical "diving" mechanism.

Another possible mechanism which is frequently advanced to explain slow chemisorption, assumes that the molecule is adsorbed rapidly with dissociation on a site of type A and that the fragments must then slowly diffuse away to some other sites of type B. Here the rate-determining step is a surface "hopping" diffusion. It has been proposed by Wicke[13] for the hydrogen–zinc oxide system. A variation of this mechanism proposes that the slow step is not surface diffusion but diffusion into the interior of the adsorbent. This interpretation of the slow rate of hydrogen uptake by zinc oxide has also been proposed.[14]

In the case of diffusion mechanisms (surface hopping or bulk diffusion) it is possible that the activation energy for deuterium be smaller than for hydrogen. Indeed the reactants here may be hydrogen or deuterium atoms, and not molecules as in the diving mechanism. Therefore, in the activated state hydrogen or deuterium will be more tightly bound than in the reactants so that $E_D < E_H$. The difference between E_D and E_H may be large enough to compensate for the isotope effect of the translational (classical) mode of motion of the diffusing atoms. Since $m_D > m_H$, the effect of the translational modes works in the opposite direction than the effect of the vibrational modes ($E_D < E_H$). It is entirely possible that at a given temperature, both effects would compensate each other exactly. At that temperature, the rates would be identical for hydrogen and deuterium. Yet above and below that temperature, they would be different. Such a case has been reported by Beebe[15] in a study of hydrogen uptake by copper powders.

(11) J. Biegeleisen, *J. Chem. Phys.*, **17**, 675 (1949).
(12) A. Sherman and H. Eyring, *J. Am. Chem. Soc.*, **54**, 2661 (1932).
(13) E. Wicke, *Z. Elektrochem.*, **53**, 279 (1949).
(14) O. Beeck, A. W. Ritchie and A. Wheeler, *J. Colloid Sci.*, **3**, 505 (1948); O. Beeck, J. W. Givens and A. W. Ritchie, *ibid.*, **5**, 141 (1950).
(15) T. Soller, S. Goldwasser and R. A. Beebe, *J. Am. Chem. Soc.*, **58**, 1703 (1936).

The diffusion mechanisms are ruled out in the case of the hydrogen–zinc oxide system. Indeed the rates for hydrogen and deuterium remain rigorously identical over a wide temperature interval from 75 to 300°. Any accidental compensation is excluded in this case.

It must be concluded that neither the "diving" mechanism nor any of the diffusion mechanisms is able to explain the negative experiment with zinc oxide.

The only alternative left open is a slow step which does not involve hydrogen, as a molecule or as adsorbed fragments. In other words, the slow step involves the generation of an active site. Adsorption can proceed only on activated sites.

Morrison's picture of zinc oxide surfaces[7] explains the slow formation of active sites in the following way. Zinc oxide is a semi-conductor because of interstitial zinc atoms in excess of stoichiometry. Interstitial zinc releases electrons readily to the conduction band of zinc oxide. When oxygen is adsorbed at the surface, it traps the conduction electrons. As a result of the presence of these charged oxygen surface traps, a space charge and an electric field barrier are set up in the vicinity of the surface.

An oxygen atom at the surface can trap two electron (O^{--}) or only one electron ($\cdot O^{-}$). It is postulated that only $\cdot O^{-}$ radical-ions provide adsorption sites for hydrogen. These are limited in number after a suitable "activation" of zinc oxide (surface evacuation or reduction). As hydrogen is adsorbed on the active sites, more sites will be created thermally by the process

$$O^{--} \longrightarrow \cdot O^{-} + \text{electron}$$

The electron must however surmount the surface barrier to get back to the bulk of the crystal and this is an activated process.

The Morrison picture is compatible with the general behavior of zinc oxide as an adsorbent for hydrogen. It is also compatible with the results of this work since it does not postulate hydrogen or deuterium in any form in the activated complex. While our isotope experiments may be considered as giving additional support to the picture of Morrison, they do not prove it unequivocally. They do however demonstrate conclusively that the surface of zinc oxide is of the "dynamic" type discussed earlier (1) and that the activated step in the adsorption of hydrogen on zinc oxide is associated with the thermal generation of new active centers. The importance of this concept of a dynamic surface in chemisorption and catalysis need not be stressed again.

To conclude, what was called prudently in a previous paper "the possible role of the solid adsorbent" may now be considered as an established experimental fact.

CATHODE CURRENT DISTRIBUTION IN SOLUTIONS OF SILVER SALTS. I. THE EQUIVALENT CONDUCTANCE OF SOLUTIONS OF SILVER NITRATE AND OF POTASSIUM ARGENTOCYANIDE AS A FUNCTION OF VOLUME CONCENTRATION AND TEMPERATURE

BY CHARLES H. ORR[1] AND HENRY E. WIRTH

Contribution from the Department of Chemistry, Syracuse University, Syracuse, N. Y.

Received December 15, 1958

The equivalent conductance of solutions of silver nitrate and of potassium argentocyanide were determined at 25, 35 and 45° in the concentration range from 0.01 to 0.5 *N*. For the solutions of silver nitrate an empirical equation of the form $\log \Lambda = \log \Lambda_0 + a_1c^{1/2} + a_2c + a_3c^{3/2} + a_4c^2$ was used to represent the data and for the solutions of potassium argentocyanide an equation of the form $\Lambda = \Lambda_0 + b_1c^{1/2} + b_2c + b_3c^{3/2} + b_4c^2$ was used. The densities of the solutions of potassium argentocyanide were determined as a function of concentration and these data were represented by equations of the form of $d^{t}_{4} = d_0 + e_1c + e_2c^{3/2}$. The values of the constants in these equations at 25, 35 and 45°, respectively, are: $\log \Lambda_0$, 2.12503, 2.20496, 2.27852; a_1, −0.28746, −0.29307, −0.30733; a_2, −0.04335, −0.03869, −0.05265; a_3, 0.35309, 0.36286, 0.45853; a_4, −0.2980, −0.3161, −0.4034; Λ_0, 123.7, 146.4, 175.9; b_1, −106.8, −92.8, −135.5; b_2, 217.8, 101.1, 194.5; b_3, −277, −66, −173; b_4, 132, 11, 55; d_0, 0.9971, 0.9941, 0.9902; e_1, 0.1348, 0.1330, 0.1312; e_2, −0.0153, −0.0150, −0.0147.

Introduction

As part of a problem on current distribution in plating baths it was necessary to know the equivalent conductance of silver nitrate and of potassium argentocyanide as a function of volume concentration and temperature. Data for silver nitrate solutions at 25° are readily available, but no data for 35 and 45° over the concentration range of interest could be found. The data at 25° were determined as a check on the equipment and procedure, after which the equivalent conductances at 35 and 45° were determined.

There are very few data available in the literature on the equivalent conductance of potassium argentocyanide. Walden[2] presented data for the range 0.00098 to 0.031 *N* at 25° with no indication of the method of measurement or of preparation of the salt. Britton and Dodd[3] presented data for the range 0.0025 to 0.01 *N* at 25°. Although the agreement with the data of Walden is fair, their values were derived from data on the conductance of mixtures of salts in solution.

In view of the lack of suitable data, a determination of the equivalent conductance of the solutions of potassium argentocyanide over a sufficiently wide concentration range to embrace most electroplating solutions and having moderate precision was undertaken. It was desired to make up the solutions by weight and to calculate the volume concentration and since very few data concerning the density as a function of volume concentration were available, densities also were determined.

Experimental

A. Apparatus.—The conductance bridge was constructed from the plans of Edelson and Fuoss[4] and the balance point was determined with earphones and with a Heath Kit Push-Pull, Extended Range Oscilloscope. The bridge resistance decade box, General Radio Type 1432M, was calibrated *in situ* against National Bureau of Standards certified resistors by a substitution method at a frequency of approximately 500 c.p.s. The two conductance cells of the design of Jones and Bollinger[5] had constants of 1.6 and 22.9. The bath temperature was maintained constant to within ±0.005°.

The density of the potassium argentocyanide solutions was determined by measuring their expansion in a dilatometer similar to a weight dilatometer,[6] except that closure was made with a three-way stopcock. The precision type cathetometer used for measuring the displacement of the liquid meniscus could be read to ±0.005 cm.

B. Materials.—The conductance water was prepared by double distillation, first from alkaline permanganate solutions and then from dilute phosphoric acid. Both distillations were carried out in a nitrogen[7] atmosphere. The terminal condenser and the receiving flasks were made of Vycor. The average specific conductance of the water used in the determinations was: 25°, 0.97; 35°, 1.36; and 45°, 1.89×10^{-6} mhos. cm.$^{-1}$.

J. T. Baker Analyzed potassium chloride was recrystallized once from a saturated boiling solution in water, then dried in porcelain evaporating dishes in a muffle furnace at about 500°.

Baker and Adamson reagent grade silver nitrate was used without further purification.

The salt, potassium argentocyanide, was prepared according to the method of Frary and Porter.[8] Since it was discovered afterward that the salt contained excess silver cyanide, corrections were applied and check determinations were made with a sample of potassium argentocyanide from Fisher Scientific Company which analyzed 99.59% pure.

C. Procedure.—The solutions were made up on a weight basis. Using the density of the solutions at 25, 35 and 45° the volume concentrations were calculated from the weights.

The density of the solutions of potassium chloride was calculated from the data of Geffcken.[9] The equations for the density of the solutions of potassium chloride are

$$d^{25}_{4} = 0.99707 + 0.048270c - 0.002403c^{3/2}$$
$$d^{35}_{4} = 0.99406 + 0.047494c - 0.002187c^{3/2}$$
$$d^{45}_{4} = 0.99025 + 0.047321c - 0.002129c^{3/2}$$

The equations for the density of the solutions of silver nitrate as a function of the volume concentration at the three temperatures were derived from the equation of Jones and Colvin[10] and the data of Bousfield and Lowry.[11] The derived equations at 35° and 45° are

(1) The Procter & Gamble Company, Miami Valley Laboratories, Cincinnati 31, Ohio.

(2) P. Walden, *Z. anorg. Chem.*, **23**, 373 (1900).

(3) H. T. S. Britton and E. N. Dodd, *J. Chem. Soc.*, 1932 (1940).

(4) D. Edelson and R. M. Fuoss, *J. Chem. Education*, **27**, 610 (1950).

(5) G. Jones and G. M. Bollinger, *J. Am. Chem. Soc.*, **53**, 411 (1931).

(6) N. Bauer, "Determination of Density. Physical Methods of Organic Chemistry," Vol. I, Part 1, ed. A. Weissberger, 2nd ed., Interscience Publishers Inc., New York, N. Y., 1949, Fig. 4, p. 277.

(7) L. B. Rogers, D. P. Krause, J. C. Griess, Jr., and D. B. Ehrlinger, *J. Electrochem. Soc.*, **95**, 34 (1949).

(8) F. C. Frary and R. E. Porter, *Trans. Am. Electrochem. Soc.*, **28**, 307 (1915).

(9) W. Geffcken, *Z. physik. Chem.*, **A155**, 1 (1931).

(10) G. Jones and J. H. Colvin, *J. Am. Chem. Soc.*, **62**, 338 (1940).

(11) W. R. Bousfield and T. M. Lowry, *Trans. Faraday Soc.*, **6**, 85 (1910).

$$d^{35}_4 = 0.99406 + 0.14154c - 0.00298c^{3/2}$$

$$d^{45}_4 = 0.99025 + 0.14131c - 0.00322c^{3/2}$$

Due to the presence of excess silver cyanide the solutions of potassium argentocyanide were analyzed for silver content and the concentration of the double salt calculated. Several solutions were analyzed, at first volumetrically by the method of Blum and Hogaboom,[12] and later by deposition of silver on a platinum gauze cathode. The concentrations of all solutions were corrected by the average value of the per cent. of the salt weighed out that was potassium argentocyanide since the contaminant, silver cyanide, was essentially insoluble.

The constant of cell I was determined by measuring the resistance of solutions of potassium chloride in that cell at 25, 35 and 45° and calculating the cell constant from these data and the equations of Shedlovsky, Brown and MacInnes,[13] and Benson and Gordon.[14] The constant of cell II was determined by comparison of the resistance of a solution of silver nitrate run simultaneously in both cells at the three temperatures. The conductivities of the silver nitrate solutions were determined at four frequencies and at temperatures of 25, 35 and 45°.

The conductance of the potassium argentocyanide solutions increased with time, so measurements at each temperature were extrapolated back to the time of filling of the cell. Electrolytic polarization was corrected for by plotting the zero time resistance *versus* the reciprocal of the square root of the frequency and extrapolating to infinite frequency.

Results

The average cell constants and their standard deviations are listed in Table I.

TABLE I

Temp., °C.	Cell constant (cm.$^{-1}$) Cell I	Cell II
25	1.5808 ± 0.0005	22.92 ± 0.02
35	1.5801 ± .0004	22.91 ± .02
45	1.5811 ± .0006	22.93 ± .02

The average values of the equivalent conductances of the solutions of silver nitrate at the three temperatures are listed in Table II.

The smoothed density, volume concentration and average equivalent conductance of the solution of potassium argentocyanide at the temperatures indicated are presented in Table III. Those values tabulated without density data are duplicate determinations. At the highest concentration the densities were obtained by extrapolation of the density equations.

TABLE III

Temp., °C.	Density, g./ml.	Volume concn., N	Λ
25	0.998	0.004944	117.0
35	.995	.004929	140.6
45	.991	.004910	168.2
25	.998	.01025	115.0
35	.995	.01022	138.5
45	.992	.01018	163.0
25	1.002	.03966	109.2
35	0.999	.03954	129.4
45	.995	.03938	152.6
25		.03946	109.3
35		.03934	131.5
45		.03918	154.9
25	1.009	.0899	104.7
35	1.006	.0896	126.0
45	1.002	.0892	148.5
25	1.017	.1581	101.5
35	1.014	.1576	121.8
45	1.010	.1569	143.5
25		.2443	98.3
35		.2435	117.7
45		.2424	138.4
25	1.028	.2458	98.6
35	1.025	.2449	118.3
45	1.020	.2439	139.2
25		.3520	95.3
35		.3507	114.2
45		.3490	134.3
25	1.042	.3531	95.2
35	1.038	.3518	114.5
45	1.033	.3502	134.1
25		.4805	92.5
35		.4787	110.9
45		.4765	130.3

Discussion

An empirical equation was found for the representation of the data on silver nitrate which represented that data with a minimum of deviation. Application of the method of least squares yielded these three equations for the equivalent conductance of the solutions of silver nitrate as a function of the volume concentration

$$\log \Lambda_{25} = 2.12503 - 0.28746c^{1/2} - 0.04335c + 0.35309c^{3/2} - 0.2980c^2$$

$$\log \Lambda_{35} = 2.20496 - 0.29307c^{1/2} - 0.03869c + 0.36286c^{3/2} - 0.3161c^2$$

$$\log \Lambda_{45} = 2.27852 - 0.30733c^{1/2} - 0.05265c + 0.45853c^{3/2} - 0.4034c^2$$

TABLE II

25° c	25° Λ	35° c	35° Λ	45° c	45° Λ
0	133.4[15]	0	160.3[16]	0	189.9[16]
.010068	124.8	.010037	149.8	.009999	176.9
.040073	117.0	.039971	140.3	.039818	165.1
.08994	110.2	.08966	132.2	.08932	155.3
.16032	104.3	.15982	125.0	.15920	146.9
.25261	98.9	.25181	118.5	.25082	139.1
.35992	94.3	.35875	112.9	.35733	132.4
.49881	89.3	.49713	106.7	.49513	125.2

(12) W. Blum and G. B. Hogaboom, "Principles of Electroplating and Electroforming," 3rd ed., McGraw-Hill Book Co., Inc., New York, N. Y., 1949, pp. 195–6.

(13) T. A. Shedlovsky, A. S. Brown and D. A. MacInnes, *Trans. Electrochem. Soc.*, **66**, 165 (1934).

(14) G. C. Benson and A. R. Gordon, *J. Chem. Phys.*, **13**, 473 (1945).

(15) T. A. Shedlovsky, *J. Am. Chem. Soc.*, **54**, 1411 (1932).

(16) Obtained by extrapolation in large scale plots of the equivalent conductance *versus* the square root of the volume concentration.

The equations for the density of the solutions of potassium argentocyanide as a function of the volume concentration are

$$d^{25}_4 = 0.9971 + 0.1348c - 0.0153c^{3/2}$$
$$d^{35}_4 = 0.9941 + 0.1330c - 0.0150c^{3/2}$$
$$d^{45}_4 = 0.9902 + 0.1312c - 0.0147c^{3/2}$$

Application of the method of averages to the conductance data yielded these three equations for the equivalent conductance of solutions of potassium argentocyanide as a function of the volume concentration

$$\Lambda_{25} = 123.7 - 106.8c^{1/2} + 217.8c - 277c^{3/2} + 132c^2$$
$$\Lambda_{35} = 146.4 - 92.8c^{1/2} + 101.1c - 66c^{3/2} + 11c^2$$
$$\Lambda_{45} = 175.9 - 135.5c^{1/2} + 194.5c - 173c^{3/2} + 55c^2$$

One of the limiting factors in these determinations is the precision with which the cell constant was determined. The maximum deviation from the average was one part in three thousand for cell I and one part in one thousand for cell II. In the case of the solutions of potassium argentocyanide the limiting factor is the determination of the concentration. The fact that there must be present a very small amount of potassium cyanide in excess of that required to make the potassium argentocyanide from silver cyanide and potassium cyanide complicates the matter a little when temperature variations are involved since there is no information available as to the temperature dependence of the solubility product of silver cyanide and the instability constant of the argentocyanide ions.

To check the procedure used to correct the volume concentrations, a sample of potassium argentocyanide was purchased. This sample, from Fisher Scientific Company, catalog number S-186, lot number 522873, was analyzed electrolytically for silver content and volumetrically for free cyanide. It was found to contain 99.59% $KAg(CN)_2$ and 0.231% KCN. Solutions having concentrations of about 0.04, 0.25 and 0.36 *N* $KAg(CN)_2$ were made up with the Fisher salt and the weights used in making the solutions were adjusted by the factor 0.9959 in calculating the volume concentration.

To one of the solutions, after its conductance had been determined, was added 0.231% KCN and the resistance of the altered solution was determined at all three temperatures. The difference between the specific conductances of the altered and the unaltered solutions was taken as the increase in specific conductance due to the presence of an excess of 0.231% potassium cyanide. The increase in specific conductance was found to be 59.8% of that calculated for a solution of pure potassium cyanide as reported by Bodensiek.[17] The specific conductances of the potassium argentocyanide solutions then were corrected for the amount of potassium cyanide present, assuming that the specific conductance of the KCN was 59.8% of that of the pure salt.

A large scale plot of the equivalent conductance *versus* the square root of the volume concentration was made from the previous data and the best smooth curve drawn through those points. The test values obtained by the method above were plotted on the same graph. The deviations from the curve were of the order of ± 0.0 to 0.3 unit. In determining the equations for the variation of the equivalent conductance of the solutions as a function of the volume concentration, these points were included with the other data.

In view of the difficulties encountered in this work on solutions of potassium argentocyanide it is estimated that the values of the density and of the equivalent conductance are reliable to about 3 to 5 parts per 1000.

The values of the equivalent conductance at infinite dilution at 35 and 45° for the solutions of silver nitrate and at all three temperatures for the potassium argentocyanide were obtained by extrapolation of large scale plots of the equivalent conductance *versus* the square root of the volume concentration and since the concentrations were still relatively large, the extrapolated values are not considered reliable. They are, however, reasonable in terms of the expected behavior of solutions of electrolytes.

The equivalent conductance at 25° of solutions of silver nitrate calculated from the appropriate equation above agree with values[15] in the literature to within 4 parts in 10,000.

The equations representing the data are good representations of the data for the range of concentration studied (0.01 to 0.5 *N*) but should not be expected to give reliable values outside this range.

Acknowledgment.—The authors wish to express their appreciation for a du Pont fellowship during the academic year 1951–1952.

(17) A. Bodensiek, Dissertation. Hannover T. H., 1925, p. 10a ("Gmelin," Vol. 8, System 22K, part 27, page 885).

CATHODE CURRENT DISTRIBUTION IN SOLUTIONS OF SILVER SALTS. II. CATHODE CURRENT DISTRIBUTION OVER A PLANE CATHODE, PARALLEL TO AND SOME DISTANCE FROM A PLANE ANODE

BY CHARLES H. ORR[1] AND HENRY E. WIRTH

Contribution from the Department of Chemistry, Syracuse University, Syracuse, N. Y.

Received December 15, 1958

Wagner has developed a theory based on fundamental ideas in electrostatics and electrochemistry which permits predictions of current distribution at cathodes. For simple configurations such as two plane parallel electrodes, his method presents a relatively easy way of predicting changes in current distribution as a function of changes in the conductance of the solution and the electrolytic polarization at the metal cathode. Using this theory, the current distribution on a plane silver cathode parallel to a plane anode was predicted for solutions of silver nitrate and of potassium argentocyanide and then was determined experimentally. The results indicate that qualitatively the theoretical method is correct. Both indicate more uniform current distribution on increasing conductance, where polarization is not decreased markedly, by increasing either temperature or concentration or both. Both also indicate that the absence of significant polarization in the case of silver nitrate leads to very non-uniform current distribution. The electrolytic polarization of a silver cathode in solutions of potassium argentocyanide at about 0.1 and 0.5 *N* at 25 and 45°, and of a solution of silver nitrate at about 0.15 *N* at 25° has been determined with a precision of ±2%. A new application of an older method for making the measurements has been described.

Introduction

The problem of the distribution of current in solutions of electrolytes has been of interest since at least 1825.[2] In a number of cases attempts have been made to calculate the current distribution. Generally the procedure has been to make assumptions about the variables which have the most pronounced effect on current distribution, as evidenced by the distribution and quality of a metal plate. A scheme is then devised to represent the behavior of a given plating bath as a function of these variables. Predictions for given conditions, arrangement and shape of the electrodes are then made from the scheme, or else measurements are made and conclusions drawn about the effect of the variables for the prescribed configurations. Sometimes, general predictions are made concerning the effects of changes in a given variable on current or metal distribution. However, these methods are very restrictive; they lack the general aspects of a formulation of distribution based upon the fundamentals of electrostatics and electrochemistry and the basic properties of electrolytic solutions.

Wagner[3] has developed a theory based on fundamental ideas in electrostatics and electrochemistry which permits predictions of current distribution at cathodes. For simple configurations such as two plane parallel electrodes, this method presents a relatively easy way of predicting changes in current distribution as a function of changes in the conductance of the solution and the electrolytic polarization at the metal cathode.

The purpose of this research was to apply the theory of Wagner to a simple case. The current distribution on a plane silver cathode parallel to a plane anode was predicted for solutions of silver nitrate and potassium argentocyanide.

Theoretical

A. Cathode Polarization.—One of the important parameters in determining current distribution, by Wagner's method[3] and those of others, is the electrolytic polarization of a metal cathode in a given solution as a function of current density. The polarization includes all effects opposing the flow of current through a solution and into an electrode except the *IR*-drop in the solution. The resistance of the solution is assumed to remain constant.

A variety of methods[4] have been used in the past to measure the polarization of a silver cathode in solutions of potassium or sodium argentocyanide. None were applied under the conditions used in this investigation and therefore the data available in the literature did not permit the necessary calculations of the current distribution to be made.

Assuming that the resistance in a solution between two points varies directly as the distance, then in Fig. 1 the ratio, r, of the distances between the cathode and nearest probe, and between the two probes should be the ratio of the resistances. If the polarization at the probe electrodes is negligible, then the potential E_1 measured between the two probes when current is flowing is equal to the *IR*-drop in the solution between the probes. If this potential is multiplied by the ratio r and the product subtracted from the potential E_2, between the near probe and the cathode, the resulting potential E_p should be the polarization of the electrode.

The polarization as measured in this way is fully consistent with the assumptions made above concerning the effects lumped under the heading of polarization and with the conditions as they would exist in a plating cell.

B. Current Distribution.—Wagner[3] worked out the current distribution over parallel electrodes at a distance great in comparison to their breadth for a configuration such as in Fig. 2. In doing so he assumed a plot of the total cathode potential, $E_c + E_p$, *versus* the current density I of the form in Fig. 3 and finally assumed that there was a linear relationship between E_p and I over the range of current densities involved.

(1) The Procter & Gamble Company, Miami Valley Laboratories, Cincinnati 31, Ohio.

(2) A. de la Rive, *Ann. chim. phys.*, **28**, 110 (1825).

(3) C. Wagner, *J. Electrochem. Soc.*, **98**, 116 (1951).

(4) S. Glasstone, *J. Chem. Soc.*, 690 (1929); F. Foerster, *Z. Elektrochem.*, **13**, 561 (1907); B. Egeberg and N. Promisel, *Trans. Electrochem. Soc.*, **59**, 293 (1931); H. E. Haring, *Trans. Am. Electrochem. Soc.*, **49**, 417 (1926); E. B. Sanigar, *Rec. trav. chim.*, **44**, 549 (1925).

Defining $h = |dE_p/dI|$, the parameter $k = hL$ is introduced, where L is the specific conductance. The dimensionless variables $u = x/A$ and $v = y/A$ were introduced for the sake of simplifying later computations. Solution of La Place's equation for two dimensions and application of the appropriate boundary conditions leads to an equation of the form

$$G_1(u) = 1 - \left(\frac{A}{\pi k}\right) \int_{-1}^{+1} G_1(u) \, [-\ln |u - w|] \, dw \quad (1)$$

where $G_1(u)$ is proportional to the local current density along the face of the cathode. Now

$$\frac{I}{I_{ave}} = \frac{G_1(u)}{\int_0^1 G_1(u) \, du}$$

and a plot of I/I_{ave} *versus* x/A will give the current distribution over the surface of the electrode. Values of $G_1(u)$ from equation 1 were obtained by the method decribed by Wagner.[5]

The technique used in measuring the current distribution over a subdivided cathode was that due to Mantzell.[6] Referring to Fig. 4, if measurements are begun with all of the resistances in series with the individual cathodelets at the same value the *IR*-drops across these resistances will not be the same since the amount of current going to the cathodelets near the outer edges is known to be greater than that going to those in the center. The current distribution observed in this case will not be the same as if the cathode were one continuous piece of metal since the presence of the resistance in series with the cathodelets has a tendency to make the current distribution more uniform. If the values of these resistances are changed until the *IR*-drops are all equal then the value of the current flowing through each cathodelet can be calculated. This process is roughly equivalent to joining the subdivided electrodes. Once the data on the variation of current with different cathodelets is determined it is then possible to compare the experimental results with those predicted by theory.

Experimental

Cathode Polarization. A. Apparatus.—The cell used in making the measurements is indicated in Fig. 1. The cathode was cut from a sheet of silver and its area was approximately 3.63 cm.^{2}. It was sealed into the cell with medium grade DeKhotinsky cement. The probe electrodes were silver wires which were plated in a potassium cyanide–potassium argentocyanide solution. The anode was a strip of platinized platinum foil.

A type K potentiometer was used to measure the potentials in the polarization experiments. A Weston Standard Cell and a Leeds and Northrup type HS moving coil reflecting galvanometer were used with the type K potentiometer. A type S potentiometer made by Fisher Scientific Company was used to measure the total current. An Eppley Students Cell and a Leeds and Northrup type R moving coil reflecting galvanometer were used with the type S potentiometer.

B. Materials.—The solutions of potassium argentocyanide were prepared from the salt sold by Fisher Scientific Company, which was analyzed electrolytically for silver content and volumetrically for free cyanide. The conductance water used was prepared as previously described.[7] The water pumped nitrogen used was taken direct from the cylinder without further treatment. The silver nitrate was Baker and Adamson, reagent grade, used without further purification.

C. Procedure.—The solutions were made up by weighing out a known amount of the salt and diluting to a volume of one liter in a volumetric flask. The concentration at 45° was calculated using the density data previously determined.[7]

To make a determination, the cell was rinsed several times with distilled water, then once very quickly with acetone. The cell then was permitted to stand about 30 minutes with a stream of nitrogen passing through it. After this period of time the cell was filled with a solution which had been saturated with nitrogen and the cell was sealed and permitted to stand overnight. The following morning the cell was placed in the constant temperature bath and the anode inserted in the cell.

After standing in the bath for about three hours, the determination was begun. The electrodes were connected to the terminals of the measuring circuit and the smallest current applied. The potentiometer was standardized against its standard cell, then readings of E_1 and E_2 were made.

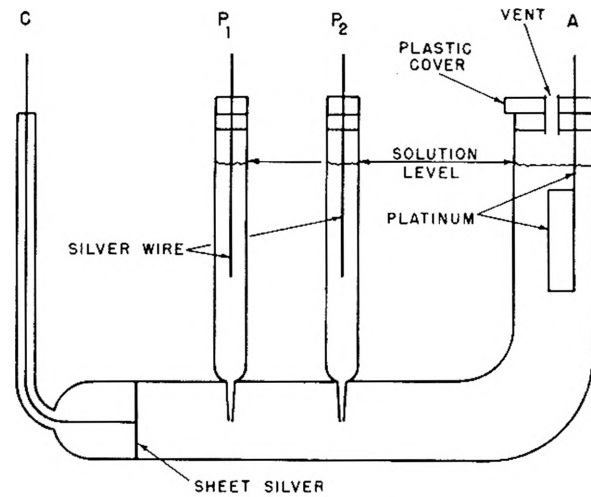

POLARIZATION CELL

Fig. 1.—Cell used for measuring electrolytic polarization.

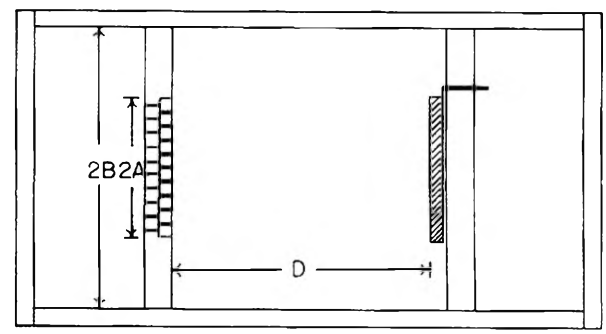

Fig. 2.—Top view of the current distribution cell: 2A = 4.9 cm.; 2B = 10.0 cm.; and D = 10.0 cm.

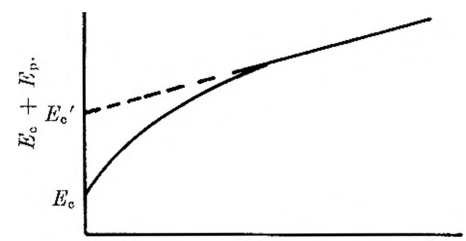

Fig. 3.—$E_c + E_p$ *vs.* I, where E_c is the cathode potential with respect to the standard hydrogen electrode, E_p is the polarization potential and I is the current density.

(5) C. Wagner, *J. Math. Phys.*, **30**, 23 (1951).
(6) E. Mantzell, *Z. Elektrochem.*, **41**, 10 (1935).
(7) C. H. Orr and H. E. Wirth, THIS JOURNAL, **63**, 1147 (1959).

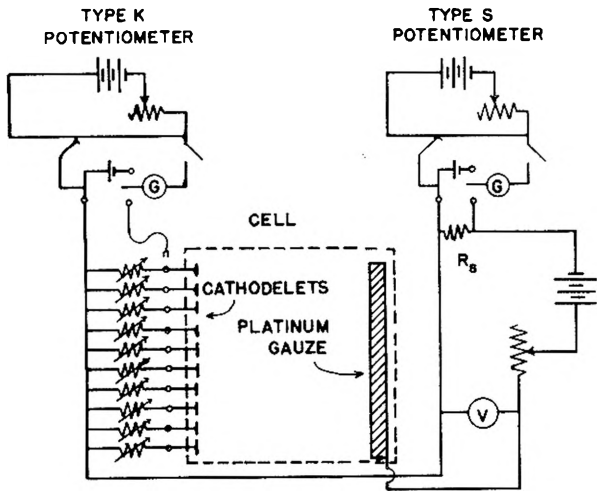

Fig. 4.—Current distribution measuring circuit.

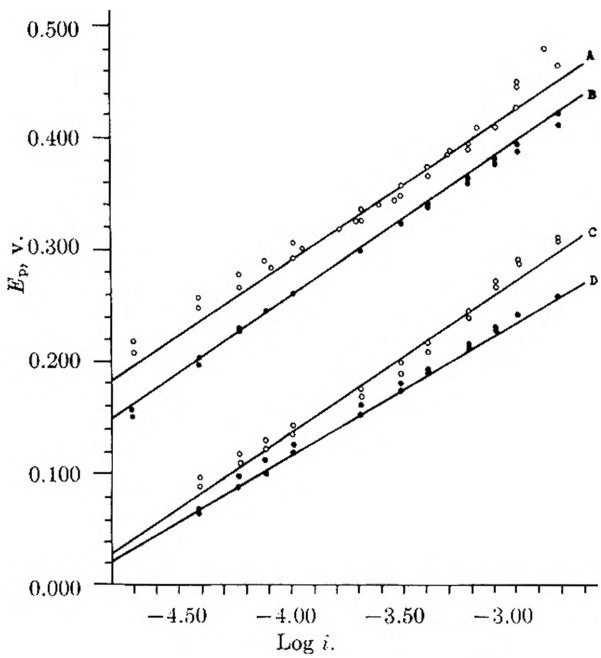

Fig. 5.—Polarization potential *vs.* log current for solutions of potassium argentocyanide: curve A, t = 25°, c = 0.1002 N; B, t = 45°, c = 0.0995 N; C, t = 25°, c = 0.5005 N; D, t = 45°, c = 0.4963 N.

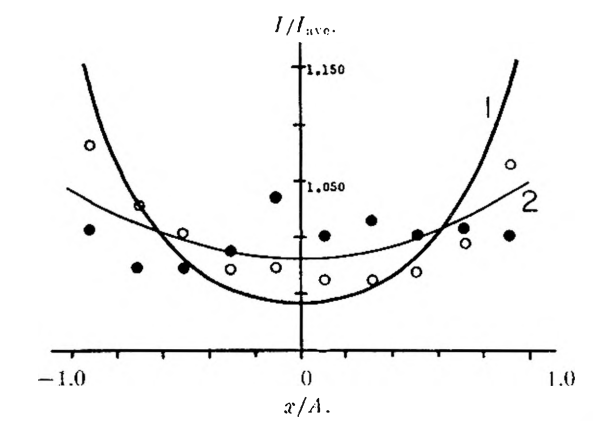

Fig. 6.—I/I_{ave} *vs.* x/A in solutions of potassium argentocyanide at 25°: open circles and curve 1, c = 0.0997 N; shaded circles and curve 2, c = 0.4985 N.

This was repeated two more times. The potentiometer was standardized again and then a measurement of E_1 with no current flowing was made. This reading of E_1 was designated ${}_0E_1$. The values of ${}_0E_1$ were always within a few tenths of a millivolt of each other before and after a determination. The average time for a determination was about six to seven minutes. After taking the last reading above, the current was adjusted to the next higher value and the series of readings repeated. This procedure was repeated until readings at the maximum current had been taken.

After completing runs on potassium argentocyanide, a run was made using silver nitrate, following the same procedure as for the potassium argentocyanide.

D. Calculations.—The exposed diameter of the silver cathode was 2.15 cm. and the distance from P_1 to C was 3.90 cm. and from P_1 to P_2 was 3.45 cm. The surface area of the cathode was 3.63 cm.^{2}. Assuming that the resistance in the solution between two points varies directly as the distance, then the ratio of the distance C-P_1 to the distance P_1-P_2 is the ratio of the respective resistances. That ratio is 1.130.

If polarization at the probe electrodes is negligible, then the potential E_1 is the IR-drop through a cylinder of solution 3.45 cm. × 3.63 cm.^{2} when a current is passed through the cell. The potential E_2 is a sum of potentials, the IR-drop through a cylinder of solution 3.90 cm. × 3.63 cm.^{2}, plus a polarization potential at the electrode. Therefore, if E_1 is multiplied by the ratio 1.130, and the resulting value subtracted from E_2, then the remainder should be the polarization potential of the electrode.

Since E_1 was not zero at the beginning of a run or during a run when no current was flowing, the value of E_1 when no current was passing, ${}_0E_1$, was subtracted from the value of E_1 for the previous determination.

An indication of the fact that the concentration remained fairly constant in the compartment between P_1 and P_2 is the relative constancy of the resistance R, calculated from the value of $E_1 - {}_0E_1 = E_r$ and the current i.

The fact that initially the potential E_1 differed from zero and also differed from run to run had no effect on the value of the polarization potential as calculated.

The polarization potential at each current density was calculated from the third values of E_1 and E_2 in each determination, since these terminal values seemed to represent the best estimate in each case of the polarization potential existing. These equations were used in the calculations

$$E_r = E_1 - {}_0E_1 \qquad (1)$$

$$E_p = E_2 - 1.130E_r \qquad (2)$$

and

$$R = E_r/i \qquad (3)$$

E. Data.—The values of the current densities and the polarization potentials for the solutions of potassium argentocyanide are plotted in Fig. 5. Those for the solution of silver nitrate at t = 25° and c = 0.1604 N are presented in Table I.

TABLE I

$i \times 10^4$, amp./cm.^{2}	E_p, v.	$i \times 10^4$, amp./cm.^{2}	E_p, v.
0.38	0.004	4.00	0.006
.57	.002	6.00	.003
.75	.005	8.0	.004
1.00	.004	10.0	.004
2.00	.004	15.0	.005
3.00	.006		

TABLE II

c	Temp., °C.	M	S
0.1002	25	0.829	0.135
.0995	45	.766	.129
.5005	25	.671	.134
.4963	45	.587	.118

Applying the method of averages to the polarization data for potassium argentocyanide and using the equation

TABLE III

No.	Temp., °C.	Volume concn., equiv./l.	L, mhos cm.$^{-1}$	h, v./amp./cm.^{2}	k, cm.	$\frac{a}{\pi k}$
1	25	0.0997	0.01040	338	3.52	0.222
2	25	.4985	.04596	335	15.41	.0506
3	45	.0990	.01462	322	4.70	.166
4	45	.4943	.06431	295	18.97	.0411
5	25	.1604	.01672	7.1	0.119	6.60

$$E_p = M + S \log i \qquad (4)$$

yielded the values listed in Table II for the constants.

The polarization potential for the solution of silver nitrate was small and essentially constant and the precision of the data thus obtained was not sufficient to warrant deriving an equation to represent it.

There are no data available in the proper range to compare with the polarization values for the solutions of potassium argentocyanide. However, the shape and course of the curve from the data of Glasstone[4] on 0.1 N $NaAg(CN)_2$ at 15° agree very well with the shape and course of the curve for 0.1 N $KAg(CN)_2$ at 25°.

The data of Piontelli and Poli[8] for 0.5 N $AgNO_3$ plus 1 N HNO_3 at 25° indicate that up to a current density of 20 × 10^{-4} amp./cm.^{2} the polarization potential lies somewhere between 0.009 and 0.016 volt, in good agreement with the results of this investigation.

If it is assumed that the dimensions of the cell do not change with time and with temperature, and that the probe electrodes are unpolarized, then the average resistance of the solution between those probe electrodes should permit calculation of the equivalent conductance of that solution. Using the average resistance of the 0.1604 N silver nitrate solution, 56.2 ohms, and the calculated equivalent conductance[5] of that solution, 104.2, a cell constant of 0.939 reciprocal centimeter was calculated for the cell. Using the average resistance in the case of two solutions of potassium argentocyanide each at two temperatures, 90.3, 63.7, 20.1 and 14.4 ohms (in the order in which the solutions are listed in Table II), and that cell constant, values of the equivalent conductances of the solutions were calculated 103.8, 148.2, 93.3 and 131.4, and compared with the calculated equivalent conductances using the data previously determined,[7] 104.2, 147.6, 92.1 and 130.0.

These data tend to indicate that the probe electrodes remained unpolarized during the course of a determination. The constancy of the central compartment resistance (average variation for resistances from the mean resistance amounted to about ±2%) between the two probe electrodes indicates that within the limits of experimental error, the composition in that compartment did not change in the course of a determination.

On the basis of this analysis it is felt that the polarization potential as defined herein has been determined for the solutions and at the temperatures indicated as a function of current density to within ±2%.

Current Distribution

A. Apparatus.—The cell used for measuring the current distribution was as indicated in Fig. 2. The body of the cell was made from Lucite. The block holding the cathodelets was machined from Lucite and the cathodelets were machined from block silver. Each cathodelet was 0.4 × 0.4 × 1.0 cm. and the mounting block provided a spacing of 0.1 cm. between adjacent electrodes. The anode was made by folding up a platinum gauze electrode which was coated with platinum black before runs were made.

All joints were sealed with a cement made by dissolving Lucite in chloroform. A thin layer of paraffin was poured on the bottom of the cell to assure complete sealing.

The measuring circuit is shown in Fig. 4. During measurements the cell was suspended in a constant temperature bath.

B. Procedure.—The solutions were prepared by weighing out the approximate weight of salt which then was diluted to a volume of one liter with conductance water.

After the solution was placed in the cell, the variable resistances in series with the individual cathodelets were all set to the same value. The current was applied at a predetermined value (0.00160 ampere) and after about three or four minutes the potential drop across the variable resistors was measured. From the known value of the resistance and the determined value of the potential drop, the current passing through each electrode could be calculated. Selecting the potential which corresponded to the least current, that potential was divided by the values of the current indicated on the other nine electrodes and new values for the resistances in series with the electrodes were calculated. These calculated values were set on the resistances and the current applied again. The potential drop across the re-

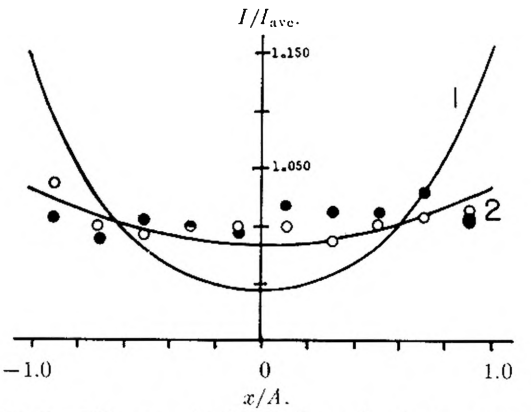

Fig. 7.—I/I_{ave} *vs.* x/A in solutions of potassium argentocyanide at 45°: open circles and curve 1, c = 0.0990 N; shaded circle and curve 2, c = 0.4943 N.

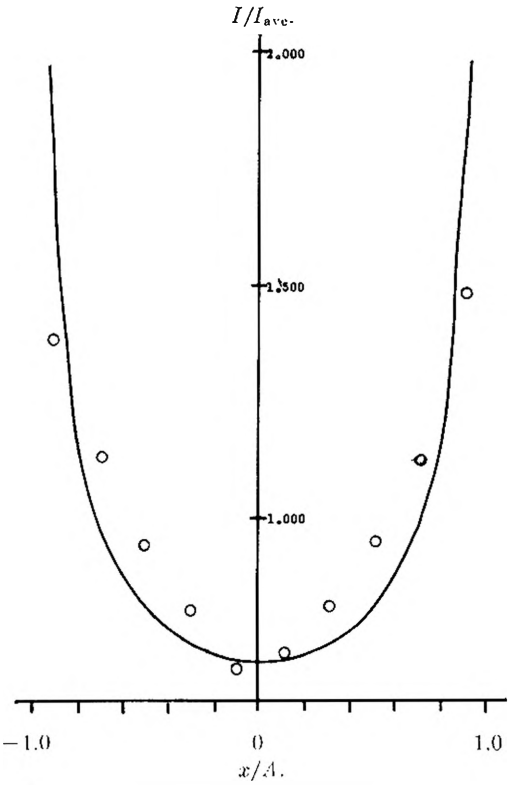

Fig. 8.—I/I_{ave} *vs.* x/A in a solution of silver nitrate at 25°, c = 0.1604 N.

(8) R. Piontelli and G. Poli, *Gazz. chem. ital.*, **80**, 107 (1950).

sistances was measured and new current and resistances were calculated. This process was continued until the difference in the potential drop between adjacent resistors was less than experimental variations in the current.

C. Data.—The information recorded in Table III for solutions of potassium argentocyanide (numbers 1–4) and of silver nitrate (number 5) was obtained from this and the previous paper in this series.[7] These data were used to calculate the theoretical current distributions using Wagner's method.

The dimensionless variable $a/\pi k$ is the ratio of an electrochemical term and a geometrical term. In this case, with a rectangular configuration of the bath and the electrodes, the geometrical term is the half-width of the cathode. As may be seen from the plots in Fig. 6–8, the smaller this ratio becomes the more uniformly the current is distributed over the cathode. Since for a given cell the parameter a is fixed, the ratio can get smaller either by the polarization or the specific conductance of the solution increasing. This too is apparent from the plots since increasing the concentration increases the specific conductance without appreciably lowering the polarization and the plots show a corresponding shift toward uniformity. Increasing the temperature has little effect on the polarization and only a moderate effect on the specific conductance so that with solutions of approximately the same concentration the increase in uniformity on increasing the temperature is not as great as in the case where the concentration is increased.

The effect of very low polarization on lack of uniformity of distribution is vividly shown on the plot for the solution of silver nitrate.

Qualitatively the method proposed by Wagner for predicting current distribution over a plane cathode is correct. The errors in these results prevent the experimental data from being a rigorous check of his theory.

Acknowledgment.—The authors wish to express their appreciation for a du Pont Fellowship during the academic year 1951–1952.

RATE OF REACTION IN HYDROGEN, NITROUS OXIDE AND IN SOME OTHER FLAMES

BY C. P. FENIMORE AND G. W. JONES

General Electric Research Laboratory, Schenectady, N. Y.

Received December 16, 1958

Flat, premixed nitrogen, nitrous oxide, hydrogen flames (some with added air) were burnt on a cooled porous burner at 6 to 41 cm. pressure, and at 1260 to 1780°K. final flame temperature. Thermocouple traverses were made, and composition profiles through the flame established by probe sampling. Hydrogen atoms were estimated from the rate of formation of HD when heavy water was added to the reactants. Diffusion was approximately corrected for by binary diffusion coefficients to get the rate of reaction through the flame. $d[N_2]/dt$ was considerably faster than the pseudo-unimolecular decomposition of nitrous oxide in the absence of hydrogen, and faster the greater the concentration of hydrogen atoms. The chain reactions $H + N_2O \rightarrow N_2 + OH$, $OH + H_2 \rightarrow H_2O + H$ therefore were assumed to occur. The measurements of [H], $[N_2O]$ and $d[N_2]/dt$ were consistent with the rate constant $k = 4 \times 10^{11} e^{-(16{,}300 \pm 2{,}000)/RT}$ l. mole^{-1} sec.$^{-1}$ for the reaction of hydrogen atoms with nitrous oxide. Similar experiments on other flames gave a rate constant for $H + O_2 \rightarrow OH + O$ consistent with the literature; and a rate constant for $OH + H_2 \rightarrow H_2O + H$ about 8 times larger than for $OH + CO \rightarrow CO_2 + H$, whereas a ratio of 12 times was expected from the literature, and these agreements show that the method is fairly accurate.

Introduction

In the last two years, a good deal of effort has gone into measuring radical concentrations in hot gases in this Laboratory. We have applied one of these techniques to a study of the hydrogen, nitrous oxide flame, along with temperature measurements and analyses of samples probed through the flame. Our results allow estimates of the rate constant for the reaction between hydrogen atoms and nitrous oxide.

Similar experiments on other flames checked the method by giving rate constants which agreed moderately well with expected values from the literature.

Experimental

A water cooled porous metal burner[1] of 31.1 cm.^{2} surface area was mounted in a brass plate with connections through the plate for a spark igniter, manometer, a movable sampling probe and a movable quartz coated thermocouple of butt-welded platinum and platinum-rhodium wires, 0.0012 cm. diameter.[1] A bell jar over this assembly could be evacuated and allowed burning at any desired pressure. Distances between the flat burner surface and the probe or thermocouple were measured by a cathetometer mounted outside the bell jar. The outside diameter of the quartz probe tip was 0.01 cm. or less and we did not attempt to sample closer than 0.1 cm. to the burner surface. Reactant gases were metered through critical flow orifices, and the samples were taken into a sample bulb at 1 mm. pressure or less and analyzed on a mass spectrometer.

Correction of the Data.—The method of calculating a rate constant from our results is described in this and in the next section. Figure 1 displays the temperature and composition measurements through three flames, all of the same final temperature, 1700°K., and with the same reactant composition, $H_2 + 0.86\ N_2O + 1.84\ N_2$. Pressure in cm. of mercury and burning velocity in cm./sec. at the pressure used and at 300°K. are indicated for each flame.

Obviously, large diffusion currents exist. For example, the gas contains more nitrous oxide than hydrogen over the first few mm. from the burner surface and this is possible only because hydrogen diffuses downstream faster than does nitrous oxide. After the gas has traversed the flame, of course, diffusion becomes negligible.

The diffusion velocity of the ith species is

$$V_i = -(D_i/X_i)dX_i/dZ$$

and is evaluated by replotting the analyses as mole fractions *versus* distance, X_i *versus* Z, and determining the gradient graphically. The diffusion coefficients D_i are taken from Hirschfelder, *et al.*,[2] under the approximation that the gas is a binary

(1) W. E. Kaskan, "6th Symposium on Combustion," Reinhold Publ. Corp., New York, N. Y., 1957, p. 134.

(2) J. O. Hirschfelder, C. F. Curtis and R. B. Bird, "Molecular Theory of Gases and Liquids," John Wiley and Sons, New York, N. Y., 1954.

mixture of nitrogen plus whichever species is being considered. The V_i so obtained have maximum values of the order of the gas velocity v for most components. For nitrogen, however, the gradient is moderate and X_{N_2} always large, so V_{N_2} is always less than 16% of v. The gas velocity v is obtained from a knowledge of the mass flow ρv, which is constant through the flame, and from the density ρ which can be evaluated at any point since temperature, pressure and composition are known.

Given V_i and X_i, the fraction of mass flow contributed by the ith species

$$G_i = X_i M_i(v + V_i)/Mv$$

can be calculated. M_i is molecular weight of the ith species and M the average molecular weight in this formula. G_i is needed because its rate of change with distance through the flame is proportional to the rate of appearance of the ith species due to chemical reaction. More exactly, the reaction rate of the ith species is

$$(\rho v/M_i)dG_i/dZ$$

G_{N_2} is the best known of the G_i because V_{N_2} is the smallest of the diffusion velocities; and whenever possible, the evaluation of a rate constant is done from G_{N_2}.

G_{N_2} and G_{NO} are plotted in Fig. 2 for the flames described by Fig. 1. It is evident that the rate of formation of nitrogen

$$[\dot{N}_2] = (\rho v/28)dG_{N_2}/dZ \backsimeq -[\dot{N}_2O]$$

is smaller below 1600°K. than above. On each G_{N_2} curve, the 1600° position is indicated. The reaction rate is greatest in all three flames at about 1680°K., and then decreases again as the temperature approaches 1700°K.

The Chain Decomposition of Nitrous Oxide.—If the maximum value of $d[N_2]/dt$ deduced from Fig. 2, $[\dot{N}_2]_{max}$, is divided by the nitrous oxide concentration at this point, one gets a first-order reaction constant for the decay of nitrous oxide in the flame. The value of this quotient does not change appreciably as one goes farther downstream from $[\dot{N}_2]_{max}$. At 12, 21 and 41 cm. pressure, $[\dot{N}_2]_{max}/[N_2O]$ is 2720, 2200, 1390 sec.$^{-1}$, respectively.

These values are larger than one would find in the absence of hydrogen. In earlier work[3] a considerable number of decompositions of nitrous oxide were measured in the combustion products of lean flames at 1 atm. pressure and at 1500 to 1760°K. with $[N_2O]$ about the same as in the present work. The results of the earlier work are correlated by

$$k_1 = 4 \times 10^{10}e^{-61,000/RT} = [\dot{N}_2]/[N_2O]$$

when $[H_2]$ is small, and this, or similar expressions from the literature, can be taken as an upper limit for the rate of decomposition in the absence of hydrogen. At 1680°K., the equation above predicts $k_1 = 450$ sec.$^{-1}$; while the rate expression of Nagasako and Volmer,[4] for example, would give $k_1 < 500$ sec.$^{-1}$. The larger values observed in the flames for $[\dot{N}_2]_{max}/[N_2O]$ indicate a chain reaction of average chain length at least 3 to 6 and perhaps much longer.

(3) C. P. Fenimore and G. W. Jones, THIS JOURNAL, **62**, 178 (1958).

(4) N. Nagasako and M. Volmer, *Z. physik. Chem.*, **10**, 414 (1930).

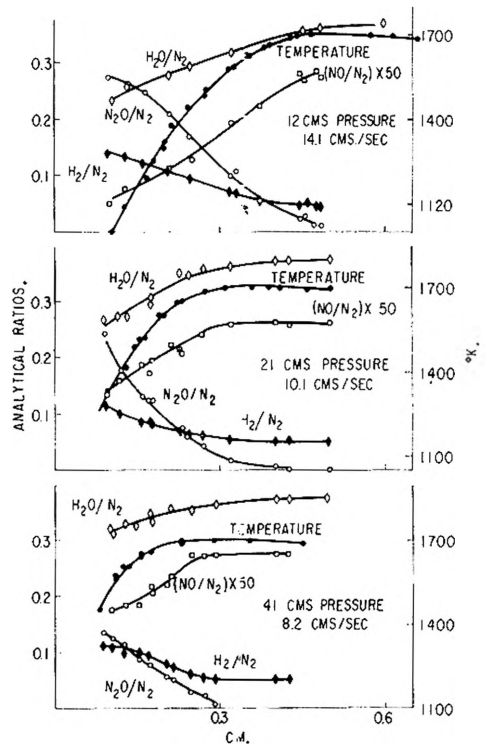

Fig. 1.—Temperatures and composition traverses through three flat flames. Reactant composition = $H_2 + 0.86N_2O + 1.84N_2$.

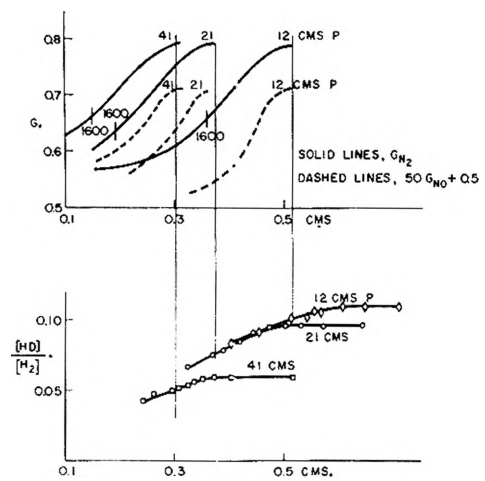

Fig. 2.—Upper curves, G-values derived from Fig. 1 for three flames; lower curves, approach of $[HD]/[H_2]$ to its equilibrium value when heavy water is added to the reactants of the same three flames.

If the chain decomposition involves reaction 2

$$H + N_2O \longrightarrow N_2 + OH \qquad (2)$$

then neglecting the little nitric oxide formed, one can write

$$[\dot{N}_2]_{max}/[N_2O] = k_1 + k_2[H]$$

and k_2 can be determined, since $[H]$ can be measured by adding heavy water to the reactants and following the rate of formation of the species HD.[5] The method of $[H]$ determination requires that reaction 3 be equilibrated

(5) C. P. Fenimore and G. W. Jones, THIS JOURNAL, **62**, 693 (1958).

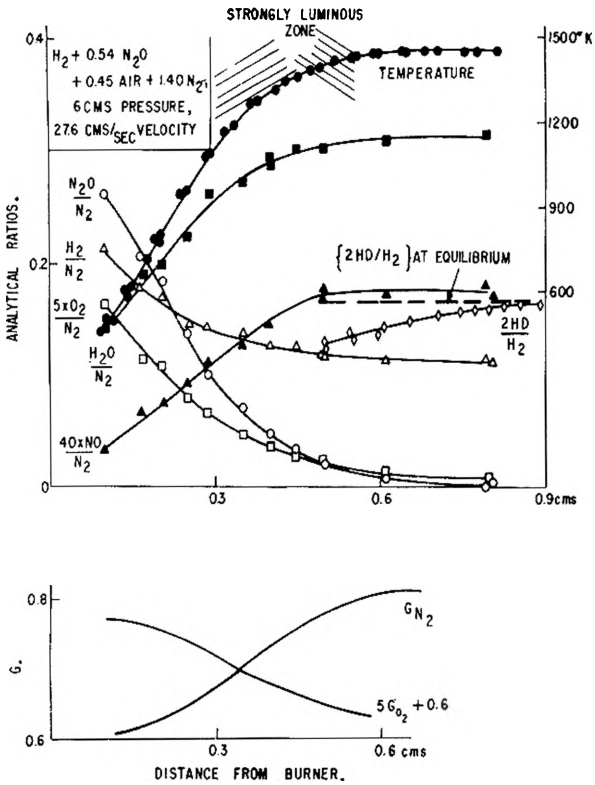

Fig. 3.—Traverses and G-values for a flame containing added air.

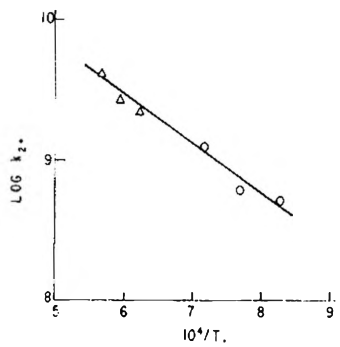

Fig. 4.—Arrhenius plot, log k_2 *vs.* $1/T$: Δ indicates values obtained from oxygen free flames; O are values from flames containing air.

$$H + H_2O \underset{k_{-3}}{\overset{k_3}{\rightleftharpoons}} H_2 + OH \qquad (3)$$

as it is in the post-flame gas, but not in the flame itself. Therefore [H] is measured in the burnt gas just beyond the flame rather than in the flame itself.

The lower curves of Fig. 2 give the [HD]/[H_2] ratios obtained when a little D_2O is swept into the reactant mixture using the nitrogen as a carrier gas. The vertical lines show that [HD]/[H_2] is still increasing after G_{N_2} and G_{NO} have become constant, so [H] can be determined in the post-flame gas. From the data plotted, we calculate [H] = 0.85×10^{-6} mole/l. at 12 cm. pressure, 0.7×10^{-6} at 21 cm. and 0.4×10^{-6} at 41 cm. pressure. A plot of $[\dot{N}_2]_{max}/[N_2O]$ *vs.* [H] then gives a slope of $k_2 = 2.5 \times 10^9$ l. mole^{-1} sec.$^{-1}$ at 1680°K. In estimating the slope, some weight is given to the requirement that the intercept at [H] = 0 lie between 450 sec.$^{-1}$ and zero.

One error in calculating k_2 is that [H] is measured farther downstream than is $[\dot{N}_2]_{max}/[N_2O]$. The easy diffusion of hydrogen atoms suggests that this error should not be serious, however, and some evidence will be given below that [H] is essentially constant across most of the flame. The error due to the approximate nature of the diffusion corrections will be considered in the last section.

Other Nitrous Oxide Flames.—Flames of the same reactant composition were examined at two other temperatures and k_2 evaluated just as above at 1600° and at 1760°K. This limited temperature range is all that is available by our method for pure nitrogen, nitrous oxide, hydrogen flames; because the flames are unstable below 1600°, and [H] cannot be determined in these post-flames gases at temperatures much above 1760°.

Flames containing added air are stable to temperatures several hundred degrees lower, however, and can be used to increase the temperature range and, hence, to increase the precision in determining k_2. In flames containing air, the chain carriers are mostly generated by combustion of the added oxygen, [H] is larger than in oxygen free flames and k_1 is negligible compared to k_2[H].

Figure 3 shows the results for one typical mixture containing added air. The upper part of the figure displays the measured temperatures and analytical ratios. The argon, 0.2 to 0.3% of the nitrogen, is not plotted. The lower part of the figure shows the derived G_{N_2} and G_{O_2}. The hydrogen atom concentration in the post-flame gas was [H] = 2.6×10^{-6} mole/l., obtaining from the HD/H_2 ratios on adding heavy water. The values of $k_2 = [\dot{N}_2]/[N_2O][H]$ are 12×10^8 at 1400°K., 6×10^8 at 1310°, and 3×10^8 at 1100°.

The highest temperature value of k_2 derived from Fig. 3 and those from two other similar runs are plotted in Fig. 4, along with the data obtained from oxygen free flames. The k_2 values derived at 1310 and 1100° from Fig. 3 are not included in Fig. 4, nor are additional lower temperature values found similarly from the other runs. If these additional values were plotted, they would lie close to the curve in Fig. 4; and this fact is evidence that, at 6 to 10 cm. pressure at least, [H] is essentially constant through most of the flame.

From Fig. 4, one obtains $k_2 = 4.2 \times 10^{11} e^{-16,300/TR}$ l. mole^{-1} sec.$^{-1}$. The error in this expression should not exceed 2 kcal. in the activation energy. It should be stated that the values of k_2, involving as they do the determination of [H] by the addition of heavy water, depend on the value of the rate constant for reaction 3. If the latter constant were revised from its estimated $10^{12} e^{-25,500/RT}$, then k_2 as determined here would change in the same direction and by the same amount. We would be surprised, however, if k_2 were wrong by more than a factor of two on this account; for [H] as determined by heavy water is consistent with other determinations by different methods. The next section gives some new evidence on the reliability of the [H] determination.

The activation energy which we obtain is near an old estimate of Melville who studied reaction 2 at lower temperatures and obtained rather widely dif-

fering values by different means. He estimated an activation energy of 15 to 20 kcal.,[6] and he did not propose a frequency factor.

Some Tests of the Method.—The approximate nature of the diffusion corrections may introduce an error into the rate constant and, though the small gradients of nitrogen should make a 50% error in the diffusion coefficient for nitrogen not too serious, there is no easy way to estimate how great the errors might be. One test of the method would be to determine known rate constants, and two checks of this sort have been carried out.

The first check was suggested by Fig. 3 which shows that when $[O_2]$ is about $^1/_5$ of $[N_2O]$, the slope of G_{O_2} *vs.* distance is about $^1/_5$ that of the negative of G_{N_2} *vs.* distance. Consequently if oxygen disappears at flame temperatures only *via* reaction 4

$$H + O_2 \longrightarrow OH + O \qquad (4)$$

as is quite well accepted, the rate constant of reaction 4 must be of the same order as k_2 at 1100 to 1400°K. We examined three hydrogen–air flames in order to determine k_4 more accurately and found from the early rate of decay of G_{O_2}, and with [H] measured as before in the post-flame gas, that the average value of $k_4 = 1.5 \times 10^8$ l. mole^{-1} sec.$^{-1}$ at 1100°K. The variation with temperature corresponded to an activation energy of 18 ± 3 kcal. These results are of the same order as other recent estimates.[7]

A second check involved a comparison of the rates of formation of water and carbon dioxide from mixed hydrogen and carbon monoxide fuel. The point of this test was that in earlier work[8] we measured the rate of reaction 5 in the post-flame gas where diffusion effects are smaller than in the reaction zone of flames

$$H + CO_2 \underset{k_{-5}}{\overset{k_5}{\rightleftharpoons}} CO + OH \qquad (5)$$

The ratio of k_5 to the rate constant for the reaction of hydrogen atoms with H_2O or D_2O was $k_5/k_3 = 3e^{-7800/RT}$. If this ratio is divided by the water gas constant, one gets the ratio of the reverse rate constants and concludes that at 1000 to 1200°K. the rate constant for OH + H_2 → H_2O + H should be 12 times larger than that for OH + CO → CO_2 + H. Consequently, if H_2O and CO_2 are formed only *via* these reactions, the ratio $d[H_2O]/[H_2]dt$ to $d[CO_2]/[CO]dt$ should equal 12 in the early part of the flame.

In Fig. 5 the results are plotted for a flame of reactant composition H_2 + 0.21CO + 0.46O_2 + 1.95A burnt at 6 cm. pressure with $\rho v = 5.35 \times 10^{-3}$ g./cm.^{2} sec. The upper graphs display analytical ratios, the lowest one gives derived *G*-values. The diffusion coefficient for CO_2 was calculated for binary CO_2–A mixtures by Westenberg's approximation[9] to Hirschfelder, *et al.*[2] The other *D* were taken from D_{CO_2} simply by assuming an inverse

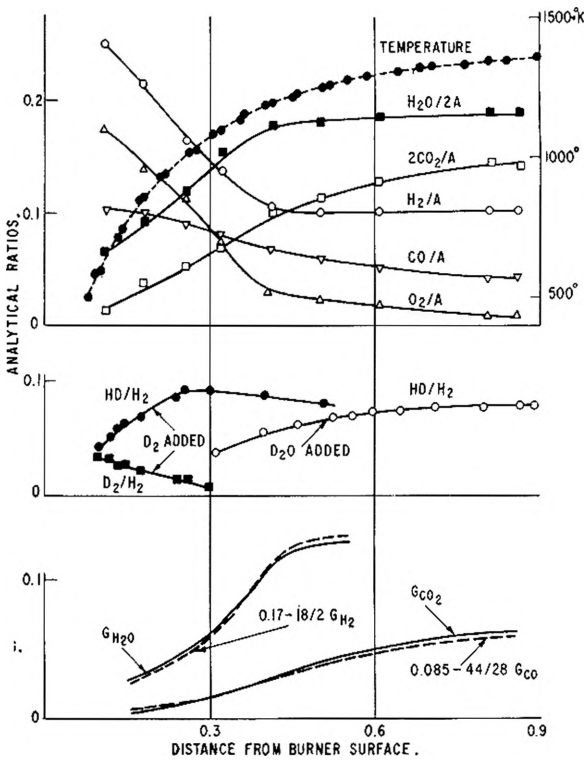

Fig. 5.—Traverses and *G*-values for a hydrogen, carbon monoxide, oxygen, argon flame. The dashed and solid *G*-curves should coincide if $d[H_2O]/dt = -d[H_2]/dt$ and if $d[CO_2]/dt = -d[CO]/dt$.

proportionality to the square root of molecular weight; $D_{H_2O} = (44/18)^{1/2} D_{CO_2}$, etc. $d[H_2O]/[H_2]dt$ increases out to 0.4 cm. from the burner surface, but beyond this point the rate falls catastrophically because the reverse reaction increases rapidly. Similarly, $d[CO_2]/[CO]dt$ decreases at distances beyond 0.5 cm. From 0.2 to 0.35 or 0.4 cm., however, the relative rates should not be influenced much by the reverse processes, and one finds a ratio of 7 to 9 over this range as compared with the expected value of 12.

It seems reasonable to conclude from these two tests that the value obtained for k_2, the rate constant for H + N_2O → N_2 + OH, is not seriously impaired by the approximate nature of the diffusion corrections.

With reference to the trustworthiness of the [H] determination, the effect of replacing a little of the hydrogen by deuterium is shown in Fig. 5. This interested us because the exchange reaction 6

$$H + D_2 \longrightarrow HD + D \qquad (6)$$

equilibrates too rapidly to use as a measure of [H] in the post-flame gas. But early in the reaction zone, it is evident that the build up of HD can be followed from added D_2. HD should build up at a rate $d[HD]/dt = k_6[H][D_2]$ approximately. More exactly, if all possible reactions of type (6) are considered and isotope effects on the rate constants ignored

$$d[HD]/dt = k_6\left\{[H][D_2] + [D][H_2] - \frac{[HD]([H] + [D])}{2}\right\}$$

If $[D] = [H][HD]/2[H_2]$, and if a region is con-

(6) H. W. Melville, *J. Chem. Soc.* 1243 (1934).

(7) D. E. Hoare and A. D. Walsh, "Reaction of Free Radicals in the Gas Phase," Special Publication No. 9, p. 22, The Chemical Society, London, 1957.

(8) C. P. Fenimore and G. W. Jones, THIS JOURNAL, **62**, 1578 (1958).

(9) A. A. Westenberg, *Combustion & Flame*, **1**, 346 (1957).

sidered where $D_2 >> [HD]^2/4[H_2]$ as in the present case, the simpler expression is adequate.

In Fig. 5, [HD] does not continue to increase; it attains a maximum at $Z = 0.25$ cm., $T = 1000°K.$, and then decreases again. At the maximum, the formation of [HD] due to reaction 6 is equal to its destruction which can be supposed to occur at a rate $([HD]/[H_2])\ d[H_2O]/dt$. Then measured quantities can be combined to give the left-hand side of the equality

$$\left(\frac{[HD]}{[D_2][H_2]}\right)\frac{d[H_2O]}{dt} = k_6[H]$$

$$\frac{d[HD]}{dt} = 0$$

and taking k_6 at 1000°K. from the recent literature,[10] one gets $[H] = 2.3 \times 10^{-5}$ mole/l. at $Z = 0.25$ cm.

This value of [H] can be compared with [H] as measured farther downstream by the heavy water method. At $Z = 0.5$ cm. [H] *via* heavy water was 91% of [H] at 0.25 cm. as determined *via* reaction 6. Assuming that [H] is fairly constant across the flame, one can conclude that the heavy water method gives [H] values which are also consistent with values determined *via* reaction 6.

(10) G. Boato, G. Careri, A. Cimino, E. Molinari and G. G. Volpi, *J. Chem. Phys.*, **24**, 783 (1956).

Another indication of the degree of reliability of the radical determinations was obtained by Dr. W. E. Kaskan of our group who measured [OH] by absorption spectroscopy[11] through the flame and the post-flame gas described by Fig. 5. In the post-flame gas, Kaskan infers [H] from [OH] under the assumption that reaction 3 is equilibrated; and here [H] *via* optical measurements proved to be 2.0 ± 0.1 times larger than [H] obtained *via* the heavy water method. In the early part of the flame, [OH] can be estimated from the rate of formation of carbon dioxide under the assumption that it is formed only *via* the reverse of reaction 5; and over the range $Z = 0.25$ to 0.4 cm. [OH] *via* optical measurements was 0.8 ± 0.1 of [OH] *via* the rate of carbon dioxide formation. This comparison of [OH] is also a comparison of the heavy water method of [H] determination with optical [OH], because the rate constant k_{-5} was obtained from measurements of k_5 which involved [H] determinations *via* heavy water. The two comparisons suggest that some error may afflict one or both of [H] *via* heavy water, or [OH] optically. But it would seem unlikely that errors in [H] could cause an error of more than a factor of two in k_2, k_4, k_5 as obtained in this or in a previous paper.[8]

(11) W. E. Kaskan, *Combustion & Flame*, **2**, 229 (1958).

THERMODYNAMICS OF THE LEAD–TIN SYSTEM

BY WESTON B. KENDALL AND RALPH HULTGREN

Institute of Engineering Research, University of California, Berkeley, Calif.

Received December 16, 1958

The heats of formation of solid solutions of tin in lead have been measured at 450°K. by liquid tin solution calorimetry. These data have been correlated with published thermodynamic data and with the phase diagram in order to establish a complete and reliable set of thermodynamic properties for both the liquid and the solid alloys.

Introduction

Alloy systems for which complete thermodynamic data are available are few in number. In fact, of those simple eutectic systems of limited solid solubility listed in Kubaschewski and Catterall[1] the only one for which the entropies of the solid can be computed with reasonable accuracy is Bi–Sn. Data of this type are certainly desirable because of the important role they play in the development of theories concerning the physical properties of alloys.

Up to the present time the only significant measurements which were lacking for an accurate determination of the entropies of solid lead–tin alloys were the heats of formation of these alloys. By measuring these in a liquid tin solution calorimeter it was found possible to establish for the entire system a complete and self-consistent set of thermodynamic properties. For the phase diagram[2] see Fig. 1.

(1) O. Kubaschewski and J. A. Catterall, "Thermochemical Data of Alloys," Pergamon Press, New York, N. Y., 1956.

(2) M. Hansen, "Constitution of Binary Alloys," 2nd Edition, McGraw-Hill Book Co., Inc., New York, N. Y., 1958.

Experimental

Materials.—The lead used in this investigation was obtained from the Consolidated Mining and Smelting Co., Ltd., Canada. The manufacturer gave the purity as 99.999%. The tin was procured from the National Bureau of Standards, Washington, and had a reported purity of 99.997%. Spectrographic analyses made in this Laboratory tended to support the reported purities.

Preparation of Alloys.—A 10-g. ingot of each alloy was prepared by melting together at 360° weighed amounts of the pure components in sealed, evacuated Vycor tubes. The tubes containing the completely molten samples were agitated for ten minutes to ensure thorough mixing of the components, then they were quenched in ice water to prevent macrosegregation. The weight losses encountered during the alloying process were in all cases less than 0.01%, so the compositions of the resulting ingots were taken to be the same as those of the mixtures from which they were prepared. The ingots were cold-worked, resealed into Pyrex tubes, homogenized for two weeks at temperatures ranging from 20 to 35° below the solidus, and quenched in a mixture of Dry Ice and acetone. Microscopic examination disclosed no traces of a second phase, and X-ray diffraction studies confirmed the homogeneity of the alloys.

Calorimetry.—The heats of formation of the alloys were determined by liquid tin solution calorimetry. A detailed description of the experimental method and apparatus may be found in a recent publication[3] and will not be repeated

TABLE I

EXPERIMENTAL RESULTS

Sample comp. (at.-% tin)	Run no.	T_i (°K.)	T_i (°K.)	Bath concn. (at.-% lead)	ΔH_{soln} (cal./g.-atom)	$\Delta H_{f,\ 450°K.}$ (cal./g.-atom)
Pure lead	58-3	449.9	612.0	0.144	3748	
	59-3	450.8	613.0	.146	3742	
	59-15	450.5	613.0	.960	3693	
	60-15	451.3	611.0	1.021	3691	
5.00	59-5	448.6	613.0	0.346	3529	+179
	59-7	448.9	613.0	.552	3542	+154
10.00	58-5	450.3	612.0	.317	3385	+263
	59-13	451.6	613.0	.867	3245	+375
14.10	58-7	450.9	611.9	.477	3197	+404
	59-11	447.2	613.0	.727	3180	+442
20.00	60-5	454.6	611.0	.338	3021	+505
	60-13	451.5	611.1	.800	3007	+520
25.00	60-7	454.6	611.0	.506	2883	+592
	60-11	452.4	611.0	.659	2893	+591

here. The samples were all dropped from a temperature of ~450°K. into a tin-bath at ~612°K. During the alloy runs the concentration of lead in the tin-bath was never allowed to exceed 1 at. %. In these dilute solutions the heat of solution of the samples was found to be nearly independent of the lead concentration so that only a small correction was necessary. The concentration effect was determined by dropping pure lead samples into the bath and plotting the results as a function of concentration.

Experimental Data.—The results of the heat of solution measurements are given in Table I together with the calculated integral heats of formation of the alloys at 450°K. In these calculations ($H_{612} - H_{450}$) for tin has been taken as 2885 cal./g.-atom. This value is about 25 cal./g.-atom smaller than that derived from Kelley,[4] as suggested by the recent work of Heffan[5] on the heat capacity of liquid tin.

From these data the partial molar heat of solution of liquid lead in liquid tin at infinite dilution is calculated to be $(\Delta\bar{H}_{Pb})_{612°K.,\ x_{Sn}=1} = 1490$ cal./g.-atom.

Evaluation of Thermodynamic Data. Liquid Alloys.—Kleppa[6] recently has measured the integral heats of formation of liquid lead–tin alloys at both 623 and 723°K. His results indicate that the heats of formation are independent of temperature over the range studied. By extrapolating his curve from 4 to 0% lead he obtained $(\Delta\bar{H}_{Pb})_{x_{Sn}=1} = 1350$ cal./g.-atom, in good agreement with our more directly measured value. An earlier set of measurements by Kawakami[7] shows more scatter and much poorer agreement with our above value of $(\Delta\bar{H}_{Pb})_{x_{Sn}=1}$; hence the data of Kleppa have been selected without modification.

Vapor pressure measurements on this system are not yet available, and e.m.f. measurements[8] are unreliable due to the very small difference between the electropositivities of lead and tin. However, Elliott and Chipman[9] made cell measurements of $\Delta\bar{F}_{Cd}$ in the ternary system Pb–Sn–Cd, and performed a Gibbs–Duhem integration of the activity of cadmium at 773°K. for the ratios Pb:Sn = 1:2 and 2:1. In this manner they were able to obtain the integral free energies of formation at two points on the Pb–Sn binary side of the diagram. If Elliott and Chipman's values of ΔF are combined with Kleppa's values of ΔH, the entropies of formation of $PbSn_2$ and Pb_2Sn are found to be ideal within ± 0.03 e.u. Until further data become available it seems reasonable to assume that the entropies of formation of the liquid alloys are ideal at all compositions (regular solution), and to compute the thermodynamic functions of the liquid alloys at all temperatures and compositions from Kleppa's heats of formation.

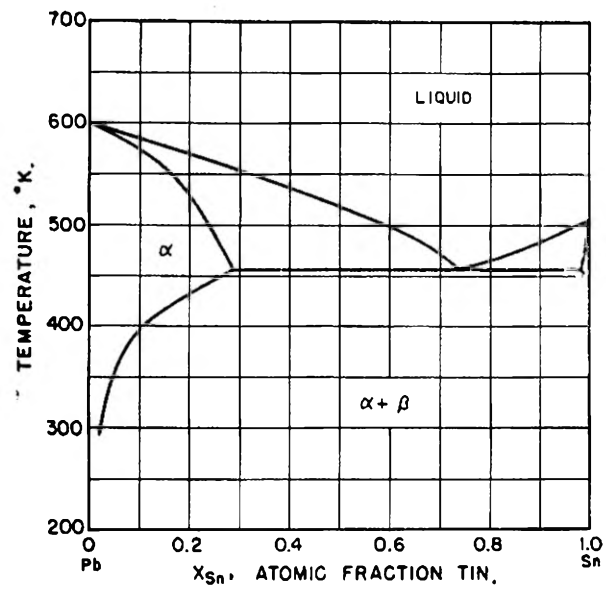

Fig. 1.—Phase diagram of the lead–tin system.

Solid α-Phase Alloys.—The experimental results given in Table I are shown in Fig. 2 along with some more recently completed measurements of Murphy and Oriani[10] which agree excellently.

One method of establishing the thermodynamic functions of the solid alloys would be to make use of the phase diagram and the free energies of fusion of lead and tin to transfer the liquid free energies across the two-phase region to the solidus. If it is assumed that the heats of formation do not vary with temperature (an assumption supported by the

(3) R. L. Orr, A. Goldberg and R. Hultgren, *Rev. Sci. Instr.*, **28**, 767 (1957).

(4) K. K. Kelley, U. S. Bur. Mines Bull. 476, 1949.

(5) H. Heffan, Master's Thesis, University of California, 1958.

(6) O. J. Kleppa, THIS JOURNAL, **59**, 175 (1955).

(7) M. Kawakami, *Sci. Rep. Tohoku Imp. Univ.*, [I], **16**, 915 (1927).

(8) R. Schaefer and F. Hovorka, *Electrochem. Soc.*, Reprint No. 87 **23**, 267 (1945).

(9) J. Elliott and J. Chipman, *J. Am. Chem. Soc.*, **73**, 2682 (1951).

(10) W. Murphy and R. Oriani, *Acta Met.*, **6**, 556 (1958).

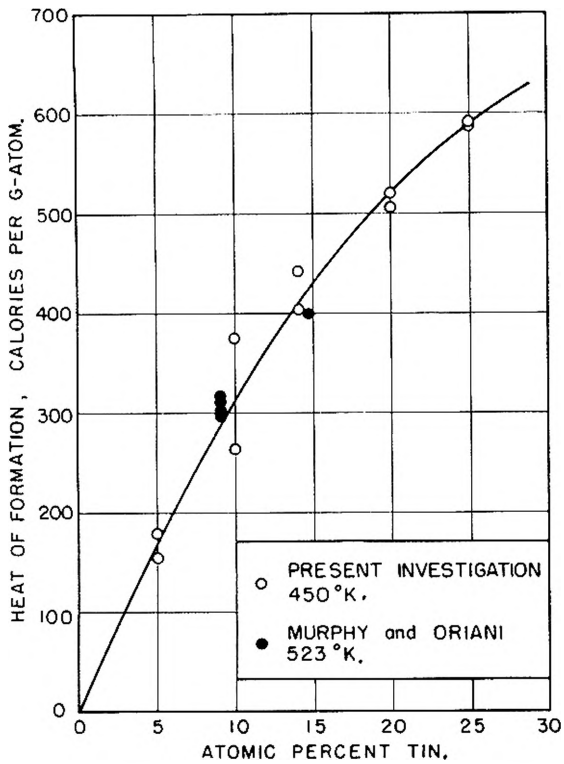

Fig. 2.—Integral heats of formation of α-phase lead–tin alloys.

close agreement of the two sets of measurements shown in Fig. 2) these values can be combined with the free energies along the solidus to obtain integral entropies of formation of the solid α-phase alloys.

There is an additional and independent means of utilizing the present heat of formation data to obtain the entropies of these alloys. $\Delta\bar{F}_{Sn}$ along the solvus is for all practical purposes zero because the alloys are in equilibrium with essentially pure tin. Values of $\Delta\bar{H}_{Sn}$ derived from the present results may be combined with $\Delta\bar{F}_{Sn}$ to obtain $\Delta\bar{S}_{Sn}$ along the solvus. $\Delta\bar{S}_{Pb}$ and subsequently ΔS may be obtained from a Gibbs–Duhem integration of $\Delta\bar{S}_{Sn}$.

An analysis of the uncertainties involved in these calculations would seem to indicate that it is somewhat better to accept the solvus line given in Hansen as correct and assume that any resulting small inconsistency between the thermodynamic functions of the liquid and the solid can be attributed mainly to the assumption of ideal entropies in the liquid. That such an inconsistency is indeed negligibly small can be demonstrated as follows: if the free energies of the solid as calculated from the solvus line using the measured heats of formation are transferred into the liquid and combined with Kleppa's heats, the entropies obtained are less than ideal by only 0.05 e.u. at $x_{Sn} = 0.25$ and by only 0.07 e.u. at $x_{Sn} = 0.50$.

Tabulated Values of Thermodynamic Properties.—Selected values of the thermodynamic properties of solid and liquid lead–tin alloys are summarized in Tables II and III. The units of ΔF and ΔH are cal./g.-atom, and those of ΔS are cal./(g.-atom × deg.).

TABLE II

LIQUID ALLOYS AT 623°K.

$(1 - x)\mathrm{Pb(l)} + x\mathrm{Sn(l)} = [\mathrm{Pb}_{(1-x)}\mathrm{Sn}_x](\mathrm{l})$

x_{Sn}	ΔF	ΔH	ΔS	a_{Pb}	a_{Sn}
0.00	0	0	0.00	1.000	0.000
.10	−270	130	.65	0.915	.246
.20	−400	220	.99	.847	.390
.30	−470	280	1.21	.785	.495
.40	−510	320	1.34	.721	.575
.50	−530	330	1.38	.657	.646
	(±40)	(±40)	(± .13)	(± .021)	(± .021)
.60	−520	310	1.34	.584	.709
.70	−480	270	1.21	.499	.772
.80	−410	210	0.99	.390	.840
.90	−280	120	.65	.236	.911
1.00	0	0	.00	.000	1.000

TABLE III

SOLID α-PHASE ALLOYS AT 456°K.

$(1 - x)\mathrm{Pb(s)} + x\mathrm{Sn(s)} = [\mathrm{Pb}_{(1-x)}\mathrm{Sn}_x](\mathrm{s})$

x_{Sn}	ΔF	ΔH	ΔS	a_{Pb}	a_{Sn}
0.00	0	0	0.00	1.000	0.000
.05	− 80	170	.55	0.957	.375
.10	−105	315	.92	.921	.647
.15	−115	430	1.20	.895	.793
.20	−120	520	1.40	.871	.906
.25	−120	590	1.56	.857	.962
.29	−105	630	1.61	.847	.986
	(±50)	(±40)	(±0.23)	(±0.045)	(±0.065)

Summary and Conclusion

Heats of formation of solid solutions of tin in lead have been determined in a liquid tin solution calorimeter. From these data together with the phase diagram, and previous thermodynamic measurements of liquid alloys, a consistent set of thermodynamic functions has been derived for both solid and liquid alloys. The self-consistency serves to confirm not only the thermodynamic measurements, but also the positions of solidus, liquidus, and solvus lines of the Pb-rich alloys.

Acknowledgment.—The authors are indebted to the Office of Ordnance Research, U. S. Army, for support of the experimental work described in this paper. In addition, they wish to express their appreciation to the Atomic Energy Commission for support of the literature search and evaluation of the lead–tin system, since it was from this evaluation, done by Linda Warner, that the need for the present study was suggested. The authors also wish to acknowledge the assistance of Raymond L. Orr in the experimental work, and the many helpful suggestions of Raymond L. Orr and Philip D. Anderson in the evaluation.

ADSORPTION OF INERT GASES BY MODIFIED CARBONS

BY W. F. WOLFF AND PHILIP HILL

Research Department, Standard Oil Company (Indiana), Whiting, Indiana

Received December 18, 1958

The adsorption of nitrogen and argon by modified active carbons has been studied by a simple desorption technique. Active carbons modified by the deposition of lithium and various inorganic compounds behave normally; the amount of gas adsorbed at ordinary temperatures and pressures decreases linearly as a function of the amount of modifier. Sodium and potassium cause the development of an unexpected maximum in the adsorption capacity. This anomalous behavior appears to be associated with the formation of new pores.

Introduction

Active carbons have been used as supports for a variety of catalytically and chemically active substances. Interest in these modified carbons has centered on use of them as catalysts and treating agents; unlike the unmodified active carbons, little attention has been given to their physical adsorption characteristics.[1] Such information could be of value both in extending our understanding of the nature of adsorption, and in developing improved adsorbents.

To study this type of adsorption, modified carbons have been prepared by depositing alkali metals and various inorganic compounds on commercial active carbons. The adsorption of nitrogen and argon by these modified carbons at ordinary temperatures and pressures was measured to determine changes in physical adsorption caused by the modifying agent.

Experimental

Commercial active carbons, designated as A, B, C and D, were used without purification. Carbons A and B were separate batches of an 8-to-14-mesh coconut charcoal supplied by E. H. Sargent and Company. Carbon C was a 12-to-20-mesh active carbon from the Burrell Corporation. Carbon D was a 20-to-50-mesh coal-based carbon from Pittsburgh Coke and Chemical Company.

Substances deposited on the active carbons included lithium, sodium and potassium metals, sodium acetate, anhydrous aluminum chloride, sodium hydroxide and a sodium trisulfide solution prepared by boiling an aqueous sodium sulfide solution with an equivalent of sulfur. Gases employed were high-purity nitrogen and standard-grade argon from Linde Air Products Company. Desorbents used in measuring gas adsorption were *n*-heptane of 99+% purity from Phillips Petroleum Company and *n*-dodecane from Humphrey–Wilkinson.

The modified carbons were prepared by contacting the active carbon with the modifier in either a molten or gaseous state. This procedure is conventionally used to disperse sodium on inert supports.[2] Glass equipment was used except for surfaces in contact with aqueous caustic or molten lithium; here, stainless-steel equipment was used. All operations were carried out under an atmosphere of the gas to be adsorbed by the finished composition.

Before depositing alkali metals, anhydrous aluminum chloride, or anhydrous sodium acetate, the carbons were dried by heating to 300° under a stream of the inert gas. The carbon was cooled, and a weighed amount of the modifier was added. The mixture was reheated, with stirring, under a static gas blanket to a temperature above the melting or sublimation point of the modifier. Heating and stirring were continued for about one-half hour beyond the time required to obtain a visually homogeneous product.

Deposition of sodium hydroxide, sodium trisulfide and sodium acetate from aqueous solutions was carried out in a slightly different manner. In each case, enough solution to wet all of the carbon was added, and the mixture was heated under a stream of nitrogen until water removal was complete. A temperature above the melting point of the modifier was maintained for one-half hour.

The modified carbons were cooled to room temperature under a static gas blanket. The amount of adsorbed nitrogen or argon at room temperature and atmospheric pressure was measured by desorption with either *n*-heptane or *n*-dodecane; this procedure has been used in studying the molecular-sieve properties of active carbons.[3] Values given for the volumes of gas desorbed are uncorrected for temperature or pressure; such gas law corrections did not significantly affect the relative size or shape of the desorption curves.

Surface areas and micropore volumes of the active carbons were determined by conventional Brunauer–Emmett–Teller (B.E.T.) nitrogen-adsorption techniques.[4] Gas mixtures were analyzed by mass spectrometry.

Results

Differing amounts of aluminum chloride, sodium acetate, sodium hydroxide and sodium trisulfide were deposited on Carbon A. Nitrogen adsorptions were determined for two or more compositions of each modifier. Figure 1 shows the change in nitrogen adsorption with composition. With the possible exception of sodium hydroxide, the amount of nitrogen adsorbed decreased linearly with increasing concentration of the modifier.

Similar runs were carried out with lithium and with potassium deposited on Carbon A. In runs with lithium, only argon was used, to avoid complications due to chemisorption. The results are plotted in Fig. 2. Lithium showed the expected linear decrease in adsorption, but, with potassium, the amount of argon adsorbed increased linearly to a maximum and then sharply decreased. On replacement of argon by nitrogen, an even more pronounced maximum was obtained.

The results obtained when different carbons were used as supports for the potassium are plotted in Fig. 3. In all cases maxima were obtained, indicating that this phenomenon is general for potassium on active carbon. The differences in size and shape are probably associated with factors such as the differing surface areas and ash contents of the carbons.

Sodium as the modifying agent also gave curves with maxima. The data for sodium on Carbons A and C are plotted in Fig. 4. The plots are significantly different from those for the sodium compounds as given in Fig. 1; only with sodium hydroxide was there any evidence for even the slightest of maxima.

(1) P. H. Emmett, *Chem. Revs.*, 43, 69 (1948).

(2) "High Surface Sodium on Inert Solids," National Distillers Chemical Co., New York, N. Y., 1953.

(3) W. F. Wolff, "The Structure and Activation of Gas-Adsorbent Carbons," presented at the 133rd meeting of the American Chemical Society, San Francisco, Calif., April, 1958.

(4) S. Brunauer, "The Adsorption of Gases and Vapors. Vol. I. Physical Adsorption," Princeton Univ. Press, Princeton, N. J., 1943, pp. 285–299.

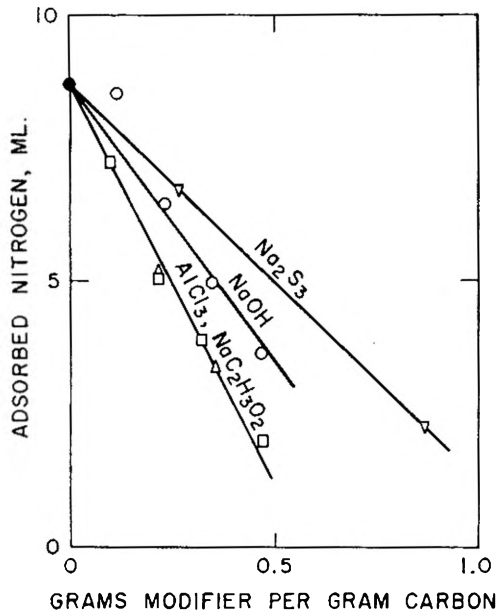

Fig. 1.—Adsorption of nitrogen with inorganic compounds on Carbon A.

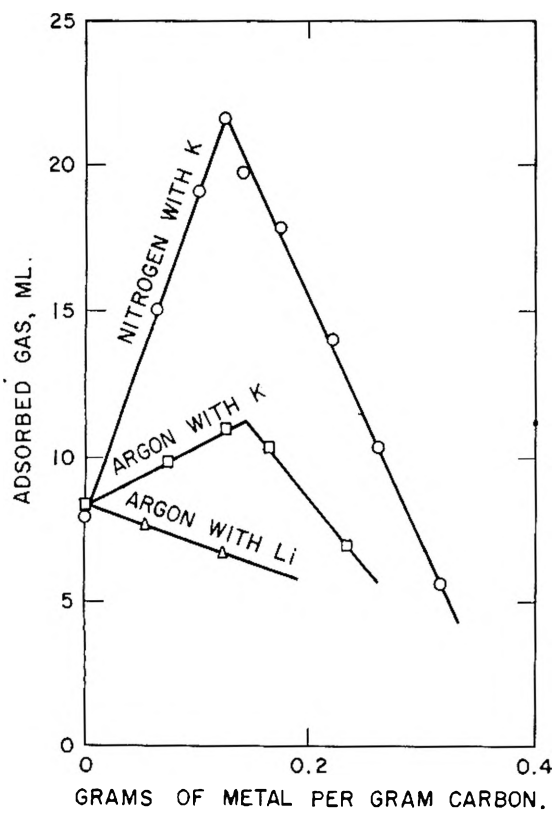

Fig. 2.—Adsorption of inert gases with alkali metals on Carbon A.

In an attempt to establish the cause of the anomalous behavior of the sodium- and potassium-modified carbons, surface areas and micropore volumes were determined for three products obtained after treating Carbon A with the alkali metals. The concentrations of metal used were those that had given compositions with maximum adsorption. Values obtained were

	Surface area, m.²/g. carbon	Micropore vol., cc./g. carbon
Carbon A	1035	0.434
Potassium-modified	1126	.394
Potassium-modified, water-washed	1189	.540
Sodium-modified, water-washed	1144	.559

The surface area was increased by all treatments, although the presence of unremoved metal might have been expected to cause a decrease. The corresponding micropore volume did show the expected decrease. The increases in both surface area and micropore volume of the water-washed products are consistent with earlier results.[5] They suggest that the treatments cause substantial changes in the structure of the carbon. However, these metal-free carbons were almost identical with the original carbon in their adsorption properties.

Additional runs were carried out to check the selectivity of potassium-modified carbon as a nitrogen adsorbent. The data plotted in Fig. 2 indicate that the potassium-containing compositions should adsorb nitrogen preferentially from a nitrogen–argon mixture, whereas the original carbon should show little or no selectivity. Accordingly, mixtures of nitrogen and argon were passed through Carbon A and through the same carbon modified by enough potassium to give the adsorption maximum. The adsorbed gases then were desorbed. Nitrogen:argon ratios of the gas mixtures charged and of the adsorbed gases were

	Charged	Adsorbed
Carbon A	1.11	1.13
Potassium-modified	1.10	1.82

The selectivities are in qualitative accord with those expected on the basis of the individual plots.

Discussion

Although the adsorption plots obtained with the various modified carbons show differences in detail, all consist of linear segments. Their regularity shows that the procedure employed in preparing the modified carbons and the method of measuring adsorbed gas are both reproducible.

The plots obtained with modifiers other than sodium and potassium are the simplest, each being defined by a single line. If the amounts of nitrogen adsorbed and of modifier added are calculated on a molar basis the data show that many molecules of the modifying agent are required to prevent the adsorption of a single nitrogen molecule. This molar ratio remains constant over the entire region studied, where a linear relationship is valid. Accordingly, the modifying agent must be neither particularly attracted to nor restricted from the sites active in the adsorption of inert gas.

The high modifier:nitrogen ratio can be explained on the basis that whole regions of the carbon surface are involved in the inert-gas adsorption. The constancy of the ratio may be interpreted in terms of all possible adsorption sites in these regions being equivalent. Presumably, a specific number of sites are associated with an equal or smaller

(5) E. Berl, *Trans. Faraday Soc.*, **34**, 1040 (1938).

number of modifying-agent molecules, and with a much smaller number of nitrogen molecules or argon atoms.

The structures of active carbons apparently are such that essentially all of the surface is furnished by graphitic planes.[3] This type of surface is uniform and could, in its entirety, constitute a region over which all adsorption sites show equal activity. Alternatively, the nitrogen and argon adsorption may preferentially occur in the narrowest pores. Such pores are believed to be fissures with widths of the same magnitude as the effective diameter of the nitrogen molecule. In such an environment, the freedom of a gas molecule for translational motion would be severely restricted, and it would be subjected to the van der Waals forces of the bounding solid at distances approaching those in a liquid.

Either of these considerations might provide a satisfactory basis for explaining the adsorption plots given by most modifying agents. The same considerations should apply in some degree to the adsorption plots given by sodium- and potassium-modified carbons. Thus, one possible explanation for the development of the characteristic adsorption maxima is that they reflect changes in the electronic structure of the system caused by the modifying agent, the initial filling of adsorption sites being more than counterbalanced by the increased activity of the remaining sites. However, such an explanation does not account for the failure of lithium to behave like either sodium or potassium.

An alternative explanation is that the adsorption maxima are associated with the formation of new regions active in the adsorption of inert gas. With sodium- and potassium-modified carbons, new pores could be formed by penetration of the alkali metal between previously unseparated graphitic planes. The penetration of potassium between the large and closely packed planes that make up crystalline graphite is well established.[6] Sodium fails to penetrate between such large planes, although a combination of sodium and ammonia is effective.[7] For the smaller less-closely packed planes of active carbon,[3] this type of penetration would be facilitated. Thus, despite failure to react with graphite, sodium will react with soot.[8]

The B.E.T. data support the view that sodium- and potassium-treatment cause significant changes in the structure of active carbon. In the case of the potassium-modified carbon a 9% increase in surface area was obtained, accompanied by a more than 100% increase in room temperature adsorption of nitrogen. The results are consistent with the assumptions that interplanar penetration by the alkali metal forms new pores and that such narrow pores provide sites particularly active in the adsorption of nitrogen and argon. Pores of these dimensions have been postulated to account for high initial heats of adsorption of inert gases on graphite.[9]

(6) A. Hérold, *Bull. soc. chim. France*, 999 (1955).

(7) M. L. Dzurus and G. R. Hennig, "Chemistry of the Lamellar Graphite Compounds," presented at the 129th meeting of the American Chemical Society, Dallas, Texas, April, 1956.

(8) K. Fredenhagen and G. Cadenbach, *Z. anorg. Chem.*, **158**, 249 (1926).

(9) R. M. Barrer, *Proc. Roy. Soc. (London)*, **A161**, 476 (1937).

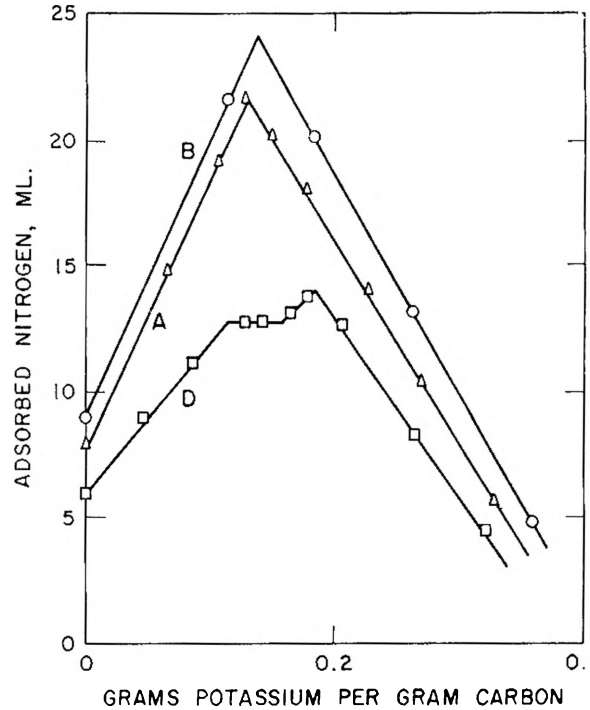

Fig. 3.—Adsorption of nitrogen with potassium on active carbon.

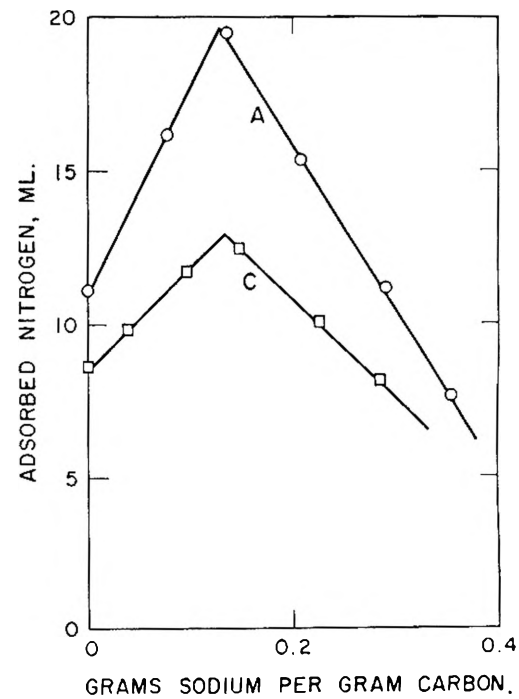

Fig. 4.—Adsorption of nitrogen with sodium on active carbon.

The apparent failure of lithium to give new pores of this type can be attributed to the small size of the lithium atom.

Conclusion

Results obtained thus far seem to favor the view that the effect of modifiers on the adsorptive properties of active carbons is more structural than electronic. The selectivity of potassium-modified char-

coal for nitrogen adsorption, in preference to argon adsorption, can be explained on this dimensional basis, although an electronic interpretation would be equally satisfactory. Further studies of these systems, with respect to the causes of this selectivity and to the nature and spacing of the supported modifying agent, should help to develop a better understanding of the actual forces involved.

SOLUBILITY OF NOBLE GASES IN MOLTEN FLUORIDES. II. IN THE LiF–NaF–KF EUTECTIC MIXTURE

BY M. BLANDER, W. R. GRIMES, N. V. SMITH AND G. M. WATSON

Oak Ridge National Laboratory,[1] *Reactor Chemistry Division, Oak Ridge, Tennessee*

Received December 19, 1958

Solubilities of He, Ne and A were measured at pressures from 1 to 2 atmospheres in a mixture of LiF, NaF and KF (46.5–11.5–42.0 mole %) at 600, 700 and 800°. The solubilities increase linearly with gas pressure, decrease with increasing atomic weight (radius) of the solute and increase with increasing temperature. Henry's law constants in moles of solute/(cm.^{3} of solution)(atmosphere) at 600° are 11.3 ± 0.7 × 10^{-8}, 4.36 ± 0.20 × 10^{-8} and 0.90 ± 0.04 × 10^{-8} and the enthalpies of solution are 8.0, 8.9 and 12.4 kcal./mole for He, Ne and A, respectively. A model which equates the free energy of solution of the gas to the free energy of formation of holes the size of the gas molecules in a continuous fluid having the same surface tension as the solvent yields solubility values which are in good agreement with those observed.

Introduction

Fused salts offer a radically different solvent medium for the study of gas solubilities. In this investigation the solubilities of helium, neon and argon were measured in the eutectic mixture LiF–NaF–KF (46.5–11.5–42.0 mole %) at 600, 700 and 800°. This eutectic mixture is convenient for study because of its relatively low melting point[2] and because of the low partial pressures of its constituents over a wide range of temperatures. This enables one to make measurements over a considerable range of temperatures and leads to a more accurate separation of the enthalpy and entropy of solution.

A previous publication[3] from this Laboratory described the measurements of the solubility of noble gases in molten fluoride mixtures. In that report, values were given for the solubility at 600 to 800° of He, Ne, A and Xe in a NaF–ZrF_4 mixture containing 47 mole % ZrF_4 and a NaF–ZrF_4–UF_4 mixture containing 4 mole % UF_4 and 46 mole % ZrF_4. This work is a continuation of the systematic study of gas solubilities in molten fluoride mixtures in progress at this Laboratory with the aim of elucidating the solvent properties which have an effect on gas solubilities.

Experimental

The rare gases used were obtained in cylinders from commercial sources. He was obtained from the Bureau of Mines at Amarillo, Texas; Ne and A were from Linde Air Products Company. All gases used were shown by mass spectrometric analysis to exceed 99.9% purity. The molten fluoride mixture was prepared from Reagent grade LiF, NaF and KF and purified in a closed system of nickel at 800° by alternate flushing with anhydrous HF and H_2. Chemical analysis of such samples yielded these data

LiF–NaF–KF (46.5–11.5–42.0 MOLE %)

	% by wt. Theor.	Obsd.
Na	6.4	7.5
K	39.8	40.1
Li	7.8	7.1
F	46.0	45.3
Ni	0	30[a]
Fe	0	170[a]

[a] Parts per million.

The apparatus and procedure are identical to those described in a previous publication.[3]

Results

The solubilities and Henry's law constants for He, Ne and A in the molten LiF–NaF–KF eutectic at 600, 700 and 800° are shown in Tables I, II and III. Figure 1 is a plot of Henry's law constants as a function of temperature. The solubility values could be duplicated in separate experiments to about ±5%. The solubility values are in moles of gas per cubic centimeter of solvent and may be converted to other units as desired by use of solvent densities calculated from the equation[4]

$$\rho\ (\text{g./cm.}^3) = 2.47 - 0.68 \times 10^{-3}\, t\ (°\text{C.})$$

Discussion

Solutions of noble gases afford the simplest systems for the interpretation of gas solubilities. The solubilities of the gases studied, all of which obey Henry's law within the experimental precision of ±5%, increase with increasing temperature and with decreasing molecular weight (or atomic radius) of the gas. The enthalpies of solution of all the gases are positive and larger the larger the atomic weight (radius).

It is important to calculate the thermodynamic properties of the solution in such a way that the entropy of solution of a gas is purely a function of solvent–gas interactions. To do this a standard

(1) Operated for the United States Atomic Energy Commission by the Union Carbide Corporation.

(2) A. G. Bergman and E. P. Dergunov, *Compt. rend. Acad. Sci. URSS*, **31**, 754 (1941).

(3) W. R. Grimes, N. V. Smith and G. M. Watson, THIS JOURNAL, **62**, 862 (1958).

(4) S. I. Cohen, W. D. Powers, N. D. Greene and H. F. Poppendiek, Oak Ridge National Laboratory, personal communications.

TABLE I

SOLUBILITY OF HELIUM IN LiF-NaF-KF (46.5-11.5-42.0 MOLE %)

Temp. (°C.)	Saturating pressure (atm.)	Solubility $\times 10^8$ (moles He)/ (cc. melt)	$K_p = c/p \times 10^8$ (moles He)/ (cc. melt) (atm.)
600	2.08	22.1	10.6
	1.77	19.0	10.7
	1.51	16.9	11.2
	1.00	11.0	11.0
	1.00	12.8	12.8
			Av. 11.3 ± 0.7
650	2.08	28.5	13.7
700	2.05	35.5	17.3
	2.04	34.8	17.1
	1.75	30.8	17.6
	1.51	26.3	17.4
	0.98	17.6	17.9
			Av. 17.5 ± 0.2
800	2.06	48.3	23.5
	2.04	48.2	23.6
	1.77	41.8	23.6
	1.51	33.6	22.3
	0.99	21.7	21.9
			Av. 23.0 ± 0.7

TABLE II

SOLUBILITY OF NEON IN LiF-NaF-KF (46.5-11.5-42.0 MOLE %)

Temp. (°C.)	Saturating pressure (atm.)	Solubility $\times 10^8$ (moles Ne)/ (cc. melt)	$K_p = c/p \times 10^8$ (moles Ne)/ (cc. melt) (atm.)
600	2.07	9.57	4.61
	1.49	6.42	4.30
	1.01	4.20	4.16
			Av. 4.36 ± 0.20
700	2.05	15.06	7.36
	1.51	11.04	7.33
	1.02	7.99	7.84
			Av. 7.51 ± 0.22
800	2.07	22.53	10.89
	1.50	16.53	11.00
	1.03	12.05	11.66
			Av. 11.18 ± 0.26

state is chosen in terms of a number of moles per unit volume in both the gas and the liquid and the standard entropy change for the dissolution of a gas is that for the process

$$X_{(g,C_d)} \longrightarrow X_{(d,C_d)} \qquad (A)$$

where X represents one mole of gas. The subscripts g and d denote the gas and liquid phases and C_d is the concentration of the gas dissolved in the liquid which is in equilibrium with the gas at concentration C_g.

In the range of concentrations where the behavior of the gas phase is ideal and where the solubility follows Henry's law in solution, the entropy change for this process is independent of the value or units of C_d. This choice of standard state, which is not the usual one,[5] eliminates the trivial contribution

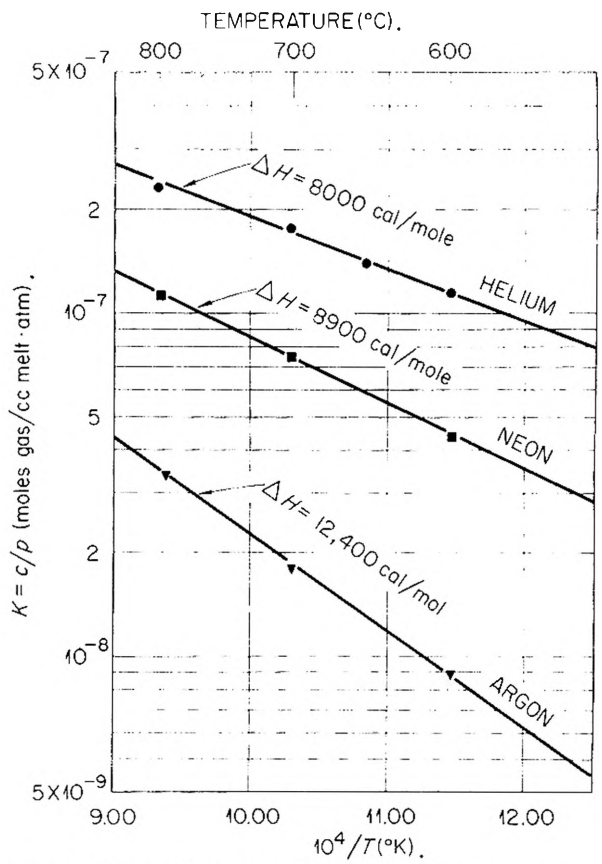

Fig. 1.—Temperature dependences of Henry's law constants for He, Ne and A in LiF-NaF-KF eutectic mixture.

TABLE III

SOLUBILITY OF ARGON IN LiF-NaF-KF (46.5-11.5-42.0 MOLE %)

Temp. (°C.)	Saturating pressure (atm.)	Solubility $\times 10^8$ (moles A)/ (cc. melt)	$K_p = c/p \times 10^8$ (moles A)/ (cc. melt) (atm.)
600	2.02	1.93	0.96
	1.50	1.38	0.92
	1.01	0.83	0.83
			Av. 0.90 ± 0.04
700	2.04	3.81	1.87
	1.50	2.71	1.80
	1.00	1.74	1.74
			Av. 1.80 ± 0.04
800	2.03	6.84	3.37
	1.51	5.16	3.42
	1.00	3.41	3.40
			Av. 3.40 ± 0.03

to the standard entropy of solution which arises from the arbitrary choice of the concentration scale. The standard entropy change ΔS^0 is by this choice purely a function of the properties of the gas in the solvent studied since the only change of significance is the environment of the gas atoms. The total entropy of solution of the gas, which is the entropy change for the equilibrium process

$$X_{(g,C_g)} \rightleftharpoons X_{(d,C_d)} \qquad (B)$$

(5) H. S. Frank and M. W. Evans, *J. Chem. Phys.*, **13**, 478 (1945).

is given by $\Delta S = \Delta H/T$, where ΔH for this process in the LiF–NaF–KF solvent as calculated from Fig. 1 is 8000, 8900 and 12400 cal./mole for He, Ne and A, respectively. C_g is the concentration of gas in the gas phase in equilibrium with the liquid at a concentration C_d. To calculate the standard entropy of solution from this one subtracts the entropy change for the isothermal expansion of the gas

$$X_{(g,C_g)} \longrightarrow X_{(g,C_d)} \qquad (C)$$

from (B) to get

$$\frac{\Delta H}{T} + R \ln \frac{C_d}{C_g} = \Delta S^0 \qquad (1)$$

Values of ΔS^0 for the noble gases are listed in Table IV and prove to be small as had been observed previously[3] in fused salt solutions. Recalculation of data in the literature[5] indicates that this is true in other solvents.

TABLE IV

ENTHALPY AND ENTROPY CHANGES ON SOLUTION OF NOBLE GASES IN MOLTEN FLUORIDE MIXTURES AT 1000°K.

Solvent	Gas	ΔH, cal./mole	ΔS^0, e.u.	Ideal gas expansion $T\Delta S$, cal./mole
NaF–KF–LiF	He	8000	−0.3	8300
(11.5–42–	Ne	8900	−1.0	9900
46.5 mole %)	A	12400	−0.1	12500
NaF–ZrF_4[1]	He	6200	−1.0	7200
(53–47	Ne	7800	−0.4	8200
mole %)	A	8200	−1.5	9700
	Xe	11100	−0.1	11200

The interpretation of these gas solubilities can be made using a model similar to that of Uhlig.[6] Although the model is naive it yields an interesting correlation with experiment. If a gas does not interact with a liquid in which it is dissolved, then the free energy change upon solution is related to the "surface" energy of the hole created by the gas. The solubility of such a gas in a continuous fluid medium can be estimated from the free energy changes in the following steps.

1. Expand the gas from the concentration C_g to C_d.

$$\Delta F_1 = +RT \ln \frac{C_d}{C_g} \qquad (2)$$

2. Shrink the gas atoms to a point and pour in the liquid. The free energy change for this is ΔF_2.

3. Expand the point particles[7]: The free energy change for this is

$$\Delta F_3 = kA\gamma_{mic} - \Delta F_2 \qquad (3)$$

where A is the area of the hole created by the particle, γ_{mic} is a microscopic "surface" tension and k is a constant necessary to obtain the correct units of energy. For spherical atoms $A = 4\pi r^2 N$ and $kA = 18.08r^2$ where r is in Å. The sum of the free energy changes of steps 1–3 is zero if the gas phase is at equilibrium with the gas in the liquid and

$$-RT \ln \frac{C_d}{C_g} = kA\gamma_{mic} \qquad (4)$$

Although a real liquid cannot be considered a continuous fluid it is interesting to speculate that it behaves as if it were one and that γ_{mic} is related to the macroscopic surface tension γ_{mac}.

The area A is at least as large as the surface area of the spherical gas molecules. Because of thermal motions one would expect the size of the hole to be larger than the gas atom. The radii of the rare gas atoms in the solid[9] will be a lower limit of the radius of the hole and the solubility calculated on this basis would be high. In Table V are listed the values of C_d/C_g calculated for the rare gases assuming that $\gamma_{mic} = \gamma_{mac}$ and using the radii of the rare gas atoms in the solid.[9] The numerical values for the surface tensions of the solvent and of the atomic radii of the noble gases are given in Tables VI and VII. A comparison in Table V of the calculated and measured values of C_d/C_g for solutions of noble gases in LiF–NaF–KF and NaF–ZrF_4[3] shows good agreement in view of the oversimplified nature of the model. The magnitude and the variation of the solubility with size of the gas molecule are correctly predicted. This order of the solubility has not often been observed experimentally as most other liquids have surface tensions so low that other solution effects predominate. The difference between the calculated and experimental values is in the direction one would expect if the estimated size of the hole were too small except for argon in LiF–NaF–KF).

TABLE V

COMPARISON OF CALCULATED AND OBSERVED VALUES OF HENRY'S LAW CONSTANTS

Solvent	Gas	Temp. (°C.)	K_c[a] × 10^3 Exptl.	Calcd.	$\frac{K_c \text{ exp.}}{K_c \text{ calcd.}}$
NaF–ZrF_4	He	600	15.5	137	0.11
		700	23.3	188	.12
		800	37.0	243	.15
	Ne	600	8.09	45.9	.18
		700	14.7	74.9	.20
		800	21.7	112	.20
	A	600	3.62	7.33	.49
		700	6.44	16.0	.40
		800	10.6	30.2	.35
	Xe	600	1.39	1.77	.79
		700	2.84	4.84	.59
		800	5.56	10.7	.52
NaF–KF–LiF	He	600	8.09	(28.3)	(.29)
		700	14.0	(46.8)	(.30)
		800	20.3	(70.7)	(.29)
	Ne	600	3.12	(3.94)	(.79)
		700	6.00	(8.63)	(.70)
		800	9.84	(16.4)	(.60)
	A	600	0.645	(0.146)	(4.4)
		700	1.43	(0.509)	(2.8)
		800	2.99	(1.41)	(2.1)
	Xe	600	...	(0.011)	
		700	...	(0.057)	
		800	...	(0.212)	

[a] $K_c = C_d/C_g$.

Thus far solvation effects have been neglected. Polarization of the rare gas atoms by the highly

(6) H. H. Uhlig, THIS JOURNAL, 41, 1215 (1937).

(7) Another path is to decrease the surface tension of the liquid, mix it with the atoms and then increase the surface tension to obtain this same result as suggested by Scatchard.[8]

(8) G. Scatchard, private communication.

(9) V. M. Goldschmidt, "Geochemistry," Oxford University Press, London, 1954.

TABLE VI

SURFACE TENSIONS OF MOLTEN FLUORIDE MIXTURES, DYNES/CM.

Temp. (°C.)	LiF-NaF-KF[a]	NaF-ZrF_4[10]
600	(230)	128
700	(220)	120
800	(210)	112

[a] Surface tension of mixtures estimated from extrapolated values of surface tension of pure components[11] assuming additive surface tension. Surface tension measurements of this mixture have not as yet been made.

TABLE VII

ATOMIC RADII OF NOBLE GASES[9]

	He	Ne	A	Xe
Radius (Å.)	1.22	1.52	1.92	2.18

ionic salt would lead to a smaller standard free energy of solution and greater solubility of the gases. As the polarizability of the rare gas atoms increases in the order He, Ne, A, Xe, an ion induced dipole interaction would cause an increasing trend in the ratio $(C_d/C_g)_{expt}/(C_d/C_g)_{calcd}$ in this same order. The last column in Table V illustrates this trend which may be a consequence of the polarization of the rare gas atom.

Although the values of the solubility may be estimated in this manner, relatively large errors in the temperature coefficients of solubility can enter from even small effects which have been neglected since the derivative of a small number may be large. In the relation

$$\frac{d\Delta F_3}{dT} = -\Delta S^0 = kA\frac{d\gamma}{dT} + k\gamma\frac{dA}{dT} \qquad (5)$$

$d\gamma/dT$ is always negative. In Table IV the standard entropy of solution of the gases listed is small. Since thermal motions of the atoms of the liquid and expansion of the liquid lead to the decrease of γ with temperature one might speculate that the "surface area" of the hole created by the gas atom increases with the liquid expansion so that the product γA is relatively constant in the solvents studied.

Equation 5 leads to another interesting speculation. For a non-spherical molecule dissolved in a liquid, the increase of the "surface area" of the hole created with an increase of temperature will be due not only to thermal translatory motions but will also be increased by the rotation of the gas molecules. At higher temperatures the rotation of the gas molecules becomes more free and the hole becomes larger. This would lead to a more negative entropy of solution for non-spherical molecules than for the spherically symmetric rare gases. This conclusion is consistent with observation in organic solvents.[5]

Conclusions

The model described, in which the free energy of solution of noble gases in molten salts is equated to the free energy of formation of holes the size of the noble gas atom in a continuous fluid which has the same surface tension as the solvent, yields solubility values for the noble gases which agree with the measured values within an order of magnitude. Measurements in other solvents presently in progress at this Laboratory will be needed to test the usefulness of this correlation.

Acknowledgments.—The authors are especially indebted to Dr. P. H. Emmett who first suggested to them the surface tension model used in the present correlation. Many interesting and valuable discussions with Drs. F. F. Blankenship and R. F. Newton are gratefully acknowledged. We are also grateful to Mr. W. D. Harman and associates who were responsible for mass-spectrometric analysis of the many samples submitted.

(10) F. W. Miles and G. M. Watson, Oak Ridge National Laboratory, unpublished work.

(11) F. M. Jager, *Z. anorg. Chem.*, **101**, 177, 180, 185 (1917).

HYDRIDE TRANSFER AND THE MOLECULAR WEIGHT DISTRIBUTION OF POLYPROPYLENE

BY C. M. FONTANA[1]

Contribution from the Research Department of the Socony Mobil Oil Company, Inc., Paulsboro, New Jersey

Received December 19, 1958

Evidence is presented for the occurrence of a hydride transfer reaction in the low temperature polymerization of propylene. The theoretical molecular weight distribution assuming equilibrium hydride transfer agrees closely with the observed distribution. The results are discussed with reference to the mechanism of Friedel–Crafts reactions and the form of alkyl halide–metal halide complexes.

In previous work on the polymerization of 1-olefins with promoted aluminum bromide catalysts,[2,3] it was postulated that a hydride transfer reaction occurs in which the growing carbonium ion abstracts a hydride ion from a tertiary carbon atom in a formed polymer chain. This reaction leads to the formation of a tree-branched polymer of wide molecular weight distribution. The purpose of this paper is to present the evidence for hydride transfer gathered from a careful study of the molecular weight distribution of a sample of polypropylene. Theoretical treatments of the molecular weight distributions to be expected with and without hydride transfer under various conditions of polymerization are also presented and compared to the observed distribution.

(1) Celanese Corporation of America, Summit Research Laboratories, Summit, New Jersey.

(2) C. M. Fontana, G. A. Kidder and R. J. Herold, *Ind. Eng. Chem.*, **44**, 1688 (1952).

(3) C. M. Fontana, R. J. Herold, E. J. Kinney and R. C. Miller, *ibid.*, **44**, 2955 (1952).

Experimental

The preparation of the polymer sample has been previously described.[3] The conditions of synthesis may be summarized briefly as follows: Semi-continuous method, temperature −44°; continuous stage, residence time 30 minutes, HBr/$AlBr_3$ (mole ratio) 0.75, C_3H_6/$AlBr_3$ (mole ratio) 20; batch stage, residence time 150 minutes, C_3H_6/$AlBr_3$ (mole ratio) 100. The polymer was separated initially into sixteen fractions by a fractional precipitation method using acetone and benzene mixed solvents.

The fractionation procedure was not uniform. A fraction containing the highest molecular weight material was prepared by three successive precipitations, each time retaining the precipitate and adding the extract to the remaining solution. This fraction then was separated into two fractions (15 and 16 in Table II) with one additional fractional precipitation. The remaining fractions (14-1) were obtained uniformly in single precipitation steps, fraction 1 being the material finally left in solution. Subsequently, some fractions were separated into components but the molecular weights of these components were not determined. These additional fractionations need not be considered for the purposes of the analysis.

The molecular weights of the lower fractions (1–6) were determined by boiling point rise in benzene using the modified Menzies–Wright apparatus and method described by Barr and Anhorn.[4] Osmotic pressure molecular weight determinations on the higher fractions (7–16) were made using the apparatus and procedure described by French and Ewart.[5] Toluene solvent at 26.9° was used. The membrane material was No. 600 Cellophane obtained from Sylvania Industrial Corporation, Fredericksburg, Va.

TABLE I

MOLECULAR WEIGHT MEASUREMENTS BY THE METHOD OF BOILING POINT RISE

Fraction j	Concn. (wt. %)	Apparent mol. wt.
1	6.15	570
	5.00	575
	4.00	585
	3.20	575
	2.40	590
	(0)	(597)
2	7.00	950
	5.33	970
	3.36	1000
	1.80	1030
	(0)	(1055)
3	7.25	1290
	5.60	1350
	4.05	1400
	1.75	1470
	(0)	(1529)
4	6.33	1560
	4.55	1640
	2.75	1750
	1.05	1780
	(0)	(1843)
5	7.30	2045
	4.15	2250
	2.10	2550
	(0)	(2708)
6	7.00	2550
	4.60	2870
	2.19	3270
	(0)	(3585)

Experimental Results and their Correlation

The ebullioscopic measurements are given in Table I. The molecular weights were determined by extrapolating a straight line obtained by the method of least squares to zero concentration, on a plot of apparent molecular weight *versus* concentration.

The osmotic pressure measurements are given in Table II. The molecular weights were calculated from the limiting values of h/c at zero concentration using the method of least squares on a plot of h/c *versus* c. Experimental results of the fractionation are summarized in Table III. A plot of log (TP_{210}) *versus* log (molecular weight) is shown in Fig. 1.

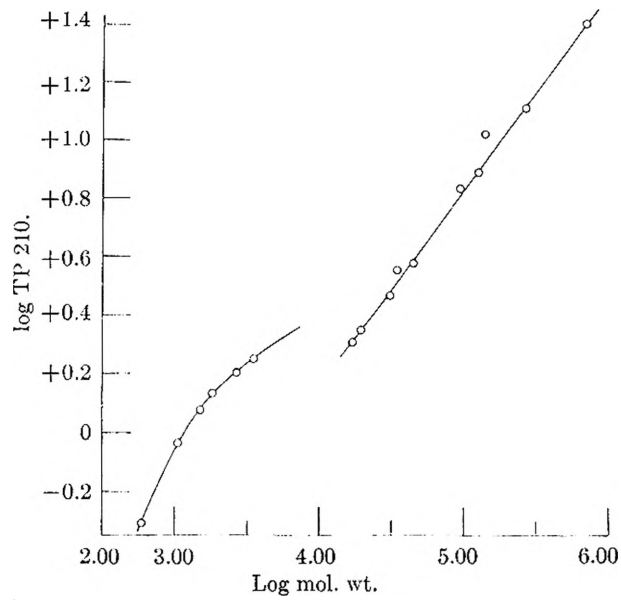

Fig. 1.—Relationship of thickening power (TP 210) to molecular weight for polypropylene fractions.

From Fig. 1 it is immediately apparent that a discontinuity exists between the molecular weight determinations of the two methods. As will be seen later, this is assumed to be due to the presence of low molecular weight material in the higher fractions. The method of treatment thus involves a correction to the osmotic pressure molecular weights, the correction being designed to remove error due to the diffusion of low molecular material through the membrane.

A general method of treating and combining these results to yield the molecular weight distribution is that given by Beall.[6] For the higher fractions the method was modified to simplify the calculations and to take into account the diffusion error in the molecular weights.

In the Beall treatment it is assumed that the molecular weight distribution of each fraction can be characterized by a binomial distribution with negative coefficients

$$\varphi_{j\lambda} = S \frac{n!}{(n-\lambda)!\lambda!} q^{(n-\lambda)} p^{\lambda} \qquad (1)$$

where S is the mole fraction of total sample in the jth fraction, λ is the number of monomer–monomer bonds (DP-1), n and p are the negative binomial coefficients characteristic of each fraction, and $q = 1 - p$. For any given separation a solubility law

(4) W. E. Barr and V. J. Anhorn, *Instruments*, **20**, 342 (1947).

(5) D. M. French and R. H. Ewart, *Anal. Chem.*, **19**, 165 (1947).

(6) G. Beall, *J. Polymer Sci.*, **4**, 483 (1949).

TABLE II

OSMOTIC PRESSURE MEASUREMENTS

Fraction j	Concn., c (g./g. solvent × 10²)	Height, h (cm.)	h/c	Mol. wt.
7	0.392	9.31	2375	
	.294	6.52	2218	
	.196	3.66	1867	
	.098	1.69	1724	
	(0)		(1470)	17,300
8	0.582	11.17	2012	
	.388	7.15	1843	
	.194	2.93	1510	
	(0)		(1286)	19,780
9	0.745	6.72	902.0	
	.561	4.77	850.2	
	.373	3.40	911.5	
	.190	1.50	789.5	
	(0)		(794.1)	32,020
10	1.043	7.25	695.1	
	0.849	5.85	689.0	
	.647	4.43	684.7	
	.198	1.41	712.1	
	(0)		(710.6)	35,790
11	1.201	7.04	586.2	
	1.009	6.20	614.5	
	0.496	2.85	574.6	
	.438	2.42	552.5	
	.202	1.12	554.5	
	(0)		(543.7)	46,770
12	1.401	3.95	281.9	
	1.098	3.03	276.0	
	0.800	2.16	270.0	
	.501	1.30	259.5	
	.206	0.53	257.3	
	(0)		(251.3)	101,200
13	1.327	2.99	225.3	
	1.320	2.73	206.8	
	1.112	2.28	205.0	
	1.028	2.16	210.1	
	0.799	1.61	201.5	
	.738	1.45	196.5	
	.507	1.03	203.2	
	.474	0.91	192.0	
	.201	.44	218.9	
	.184	.30	163.0	
	(0)		(185.7)	136,900
14	1.448	2.65	183.0	
	1.084	1.98	182.7	
	0.764	1.34	175.4	
	.482	0.81	168.0	
	.201	.34	169.2	
	(0)		(164.8)	154,300
15	1.095	0.98	89.50	
	.782	.67	85.68	
	.507	.42	82.84	
	.216	.19	87.96	
	(0)		(84.78)	300,000
16	0.954	0.29	30.40	
	.669	.19	28.40	
	.482	.15	31.12	
	.281	.08	28.47	
	.094	.03	31.91	
	(0)		(30.67)	829,000

TABLE III

SUMMARY OF EXPERIMENTAL RESULTS ON THE FRACTIONATION OF POLYPROPYLENE

Fraction j	Weight,[a] %	TP_{210}[b]	RTP[b]	Mol. wt.
1	3.97	0.49	0.441	597
2	6.39	.92	.614	1,055
3	3.66	1.19	.646	1,529
4	5.00	1.36	.667	1,843
5	5.00	1.60	.690	2,708
6	3.04	1.78	.693	3,585
7	4.62	2.04	.716	17,300
8	7.94	2.24	.747	19,780
9	4.64	2.93	.787	32,020
10	4.87	3.58	.822	35,790
11	12.64	3.76	.827	46,770
12	5.18	6.72	.866	101,200
13	9.36	7.60	.872	136,900
14	9.27	10.33	.918	154,300
15	4.76	12.6	.923	300,000
16	9.66	24.6	.998	829,200

[a] Adjusted to 100% yield. Actual yield 97.4%. Sample weight 455.0 g. [b] Thickening power and relative thickening power previously defined.[3]

of the form

$$X_\lambda = e^{-a\lambda} \tag{2}$$

is assumed, where X_λ is the fraction of molecules of size λ remaining in solution and a is a constant characteristic of the given fractionation.

According to the method of moments, the three equations to be satisfied by the parameters for any given fractionation where the jth fraction is obtained, are

$$S_j = \sum_{j=1}^{j} S[1 - R^n] \tag{3}$$

$$S_j u_j = \sum_{j=1}^{j} Su[1 - e^{-a}R^{n-1}] \tag{4}$$

$$S_j(u + 1 - p_j) = \sum_{j=1}^{j} Su[u + 1 - p - e^{-a} (ue^{-a} + 1 - p)R^{n-2}] \tag{5}$$

where j denotes the fraction numbered from that of lowest molecular weight, $R = 1 + p(e^{-a} - 1)$, $u = np$, and where it is understood that S, R, n, p and u are functions of j. For the last two fractions separated, $j = 1$ (solution), $j = 2$ (precipitate), the three equations are solved for three unknowns: a, n_1 and n_2. For each of the preceding fractions there are only two new unknowns, a and n_j. Beall proposed that the equations to be satisfied then be equation 3

$$bS_j u_j = \sum_{j=1}^{j} Su[1 - e^{-a}R^{n-1}] \tag{6}$$

and

$$b^2 S_j u_j(u_j + 1 - p_j) = \sum_{j=1}^{j} Su[u + 1 - p - e^{-a} (ue^{-a} + 1 - p)R^{n-2}] \tag{7}$$

where b is a new arbitrary parameter.

The values of S and u are calculated readily from the experimental data from the relationships $S_j =$

W_j/kM_j, $k = \sum_j W_j/M_j$, and $u = \overline{DP} - 1 = M_j/42.08 - 1$, where W_j is the weight of the fraction, M_j is the molecular weight and k is determined by summing over all the fractions.

The Beall procedure was used for the two lowest and the two highest fractions. Because of the method of separation the two highest fractions formed an independent sample.

Instead of using the Beall procedure for the higher fractions, it is possible to find values of the constants, a and n_j, which satisfy equations 3 and 4 alone.[7] The procedure adopted for this calculation was as follows: for various likely values of $e^{-a} - 1$ the functions

$$A = \sum_{j=1}^{j-1} S(1 - R^n)$$

and

$$B = \sum_{j=1}^{j-1} Su(1 - e^{-a}R^{n-1})$$

were calculated. From these, values of $R' = ue^{-a}A/B$ were determined with corresponding values of n' obtained from the relationships $R' = 1 + p'(e^{-a} - 1)$ and $u = n'p'$. Using the values of A and n', the values of the function $R'' = (A/S)^{1-n'}$, are determined. The functions R' and R'' are plotted against $e^{-a} - 1$ and the point of intersection gives the true value of $e^{-a} - 1$. Values of R were then found by linear interpolation of R' and the corresponding values of p and n were determined. The final values were checked by equations 3 and 4 in the form

$$\sum_{j=1}^{j-1} S = \sum_{j=1}^{j} SR^n \qquad (8)$$

and

$$\sum_{j=1}^{j-1} Su = \sum_{j=1}^{j} Sue^{-a}R^{n-1} \qquad (9)$$

To treat the higher fractions involving diffusion error in the osmotic pressure molecular weights, the following procedure was used: For the first such fraction ($j = 7$) the true molecular weight was approximated by extrapolating from lower molecular weight values in Fig. 1. This value (mol. wt. = 4,876) was used to obtain the distribution $\varphi\lambda$ for fraction 7, using S and u values calculated by means of the same value of k as used previously. The measured and corrected molecular weights are related by

$$M_c = \left[1 - \sum_{\lambda=0}^{c} \varphi\lambda \Big/ \sum_{\lambda=0}^{\infty} \varphi\lambda\right] \bar{M}_m \qquad (10)$$

where $\bar{M}_c$ is the corrected number average molecular weight and $\bar{M}_m$ is the molecular weight measured by osmotic pressure. From this relationship the value $c = 129$ was determined. This is the critical value of λ corresponding to a molecular weight of 5470 and corresponds to the largest size molecule capable of diffusing through the membrane in order to account for the observed osmotic pressure. This critical size is assumed constant for all higher molecular weight fractions through $j = 14$.

For the higher fractions, starting with $j = 8$, the procedure was as follows: Three or four reasonable values of M (assumed) were taken. For each of these values the parameters and the distributions were obtained as in the foregoing procedure, again using the same value of k. Values of M(calcd.) then were determined by

$$M(\text{calcd.}) = (1 - F)\bar{M}_m$$

where

$$F = \sum_{\lambda=0}^{129} \varphi\lambda \Big/ \sum_{\lambda=0}^{\infty} \varphi\lambda$$

Values of M(calcd.) and M(assumed) were plotted against n and the intersection of the two curves fixed both $\bar{M}_c$ and n. From $\bar{M}_c$ the parameters S, u, n, p and $e^{-a} - 1$ were determined readily as before.

Finally, a new value of k was determined for the whole sample using values of $\bar{M}_c$ in order to determine values of S_j such that $\sum_j S_j = 1$. The final values of the parameters, S, u, n, p, $1 - e^{-a}$ and $\bar{M}_c$ are summarized in Table IV.

The distribution functions for each sample were calculated and summed to about 200 terms in the series

$$1 + \frac{(1 - \epsilon)x}{1!} + \frac{(2 - \epsilon)(1 - \epsilon)x^2}{2!} + \ldots + \frac{(\lambda - \epsilon)(\lambda - \epsilon - 1)\ldots(1 - \epsilon)x^\lambda}{\lambda!} \qquad (11)$$

where $\epsilon = n + 1$ and $x = -p/(1 - p)$, by means of the International Business Machines' "Card Programmed Calculator." Each term multiplied by $S(1 - p)^n$ gives the value of $\varphi\lambda$ at any given λ. Values of the function $\varphi\lambda$ at high λ values were calculated by

$$\varphi\lambda = S\frac{\bar{n}e^{-\bar{n}}}{\Gamma(\bar{n} + 1)}\left(\frac{1}{1 + \bar{p}}\right)^{\bar{n}}\sqrt{\frac{1}{\lambda(\bar{n} + \lambda)}}\left[\frac{(\bar{n} + \lambda)\bar{p}}{\lambda(1 + \bar{p})}\right]^\lambda(\bar{n} + \lambda)^{\bar{n}} \qquad (12)$$

where $\bar{n}$ and $\bar{p}$ are the absolute values of n and p and Γ is the gamma function. The distributions are shown in Fig. 2, together with the over-all sample distribution (circles) obtained by summing the fraction distributions. It may be observed from Fig. 2 that the number distribution follows closely an inverse square law with increasing molecular weight over the range of DP from 20 to about 20,000.

Theoretical Molecular Weight Distributions.—Theoretical molecular weight distributions were derived for two extreme cases (1) assuming no hydride transfer and (2) assuming hydride transfer to be sufficiently rapid that the carbonium ion carbon may be considered to be statistically distributed over all polymer molecules. Both treatments presume a slow growth of many polymer chains throughout the reaction time, a picture consistent with the results of a previous kinetic study of the polymerization of propylene with promoted

(7) An alternative procedure would be to generalize the solubility law to include two arbitrary constants and use equations corresponding to (3), (4) and (5).

TABLE IV

VALUES OF CONSTANTS CALCULATED FROM THE EXPERIMENTAL DATA

	S	u	$-n$	$-p$	$(1 - e^{-q})$	M_c
1	0.2773	13.18	2.207	5.972	40.84	597
2	.2525	24.07	3.542	6.796	40.84	1,055
3	.09981	35.34	0.9653	36.61	8.76	1,529
4	.1131	42.80	1.699	25.19	7.28	1,843
5	.07696	63.35	0.5844	108.4	3.78	2,708
6	.03535	84.19	.5609	150.1	1.45	3,585
7	.03950	114.9	.4478	256.6	1.40	4,876
8	.04438	176.3	.4446	396.5	1.303	7,460
9	.01560	293.8	.2661	1,104	0.387	12,405
10	.01177	409.2	.3253	1,258	.261	17,260
11	.01971	634.7	.3705	1,713	.373	26,750
12	.004445	1,154	.1910	6,042	.0712	48,600
13	.005035	1,841	.2235	8,238	.0730	77,500
14	.003410	2,693	.3553	7,580	.0433	113,350
15	.0006617	7,128	.9751	7,310	.5908	300,000
16	.0004857	19,704	1.925	10,238	.5908	829,200

aluminum bromide at low temperatures.[8] Both treatments also imply no chain termination or other chain transfer mechanism.

(a) **Without Hydride Transfer.**—Consider the statistical distribution of N molecules of monomer among c growing chains, the probability for any given monomer adding to a given chain being $1/c$. In a batchwise polymerization, the probability of obtaining the nth-mer, which is the resulting mole fraction of nth-mer in the polymer, is given by Bernouilli's theorem

$$P_n = \frac{N!}{n!(N-n)!}\left(\frac{1}{c}\right)^n\left(\frac{c-1}{c}\right)^{N-n} \qquad (13)$$

where n is the degree of polymerization.

Applying the Stirling approximation to the factorials in the form $n! = n^n e^{-n}\sqrt{2\pi n}$, and letting $N \to \infty$, $c \to \infty$, and $N/c = s$, (the olefin-to-catalyst ratio) the resulting distribution function becomes

$$P_n = \frac{e^{n-s}}{\sqrt{2\pi n}}\left(\frac{s}{n}\right)^n \qquad (14)$$

For a continuous polymerization stage (CFSTR), the distribution may be obtained from equation 14 by multiplying by $e^{-s/s'}/s'$ and integrating over s, where s' is the olefin-to-catalyst mole ratio. The result is

$$P_n' = \frac{s'^n}{(s'+1)^{n+1}} \qquad (15)$$

If the continuous stage is followed by a batch stage (semi-continuous method) the final distribution is

$$P_n'' = \sum_{r=0}^{n} P_{n-r}P_r' = \sum_{r=0}^{n} \frac{e^{-t}t^{n-r}s^r}{(n-r)!(s+1)^{r+1}}$$

$$= \frac{s^n e^{-t}}{(s+1)^{n+1}} \sum_{r=0}^{n} A^r/r! \qquad (16)$$

where $A = t(s+1)/s$, t is the ratio of olefin-to-catalyst in the batch stage and s is the ratio of olefin to catalyst in the continuous stage.

The distribution (16) was calculated using the parameters corresponding to the experimental conditions $t = 133.3$, $s = 26.67$ and the results are given in Fig. 2 as curve A.

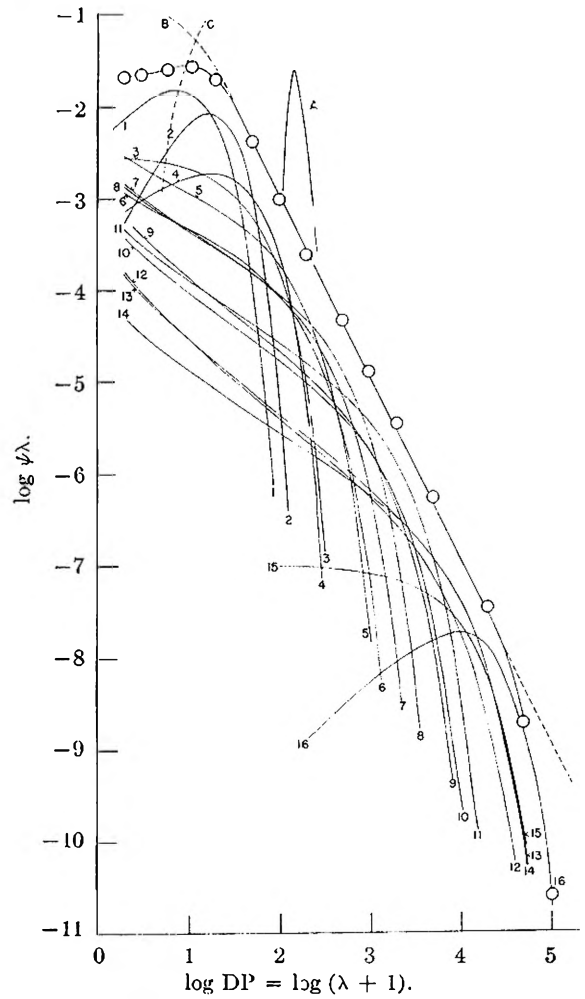

Fig. 2.—The distributions: circles represent the most probable experimental distribution obtained by summing the individual probable distributions of the fractions.

(b) **With Equilibrium Hydride Transfer.**—In a continuous flow reactor under conditions of equilibrium with respect to hydride transfer, there are n/s carbonium ion carbons associated with the P_n, nth-mers. At steady-state conditions

(8) C. M. Fontana and G. A. Kidder, *J. Am. Chem. Soc.*, **70**, 3745 (1948).

$$\frac{dP_n}{dt} = k_1 \frac{n-1}{s} P_{n-1} - k_1 \frac{n}{s} P_n - k_4 P_n = 0 \quad (17)$$

where k_1 is the rate constant for the addition of monomer, and k_4 is the rate constant for removal of macromolecules (= rate constant for addition of catalyst). The distribution function is the solution of equation 17, or

$$P_n = \frac{A}{n(n+1)} \quad (18)$$

where A is a normalization constant ($A = 1$ for $\sum_1^\infty P_n = 1$).

If the continuous stage is followed by a batch stage, the differential equation to be solved is

$$\frac{dP_n}{dt} = \frac{n-1}{s+t} P_{n-1} - \frac{n}{s+t} P_n \quad (19)$$

and its solution is

$$P_n = A \frac{[1-(1-y)^n(1+ny)]}{n(n+1)y} \quad (20)$$

where $y = s/(s+t)$, s and t are the olefin-to-catalyst ratios in the continuous and batch stages, respectively, and A is a normalization constant ($A = 1$ for $\sum_1^\infty P_n = 1$). This is the distribution function for semi-continuous polymerization assuming equilibrium hydride transfer.

Discussion

Following its initial discovery,[9] the hydride transfer reaction is now generally recognized in various high temperature carbonium ion reactions such as catalytic cracking, isomerization and conjunct polymerization of hydrocarbons.[10] In alkylation it forms an essential step of the carbonium-ion mechanism. Recently, it has been postulated to occur at low temperatures (−80°) in the self-alkylation of isobutane in the system HF–BF_3.[11] However, its occurrence in low temperature polymerization with promoted aluminum bromide appears to be unique and forms the basis for the synthesis of some novel polymers from 1-olefins.[2,3] Heretofore, the evidence for the occurrence of hydride transfer in low temperature polymerization, although convincing, has been mainly qualitative. In this paper more quantitative evidence is considered.

On comparison of the theoretical curve A, assuming no hydride transfer, with the experimental distribution it is found that this theory is wholly inadequate to account for the wide molecular weight distribution observed. Moreover, it is difficult to find reasonable reactions, other than hydride transfer, which can account for such a high poly-dispersity.

The theoretical curve B, assuming equilibrium hydride transfer, agrees very well with the observed distribution except at very low and at very high molecular weights. The discrepancy at the low molecular weight end (which results in $A = 2$ instead of $A = 1$), can be largely accounted for by the prior removal of small molecules in the stripping operation. Thus, assuming that the partial pressure of any one component is no greater than about 1 mm. at 250°, the mole fraction of each component in the finished polymer would be limited approximately to curve C (Fig. 2). This result is strongly suggestive that the observed maximum in the molecular weight distribution was caused by removing the polymer product. If it is assumed that the distribution of unremoved polymer is correctly given by the distribution law (equation 24) with $A = 1$ at the low end, and that low molecular weight components were removed under the conditions described above, the amount of polymer removed can be calculated readily. The result shows that 45.5 mole % or 3.1 weight % of the original polymer could have been removed in this way. This would account for the observed discrepancy at the low molecular weight end.

It is instructive to compare the observed average degree of polymerization ($\overline{DP}$) with the experimental monomer-to-catalyst ratio. From the results in Table IV, $\overline{DP} = \sum_j \bar{S} M_c = 99.1$. Assuming the original distribution to be given by equation 20 with $A = 1$, $\overline{DP} = \sum_1^n nP_n = 1 + \frac{1}{y}\left(\sum_1^n \frac{1}{n+1} - 1\right)$ = 54.8 (n_f = 30,000). Correcting the observed distribution for loss of light material as above, the corrected value for the original polymer becomes $\overline{DP}$ = 55.7. Thus, while the average degree of polymerization is somewhat uncertain, due to the uncertainties in the distribution at the low end, the more probable figure is about 55. This is nearly one-third the monomer-to-catalyst (promoter-limited) ratio used experimentally. (This means that possibly three macromolecules were formed per promoter-catalyst couple). This may indicate a slow inactivation of randomly situated carbonium ions due to the formation of resonating carbonium ions of the type

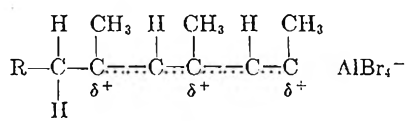

a process which requires two proton transfers (presumably to monomer, starting a new chain) for each catalyst–promoter couple inactivated. It is also indicated that other proton transfer reactions are not predominant under these conditions of polymerization.

The discrepancy between theory and experiment at the high molecular weight end of the distribution is believed to be due to failure to establish equilibrium with respect to hydride transfer during chain growth. Since the hydride transfer reaction is one between macromolecules, the rate of reaction must decrease with increasing size as a result of steric effects. At some size the rate of hydride transfer will not be sufficiently high to enable the macromolecule to accumulate its equilibrium portion of carbonium ions. This should result in a slight positive deviation from theory at molecular weights below a critical limit and a large negative deviation

(9) P. D. Bartlett, F. E. Condon and A. Schneider, *ibid.*, **66**, 1531 (1944).

(10) For a recent review see L. Schmerling, *Ind. Eng. Chem.*, **45**, 1447 (1953).

(11) C. K. Donnell and R. M. Kennedy, *J. Am. Chem. Soc.*, **74**, 4162 (1952), and previous papers of this series.

above this limit. This is approximately what is observed.

The extent of isomerization of carbonium ions during chain growth in this polymerization system remains an open question. Certain limitations in the rate of isomerization, however, are indicated. Thus it may be seen readily that a catalyst which isomerizes sufficiently rapidly during chain growth so as to eliminate all tertiary hydrogens, could not subsequently promote an intermolecular hydride transfer reaction and would not yield polymers of this type.

The present picture of polymer growth, if accepted, does lead to some interesting conclusions with respect to the nature of carbonium ion complexes in hydrocarbon media. It is clear that no appreciable concentration of free carbonium ions is allowed, otherwise equilibration with respect to hydride transfer would involve a very different distribution due to the accumulation of positive charge on a single molecule. Of course, energetic considerations alone rule out this possibility in hydrocarbon media.

The requirement of random distribution of carbonium ion complexes can be met if it is assumed that the complexes exist either as ion pairs or as coördinated complexes, or both. However, if more than one form of the complex exists and it is assumed that only one form reacts, then it is necessary that a reasonably rapid rate of interconversion exists, otherwise the postulate of random addition of monomer could not possibly be valid. If the two forms are assumed to be essentially at equilibrium, the picture is inconsistent with the previous kinetic results.[8]

The kinetics of polymerization are explained on the basis of a rapid and reversible association of monomer with complex, followed by an unimolecular, rate-determining rearrangement step. The sum of the concentration of complex and monomer-associated complex is assumed constant. This sum will not be constant if the active complex is in equilibrium with an appreciable amount of a non-reactive complex. One is thus led to examine the validity of the postulate, commonly assumed, that alkyl halide–aluminum halide complexes exist in two forms.

From a theoretical standpoint, Fairbrother[12] considered the question of the existence of the transition of covalent alkyl halide to ionic alkyl halide brought about by electrophilic metal halides. In considerations of this kind it is generally assumed that if the hypothetical potential energy curve for the ionic state is lowered sufficiently by solvation so that it crosses the hypothetical potential energy curve for the covalent state, there exists the possibility of two states with a potential energy hump between them. These theoretical considerations all seem to be inconclusive because it apparently is impossible to determine whether or not the resonance interaction between the hypothetical states will be high enough to yield only one minimum in the potential energy curve as a function of carbon–halogen distance.

On the other hand, all the experimental evidence of which this author is aware is consistent with the view that only one form exists for any given complex. Fairbrother[12] interpreted the substantial increase in polarization of ethyl bromide upon addition of aluminum bromide in cyclohexane solution to be due to the formation of a relatively small percentage of ion pairs. Alternately, these results could be interpreted by assuming the formation of a substantial amount of a less polar complex. Fairbrother and Wright[13] find the trityl bromide–stannic bromide complex to be mainly ionic. There was no evidence for the covalent complex, although a relatively small amount was considered possible. Bentley and Evans[14] report the trityl chloride–mercuric chloride complex to be mainly ionic. From an examination of the properties of 1:1 complexes of gallium chloride and aluminum halides with primary alkyl halides, Brown, *et al.*,[15] conclude these addition compounds exist primarily in non-ionic form and undergo ionization only slowly, if at all. However, in this same paper, two different mechanisms of alkylation of aromatic hydrocarbons are proposed, based essentially on the premise that two types of alkyl halide–metal halide complexes exist. The existence of only one such complex would clearly result in one mechanism of alkylation, a mechanism identifiable with Swain's concerted displacement mechanism.[16] After about seventeen more papers on the catalytic halides, Brown, *et al.*,[17] still have not found positive evidence for the existence of two distinct forms of the metal halide–alkyl halide complexes.

More recently, the idea of two separate forms of certain complexes has been invoked more generally. For example, Winstein's[18] formulation into classes I (covalent) and II (internal ion pair) is analogous to the above. The same question is also involved in controversial mechanisms of substitution[19] at a saturated carbon atom. However, further discussion of this question is beyond the scope of this paper.

On the basis of presently available evidence, it is believed that, in general, only one form of a metal halide–alkyl halide complex exists, a form which is neither purely ionic, nor purely coördinated, but a resonance hybrid of these two extremes. This view is consistent with the previously expressed views on the nature of carbonium ion–anion bonds discussed in connection with the mechanism of hydride transfer.[3]

(12) F. Fairbrother, *J. Chem. Soc.*, 503 (1945).

(13) F. Fairbrother and B. Wright, *ibid.*, 1058 (1949).

(14) A. Bentley and A. G. Evans, *Research*, **5**, 535 (1952).

(15) H. C. Brown, H. W. Pearsall, L. P. Eddy, W. J. Wallace, M. Grayson and K. L. Nelson, *Ind. Eng. Chem.*, **45**, 1462 (1953), and previous papers.

(16) C. G. Swain and W. P. Langsdorf, Jr., *J. Am. Chem. Soc.*, **73**, 2813 (1951), and previous papers of this series.

(17) F. R. Jensen and H. C. Brown, *J. Am. Chem. Soc.*, **80**, 3039 (1958).

(18) S. Winstein, E. Clippinger, A. H. Fainberg and G. C. Robinson, *Chemistry and Industry*, 664 (1954).

(19) E. P. Hughes, C. K. Ingold, S. F. Mok, S. Patai and Y. Pocker, *J. Chem. Soc.*, 1265 (1957) and related papers.

PARTIAL VAPOR PRESSURE AND ENTROPY OF SOLUTION OF IODINE

BY JOHN WALKLEY AND JOEL H. HILDEBRAND

Contribution from the Department of Chemistry, University of California, Berkeley, California

Received December 20, 1958

Measurements of the partial vapor pressure of iodine at 25° from its solutions in CCl_4 and CS_2 are reported giving values for $(\partial \ln p_2/\partial \ln x_2)_T$ of 0.98 and 0.86, respectively. These are combined with values of $R(\partial \ln x_2/\partial \ln T)$ from solubility to give for the entropy of solution of solid iodine, 21.5 and 16.2 cal. deg.$^{-1}$ mole^{-1}, respectively. These values are independent of the assumptions contained in regular solution theory, including extrapolated properties of liquid iodine.

The senior author,[1] in 1952, called attention to the straight lines obtained by plotting log x_2, where x_2 is the solubility of a non-polar solid, such as iodine, against log T, instead of the usual $1/T$, and he and Scott[2] in the same year discussed the entropy of solution of the solid as given by the purely thermodynamic relation

$$\bar{s}_2 - s_2^S = R\left(\frac{\partial \ln a_2}{\partial \ln x_2}\right)_T\left(\frac{\partial \ln x_2}{\partial \ln T}\right)_{sat} \qquad (1)$$

a denotes activity referred to pure liquid solute as standard state. The factor, $\partial \ln a_2/\partial \ln x_2$ was estimated by aid of the regular solution equation

$$\ln a_2 - \ln x_2 + v_2\phi_1^2(\delta_2 - \delta_1)^2/RT \qquad (2)$$

v_2 denotes molal volume of the solute as supercooled liquid; the δ's are solubility parameters. This factor is unity when Henry's law is obeyed, which is practically the case where the solubility is small. We calculated 0.96 in CCl_4, 0.98 in C_7H_{16} and 0.998 in C_7F_{16}. In CS_2, however, it fell to 0.81.

Hildebrand and Glew[3] found that a plot of $R(\partial \ln x_2/\partial \ln T)$ against $-\log x_2$ for iodine solutions gives a straight line, beginning with CS_2, through a tenfold range in x_2. The linear range was later extended to 50-fold by Shinoda and Hildebrand.[4]

The present study was undertaken in order to convert $R(\partial \ln a_2/\partial \ln T)_{sat}$ to entropy in the case of the CS_2 solution by a direct, experimental evaluation of the Henry's law factor. For this, we replace $\partial \ln a_2/\partial \ln x_2$ by $\partial \ln p_2/\partial \ln x_2$, where p_2 is the partial vapor pressure of iodine from its solution.

Experimental

The partial vapor pressure of iodine was determined by extracting and titrating the iodine vapor from a large flask, 3.126-liters capacity, connected by a wide neck with a small bulb, 200 cc., holding the solution. The latter was immersed in a thermostat maintained at 25.000 ± 0.001°; the flask was above the water in an air thermostat held at 26.00 ± 0.05° to prevent condensation upon its walls. This difference of 1° was found to be adequate.

The two vessels were connected by a ground-glass joint, sealed vacuum tight with Apiezon wax. Both vessels were thoroughly cleaned and dried. A solution was placed in the lower one; the two vessels were connected and sealed; the solution was frozen in a Dry Ice–alcohol bath, and the apparatus was evacuated through a capillary tube in the neck, which was then sealed off. The apparatus was placed in position in the double thermostat. After about 24 hours, with frequent agitation, equilibrium was reached. The apparatus was removed, and the bulbs quickly separated. The mole fraction of iodine in the solution was determined by titration in the usual manner. The vapor of iodine was absorbed in KI solution, using successive portions until there was no further coloration. The vapor pressure of iodine was calculated upon the assumption that at these dilutions it obeys the ideal gas law. The validity of this assumption is attested by the fact that our value for the saturated solution, 0.305 mm., agrees well with the vapor pressure of solid iodine, 0.309 mm., determined by Gillespie and Frazer,[5] using a flexible diaphragm.

We made preliminary measurements with CCl_4 solutions, and also with solutions in $CHBr_3$. The results in the latter were somewhat scattered, possibly on account of instability of the solvent, and were not sufficiently reliable for our purpose. The data for the other two solutions are given in Table I.

TABLE I

PARTIAL VAPOR PRESSURES AND MOLE FRACTIONS OF IODINE AT 25°

CCl_4		CS_2	
p_2 (mm.)	$100x_2$	p_2 (mm.)	$100x_2$
0.076	0.271	0.086	1.38
.138	.518	(.172)	2.29
.181	.679	.191	3.22
.234	.893	.264	4.63
.305	1.148	.282	5.00
		.305	5.46

A plot of log p_2 against log x_2 gives a curved line in the case of the CS_2 solution, but log (p_2/x_2) against x_1^2 gives a straight line with a slope of 0.60. All points except the one in parentheses in Table I fall closely upon this line. From this we calculate $\partial \ln p_2/\partial \ln x_2 = 0.86$, with which the earlier, indirect figure, 0.81, is in fair agreement.

Table II gives the entropy of solution of solid iodine as determined from these data.

TABLE II

ENTROPY OF SOLUTION OF SOLID IODINE AT 25°

Solvent	$\left(\frac{\partial \ln p_2}{\partial \ln x_2}\right)_T$	$R\left(\frac{\partial \ln x_2}{\partial \ln T}\right)_{sat}$	$\bar{s}_2 - s_{2,}$ cal. deg.$^{-1}$ mole^{-1}
CCl_4	0.98	21.9	21.5
CS_2	0.86	18.8	16.2

We defer discussion of these values of entropy till we have the results of a study nearly completed which will enable us to take into account the contribution of expansion to entropy of solution in these and other cases.

This research has been supported by the National Science Foundation.

(1) J. H. Hildebrand, *J. Chem. Phys.*, **20**, 190 (1952).

(2) J. H. Hildebrand and R. L. Scott, *ibid.*, **20**, 1520 (1952).

(3) J. H. Hildebrand and D. N. Glew, THIS JOURNAL, **60**, 618 (1956).

(4) Kōzō Shinoda and J. H. Hildebrand, *ibid.*, **62**, 292 (1956).

(5) L. J. Gillespie and L. H. D. Frazer, *J. Am. Chem. Soc.*, **58**, 2260 (1936).

THE DISSOCIATION PRESSURE OF ALUMINUM CARBIDE[1]

BY DAVID J. MESCHI AND ALAN W. SEARCY

Department of Mineral Technology, University of California, Berkeley, California

Received December 27, 1958

The vapor pressure of Al_4C_3 has been measured in the region from 1500 to 1800°K. by means of the Knudsen effusion method and of a torsion method. ΔH^0 at 1600°K. was calculated for the reaction $Al_4C_3(s) \rightarrow 4Al(g) + 3C(s)$ by means of the second law and the third law, and respective values of 89 (±3) kcal./mole Al and 87 (±3) kcal./mole Al were obtained. The results indicate carbon content of no more than 2% in the vapor when aluminum carbide is dissociated at 1600°K.

Some years ago, attempts were made to prepare aluminum by reaction of the oxide with carbon and subsequent distillation of aluminum from the product carbide.[2-4] The metal thus obtained contained a high percentage of carbon as an impurity. Since carbon has a low vapor pressure at the temperature of the experiments, the presence of so much carbon in the condensate appeared to indicate an important gaseous aluminum carbide molecule. Zeeman has since found and analyzed the spectrum of AlC,[5] but the dissociation energy that he reported for this molecule was much too low to account for the reported concentration of carbon in the vapor from aluminum carbide dissociation.

Because no other metal was known to form a gaseous carbide molecule, further investigation of the vaporization of aluminum carbide appeared to be of great interest. Dissociation pressure measurements, vapor molecular weight determinations and material balance studies accordingly were initiated. While this work was in progress, a mass spectrographic investigation of the existence and stabilities of gaseous aluminum carbides was reported by Chupka and his co-workers.[6] Their work will be referred to in the course of the paper.

Experimental

Dissociation pressures for aluminum carbide were measured by two techniques: the Knudsen technique and the torsion cell technique as described by Searcy and Freeman.[7]

The Knudsen method requires a knowledge of the molecular species present; the torsion method does not. Theoretically, then, these two methods used together would give both the vapor pressure and an average molecular weight of the vapor. However, the inaccuracies inherent in the two methods are great enough so that a small percentage of a particular species cannot be detected unless its molecular weight is very different from that of the other species present.

The cell used in the Knudsen studies consisted of a graphite crucible fitted with a graphite lid through which an orifice had been drilled. The crucible itself was placed in a graphite casing and covered with a thin disk of graphite. This disk had a hole centered over the orifice in the lid to allow the vapor to escape. Thus, with the exception of the small area immediately surrounding the orifice, the cell proper was completely covered.

The assembly was heated *in vacuo* by means of a radio-frequency induction heater. In an effusion cell of uniform diameter the lid tended to be somewhat cooler than the bottom of the crucible. To reduce this temperature gradient and thus prevent aluminum carbide formation on the under surface of the lids, the upper part of the graphite casing was made larger in diameter than the lower part and was covered with tantalum sheet which acted both as a radiation shield and a susceptor. When these precautions had been taken, no deposit could be detected on the lid. To test the background cell weight losses, a casing which permitted two cells to be heated at once was used in one of the series of runs. An empty cell was placed in the casing upside down, followed by a graphite spacer. The cell containing the sample was then placed on top. Experiments with two empty cells in this assembly demonstrated that both cells gained or lost approximately the same weight in a given cycle. The empty lower cell thus provided a correction for cell weight changes due to background effects.

Techniques and apparatus used in determining the vapor pressure by the torsion method were essentially those described by Searcy and Freeman,[7] except that resistance heating was substituted for induction heating. This change was made to avoid the erratic oscillations caused by the strong electromagnetic field of an induction heater.

A vertical tube of 10 mil tantalum sheet served as the resistance element. The heating element and cell were encased in a water-cooled metal can to the top of which was attached a vertical glass tube about three feet long and approximately four inches in diameter. A side arm on this tube connected the system to the vacuum pumps. A vacuum of approximately 10^{-5} mm. could be obtained.

The torsion wire was attached to a glass cap which was fitted to the top of the tube by a standard taper joint. Angular deflections were read by means of a mirror mounted on the cell suspension.

The torsion cell itself was identical in design to that described by Searcy and Freeman, except that the cell was not covered by a metal radiation shield.

Torsion fibers were 2 mil tungsten wires approximately 34 cm. long. The torsion constants of the fibers were usually about 3 dyne cm. per radian.

Torsion experiment pressures were calculated by means of the formula: $P = 2DY/(d_1a_1 + d_2a_2)$, where P is pressure, D is the torsion constant of the wire, Y is angular deflection, d is the moment arm of the orifice, and a is the area of the orifice.

In both the Knudsen and torsion techniques, account must be taken of the fact that the orifice is not a hole in an infinitely thin plate, but is actually a channel of finite length. The channel length corrections are different for the two techniques. Derivation and evaluation of the correction factors are discussed by Freeman and Searcy in a previous paper.[8]

Aluminum carbide was synthesized in the cells from aluminum powder and excess graphite powder. The aluminum, a sample kindly provided by the Aluminum Company of America, contained no more than 0.005% impurities, these being mostly Cu, Fe and Si. The graphite was National Carbon, grade SP-2, special spectroscopic quality powder. The powders were mixed directly in the cells and heated *in vacuo* to 1000° or higher for approximately a half-hour in order to form the carbide. An X-ray powder photograph made of a sample prepared in this manner showed only lines due to Al_4C_3 and graphite. To prevent hydrolysis of the carbide, exposure to atmospheric moisture was avoided except for the brief periods necessary to transfer the cells to and from the vacuum line.

All temperature readings were made by means of a Leeds and Northrup optical pyrometer.

(1) This work was supported by the Metallurgy and Materials Branch of the Atomic Energy Commission.

(2) W. D. Treadwell and A. Gyger, *Helv. Chim. Acta*, **16**, 1214 (1933).

(3) W. D. Treadwell and J. Hartnagel, *ibid.*, **17**, 1384 (1934).

(4) O. Ruff, E. Jellinek and T. Foehr, *Z. Elektrochem.*, **24**, 157 (1918).

(5) P. B. Zeeman, *Can. J. Phys.*, **32**, 9 (1954).

(6) W. A. Chupka, J. Berkowitz, C. F. Giese and M. G. Inghram, THIS JOURNAL, **62**, 611 (1958).

(7) A. W. Searcy and R. D. Freeman, *J. Am. Chem. Soc.*, **76**, 5229 (1954).

(8) R. D. Freeman and A. W. Searcy, *J. Chem. Phys.*, **22**, 762 (1954).

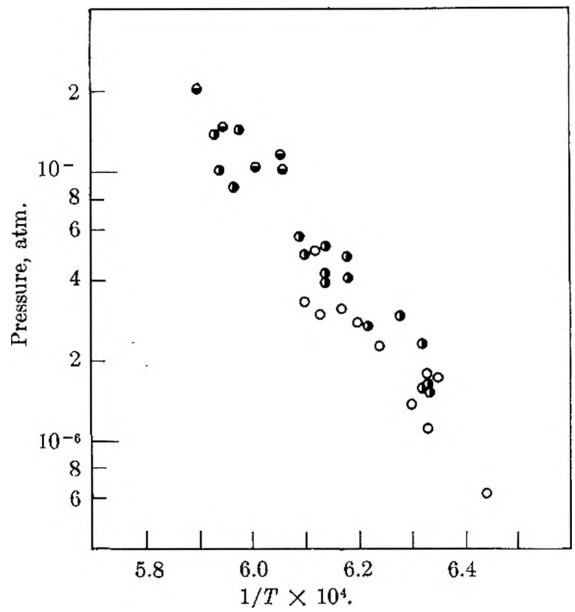

Fig. 1.—$1/T$ *vs.* pressure.

Orifice { A B C

Area, cm.² 0.0460 0.0165 0.00477

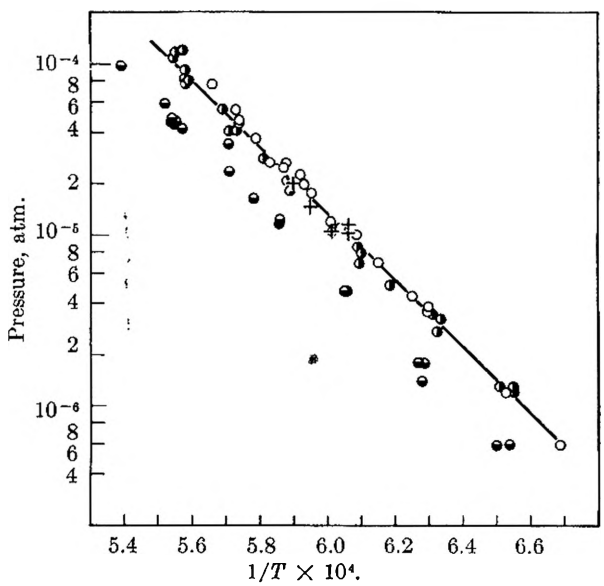

Fig. 2.—$1/T \times 10^4$ *vs.* pressure: ○, torsion run 1; ◒, torsion run 2; ◑, torsion run 3; +, Knudsen run, orifice C.

Dissociation Pressure Results.—Knudsen vapor pressure measurements were made on four different samples with the use of three different orifice sizes. Results of these three runs are plotted in Fig. 1. Pressures were calculated on the assumption that the vapor was monoatomic aluminum. The quoted orifice areas are the actual areas multiplied by a Clausing factor which corrects the Knudsen equation for the effect of a wall of finite thickness.[8,9]

The Knudsen method requires the assumption that the amount of vapor which effuses through the orifice is too small to lower the pressure within the cell appreciably below the equilibrium value. Either the formation of a protective coating of graphite on the aluminum carbide or a slow step in the evaporation process could reduce the rate of evaporation of aluminum enough to render the assumption invalid. It is evident from the plot that, with the two larger orifices at least, the equilibrium pressure was not attained.

After each of the series of runs, the sample in the Knudsen cell was examined. In all cases a layer of graphite several millimeters thick was found at the top of the sample. Under this the yellow aluminum carbide could be seen. Thus a barrier to evaporation of aluminum was present, as the variation in apparent pressure with hole area suggests and, with the two larger orifices at least, this barrier was enough to cause a significant drop in the measured vapor pressure. Calculation of the pressures for zero orifice area by the method of Searcy and Peavler[10] yields values that are, to the limits of the random error, identical with the pressures obtained with the smallest orifice. Those pressures obtained with the smallest orifice are listed in Table I.

Column 3 of the table, headed "Blank wt. change," gives the weight loss or gain of an empty cell which was heated simultaneously with the cell that contained the sample. Sample weight losses in column 4 have been corrected for the weight fluctuation of the empty cell. The runs are listed in the order in which they were made.

TABLE I

KNUDSEN RUNS USING ORIFICE C (AREA = 4.77×10^{-3} CM.²)

Temp., °K.	Duration, sec.	Blank wt. change, mg.	Sample wt. loss, mg.	Pressure, atm. × 10^6
1695	6300	+0.01	3.40	20.2
1681	6420	+ .02	2.55	14.8
1664	9840	+ .06	2.77	10.4
1650	11460	− .02	3.14	10.1
1651	7680	+ .08	2.39	11.5

Three samples were run by means of the torsion technique. Cells and samples were initially heated to about 1800°K. and were held at that temperature for outgassing until the angular deflection reading became reasonably steady. Starting with this temperature, a series of readings was made at successively lower temperatures until no deflection could be observed. This sequence was repeated three or more times for each run.

The results are plotted in Fig. 2. Pressure curves measured in runs 1 and 3 agree with each other quite well, but those of run 2 fall considerably lower. Depletion of the more volatile constituent is probably to blame for the lower results. When the sample used in run 2 was examined after the run, none of the typical yellow color of Al_4C_3 could be seen, although a powder X-ray photograph proved the presence of this compound in the sample. Apparently the crystals of the carbide had become completely covered with layers of graphite. In sample 1 the presence of the yellow carbide was easily visible after the run.

High temperature deflections were observed to fall off slowly with time, probably because of depletion of aluminum from the surface. In run 2,

(9) S. Dushman, "Scientific Foundations of Vacuum Technique," John Wiley and Sons, New York, N. Y., 1949, p. 99.

(10) A. W. Searcy and R. J. Peavler, *J. Am. Chem. Soc.*, **78**, 2076 (1956).

outgassing probably was carried too far, with the result that the sample was depleted at the start of the measurements.

The Knudsen data obtained with the smallest orifice are also plotted on Fig. 2. These data agree well with those of runs 1 and 3. Calculated pressures from torsion measurements thus were as high as those of the Knudsen determinations despite a less favorable ratio of hole-to-sample surface area in the torsion experiments. The diameter of the holes was approximately 2 mm., about the same as the intermediate diameter of the Knudsen experiments, but the cross-sectional area of the torsion cells was less than half that of the Knudsen cells.

Probably this unexpected agreement is due to the different methods of heating the cells. The torsion cells were suspended inside the tubular heating element and were heated very uniformly by radiation. Between different parts of the cell the greatest observable temperature difference was less than 3°, and any temperature gradient present would tend to make the upper surface of the sample cooler than the cell walls. Natural distillation thus tended to replenish the aluminum carbide at the upper sample surface.

Induction-heated Knudsen cells, on the other hand, are almost impossible to heat uniformly. Asymmetric construction of the cell or asymmetric placement of the induction coil is necessary to keep the lid surface about the effusion hole as hot as the sample in order to prevent obstruction of the orifice by condensed vapor. An arrangement that keeps the lid as hot as the upper surface of the sample almost inevitably must leave the upper surface of the sample hotter than the lower. The difference in cell temperature was of the order of 10° at most, and in the sample itself the temperature difference from top to bottom probably was less. Even so, such a gradient would favor vapor transport from the hotter top to the cooler bottom, from whence aluminum and aluminum carbide vapor molecules could escape only by diffusion through the pores of the residual graphite of the sample.

Data of torsion runs 1 and 3 and the Knudsen run with the smallest orifice were used in calculating thermodynamic data. If torsion run 2 were also included, the resulting thermodynamic values would be changed by less than 2 kcal. per mole of aluminum.

Dissociation pressures were calculated from the experimental data on the assumption that all vaporization took place by the reaction $Al_4C_3(s) \rightarrow 4Al(g) + 3C(s)$. The dissociation pressure calculated for torsion runs 1 and 3 is then given by the equation $\log P = -(1.95 \times 10^{-4})/T + 6.79$. Justification for the assumption is discussed later.

From the dissociation pressures, ΔH^0 was calculated at 1600°K. by two methods: the first of these utilizes the relation

$$\frac{d \ln P}{d\, 1/T} = \frac{-\Delta H^0}{R}$$

A least squares solution yields $\Delta H = 92$ kcal./mole Al for run 1 and 87 kcal./mole Al for run 3. The weighted average is 89.1 kcal./mole Al or 356 kcal./mole Al_4C_3.

In the second method, ΔF^0 was found from the measured pressure by means of the reaction $\Delta F^0 = -RT \ln P$, and ΔS^0 for the reaction was calculated from tabulated or estimated values of entropies.

A value of ΔH^0 was then calculated at 1600°K. from the entropy of the reaction and the free energy determination. The various numerical values used in the calculation are given in Table II.

TABLE II

Substance	S^0_{1600}, e.u.	$H^0_{1600} - H^0_{298}$, kcal.
$Al_4C_3(s)$	71 (±3)	57 (±3)
C (graphite)	8.44	6.142
Al(g)	47.72	6.501

Necessary data for C(s) and Al(g) were obtained from Stull and Sinke.[11] The values for Al_4C_3 were obtained as follows: $S^0_{298} = 25$ e.u. from Circular 500[12]; $S^0_{600} - S^0_{298} = 26.35$ e.u., $H^0_{600} - H^0_{298} = 11.53$ kcal. from Kelley.[13]

Entropies and heat contents for Al_4C_3 above 600°K. were calculated by use of the estimated equation,[14] $C_p = 40.04 + 5.0 \times 10^{-3}\, T$ cal./deg. mole. The average vapor pressure of Al over the system at 1600°K. was 4.2×10^{-6} atm.

Using these values, ΔH^0_{1600} for the reaction is calculated to be +349 (±10) kcal./mole Al_4C_3 or +87 (±3) kcal./mole Al. At 1700° the pressure of aluminum was 2.2×10^{-5} atm. and ΔH^0 was +87 kcal./mole Al. From these values and a heat of sublimation of 77.5 kcal./mole for aluminum,[11] the heat of formation of Al_4C_3 at 298°K. is calculated to be +51 (±10) kcal. This is somewhat higher than the +40 kcal. obtained by Roth,[15] but the large uncertainty removes most of the significance from this discrepancy.

The values of ΔH^0 obtained by this second method agree well with the value of 89 kcal./mole Al obtained from the slope.

Vapor Carbide Concentration.—In attempts to determine the amount of gaseous carbide molecules in the vapor, various arrangements were devised whereby some of the vapor effused from a Knudsen cell was condensed on a cooled target. The sample thus collected was analyzed for carbon. The results obtained were inconclusive because of the difficulty in obtaining enough sample. The amount of carbon found in the samples decreased as the sample size was increased, varying from approximately 3% for two samples of less than a milligram total weight to about 0.8% for two 3-mg. samples. The temperature of the Knudsen cell was approximately 1600°K. for all samples. To judge from this variation, the carbon found in the samples was due largely to contamination. One can conclude that the carbon content of the vapor is no more than 2% and probably considerably lower. The results of Chupka, *et al.*, provide a more sensitive limit.[6] They found by mass spectrometry that Al_2C_2, which

(11) D. R. Stull and G. C. Sinke, "Thermodynamic Properties of the Elements," American Chemical Society, Washington, D. C., 1956.

(12) Circular 500, National Bureau of Standards.

(13) K. K. Kelley, "Contributions to the Data on Theoretical Metallurgy, X. High Temperature Heat Content, Heat Capacity, and Entropy Data for Inorganic Compounds," Bulletin 476, Bureau of Mines, U. S. Government Printing Office, Washington, D. C., 1949.

(14) O. Kubaschewsky and E. L. Evans, "Metallurgical Thermochemistry," Pergamon Press, London, 1956, pp. 180-187.

(15) W. A. Roth, *Z. Elektrochem.*, **48**, 267 (1942).

was present to the extent of approximately 10^{-1} mole % at 2100°K., is the most important carbide species. From this concentration and estimated thermodynamic data, the Al_2C_2 concentration at 1600°K. is calculated to be of the order of 10^{-2} mole %.

In light of these results, it seems unlikely that a gaseous aluminum carbide molecule would account for the high percentage of carbon found by the early investigators in the aluminum distilled from aluminum carbide. That transport of carbon is probably due to partial hydrolysis of the carbide with the formation of CO followed by reaction of the CO with the distilled aluminum at the condensing surface has been suggested in two recent papers.[6,16]

Some observations made in the course of these experiments substantiate this explanation. When a sample which had been allowed to stand for some time was reheated, gas was evolved in quantities too large to be attributed to mere outgassing. The vapor from such a sample was condensed, collected, and analyzed. Carbon was present to the extent of 13% by weight.

Acknowledgment.—The authors wish to acknowledge the assistance of Dr. William L. Korst in the construction and evaluation of the torsion apparatus.

(16) L. Brewer and A. W. Searcy, "Annual Review of Physical Chemistry," Vol. 7, Annual Reviews, Inc., Palo Alto, Calif., 1956, p. 266.

THE BINDING OF CHLORIDE IONS TO ALKYL AMINES

BY H. A. SAROFF AND J. W. HEALY

National Institute of Arthritis and Metabolic Diseases, National Institutes of Health, Public Health Service, U. S. Department of Health, Education and Welfare, Bethesda, Maryland

Received December 27, 1958

Complexation constants were measured for the binding of chloride ions to decyl- and dodecylammonium ions at concentrations greater and less than critical. The apparent constants were found to be 1.5 and 6 for the decyl- and dodecylammonium ions, respectively. The electrostatic contribution of the micelle to the binding was evaluated to be a factor varying from about 1.2 to 4.2 depending upon the size of the micelle. Comparisons were made with the chloride binding constants to proteins.

In evaluating the data for the binding of chloride ions to serum albumin, Scatchard, Coleman and Shen[1] divided the hundred binding sites of serum albumin into four sets with the following intrinsic equilibrium constants and number of binding sites per set: $k_1 = 2400$, $n_1 = 1$; $k_2 = 100$, $n_2 = 8$; $k_3 = 3.3$, $n_3 = 18$, and about 70 groups with smaller constants. In another analysis[2] three sets of sites with the following values were proposed: $k_1 = 2500$, $n_1 = 4$; $k_2 = 50$, $n_2 = 12$; and $k_3 = 1$, $n_3 = 84$. The basic sites of serum albumin available for binding anions are the 16 imidazole groups of histidine, the 56 ϵ-amino groups of lysine, the 25 guanidyl groups of arginine and the small number, 1 to 4, of α-amino groups. In order to investigate the characteristics of the amino group as a binding site for anions we have chosen as a pair of model compounds decyl- and dodecylamine. With these model compounds, there is the possibility of studying the binding of anions to the protonated amino group with the compounds both in the monodisperse and clustered or micellar form. This communication reports on the study of the binding of chloride ions to these compounds.

Experimental

The dodecylamine used in this study was the Armour product lot number RA-1. The free base was converted into the hydrochloride and recrystallized five times from methyl alcohol by Dr. L. Kushner of the National Bureau of Standards who kindly furnished us with this purified sample. *Anal.*[3] Calcd.: C, 64.97; H, 12.64; Cl, 15.98. Found: C, 64.81; H, 12.64; Cl, 16.04.

The *n*-decylamine was purchased from the Matheson Co., Rutherford, N. J. It was converted to the hydrochloride and recrystallized twice from methyl alcohol. *Anal.*[3] Calcd.: C, 61.93; H, 12.49; Cl, 18.30. Found: C, 61.84; H, 12.43; Cl, 18.54.

Binding of chloride ion was measured at 25° by the method previously described[4] in a cell equipped with a collodion membrane made permselective to anions by the incorporation of polyvinyl N-methylpyridine.[5] The resistance of the membranes used was in the range of from 200 to 500 ohms cm.^{2}. Potentials were measured with at least two solutions of KCl with known concentrations to give small (0 to 3 mv.) positive and negative e.m.f. values. The concentration of KCl with an activity of chloride ion equal to the activity of the chloride ion in the solution with the decyl- and dodecylammonium ions was determined by interpolation of the logarithm of the concentration to a zero potential.

The cell employed in these measurements was constructed from two Lucite blocks. Matching holes of about 15-ml. capacity were milled into the face of each block and additional holes were drilled to serve as connectors for saturated KCl–agar bridges from the saturated calomel electrodes. The two blocks were clamped together with the permselective membrane placed between the matching holes to form a two compartment cell.

E.m.f. measurements were made with a vibrating reed electrometer (Model 31, Applied Physics Corporation, Pasadena, California) connected to a recording potentiometer. The electrometer and recording potentiometer were employed in place of the Leeds and Northrop Type K potentiometer used previously in order to follow more accurately the drifts which sometimes occur in the potentials.

The precision of measurements of chloride concentration in KCl solutions employing known solutions of KCl was about four parts in a thousand in concentrations varying from 0.001 to 1.0 *M*. This precision was obtained without thermostating the calomel electrodes. More precise measurements can be made with careful control of the temperature of the calomel electrodes.[6]

(1) G. Scatchard, J. S. Coleman and A. L. Shen, *J. Am. Chem. Soc.*, **79**, 12 (1957).

(2) H. A. Saroff, THIS JOURNAL, **61**, 1364 (1957).

(3) We wish to thank Dr. W. Alford for the analysis of this compound.

(4) M. S. Lewis and H. A. Saroff, *J. Am. Chem. Soc.*, **79**, 2112 (1957).

(5) M. H. Gottlieb, R. Neihof and K. Sollner, THIS JOURNAL, **61**, 154 (1957).

(6) K. A. Kraus, R. W. Holmberg and C. J. Borkowski, *Anal. Chem.*, **22**, 341 (1950).

Measurements made on the amine solutions were found to be less precise than those on the known KCl solutions because of the slight drifts encountered in the e.m.f. values. The drift was less at the higher concentrations.

Results

The binding of chloride ion was measured at concentrations of decyl- and dodecylammonium chloride which were both greater and less than the critical micelle concentration. The critical micelle concentrations in salt free solutions are 0.048[7] and 0.0131 M[8] for decyl- and dodecylammonium chloride, respectively. For the dodecylammonium chloride measurements the concentrations less than critical were about 0.010 M, and the concentrations greater than critical were about 0.020 M. For decylammonium chloride the concentrations chosen were about 0.02 to 0.03 M for the low concentrations and 0.080 M for the high concentrations.

Solubility of the dodecylammonium chloride limited the range of concentrations which could be measured. A 0.04 M dodecylammonium chloride solution in water could be prepared with ease on warming to 40°. The 0.04 M solution allowed to cool to 25° formed crystals after about three days. A 0.08 M solution of the chloride in warm water precipitated crystals within a few minutes after cooling to 25°. Solutions of dodecylammonium chloride above 0.01 M precipitated crystals of the amine hydrochloride at 25° when the KCl concentration was above 0.10 M. Kushner, Hubbard and Parker[9] reported measurements on dodecylammonium chloride at concentrations as high as 0.05 M in salt solutions at 30°.

The time required for the formation of the crystals was usually about 10 to 15 minutes, although some of the solutions remained clear for a few hours. Measurements of binding in KCl solutions were made on the clear solutions.

The experimental points of Figs. 1 and 2 summarize the data obtained from the measurements on the two amines. The symbol $\bar{\nu}$ represents the fraction of each mole of alkylammonium ion complexed with the chloride ion. The value of $\bar{\nu}$ was calculated on the assumption that the activity coefficient of the chloride ion in the KCl solution is the same as the activity coefficient of the free (uncomplexed to the alkylammonium ion) chloride ion in the alkylammonium chloride solution. For both alkylammonium chlorides in water the binding of the chloride ion is greater in the micellar form than in the monodisperse form. The enhanced binding is interpreted to be a function of the electrostatic contribution arising from the positive charges of the micelle.

While the values of $\bar{\nu}$ give the charge on a molecule of amine at various concentrations of KCl, it is of interest to calculate an association constant from these data. We consider the equations

$$R{-}NH_3^+ + Cl^- = R{-}NH_3Cl \qquad (1)$$

$$K = \frac{c_{R-NH_3Cl}\, y_{R-NH_3Cl}}{c_{R-NH_3^+}\, y_{R-NH_3^+}\, c_{Cl^-}\, y_{Cl^-}} \qquad (2)$$

(7) H. B. Klevens, *J. Am. Oil Chemists Soc.*, **34**, 74 (1953).

(8) M. L. Corrin and W. D. Harkins, *J. Am. Chem. Soc.*, **69**, 683 (1947).

(9) L. M. Kushner, W. D. Hubbard and R. A. Parker, *J. Research Natl. Bur. Standards*, **59**, 113 (1957).

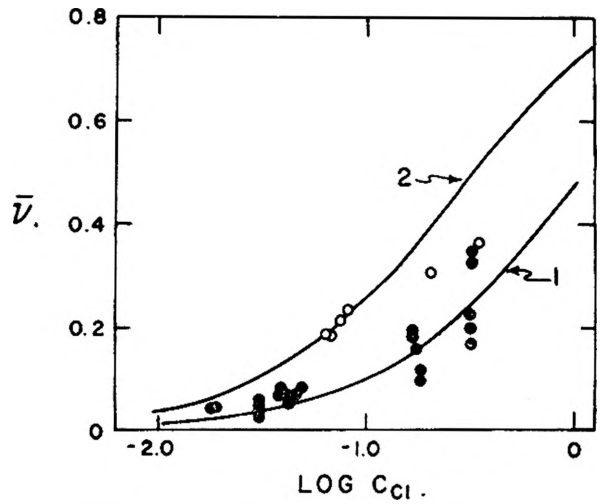

Fig. 1.—The concentration dependence of the binding of chloride ion to the decylammonium ion: ○, concentration of decylammonium chloride was 0.0800 M; ●, concentration of decylammonium chloride varied from 0.016 to 0.032 M. The chloride concentration was increased by adding KCl. Curves 1 and 2 calculated as indicated in the text from equation 3 with $k' = 1.5$ and 4.5, respectively.

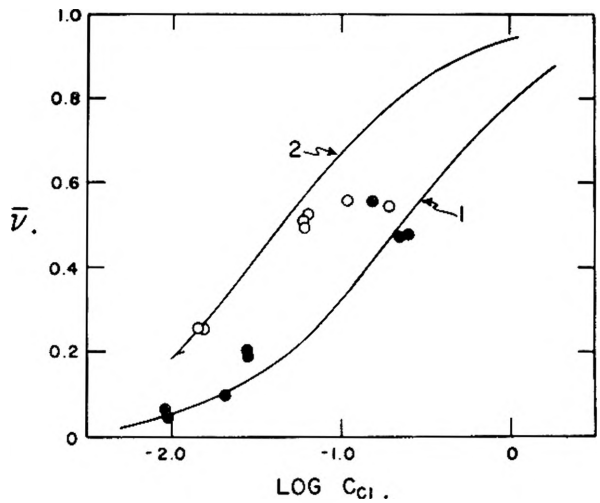

Fig. 2.—The concentration dependence of the binding of chloride ion to the dodecylammonium ion: ○, concentration of dodecylammonium chloride was 0.0202 M; ●, concentration of dodecylammonium chloride varied from 0.0192 to 0.0101 M. The chloride concentration was increased by adding KCl. Curves 1 and 2 calculated from equation 3 with $k' = 6$ and 25, respectively.

The symbols $c_{R-NH_3^+}$, c_{R-NH_3Cl} and c_{Cl^-} represent concentrations of ammonium ions, ammonium ion–chloride complex and chloride ions, respectively, and $y_{R-NH_3^+}$, y_{R-NH_3Cl} and y_{Cl^-} are the corresponding activity coefficients. K represents the association constant for the reaction defined by equation 1. If the apparent association constant k' is defined as

$$K\frac{y_{R-NH_3^+}}{y_{R-NH_3Cl}}$$

then we may write

$$\bar{\nu} = \frac{k' c_{Cl^-}\, y_{Cl^-}}{1 + k' c_{Cl^-}\, y_{Cl^-}} \qquad (3)$$

An evaluation of the apparent association constant k' from the above equations was made on the

alkylammonium chloride solutions containing concentrations to 0.02 *M* added KCl. The activity coefficient y_{Cl^-} was taken as $y_{\pm}$ for KCl from the data compiled by Harned and Owen.[10] Decyl- and dodecylammonium chloride in concentrations below critical exhibit complexation with chloride ion with an apparent constant of 1.5 and 6, respectively. At concentrations above critical, decyl- and dodecylammonium ion in water complexes chloride ion with an apparent constant of 4.3 and 25, respectively.

In order to illustrate graphically the effect of added KCl on the complex formation, the experimental values of $\bar{\nu}$ are plotted as a function of log c_{Cl^-} in Figs. 1 and 2 along with curves calculated from equation 3 with the constants found for the salt-free and low salt solutions. Salt added to solutions of dodecylammonium chloride has been demonstrated by Corrin and Harkins[11] to decrease the critical micelle concentration. The added salt also increases the micellar weight according to the data of Debye,[12] Mysels,[13] and Kushner, Hubbard and Parker.[9]

The salt effect is particularly apparent in the binding of chloride to the micellar forms. As the salt concentration is increased the apparent binding constant decreases and approaches that of the lower concentration of alkyl derivative. This change in apparent association constant is consistent with the change in micellar size if it is assumed that, as the micelle grows, the average effective distance between charges increases with the result that the electrostatic effect becomes smaller.

The electrostatic effect can be evaluated by taking the ratio of the apparent association constant in the micelle to that in the monodisperse form. For the dodecylammonium chloride in water, the electrostatic effect is a factor of 4 and this factor decreases with added salt. Table I summarizes the electrostatic contributions to the association constants of the micellar forms of both decyl- and dodecylammonium chlorides in water and in salt solutions.

Ammonium chloride, in a 0.0800 *M* solution, showed no complexation within the experimental error of our apparatus. (The free chloride ion was measured at 0.0797 *M*.)

Discussion

The binding of chloride ion to the alkyl amines increases as the chain length of the alkyl group increases. The constant for the ammonium ion is too small for measurement in our apparatus. Preliminary studies in this Laboratory with hexylammonium chloride gave a constant (k') of 0.5[14]; decylamine at concentrations below critical gave a value of 1.5 and dodecylamine at concentrations below critical gave a value of 6. These constants, of course, include the ratio of activity coefficients, $y_{R\text{-}NH_3^+}/y_{R\text{-}NH_3Cl}$, as well as any electrostatic effect of small aggregates below the critical micelle concentration. The question of small aggregates is difficult to evaluate unequivocally on the basis of the presently available data for decyl- and dodecylamine. Ralston and Hoerr[15] interpreted their equivalent conductance data on octyl- and decylammonium salts to indicate that these salts behaved as ordinary strong electrolytes and were unaggregated. Similar data for dodecylamine indicated some aggregation. In a later paper, Hoerr and Ralston[16] interpreted the cationic conductance data of these same salts to show some aggregation. A comparison was made between these amines and the carboxylic acids. Aggregation occurring in the carboxylic acids is reflected in the pK's of these acids. The data on the carboxylic acids and their aggregation constants, attributed to hydrogen bonding, have been summarized by Katchalsky, Eisenberg and Lifson.[17] If hydrogen bonding were to cause the small aggregation, such an aggregation would be much weaker for the free amine due to the smaller electronegativity of the nitrogen in the amine compared to that of oxygen[18] in the carboxylic acid. The aggregation *via* hydrogen bonding of the charged ammonium ion would be negligible. With small aggregates (brought about by the reduction of the water–alkyl chain interface) occurring in the alkylamine solution, the differences in pK's (at zero ionic strength) should parallel the differences in chloride binding constants. The difference between the pK values[19] of hexyl- and dodecylamines in the absence of salt is 0.1, corresponding to a ratio of 1.26 in the constants. We find the ratio of the chloride binding constants of decyl- and dodecylammonium ions to be 4 and that for the hexyl- and dodecylammonium ions to be about 10. Thus, from these data on the amines, the constants

TABLE I

ELECTROSTATIC CORRECTION TERM k'(MICELLE)/k'(MONODISPERSE) FOR THE ASSOCIATION CONSTANTS OF DODECYL- AND DECYLAMMONIUM CHLORIDES

Decylammonium chloride 0.0800 *M*

Added KCl, *M*	c_{Cl^-}, *M*		$\bar{\nu}$	k'	$k'/1.5$
0.00	0.0650	...	0.19	4.3	2.9
.01222	.0753	...	.21	4.4	2.9
.02038	.0817	...	.23	4.4	2.9
.1503	.206$_0$	...	.30	2.8	1.9
.3006	.351$_6$	...	.36	2.2	1.5

Dodecylammonium chloride 0.0202 *M*

Added KCl, *M*		Mol. wt. of micelle[9]	$\bar{\nu}$	k'	$k'/6$
0.00	0.0151	17,800	0.25	25	4.2
.05105	.0610	30,000	.51	20	3.4
.1021	.111$_0$	85,500	.56	14	2.4
.2041	.213$_3$	665,000	.54	7.4	1.2

(10) H. S. Harned and B. B. Owen, "Physical Chemistry of Electrolytic Solutions," Reinhold Publ. Corp., New York, N. Y., 1958, p. 498.

(11) M. L. Corrin and W. D. Harkins, *J. Am. Chem. Soc.*, **69**, 683 (1947).

(12) P. Debye, *Ann. N. Y. Acad. Sci.*, **51**, 575 (1949).

(13) K. J. Mysels, THIS JOURNAL, **58**, 303 (1954).

(14) Studies on hexylamine will be presented in another communication.

(15) A. W. Ralston and C. W. Hoerr, *J. Am. Chem. Soc.*, **64**, 772 (1942).

(16) C. W. Hoerr and A. W. Ralston, *ibid.* **65**, 976 (1943).

(17) A. Katchalsky, H. Eisenberg and S. Lifson, *ibid.*, **73**, 5889 (1951).

(18) L. Pauling, "The Nature of the Chemical Bond," Cornell University Press, Ithaca, N. Y., 1940, p. 291.

(19) C. W. Hoerr, M. R. McCorkle and A. W. Ralston, *J. Am. Chem. Soc.*, **65**, 328 (1943).

for the binding of chloride ion to the alkylammonium ion appear to require but little correction for the effects of aggregation.

The recent studies of Mukerjee, Mysels and Dulin[20] on sodium dodecyl sulfate indicate that the dimer is the main stable aggregate at low concentrations. At a 0.01 *M* concentration, about 25% of the dodecyl sulfate ion exists in the form of the dimer (calculated for a dimerization constant of 120). If the dimer is formed with the charge heads separated and the tails interwoven,[20] then we may readily estimate the electrostatic effect of the charted heads. If we take the separation of charged heads to be that equivalent to a six carbon atom distance, the data on the *pK*'s of the two carboxyl groups of suberic acid may be used. The difference in the two *pK* values is 1.03.[21] After subtracting from this difference the statistical effect (logarithm of 4) we find the electrostatic effect to be the factor 2.7. Thus the dimer would impose a relatively small correction on the association constants of the alkylammonium ions and the chloride ion.

The effective chain length for the amino group of lysine incorporated in a protein is, of course, a difficult quantity to estimate. However, a length of from 6 to 12 would seem reasonable giving values of k' varying from 0.5 to 6. Thus the value of 3.3 proposed by Scatchard for 18 sites and the value, 1, proposed by Saroff for 84 sites fall in the proper range.

The higher values of association constant ranging from 2500 to 50, undoubtedly arise from some steric or structural effect.[1] A specific structure involving the clustering of 16 sites has been suggested for serum albumin.[2]

(20) P. Mukerjee, K. J. Mysels and C. I. Dulin THIS JOURNAL, **62**, 1390 (1958); P. Mukerjee, *ibid.*, **62**, 1397 (1958); P. Mukerjee and K. J. Mysels, *ibid.*, **62**, 1400 (1958), and P. Mukerjee, *ibid.*, **62**, 1404 (1958).

(21) R. Gane and C. K. Ingold, *J. Am. Chem. Soc.*, **50**, 1594 (1928)

THE HEATS OF VAPORIZATION OF PARA-HYDROGEN AND ORTHO-DEUTERIUM FROM THEIR BOILING POINTS TO THEIR CRITICAL TEMPERATURES[1]

BY DAVID WHITE, JIH-HENG HU AND HERRICK L. JOHNSTON

Contribution of the Cryogenic Laboratory and Department of Chemistry, The Ohio State University, Columbus, Ohio

Received January 8, 1959

The heats of vaporization of hydrogen and deuterium have been measured from their boiling points to their critical points. The heats of vaporization of hydrogen deuteride and tritium have been predicted from the data, using a simple mass relationship.

Introduction

The heats of vaporization of hydrogen and deuterium have been measured, in this Laboratory,[2] in the vicinity of the boiling points. In the case of hydrogen the heat of vaporization was calculated at temperatures up to the critical[3] from vapor pressure data and the molar volumes of the saturated liquid and gas. However, lack of experimental values for the saturated molar volumes of deuterium has prevented a similar extension of its heat of vaporization from vapor pressure data.[4]

In the hydrogen isotopes, the thermodynamic properties at low temperatures differ considerably due to quantum effects. In order to determine the magnitude of these effects, an attempt has been made to determine directly the heats of vaporization of hydrogen and deuterium between their respective boiling points and critical temperatures. Although, even in the direct determination, the results, in the vicinity of the critical point, depend largely on a knowledge of the saturated molar volumes of the liquid and gas, the measured values for hydrogen and its isotopes can be considered, in general, far more reliable than those calculated from vapor pressure data.

Apparatus.—Owing to the high pressures attained during these experiments, the calorimeter employed was the modified condensed gas calorimeter designed by Rifkin, Kerr and Johnston[5] for the measurement of the heat capacity and vapor pressure of liquid diborane above its boiling point. This apparatus already has been described in considerable detail.

A standard thermocouple, which had been calibrated against a helium thermometer,[3] was used for temperature measurements. To ensure the constancy of the calibration, the thermocouple readings were intercompared with temperatures calculated from the vapor pressures of normal hydrogen, measured in the calorimeter.

Three Bourdon gages, each covering different ranges, were used to measure the pressure during the heat of vaporization experiments. These gages were calibrated at close intervals against a precision dead-weight gage.

Procedure.—Pure hydrogen or deuterium was first condensed into an ortho–para converter containing chromic oxide gel and allowed to stand for approximately six hours. Since the half-life for the ortho–para conversion of hydrogen or deuterium on the catalyst is of the order of only a few minutes, the 20.4°K. equilibrium mixture is certain to be attained after six hours. Although no ortho–para analyses were made, the hydrogen was assumed to consist of 99.8% of the para- and 0.2% of the ortho-form, and the deuterium 2.2% and 97.8% of these forms, respectively.

(1) This work was supported by the United States Atomic Energy Commission.

(2) (a) H. L. Johnston, J. T. Clarke, E. B. Rifkin and E. C. Kerr, *J. Am. Chem. Soc.*, **72**, 3933 (1950); (b) E. C. Kerr, E. B. Rifkin, H. L. Johnston and J. T. Clarke, *ibid.*, **73**, 282 (1951).

(3) D. White, A. S. Friedman and H. L. Johnston, *ibid.*, **72**, 3927 (1950).

(4) A. S. Friedman, D. White and H. L. Johnston, *ibid.*, **73**, 1310 (1951).

(5) E. B. Rifkin, E. C. Kerr and H. L. Johnston, *ibid.*, **75**, 785 (1953).

(6) T. Rubin, H. L. Johnston and H. Altman, *ibid.*, **73**, 3401 (1951).

TABLE I

HEATS OF VAPORIZATION OF PARA-HYDROGEN

Temp. (°K.)	T/T_c	Heat input (cal.)	Heat input cor. (cal.)	n_r (mole)	$V_l/(V_g - V_l)$	n_T (mole)	ΔH_v (cal./mole)
24.41	0.7344	42.01	42.39	0.1958	0.0552	0.2066	205.2
26.33	.7921	43.64	43.79	.2073	.0887	.2257	194.0
28.12	.8460	43.74	45.69	.2246	.1398	.2560	178.5
29.65	.8920	39.87	39.24	.2203	.2450	.2676	146.7
30.97	.9317	36.92	36.42	.2298	.3385	.3076	118.4
31.85	.9582	33.74	33.01	.2260	.5030	.3396	97.2
32.69	.9835	27.41	24.22	.2073	1.0000	.4146	58.4

TABLE II

HEATS OF VAPORIZATION OF ORTHO-DEUTERIUM

Temp. (°K.)	T/T_c	Heat input (cal.)	Heat input cor. (cal.)	n_r (mole)	$V_l/(V_g - V_l)$	n_T (mole)	ΔH_v (cal./mole)
24.25	0.6323	57.57	58.00	0.1988	0.0172	0.2022	287.3
26.83	.6996	55.03	55.84	.1964	.0327	.2028	275.7
28.58	.7439	60.71	61.03	.2219	.0489	.2328	262.5
30.53	.7961	57.81	58.42	.2208	.0768	.2378	245.9
32.48	.8469	54.30	54.95	.2194	.1178	.2453	224.1
34.10	.8892	53.18	53.14	.2285	.1722	.2679	198.4
35.43	.9239	46.70	45.52	.2117	.2395	.2624	173.5
36.57	.9536	39.92	40.11	.1990	.3405	.2668	150.3
37.52	.9784	32.71	32.53	.1803	.5030	.2710	120.0

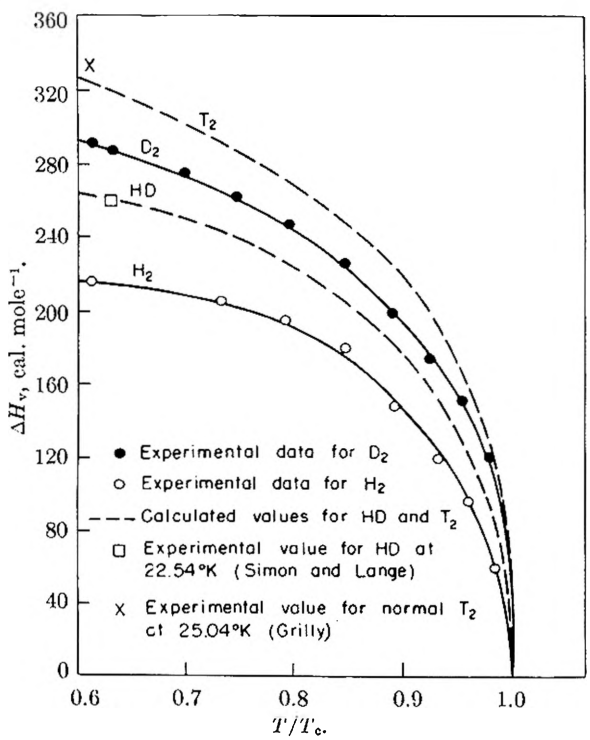

Fig. 1.—Heats of vaporization of the isotopes of hydrogen between the boiling point and critical point.

After the conversion had taken place approximately four moles was condensed into the calorimeter. The vaporizations then were carried out at various temperatures, using the procedure employed by Giauque and Johnston[7] and by Johnston, Clarke, Rifkin and Kerr.[1] The time of energy input varied from 12 to 30 minutes, and during this time the pressure was held constant to within ±10 mm. at the lower pressures and to within ±25 mm. at the highest pressures, by means of a manually controlled needle valve. A correction was made for the small temperature differences between the initial and final states of the calorimeter by means of the heat capacity data of Smith, Hallett and Johnston.[8,9] A considerable effort was made to arrive at a final temperature very close to the initial temperature in order to minimize this correction. Such a precaution is of particular importance in the vicinity of the critical point, where owing to the enormous heat capacity of the system, even a few hundredths of a degree difference leads to a sizeable correction. Corrections also were applied for the heat transfer, during the experiments, between the calorimeter and its surroundings.

Materials Used.—The hydrogen used in this investigation was prepared electrolytically, and purified by triple distillation. After compression in a storage cylinder, a mass spectroscopic analysis of the gas showed less than 0.01 mole % of impurity.

The deuterium was supplied by the U.S. Atomic Energy Commission. After purification by distillation, it was found to contain 99.01% deuterium and 0.99% hydrogen deuteride. Other impurities amounted to less than 0.01%.

Experimental Results

The heats of vaporization of hydrogen and deuterium are given in Tables I and II, respectively.

The heats of vaporization for hydrogen show considerably more scattering than those for deuterium. In some of these runs the heating period was so short that a large superheating resulted. This effect tends to make the total heat input somewhat uncertain. Furthermore, in the earliest experiments there was some difficulty in controlling the pressure during the vaporization. The most serious uncertainty, however, is in the determination of the total number of moles vaporized in a given experiment. Not only must the number of moles removed from the calorimeter (Tables I and II, column 4) be considered, but also the number of moles vaporized in the dead space of the calorim-

(7) W. F. Giauque and H. L. Johnston, *ibid.*, **51**, 2300 (1929).

(8) A. L. Smith, N. C. Hallett and H. L. Johnston, *ibid.*, **76**, 1486 (1954).

(9) A. L. Smith, N. C. Hallett and H. L. Johnston, Contract SC-4, W-7405, Eng. 36 between the Regents of The University of California and The Ohio State University Research Foundation, TR-436-3 (March 15, 1952).

eter. Let n_r be the number of moles removed from the calorimeter of volume V, let n_1^g and n_1^l be the initial number of moles of gas and liquid, respectively, in the calorimeter; and let n_2^g and n_2^l be the corresponding final amounts of gas and liquid. Since the volume of the calorimeter is constant, *i.e.*

$$V_g n_1^g + V_l n_1^l = V_g n_2^g + V_l n_2^l$$

and the number of moles removed from the calorimeter is given by the expression

$$n_1^g + n_1^l - n_2^g - n_2^l = n_r$$

it can be shown that the total number of moles vaporized n_T is given by the relation

$$n_T = n_r + n_r \left(\frac{V_l}{V_g - V_l} \right)$$

where V_l and V_g are the molar volumes of the liquid and gas,[10] respectively, at the temperature and pressure of the vaporization. No experimental data exist for the molar volumes of liquid and gaseous deuterium along the saturation curve. Therefore, V_l was obtained by extrapolation, to the saturation curve, of the pressure–volume–temperature data of liquid deuterium,[11] and V_g was obtained in a similar manner from gaseous pressure–volume–temperature data.[12] Since such extrapolations are not too accurate, particularly in the vicinity of the critical point, the uncertainty in the heat of vaporization at the highest temperatures can be as much as 5%. The values of $V_l/(V_g - V_l)$ used in the calculations were tabulated for both hydrogen and deuterium (column 5 of Tables I and II), so that the total number of moles can be recalculated in the event that new liquid and gas densities become available.

The heats of vaporization of deuterium have been corrected for the presence of the 1% hydrogen deuteride. In making this correction, it was assumed that a solution of hydrogen deuteride and deuterium behaves ideally. Although the heat of vaporization of hydrogen deuteride between the boiling point and the critical point has not been determined, it was estimated from the results of these experiments (see below).

(10) E. Mathias, C. A. Crommelin and H. K. Onnes, *Leiden Comm.*, 154b (1918).

(11) A. S. Friedman, M. Trzeciak and H. L. Johnston, *J. Am. Chem. Soc.*, **76**, 1552 (1954).

(12) Unpublished results of this Laboratory.

Discussion of Results

The large isotope effect obtained in the heat of vaporization is of considerable interest, particularly if the results can be used to predict the properties of all the other hydrogen isotopes. Since the intermolecular forces for all the hydrogen isotopes can be considered to be nearly the same, no correlation can be expected from any classical law of corresponding states. Deviations from such a law, as a result of quantum effects, have already been discussed by DeBoer and Lunbeck.[13]

An empirical relationship developed by Friedman, White and Johnston[14] states that when a thermodynamic quantity of an isotope series is plotted against the reciprocal of square root of the mass, a straight line is obtained. By applying this relationship to the heats of vaporization at the boiling point of hydrogen, deuterium and hydrogen deuteride,[15] a straight line plot is obtained which, when extrapolated to the mass of tritium, leads to a value of 323 ca./mole. From vapor pressure data, Grilly[16] has calculated a value of 333 cal./mole for the heat of vaporization of tritium at 25.04°K. Thus the predicted value agrees to within 3% of the experimental value. Assuming that for each value of T/T_c (column 8 of Tables I and II) between the boiling point and critical point, such a linear relationship holds for all the isotopes, the heats of vaporization of hydrogen deuteride and tritium were calculated. The results of these calculations are shown by the dotted lines in Fig. 1; the solid lines represent the experimental results for hydrogen and deuterium.

(13) J. DeBoer and R. J. Lunbeck, *Physica*, **14**, 520 (1938).

(14) A. S. Friedman, D. White and H. L. Johnston, *J. Chem. Phys.*, **19**, 126 (1951).

(15) F. Simon and F. Lange, *Z. Physik*, **15**, 312 (1923).

(16) E. R. Grilly, *J. Am. Chem. Soc.*, **73**, 843 (1951).

THE SOLUBILITY OF SILVER SULFATE IN ELECTROLYTE SOLUTIONS. PART 1. SOLUBILITY IN POTASSIUM NITRATE SOLUTIONS[1]

BY M. H. LIETZKE AND R. W. STOUGHTON

Contribution from the Chemistry Division, Oak Ridge National Laboratory, Oak Ridge, Tenn.

Received January 10, 1959

The solubility of Ag_2SO_4 has been measured in water to 230°, in 0.1 and 0.6 *m* KNO_3 to 200°, and in 1 *m* KNO_3 to 150°. Based on the solubilities in pure water and a Debye–Hückel expression for the variation in the activity coefficient of Ag_2SO_4 with ionic strength at any temperature, solubilities were calculated at various temperatures and KNO_3 concentrations. The agreement between observed and calculated values was good. It is concluded that in this case the Debye–Hückel equation holds as well at elevated temperatures as at room temperature and that it is not necessary to assume any complexing in these solutions to explain the data.

In a previous paper[2] it was shown that at 25° a plot of the log of the stoichiometric solubility product S of Ag_2SO_4 (on a molality basis) *versus* the square root of the ionic strength I was essentially independent of the electrolyte medium. This was true on the basis of assumed complete dissociation

(1) This paper is based upon work performed for the United States Atomic Energy Commission at the Oak Ridge National Laboratory operated by Union Carbide Corporation.

(2) M. H. Lietzke and R. W. Stoughton, *J. Am. Chem. Soc.*, **79**, 2067 (1957).

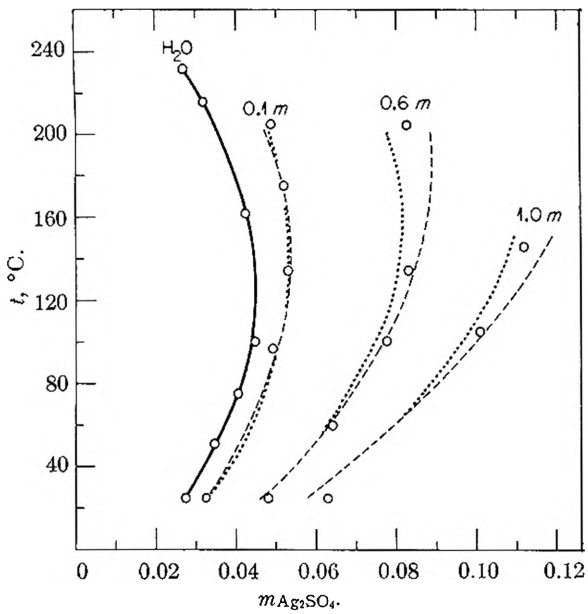

Fig. 1.—The solubility of Ag_2SO_4 in KNO_3 solutions: O, obsd. solubility; ——, calcd. solubility assuming A_s is constant at each KNO_3 concn.; – – – –, calcd. solubility assuming A_s varies as $(DT)^{-1/2}$.

whether or not the supporting electrolyte contained a common ion and regardless of valence type. Moreover, the curves, which showed a monotonic increase with $\sqrt{I}$, all fell below the limiting (Debye–Hückel) slope, *i.e.*, they showed a smaller dependence on ionic strength. These facts suggested that (1) no sulfate complexing need be postulated in these systems and that (2) a Debye–Hückel expression of the type

$$\ln S = \ln S_0 + s_T \left[\frac{\sqrt{I}}{1 + A_s\sqrt{I}} - \frac{\sqrt{3s_0}}{1 + A_s\sqrt{3s_0}} \right] \quad (1)$$

could be used to describe the data. In this equation s_0 and S_0 represent the molal solubility and the molal solubility product of Ag_2SO_4, respectively, in pure water at temperature T; s_T is the Debye–Hückel limiting slope for a 1–2 electrolyte (Ag_2SO_4) at that temperature; A_s is either a constant or a term which varies inversely as the square root of the DT product, where D is the dielectric constant of water. The value of D is assumed to vary with temperature in accordance with the equation given by Akerlof and Oshry.[3] In the case of Ag_2SO_4 solubility in pure water $S_0 = 4s_0^3$ at ionic strength $I_0 = 3s_0$, while the expression for I depends upon the supporting electrolyte.

In order to test the validity of the two assumptions a study of the solubility of Ag_2SO_4 in a variety of electrolyte media was initiated as a function of temperature and ionic strength. Ag_2SO_4 was chosen because the solubility range in water and in a variety of electrolyte media is sufficiently high so the measurements can be made visually. Furthermore, the compound is sufficiently stable over the temperature range used that one does not encounter insurmountable difficulties with side reactions.

The present paper describes the solubility of Ag_2SO_4 in KNO_3 solutions; subsequent papers in the series will describe the solubility of Ag_2SO_4 in other media. In all cases the measurements have been extended over a wide range of ionic strength and from 25° to at least 200°. Since the calculations involved in testing the above assumptions would be extremely tedious on a desk calculator a high speed computer has been used in all cases.

(3) G. C. Akerlof and H. I. Oshry, *ibid.*, **72**, 2844 (1950).

Experimental

The solubility measurements were carried out using the same technique described previously.[4] The determinations could be made only on a heating cycle since the solutions supersaturated upon cooling. In the present work Ag_2SO_4 crystals and aliquots of previously analyzed KNO_3 solutions were weighed into the fused silica tubes. Since the Ag_2SO_4 molality could be calculated directly, subsequent analysis of the contents of every tube was unnecessary.

In contrast to systems containing Ag_2SO_4 dissolved in acid,[4] where the tubes could be heated many times to check a given point, the tubes containing Ag_2SO_4 crystals and KNO_3 solution could usually be heated only once. Even after one heating it was evident that a very small amount of Ag_2O had formed by hydrolysis. As long as a tube was heated only once and the work was conducted relatively rapidly consistent and reproducible results were obtained. A second heating of the same tube showed a slightly different solubility and a darkening of the appearance of the precipitate, clearly indicating the formation of Ag_2O. The solubilities reported therefore do not strictly represent equilibrium conditions. However the authors are convinced that the reported data are those which obtain in the absence of hydrolysis and that the hydrolysis reaction is significantly slower than the dissolution of Ag_2SO_4 to produce a metastable condition. Slow hydrolysis also was observed even when a small amount of HNO_3 had been added. This situation is as should be expected in view of the calculated decrease of the acid quotients for HSO_4^- and HNO_3 with temperature;[5] in order to increase appreciably the H^+ concentration, enough HNO_3 would have to be added to change markedly the various concentrations of species assumed to exist.

Hence it was necessary to use several tubes to determine each point on the solubility diagram. The solubility points were reproducible to ±2° in 0.1 and 0.6 *m* KNO_3 and to about ±5° in 1.0 *m* KNO_3.

Results and Discussion

In Fig. 1 the circled points represent the experimentally observed solubilities of Ag_2SO_4 in H_2O and in 0.1, 0.6 and 1.0 *m* KNO_3 solutions. The points at 25° are lower than those observed by Harkins[6] and are in better agreement with the calculated values. The results in H_2O up to 100° were obtained from the work of Barre.[7] The curves in Fig. 1 represent the calculated values using the best A_s at each concentration.

The stoichiometric ionic strength I of the Ag_2SO_4–KNO_3 solutions is given at any molality m of KNO_3 by m plus three times the molal solubility of Ag_2SO_4, s, in the same medium, *i.e.*

$$I = m + 3s \quad (2)$$

Under the same conditions the solubility product of the Ag_2SO_4 on a molality basis is given by

$$S = 4s^3 \quad (3)$$

In starting the calculations at each concentration of KNO_3 the observed solubility of Ag_2SO_4 at a given temperature was used to compute a value of I. Then using equations 1 and 3 a value of s_{calcd} (the calculated solubility of Ag_2SO_4) was obtained. This

(4) M. H. Lietzke and R. W. Stoughton, *ibid.*, **78**, 3023 (1956).

(5) See M. H. Lietzke and R. W. Stoughton, THIS JOURNAL, **63** 1190 (1959).

(6) W. D. Harkins, *J. Am. Chem. Soc.*, **33**, 1807 (1911).

(7) M. Barre, *Ann. chim. phys.*, [8] **24**, 211 (1911).

value of s_{calcd} was used to correct I and the process repeated until successive values of s_{calcd} agreed to within 0.1%. The calculations were carried out at 25° intervals from 25 to 200° at each concentration of KNO_3 using three different values of A_S, *viz.*, 0.9, 1.1 and 1.3. A plot of s_{calcd} *vs.* A_s was then made at each temperature in order to determine the value of A_s which gave best agreement with the observed value. It was found that at each concentration of KNO_3 the value of A_s was practically temperature independent; this implies that $\mathring{a}/(DT)^{1/2}$ is temperature independent, where $\mathring{a}$ is the $\mathring{a}$ parameter of the Debye–Hückel theory.[8] Hence the values were averaged at each concentration of KNO_3 and the s_{calcd} value corresponding to the average value was read from each graph. In addition an over-all average A_s was calculated and the corresponding values of s_{calcd} also were obtained from the graphs. Both sets of s_{calcd} values are given in Table I.

TABLE I

THE SOLUBILITY OF Ag_2SO_4 IN KNO_3 SOLUTIONS

KNO_3, m	t, °C.	s_{obsd}	s_{calcd} $A_s = 1.33$	s_{calcd} $A_s = 1.11$	s_{calcd} $A_s = 1.33$ $\left(\frac{D'T'}{DT}\right)^{1/2}$[a]
0.1	25	0.0329	0.0320	0.0327	0.0320
	50	.0404	.0407	.0416	.0406
	75	.0463	.0471	.0482	.0469
	100	.0505	.0514	.0528	.0509
	125	.0530	.0536	.0552	.0528
	150	.0538	.0538	.0556	.0527
	175	.0529	.0518	.0539	.0516
	200	.0461	.0479	.0501	...
			$A_s = 1.07$	$A_s = 1.11$	$A_s = 1.07$ $\left(\frac{D'T'}{DT}\right)^{1/2}$[a]
0.6	25	0.0488	0.0463	0.0455	0.0463
	50	.0605	.0590	.0579	.0584
	75	.0699	.0691	.0678	.0678
	100	.0771	.0770	.0755	.0746
	125	.0821	.0831	.0813	.0792
	150	.0849	.0870	.0849	.0812
	175	.0855	.0889	.0865	.0808
	200	.0838	.0888	.0860	.0776
			$A_s = 0.88$	$A_s = 1.11$	$A_s = .88$ $\left(\frac{D'T''}{DT}\right)^{1/2}$[a]
1.0	25	0.0628	0.0580	0.0512	0.0580
	50	.0760	.0746	.0653	.0739
	75	.0880	.0884	.0769	.0864
	100	.0990	.100	.0862	.0964
	125	.107	.111	.0936	.104
	150	.113	.119	.0992	.109

[a] $D'T'$ is the DT product at 25°.

Solubility values calculated on the assumption that at each m, $A_s = A_s'(D'T'/DT)^{1/2}$, *i.e.*, that the $\mathring{a}$ parameter is temperature independent, also are shown in Table I. Here A_s' is independent of D and T, and $D'T'$ is the DT product at 25°. On this assumption A_s increases by about 16% in going from 25 to 200°.

As can be seen in Fig. 1 the calculated and observed plots are all concave to the left even at 1.0 m KNO_3. It will be shown in subsequent papers that this is not true when Ag_2SO_4 is dissolved in solutions involving more than a pure ionic strength effect.

It is evident from Table I that the Ag_2SO_4 solubilities based on a value of A_s which decreases with increasing concentration of KNO_3 show close agreement with the experimentally observed values, while those based on an over-all average A_s are not as good at 1 m KNO_3. The greatest difference between the observed and calculated solubilities in the latter case was 18%, and the average at all concentrations was about 4%. The $\mathring{a}$ parameters corresponding to the values of A_s at 25° are as follows: 0.1 m KNO_3, $A_s = 1.33$, $\mathring{a} = 4.0$ Å.; 0.6 m KNO_3, $A_s = 1.07$, $\mathring{a} = 3.3$ Å.; and 1.0 m KNO_3, $A_s = 0.88$, $\mathring{a} = 2.7$ Å. The decrease in the value of $\mathring{a}$ is consistent with an hypothesis involving smaller hydration spheres for the ions as the concentration of KNO_3 increases. Since temperature independent values of A_s give calculated solubilities which agree more closely with the observed solubilities than do values of A_s which vary as $(DT)^{-1/2}$ (Table I) it appears that the $(DT)^{-1/2}$ variation may be just about offset by a decrease in the $\mathring{a}$ values (or the solvent density) with increasing temperature.

The attainment of solubility equilibrium in the 1.0 m KNO_3 solution at the higher temperatures was slow. Yet it was necessary to heat the tubes sufficiently rapidly so that the Ag_2SO_4 did not hydrolyze to any large extent. Since no single A_s value fits the data as well in 1 m KNO_3 over the entire temperature range as in the 0.1 and 0.6 m KNO_3 solutions, and since the 25° value was easy to check within 1%, it appears that the solubilities observed in 1 m KNO_3 solution at the elevated temperatures are too high. However, they represent the best measurements that could be made under the restricting condition of competitive hydrolysis. The data obtained above 150° in the 1.0 m KNO_3 solution were meaningless and hence the values are reported only to 150°.

Any tendency of the sulfate ion to hydrolyze should be maximized at the highest temperatures and the lowest ionic strengths, *i.e.*, where the bisulfate acid quotient is lowest. The conditions of lowest ionic strengths obtain in pure water. At 200° in pure water the ionic strength is about 0.1; using the appropriate value S and an estimated value for the concentration product[9] for water dissociation under these conditions, the ratio of HSO_4^-/SO_4^{--} is only about 0.002, on the assumption of no hydrolysis of silver ion. Any hydrolysis of the latter ion would of course tend to enhance bisulfate formation.

It is evident that with the assumption of complete dissociation of both the Ag_2SO_4 and KNO_3 a Debye–Hückel type of expression for the solubility product of Ag_2SO_4 in KNO_3 solutions can be used to fit the solubility data over a wide range of concentration and temperature. It is further evident that

(8) NOTE ADDED IN PROOF.—Actually the Debye-Hückel equation was derived in terms of molar concentrations c rather than molal concentrations m, and c is approximately equal to the product of m times the solvent density d_0. Further, the quotient $(d_0/DT)^{1/2}$ is nearly independent of temperature. Hence a nearly temperature independent A_s is consistent with a temperature independent $\mathring{a}$.

(9) H. S. Harned and B. B. Owen, "The Physical Chemistry of Electrolytic Solutions," Reinhold Publ. Corp., New York, N. Y., Third Edition, 1958, pp. 643–649.

at least in this case the Debye–Hückel equation holds as well at elevated temperatures as at room temperature.

Acknowledgment.—The authors wish to express their appreciation to G. R. North for performing the experimental solubility measurements and to M. P. Lietzke for programming the equations for the IBM-704 Computer.

THE SOLUBILITY OF SILVER SULFATE IN ELECTROLYTE SOLUTIONS. PART 2. SOLUBILITY IN POTASSIUM SULFATE SOLUTIONS[1]

BY M. H. LIETZKE AND R. W. STOUGHTON

Contribution from the Chemistry Division, Oak Ridge National Laboratory, Oak Ridge, Tenn.

Received January 10, 1959

The solubility of Ag_2SO_4 was measured in 0.1, 0.3, 0.5 and 0.8 *m* K_2SO_4 solutions to about 200°. Based on the values in pure water the solubilities were calculated as a function of K_2SO_4 concentration and temperature on the assumptions that (1) both electrolytes were completely dissociated and (2) the activity coefficient of Ag_2SO_4 varied with ionic strength according to an equation of the Debye–Hückel type. The agreement between observed and calculated solubilities was good.

A previous paper[2] in this series described the solubility of Ag_2SO_4 in KNO_3 solutions. It was shown that an equation of the Debye–Hückel type could be used to describe the solubility data in that system over a wide range of temperature and concentration. The present paper describes the solubility of Ag_2SO_4 in K_2SO_4 solutions.

In contrast to the Ag_2SO_4–KNO_3 system, which involves a pure solvent medium effect in enhancing the solubility of Ag_2SO_4 over the solubility in pure H_2O, the Ag_2SO_4–K_2SO_4 system involves a common ion effect as well as a medium effect. The measurements have been extended over the range 0.1 to 0.8 *m* K_2SO_4 from 25 to 200°. Again a high speed digital computer was used to check the applicability of the Debye–Hückel equation to the solubility system.

Experimental

The solubility measurements were carried out using the same technique described previously.[2,3] The same observations in regard to hydrolysis of the Ag_2SO_4 made in the case of the Ag_2SO_4–KNO_3 system apply to the present system. Again the measurements were reproducible to ±2°.

Results and Discussion

In Fig. 1 the circled points represent the experimentally observed solubilities of Ag_2SO_4 in H_2O and in 0.1, 0.3, 0.5 and 0.8 *m* K_2SO_4 solutions. The points from 25 to 100° in H_2O and from 33 to 100° in the K_2SO_4 solutions are from the work of Barre.[4]

On the assumption of complete dissociation of both electrolytes, the stoichiometric ionic strength I of the Ag_2SO_4–K_2SO_4 solutions is given at any molality m of K_2SO_4 by equation 1

$$I = 3m + 3s \qquad (1)$$

where s represents the molal solubility of Ag_2SO_4 in the K_2SO_4 solution. As in the previous paper in this series[2] the stoichiometric solubility product of Ag_2SO_4 on a molality basis S at any molality m of K_2SO_4 was assumed to be given in terms of the solubility product in pure H_2O by a Debye–Hückel expression of the type

$$\ln S = \ln S_0 + s_T \left[\frac{\sqrt{I}}{1 + A_s\sqrt{I}} - \frac{\sqrt{3s_0}}{1 + A_s\sqrt{3s_0}} \right] \qquad (2)$$

In this equation S_0, the molality solubility product of Ag_2SO_4 in pure H_2O, equals $4s_0^3$ at ionic strength $I_0 = 3s_0$; s_T is the Debye–Hückel limiting slope at the given temperature; and A_s is either a constant or a term which varies inversely as the square root of the DT product, where D is the dielectric constant of H_2O. The value of D was computed at each temperature using the equation given by Akerlof and Oshry.[5] According to the Debye–Hückel theory the value of s_T varies with temperature inversely as the three halves power of the DT product. At any temperature and concentration of K_2SO_4 the solubility product S of the Ag_2SO_4 is given by equation 3

$$S = 4s^2(s + m) \qquad (3)$$

In starting the calculations at each concentration of K_2SO_4 the observed solubility of Ag_2SO_4 at each temperature was used to compute a value of I. Then using equations 2 and 3 a value of s_{calcd} (the calculated solubility of Ag_2SO_4) was obtained. This value of s_{calcd} was used to correct I (equation 1) and the process repeated until successive values of s_{calcd} agreed to within 0.1%. The calculations were carried out at 25° intervals from 25 to 200° at each concentration of K_2SO_4 using three different values of A_s, *viz.*, 0.45, 0.65 and 0.85. From a plot of s_{calcd} *vs.* A_s at each temperature and concentration of K_2SO_4 it was possible to find the value of A_s which gave closest agreement with the observed solubility. It was found that the value of A_s varied little with temperature at each concentration of K_2SO_4 but did show a small decrease with increasing concentration of K_2SO_4. Table I shows the calculated solubilities of Ag_2SO_4 corresponding to the values of A_s averaged at each concentration of K_2SO_4 and also to an over-all average value of 0.7. Using a single average value of A_s is equivalent to assuming that $\mathring{a}/(DT)^{1/2}$ is independent of concentration

(1) This paper is based upon work performed for the United States Atomic Energy Commission at the Oak Ridge National Laboratory operated by Union Carbide Corporation.

(2) M. H. Lietzke and R. W. Stoughton, THIS JOURNAL, **63**, 1183 (1959).

(3) M. H. Lietzke and R. W. Stoughton, *J. Am. Chem. Soc.*, **78**, 3023 (1956).

(4) M. Barre, *Ann. chim. phys.*, [8] **24**, 202 (1911).

(5) G. C. Akerlof and H. I. Oshry, *J. Am. Chem. Soc.*, **72**, 2844 (1950).

TABLE I

THE SOLUBILITY OF Ag_2SO_4 IN K_2SO_4 SOLUTIONS

m K_2SO_4	t, °C.	s_{obsd}	Scaled $A_s = 0.766$	Scaled $A_s = 0.7$	Scaled $A_s = 0.60$ $\left(\frac{D'T''}{DT'}\right)^{1/2}$[a]
0.1	50	0.0343	0.0326	0.0338	0.0352
	75	.0412	.0402	.0416	.0432
	100	.0461	.0463	.0476	.0489
	125	.0491	.0504	.0519	.0533
	150	.0506	.0531	.0544	.0554
	175	.0509	.0541	.0556	.0556
	200	.0501	.0530	.0550	.0544
			$A_s = 0.665$		
0.3	50	0.0372	0.0385	0.0373	0.041
	75	.0464	.0497	.0476	.052
	100	.0565	.0595	.0572	.0618
	125	.0675	.0691	.0663	.071
	150	.0795	.0781	.0752	.079
	175	.0925	.0875	.0843	.0843
	200	.107	.099	.0941	.092
			$A_s = 0.643$		
0.5	50	0.0431	0.0438	0.0402	0.0464
	75	.0541	.0575	.0523	.0594
	100	.0668	.0704	.0644	.0715
	125	.0814	.085	.0766	.083
	150	.0977	.0999	.0895	.0945
	175	.116	.119	.104	.104
	200	.135	.138	.121	.117
			$A_s = 0.648$		
0.8	50	0.0515	0.0478	0.0433	0.0490
	75	.0652	.0640	.0576	.0681
	100	.0819	.0805	.0724	.0805
	125	.101	.0995	.0883	.101
	150	.122	.122	.106	.113
	175	.144	.147	.127	.127
	200	.167	.182	.153	.146

[a] $D'T''$ is the DT' product at 25°.

and temperature[6]; here $\mathring{a}$ is the "distance of closest approach" parameter of the Debye–Hückel theory. Shown also are the calculated solubilities of Ag_2SO_4 corresponding to an over-all average value of A_s which varies with temperature as $(DT)^{-1/2}$; in these calculations it is assumed that $\mathring{a}$ is independent of concentration and temperature. The solubilities calculated with the values of A_s averaged at each concentration of K_2SO_4 are also plotted in Fig. 1.

A comparison of the observed and calculated solubilities in Table I indicates that the temperature-independent values of A_s averaged at each concentration of K_2SO_4 give calculated solubilities agreeing most closely with the observed. In all cases above 0.1 m K_2SO_4 the value of A_s which varies as $(DT)^{-1/2}$ gives calculated solubilities which are too low at the highest temperatures. These same observations also were made in the Ag_2SO_4–KNO_3 solubility system.[2] However, in contrast to the Ag_2SO_4–KNO_3 system the direction of curvature of both the observed curves and the calculated curves changes at higher concentrations of K_2SO_4. The $\mathring{a}$ parameters corresponding to the A_s values at 25° are as follows: for 0.1 m K_2SO_4, $A_s = 0.766$, $\mathring{a} = 2.3$ Å.; for the higher concentrations of K_2SO_4 the values of A_s decrease slightly with $\mathring{a} = 2.0$ Å. As in the Ag_2SO_4–KNO_3 system, the decrease in the value of $\mathring{a}$ is consistent with an hypothesis involving smaller hydration spheres for the ions as the concentration of K_2SO_4 increases. Also, the temperature-independent values of A_s give calculated solubilities which agree more closely with the observed solubilities than do values of A_s which vary as $(DT)^{-1/2}$ (Table I); this fact may be interpreted on the basis of the Debye–Hückel equation by concluding that the $(DT)^{-1/2}$ variation tends to be offset by a decrease in the $\mathring{a}$ value (or the solvent density) with increasing temperature.

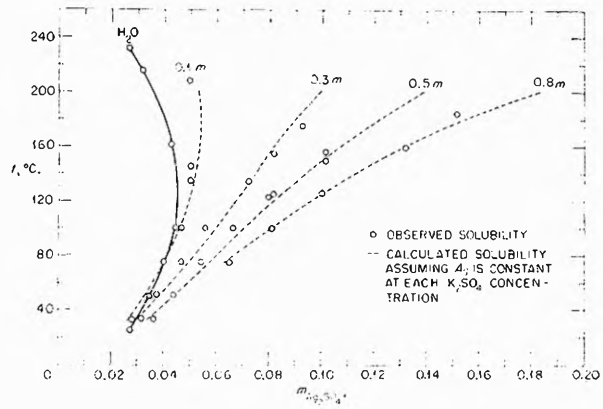

Fig. 1.—The solubility of Ag_2SO_4 in K_2SO_4 solutions.

It is evident that with the assumption of complete dissociation of both the Ag_2SO_4 and K_2SO_4 a Debye–Hückel type of expression for the variation in the molality solubility product of Ag_2SO_4 with ionic strength in K_2SO_4 solutions can be used to fit the solubility data over a wide range of concentration and temperature.

Acknowledgment.—The authors wish to express their appreciation to L. N. Cain for performing the experimental solubility measurements.

(6) Using a constant value of A_s is more nearly equivalent to assuming that $\mathring{a}(d_0/DT)^{1/2}$ is independent of concentration and temperature; here d_0 is the density of the solvent.

THE SOLUBILITY OF SILVER SULFATE IN ELECTROLYTE SOLUTIONS. PART 3. SOLUBILITY IN SULFURIC ACID SOLUTIONS[1]

By M. H. Lietzke and R. W. Stoughton

Contribution from the Chemistry Division, Oak Ridge National Laboratory, Oak Ridge, Tenn.

Received January 10, 1959

The solubility of Ag_2SO_4 was calculated as a function of H_2SO_4 concentration and temperature to 250° based on (1) the solubility in pure water, (2) T. F. Young's equation for the variation of the HSO_4^- acid constant with temperature, and (3) the assumption that the Ag_2SO_4 molality solubility product and the HSO_4^- acid quotient varied with ionic strength according to Debye–Hückel expressions. After redetermining solubilities under conditions where the observed and calculated values were incompatible, general good agreement was obtained.

Two previous papers in this series have described the solubility of Ag_2SO_4 in KNO_3[2] and K_2SO_4 solutions.[3] The present paper describes a study of the solubility of Ag_2SO_4 in H_2SO_4 solutions primarily through the medium of a high speed digital computer. In addition, new experimental results are presented correcting certain inconsistencies in previously reported high temperature data.[4]

Experimental

All the solubility measurements were carried out using the synthetic method described previously.[4] In contrast to the measurements in KNO_3 and K_2SO_4 media, the solubility points in acid solution were sharp and reproducible to about ±1°.

Results and Discussion

In accordance with the earlier papers in this series it was assumed that the molality solubility product S of Ag_2SO_4 in the H_2SO_4 solutions could be expressed by equation 1

$$\ln S = \ln S_0 + \mathcal{S}_T\left[\frac{\sqrt{I}}{1 + A_s\sqrt{I}} - \frac{\sqrt{I_0}}{1 + A_s\sqrt{I_0}}\right] \quad (1)$$

where $\mathcal{S}_T$ is the Debye–Hückel limiting slope for a 1–2 electrolyte at absolute temperature T; S_0 is the molality solubility product of Ag_2SO_4 in pure water at that same temperature; I is the ionic strength of the solution; I_0 is the ionic strength of Ag_2SO_4 in pure water; and A_s is either a constant or a term that varies as $(DT)^{-1/2}$. The dielectric constant D of water was computed at each temperature using the equation given by Akerlof and Oshry.[5]

In calculating the ionic strength of the solution it was assumed that only the species Ag^+, $SO_4^=$ and HSO_4^- existed in solution. If s is the molal solubility of Ag_2SO_4 in H_2SO_4 of molality m, then the ionic strength of the solution is given by equation 2

$$I = m + s + \frac{S}{2s^2} \quad (2)$$

where S is given by equation 1.

An equation for the variation in the bisulfate dissociation constant K_2^0 with temperature was obtained from T. F. Young[6]

$$\log K_2^0 = -\frac{775.3835}{T} + 6.947210 - 0.021247_2T \quad (3)$$

The bisulfate acid quotient K_2 in the Ag_2SO_4 solutions was assumed to vary with ionic strength at any temperature according to equation 4

$$\ln K_2 = \ln K_2^0 + \frac{\mathcal{S}_T'\sqrt{I}}{1 + A_K\sqrt{I}} \quad (4)$$

where $\ln K_2^0$ is given by equation 3, $\mathcal{S}_T'$ is the Debye–Hückel limiting slope at temperature T for the quotient of ions involved in the reaction $HSO_4^- = H^+ + SO_4^=$, and A_K is either a constant or a term that varies as $(DT)^{-1/2}$.

To derive an equation relating m, s, S and K_2 as previously defined, let $m_{Ag^+} = 2s$, $m_{H^+} = m + x$, $m_{SO_4^=} = s + x$, and $m_{HSO_4^-} = m - x$. Then

$$S = (m^2_{Ag^+})(m_{SO_4^=}) = 4s^2(s + x) \quad (5)$$

and

$$K_2 = \frac{(m_{H^+})(m_{SO_4^=})}{m_{HSO_4^-}} = \frac{(m + x)(s + x)}{(m - x)} \quad (6)$$

Eliminating x between equations 5 and 6 one obtains

$$\frac{S}{4s^2}\left(m - s + \frac{S}{4s^2}\right) = K_2\left(m + s - \frac{S}{4s^2}\right) \quad (7)$$

In calculating the solubility of Ag_2SO_4 at any given temperature and molality of H_2SO_4 values of A_s and A_K were assumed. Then an initial arbitrary value of I was substituted into equations 1 and 4 to give initial values of S and K_2. Equation 7 was then solved by successive approximations to obtain a value of s_{calcd} (the calculated solubility of Ag_2SO_4 in the H_2SO_4 solution). The value of s_{calcd} was used to correct I by means of equation 2. The process was repeated until successive values of s_{calcd} agreed to within 0.1%. This method yielded a consistent set of values of s, S, K_2 and I.

The calculations were carried out at 25° intervals from 25 to 250° at each concentration of H_2SO_4 using various combinations of A_s and A_K. It was found that the calculated solubilities were very sensitive to the values of A_s and A_K chosen and that best fit was obtained with $A_s = 0.7$ and $A_K = 0.4$. Making A_s and A_K vary as $(DT)^{-1/2}$ did not produce a better fit; this same observation was made in the cases of Ag_2SO_4 solubility in KNO_3 and K_2SO_4 solutions.

Figure 1 shows a plot of the observed solubility of Ag_2SO_4 in H_2SO_4 solutions and solubilities calculated with $A_s = 0.7$ and $A_K = 0.4$. The agreement is very close except at the highest temperatures in 1.0 m H_2SO_4 where at a given temperature the calculated solubility is too low. In Table I is shown the effect of changing A_K from 0.4 to 2.0: in all cases the agreement becomes much poorer.

(1) This paper is based upon work performed for the United States Atomic Energy Commission at the Oak Ridge National Laboratory operated by Union Carbide Corporation.

(2) M. H. Lietzke and R. W. Stoughton, This Journal, **63**, 1183 (1959).

(3) M. H. Lietzke and R. W. Stoughton, *ibid.*, **63**, 1186 (1959).

(4) M. H. Lietzke and R. W. Stoughton, *J. Am. Chem. Soc.*, **78**, 3023 (1956).

(5) G. C. Akerlof and H. I. Oshry, *ibid.*, **72**, 2844 (1950).

(6) T. F. Young, private communication.

TABLE I

THE SOLUBILITY OF Ag_2SO_4 IN H_2SO_4 SOLUTIONS

	s_{obsd}	$A_S = 0.7$ $A_K = 0.4$	$A_S = 0.7$ $A_K = 2.0$
	$m_{H_2SO_4} = 0.1$		
25	0.0292	0.0306	0.0350
50	.0463	.0462	.0537
75	.0615	.0613	.0717
100	.0747	.0765	.0884
125	.0858	.0893	.100
150	.0946	.0985	.107
175	.101	.104	.110
200	.105	.106	.109
225	.106	.105	.106
250	.104	.103	.103
	$m_{H_2SO_4} = 0.5$		
25	0.0332	0.0350	0.0546
50	.0510	.0578	.0975
75	.0803	.0862	.155
100	.120	.123	.231
125	.167	.168	.316
150	.218	.218	.394
175	.272	.269	.449
200	.323	.315	.478
225	.370	.351	.489
	$m_{H_2SO_4} = 1.0$		
25	0.0347	0.0369	0.0723
50	.0514	.0617	.136
75	.0835	.0939	.228
100	.134	.139	.363
125	.201	.195	.533
150	.280	.265	.712
175	.370	.346	.852
200	.468	.435	.931
225	.572	.517	.965
250	.677	.562	.972

While the calculations were in progress it was evident that no reasonable assumptions regarding the variation of K_2 and S with temperature and ionic strength gave calculated values agreeing with several of the observed values previously reported.[4] Hence the measurements were repeated using accurately weighed quantities of Ag_2SO_4 and H_2SO_4 solution in each tube to yield the observed values reported in this paper. It is believed that several of the former results were in error due to analytical inaccuracies in the silver determinations.

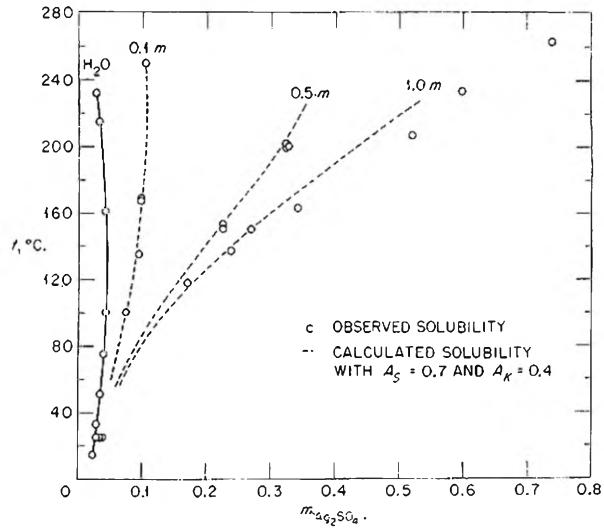

Fig. 1.—The solubility of Ag_2SO_4 in H_2SO_4 solutions.

The value $A_S = 0.7$ observed in this work agrees with the average value of A_S giving best fit in the solubility of Ag_2SO_4 in K_2SO_4 solutions.[3] The value $A_K = 0.4$ agrees with the value found by C. F. Baes, Jr.,[7] when using the data of T. F. Young in fitting the variation of the log of the bisulfate concentration quotient in pure H_2SO_4 media at 25° against the square root of the ionic strength. In general, decreasing the value of A_S increases the calculated solubility of Ag_2SO_4 in H_2SO_4 and decreasing the value of A_K decreases the calculated value. Thus to some extent a simultaneous decrease or increase of both these parameters is self-compensating, although by no means completely so with varying m and T.

The present paper shows in a striking manner how the use of a high speed digital computer can be used not only to fit solubility data with expressions of the Debye–Hückel type but also to show up inconsistencies in a set of solubility data.

Acknowledgment.—The authors wish to express their appreciation to M. P. Lietzke for assistance in programming the equations for the ORACLE (the high speed digital computer at ORNL) and to L. N. Cain for performing the experimental solubility measurements.

(7) C. F. Baes, Jr., private communication.

THE SOLUBILITY OF SILVER SULFATE IN ELECTROLYTE SOLUTIONS. PART 4. SOLUBILITY IN NITRIC ACID SOLUTIONS[1]

By M. H. Lietzke and R. W. Stoughton

Contribution from the Chemistry Division, Oak Ridge National Laboratory, Oak Ridge, Tenn.

Received January 10, 1959

The solubility of Ag_2SO_4 has been measured in 0.03, 0.1, 0.5, 0.8 and 1.0 *m* HNO_3 to about 200°. Using the solubility in pure water; T. F. Young's equations for the dissociation constants of HSO_4^- and HNO_3 *vs.* temperature; and the assumption that all activity coefficients vary with ionic strength according to Debye–Hückel expressions; solubilities were calculated at 25° intervals to 200° for the concentrations of HNO_3 used in the measurements. The good agreement obtained in this and previous work led to the conclusions that (1) the principal species assumed to exist are correct and (2) the Debye–Hückel equation is as applicable at elevated temperatures as at room temperature in nitrate and sulfate media.

Previous papers in this series have described the solubility of Ag_2SO_4 in KNO_3,[2] K_2SO_4[3] and H_2SO_4[4] solutions. The present paper describes the solubility of Ag_2SO_4 in HNO_3 solutions over a wide range of temperature and ionic strength. As in the previous papers a high speed digital computer has been used to show the application of expressions of the Debye–Hückel type in describing the solubility data. In fact, in systems as complex as this one such calculations could hardly be carried out on a desk calculator.

Experimental

The solubility measurements were carried out using the synthetic method described previously.[5] The solubility points were sharp and reproducible to about ±1°.

Results and Discussion

In Fig. 1 the circled points represent the experimentally determined solubility values for Ag_2SO_4 in HNO_3 solutions. The values for the solubility of Ag_2SO_4 in H_2O were reported in the first paper in this series.[2]

As in the previous papers it is assumed that the molality solubility product S of Ag_2SO_4 in HNO_3 solutions can be expressed by equation 1

$$\ln S = \ln S_0 + s_T\left[\frac{\sqrt{I}}{1 + A_s\sqrt{I}} - \frac{\sqrt{I_0}}{1 + A_s\sqrt{I_0}}\right] \quad (1)$$

where s_T is the Debye–Hückel limiting slope at temperature T for a 1–2 electrolyte; S_0 is the molality solubility product of Ag_2SO_4 in pure water at the same temperature; I is the ionic strength of the solution; I_0 is the ionic strength of Ag_2SO_4 in pure water; and A_s is either a constant or a term that varies as $(DT)^{-1/2}$. The dielectric constant D of water was computed at each temperature using the equation given by Akerlof and Oshry.[6]

In all subsequent calculations it was assumed that only the species Ag^+, $SO_4^=$, H^+, NO_3^-, HNO_3 and HSO_4^- exist in solution. The molal concentrations of these species are related to each other by the definitions of the molality solubility product S and of the concentration quotients $K_{HSO_4^-}$ and K_{HNO_3}

$$S = (m^2_{Ag^+})(m_{SO_4^=}) \quad (2)$$

$$K_{HSO_4^-} = \frac{(m_{H^+})(m_{SO_4^=})}{m_{HSO_4^-}} \quad (3)$$

$$K_{HNO_3} = \frac{(m_{H^+})(m_{NO_3^-})}{m_{HNO_3}} \quad (4)$$

Using these equations and the new variables $u = S/4s^3$, the molalities of the various species are expressible in terms of the calculated solubility s, u, $K_{HSO_4^-}$ and K_{HNO_3}. The ionic strength becomes

$$I = \frac{K_{HSO_4^-}}{u}(1 - u) + s(u + 2) \quad (5)$$

Equations 2, 3 and 4 may also be combined to give equation 6, which the calculated s must satisfy

$$s(1 - u)\left[1 + \frac{K_{HSO_4^-}}{uK_{HNO_3}}(1 - u)\right] = m - \frac{K_{HSO_4^-}}{u}(1 - u)\left[1 + \frac{K_{HSO_4^-}}{uK_{HNO_3}}(1 - u)\right] \quad (6)$$

where m is the molality of HNO_3.

Equations for the variation of the acid dissociation constants $K^0_{HSO_4^-}$ and $K^0_{HNO_3}$ with temperature were obtained from T. F. Young.[7]

$$\ln K^0_{HSO_4^-} = 15.99658 - \frac{1785.390}{T} - 0.04892367T \quad (7)$$

$$\ln K^0_{HNO_3} = 15.09843 - \frac{738.8574}{T} - 0.03130147T \quad (8)$$

The concentration acid quotients $K_{HSO_4^-}$ and K_{HNO_3} in the Ag_2SO_4 solutions were assumed to vary with ionic strength at any temperature according to equations 9 and 10.

$$\ln K_{HSO_4^-} = \ln K^0_{HSO_4^-} + S'\frac{\sqrt{I}}{1 + A_K\sqrt{I}} \quad (9)$$

$$\ln K_{HNO_3} = \ln K^0_{HNO_3} + S''\frac{\sqrt{I}}{1 + A_N\sqrt{I}} \quad (10)$$

where $\ln K^0_{HSO_4^-}$ and $\ln K^0_{HNO_3}$ are given by equations 7 and 8; S' and S'' are the corresponding Debye–Hückel limiting slopes for the ion quotients involved in equations 3 and 4, respectively; and A_K and A_N are either constants or terms that vary as $(DT)^{-1/2}$.

In calculating the solubility of Ag_2SO_4 at any given temperature and molality of HNO_3 values of A_s, A_K and A_N (as previously defined) were assumed. An initial arbitrary value of I was substituted into equations 1, 9 and 10 to give initial values of S, $K_{HSO_4^-}$ and K_{HNO_3}. Equation 6 then was solved by successive approximations to obtain a

(1) This paper is based upon work performed for the United States Atomic Energy Commission at the Oak Ridge National Laboratory operated by Union Carbide Corporation.

(2) M. H. Lietzke and R. W. Stoughton, This Journal, **63**, 1183 (1959).

(3) M. H. Lietzke and R. W. Stoughton, *ibid.*, **63**, 1186 (1959).

(4) M. H. Lietzke and R. W. Stoughton, *ibid.*, **63**, 1188 (1959).

(5) M. H. Lietzke and R. W. Stoughton, *J. Am. Chem. Soc.*, **78**, 3023 (1956).

(6) G. C. Akerlof and H. I. Oshry, *ibid.*, **72**, 2844 (1950).

(7) T. F. Young, private communication.

TABLE I

THE SOLUBILITY OF Ag_2SO_4 IN HNO_3 SOLUTIONS

t, °C.	s_{obsd}	s_{calcd}: $A_s = 0.65$, $A_K = 0.4$, $A_N = 0.5$	s_{calcd}: $A_s = 0.7$, $A_K = 0.4$, $A_N = 2.0$
	0.03 m HNO_3		
25	0.0328	0.0331	0.0330
50	.0393	.0429	.0429
75	.0445	.0505	.0504
100	.0482	.0555	.0554
125	.0506	.0580	.0578
150	.0515	.0580	.0578
175	.0511	.0558	.0556
200	.0493	.0516	.0515
	0.1 m HNO_3		
25	0.0428	0.0446	0.0443
50	.0590	.0605	.0601
75	.0725	.0755	.0751
100	.0830	.0887	.0883
125	.0920	.0990	.0985
150	.100	.106	.105
175	.105	.109	.108
200	.110	.109	.108

t, °C.	s_{obsd}	s_{calcd}: $A_s = 0.65$, $A_K = 0.4$, $A_N = 0.5$	s_{calcd}: $A_s = 0.7$, $A_K = 0.4$, $A_N = 2.0$	s_{calcd}: $A_s = 0.7$, $A_K = 0.4$, $K_N = \infty$
		0.5 m HNO_3		
25	0.0786	0.0779	0.0779	0.0781
50	.106	.115	.112	.112
75	.146	.154	.150	.151
100	.194	.199	.193	.195
125	.243	.248	.239	.244
150	.291	.298	.284	.294
175	.339	.345	.325	.341
200	.386	.384	.356	.381
		0.8 m HNO_3		
25	0.0929	0.0958	0.0924	0.0928
50	.135	.138	.133	.134
75	.185	.188	.180	.183
100	.245	.246	.234	.239
125	.315	.311	.293	.303
150	.387	.382	.354	.372
175	.458	.452	.410	.442
200	.530	.516	.455	.507
		1.0 m HNO_3		
25	0.108	0.104	0.100	0.101
50	.151	.151	.144	.146
75	.205	.206	.196	.199
100	.270	.271	.255	.261
125	.340	.344	.321	.333
150	.416	.425	.388	.412
175	.500	.507	.452	.494
200	.605	.585	.503	.571

value of s_{calcd} (the calculated solubility of Ag_2SO_4 in the HNO_3 solution). The value of s_{calcd} was used to correct I by means of equation 5. The process was repeated until successive values of s_{calcd} agreed to within 0.1%. This method yielded a consistent set of values of s, S, $K_{HSO_4^-}$, K_{HNO_3} and I.

The calculations were carried out at 25° intervals from 25 to 200° at each concentration of HNO_3 using various combinations of A_s, A_K and A_N. It was found that increasing A_s or decreasing A_K decreases the calculated solubility of silver sulfate. If A_s and A_K are decreased together, essentially the same results are obtained. Hence, it is more difficult in nitric acid solutions to get a unique set of the constants than in the other systems studied where only one or two of the parameters were involved. The closest agreements between the calculated and observed solubilities were obtained with $A_s = 0.65$, $A_K = 0.4$ and $A_N = 0.5$; or with $A_s = 0.55$, $A_K = 0.3$ and $A_N = 0.5$. Undoubtedly values of A_s between 0.55 and 0.65 with corresponding best-fit values of A_K between 0.3 and 0.4 would give equally good results. The calculated solubilities plotted in Fig. 1 correspond to the first set mentioned. These values are also given in Table I along with solubilities calculated using $A_s = 0.7$, $A_K = 0.4$ and $A_N = 2.0$. The value of A_N is not very important except at the highest temperatures. This effect is as expected in view of the fact that HNO_3 is a relatively strong acid at the lower temperatures, and at any temperature its acid quotient K_{HNO_3} is much larger than the acid constant $K^0_{HNO_3}$ at the ionic strength values obtaining here. From room temperature activity coefficient data the value corresponding to A_N in the equation for ln $\gamma^{\pm}$ is about 2.0; the value of A_N in equation 10 found to give the best over-all fit in the present work, however, was about 0.5, although the value of this parameter was not as critical as those in equations 1 and 9.

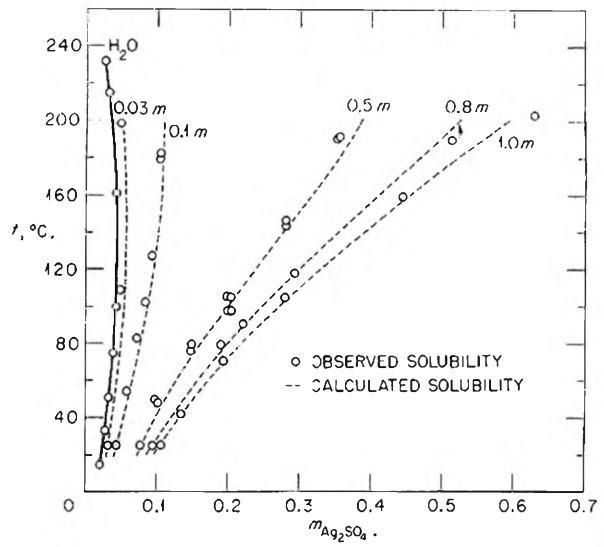

Fig. 1.—The solubility of Ag_2SO_4 in HNO_3 solutions.

Calculations also were performed assuming HNO_3 is a strong acid over the entire temperature range. These values are given in Table I for the three highest concentrations of HNO_3. As can be seen, a slightly better fit is obtained if equations 8 and 10 are used at the highest temperatures. If the incomplete dissociation of HNO_3 is ignored, then the value of A_s giving the best fit is larger, *i.e.*, $A_s = 0.7$ with $A_K = 0.4$.

If the values of A_s, A_K and A_N which give best fit are made to vary as $(DT)^{-1/2}$, *i.e.*, if the value of $\hat{a}$ is assumed to be constant, the net effect is to produce poorer calculated solubilities of Ag_2SO_4 than if the $(DT)^{-1/2}$ variation is omitted. This is especially true at the higher temperatures where the calculated values become too low.

As in the previous solubility systems studied the

temperature independence of the A-parameters may imply that the $(DT)^{-1/2}$ variation of the A-values may be just about offset by a decrease in the $\mathring{a}$ ("distance of closest approach") values or in the solvent density with temperature.

Hence it appears that expressions of the Debye–Hückel type can be used to describe the solubility of Ag_2SO_4 in HNO_3 solutions over a wide range of concentration and temperature. It is further concluded that the principal species obtaining in solution are those assumed to exist.

Acknowledgment.—The authors wish to express their appreciation to L. N. Cain for performing the experimental solubility measurements.

THE SOLUBILITY OF TANTALUM AND COBALT IN SODIUM BY ACTIVATION ANALYSIS[1]

BY J. A. GRAND, R. A. BAUS, A. D. BOGARD, D. D. WILLIAMS, L. B. LOCKHART, JR., AND R. R. MILLER

Chemistry Division, Naval Research Laboratory, Washington 25, D. C.

Received January 10, 1959

The solubilities of tantalum and cobalt were determined by equilibrating sodium in tantalum and cobalt vessels at three temperatures. The sodium was irradiated in the Materials Testing Reactor. The solubility values were determined from a separation and counting of active isotopes in the sodium metal. Tantalum solubility ranged from 0.032 to 2.9 parts per million from 325 to 525°. The range on cobalt was from 0.28 to 0.1 part per million from 365 to 525°.

A coöperative study of activity transport in sodium-cooled systems was conducted by a group of laboratories.[2-4] These investigations were concerned with radioactivity produced in the structural materials of a power reactor and transferred by the sodium coolant to other parts of the system. Radioactivity deposited in parts of the system outside of the reactor proper could limit personnel accessibility for repair or maintenance. Although this problem was found to be of only limited importance, radioactivity was produced in type 347 stainless steel that could have been serious if transported in large amounts. The isotopes of most importance were formed by these reactions: $Fe^{54}(n,p)Mn^{54}$, $Co^{59}(n,\gamma)Co^{60}$, $Ta^{181}(n,\gamma)Ta^{182}$ and $Cr^{50}(n,\gamma)Cr^{51}$. As part of this program the solubility of tantalum and cobalt in sodium was determined at the Naval Research Laboratory.

Experimental

Method.—The solubility determinations were made by equilibrating sodium in tantalum and in cobalt vessels in a series of runs at three temperatures. At the end of the equilibration period, the sodium was withdrawn at temperature in a quartz pipet. Each sodium sample, with monitors of tantalum, cobalt and iron, was sent to the Materials Testing Reactor for irradiation. Subsequent radiochemical analysis of the sodium and the monitors permitted the solubility to be calculated.

The runs were made by distilling sodium in a stainless steel still, at a pot temperature of 450–500° and a pressure of 0.1 μ, into a Pyrex receiver fitted with a filter. The sodium was filtered at just above the melting point into a stainless steel equilibration apparatus containing a cobalt or a tantalum vessel. These vessels were in the form of test-tubes approximately 2.2 cm. i.d. and 17 cm. long and were inserted in a Type 347 stainless steel container approximately 3 cm. i.d. and 19 cm. long. The upper part of the container was fitted with a stainless steel filling tube and a stainless steel vertical arm connected through Kovar to a glass assembly for sampling purposes. The filling tube extended into the tantalum or cobalt vessel to minimize splattering. The apparatus was sealed off with 300–400 mm. pressure of argon in the vessel and transferred to a controlled furnace, maintained at the desired temperature. The tantalum runs were made at 325, 425 and 525° and the cobalt runs at 365, 425 and 525°. The samples were equilibrated 24 hours with electromagnetic stirring and then connected to auxiliary apparatus by a side-arm spherical joint. The system was opened through a "break-offski" in the side-arm and argon admitted. With argon flowing through the system, a quartz pipet was inserted through the vertical arm and all of the sodium (approximately 35 g.) withdrawn at temperature. Monitors forwarded with each sodium sample for irradiation were individually sealed in quartz. The conditions of the experiments precluded the taking of sodium samples for oxygen analysis. Similar experiments at this Laboratory lead to the assumption that the oxygen content of the sodium was in the range 0.001–0.002 wt. %.

Chemical Procedures.—The analytical procedures involved complete solution of the sample, addition of inactive carriers in known amounts, and treatment with HF–HNO_3–H_2SO_4 and later H_2O_2. Following this, gross separations of the elements were made, followed by rigorous decontamination steps. These procedures previously had been tested and found to give excellent decontamination from other activities present or suspected. The separations were adapted from the work of Meinke[5] and others.[6] A known weight of the separated material (usually 50 mg.) was mounted in a reproducible manner on a plastic holder using a trace of collodion as binder. Aliquot size was adjusted so that the counting rate of the mounted sample fell in the range 100–5000 c./m.

Counting Techniques.—The samples were counted on standard β-counting equipment (the γ from Zn^{65} was counted with low efficiency) using halogen-filled, end-window G–M tubes. The equipment was calibrated using standards prepared from National Bureau of Standards solutions of C^{14}, Co^{60}, Sr^{90} (Y^{90}), RaD-E and P^{32}. Corrections for sample weight, absorption, back-scattering, geometry and window thickness were applied.

Results

The results of the radiochemical analyses of the sodium samples from the tantalum studies are given in Table I. All activities are corrected to the out-of-pile date. In Table II is given the Ta^{182} activity found in the corresponding monitors. Fe^{59}, Co^{60} and Sn^{123} activities also were found but were a factor of 10^7 lower than the tantalum ac-

(1) Presented at the Division of Analytical Chemistry, 133rd Meeting, ACS, San Francisco, Calif., April, 1958.

(2) F. G. Haag, *Chem. Eng. Progr. Symp. Series*, **53**, 43 (1957).

(3) U. Hashimoto, *Nippon Kunzoku Gakkai-Si*, **2**, 67 (1938).

(4) C. B. Jackson, *et al.*, "Liquid Metals Handbook," 3rd ed., pages 134–151, Government Printing Office, 1955.

(5) W. W. Meinke, U. S. Atomic Energy Comm. AECD-2738 (Aug. 1949), AECD-3084 (Mar. 1951).

(6) Los Alamos Scientific Laboratory. "Collected Radiochemical Procedures." LA-1721 (Dec. 1954).

tivity. The sodium samples and monitors were irradiated for 16.6 days at a reported flux of 1×10^{14} thermal neutrons/cm.^{2}/sec. Calculations of the flux from the tantalum monitor activity found, and substantiated by the activity levels of the cobalt and iron monitors, gave values of 2.8, 2.8 and 1.3×10^{13} for the three experiments. The calculated reduction in flux due to the irradiation containers was approximately 10%. The flux difference encountered may have been due to shadowing by other samples. This information is cited only to inform other experimenters of the necessity of using adequate monitors.

TABLE I

RADIOACTIVITY FOUND IN SODIUM FROM TANTALUM EXPERIMENTS

Isotope	Expt. no. 1 (325°), d./m./g. Na	Expt. no. 2 (425°), d./m./g. Na	Expt. no. 3 (525°), d./m./g. Na
Ag^{110}	6.5×10^5	9.9×10^5	2.9×10^6
Cd^{115}	8.5×10^4	1.1×10^5	3.0×10^4
Co^{60}	6.6×10^3	7.8×10^3	3.3×10^4
Fe^{59}	3.5×10^3	4.0×10^3	2.4×10^4
Sb^{124}	9.4×10^3	1.4×10^4	6.0×10^4
Sn^{123}	6.6×10^2	1.1×10^3	8.1×10^2
Zn^{65}	1.1×10^5	2.1×10^5	1.9×10^5
Ta^{182}	3.7×10^5	2.1×10^6	1.6×10^7

TABLE II

RADIOACTIVITY FOUND IN TANTALUM MONITORS

Isotope	Expt. no. 1 d./m./g. Ta	Expt. no. 2 d./m./g. Ta	Expt. no. 3 d./m./g. Ta
Ta^{182}	1.14×10^{13}	1.13×10^{13}	0.55×10^{13}

The solubility of tantalum in sodium in grams/gram may be calculated by dividing the d./m. of Ta^{182} per gram of sodium in Table I by the corresponding d./m. of Ta^{182} per gram of tantalum. The concentration of the other elements present whose isotopes are reported in Table I may be calculated from cross section and flux data. These results with a sub-total of the impurities are given in Table III. It should be emphasized that the tantalum solubility figures are not dependent on flux or cross section data.

TABLE III

EFFECT OF TEMPERATURE ON THE CONCENTRATION OF IMPURITIES AND SOLUBILITY OF TANTALUM IN SODIUM

Element	Expt. no. 1 (325°), p.p.m.	Expt. no. 2 (425°), p.p.m.	Expt. no. 3 (525°), p.p.m.
Ag	0.04	0.06	0.4
Cd	.1	.1	.08
Co	.002	.002	.02
Fe	.4	.4	5
Sb	.004	.006	0.05
Sn	.2	.3	.4
Zn	.6	1.1	2
Total	1.35	1.97	7.95
Ta	0.032	0.19	2.9

The corresponding data for the cobalt experiments are shown in Tables IV, V and VI. The samples for these experiments were irradiated 15.4 days at a reported flux of 1×10^{14} thermal neutrons/cm.^{2}/sec. Calculation of the flux from the monitors gave values of 3.5, 4.2 and 2.0×10^{13}. Activities in the cobalt monitors other than Co^{60} were of the order of 10^5 lower than the Co^{60} activity.

TABLE IV

RADIOACTIVITY FOUND IN SODIUM FROM COBALT EXPERIMENTS

Isotope	Expt. no. 4 (365°), d./m./g. Na	Expt. no. 5 (425°), d./m./g. Na	Expt. no. 6 (525°), d./m./g. Na
Ag^{110}	5.9×10^7	5.6×10^7	2.7×10^7
Cd^{115}	9.9×10^5	5.0×10^5	5.0×10^5
Fe^{59}	1.5×10^3	5.6×10^3	8.5×10^3
Sb^{124}	9.0×10^3	8.1×10^4	3.0×10^4
Sn^{123}	1.8×10^2	1.0×10^2	1.6×10^2
Zn^{65}	3.5×10^5	1.6×10^5	5.5×10^5
Co^{60}	1.2×10^5	1.1×10^5	2.4×10^6

TABLE V

RADIOACTIVITY FOUND IN COBALT MONITORS

Isotope	Expt. no. 4, d./m./g. Co	Expt. no. 5, d./m./g. Co	Expt. no. 6, d./m./g. Co
Co^{60}	4.27×10^{12}	5.19×10^{12}	2.40×10^{12}

TABLE VI

EFFECT OF TEMPERATURE ON THE CONCENTRATION OF IMPURITIES AND SOLUBILITY OF COBALT IN SODIUM

Element	Expt. no. 4 (365°), p.p.m.	Expt. no. 5 (425°), p.p.m.	Expt. no. 6 (525°), p.p.m.
Ag	3	3	3
Cd	1	0.5	1
Fe	0.1	.4	1.4
Sb	.003	.02	0.02
Sn	.04	.02	0.07
Zn	1.7	.6	5
Total	5.8	4.5	10.5
Co	0.028	0.021	1.00

Discussion

The solubility data for tantalum in sodium gives a fair straight line presentation when the log of the solubility is plotted against the reciprocal of the temperature. The presence of impurities shown in Table III would tend to throw some question on the validity of the experiments. The impurities found are typical for sodium exposed to stainless steel. Elements such as silver, cadmium, antimony, tin and zinc are soluble in sodium and are readily leached from stainless steel. Presumably they were present from the distillation and filling operation. However, the over-all increase in impurities with temperature indicates refluxing and leaching from the stainless steel filling tube. Unfortunately a blank on the filling operation was not made as this would have given information on the extent of leaching. Difficulty might be obviated by the use of an all tantalum system. A point of conjecture too, is the question as to whether the measurement of solubility, in the case of relative insoluble components such as iron, nickel, cobalt and tantalum, is a measure of the solubility of the metal or of possibly a double oxide of sodium and the metal. This may be significant in consideration of the fact that the low oxygen content of these systems is still sufficient to account for these oxides.

A plot of the log solubility of cobalt against the

reciprocal of temperature indicates a possible error in the 425° point. This could be due to the α–β transformation of cobalt occurring in the range 420–486°.[2] The values at 365 and 425° are of the same magnitude as the value for cobalt as an impurity in sodium–potassium alloy reported by Smales.[7]

(7) A. A. Smales, Proc. Int. Conf. Peaceful Uses Atomic Energy (Geneva, Aug. 8–20, 1955), 9, 273 (1956).

ON A MODEL FOR THE HELIX–RANDOM COIL TRANSITION IN POLYPEPTIDES.[1,2] I. THE MODEL AND ITS THERMAL BEHAVIOR

BY LEONARD PELLER[3]

Frick Chemical Laboratory, Princeton University, Princeton, New Jersey

Received January 15, 1959

An Ising partition function is employed to describe a range of configurational states of a long polypeptide chain in dilute aqueous solution. A thermal transition from an essentially helical to an essentially random coil state occurs in a coöperative fashion. The transition temperature depends only on the magnitude of the difference in nearest neighbor interaction enthalpies and the difference in entropy between the amino acid residues in the helical and random coil forms. An extremely sharp transition occurs when the likelihood of adjoining units being in different configurational states is small. Operationally defined enthalpies and entropies for the transition are discussed.

Introduction

The studies of Doty, Blout and their collaborators[4–6] have strikingly demonstrated the existence of structural transitions for a number of synthetic polypeptides in solution. These structural changes have been interpreted as reversible transformations between helical and randomly coiled states for the macromolecules. Concurrent with this experimental work there has been an interest in the development of models to explore certain thermodynamic aspects of this transition as influenced by various factors, *e.g.*, temperature, solvent composition and charge interactions.[7a,b,8–11]

While these transformations are of enormous interest in themselves, their discovery has had the further important result of focusing attention on the possible occurrence of similar transitions in many proteins.[12–14] The phenomena of protein denaturation, while undoubtedly involving effects not encountered in single polypeptide chains, do exhibit a number of interesting parallels with the helix–coil transitions. Some of these similarities may be illuminated by consideration of a simple model for the polypeptide transformations.

The Partition Function for the Polypeptide.—In developing a model for the helix–random coil transition of a single polypeptide chain, the central problem is the construction of a partition function which will be applicable to a range of configurational states. In Fig. 1 three such states are illustrated. Figure 1a depicts the helical or completely ordered state with the maximum number of intramolecular hydrogen bonds. So far as these short range interactions are concerned, this form represents the state of minimum internal energy. Figure 1c depicts the random coil or completely disordered state with the maximum rotational freedom about the polypeptide backbone. This form represents the state of maximum configurational entropy. Figure 1b depicts an intermediate configurational state with alternating random coil and helical regions. Under given conditions this form may be the most probable state for the system, *i.e.*, the state of minimum free energy.[15]

At the junctions between helical and random coil regions there will be a certain number of residues which are hydrogen bonded to only *one* nearest neighbor residue. The residues in the body of a helical region are hydrogen bonded to *two* nearest neighbors while those in random coil regions are considered not to be intramolecularly hydrogen bonded. However, these terminal helical residues with one broken hydrogen bond have presumably acquired little more librational entropy than those in the body of a helix. We assume that there will be three such residues at each junction between a helical and a random coil region for an α-helix.

(1) Taken in part from a thesis presented to Princeton University in partial fulfillment of the requirements for the Ph.D. degree, November, 1957.

(2) Presented in part before the Division of Biological Chemistry, 133rd National Meeting of the American Chemical Society, San Francisco, April 13–18, 1958, and more extensively before the Division of Physical Chemistry—Symposium on the Statistical Mechanics of the Helix-Random Coil Transitions in Polypeptides and Polynucleotides, 134th National Meeting of the American Chemical Society, Chicago, September 7–12, 1958.

(3) Department of Chemistry, University of Wisconsin, Madison, Wisconsin.

(4) P. Doty and J. T. Yang, *J. Am. Chem. Soc.*, **78**, 498 (1956).

(5) P. Doty, A. Wada, J. T. Yang and E. R. Blout, *J. Polymer Sci.*, **23**, Symposium on Macromolecules Part 2, 85 (1957).

(6) P. Doty, K. Imahori and E. Klemperer, *Proc. Nat. Acad. Sci.*, **44**, 424 (1958).

(7a) J. A. Schellman, *Compt. rend. trav. lab. Carlsberg. Sér. chim.*, **29**, 230 (1955).

(7b) J. A. Schellman, THIS JOURNAL, **62**, 1485 (1958).

(8) B. H. Zimm and J. K. Bragg, *J. Chem. Phys.*, **28**, 1246 (1958).

(9) J. H. Gibbs and E. A. DiMarzio, *ibid.*, **28**, 1247 (1958).

(10) S. A. Rice, A. Wada and E. P. Geiduschek, *Disc. Faraday Soc.*, in press.

(11) T. L. Hill, *J. Chem. Phys.*, **30**, 383 (1959).

(12) W. F. Harrington and J. A. Schellman, *Compt. rend. trav. lab. Carlsberg, Sér. chim.*, **30**, 21 (1956).

(13) J. T. Yang and P. Doty, *J. Am. Chem. Soc.*, **79**, 761 (1957).

(14) For a recent review which discusses configurational changes in proteins and their relation to the helix-coil transitions in polypeptides see W. Kauzmann, The Physical Chemistry of Proteins in "Annual Review of Physical Chemistry," Annual Reviews, Inc., Palo Alto, Calif., 1957, Vol. 8, pp. 413–438.

(15) Evidence in support of the existence of this interrupted helix was presented by P. Doty, J. T. Yang and J. R. Fresco before the Division of Physical Chemistry—Symposium on the Statistical Mechanics of the Helix-Random Coil Transitions in Polypeptides and Polynucleotides, 134th National Meeting of the American Chemical Society, Chicago, September 7–12, 1958.

Schellman[7a] has earlier pointed out the significance of these atypical residues in determining the minimum sized helix which is more stable than the corresponding random coil.

The isothermal-isobaric partition function (Δ) for a polypeptide can be written formally as

$$\Delta = \sum_{(N_h, N_c, N_{hh}, N_{cc}, N_{hc})} g(N_h, N_c, N_{hc}) \; f_h^{x(N_h - N_{hc})} \; f_h'^{xN_{hc}} \; f_c^{xN_c} \; e^{-x(\omega_{hh}N_{hh} + \omega_{cc}N_{cc} + \omega_{hc}N_{hc})/RT} \tag{1}$$

N_h and N_c are, respectively, the numbers of helical and random coil units where a unit consists of x residues taken to be three for an α-helix. f_h and f_c are the partition functions for the internal degrees of freedom of helical and random coil residues, respectively. f_h' is the partition function for the terminal helical residues. N_{hh} and N_{cc} are the number of pairs of neighboring helical and random coil units, respectively. N_{hc} is the number of pairs of units, one of which is helical and the other random coil. w_{hh}, w_{cc} and w_{hc} are the corresponding heats of interaction per mole for these pairs of nearest neighbors.

For a polypeptide chain consisting of N amino acid residues, it follows from the definition of N_h and N_c that

$$x(N_h + N_c) = N \tag{2a}$$

Moreover, regarding each residue as having two nearest neighbors we have

$$2N_{hh} + N_{hc} = 2N_h \tag{2b}$$

$$2N_{cc} + N_{hc} = 2N_c \tag{2c}$$

Utilizing equations 2b and 2c the expression for Δ can be given in terms of N_h, N_c and N_{hc} as

$$\Delta = \sum_{(N_h, N_c, N_{hc})} g(N_h, N_c, N_{hc})(j_h)^{N_h}(j_c)^{N_c}(y_{hc})^{N_{hc}} \tag{3}$$

where

$j_h \equiv (f_h e^{-w_{hh}/RT})^x$, $j_c \equiv (f_c e^{-w_{cc}/RT})^x$, and

$$y_{hc} \equiv \left[\frac{f_h'}{f_h} e^{-(w_{hc} - w_{hh}/2 - w_{cc}/2)/RT}\right]^x$$

The appropriate combinatorial factor (g) for a long polypeptide chain is given in the usual form for a one dimensional Ising model as

$$g(N_h, N_c, N_{hc}) = \left[\frac{N_h!}{\left(N_h - \frac{N_{hc}}{2}\right)!\left(\frac{N_{hc}}{2}\right)!}\right] \left[\frac{N_c!}{\left(N_c - \frac{N_{hc}}{2}\right)!\left(\frac{N_{hc}}{2}\right)!}\right] \tag{4}$$

There are $N_{hc}/2$ helical and random coil regions among which the N_h and N_c helical and random coil units are distributed.

Equilibrium State.—The free energy per mole of the polypeptide chain is given by

$$F = -RT \ln \Delta \tag{5}$$

Δ may be approximated by its maximum term (t_{max}) in equation 3 which is obtained from the two conditions[16]

$$\left[\frac{\partial(\ln t)}{\partial N_{hc}}\right]_{N_c} = 0 \tag{6a}$$

(16) For general methods of treating the one dimensional Ising model see T. L. Hill, "Statistical Mechanics," McGraw-Hill Book Co., Inc. New York, N. Y., 1956, pp. 318-327.

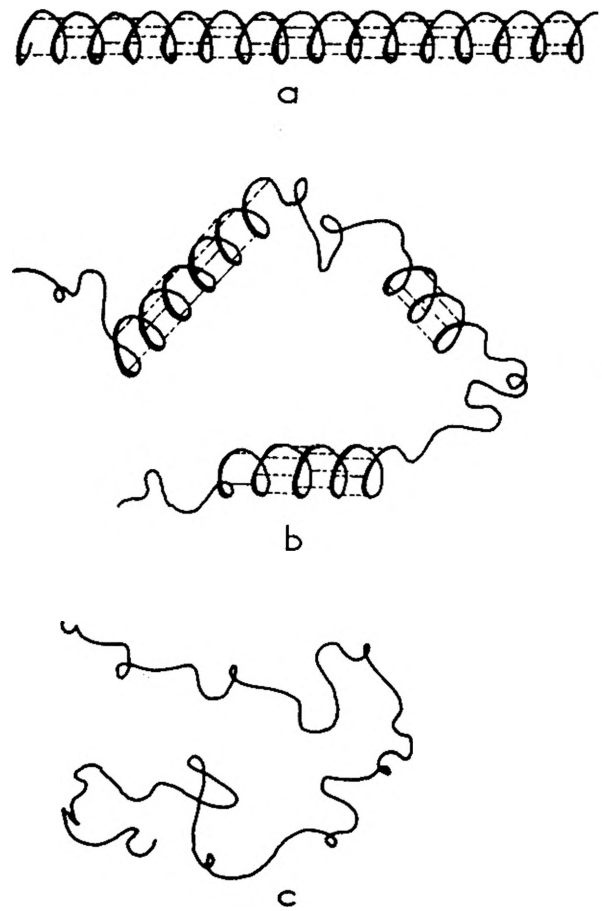

Fig. 1.—The two extreme configurational states (a and c) and an intermediate configuration (b) of the polypeptide.

$$\left[\frac{\partial(\ln t)}{\partial N_c}\right]_{N_{hc}} = 0 \tag{6b}$$

Employing Stirling's approximation for $\ln t$ and equating the derivative with respect to N_{hc} to zero as in equation 6a yields

$$\frac{(N_{hc})^2}{\left(N_h - \frac{N_{hc}}{2}\right)\left(N_c - \frac{N_{hc}}{2}\right)} = \frac{(N_{hc})^2}{(N_{hh})(N_{cc})} = 4(y_{hc})^2 \tag{7a}$$

Similarly equation 6b combined with equation 2a yields

$$\frac{N_h\left(N_c - \frac{N_{hc}}{2}\right)}{N_c\left(N_h - \frac{N_{hc}}{2}\right)} = \frac{j_c}{j_h} \tag{7b}$$

These two simultaneous quadratic equations in N_h, N_c and N_{hc} coupled with equation 2a can be solved for the variables in terms of the parameters j_c/j_h and y_{hc}^2. It is first convenient to define the quantities $X_c = xN_c/N$ and $X_h = xN_h/N$ where X_c is the fraction of random coil residues and X_h the fraction of helical residues. The quantity xN_{hc}/N is the fraction of terminal helical residues which are hydrogen bonded to only one nearest neighbor.

The solution of the above equations for X_c is

$$X_c = \tfrac{1}{2}\left[1 \pm \left(\frac{q}{q+4}\right)^{1/2}\right] \tag{8a}$$

where the composite parameter q is equal to $[1 - (j_c/j_h)]^2/(y_{hc})^2\,(j_c/j_h)$. The correct sign to choose

corresponding to the state of lower free energy will be indicated below. The fraction of atypical helical residues is given by

$$\frac{xN_{hc}}{N} = \frac{\left[(y_{hc})^1\left(\frac{q}{q+4}\right) + (y_{hc})^2\left(\frac{4}{q+4}\right)\right]^{1/2} - (y_{hc})^2}{[1-(y_{hc})^2]} \quad (8b)$$

A positive sign for the square root must be taken for xN_{hc}/N to be greater than zero when y_{hc} is less than one as will be the case throughout this discussion.

The difference in free energy between the polypeptide in its equilibrium state and in the completely helical state ($X_c = xN_{hc}/N = 0$) is given by

$$\Delta F = -\frac{RTN}{x}\left[(1-X_c)(\ln(1-X_c) + (X_c)\ln X_c - \left(1 - X_c - \frac{xN_{hc}}{2N}\right)\ln\left(1 - X_c - \frac{xN_{hc}}{2N}\right) - \left(X_c - \frac{xN_{hc}}{2N}\right)\ln\left(X_c - \frac{xN_{hc}}{2N}\right) - \frac{xN_{hc}}{N}\ln\left(\frac{xN_{hc}}{2N}\right) + \frac{xN_{hc}}{N}\ln(y_{hc})\right] - \frac{RTN}{x}X_c\ln\left(\frac{j_c}{j_h}\right) \quad (9)$$

where the maximum term has been utilized in equation 5. For a given value of $xN_{hc}/2N$, the term in brackets is obviously unchanged in value when X_c is replaced by $1 - X_c$, *i.e.*, if either root of equation 8 is substituted. However, for $j_c/j_h < 1$ the last term will make a smaller positive contribution to the free energy change if $X_c < 1/2$, *i.e.*, if the negative root is chosen. Similarly for $j_c/j_h > 1$, $X_c > 1/2$ and the positive root must be chosen. For $j_c/j_h = 1$, then $X_c = 1/2$. This sign ambiguity can be removed by writing equation 8a in a somewhat less compact form

$$X_c = 1/2\left\{1 + \frac{\left[\left(\frac{j_c}{j_h}\right) - 1\right]}{\left(\frac{j_c}{j_h}\right)^{1/2}(q+4)^{1/2}(y_{hc})}\right\}$$

The over-all free energy difference between the completely random coil and the completely helical states is given by equation 9 with $X_c = 1$ and $xN_{hc}/N = 0$.

$$\Delta F = -\frac{RTN}{x}\ln\left(\frac{j_c}{j_h}\right) = N(w_{cc} - w_{hh}) - NRT\ln\left(\frac{f_c}{f_h}\right) = N(\Delta h - T\Delta s) \quad (10)$$

The assumption that the free energies of helical and random coil residues are *independent* of the size of the regions in which they are located permits the expression of the parameter j_c/j_h in terms of an over-all heat (Δh) and entropy (Δs) of reaction per amino acid residue as in the above equation.

When $j_c/j_h = 1$, ΔF given by equation 10 is zero. The temperature where this occurs is designated the transition temperature (T_t) and is given by $\Delta h/\Delta s$. This definition of the transition temperature is identical to Schellman's[7a] for a very long polypeptide chain.

Thermal Behavior of the Model.—In order to describe the thermal behavior of the configuration of the polypeptide, the temperature dependence of the two parameters j_c/j_h and y_{hc} must be specified.[17]

(17) The parameters j_c/j_h and y_{hc} play the same role as the quantities s and σ which appear in the treatment of Zimm and Bragg.[8]

We identify the heat of reaction (Δh) with the enthalpy change on severance of a peptide–peptide hydrogen bond in water and choose a value of 2 kcal. for this quantity. This is to be compared with a value of 1.5 kcal. suggested by Schellman[18] for this quantity from the estimated heat of dimerization of urea in aqueous solution. With a strongly hydrogen bonded solvent such as water this quantity might be better described as a heat of hydrogen bond interchange in accordance with the following chemical reaction where the number of hydrogen bonds is conserved[19]

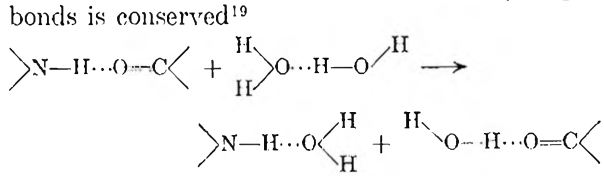

The heat of the above reaction might be slightly positive, but it may be substantially smaller than the energies of hydrogen bonds usually quoted.[20] The latter refer to a process in which such a bond is ruptured leading to a state with no intact hydrogen bonds.

For these purely illustrative calculations we utilize a value for Δs of 6 e.u. Schellman[7a] has pointed out that an upper limit to this entropy due to internal rotation about the polypeptide backbone is given by $R\ln(\prod_{i=1}^{3} m_i)$ where m_i is the number of rotational minima for each of the three bonds in each amino acid residue in the chain. From the work of Pauling and Corey[21] $\prod_{i=1}^{2} m_i = 36$ where the *trans* form of the amide bond is regarded as being substantially more stable than the *cis*. This of course assumes all the rotational minima for a given bond are of equal depth—an approximation which is justified in determining an upper limit for Δs. However, this neglects the contribution to the entropy change of the difference in solvent interactions with the helical and the random coil states. Perhaps as important is the fact that many configurations of the chain consistent with the rotational minima must be ruled out because they permit overlap of remote segments of the chain—the so-called excluded volume effect of polymeric coils. This last complication which cannot be described as a nearest neighbor interaction may vitiate the assignment of a rotational entropy per residue independent of the size of the random coil region and indeed of the size of the chain itself. In any event, all these considerations coupled with the neglect of librational entropy in the helix combine to justify an upper limit of about 7–8 e.u. for Δs due to increased rotational freedom of the *backbone*.[7a] However, an increase in rotational freedom of the amino acid side chains in the random coil over the helical form

(18) J. A. Schellman, *Compt. rend. trav. lab. Carlsberg, Sér. chim.*, **29**, 223 (1955).

(19) W. Kauzmann, in W. D. McElroy and B. Glass, "The Mechanism of Enzyme Action," Johns Hopkins Press, Baltimore, Md., 1954, p. 73.

(20) C. A. Coulson, "Valence," Oxford University Press, London, 1952, p. 301.

(21) L. Pauling and R. Corey, *Proc. Natl. Acad. Sci.*, **37**, 729 (1951).

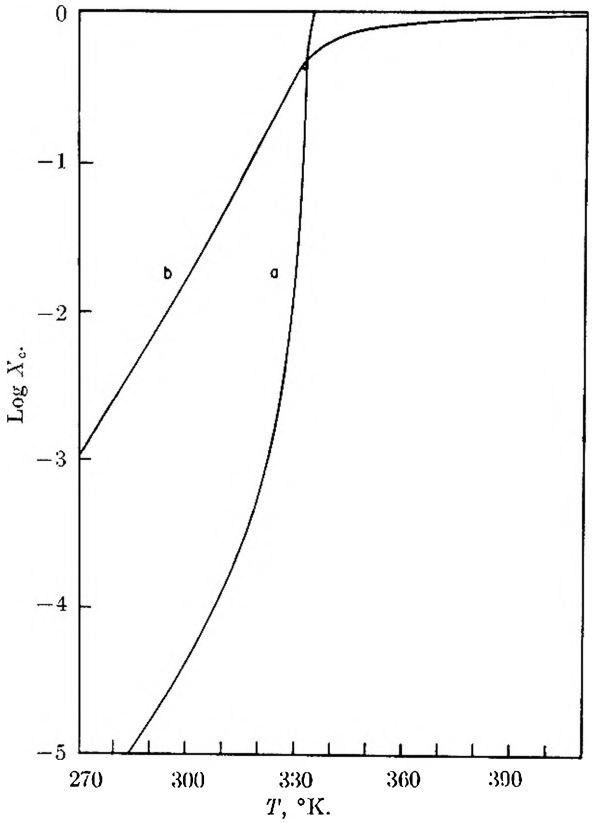

Fig. 2.—The logarithm of the fraction of residues in the random coil configuration (X_c) plotted against the absolute temperature (T, °K.): curve a, terminal helical residues having no librational entropy; curve b, terminal helical residues having a librational entropy of 2 e.u.

would be expected to make a further positive contribution to Δs.

The above values of Δh and Δs suffice to define the temperature dependence of j_c/j_h as well as the transition temperature. At the junctions between helical and coil regions there are no intact hydrogen bonds so

$$w_{cc} - w_{hh} = w_{hc} - w_{hh}$$

If Δh is identified with $w_{cc} - w_{hh}$, *i.e.*, the temperature dependence of f_c/f_h is ignored, we have a partial specification of y_{hc}. Only the magnitude of f'_h/f_h remains to be determined.

In Fig. 2 log X_c is plotted against the absolute temperature for two values of f'_h/f_h. Curve a which has been calculated for f_h equal to f'_h indicates a sharper transition than curve b where $R \ln f'_h/f_h$ has been set equal to 2 e.u. The transition temperature is the same for both plots being equal to $\Delta h/\Delta s$ or about 60°. Allowing the terminal helical residues some measure of librational entropy has the expected effect of broadening the temperature range in which conversion of the helix to a random coil takes place. At temperatures well below the transition temperature where helical imperfections first begin to appear $q >> 4$ and X_c equals $1/q$ as can be seen by expansion of the square root in equation 8a. Similarly at temperatures well above T_t where the polypeptide is essentially a random coil, X_h is given approximately by $1/q$.

In Fig. 3 X_c is plotted against the absolute temperature for f_h equal to f'_h, *i.e.*, assuming no en-

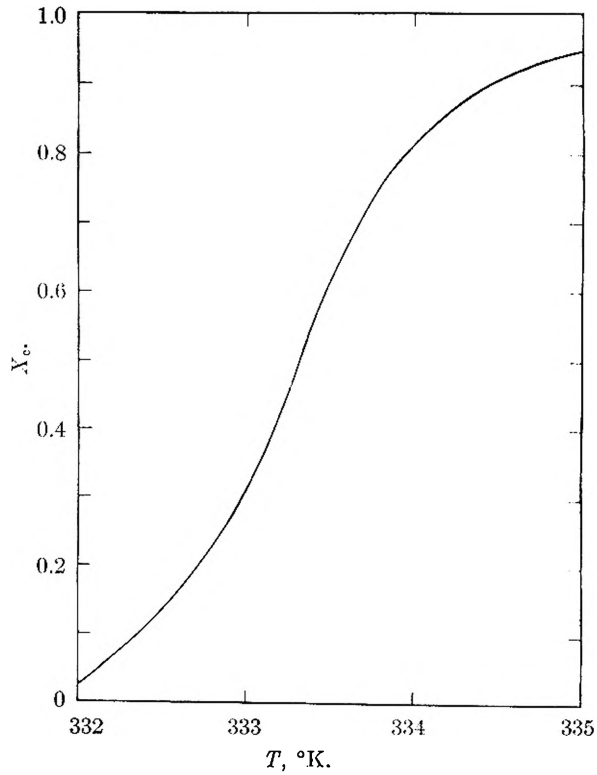

Fig. 3.—The fraction of residues in the random coil configuration (X_c) plotted against the absolute temperature (T, °K.) in the vicinity of the transition temperature. The parameters are the same as for curve a of Fig. 2.

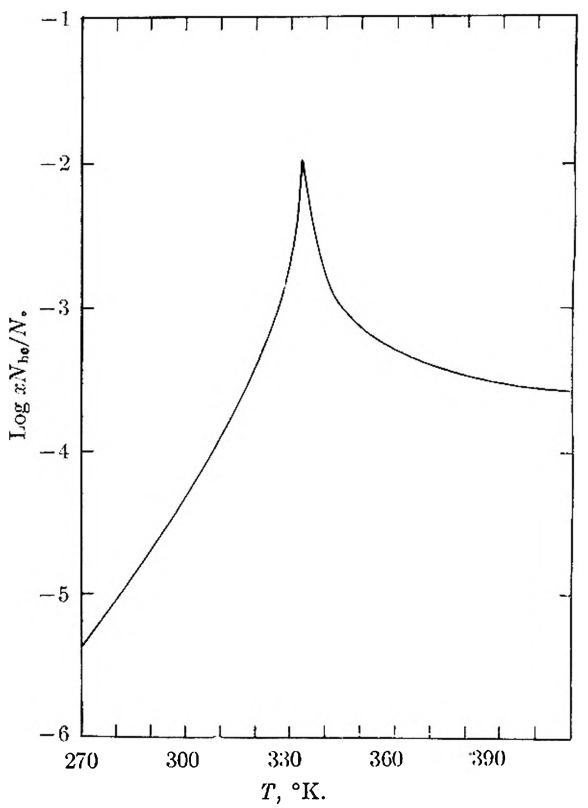

Fig. 4.—The logarithm of the fraction of terminal helical residues (xN_{hc}/N) plotted against the absolute temperature (T, °K.). The parameters are the same as for curve a of Fig. 2.

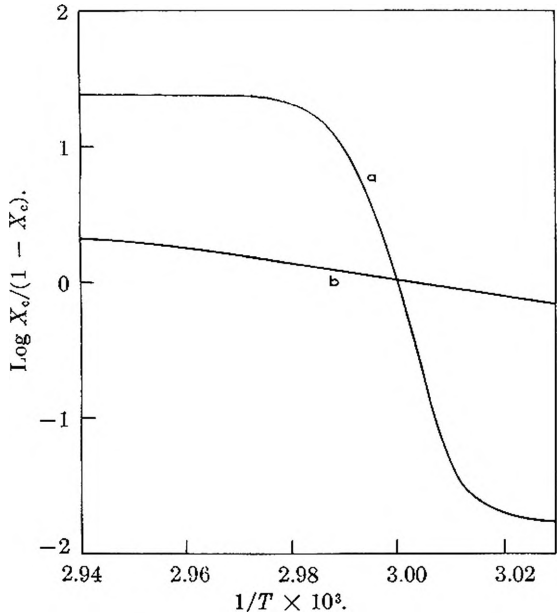

Fig. 5.—The logarithm of the "equilibrium constant" $X_c/(1 - X_c)$ for the hypothetical reaction: helical residue $\rightleftarrows$ random coil residue, plotted against the reciprocal of the absolute temperature (T, °K.). Curves a and b have been calculated employing the same parameters as for curves a and b, respectively, of Fig. 2.

hanced librational entropy for the terminal helical residues over those in the body of a helical region. It is apparent that the transition from helix to random coil is essentially complete within a range of about 3°. Increasing the magnitude of Δh sharpens the transition and also elevates the transition temperature. For Δh equal to 3 kcal. and the same estimate of Δs, T_t would be equal to 227°. Hence the polypeptide would be essentially helical at all temperatures below the normal boiling point of water. The extreme sharpness of such a transition would militate against its detection. Such a system would give no evidence of undergoing a transformation unless it were accessible to study in a narrow temperature region about T_t. The qualitative distinctions often made regarding the thermal stability of proteins may have their roots in relatively small variations in the nearest neighbor interactions of the different amino acid residues which could greatly influence the temperature region where such transitions occur.

The transition is exemplified quite clearly in Fig. 4 where the logarithm of the fraction of atypical helical residues as given in equation 8b is plotted against the absolute temperature. At temperatures well below the transition temperature, the polypeptide is predominantly helical with a small number of random coil regions and hence few junctions and few atypical helical residues. Well above the transition temperature the reverse situation holds. The maximum occurs at about T_t where xN_{hc}/N is given approximately by y_{hc}. As we have remarked above, the temperature range of the transformation is narrowed by decreasing y_{hc} so the height of the maximum in Fig. 4 is an inverse measure of the sharpness of the transition.

"Enthalpies and Entropies" of Reaction.—The ratio $X_c/(1 - X_c)$ represents the mass action expression for the equilibrium

helical residue $\rightleftarrows$ random coil residue

There are some conceptual advantages to defining enthalpies (ΔH^*) and entropies (ΔS^*) for the above "reaction" as

$$\Delta H^* \equiv RT^2 \frac{d\left[\ln\left(\frac{X_c}{1 - X_c}\right)\right]}{dT} \qquad (11)$$

$$\Delta S^* \equiv R \ln\left(\frac{X_c}{1 - X_c}\right) + \frac{\Delta H^*}{T} \qquad (12)$$

From equation 8a, ΔH^* may be written as

$$\Delta H^* = \frac{2x\Delta h}{(y_{hc})\left[\left(\frac{j_c}{j_h}\right)(q + 4)\right]^{1/2}} \qquad (13)$$

where

$$\Delta h = w_{cc} - w_{hh} = \frac{RT^2}{x} \frac{d\left[\ln\left(\frac{j_c}{j_h}\right)\right]}{dT} = \frac{2RT^2}{x} \frac{d\left[\ln\left(y_{hc}\right)\right]}{dT}$$

At temperatures far below the transition range, $j_c/j_h << 1$ and $q >> 4$ so equation 13 becomes

$$\Delta H^* = 2x\Delta h \qquad (14)$$

This is consonant with the necessity of breaking $2x$ or 6 consecutive hydrogen bonds to convert the minimal sized helical unit of three residues to a random coil unit. At the transition temperature $j_c/j_h = 1$ and $q = 0$ so the heat of reaction is given by

$$\Delta H^* = \frac{x\Delta h}{y_{hc}} \qquad (15)$$

At the transition temperature X_c equals one-half so equation 12 becomes

$$\Delta S^* = \frac{\Delta H^*}{T_t}$$

which is the usual relation between the heat and entropy change for a first-order phase transition. The small size of y_{hc} results in large values of ΔH^* and ΔS^* at T_t.

In Fig. 5 there are customary van't Hoff plots of the log of the apparent equilibrium constant against the reciprocal of the absolute temperature over a range of about 10° in the vicinity of the transition temperature. The ordinate in the plot might be obtained from an analysis of residue optical rotations. As is to be expected, the slope and hence the defined enthalpy of reaction at T_t is larger for the sharper transition (curve a). In the neighborhood of T_t where X_c is measurably different from zero and one, experimental data may give an effectively constant slope when plotted in this fashion. It is possible that the large heats and entropies which are characteristic of reversible protein denaturation as well as polypeptide transitions might be better associated with small values of a parameter such as y_{hc} rather than with a certain large number of hydrogen bonds being severed in an "all or none" manner.

Conclusion

In the previous discussion it has been pointed out that a polypeptide whose configurational state can be described by an Ising nearest neighbor model can undergo a coöperative thermal transition in a

very narrow temperature range. The coöperative nature of the transition derives from the fact that a single helical region will be more stable, *i.e.*, have a lower internal energy than several such regions with the same total number of residues. This situation arises because of the increased number of terminal residues with only one intact hydrogen bond in the latter case. Opposed to this tendency to accumulate all the helical residues in one portion of the chain, there will be the inevitable tendency to increase the entropy of the system through the greater measure of disorder provided by the dispersal of the residues in a number of regions. The free energy minimum for the system with respect to the number of regions represents a compromise between these two opposing tendencies. If the likelihood of junctions between helical and random coil regions as determined by the magnitude of y_{hc} is small, then the polypeptide will always be either predominantly a helix or a random coil except in a very narrow temperature interval. Viewed in a somewhat different way, after the appearance of initial breaks in the helical structure, there will be a tendency for the random coil content to increase by the growth of existing random coil regions through the accretion of residues from the neighboring helical regions rather than by the creation of new random coil regions. The propagation of imperfections in the helical structure will thus occur in a coöperative manner at the boundaries of existing disordered regions.

A system described by a one dimensional Ising model will never undergo a transition where discontinuities appear at a specific temperature in measurable properties. Moreover, as Zimm and Bragg[8] have remarked, one dimensional system in general cannot manifest this type of behavior—a fact pointed out a number of years ago by Landau and Lifshitz.[22] Nonetheless one may encounter arbitrarily sharp transitions in such systems—transformations which may aptly be viewed as phase transitions in a somewhat broader context for this phenomenon.

The description of the polypeptide as a one-dimensional system is justified in so far as hydrogen bond formation is concerned because each residue can interact with at most two nearest neighbors. Such interactions alone suffice to give a coöperative character to the helix–random coil transition. Departure from a strictly linear dependence of the configurational entropy in a random coil region on the number of residues in such a region might create the possibility of another coöperative effect—one which could not be represented by nearest neighbor interactions.

Acknowledgment.—The author wishes to thank Professor Walter Kauzmann for advice and encouragement during the progress of this work. He is also grateful for financial assistance from the National Science Foundation for the summers of 1956 and 1957 through a grant to Professor Kauzmann.

(22) L. Landau and E. Lifshitz, "Statistical Physics," Oxford University Press, New York, N. Y., 1938, p. 232.

ON A MODEL FOR THE HELIX–RANDOM COIL TRANSITION IN POLYPEPTIDES.[1,2] II. THE INFLUENCE OF SOLVENT COMPOSITION AND CHARGE INTERACTIONS ON THE TRANSITION

BY LEONARD PELLER[3]

Frick Chemical Laboratory, Princeton University, Princeton, New Jersey

Received January 15, 1959

The one-dimensional Ising model employed in the previous paper (I) has been extended to examine the influence of solvent composition and charge interactions in the helix–random coil transition in a long polypeptide chain. Increasing the activity of a second component in water, *e.g.*, urea, which interacts preferentially with the random coil residues, produces a coöperative transition from helix to random coil in a quite narrow activity range. For a very strongly interacting component an inverted thermal transition may occur: random coil → helix with increasing temperature. An approximate calculation of the influence of charge repulsions indicates a helix–coil transition in a polyglutamic acid on increasing the *p*H. The transition is accompanied by a considerable ionization of carboxyl groups in a very narrow *p*H range. The possible significance of this type of ionization for the anomalous titration behavior of some proteins is discussed.

Introduction

In the preceding paper[4] a one-dimensional nearest neighbor model was proposed to examine the thermally induced helix–coil transition in a long polypeptide chain. This model can be extended to consider in an approximate fashion the influence of solvent composition and charge interactions on this transition. The recent experimental work of Doty, Blout and their collaborators has indicated the importance of these factors in the structural transformations of synthetic polypeptides in solution.[5–7] Moreover, the properties of proteins

(1) Taken in part from a thesis presented to Princeton University in partial fulfillment of the requirements for the Ph.D. degree, November, 1957.

(2) Presented in part before the Division of Biological Chemistry, 133rd National Meeting of the American Chemical Society, San Francisco, April 13–18, 1958, and more extensively before the Division of Physical Chemistry—Symposium on the Statistical Mechanics of the Helix-Random Coil Transitions in Polypeptides and Polynucleotides, 134th National Meeting of the American Chemical Society, Chicago, September 7–12, 1958.

(3) Department of Chemistry, University of Wisconsin, Madison, Wisconsin.

(4) L. Peller, THIS JOURNAL, **63**, 1194 (1959).

(5) P. Doty and J. T. Yang, *J. Am. Chem. Soc.*, **78**, 498 (1956).

(6) P. Doty, A. Wada, J. T. Yang and E. R. Blout, *J. Polymer Sci.*, **23**, Symposium on Macromolecules, Part 2, 85 (1957).

(7) P. Doty, K. Imahori and E. Klemperer, *Proc. Natl. Acad. Sci.*, **44**, 424 (1958).

which are dependent on their configurational state display a great sensitivity to these same factors.[8] The behavior of a simple model for a polypeptide as discussed below emphasizes the possibility of a common origin for the experimentally observed phenomena in the polypeptides and the proteins.

Studies of the effect of solvent composition on the state of "folding" of proteins have been in the main restricted to aqueous solutions with some added denaturant present. Many of these denaturants such as urea, guanidine salts, and the various α-halo-acetic acids have been presumed to affect the configuration of the protein through their capacity to form hydrogen bonds with groups which are exposed in the "unfolded" state. These denaturants manifest fairly sharp concentration thresholds in regard to their effectiveness. Such thresholds argue for the existence of coöperative effects.

It is tempting to explain the influence of charge interactions on protein configuration on the basis of the tendency of the net charge repulsions to favor an expanded state for the molecule.[8] However, it should not be concluded that the isoelectric point would then necessarily be the *p*H of maximum stability. Clusters of charged groups deviating from the over-all distribution of polar amino acids may produce a structural lability in limiting regions of the molecule. These regions may be of chief significance in regard to helix–coil transitions in proteins. The limited extent of helical character in the compact globular proteins, which has been the subject of recent investigations,[9,10] points to the possibility that localized charge interactions in these regions may be the principal determinants of *p*H dependent configurational changes. The approximate electrostatic calculations for a single polypeptide chain which are presented below may then have some applicability to proteins.

A. Influence of Solvent Composition on the Configurational State of the Polypeptide.—It is readily apparent that any molecule which will interact preferentially with either a helical or a random coil residue in the polypeptide will strongly influence the equilibrium number of these residues. The action of water discussed in the previous paper can be viewed in terms of a preferential interaction of this solvent through hydrogen bonds with the random coil residues and the terminal helical residues. This interaction manifests itself through a lowering of the energy necessary to break a peptide–peptide hydrogen bond as compared to that required in a less polar solvent. With the polypeptide at infinite dilution in a single solvent there are of course no concentration effects on the transition.

The role of solvent composition may be considered in an approximate way by assuming that a second solvent component binds preferentially to the CO and NH groups of those amino acid residues whose internal hydrogen bonds have been broken, *i.e.*, residues in the random coil regions and terminal helical residues. The mode of interaction of the hydrogen bond forming denaturants mentioned above might reasonably be of this type. The number of "binding sites" (M) in the polypeptide then is given by

$$M = 2xN_c + xN_{hc} \qquad (1)$$

where each random coil residue contributes two possible sites and each terminal helical residue contributes only one.

The Free Energy of Binding.—The preferential binding of a molecule to the polypeptide adds another term to the free energy of the system. A partition function for this term can be written in the following form if there is *no interaction* between the bound molecules

$$\Delta_b = \frac{M!}{(M-m)!m!} j^m k^{M-m} \qquad (2)$$

M is the total number of sites while m is the average number of bound molecules. j and k are partition functions for filled and empty sites, respectively. Δ_b represents the partition function for the system polypeptide plus bound molecules. No distinction has been made between the NH and CO groups with respect to their interactions with the solvent system.

The average number of bound molecules is determined by equating the partial molal free energy of a bound molecule to one free in solution, *i.e.*

$$\mu = \left(\frac{\partial F_b}{\partial m}\right)_M = -RT\left\{\frac{\partial[ln\,(\Delta_b)]}{\partial m}\right\}_M =$$
$$-RT\left[\ln\left(\frac{M-m}{m}\right) + \ln\left(\frac{j}{k}\right)\right] = \mu_0 + RT\ln a \qquad (3)$$

where Stirling's approximation has been employed for the factorials in equation 2. The activity of the preferentially bound molecule when free in solution is a, and μ_0 is the standard state partial molal free energy for this molecule. Equation 3 if solved for m yields

$$m = \frac{KaM}{1+Ka} \qquad (4)$$

where K is defined as $(j/k)e^{\mu_0/RT}$ and may be regarded as an equilibrium constant for association.

The free energy change per mole (ΔF_b) on binding m molecules to one molecule of the polypeptide is given by the free energy of the polypeptide minus the free energy of the m bound molecules and the free energy of the polypeptide with all M sites empty, *i.e.*, $m = 0$.

$$\Delta F_b = -RT\ln\Delta_b - (m\mu_0 + mRT\ln a - MRT\ln k)$$
$$= -MRT\ln(1+Ka) \qquad (5)$$

where equation 4 has been used for m, and μ has been expressed in terms of the activity as in equation 3. Schellman[11] has employed an equation of this form to discuss the influence of urea on the "all or none" transformation of the polypeptide.

The Equilibrium Configurational State of the Polypeptide.—The equilibrium configurational state for the polypeptide in a binary solvent may be determined by minimizing the total free energy with respect to N_c (or X_c) and N_{hc} (or xN_{hc}/N).

(8) W. Kauzmann, in W. D. McElroy and B. Glass, "The Mechanism of Enzyme Action," Johns Hopkins Press, Baltimore, Md., 1954, pp. 70–110.

(9) W. F. Harrington and J. A. Schellman, *Compt. rend. trav. lab. Carlsberg, Sér. chim.*, **30**, 21 (1956).

(10) J. T. Yang and P. Doty, *J. Am. Chem. Soc.*, **79**, 761 (1957).

(11) J. A. Schellman, *Compt. rend. trav. lab. Carlsberg, Sér. chim.*, **29**, 230 (1955).

The total free energy is the sum of equation 9 of the preceding paper and equation 5 above with M given by equation 1.

$$\Delta F = -\frac{RTN}{x}\left[(1 - X_c)\ln(1 - X_c) + (X_c)\ln(X_c) - \left(1 - X_c - \frac{xN_{hc}}{2N}\right)\ln\left(1 - X_c - \frac{xN_{hc}}{2N}\right) - \left(X_c - \frac{xN_{hc}}{2N}\right)\ln\left(X_c - \frac{xN_{hc}}{2N}\right) - \left(\frac{xN_{hc}}{N}\right)\ln\left(\frac{xN_{hc}}{2N}\right) + \left(\frac{xN_{hc}}{N}\right)\ln(y_{hc}) + \left(\frac{x^2N_{hc}}{N}\right)\ln(1 + Ka)\right] - \frac{RTN}{x}X_c\left[\ln\left(\frac{j_c}{j_h}\right) + 2x\ln(1 + Ka)\right] \quad (6)$$

These two minimization conditions yield the following expressions for the fraction of random coil residues (X_c) and the fraction of terminal helical residues (xN_{hc}/N)

$$X_c = {}^1/_2\left[1 \pm \left(\frac{r}{r + 4}\right)^{1/2}\right] \quad (7a)$$

$$\frac{xN_{hc}}{N} = \frac{\left[(y_{hc})^4\left(\frac{r}{r+4}\right)^2(1 + Ka)^{4x} + (y_{hc})^2\left(\frac{4}{r+4}\right)(1 + Ka)^{2x}\right]^{1/2} - (y_{hc})^2(1 + Ka)^{2x}}{[1 - (y_{hc})^2(1 + Ka)^{2x}]} \quad (7b)$$

assuming that $1 > y_{hc}(1 + Ka)^x$. The composite parameter r is equal to

$$\frac{\left[1 - \left(\frac{j_c}{j_h}\right)(1 + Ka)^{2x}\right]^2}{(y_{hc})^2\left(\frac{j_c}{j_h}\right)(1 + Ka)^{4x}}$$

Inspection of equation 6 shows that for a given value of xN_{hc}/N the state of lower free energy will be given by the root corresponding to the negative sign in equation 7a, *i.e.*, $X_c < {}^1/_2$, if $(j_c/j_h)(1 + Ka)^{2x} < 1$. Similarly for $(j_c/j_h)(1 + Ka)^{2x} > 1$, the positive root, *i.e.*, $X_c > {}^1/_2$ corresponds to the state of lower free energy.

Helix–Coil Transition Induced by Preferential Binding.—A coöperative transition from an essentially helical to an essentially random coil state of the polypeptide can be produced by increasing the activity of the bound molecule. In Fig. 1 X_c is plotted against the activity of the bound molecule for such a transition at 300°K. The values of the parameter r in equation 7a have been calculated using the values of j_c/j_h and $y_{hc}(f'_h/f_h = 1)$ given in the previous paper. The value of K has been chosen as 2×10^{-2} at 300°K. with the standard state of the bound molecule being a one molar aqueous solution. The value of the association constant is of the order of magnitude suggested by Schellman's[12] estimate of the dimerization constant for urea of 4.1×10^{-2} at 298°K.

The range of activity of the bound molecule in which the polypeptide is transformed from the helical to the random coil configuration is quite small. This should be compared with the narrow temperature range in which this transition is effected, which was discussed in the preceding paper. The sharpness of both transitions is a consequence of the small size of y_{hc}, *i.e.*, the small likelihood of junctions between helical and random coil regions. The mid-point of the transition ($X_c = X_h = {}^1/_2$) depicted in Fig. 1 occurs at an activity of about 9.1. This may be designated conveniently as the transition activity (a_t) following Schellman.[11] From equation 7a, the transition mid-point is located at r equal to zero or

$$\left(\frac{j_c}{j_h}\right)(1 + Ka_t)^{2x} = 1 \quad (8)$$

At a_t the fraction of terminal helical residues (xN_{hc}/N) is given approximately by $y_{hc}(1 + Ka_t)^x$. Interaction of the second solvent component with these terminal residues thus increases the likelihood of junctions between the helical and random coil regions and broadens the transition.

From equation 8 it is apparent that the exact location of the mid-point of the transition depends strongly on the magnitude of K. For example, for a value of K of 10^{-2} at 300°K., a_t equals approximately 18. The sharpness of the transformation necessitates observations in the vicinity of a_t for its detection as in the case of the thermal transition. At a given temperature a_t is also greatly affected by the magnitudes of Δh and Δs in the pure solvent through their influence on j_c/j_h in equation 8. The fact that for many proteins changes in urea concentration from 4 to 8 M are sufficient to bring about an increase in the rate of denaturation from immeasurably slow to extremely rapid is therefore strong evidence for both a qualitative and *quantitative* similarity in its mode of action on these pro-

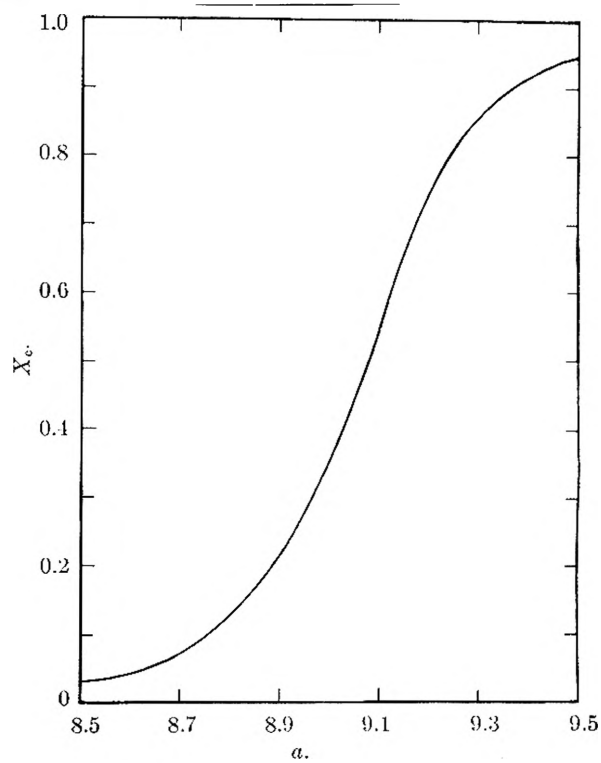

Fig. 1.—The fraction of residues in the random coil configuration (X_c) plotted against the activity (a) of a second solvent component.

(12) J. A. Schellman, *ibid.*, **29**, 223 (1955).

(13) H. Neurath, J. P. Greenstein, F. W. Putnam and J. O. Erickson, *Chem. Revs.*, **34**, 157 (1944).

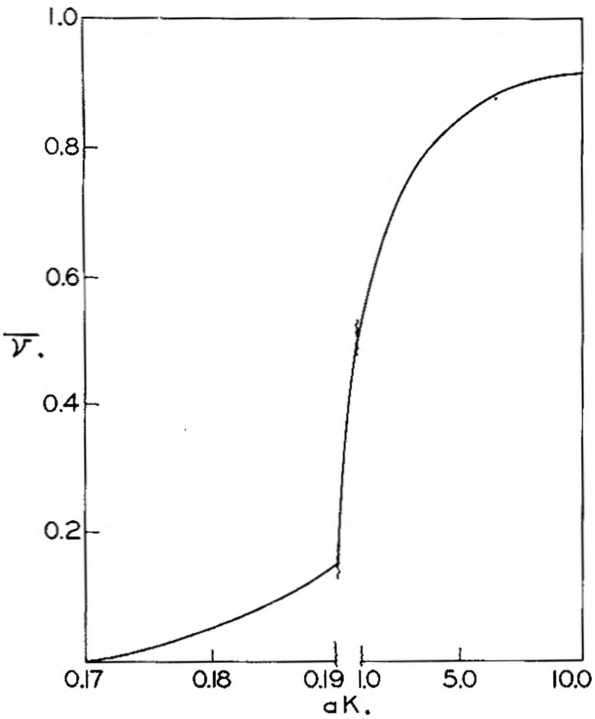

Fig. 2.—The extent of preferential binding ($\bar{\nu}$) to the polypeptide of a second solvent component plotted against the product of the activity (a) of the component and its association constant (K).

teins.[13,14] This great variation in rate with relatively small change in urea concentration has been interpreted as a high order of reaction for the urea.[15] These high orders of reaction are evidence for coöperative effects perhaps of the type discussed above.

The influence of a second solvent component on the helix–coil transition has been examined from a point of view commonly employed to interpret the preferential binding of small molecules to proteins in aqueous media. It is perhaps useful to pursue this approach somewhat further. From equations 1 and 4 the fraction of filled sites (ν) is given by

$$\bar{\nu} \equiv \frac{m}{2N} = \left(X_c + \frac{xN_{hc}}{2N}\right)\frac{Ka}{1 + Ka} \qquad (9)$$

where there are two potential binding sites for each residue (the CO and NH groups) and a total of $2N$ such sites for the polypeptide.

In Fig. 2, $\bar{\nu}$ is plotted against Ka for the values of the relevant parameters described previously. For Ka greater than about 0.2, the binding curve is the characteristic Langmuir isotherm for non-interacting adsorption. Below this value of Ka the binding plot exhibits an upward curvature because of the increase of available sites with increasing activity of the bound molecule. Such sigmoidal binding curves have been found with some proteins[16] and interpreted as arising from attractive interactions between the bound molecules. It is well to realize that such behavior may occur because of configurational changes in the protein exposing more sites for binding even in the absence of interactions between the bound molecules. This is clearly the case for the polypeptide with the maximum number of available sites created at a relatively low degree of saturation ($\bar{\nu} = 0.15$).

Thermal Transition in a Binary Solvent System.—For a given value of the activity of the bound molecule (approximately a given solvent composition), equation 8 defines a transition temperature for the system. Using the relation between j_c/j_h in terms of the heat of severance of a peptide–peptide hydrogen bond (Δh) and the transition temperature ($T_t^0 = \Delta h/\Delta s$) in the absence of the second solvent component (a equal to zero) as given in equation 10 of the previous paper, we obtain the expression

$$T_t = \frac{T_t^0}{1 + \left(\frac{2RT_t^0}{\Delta h}\right)\ln(1 + Ka_t)} \qquad (10a)$$

If $(2RT_t/\Delta h)\ln(1 + Ka_t) << 1$ and $Ka_t << 1$, then the denominator in equation 10a can be expanded yielding

$$T_t^0 - T_t \cong \frac{R(T_t^0)^2}{\Delta h}(2K)(a_t) \qquad (10b)$$

Ignoring the temperature dependence of K, $T_t^\circ - T_t$ varies directly with a or with the concentration (c) if $a \cong c$. Save for the factor $2K$, equation 10b is identical to the usual expression for the depression of the freezing point for macroscopic phases. Choosing a one molar solution as the standard state for the bound molecule and setting $a = c$, then the quantity $R(T_t^0)^2(2K/\Delta h$ represents a "molar transition point depression constant." The combination of small values of $K(2 \times 10^{-2}$ at 300°K.) and Δh (2 kcal.) yields a value for this "constant" of 4.44 which is of comparable magnitude to that encountered for freezing point depressions, *e.g.*, water—1.86 and benzene—5.12. If K has a small temperature dependence as for urea binding ($\Delta h_b = RT^2\mathrm{d}(\ln K)/\mathrm{d}T = -1.5$ kcal. from Schellman's analysis[12]), equation 10a shows an almost linear decrease in T_t with increasing a for a 30° temperature range below T_t° (333°K.).

It is interesting to note that the lowering of the "shrinkage temperature" of the fibrous protein collagen has been found to be a linear function of the volume fraction of the ethylene glycol present.[17] This similarity to the behavior expected for the depression of a melting point has been adduced as evidence for the shrinkage process being a true first-order phase transition.[17] Such behavior may, however, arise in structural transformations of macromolecules which are to be regarded as phase transitions only in a broader definition of the phenomenon than has been commonly employed.

The preceding discussion has been intended to apply to thermal transitions in a polypeptide in aqueous solution as influenced by denaturants such as urea. The character of the thermal transition can be altered more profoundly by a second solvent component which interacts very strongly with the free NH and CO groups.

This may be seen quite clearly by examining the temperature dependence of X_c at a given value of a.

(14) F. W. Putnam, in H. Neurath and K. Bailey, "The Proteins," Vol. I, Part B, Academic Press, New York, N. Y., 1953, pp. 807–892.

(15) R. B. Simpson and W. Kauzmann, *J. Am. Chem. Soc.*, **75**, 5139 (1953).

(16) J. R. Colvin, *Canadian J. Chem.*, **30**, 320 (1952).

(17) P. J. Flory and R. R. Garrett, *Nature*, **177**, 176 (1956).

The behavior of the quantity dX_c/dT as obtained from equation 7a

$$\frac{d(X_c)}{dT} = \left[\frac{1}{(r+4)^{3/2}}\right]\left[\frac{1}{(y_{hc})\left(\frac{j_0}{j_h}\right)^{1/2}(1+Ka)^{2x}}\right]\left(\frac{2x}{RT^2}\right)\left[\Delta h + \left(\frac{2Ka}{1+Ka}\right)\Delta h_b\right] \quad (11)$$

illustrates some of these complexities. Whether dX_c/dT is positive or negative clearly depends on the sign of the factor $\Delta h + (2Ka/1 + Ka)\Delta h_b$. In the absence of any binding (K or a equal to zero) this quantity reduces to Δh. The heat of rupture of the peptide–peptide hydrogen bond in the single solvent has been assumed to be positive, otherwise the polypeptide would never be in the helical form at any temperature. The conversion of helix to random coil in this solvent is then an endothermic process with increasing temperature shifting the equilibrium from helix to random coil.

However, as Δh_b would be expected generally to be negative, conditions may arise where the factor $\Delta h + (2Ka/1 + Ka)\Delta h_b$ will also be negative. dX_c/dT would then be less than zero, and *the fraction of the polypeptide in the random coil form would decrease with increasing temperature.* The operationally defined enthalpies and entropies discussed in the preceding paper would then have large negative values at the transition temperature as can be seen from equation 12

$$\Delta H^* = \frac{x}{y_{hc}}\left(\Delta h + \frac{2Ka_t}{1+Ka_t}\Delta h_b\right) = T_t\Delta S^* \quad (12)$$

Conversion of helix to random coil in this solvent system can be described therefore as an *exothermic* process inasmuch as ΔH for the over-all process equals $N(\Delta h + (2Ka/1 + Ka)\Delta h_b)$. The inverted transition for poly-γ-benzyl-L-glutamate in a 4:1 by weight dichloroacetic acid–ethylene dichloride solvent system found by Doty and Yang[5] can be explained on this basis. For example, taking $\Delta h =$ 4 kcal. in pure ethylene dichloride and assuming Ka for binding the dichloroacetic acid is sufficiently great for $Ka/(1 + Ka) \sim 1$, then for the observed behavior $-\Delta h_b$ must be greater than 2 kcal.

The transition temperature for the inverted transition is *increased* by increasing the activity of the strongly interacting solvent component as can be seen from the sign of dT_t/da_t

$$\frac{dT_t}{da_t} = -\frac{T_t^2(2RK)}{\Delta h(1+Ka_t) + 2\Delta h_b(Ka_t)} \quad (13)$$

when $\Delta h + (2Ka_t/1 + Ka_t)\Delta h_b < 0$. For a given value of a the quantity $\Delta h + (2Ka/1 + Ka)\Delta h_b$ may be less than zero at low temperatures, and greater than zero at higher temperatures, owing to K decreasing with increasing temperature ($\Delta h_b <$ 0). The possibility then arises for a low temperature inverted transition and a high temperature normal transition with helix going to random coil on increasing the temperature. The likelihood of observing this high temperature transition is restricted by the temperature range for the existence of the solvent system in the liquid state. However, the occurrence of temperature minima in the rate of urea denaturation of ovalbumin[15] and tobacco mosaic virus[18] may be manifestations of such a phenomenon and have been analyzed in essentially these terms.

The foregoing discussion has emphasized the importance of preferential interactions of the components of a binary solvent system in influencing the helix–coil transition. In particular, the random coil configurational state must be given a somewhat wider meaning in the light of these interactions which are dependent on both solvent composition and temperature.

B. Influence of Electrostatic Interactions on the Configurational State of the Polypeptide

Polypeptides consisting of amino acid residues with terminal acidic or basic groups, *e.g.*, glutamic acid and lysine, have been shown to undergo the transition from helix to random coil by altering the *p*H of the solution in such a way as to increase the net charge on the macromolecule.[6,7] Presumably the free energy due to these electrostatic interactions increases with net charge more rapidly for the residues in the helical configuration than for those in the random coil configuration. Eventually the charge repulsions become of such magnitude that they disrupt the hydrogen bonded network of the helix converting it to a more or less random coil.

Two causes may be cited for the greater importance of charge repulsions in helical regions as compared to random coil regions. Firstly, the charged groups in helical regions are distributed on an approximately cylindrical surface which is impermeable to mobile ions, while those in a random coil region are distributed throughout a volume permeable to these mobile ions. Secondly, a charged random coil may expand in such a way as to increase the separation of charged groups and thus effectively diminish the magnitude of the electrostatic interactions. This expansion must come of course at the expense of rotational entropy for the random coil regions.

Incorporation of these electrostatic effects in a model for the helix-coil transition involves certain difficulties. These difficulties are connected with a suitable expression for the partition function and hence the free energy of the system. The charge interactions are long range in nature and thus are not easily taken into account in an essentially nearest neighbor model. However, when the fixed charges in the polypeptide are screened from one another by added electrolyte, the charge interactions between nearest neighbors may become of supervening importance. Further, these electrostatic repulsions influence the rotational freedom of the random coil residues and hence the configurational entropy. This complication requires inclusion of an entropy of elastic deformation for the random coil regions.

In the following development we make the simplifying but drastic approximation of neglecting the charge interactions save within the helical regions. This tends to sidestep some of the difficulties enumerated above but permits an examination of certain maximal electrostatic effects. Moreover, such an approximate calculation of the effect of *p*H on configurational state does reveal some interesting properties of the electrostatically induced transition.

(18) M. A. Lauffer, *J. Am. Chem. Soc.*, **65**, 1793 (1943).

Electrostatic Free Energy of the Charged Polypeptide.—For a system containing M groups capable of dissociating a proton, *e.g.*, carboxyl groups, the free energy (F_e') may be written as

$$F_e' = -RT \ln \frac{M!}{m!(M-m)!} j^m k^{M-m} + (M-m)^2 W \quad (14)$$

where $M - m$ is the average number of charged groups, *e.g.*, carboxylate ions. j and k are the partition functions for the isolated groups in the uncharged and charged states, respectively. The electrostatic repulsions between the charged groups contribute the second term in equation 14 where W is a function of the geometry of the system, ionic strength, etc. This expression may be simply described as a free energy of binding protons including interactions between the empty sites.

The average number of bound protons (m) is given by the relation stating the equality of the partial molal free energy of a bound proton and one free in solution

$$\mu = \left(\frac{\partial F_e'}{\partial m}\right)_M = -RT\left[\ln\left(\frac{M-m}{m}\right) + \ln\left(\frac{j}{k}\right) + 2\frac{(M-m)W}{RT}\right] = \mu_0 + RT \ln a \quad (15a)$$

μ_0 is the standard state partial molal free energy of a hydrogen ion, and a is its activity under given conditions. This expression can be written in terms of the degree of dissociation (α) as

$$\alpha \equiv \frac{M-m}{M} = \frac{1}{1 + \frac{a}{K} e^{2\alpha MW/RT}} \quad (15b)$$

where $K = (k/j)e^{-\mu_0/RT}$ and is the so-called intrinsic dissociation constant for the isolated group. Equation 15b is the usual titration expression for a polyelectrolyte with one type of dissociable group.

The free energy of the polypeptide (F_e) with m bound protons referred to the uncharged polypeptide ($M = m$) as a standard is given by F'_e plus the free energy of $M - m$ protons minus the free energy of the uncharged polypeptide

$$F_e = F_e' + (M-m)\mu + MRT \ln j = MRT \ln (1-\alpha) - \alpha^2 M^2 W \quad (16)$$

It is clear that F_e represents the free energy of ionization of $M - m$ protons from the completely undissociated polypeptide at constant pH, *i.e.*, constant a.

In order to apply equation 16 to the examination of the effect of charge interactions on the helix–coil transition, a suitable expression must be found for W. Considering the charge on the dissociated groups in a helical region as smeared out on the surface of a cylinder of radius b and length L which is impermeable to salt ions, we can write for W_h[19]

$$W_h = \frac{N_a(\epsilon)^2}{\lambda D b L}\left[\frac{K_0(\lambda b)}{K_1(\lambda b)}\right] \quad (17)$$

N_a is Avogadro's number, ϵ is the electronic charge and D is the bulk dielectric constant of the medium external to the cylinder. λ is the Debye–Hückel screening parameter equal to $[4\pi N_a{}^2\epsilon^2\Sigma c_i z_i{}^2/1000\,DRT]^{1/2}$ where the ionic strength ($\Gamma/2$) equals $\Sigma c_i z_i{}^2/2$. K_0 and K_1 are modified Bessel functions of the second kind of zero and first order, respectively. The modified Bessel functions are characteristic solutions of the linearized cylindrically symmetric Poisson–Boltzmann equation.

For a given helical region L is a linear function of the number of residues, and the quantity L/xN_h is approximately the repeat distance per residue in the α-helix (about 1.5 Å.[20]). The radius of the cylinder (b) equivalent to the α-helix of polyglutamic acid is about 5 Å.[21]

Setting M equal to xN_h, it is apparent from equation 15b that α is independent of the size of the helical region as MW_h (or xN_hW_h) is independent of the length of the equivalent cylinder. Then F_e as given by equation 16 is a linear function of the number of helical residues. This is approximately true provided the different electrostatic environment of the terminal helical residues is neglected. The electrostatic free energy for the polypeptide referred to the uncharged polypeptide as a standard state can be written as

$$\Delta F_e = xN_h[RT \ln (1-\alpha_h) - \alpha_h{}^2(xN_hW_h)] + xN_c \ln\left(\frac{a/K}{1+a/K}\right) \quad (18)$$

where α_h is given by equation 15b. The last term in equation 18 is the purely statistical contribution to the electrostatic free energy made by the distribution of bound protons within the random coil regions. When W_h is zero, $1 - \alpha_h$ equals $(a/K)/(1 + a/K)$. Hence ΔF_e as given by equation 18 is independent of the configurational state of the polypeptide as is to be expected physically.

The Equilibrium Configurational State of the Charged Polypeptide.—The fraction of residues in the random coil configuration is obtained readily by minimizing the total free energy of the polypeptide with respect to N_c and N_{hc}. The total free energy is given by the sum of equation 9 of the preceding paper and equation 18 above. As charge interactions have been neglected everywhere except in the helical regions, equation 18 does not depend explicitly on the number of such regions but only on the distribution of residues in the two configurational states. Consequently only the expression resulting from the minimization condition with respect to N_c is modified. The solution of the simultaneous quadratic equations gives X_c in the usual form

$$X_c = {}^1/_2\left[1 \pm \left(\frac{s}{s+4}\right)^{1/2}\right]$$

where

$$s = \frac{\left[1 - \left(\frac{j_c}{j_h}\right)\left(\frac{1+a/K}{a/K}\right)^x (1-\alpha_h)^x e^{-x\alpha_h{}^2 w_h}\right]^2}{(y_{hc})^2\left(\frac{j_c}{j_h}\right)\left(\frac{1+a/K}{a/K}\right)^x (1-\alpha_h)^x e^{-x\alpha_h{}^2 w_h}} \quad (19)$$

w_h is equal to xN_hW_h/RT and is thus independent of the length of a helical region. The choice of sign is then dictated as above: for

$$1 > \left(\frac{j_c}{j_h}\right)\left(\frac{1+a/K}{a/K}\right)^x (1-\alpha_h)^x e^{-x\alpha_h{}^2 w_h}$$

the negative sign corresponds to the lower free

(19) T. L. Hill, *Arch. Biochem. Biophys.*, **57**, 229 (1955).

(20) L. Pauling and R. B. Corey, *Proc. Natl. Acad. Sci.*, **37**, 241 (1951).

(21) C. E. Hall and P. Doty, *J. Am. Chem. Soc.*, **80**, 1269 (1958).

energy state, and the positive sign applies when the inequality is reversed.

The dependence of the configurational state of a polyglutamic acid on pH at 300°K. is displayed in Fig. 3 for two rather high values of the ionic strength ($\Gamma/2$). A pK of 4.6 has been chosen for the isolated carboxyl group,[22] and a bulk dielectric constant of 80 has been employed. The other parameters are as indicated in the preceding paper with the larger value of y_{hc} employed. Raising the pH results in enhanced dissociation of the carboxyl groups and hence an increase in charge repulsions with a concomitant increase in the random coil character of the polypeptide. The transition is complete within a range of one pH unit. A transition pH at which half the residues are helical and half random coil is defined by equating s to zero. Increasing the ionic strength of the solution diminishes the magnitude of the charge repulsions and displaces this transition pH to a higher value, *i.e.*, more carboxyl groups must ionize to disrupt the helical configuration.

The transformation is well illustrated by the titration curve for the polypeptide in the vicinity of the transition pH as shown in Fig. 4. The quantity $1 - \bar{\alpha}$ is the average fraction of protons bound by the polypeptide where $\bar{\alpha}$ is given by

$$\bar{\alpha} = \alpha_h X_h + \alpha_c X_c \qquad (20)$$

α_c is given by equation 15b with W equal to zero. At pH's below the transition pH the titration curve of the polypeptide approaches that characteristic of the completely helical configuration, *i.e.*, the charged cylinder. At pH's above the transition pH the behavior of the polypeptide approaches that of the random coil. In the immediate vicinity of the transition pH there is a marked steepening of the titration curve of the polypeptide. This steepening is manifested by an appreciable ionization of the carboxyl groups in a very narrow pH range.

It can be stated quite generally that *any electrostatically induced structural transition will be accompanied by an ionization (or a binding of protons) which will result in a net charge increase.* This ionization is an inevitable consequence of a change in structure from a configuration where charge interactions are important to one where they are less so. Moreover, this ionization will be increasingly extensive with increasing electrostatic instability, *i.e.*, for the above calculations the larger w_h. The neglect of charge interactions in the random coil configurational state make the above estimated ionizations maximal within the framework of the approximate polyelectrolyte theory employed.

Such ionizations are likely to be very considerable for helix–coil transitions in synthetic polypeptides and DNA[23] for two reasons. First, *all* the monomeric units in these macromolecules carry dissociable groups. Secondly, relatively great dimensional changes occur in a transition between a highly asymmetric configuration and a spherically symmetric one. These great dimensional differences may imply substantially different electrostatic

(22) C. Tanford, S. A. Swanson and W. S. Shore, *J. Am. Chem. Soc.*, **77**, 6414 (1955).

(23) S. A. Rice and A. Wada, to be published.

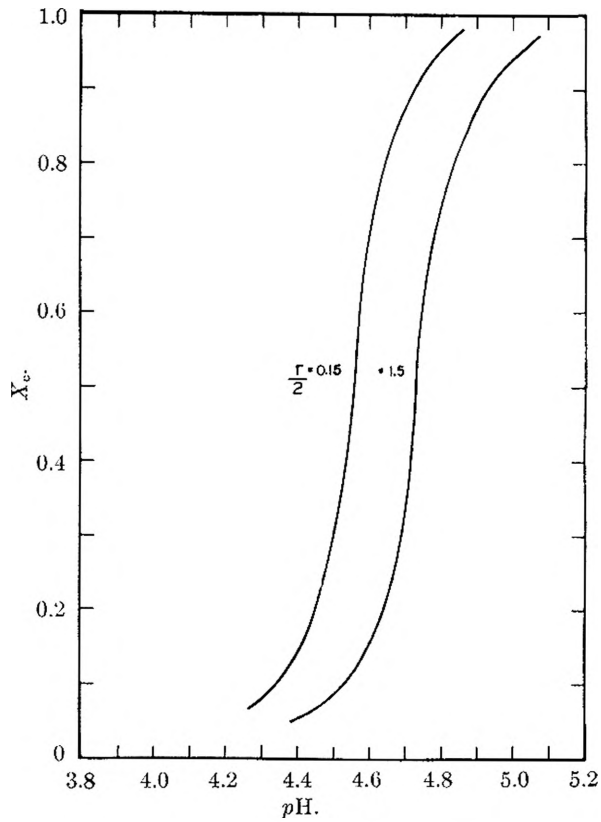

Fig. 3.—The fraction of residues in the random coil configuration (X_c) in polyglutamic acid plotted against pH for two values of the ionic strength ($\Gamma/2$).

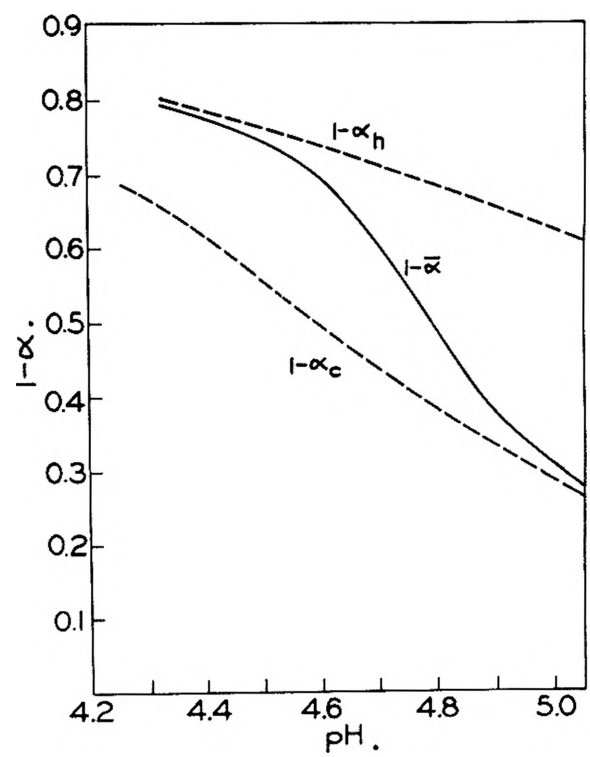

Fig. 4.—The titration curve for polyglutamic acid (solid curve) in the pH region of the helix-coil transition, $\Gamma/2$ = 1.5. The upper and lower dashed curves refer to hypothetical polypeptides which maintain the helical and random coil configurations respectively throughout this pH region.

terms in the titration equations for the two extreme states.

These remarks may have a bearing on the origin of certain phenomena observed with the denaturation of a number of proteins. A view has grown up in the past twenty years that the denaturation of many proteins is induced by the prior ionization of certain "trigger" groups. These groups, *e.g.*, carboxyls and imidazoles in the case of ferrihemoglobin[24] denaturation are presumably linked by hydrogen bridges to other basic or acidic groups in the native protein and are not titratable until the protein is exposed to extremes of *p*H. This anomalous titration behavior of a number of proteins has been reviewed and interpreted recently by Steinhardt and Zaiser[24] from substantially this point of view. It is to be noted that in the case of the hemoglobins, pepsin and other proteins cited by these authors the binding or liberation of protons occurs in a manner to increase the net charge and is accompanied by other denaturative changes which indicate a structural "loosening and expansion" of the macromolecule. Consequently gross electrostatic effects of the type discussed above must be present. Whether these considerations suffice to account completely for the titration behavior is open to question. More details concerning the extent of the configuration changes during denaturation must be obtained before it will be possible to examine this point more critically.

(24) J. Steinhardt and E. M. Zaiser in M. L. Anson, K. Bailey and J. T. Edsall, "Advances in Protein Chemistry," Vol. 10, Academic Press, New York, N. Y., 1955, pp. 151–226.

Acknowledgment.—The author wishes to extend his thanks to Professor Walter Kauzmann for much advice and encouragement throughout the course of this work. He would also like to acknowledge the financial assistance received from the National Science Foundation for the summers of 1956 and 1957 through a grant to Professor Kauzmann.

THE KINETIC ANALYSIS OF A DISTILLING SYSTEM AND ITS APPLICATION TO PRELIMINARY DATA ON THE TRANSESTERIFICATION OF DIMETHYL TEREPHTHALATE BY ETHYLENE GLYCOL[1]

BY LEIGHTON H. PEEBLES, JR., AND WILLIAM S. WAGNER

Contribution No. 52 from the Research Division, The Chemstrand Corporation, Decatur, Alabama

Received December 27, 1958

The kinetics of a reaction in which the distillation of one product of the reaction was used to follow the reaction is analyzed in terms of the amount of distillate as a function of time. The change in volume of the reacting system must be included in the rate equations in such a way that the normal rate constant includes a function of the initial concentrations. The transesterification of dimethyl terephthalate (DMT) by ethylene glycol (EG) was studied under conditions designed to yield bis-β-hydroxyethyl terephthalate (BHET) as the primary product. This reaction has been analyzed by Griehl and Schnock[2] who concluded that the reaction followed first-order kinetics. The reaction was reanalyzed because it appeared more likely to follow a mechanism of two competitive, consecutive second-order reactions. The data are consistent with two competitive, consecutive second-order reactions, but are not sufficiently inconsistent with single first-order kinetics to establish the mechanism. The analysis of Frost and Schwemer[3] for two competitive, consecutive second-order reactions has been generalized for any set of initial conditions. The resultant rate expressions were integrated with a digital computer, and selected values are presented.

Introduction

There are many reactions in which the distillation of one of the products drives the reaction toward completion. It is convenient to follow the course of many of such reactions by the distillate collected. Pratt and his co-workers[4] used distillation to follow the course of etherification of phenylcarbinols and transesterification of their alcohols, etherification of benzyl and related alcohols, etc. However, no kinetic analysis has been published for a distilling system in which the volume of the system changes appreciably with time.

In the present case, a kinetic analysis for a reacting system in which changes in volume as well as the reaction progress affect the reactant concentrations, has been devised. Interest in this problem originated in the course of studies on the kinetics of condensation reactions of which the transesterification of dimethyl terephthalate with ethylene glycol is an example.

The classical method of preparing polyethylene terephthalate involves a two-step process, the first step of which is the above transesterification.

From the organic chemistry involved, it seemed that the transesterification reaction probably would follow a mechanism comprised of two consecutive second-order reactions involving the individual transformation of each methyl ester group on the DMT molecule into a β-hydroxyethyl ester group.

It was necessary to develop a mathematical method that was capable of analyzing the data obtained from a distilling system in terms of two competitive, consecutive second-order reactions in

(1) Presented at the 134th National Meeting of the American Chemical Society, Chicago, Illinois, September, 1958.

(2) W. G. Griehl and G. Schnock, *Faserforsch. u. Textiltech.*, **8**, 408 (1957).

(3) (a) A. A. Frost and W. C. Schwemer, *J. Am. Chem. Soc.*, **74**, 1268 (1952); (b) A. A. Frost and R. G. Pearson, "Kinetics and Mechanism," John Wiley and Sons, New York, N. Y., 1953, p. 164ff.

(4) E. F. Pratt, *et al.*, *J. Am. Chem. Soc.*, **71**, 2846 (1949); **72**, 1367 (1950); **72**, 4638 (1950); **75**, 275 (1953); **75**, 3739 (1953); **78**, 76 (1956).

which a volume change occurs. The equations developed resemble Frost and Schwemer's[3] expressions, but are generalized to handle other than equivalent amounts of reactants and include a correction for the volume change. An experimental technique also had to be devised that would give suitable, reproducible data.

Mathematical Treatment

1. The Volume of the System Remains Constant with Time.—A reaction system consisting of two competitive, consecutive second-order reactions can be represented by

$$A + B \longrightarrow C + E \quad (1)$$
$$A + C \longrightarrow D + E \quad (2)$$

The problem of two competitive, consecutive second-order reactions has been considered many times by different people[5-14]. As yet there is no closed analytical integrated expression to indicate the concentrations of the various species with time. A general method of obtaining the two rate constants is to determine k_2 in one experiment, then evaluate k_1 by another experiment, generally with rather involved series approximations, or with graphical integrations.

Frost and Schwemer[3] have developed a method of evaluating both k_1 and k_2 simultaneously in a single experiment, under specified initial concentrations so that the rate expressions are analytically integrable. The first objectives in this work were the generalization of Frost and Schwemer's method to cover any set of initial concentrations and the evaluation of the resulting equations by numerical integration using a digital computer. The modification necessary for the case where the volume of the system changes with time will be considered later.

The differential equations for the system represented by equations 1 and 2 with a constant volume are

$$-\frac{d(A)}{dt} = k_1(A)(B) + k_2(A)(C) \quad (3)$$
$$-\frac{d(B)}{dt} = k_1(A)(B) \quad (4)$$

where (A), (B) and (C) are expressed as moles per liter.

The material balances for equations 1 and 2 are

$$A_0 = A + C + 2D \quad (5)$$
$$B_0 = B + C + D \quad (6)$$

from which the instantaneous number of moles of C may be obtained.

$$C = A - 2B - (A_0 - 2B_0) \quad (7)$$

where the subscript zero denotes the amount present at zero time. Let certain dimensionless quantities be defined as

$$\alpha = \frac{(A)}{(A)_0}, \beta = \frac{(B)}{(B)_0}, \mu = \frac{(A)_0}{(B)_0}, \kappa = k_2/k_1$$
$$\tau \text{ for the present} = k_1(B)_0 t \quad (8)$$
$$\epsilon = \frac{E}{E_\infty} = (\mu/2)(1 - \alpha) \text{ for } \mu \geq 2$$
$$= (1 - \alpha) \quad \text{for } \mu \leq 2$$

By substituting the first line of equations 8 into (3) and (7) and then dividing (3) by (4), there is obtained

$$\mu d\alpha/d\beta = (1 - 2\kappa) + \kappa\mu\alpha/\beta + (\mu - 2)\kappa/\beta \quad (9)$$

Equation 9 can be integrated to give

$$\mu\alpha = \mu - 2 + \frac{1 - 2\kappa}{1 - \kappa}\beta + \frac{\beta^\kappa}{1 - \kappa} \quad (10)$$

Equation 4 can now be rewritten by use of (8) to give

$$-d\beta = \mu\alpha\beta d\tau \quad (11)$$

which on integration gives

$$\tau = -\int_1^\beta \frac{d\beta}{\beta\left[\mu - 2 + \frac{(1 - 2\kappa)}{1 - \kappa}\beta\frac{\beta^\kappa}{1 - \kappa}\right]} \quad (12)$$

Equation 12 can only be integrated analytically in two general cases: (a) when $\kappa = 2$ or $^1/_2$ and (b) when $\mu = 2$ and κ is a ratio of integers. It is possible by numerical integration to obtain $\tau(\beta, \kappa, \mu)$ for selected values of κ and μ. Intermediate values of $\tau(\beta, \kappa, \mu)$ then can be found by linear interpolation.

2. The Volume of the System Varies with Time.—If the volume of the system varies with time, the differential equations must be modified to correct for the change in concentration due to volume change as well as reaction and to impose the conditions of a material balance upon the kinetic expressions.

Consider a reacting system in which one of the products is distilled as it is formed. The volume of the reacting system then varies as a function of the volume of the material distilled. In the simplest case, the volume will vary linearly with the moles of distillate obtained, thus

$$V = V_0 - vE \quad (13)$$

where v is a molar volume of the distillate chosen so that equation 13 is true. Now consider a single second-order reaction such as

$$A + B \longrightarrow C + E \uparrow k \quad (14)$$

A material balance requires

$$E = A_0 - A = B_0 - B \quad (15)$$

and

$$A = A_0 - B_0 + B$$

so

$$V = V_0 - vA_0 + vA = V_0 - vB_0 + vB \quad (16)$$

and rearranging

$$V = \frac{V_0 - vA_0}{1 - v(A)} = \frac{V_0 - vB_0}{1 - v(B)} \quad (17)$$

so that the mass balance between A and B may be written in terms of concentration

$$(A) = \frac{A_0 - B_0}{V} + (B) \quad (18)$$

(5) C. K. Ingold, *J. Chem. Soc.*, 2170 (1931).
(6) M. Ritchie, *ibid.*, 3112 (1931).
(7) F. H. Westheimer, W. A. Jones and R. A. Lad, *J. Chem. Phys.*, **10**, 478 (1942).
(8) D. French, *J. Am. Chem. Soc.*, **72**, 4806 (1950).
(9) J. C. Morrow, *J. Chem. Phys.*, **23**, 2452 (1955).
(10) S. Wideqvist, *Arkiv Kemi*, **8**, 545 (1955).
(11) V. F. G. Cook and W. Gerrard, *J. Chem. Soc.*, 1978 (1955).
(12) T. Bak, *Acta Chem. Scand.*, **8**, 1733 (1954).
(13) R. L. Burnett and L. P. Hammett, *J. Am. Chem. Soc.*, **80**, 2415 (1958).
(14) W. G. McMillan *ibid.*, **79**, 4838 (1957).

$$(A) = \frac{(A)_0 - (B)_0}{1 - v(B)_0} + \frac{1 - v(A)_0}{1 - v(B)_0}(B)$$

and

$$\frac{d(A)}{d(B)} = \frac{1 - v(A)_0}{1 - v(B)_0} \quad (19)$$

In order that these equations may be satisfied, the rate equations must be written

$$-\frac{d(A)}{dt} = [1 - v(A)_0]k(A)(B) \quad (20)$$

$$-\frac{d(B)}{dt} = [1 - v(B)_0]k(A)(B)$$

where the rate constant must be multiplied by a function of the initial concentration of the component chosen as the dependent variable.

If either equation 19 or 20 is integrated with the aid of the mass balance equation 18, the result is

$$kt = \frac{1}{(B)_0 - (A)_0} \ln \left\{ \frac{(A)_0}{(B)_0} \times \frac{(B)}{(A)} \right\} \quad (21)$$

Equation 21 is almost an obvious result, since in this particular case the volume cancels out because of the ratio of concentrations in the logarithmic term. The important point to note, however, is that an incorrect result would have been obtained if the differential equations 20 had been used without the bracketed term, and the mass balance equation 18 had been used to eliminate the independent variable. In those cases where a ratio of concentrations in the integrated form does not occur, such as in a first-order equation, or a second-order equation with equal initial concentrations, the function in the brackets of equation 20 does appear. This is necessary so that mass balance equations of the form of equation 18 may be satisfied.

The above result applies to a single second-order reaction where one mole of A reacts with one mole of B. The same arguments can be applied to any order of reaction, and the generalized equation denoting the reaction is

$$aA + bB \longrightarrow cC + eE \uparrow \quad (22)$$

where a moles of A react with b moles of B to produce c moles of C and e moles of E are distilled. The stoichiometrical quantities a, b, c, e, can have zero or positive values, and the sum of a and b is the order of the reaction. Again the simplest case of a volume change is considered, namely

$$V = V_0 - \frac{ve}{a}(A_0 - A) = V_0 - \frac{ve}{b}(B_0 - B) \quad (23)$$

$$= V_0 + \frac{ve}{c}(C_0 - C)$$

Note the sign has changed for the case of the product C.

The rate equations are then written as

$$-\frac{d(A)}{dt} = a\left[1 - \frac{ve}{a}(A)_0\right] k(A)^a(B)^b$$

$$-\frac{d(B)}{dt} = b\left[1 - \frac{ve}{b}(B)_0\right] k(A)^a(B)^b \quad (24)$$

$$+\frac{d(C)}{dt} = c\left[1 + \frac{ve}{c}(C)_0\right] k(A)^a(B)^b$$

This result can now be used to write the differential equations for two competitive, consecutive second-order reactions

$$-\frac{d(A)}{dt} = [1 - v(A)_0][k_1(A)(B) + k_2(A)(C)] \quad (25)$$

$$-\frac{d(B)}{dt} = [1 - 2v(B)_0]k_1(A)(B)$$

The mass balance for the intermediate C, written in terms of concentrations, is

$$(C) = (A) - 2(B) - [(A)_0 - 2(B)_0]\left[\frac{1 - v(A)}{1 - v(A)_0}\right] \quad (26)$$

Equations 8 may now be used with the exception that τ is redefined

$$\tau = (1 - v(A)_0)k_1(B)_0 t$$

Then equation 10 becomes

$$\frac{\mu}{\delta}\frac{(A)}{(A)_0} = \frac{\mu\alpha}{\delta} = \frac{\mu - 2}{1 - v(A)_0} + \frac{1 + 2\kappa}{1 - \kappa}\beta + \frac{\beta^\kappa}{1 - \kappa} \quad (27)$$

where

$$\delta = \frac{1 - v(A)_0}{1 - 2v(B)_0}$$

and

$$\tau = -\int_1^\beta \frac{d\beta}{\beta\left[\frac{\mu - 2}{1 - v(A)_0} + \frac{1 - 2\kappa}{1 - \kappa}\beta + \frac{\beta^\kappa}{1 - \kappa}\right]} \quad (28)$$

Equation 28 is the same as equation 12 except for the factor of $(1 - v(A)_0)$ in the denominator of $(\mu - 2)$. Since this term is a constant in both equations for a given integration intermediate values of τ may be interpolated between given values of μ and κ.

When $\kappa = 1$, equations 10, 12, 27 and 28 are not correct. In this particular case, for constant volume

$$\mu\alpha = \mu - 2 + 2\beta - \beta \ln \beta \quad (29)$$

and for changing volume

$$\frac{\mu\alpha}{\delta} = \frac{\mu - 2}{1 - v(A)_0} + 2\beta - \beta \ln \beta \quad (30)$$

and again

$$\tau = \int_\beta^1 \frac{d\beta}{\mu\alpha\beta} \quad (31)$$

where τ has absorbed the constant δ.

The integrals were evaluated by Simpson's rule. $\tau\mu(\beta, \mu, \kappa)$ and $\beta(\epsilon, \mu, \kappa)$ are presented in Tables I and II for various values of μ and κ for conversions of 20, 30, 40, 50 and 60% from equation 12 without the volume correction. If the volume changes with time, the conversion must be calculated according to equations 32.

$$\epsilon = \frac{\mu}{2} - \frac{\mu\alpha}{2}\left[\frac{1 - v(A)_0}{1 - v(A)_{0\alpha}}\right], \mu \geq 2 \quad (32)$$

$$= 1 - \alpha\left[\frac{1 - v(A)_0}{1 - v(A)_{0\alpha}}\right], \mu \leq 2$$

The function $\beta(\epsilon, \kappa)$ does not vary with v providing $(\mu - 2) \div (1 - v(A)_0)$ is a constant. Thus to use Tables I and II when $v \neq 0$, $(\mu - 2)/(1 - v(A)_0)$ equal to one of the tabulated values, ϵ must be recalculated, that is, replacing the heading ϵ's in Tables I and II by use of equation 32.

The method of evaluating k_1 and k_2 is as follows: since in equation 8 τ is proportional to time, the ratio of τ at two conversions must be equal to the ratio of time at these same conversions, *i.e.*, τ at 60% conversion/τ at 20% conversion equals

TABLE I

$\beta(e, \kappa)$, $v = 0$

κ	$\epsilon = 0.2$	$\epsilon = 0.3$	$\epsilon = 0.4$	$\epsilon = 0.5$	$\epsilon = 0.6$
10	0.7613	0.6640	0.5686	0.4737	0.3790
7	.7486	.6499	.5551	.4619	.3693
5	.7349	.6336	.5384	.4464	.3562
4	.7252	.6213	.5252	.4336	.3449
3	.7123	.6041	.5059	.4142	.3270
2	.6938	.5780	.4753	.3820	.2958
1.5	.6810	.5589	.4519	.3564	.2702
1.0	.6641	.5322	.4177	.3178	.2308
3/4	.6533	.5139	.3933	.2896	.2015
1/2	.6400	.4900	.3600	.2500	.1600
1/3	.6292	.4691	.3290	.2118	.12006
1/4	.6231	.4563	.3089	.1862	.09364
1/5	.6191	.4476	.2947	.1675	.07469
1/6	.6163	.4412	.2839	.1530	.06040
1/7	.6142	.4364	.2755	.1414	.04929
1/8	.6126	.4326	.2687	.1318	.04044
1/9	.6113	.4295	.2630	.1236	.03330
1/10	.6102	.4270	.2583	.11667	.02746

TABLE II

$\tau(e, \kappa, \mu)$

$\mu = 1$, $v = 0$

κ	$\epsilon = 0.2$	$\epsilon = 0.3$	$\epsilon = 0.4$	$\epsilon = 0.5$	$\epsilon = 0.6$
10	0.1607	0.2454	0.3444	0.4659	0.6226
7	.1713	.2615	.3656	.4918	.6530
5	.1817	.2784	.3891	.5223	.6907
4	.1886	.2902	.4064	.5454	.7206
3	.1972	.3058	.4300	.5784	.7646
2	.2086	.3278	.4650	.6294	.8356
1.5	.2158	.3427	.4901	.6677	.8912
1.0	.2246	.3619	.5243	.7225	.9745
3/4	.2297	.3739	.5469	.7606	1.0350
1/2	.2356	.3883	.5754	.8109	1.1192
1/3	.2399	.3996	.5991	.8555	1.198
1/4	.2422	.4060	.6130	.8827	1.249
1/5	.2437	.4100	.6221	.9012	1.285
1/6	.2447	.4128	.6285	.9146	1.312
1/7	.2454	.4149	.6333	.9248	1.332
1/8	.2460	.4165	.6371	.9328	1.349
1/9	.2464	.4178	.6400	.9392	1.362
1/10	.2467	.4187	.6425	.9446	1.374

$\mu = 2$, $v = 0$

10	0.1513	0.2427	0.3626	0.5294	0.7795
7	.1607	.2552	.3769	.5449	.7955
5	.1710	.2701	.3958	.5670	.8199
4	.1784	.2818	.4116	.5865	.8430
3	.1886	.2987	.4356	.6182	.8830
2	.2036	.3255	.4765	.6762	.9622
1.5	.2142	.3462	.5102	.7271	1.0368
1.0	.2286	.3766	.5636	.8131	1.1714
3/4	.2381	.3985	.6049	.8845	1.291
1/2	.2500	.4286	.6667	1.0000	1.500
1/3	.2598	.4564	.7305	1.1334	1.770
1/4	.2656	.4741	.7756	1.239	2.011
1/5	.2694	.4865	.8098	1.327	2.235
1/6	.2720	.4957	.8368	1.404	2.449
1/7	.2740	.5028	.8589	1.471	2.657
1/8	.2755	.5085	.8773	1.531	2.862
1/9	.2768	.5131	.8929	1.586	3.066
1/10	.2778	.5170	.9064	1.637	3.270

$\mu = 3$, $v = 0$

10	0.09723	0.1520	0.2196	0.3067	0.4245
7	.10324	.1598	.2285	.3163	.4343
5	.10984	.1693	.2402	.3295	.4487
4	.11462	.1766	.2498	.3411	.4620
3	.1211	.1871	.2643	.3597	.4845
2	.1306	.2037	.2889	.3932	.5280
1.5	.1374	.2165	.3090	.4223	.5683
1.0	.1466	.2352	.3407	.4710	.6399
3/4	.1526	.2487	.3651	.5111	.7026
1/2	.1601	.2671	.4014	.5754	.8110
1/3	.1663	.2840	.4386	.6489	.9486
1/4	.1699	.2948	.4648	.7066	1.0698
1/5	.1723	.3024	.4845	.7545	1.1814
1/6	.1740	.3080	.5002	.7957	1.287
1/7	.1752	.3123	.5129	.8319	1.389
1/8	.1762	.3157	.5235	.8643	1.489
1/9	.1770	.3185	.5324	.8936	1.588
1/10	.1776	.3208	.5402	.9204	1.686

$\mu = 4$, $v = 0$

10	0.07165	0.11075	0.1578	0.2168	0.2939
7	.07608	.11649	.1643	.2237	.3010
5	.08093	.1234	.1728	.2332	.3112
4	.08445	.1287	.1797	.2415	.3206
3	.08922	.1363	.1901	.2547	.3363
2	.09622	.1484	.2077	.2783	.3666
1.5	.10118	.1576	.2221	.2988	.3943
1	.10789	.1712	.2447	.3329	.4434
3/4	.11229	.1809	.2620	.3608	.4861
1/2	.11779	.1942	.2877	.4055	.5596
1/3	.1223	.2064	.3140	.4563	.6524
1/4	.1250	.2141	.3325	.4961	.7337
1/5	.1267	.2196	.3464	.5290	.8082
1/6	.1280	.2236	.3574	.5573	.8787
1/7	.1289	.2266	.3663	.5821	.9466
1/8	.1295	.2291	.3738	.6043	1.0129
1/9	.1301	.2311	.3801	.6243	1.0783
1/10	.1306	.2328	.3854	.6426	1.1432

time for 60% conversion/time for 20% conversion. With tables of τ at 20, 30, 40, 50 and 60% conversion for selected values of κ, intermediate values of κ can be interpolated linearly. From a knowledge of the average value of κ from several time ratios, the value of τ can be computed for various conversions, and k_1 determined. Further $k_2 = \kappa k_1$. Figure 1 shows the time ratio for 60% conversion to 20% conversion as a function of $1/\kappa$ for various values of μ.

The reason for the sudden decrease in the $\mu = 1$ curve from the $\mu = 2$ curve is due to the fact that the conversion is limited by the α parameter at $\mu \geq 2$ and by the β parameter at $\mu \leq 2$. It so happens that the experimental results associated with this study are in the area of the minima, so a different method of computing the value of κ was used; the quantity τ/t was evaluated at 20, 30, 40, 50 and 60% conversion for assorted κ values. The value of κ with the minimum variance around $<\tau/t>$ average, was used to determine k_1 and k_2.

The data have been analyzed for two competitive, consecutive second-order reactions with a changing volume as outlined above and also for first- and second-order kinetics for reasons presented later. For a first-order reaction with respect to the B component with a changing volume, the integrated equation in terms of conversion is

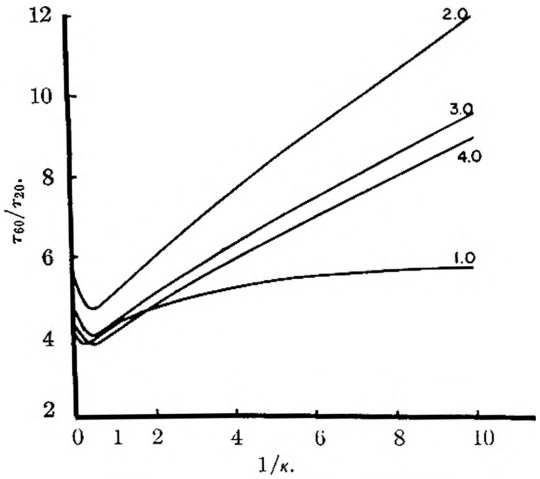

Fig. 1.—Variation of the ratio "time for 60% conversion to time for 20% conversion" against $1/\kappa$, the ratio of the rate constants, as a function of a, the ratio of initial concentrations.

$$kt = -\ln \frac{1-\epsilon}{1-2v(\mathrm{B})_0\epsilon} \qquad (33)$$

For a single second-order reaction with unequal amounts of reaction the equation is

$$kt = \frac{-1}{(\mathrm{A})_0 - (\mathrm{B})_0} \ln \frac{1-\epsilon}{1-\epsilon/\mu} \qquad (34)$$

The Transesterification Reaction

For economy of space in representing the rather complex set of reactions thought to occur when ethylene glycol (EG) and dimethyl terephthalate (DMT) react, let the abbreviations EG and DMT accompanied by one or more hyphens represent EG and DMT residues with one or more functional groups reacted, and let E represent methanol. This complex set of reactions can then be partially represented by the set of equations

$$\mathrm{EG} + \mathrm{DMT} \longrightarrow \mathrm{EG\text{-}DMT} + \mathrm{E}\uparrow \qquad (35)$$
$$(\mathrm{A} + \mathrm{B} \longrightarrow \mathrm{C} + \mathrm{E}) \qquad (1)$$
$$\mathrm{EG} + \mathrm{EG\text{-}DMT} \longrightarrow \mathrm{EG\text{-}DMT\text{-}EG} + \mathrm{E}\uparrow \qquad (36)$$
$$(\mathrm{C} + \mathrm{A} \longrightarrow \mathrm{D} + \mathrm{E}) \qquad (2)$$
$$\mathrm{EG\text{-}DMT} + \mathrm{DMT} \longrightarrow \mathrm{DMT\text{-}EG\text{-}DMT} + \mathrm{E}\uparrow \qquad (37)$$
$$\mathrm{EG\text{-}DMT\text{-}EG} + \mathrm{DMT} \longrightarrow \mathrm{EG\text{-}DMT\text{-}EG\text{-}DMT} + \mathrm{E}\uparrow \qquad (38)$$
$$\mathrm{DMT\text{-}EG\text{-}DMT} + \mathrm{EG} \longrightarrow \mathrm{EG\text{-}DMT\text{-}EG\text{-}DMT} + \mathrm{E}\uparrow \qquad (39)$$
$$\text{etc.} \qquad (40)$$
$$\text{etc.} \qquad (41)$$

Equations 35 and 36 correspond to equations 1 and 2, respectively.

In developing the kinetics of the reaction, the following simplifying assumptions are made: (1) reactions corresponding to equations 37 through 41 are suppressed under the experimental conditions employed and may be neglected. (2) The methanol was driven off instantly as it was formed. (3) No reverse reactions occurred to a significant extent. Now consider each assumption.

The concentration of EG employed was relatively large compared to the concentration of DMT; initially the EG/DMT mole ratio was 3.75. Therefore, the concentration of EG should always be relatively large compared to the sum of the concentrations of hydroxyl group bearing species such as EG-DMT, EG-DMT-EG, etc., thus the probability of further reaction beyond step 36 with DMT is low.

In early experiments, a short time lag occurred between dropping the catalyst and distillation of methanol. This was found to be due mainly to the build-up of methanol in the solution and in the reactor and condenser space. This time lag was eliminated by continuously injecting methanol from a reservoir into the reactor. After a steady state of methanol distillation occurred due to injection, no hold-up or time lag occurred. Methanol was almost explosively evolved upon addition of the catalyst. No reaction occurred prior to catalyst addition. Further, it was found that the evolution of methanol was apparently diffusion controlled unless the reacting mixture was stirred at sufficiently high speeds. Beyond a critical stirring rate, no change in methanol distillation was noted.

The error in the assumption of no reverse reaction would be almost entirely due to the small amount of dissolved methanol, less than 2.5 weight %, initially.

Experimental

Reactor.—Methanol from a reservoir is continuously injected into the glass reactor by a microbellows pump. A fine glass frit between the reservoir and pump serves to remove dust particles from the methanol to avoid fouling the pump. The reactor is heated by a refluxing bath of *p*-cymene which boils at 175°. Thermometers were located in the head space and within the reacting mixture. In order to reduce the error due to methanol evaporation the condenser of the reactor was equipped with an adapter which extended down into the collection bottles which were cooled by ice-baths. Between the adapter and the laboratory atmosphere was another condenser and a drying tube to prevent escape of methanol and admission of water vapor. Ice-water was circulated through the condensers to lower the vapor pressure of methanol and to lower the solubility of DMT in the methanol. The catalyst was contained in a closed bulb which was held by nichrome wire which passed through the nitrogen inlet tube. Nitrogen was used to flush out the reactor before catalyst addition and turned off before the reaction started.

The reaction vessel was charged with 200 ml. (3.58 moles) of EG (Carbide and Carbon's "iron and chloride free" grade), and 185 g. (0.953 mole) of DMT (Hercules "polymerization" grade). The vessel was heated to melt the charge and bring its temperature into equilibrium with the heating bath. Methanol injection was started and allowed to run 30 minutes before addition of 0.090 g. (0.05% based on DMT) of zinc acetylacetonate. The reaction was started by pulling on the wire causing the catalyst ampule to drop into the reactor and be crushed by the whirling stirrer. Sample bottles of distillate were collected prior to the catalyst drop to ensure equilibrium of the injection rate and at 2.5 minute intervals until the reaction had slowed down, and then at 5 minute intervals thereafter until apparent completion of the reaction.

Since the reactor head is not an efficient fractionating column, some EG and DMT were distilled along with the methanol. The distillate contained less than 1% of DMT due to its low solubility at 0°, but upwards to 15 weight % of the distillate was EG. Most of the EG distilled occurred from mechanical carry-over during the initial stages of violent methanol evolution. The amount of methanol produced by the reaction was determined from the weight of material distilled, corrected by refractive index measurement for the EG content and for the rate of methanol injection. The latter was determined by the weight of methanol removed from the reservoir.

The reduction in volume of the reacting mixture was shown by preliminary experiments to be equal to the volume of methanol distilled during the course of the reaction. Under the experimental conditions used here, the change in volume amounted to about 20% of the initial volume.

Zinc Acetylacetonate.[15]—Two hundred g. (2.0 moles) of acetylacetone and 31.2 g. (0.25 mole) of zinc carbonate were stirred under reflux until the evolution of carbon dioxide had ceased and a slightly turbid solution remained. The solution was filtered through a heated filter and allowed to cool slowly. The zinc acetylacetonate crystallized in a solid mass which was broken up and washed three times with isopropyl ether. After drying at room temperature under vacuum, the product melted to a clear melt at 127–128°. The yield was nearly quantitative.

Results and Discussion

The results for the transesterification reaction are presented as an example of the kinetic analysis of a distilling system which is reacting by two competitive, consecutive second-order reactions. Table III contains the analysis for four runs under identical initial conditions. The variance given in Table III is that for the selected value of κ. Since for this mechanism there is no way of obtaining a straight line plot, Fig. 2 shows conversion against time for the four runs. The solid line is calculated from the average of k_1 and k_2 and the points are the experimental conversions.

TABLE III

RATE CONSTANTS FOR TRANSESTERIFICATION OF DMT BY EG

Run	k_1, l./mole min. $\times 10^3$	k_2, l./mole min. $\times 10^3$	Variance $\times 10^3$
7	3.69	12.9	9.2
8	4.29	12.9	1.9
9	4.62	16.2	33.8
10	4.37	13.1	5.0
Av.	4.24	13.8	

In the case of hydrolysis of dibasic acid esters, there is a firm basis for expecting that κ, the ratio of k_2/k_1, should be equal to or less than $^1/_2$, since the hydrolysis of the second ester group proceeds while the first hydrolyzed carboxyl group is ionized.[5] In general, most published work on two competitive, consecutive second-order reactions gives κ values of less than one-half. The results on the transesterification of DMT by EG show that κ is around three, that is, the second step constant is three times greater than the first step constant. Whether or not any significance is to be attached to this result is, of course, contingent upon the correctness of the assumption that the mechanism involves two consecutive second-order reactions. As will be seen, the present data are not capable of unambiguously deciding this point.

Griehl and Schnock in a recent paper came to the conclusion that the transesterification reaction is first order in DMT alone.[2] The present data can be represented adequately by a first-order plot as shown in Fig. 3. However, Griehl and Schnock state that the reaction is not second order. We are not able to support the latter conclusion either from their data or from our work. With the initial concentrations used in both Griehl and Schnock's work and the present work, a second-order reaction is pseudo first order due to the excess of EG used. Figure 4 shows a second-order plot for the present data, and it is quite similar to the first-order plot. It is possible, however, to distinguish between two consecutive second-order reactions and a pseudo first-order reaction at sufficiently low values of κ. It is unfortunately true, that while the present data are reasonably consistent with kinetics of two consecutive second-order reactions, they are not sufficiently inconsistent with the first-order ki-

(15) Prepared by L. R. Hinken of this Laboratory.

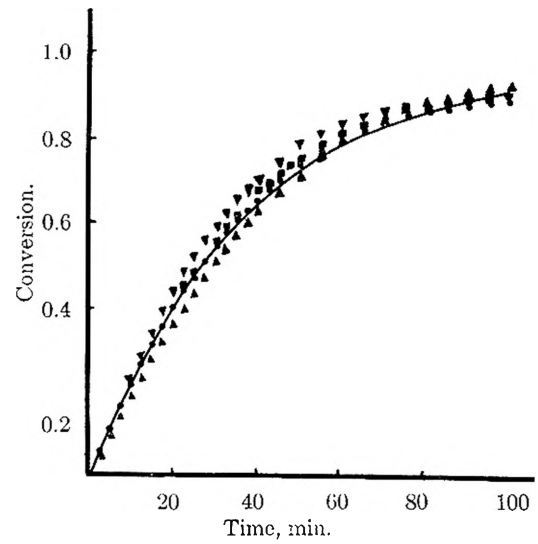

Fig. 2.—Conversion time plot for four runs. Solid line computed for average of individual rate constants.

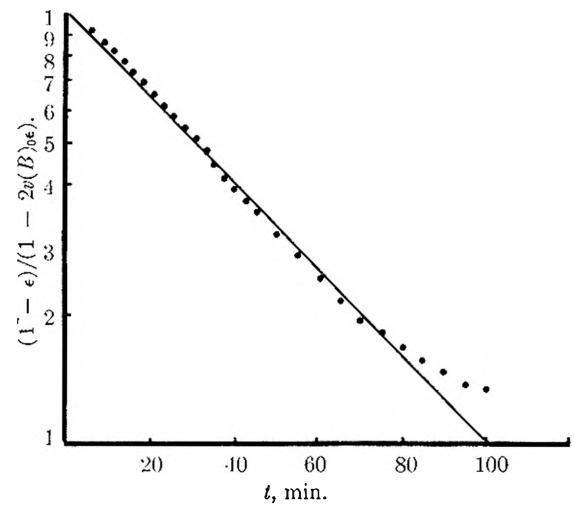

Fig. 3.—First-order plot for run 8.

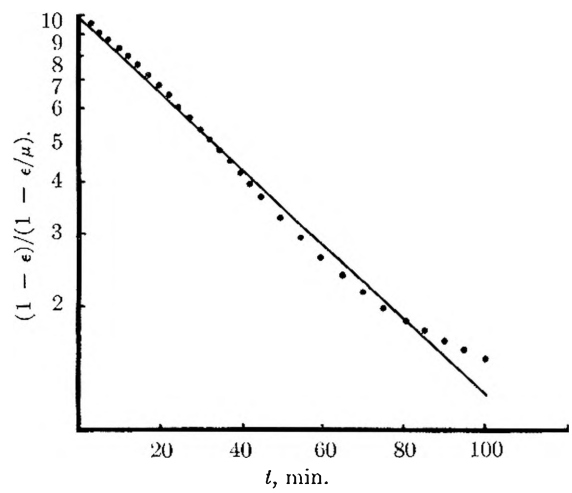

Fig. 4.—Second-order plot for run 8.

netics suggested by Grichl and Schnock or single second-order kinetics to make a decision possible.

An example of a reaction which proceeds with distillation has been given. The method is applicable to many other reactions in which an appreciable volume change occurs. Except for the case of a single second-order reaction with unequal initial reactant concentrations, the rate equations must be modified to include a function of the initial concentrations in the normal rate constant. Reactions which could be analyzed in this fashion include those where a gas is liberated, a liquid vaporized or distilled, or a precipitate formed which effectively removes the product from the locus of reaction. Examples of types of reactions which might be studied in this way are the polymerization of a monomer to an insoluble polymer (if the polymer does not enter into further reaction); certain pyrolysis reactions; and of course reactions similar to the present case. If this approach is not used when an appreciable volume change occurs, then incorrect material balances will occur, which may not be recognized due to inability to carry the reaction to completion, and incorrect rate constants will be obtained, as may be seen from equations 28 and 32–34.

Acknowledgments.—The authors wish to express their thanks to Dr. T. W. DeWitt and Dr. P. H. Hobson for many helpful discussions during the course of this work, to Mr. J. B. Cox for assistance in using the Bendix G15D Computer, to Messrs. R. F. Crafts and W. S. Ward for assistance in the experimental study, and to The Chemstrand Corporation for permission to publish this paper.

NOTES

CHROMATOGRAPHY OF DECABORANE AND SUBSTITUTED DECABORANES

BY BERNARD SIEGEL[1] AND JULIUS L. MACK

Research and Development Department, U. S. Naval Propellant Plant, Indian Head, Md.

Received December 27, 1958

Recent advances in decaborane chemistry have developed new methods for the preparation of substituted decaboranes. A vexing problem often encountered in these investigations has been the extreme difficulty in isolating decaborane derivatives from complex reaction mixtures. This is attributable to the low volatility of decaborane derivatives[2] and their extreme susceptibility to air and many solvents. Chromatography was considered an ideal solution to this problem, provided a system could be developed that would minimize the decomposition of decaborane and its derivatives.

An anhydrous system was deemed necessary since these compounds are readily hydrolyzed when in contact with organic solvents containing water. While most adsorbents ordinarily used in chromatography cannot be made anhydrous without losing their effectiveness[3,4] Florisil can be heated to high temperatures without destroying its surface.[5] Initial experiments with this "Anhydrous" adsorbent resulted in extensive loss of decaborane; in one experiment only 180 mg. of decaborane was eluted from 1.0 g. put onto a column of Florisil. It was subsequently found that losses could be minimized by previous overnight evacuation of the florisil column at 500°; this treatment removed 20–23 g. of water from the 500 g. of adsorbent used in each column and contributed to the effectiveness of the separations by preventing break-up of the column during chromatography by rising gas bubbles.

Sharp separations were obtained on mixtures of decaborane–biphenyl, decaborane–iododecaborane and decaborane–benzyldecaborane. A previously reported reaction mixture[6] was chromatographed; benzyldecaborane had previously been isolated from the reaction mixture by high vacuum distillation, but the distillation had resulted in significant decomposition. With chromatography, a larger yield of benzyldecaborane was recovered, in addition to a new benzylated product.

These separations were based on simply adsorption-type chromatography. It appeared interesting to investigate also the possibility of partition-type chromatography. Using the same adsorbent as a support for diethyl ether, decaborane was sharply separated from biphenyl, with petroleum ether serving as the mobile phase. A mixture of mono and di-iododecaboranes was also separated by this type of process.

Experimental

General Procedure.—The adsorbent used was 100/200 mesh Florisil. The column was 31 mm. Pyrex glass, packed with adsorbent to a height of four feet, and was bounded at the bottom by a fritted disc and greaseless stop-cock. The head consisted of a solvent reservoir below which was an exit to the atmosphere through a stopcock. After the column was packed to the desired height, the head was closed off and the column was wrapped with a heating jacket. The latter was heated overnight at 500° with evacuation through the bottom. The heating jacket was then removed and dried solvent was poured on the cooled column, rigidly excluding air. The sample was then introduced, followed by eluent. The eluents used were dried petroleum ether (b.p. 38–43°) and methylene chloride,

(1) Aerojet-General Corporation, Azusa, California.

(2) Decaborane has a vapor pressure of 0.3 mm. at 55° (A. Stock and E. Pohland, *Ber.*, **62**, 90 (1929)) and substituted decaboranes are generally considerably less volatile.

(3) L. H. Milligan, THIS JOURNAL, **26**, 247 (1922).

(4) F. E. Bartell and E. G. Almy, *ibid.*, **36**, 475 (1932).

(5) Florisil—a synthetic adsorbent, Floridin Co., Tallahassee, Florida.

(6) B. Siegel, J. Mack, J. Lowe and J. Gallaghan, *J. Am. Chem. Soc.*, **80**, 4523 (1958).

chosen for volatility and inertness. The eluate was collected at a rate of 30–40 cc./hr.

Separations (Adsorption).—A petroleum ether solution of 1.0 g. of decaborane and 0.5 g. of biphenyl was chromatographed with petroleum ether as eluent. The initial 600 cc. of eluate contained no solute. Decaborane was eluted over the next 500 cc. of eluate. After 200 cc. of further eluate without solvent, biphenyl was eluted quantitatively.

The separations of mixtures of decaborane–benzyldecaborane and decaborane–iododecaborane[7] were similar except that in these cases, after the elution of decaborane with petroleum ether, the substituted decaboranes could not be eluted with the latter and methylene chloride was used as the eluent.

A petroleum ether extract (8.8 g.) of the benzyl chloride–$B_{10}H_{13}MgI$ reaction[6] was chromatographed after distilling the volatile material. This yielded a trace of decaborane, eluted with petroleum ether; this was followed by 2.95 g. of benzyldecaborane, eluted with 25% methylene chloride; the last fraction (1.9 g.) was eluted with methylene chloride and had a cryoscopic molecular weight of 298 and a composition of 72.6% C, 14.7% B and 7.8% H. The latter was rechromatographed with gradually increasing concentrations of methylene chloride as eluent but no further separation was noted.

Separations (Partition).—A decaborane–biphenyl mixture was chromatographed on a column prepared with diethyl ether, using petroleum ether as eluent. Biphenyl was eluted quantitatively first, followed by decaborane. In a similar manner, a mixture of iododecaborane–di-iododecaborane[7] was chromatographed on a column prepared with methylene chloride, using petroleum ether as eluent. Iododecaborane was eluted first, followed by diiododecaborane.[8]

(7) The latter was prepared by an unpublished method. Details were made available to us by a private communication from the Reaction Motors Division, Thiokol Chemical Corp.

(8) The melting point of this compound was 268°. Since the diiododecaborane reported by Stock (A. Stock, "Hydrides of Boron and Silicon," Cornell Univ. Press, Ithaca, N. Y., 1933) melted at 230°, the compound isolated in this paper is apparently another isomer.

DISSYMMETRY OF DISCS OF NEGLIGIBLE THICKNESS

By Paul Becher

Chemical Research Dept., Atlas Powder Co., Wilmington, Delaware

Received November 10, 1958

The scattering functions and the corresponding dissymmetry corrections for a variety of molecular shapes, such as spheres, rods and coils, have been tabulated, *e.g.*, by Doty and Steiner.[1] Recently, however, we required such information for a disc-shaped scattering unit. Although no such tabulation apparently exists, Debye[2] has shown that the scattering function for a disc of negligible thickness (*i.e.*, negligible with respect to the wave length employed) is given by

$$P(\vartheta) = x^0 - x^2/6 + \sum_{n=3}^{n=\infty} [x^{2(n-1)} \cos (n+1)\pi]/b_n$$

where the coefficients b_n are given by the recursion formula

$$b_n = \left(2n + \frac{b_{n-1}}{b_{n-2}}\right) b_{n-1}$$

and where $b_1 = 1$ and $b_2 = 6$.

The quantity x is defined in the usual manner

$$x = \frac{2\pi D}{\lambda'} \sin \frac{\vartheta}{2}$$

(1) P. Doty and R. F. Steiner, *J. Chem. Phys.*, **18**, 1211 (1950).

(2) P. Debye and E. W. Anacker, This Journal, **55**, 644 (1951); *Cf.* also O. Kratky and G. Porod, *J. Colloid Sci.*, **4**, 35 (1949).

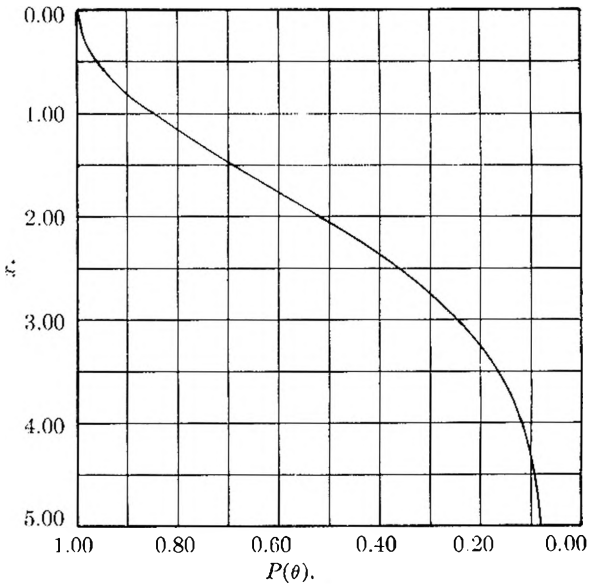

Fig. 1.—Scattering function, $P(\varphi)$ as a function of x.

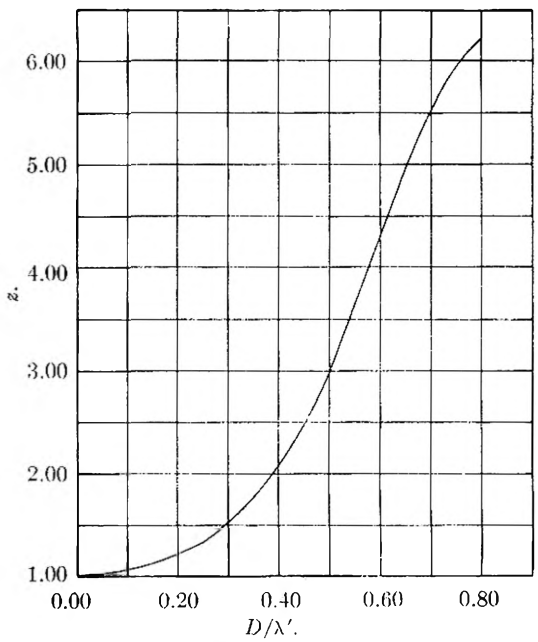

Fig. 2.—Dissymmetry, I_{45}/I_{135}, as a function of D/λ'.

Table I

Scattering Factor for Thin Discs

x	$P(\vartheta)$	x	$P(\vartheta)$
0.10	0.998	2.60	0.335
.20	.993	2.70	.309
.30	.985	2.80	.286
.40	.973	2.90	.263
.50	.961	3.00	.242
.60	.942	3.10	.225
.70	.921	3.20	.205
.80	.899	3.30	.191
.90	.874	3.40	.174
1.00	.846	3.50	.162
1.10	.817	3.60	.152
1.20	.787	3.70	.143
1.30	.756	3.80	.132
1.40	.722	3.90	.124
1.50	.687	4.00	.116

TABLE I (*Continued*)

1.60	.654	4.10	.112
1.70	.620	4.20	.109
1.80	.584	4.30	.101
1.90	.550	4.40	.097
2.00	.517	4.50	.092
2.10	.483	4.60	.088
2.20	.451	4.70	.086
2.30	.420	4.80	.083
2.40	.390	4.90	.081
2.50	.361	5.00	.079

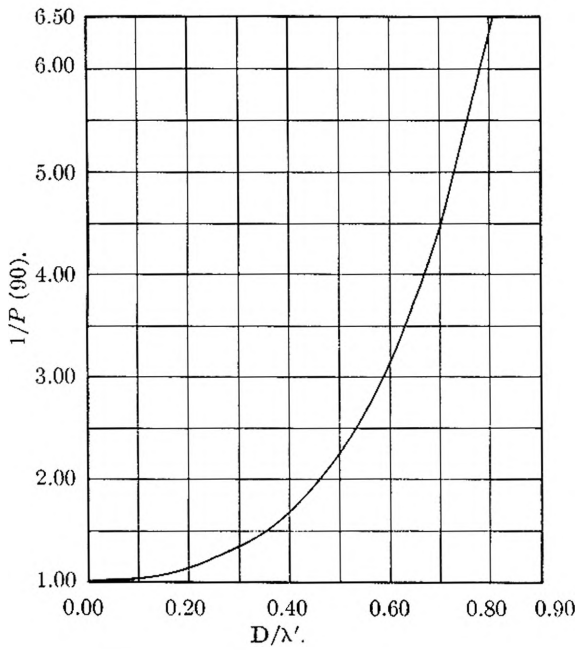

Fig. 3.—Correction function, $1/P(90)$, as a function of D/λ'.

TABLE II

DISSYMMETRY (I_{45}/I_{135}) AND CORRECTION FACTOR FOR THIN DISCS

D/λ'	[z]	$1/P$ (90)
0.05	1.011	1.009
.10	1.047	1.033
.15	1.110	1.078
.20	1.205	1.140
.25	1.338	1.229
.30	1.514	1.342
.35	1.755	1.495
.40	2.075	1.689
.45	2.476	1.934
.50	3.000	2.252
.55	3.641	2.646
.60	4.311	3.145
.65	4.933	3.759
.70	5.682	4.484
.75	5.879	5.376
.80	6.230	6.369

where D is the diameter of the disc and λ' the wave length of light in the medium.

The summations involved are straightforward, although tedious, since the series converges slowly. The scattering function is listed as a function of x in Table I, and presented graphically in Fig. 1. The dissymmetry ($[z] = I_{45}/I_{135}$) and the correction function, $1/P(90)$, are listed as a function of D/λ' in Table II, and shown graphically in Figs. 2 and 3. It is interesting to note that the behavior of the discs lie between that of a sphere and a rod, a not unexpected result.

cis–trans ISOMERIZATION AND SOLVOLYSIS OF DICHLOROBIS-(ETHYLENEDIAMINE)-CHROMIUM(III) CHLORIDE IN NEARLY ANHYDROUS METHANOL[1a]

BY LYNORE E. SLATEN[1b] AND CLIFFORD S. GARNER

Department of Chemistry, University of California, Los Angeles 24, California

Received November 24, 1958

Isomerization and substitution reactions of *cis*-$Co(en)_2Cl_2^+$ (en = ethylenediamine) have been investigated in solvent water and solvent methanol.[2] In aqueous solution the *cis–trans* isomerization is complicated by competition between chloride ion and water for the cobalt ion. However, in solvent methanol *cis*-$[Co(en)_2Cl_2]Cl$ has been shown[3–5] to isomerize quantitatively to the *trans*-isomer at 36° by a first-order reaction without net loss of ligand chloride. Trimble[6] found no spectrophotometric evidence for any change of the *trans*-complex in methanol in 12 hours at 100°. He observed that the *cis*-complex in 2-methoxyethanol ("Methyl Cellosolve") isomerizes completely at 30–50°, followed by a slower reaction between solvent and *trans*-isomer. Brasted and Hirayama[7] studied the isomerization in ethanol and propanol as well as in methanol.

Little is known about isomerization of the corresponding chromium(III) isomers. Trimble[6] found that *l-cis*-$[Cr(en)_2Cl_2]Cl$ in 2-methoxyethanol fails to isomerize in 30 minutes at reflux temperature, although he reported complete racemization in 2 minutes of boiling the solution.

We report here a partial kinetic study of the isomerization of *cis*-$[Cr(en)_2Cl_2]Cl$ in methanol. We have found that *trans*-$[Cr(en)_2Cl_2]Cl$, unlike the *cis*- and *trans*-cobalt analogs, releases ligand chloride at a measurable rate in nearly anhydrous methanol.

Experimental

***cis*-Dichlorobis-(ethylenediamine)-chromium(III) Chloride.**—$[Cr(en)_3]Cl_3 \cdot 3.5H_2O$ was synthesized[8] and converted[9] to *cis*-$[Cr(en)_2Cl_2]Cl \cdot H_2O$, which was stored in the dark. *Anal.* Calcd.: Cr, 17.54; N, 18.89; H_2O, 6.08. Found: Cr, 17.84; N, 18.87; H_2O, 6.08. Water of crystallization was removed in the dark at *ca.* 90° under vacuum just before preparing a reaction mixture.

***trans*-Dichlorobis-(ethylenediamine)-chromium(III) Chloride.**—$[Cr(en)_3](SCN)_3 \cdot H_2O$ was prepared and converted[9]

(1) (a) Supported by U. S. Atomic Energy Commission under Contract AT(11-1)-34, Project 12; (b) Research Center, International Business Machines Corp., Poughkeepsie, N. Y.

(2) For a general review see F. Basolo and R. G. Pearson, "Mechanisms of Inorganic Reactions," John Wiley and Sons, Inc., New York, N. Y., 1958.

(3) D. D. Brown, C. K. Ingold and R. S. Nyholm, *J. Chem. Soc.*, 2674 (1953).

(4) D. D. Brown and C. K. Ingold, *ibid.*, 2680 (1953).

(5) D. D. Brown and R. S. Nyholm, *ibid.*, 2696 (1953).

(6) R. F. Trimble, *J. Am. Chem. Soc.*, **76**, 6321 (1954).

(7) R. C. Brasted and C. Hirayama, *ibid.*, **80**, 788 (1958).

(8) J. C. Bailar, Jr., and J. B. Work, *ibid.*, **67**, 176 (1945).

(9) C. L. Rollinson and J. C. Bailar, Jr., *ibid.*, **66**, 641 (1944); "Inorganic Syntheses," Vol. II, W. C. Fernelius, editor, McGraw-Hill Book Co., Inc., New York, N. Y., 1946, pp. 196–200.

to *trans*-$[Cr(en)_2(NCS)_2]SCN$, from which *trans*-$[Cr(en)_2Cl_2]Cl \cdot HCl \cdot 2H_2O$ was made[10] and stored in the dark over concd. hydrochloric acid. Water and hydrogen chloride of crystallization were removed in the dark under vacuum at *ca.* 90° prior to preparing a reaction mixture. *Anal.* Calcd. for $[Cr(en)_2Cl_2]Cl$: Cr, 18.67; N, 20.11. Found: Cr, 18.30; N, 19.68.

Not more than 24 hours ahead, reagent-grade absolute methanol was refluxed over fresh magnesium filings, then distilled through a closed Pyrex system into a well-dried Pyrex flask. Brown and Ingold,[4] who used a similar procedure, found that subsequent manipulations in preparing methanolic solutions may allow the water content to increase to as much as 0.1% (0.04 *f* in H_2O) even with careful technique. Karl Fischer titrations of our purified methanol indicated <0.05% water. Chloride absence was shown by tests with silver ion. All methanolic solutions were made with dried reagents. Reagent-grade acetone used in chloride analyses was shown to be chloride-free. Other chemicals were reagent grade.

Run Procedure.—Run mixtures were prepared in dim light. Dissolution times for the *trans*- and *cis*-compounds were 10 and 45 minutes, respectively. Solutions were sealed into well-dried Pyrex ampoules and placed simultaneously in a dark constant-temperature bath at 50.0 ± 0.05°. Ampoules were removed from the bath at known intervals, cooled to *ca.* 25° and two 10.00-ml. aliquots removed for free-chloride analysis by a rapid potentiometric method[4] using standard methanolic silver nitrate. The remaining 50 ml. was stored in the dark for spectral measurements made *ca.* 1 hour later.

Absorption spectra were measured in stoppered 10.00-cm. quartz cells with a Cary Model 11 spectrophotometer; dried methanol was used in the reference cell. Absorbancies of fresh run solutions exposed to light only during the 5-minute spectral scan remained constant to ±0.01 over 2-hour periods; all solutions were measured within this time.

Results and Discussion

Solvolysis of *trans*-Dichlorobis-(ethylenediamine)-chromium(III) Chloride.—Loss of ligand chloride by the *trans*-complex in methanol at 50° in the dark appears to follow a first-order rate law up to 15 hours, at which time *ca.* 30% of the first ligand chloride is released (Fig. 1). Based on one ligand chloride released, the concentration of unreacted complex at time t was taken as $2(\text{complex})_0 - (Cl^-)$, where $(\text{complex})_0$ is the initial concentration known from the gravimetric synthesis of the solution. The "anhydrous" methanol may conceivably have been as much as 0.04 *f* in H_2O (see Experimental section), a concentration 27 × greater than $(\text{complex})_0$, which could not be increased because of solubility limitations. Hence, aquation or methanolysis could account for the chloride release. Added low concentrations of water in alcoholic solutions of metal salts cause changes in the absorption spectra interpretable in some cases in terms of consecutive formation of aquo complexes from alcohol complexes.[11] *E.g.*, Jørgensen[11] estimates that chromium(III) nitrate in ethanol 0.04 *f* in H_2O has at 25° an average equilibrium cation composition $Cr(H_2O)_{0.06}(C_2H_5OH)_{0.94}^{+3}$. In methanol thermodynamic competition between CH_3OH and H_2O for chromium might then result in much more methanolysis than aquation of *trans*-$Cr(en)_2Cl_2^+$. Basolo[12] has reported that the analogous cobalt complex shows within several weeks essentially no change in absorption spectrum in methanol made 0.4 *f* in H_2O under conditions where, in water, the complex converts to the chloroaquo complex in one hour; since *trans*-$Co(en)_2Cl_2^+$ and *trans*-$Cr(en)_2Cl_2^+$ aquate at 25° at essentially the same rate,[13] Basolo's observation suggests that the solvolysis we observe is not aquation. Moreover, Adamson's conclusion[14] that substitution reactions in solvents having an –OH group occur *via* a bimolecular front-side displacement would imply that the rate of chloride release should be first order in

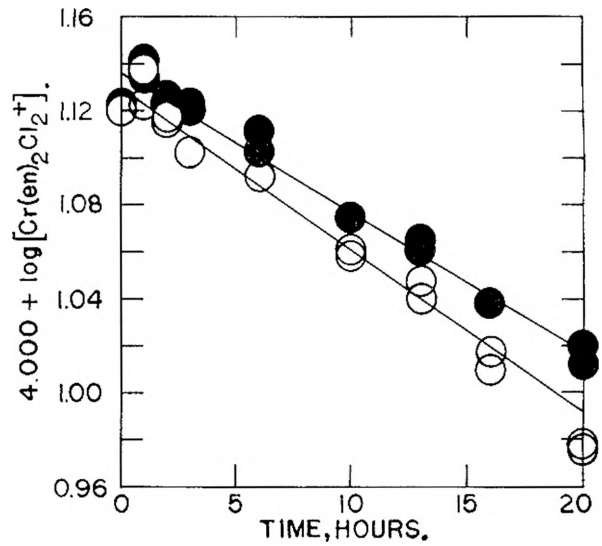

Fig. 1.—Solvolysis of 0.00152 *f* *trans*-$[Cr(en)_2Cl_2]Cl$ at 50°: in "anhydrous" methanol, <0.04 *f* in H_2O, ●; in methanol 0.22 *f* in added H_2O, ○; a run with 0.00102 *f* complex in "anhydrous" methanol gave the same initial slope as that shown for the filled circles.

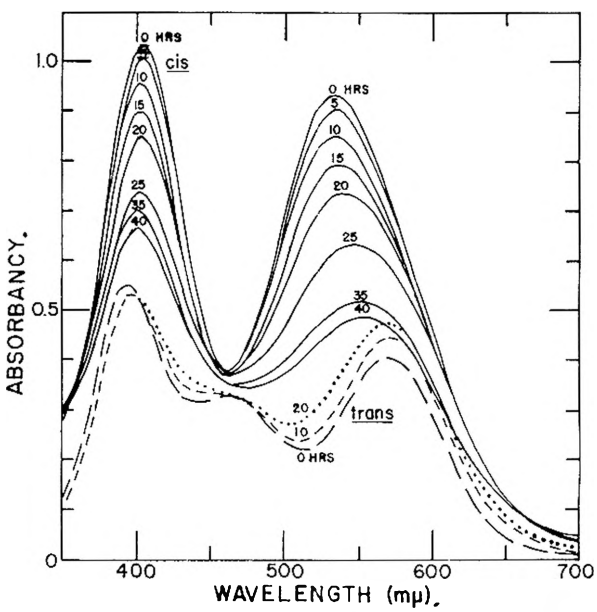

Fig. 2.—Dashed curves: change in absorption spectrum of 0.00152 *f* *trans*-$[Cr(en)_2Cl_2]Cl$ during solvolysis in methanol (<0.04 *f* in H_2O or 0.22 *f* in added H_2O) at 50°. Solid curves, change in absorption spectrum of 0.00122 *f* *cis*-$[Cr(en)_2Cl_2]Cl$ in methanol (<0.04 *f* in H_2O) at 50°. All spectra taken at room temperature.

(10) P. Pfeiffer, *Ber.*, **37**, 4255 (1904).

(11) J. Bjerrum and C. K. Jørgensen, *Acta Chem. Scand.*, **7**, 951 (1953); C. K. Jørgensen, *ibid.*, **8**, 175 (1954); L. I. Katzin and E. Gebert discussion with Jørgensen and Bjerrum, *Nature*, **175**, 425 (1955).

(12) F. Basolo, *J. Am. Chem. Soc.*, **72**, 4393 (1950).

(13) R. G. Pearson, R. A. Munson and F. Basolo, *ibid.*, **80**, 504 (1958); unpublished work of D. J. MacDonald and C. S. Garner on the *trans*-chromium complex in this Laboratory.

(14) A. W. Adamson, *ibid.*, **80**, 3183 (1958).

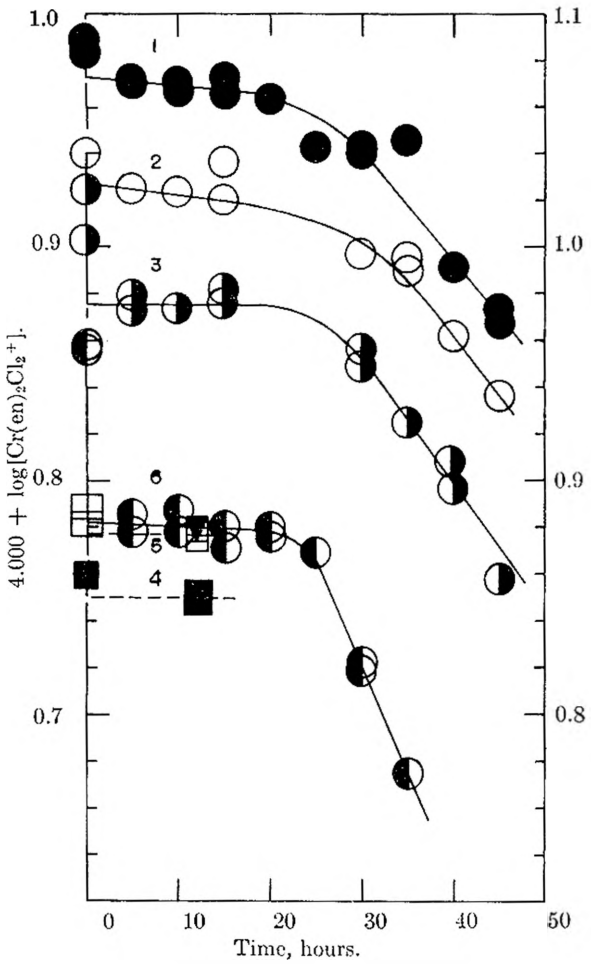

Fig. 3.—Ligand chloride release following isomerization of *cis*-$[Cr(en)_2Cl_2]Cl$ in methanol at 50°: ●, 1.22, 0; ○, 1.11, 0; ◑, 1.11, 0.22; ■, 1.00, 0.22—made 0.000974 *f* in HCl after 12-hr. point, giving ▼ point on curve 6; □, 0.976, 0.22—0.000972 *f* in HCl at start of run; ◐, 1.21, 0.44 (first number is initial milliformality of *cis* compound; second number is initial formality of added water). Left legend for curves 1, 2, 3; right legend for curves 4, 5, 6.

methanol or water; *trans*-$Cr(en)_2Cl_2^+$ should then release chloride at least 6 × faster in methanol 0.22–0.26 *f* in H_2O than in "anhydrous" methanol (<0.04 *f* in H_2O) if aquation alone were responsible, but at about the same rate if methanolysis predominates. Our pseudo first-order rate constants k_1 at 50°, $10^6\ k_1 = 3.78 \pm 0.22$ sec.$^{-1}$ in "anhydrous" methanol and $10^6\ k_1 = 4.43 \pm 0.30$ sec.$^{-1}$ in methanol 0.22 *f* in added H_2O, correspond to a rate ratio of 1.17 ± 0.11 in accord with the methanolysis hypothesis; the corresponding bimolecular rate constant k_2 would be $10^7\ k_2 = 1.59 \pm 0.22$ l. mole^{-1} sec.$^{-1}$. Bonding of methanol to chromium has been shown by the work of Adamson[14] and Koppel.[15]

Zero-time intercepts of the rate plots correspond to an initial loss of 12% of one ligand chloride, (only 6% if the 5–10 minute warm-up to 50° is omitted), both in "anhydrous" methanol and in methanol 0.22 *f* in added H_2O. Brown, Ingold and Nyholm[4,5] observed a similar rapid reaction releasing 1% of one ligand chloride from methanol solutions of the analogous *cis*-cobalt complex at 36° which they established as due to a slow attack by silver ion on the complex cation during titration for chloride.

cis–trans **Isomerization of *cis*-Dichlorobis-(ethylenediamine)-chromium(III) Chloride.**—Figure 2 (solid curves) exhibits the change with time in the absorption spectrum of the *cis*-complex in "anhydrous" methanol at 50° in the dark; the spectral changes are essentially the same in methanol 0.22 *f* in added H_2O, but are 5–7% faster in methanol 0.44 *f* in added H_2O. A first-order plot of log $[(A - A_\infty)/(A_0 - A_\infty)]$ *vs.* time (A_0, A and A_∞ are absorbancies[16] of the *cis* 530-mμ absorption peak at zero time, at time t and at isomerization equilibrium, respectively) is linear up to at least 13 hours (18% isomerization). The assumption that the principal reaction during this time is *cis–trans* isomerization is compatible with the spectra of the pure isomers, and is further supported by the fact that the slope of the first-order plot for the absorbancies at 403 mμ (main *cis* peak) agrees with that from the plot at 530 mμ. Because of solvolysis of the *trans* isomer the equilibrium isomerization spectrum could not be checked experimentally to confirm our assumption that it corresponds to all *trans* form; changes in the spectrum of the *trans* isomer during its solvolysis (dashed curves, Fig. 2) do not indicate appreciable conversion of *trans* to *cis* isomer under comparable conditions. The isomerization rate constant k is $10^6\ k = 4.13 \pm 0.11$ sec.$^{-1}$, *ca.* 100 × less than for the cobalt analog[7] in methanol at the same temperature.

Figure 3 gives the results of free-chloride analyses made concurrently with the spectral runs. As in the case of the *trans*-complex there is a zero-time loss of chloride from the *cis* cation (22–37%, depending on water content of methanol—see Fig. 3). Considered in the light of the *cis–trans* isomerization and the *trans*-solvolysis, the general shape of curve 2 (and perhaps curve 1) suggests the sequence of reactions could be *cis* → *trans* → solvolysis products. Final slopes of curves 1, 2 and 3 correspond to rate constants of *ca.* 3×10^{-6} sec.$^{-1}$, about the same as the specific rate of the *trans* solvolysis. However, the rather sharp bending over of curves 3 and 6 is incompatible with this reaction scheme alone; nor have we been able to explain the "bending" by invoking concurrent solvolysis of the *cis*-complex either with or without a concurrent back reaction of the *trans*-complex. The *cis* system is a complex one and the reactions of these chromium complexes in methanol are much more complicated than those of the cobalt analogs.

Molar Absorbancy Indices.—From the relation $a_M = A/(cl)$, where c is the molarity of the complex and l the optical path length (cm.), the molar absorbancy indices a_M for *cis*- and *trans*-$[Cr(en)_2Cl_2]Cl$ in methanol at room temperature at their absorption peaks have been found to be 84.7 at 403 mμ and 77.0 at 530 mμ for the *cis*-isomer and 34.7 at 393 mμ, 20.7 at 460 mμ and 25.2 at 570 mμ for the *trans*-isomer. For the *cis*-isomer the 403-mμ peak

(15) J. Koppel, *Z. anorg. Chem.*, **28**, 461 (1901).

(16) Beer's law was shown to be valid for the *cis* 530-mμ peak and nearby *trans* 517-mμ minimum over the respective ranges 1.02–1.22 *f* and 1.11–1.52 *f*, using fresh solutions.

is higher than the 530-mμ peak, whereas in water the relative peak heights are reversed.

Acknowledgments.—Help from Mr. Wayne A. Lavold, who prepared the *trans*-compound, and Miss Mary E. Burke, who took data during some of the night rate work, is gratefully acknowledged.

SELF-DIFFUSION COEFFICIENTS OF ISOMERIC PENTANES[1]

By E. Fishman and T. Vassiliades

Department of Chemistry, Syracuse University, Syracuse, N. Y.

Received December 4, 1958

An earlier paper by one of us[2] reported the self-diffusion coefficients of *n*-pentane and *n*-heptane measured over an extended temperature range. Interpretation of the data by the Eyring theory of rate processes[3] was undertaken, since normal hydrocarbons provide a direct test of the simple model used in that theory. It was found that the theory correlated the self-diffusion, viscosity and molecular size data quite well.

This paper reports an extension of the earlier work to a situation where molecular *shape* rather than chain length is the variable parameter whose effect is correlated by the Eyring theory. The self-diffusion coefficients of isopentane and cyclopentane were measured over an extended temperature range and found to follow the equations

$$D = 9.8 \times 10^{-4} e^{-1789/RT}$$

for isopentane and

$$D = 3.0 \times 10^{-3} e^{-2760/RT}$$

for cyclopentane. These are to be compared with

$$D = 8.1 \times 10^{-4} e^{-1587/RT}$$

for *n*-pentane.[2,4]

As in the previous work, a range of capillary lengths and diffusion times was employed in order to check for systematic error. Convincing evidence that the systematic errors in this particular capillary diffusion technique are small is shown by the comparison of the results given in ref. 2 with the self-diffusion data on the same liquids published by Douglass and McCall.[5] Although both the capillary and the spin-echo techniques are open to criticism for possible uncorrected systematic errors, the two methods are completely independent of each other and their close agreement tends to confirm both techniques.

Results and Discussion.—The results are shown in Table I; reported diffusion coefficients are averages of at least four determinations.

Figure 1 includes the data on *n*-pentane and neopentane for comparison. The straight lines were determined by the method of least squares; equations for the lines have been presented above. The frequency factors *and* the activation energies are in the order cyclo > iso > normal. Since the activation energy dominates in determining the magnitude of a rate constant at a given temperature, cyclopentane has the lowest diffusion coefficient although the frequency factor is highest. This means that diffusion of the most symmetrical molecule is favored by orientation or entropy factors, but relatively opposed by energy considerations. This idea will be explored quantitatively below.

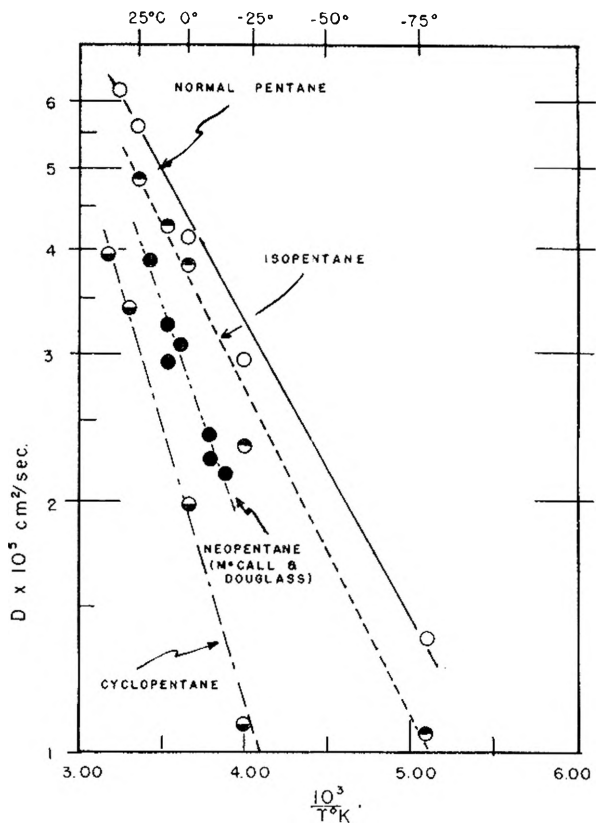

Fig. 1.—The logarithm of the self-diffusion coefficient *vs.* reciprocal temperature.

Table I

Self-diffusion Coefficients of Iso- and Cyclopentanes[a]

Isopentane		Cyclopentane	
Temp., °C.	$D \times 10^5$, cm.²/sec.	Temp., °C	$D \times 10^5$, cm.²/sec.
25.5	4.85	46.2	3.97
10.0	4.26	30.0	3.41
0.0	3.83	0.0	2.00
−22.9	2.31	−22.9	1.09
−78.5	1.06	−78.5	0.28

[a] The average error in the measurements, based on the average deviation of *D* from its mean value at each temperature, is about 5%.

It would be expected that cyclopentane, having the highest energy of vaporization, would also have the highest activation energy for diffusion; however, this alone does not account for the largeness of the activation energy. As may be seen in Table II, cyclopentane uses a larger fraction of its vaporization energy for diffusion than the less symmetrical pentanes. This ratio has been correlated with the fraction of the intermolecular bonds

(1) Based on the Master's Thesis of T. Vassiliades, Syracuse University (1958). Presented at the 134th meeting of the American Chemical Society, Chicago, Ill., September 12, 1958.

(2) E. Fishman, This Journal, **59**, 469 (1955).

(3) S. Glasstone, K. J. Laidler and H. Eyring, "The Theory of Rate Processes," McGraw-Hill Book Co., New York, N. Y., 1941.

(4) $D = 4.6 \times 10^{-3} e^{-2530/RT}$ has been reported for neopentane (private communication, David W. McCall.)

(5) D. C. Douglass and D. W. McCall, This Journal, **62**, 1102 (1958).

TABLE II

RATIO OF VAPORIZATION TO ACTIVATION ENERGIES AT 0°

Liquid	E_{vap} (kcal./mole)	E^*_{diff} (kcal./mole)	Ratio E_{vap}/E_{diff}
n-Pentane	5.7	1.6	3.6
Isopentane	5.8	1.8	3.2
Cyclopentane	6.9	2.8	2.5

existing in the liquid lattice for each molecule which must be broken in forming the activated complex for flow. Thus the data of Table II imply that, in moving through the liquid lattice, the extended chain molecule proceeds with less distortion of the lattice than the more spherical molecule, which requires nearly half of its vaporization energy to reach the activated state for diffusion.

If the usual assumptions of the Eyring rate process theory are accepted, an entropy of activation can be calculated from the diffusion coefficients and the activation energy using the equation

$$D = e\lambda^2 \frac{kT}{h} e^{\Delta S^*/R} e^{-\Delta E^*/RT}$$

Here, all constants have their conventional meaning and λ, with the dimensions of cm., is a jump distance for an individual diffusion step. The frequency factor, then, is the collection of terms $e\lambda^2 (kT/h)e^{\Delta S^*/R}$, and at any one temperature, differences in frequency factor from one system to another are contained in the term $\lambda^2 e^{\Delta S^*/R}$. There is, at present, no way of obtaining an independent value of λ; in order to calculate ΔS^* a value of λ must be assumed. Table III shows the results for ΔS^* calculated at 0° with the assumption of 1.3 Å. for λ, the length of a methylene group in a saturated hydrocarbon. Other assumptions about λ, say using the length of each molecule, lead to different numerical results for ΔS^*, but the sequence of ΔS^* values is not changed by any reasonable choice of λ's. These relative values of ΔS^* indicate a greater need for orientation in the diffusion of the normal hydrocarbon molecule than for the cyclic isomer. Thus the *n*-pentane, when compared to more symmetrical molecules, has a lower frequency of properly-oriented jumps (the jump should be along the chain axis) but a much larger proportion of the jumps leads to diffusion. The energy barrier is relatively low in this favored direction and the over-all diffusion rate is higher.

TABLE III

EVALUATION OF ΔS^* AT 0° ASSUMING 1.3 Å. FOR λ

Liquid	$D \times 10^5$ cm.²/sec.	$\lambda^2 e^{\Delta S^*/R}$ Å.	ΔS^*, e.u.
n-Pentane	4.14	0.71	−2.4
Isopentane	3.83	0.82	−1.8
Cyclopentane	2.00	2.76	0.59

In conclusion, the lattice parameters, λ_1 and $(\lambda_2\lambda_3)^{1/2}$, defined in the Eyring theory and calculated from the self-diffusion and viscosity coefficients at 0° are shown in Table IV. It is obvious that these parameters do not show the expected isomeric trends.

TABLE IV

LATTICE PARAMETERS AT 0°

Liquid	$D\eta/kT \times 10^8$, cm.$^{-1}$[a]	V(cc.)	λ_1, Å.	$(\lambda_2\lambda_3)^{1/2}$
n-Pentane	3.0	111.6	2.4	8.8
Isopentane	2.8	112.5	2.3	9.0
Cyclopentane	3.2	91.6	2.2	8.3

[a] Viscosities taken from Timmermans, "Physico Chemical Constants of Pure Organic Compounds," Elsevier Publishing Co., New York, N. Y.

Acknowledgment.—The authors are grateful to the Research Corporation for generous support of this research.

PHYSICAL CHEMISTS

NEEDED IN THE FAST GROWING

SEMICONDUCTOR INDUSTRY

- **Men with MS or PhD degrees desired, to be members of the technical staff in R & D at Fairchild Semiconductor Corporation.**

- **Fairchild is the fastest growing firm in a rapidly changing industry. Firm's success to date is attributable to a research-minded top management, all members having exceptional professional backgrounds.**

- **Company will pay relocation costs to Palo Alto, California (near San Francisco)—one of the most desirable areas in the west.**

IMMEDIATE OPENINGS

1. Surface Chemist, MS or PhD level

To conduct basic studies of surface phenomena to improve quality and stability of semiconductor devices—to improve present techniques of surface cleaning and coating—also to seek new and better surface treatments. For development of personal stature, publication of basic studies will be encouraged.

2. Electrochemist, MS or PhD level

To conduct basic research in the electrochemistry of semiconductors and related materials—to perform and supervise projects concerned with electrochemical and chemical etching of materials, developing control and selectivity—to develop electroplating and other plating with good process control. Publication of basic studies will be encouraged.

Please send detailed resume including salary requirements. Palo Alto interviews for qualified applicants will be arranged from anywhere in the U. S.

FAIRCHILD
SEMICONDUCTOR CORPORATION

844 CHARLESTON ROAD • PALO ALTO, CALIFORNIA • DAvenport 6-6695